In the Name of God
the Merciful, the Compassionate

To my Father and Mother

UNIVERSITY OF SOUTHAMPTON

THE GEOCHEMISTRY OF DEEP SEA SEDIMENTS FROM THE INDIAN OCEAN AND THE STABILITY OF THEIR SMECTITE, PALYGORSKITE AND ZEOLITE PHASES

by

POORAN SAYAD

Thesis submitted for the degree
of
Doctor of Philosophy

Department of Geology 1984

UNIVERSITY OF SOUTHAMPTON

ABSTRACT

FACULTY OF SCIENCE

GEOLOGY

Doctor of Philosophy

THE GEOCHEMISTRY OF DEEP SEA SEDIMENTS FROM THE INDIAN OCEAN AND THE STABILITY OF THEIR SMECTITE, PALYGORSKITE AND ZEOLITE PHASES

by Pooran Sayad

Cretaceous to Quaternary sediments cored in Deep Sea Drilling Project Legs 22, 23, 24, 25 and 26 in the Indian Ocean were studied. Chemical analyses of zeolites (phillipsite (phill) + clinoptilolite (clin)), palygorskite (paly), mixed layer illite/smectite (MLIS) isolated from the sediments and bulk sediments were performed by Energy Dispersive X-ray and β-probe techniques. Bulk chemistry element-comparisons (i.e. Ti vs. Al, Cr vs. TiO_2 and Fe/Ti vs. Al/(Al+Fe+Mn) indicated the basaltic and silicic volcanic material contribution to the sediments. The sediments contain authigenic minerals: mainly phillipsite (Miocene and younger), clinoptilolite (Cretaceous to Miocene), mixed layer illite/smectite and palygorskite. Palygorskite, mixed layer illite/smectite and clinoptilolite assemblages are present in Cretaceous sediments. Biogenic silica is relatively abundant everywhere. Opal-CT formed from dissolved radiolaria, diatoms and sponge spicules is mainly associated with clinoptilolite.

Phillipsite and mixed layer illite/smectite, with a high percentage of expandable layer, are thought to be derived from volcanic glass, whereas palygorskite can form from mixed layer illite/smectite. In the absence of detrital mixed layer illite/smectite (i.e. MLIS with a low percentage of expandable layer), authigenic mixed layer illite/smectite (i.e. MLIS with a high percentage of expandable layer) results from the alteration of volcanics and becomes a sink for Mg^{2+}. On moving into more siliceous interstitial waters on burial, clinoptilolite could form at the expense of mixed layer illite/smectite and silica. In the presence of detrital mixed layer illite/smectite, Mg^{2+} released from the alteration of volcanics (plus additional Mg^{2+} from sea water, or hydrothermal solutions or Mg-bearing minerals) could react with mixed layer illite/smectite to form palygorskite. Clinoptilolite could then form at the expense of palygorskite on moving into more siliceous interstitial waters on burial. The suggested reactions are:

1. $MLIS_{(authigenic)} + Silica_{(biogenic\ and/or\ volcanic)} \longrightarrow clin$
2. $Phill + Silica_{(biogenic\ and/or\ volcanic)} \longrightarrow clin$
3. $MLIS_{(detrital)} + Silica_{(biogenic\ and/or\ volcanic)} + Mg^{2+} \rightleftharpoons paly$
4. $Paly + Silica_{(biogenic\ and/or\ volcanic)} \longrightarrow clin + Mg^{2+}$

Reactions 1, 2 and 4 show negative free energies of reaction, whereas reaction 3 is almost at equilibrium using activity data for ions in interstitial waters.

Thermodynamically, phillipsite, palygorskite and mixed layer illite/smectite are unstable relative to clinoptilolite, which is favoured by high silica concentrations. The stability diagrams indicated that high Mg^{2+} and pH, and low to high silica, are necessary for palygorskite formation compared with mixed layer illite/smectite and clinoptilolite.

ACKNOWLEDGEMENTS

I gratefully acknowledge the supply of sample material from the Deep Sea Drilling Project.

My deepest gratitude is expressed to my Supervisor, Dr. M.E. Cosgrove, for valuable comments, critical suggestions and encouragement concerning my thesis.

The author's gratitude is extended to Mr. G. Jack, Mr. K. Gosdon, Mr. R.A. Saunders, Mr. B. Marsh and Mrs. A. Dunkley for technical assistance.

I would also like to thank Professor F. Hodson and Professor R.W. Nesbitt for their interest in my research.

Further, I wish to thank Mrs. K. Sharpe for typing this thesis, and for the useful suggestions she made during the typing process.

Finally, I would like to express my deepest gratitude to my parents, Mr. Mohammad Ali Sayad and Mrs. Sabrieh Kardony, for their patience and the continuous financial and moral support throughout the entire period of my studies and preparation of the present thesis. I also wish to thank all the members of my family, particularly my youngest sister and brother, Miss Parichehr Sayad and Mr. Pedram Sayad, for their moral support and co-operation throughout my research studies.

C O N T E N T S

/contd.over

CONTENTS contd.

CONTENTS contd.

/contd.over

CONTENTS contd.

/contd.over

CONTENTS contd.

/contd over

CONTENTS contd.

/contd.over

CONTENTS contd.

/contd.over

CONTENTS contd.

LIST OF ABBREVIATIONS

In the present thesis the various abbreviations used are listed as follows:

a.ss = amorphous silica saturation

B = 100 - total mineralogy (biogenic silica, opal-CT, volcanic glass and minor minerals)

bar = barite

B.M = biological matter

calc = calcite

c.c = continental crust

CL = clin = clinoptilolite

Cr = cristobalite

Dec = December

Do = Dol = Dolo = Dolomite

Feb = February

G = ethylene glycol treated

gar = garnet

Gib = Gibbsite

Go = Goethite

H = heated

Hali = Halite

Ilm = Ilmenite

Int = Interlayer

I.W = Interstitial water

Kf = K-feld = K-feldspar

mont = montmorillonite

ML = MLIS = IS = mixed layer IS = mixed layer illite/smectite

N = Normal

Oct = octahedral

Op-CT = opal-CT = disordered cristobalite/tridymite

Org C = Organic C = organic carbon

Paly = palygorskite

Pf = plag = plagioclase

Phill = phillipsite

q.s = quartz saturation

Qtz = qtz = quartz

Sample No. = Sample number

/ contd.over

List of Abbreviations contd.

smec	=	smectite
S.W	=	sea water
tet	=	tetrahedral
TM	=	terrigenous matter
tr	=	tridymite
VM	=	volcanic matter
Zir	=	zircon
ΔG_f^o	=	Standard free energy of formation
ΔG_R^o	=	free energy of reaction
%Exp	=	%E = percentage of expandable layer

CHAPTER I

INTRODUCTION

A. Object of the Present Study

The object of the present study is to investigate the relative stabilities of palygorskite, phillipsite, clinoptilolite and mixed layer illite/smectite (MLIS) as they occur in deep sea sediments.

The standard free energy of formation (ΔG^{o}_{f}) of a mineral depends on its chemical composition and the nature of its chemical bonds. Thus ΔG^{o}_{f} values are useful for comparing the stabilities of different minerals and mineral assemblage. Previously thermodynamic data for a large number of minerals were missing, but slowly this information is accumulating. Such data enable predictions to be made of the field conditions of mineral formation and to construct stability diagrams. Therefore, with these facts in mind, one of the aims of the present study is to develop thermodynamic models for predicting the formation and stability of palygorskite, zeolites and MLIS in the deep sea environment. The consideration of thermodynamic data is a powerful technique when applied to geological problems, for it is commonly possible to write reactions in terms of simple components for any given mineral assemblage. The more reactions that can be written in terms of these simple components, the greater the amounts of information that can be obtained from the mineral assemblage.

The Indian Ocean sediments were chosen for study since palygorskite and zeolites are known to occur in the basins, on the margins and on the ridges of the ocean. Consequently there are several theories for their origin. For example, palygorskite in the north-west of the Indian Ocean is thought to be of detrital origin, since its abundance increases towards the continent and it is known to form on the continents surrounding the Arabian Sea (Kolla et al., 1981; Goldberg et al., 1970). Conversely, palygorskite on the flank of the Ninetyeast Ridge is suggested to be of diagenetic origin, since it is far from the continent (Couture, 1977a).

In the present study, 90 samples from Legs 22, 23, 24, 25 and 26 in the Indian Ocean were studied. The selection of samples was based upon the presence of zeolites, palygorskite and MLIS in the cores. Chemical analyses were carried out as follows:

1) major element analyses for 9 elements (Si, Ti, Al, Fe, Mg, Ca, K, Na, P) on whole sediment samples;

2) trace element analyses for 17 elements (Mo, Nb, Zr, Y, Sr, Rb, Ni, Mn, Cr, V, Pb, As, Zn, Cu, Ba, Ce, La) on whole sediment samples;

3) major element analyses of 21 monomineralic clay minerals (mixed layer illite/smectite or smectite);

4) major element analyses of 17 clinoptilolite, 8 phillipsite and 9 palygorskite samples for 9 elements by Energy Dispersive X-ray;

5) CO_2 and organic carbon (C_{org}) determination on all whole sediment samples;

6) iron determinations, as Fe^{2+} and Fe^{3+}, on all whole sediment samples.

Mineralogical analyses were undertaken as follows:

1) bulk mineral analyses for 10 minerals (quartz, K-feldspar, plagioclase, clinoptilolite, phillipsite, total clay, calcite, dolomite, pyrite and halite);

2) clay mineral analyses of the < 2 μm fraction for 5 minerals (mixed layer illite/smectite, illite, kaolinite, palygorskite and chlorite) on 86 sediment samples;

3) clay mineral analyses of 3 fractions (2 - 0·2 μm, 0·2 - 0·08 μm and $<$ 0·08 μm) for 5 minerals on 43 sediment samples.

The stratigraphic details of each site are shown in Figs.1-1 to 1-4. The sedimentological characteristics of the present study sediments are also presented in Table 1-1. The geological time scale used is shown in Table 1-2.

B. The Indian Ocean

1. Form - Limits

The limits of the Indian Ocean which are shown in Figure 1-5 are:

a) to the west, the east coast of Africa from Cape Agulhas ($35^{\circ}S$-$20^{\circ}E$) up to Cape Guardafui which marks the southern point of the entrance of the Gulf of Aden;

b) on the north, the south coast of Arabia, Iran and the west and east coast of the Indian Peninsula;

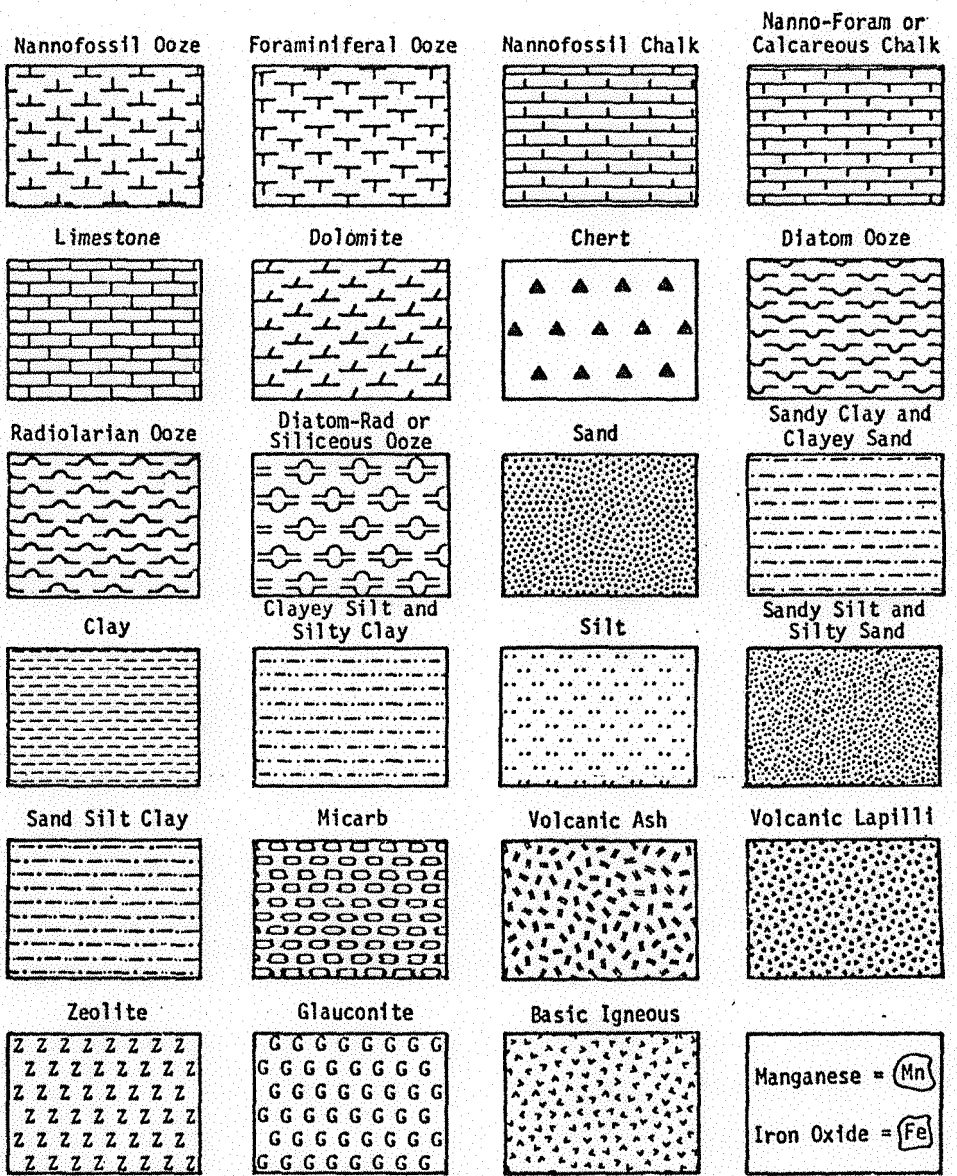

. Lithologic symbols and letters used on core and site summary forms.

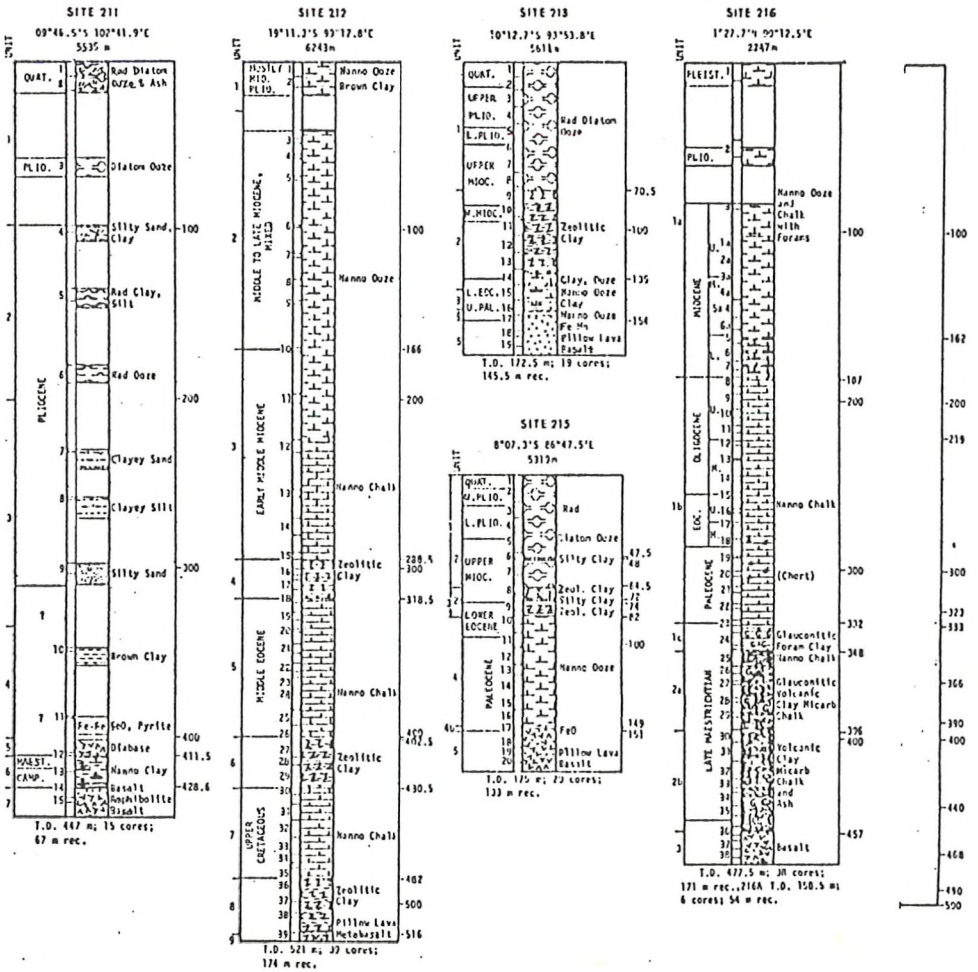

Fig1-1. Stratigraphy of sites of Leg 22. Data from Initial Report of Deep Sea Drilling Project, Leg 22.

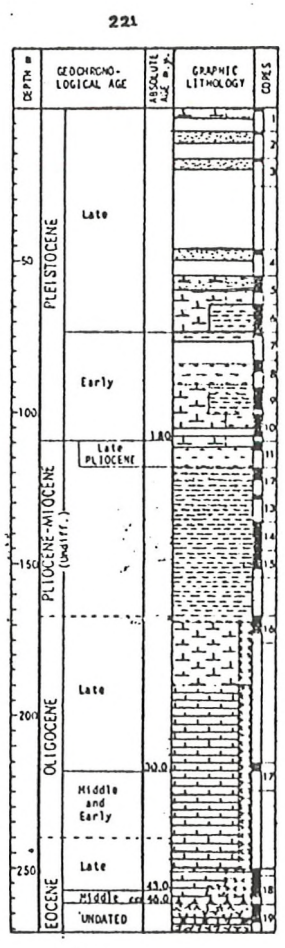

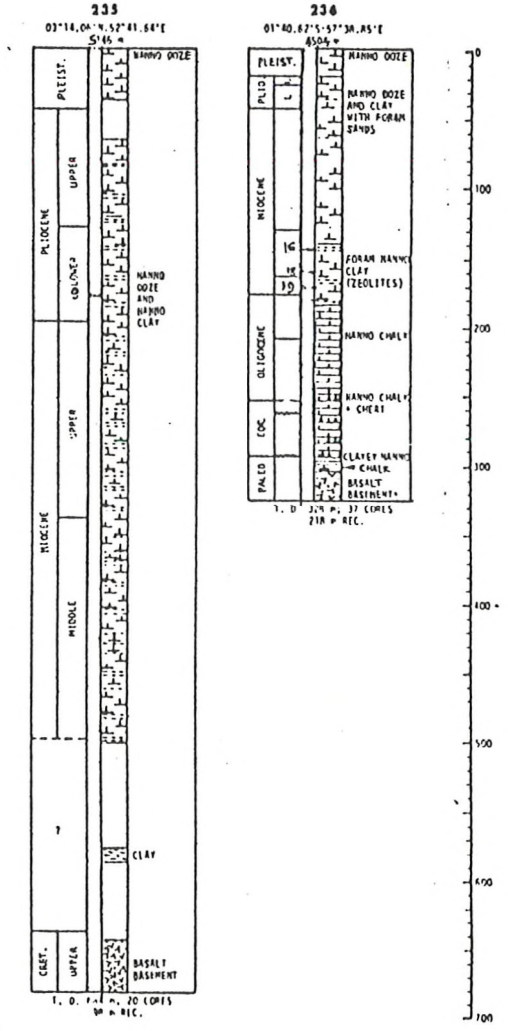

Leg 23

Leg 24

Fig.1-2. Stratigraphy of sites of Legs 23 and 24. Data from Initial Reports Deep Sea Drilling Project, Legs 23 and 24.

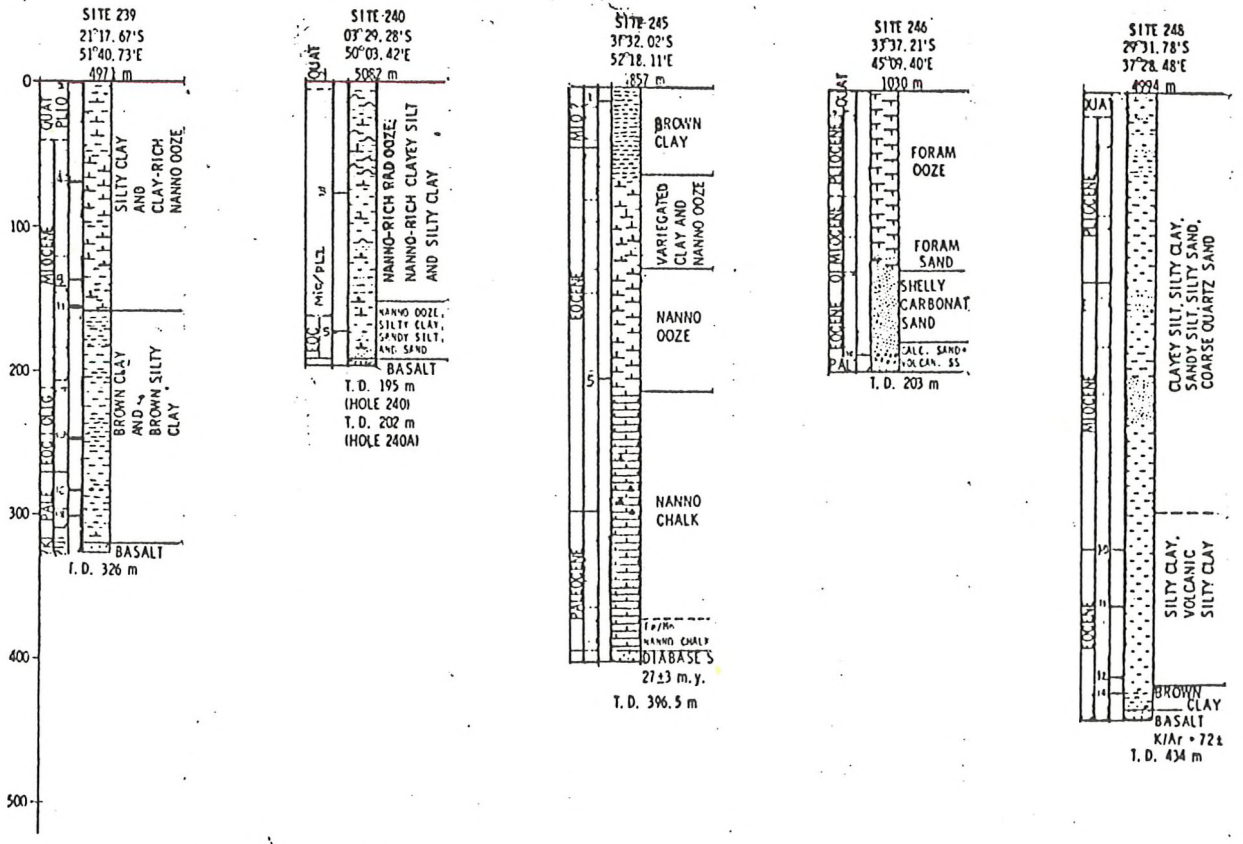

Fig-1-3.Stratigraphy of sites of Leg 25.Data from Initial Report of Deep Sea Drilling Project,Leg 25.

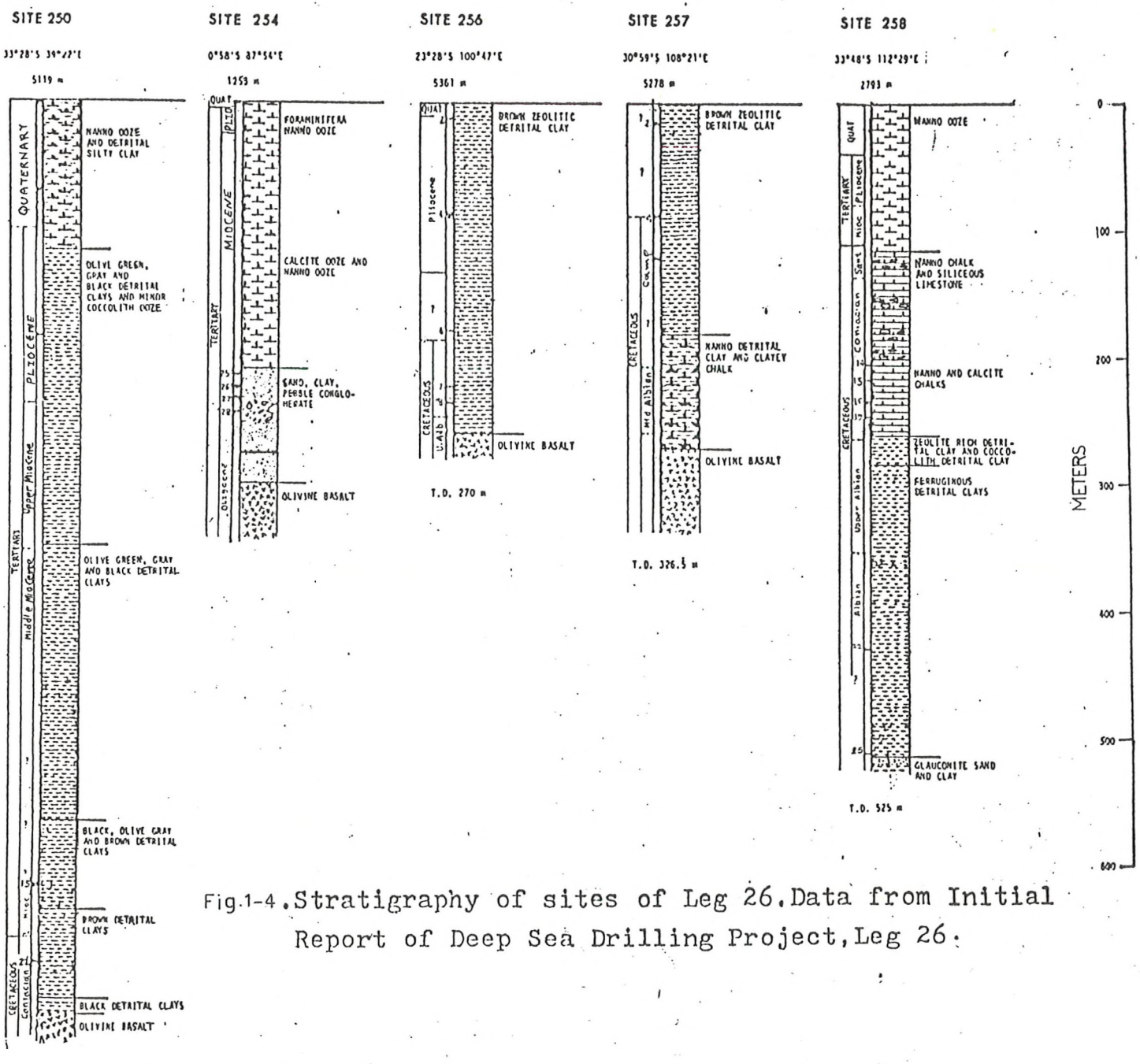

Fig.1-4. Stratigraphy of sites of Leg 26. Data from Initial Report of Deep Sea Drilling Project, Leg 26.

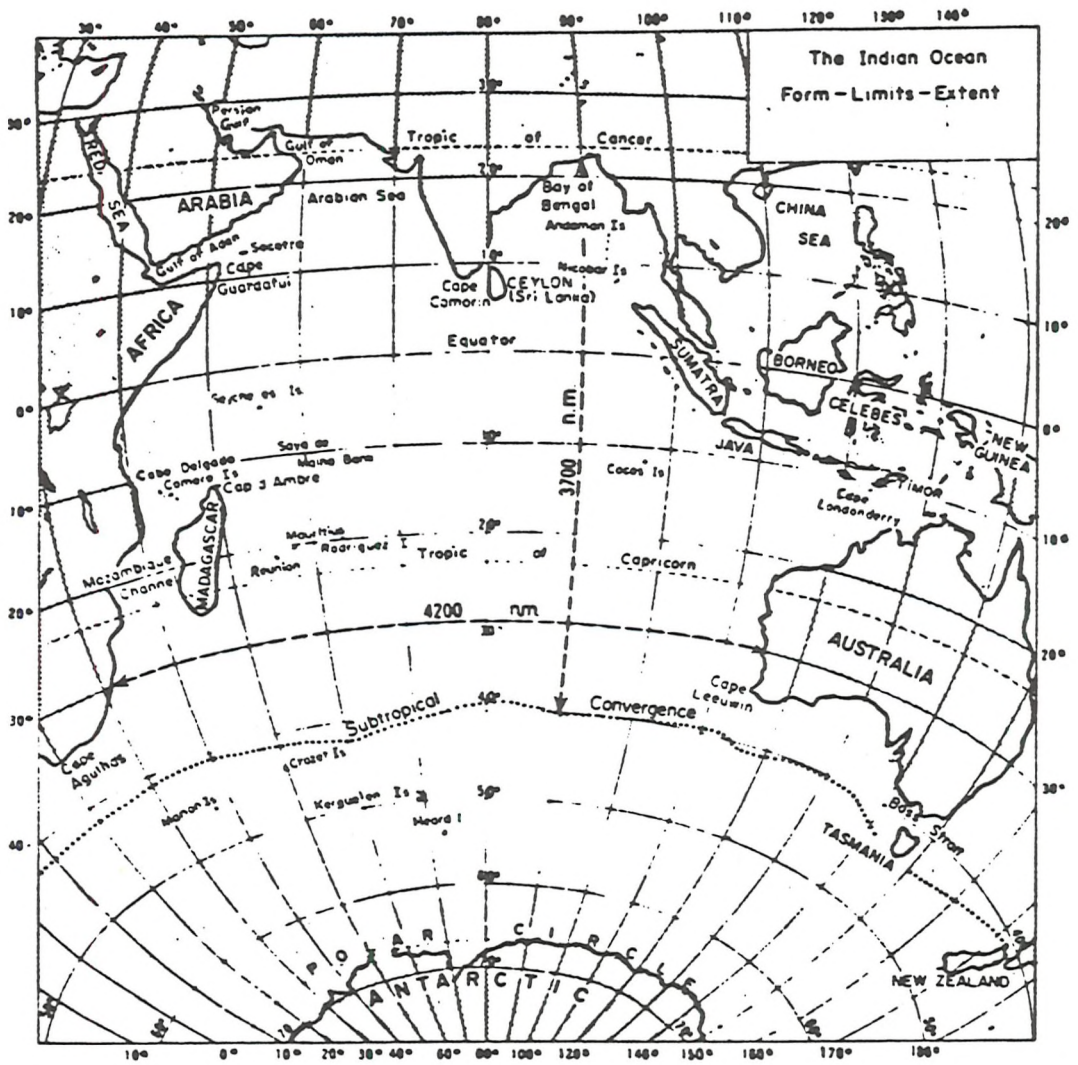

Fig·1–5 . The Indian Ocean. Form—limits—extent.
(after Tchernia ,1980)

c) to the south this ocean is in free communication with the Southern Ocean, and their separation is represented by the hydrological limit of the Sub-tropical Convergence situated at about 40°S latitude.

d) to the east, the coasts of Burma, Malaysia, the principal island arc of Indonesia and the west coast of the sub-continent of Australia.

The Indian Peninsula divides its northern part into two great gulfs: the Bay of Bengal and the Arabian Sea, which itself extends to the north of the Gulf of Oman and the Persian Gulf, and to the west by the Gulf of Aden and the Red Sea (Tchernia, 1980).

2. Depth of the Indian Ocean

The mean depth of the Indian Ocean is about 3800m. The great basins have depths of 5000-6000m, reaching even 6500m in the Wharton Deep to the north-west of Australia. The maximum depth is found in the Java Trench on the convex side of the chain of the Sunda Islands, the deepest point of which is 7700m (Tchernia, 1980).

3. Present day sedimentation

The Indian Ocean is the smallest of the three major ocean basins, but it appears to be the most geologically complex. One of the characteristics of the Indian Ocean which serves to distinguish it from the Atlantic and Pacific Oceans is the abundance of aseismic, relatively shallow, flat-topped, often sediment-covered and steep-sided ridges, or plateau-like morphological features, which have been termed 'microcontinents' by Heezen and Tharp (1965) and 'oceanic ridges' by Udintsev (1965). Its major physiographical features are shown in Figure 1-6, and they have been extensively described by Laughton et al. (1971). Information on the sediments of the Indian Ocean has only been acquired relatively recently and is derived largely from the results of the Deep Sea Drilling Project (Von der Borch et al.,1974; Whitmarsh et al.,1974; Fisher et al.,1974; Simpson et al.,1974; Davies et al., 1974). The present day pattern of sedimentation is shown in Figure 1-7.

Thick terrigenous sediments are accumulating on the Indus Cone, the Bengal Fan and the Zambezi Fan. Carbonate sediments are accumulating in the shallow areas along the Australian and African coasts, on the shallow ridges and platforms and in the shallower parts of the Somali Basin. Siliceous sediments are found in significant amounts in the sub-polar regions of the Crozet Basin and in the equatorial regions of the deep basin. Elsewhere, deep sea clays are still accumulating, except in the Wharton

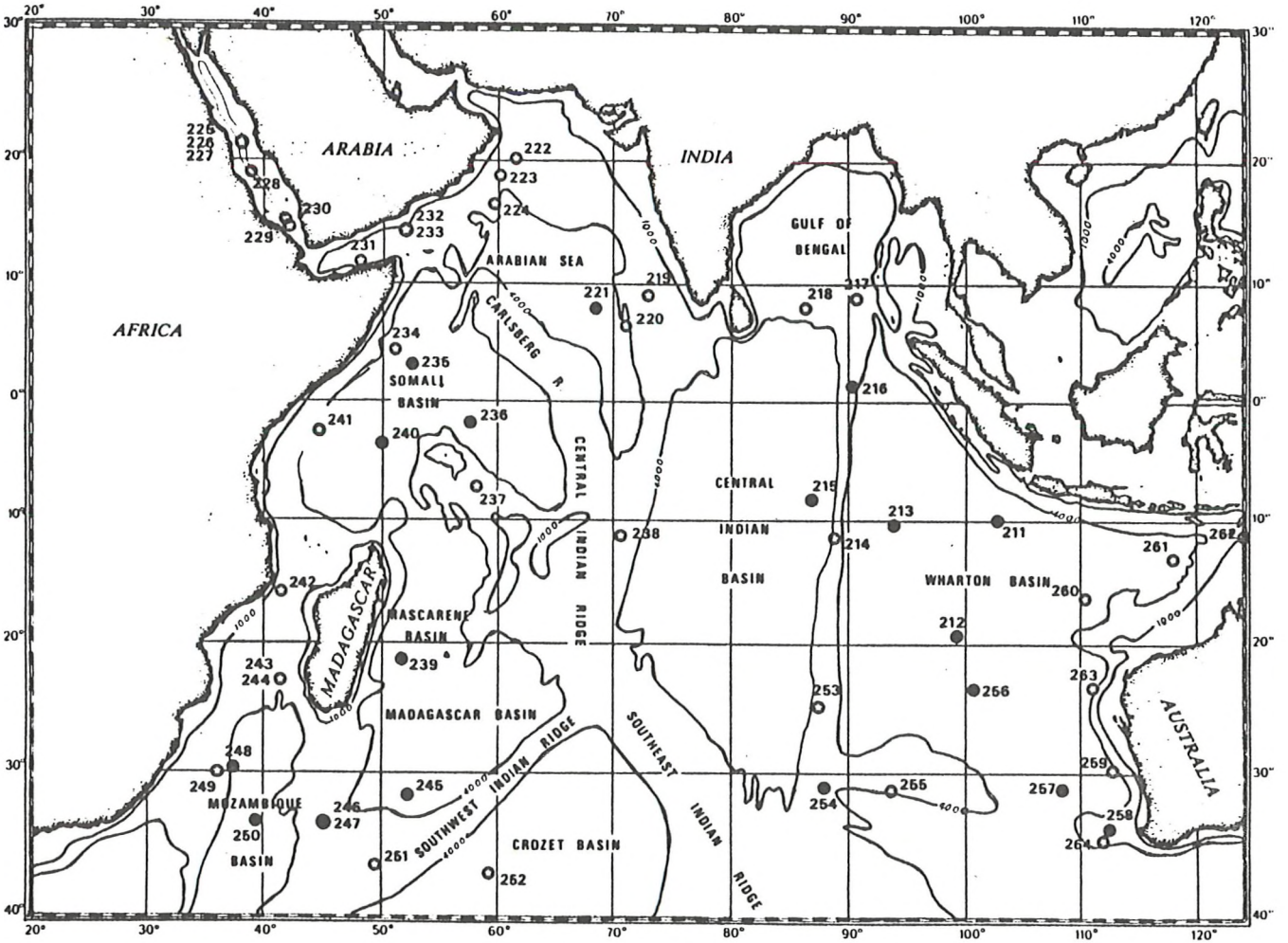

Fig 1-6 . D.S.D.P. *Glomar Challenger* drill sites in the Indian Ocean.
The present study sites are shown by filled circles.

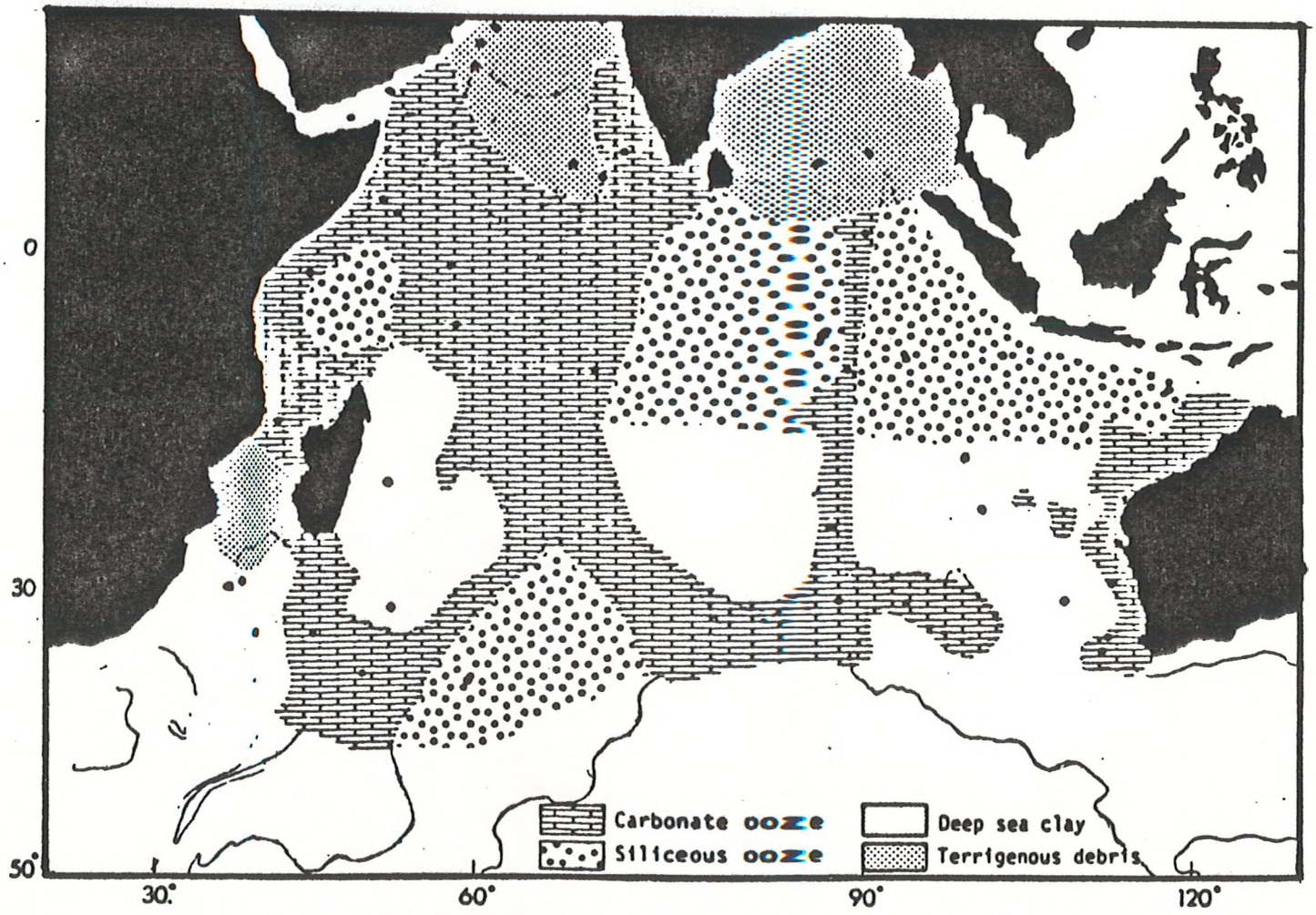

Fig.1-7 . ***Present-day sedimentation in the Indian Ocean. Solid circles represent Deep Sea Drilling Project sites.***
(From Luyendyk et al., 1974)

Basin and Southern Mascarene Basin, and parts of the Crozet Basin. Sedimentation appears to have stopped and deposition is minimal between Broken Ridge and the south-east Indian Ridge, where an extensive area of manganese nodule pavement is present (Kennett et al., 1975). The lack of deposition in these areas is presumed to be due to isolation and/or the activity of deep currents (Kidd et al., 1978).

4. Sediment sources

The nature of sediments and sedimentation processes in the Indian Ocean could be potentially complex because of the combination of an active mid-oceanic ridge, aseismic ridges, micro-continents, plateaux and deep basins in the ocean (Heezen et al., 1964) and the asymmetric distribution of the surrounding land masses. Several sediment sources and modes of sediment transport are distinguished in the Indian Ocean.

Fluvial and aeolian modes of transport of the detrital material are the most important in the Arabian Sea. The eastern Arabian Sea receives its fluvial input primarily from the Indus River, which drains the Himalayas as well as large areas of semi-arid to arid land in west Pakistan and north-west India. A number of smaller rivers, chiefly the Narbada, with a common outlet to the Arabian Sea through the Gulf of Cambay, drain the middle portion of India, where the soil is derived from the weathering of the Deccan Traps (Goldberg et al., 1970; Weser, 1974). The arid regions adjoining the northern and western Arabian Sea have a few small rivers which provide a minimum of fluvial products (Goldberg et al.,1970). The aeolian input to the Arabian Sea has been suggested by many authors. Goldberg et al. (1970) believed that the sediments could have been transported from an area to the north, perhaps the desert regions of northern India and west Pakistan to the basin. They suggested that this input is also carried to the equatorial regions of the Indian Ocean. Kolla et al. (1981) suggested the aeolian contribution to the Arabian Sea from the following region: Iran-Makran region, Arabian Peninsula and Somalia. Mallik (1974) has studied heavy minerals from Sites 223 and 224 in the Arabian Sea and suggested mixed igneous and metamorphic sources such as occur along the Arabian coastal plain and on Masira and the Kuria Muria Islands in the Arabian Sea. Papavasiliou (1979) believed that the combination of intense monsoon systems and arid climate in this area, coupled with the proximity of Sites 223 and 224 to the Semail ophiolites (Oman mountains and Masira Island) could result in a very important aeolian input of mafic detritus.

The eastern part of the Bay of Bengal and southward well beyond the Equator on both sides of the Ninetyeast Ridge, including the Java Trench, is influenced by the Ganges and Brahamaputra Rivers, draining the Himalayan region (Kolla et al., 1973a, Goldberg et al., 1970). The western part of the Bay of Bengal is influenced by the rivers discharging into the Bay from the east coast of India and carrying high contents of montmorillonite.

Kolla et al. (1973a) observed the influence of windborne volcanic material from the Indonesian Island arc in the regions landward of the Java Trench, the Cocos Roo Rise and the Ninetyeast Ridge. They also noticed the influence of the south-easterly winds on the southern part of the Wharton Basin, extending somewhat west of the Ninetyeast Ridge south of 15°C, which carry kaolinite-rich clays from the lateritic soils of western Australia. They believed that the smectite abundance in the area between west of the Ninetyeast Ridge and the Mid-Indian Ridge may be in part related to Mid-Indian Ridge volcanics. Slumping and washing of the sediments from this ridge into the adjacent deep areas may be the mechanisms of sediment dispersal. The presence of red and brown clays and the high amount of phillipsite suggest that considerable quantities of smectite may be derived from local (between the ridges) submarine volcanics or from global fall-out of volcanic dust (Lisitzin, 1972). According to Girdley et al. (1974), terrigenous contributions to the Mascarene Basin are possible from eastern Madagascar and the Mascarene Islands. Reunion and Mauritius could also contribute to the Mascarene Basin (Fisher et al., 1974; Hekinian, 1968). They also noted that Eastern Africa (Somalia and Kenya) and the Seychelles Islands contribute terrigenous material to the Somali Basin, whereas the Mozambique Basin receives terrigenous debris from eastern and south-eastern Africa (Mozambique and South Africa), as well as from western and south-western Madagascar.

5. Climatology of the Indian Ocean

Atmospheric conditions above the Indian Ocean are dominated by the fact that two-thirds of the area of this ocean is found between the two tropics (23°27'N and 23°27'S) and only one-third between the Tropic of Capricorn and 40°S (Tchernia, 1980) (Fig.1-5). According to him, one adopts as characterising the tropical climate the fact that the mean of the coldest month is above 18°; one can say that all the Indian Ocean north of a line between 30-35°S in the west near the African coast, to 25°S in the east on the Australian coast, is tropical or

equatorial in climate, representing 80% of the surface of the Indian Ocean. But this relative uniformity is only apparent. It is necessary to distinguish between the two tropical climates, north and south, for that of the north, influenced by the monsoon, is very different from that of the south.

a. Regime of winds

Wind and weather may play an important role in the current flow as well as in the nature of the transport agents and their volume of sediment discharge into the Indian Ocean. A monsoonal wind system prevails in this area. This wind results in a typical low-latitude monsoonal surface current pattern which is characterised by summer and winter flow reversals accompanied by only small variations in surface temperature (Weser, 1974).

During the northern winter (Dec. - Feb.) cooling of the landmasses of Siberia and Central Asia greatly surpasses that of the neighbouring oceans. These continental regions then become the site of one of the most important centres of atmospheric highs on the planet. Between these parts of Asia and the nearby regions of the Pacific and Indian Oceans, one finds in winter a gradient of atmospheric pressure which directs the land winds toward the sea (north-east - south-west direction) (Fig.1-8). During the northern summer (June - August) intensive warming of southern Eurasia and North Africa, particularly the whole desert arc running from Somalia to north-western India by way of Arabia, creates a zone of low pressures centred on Arabia, Pakistan and north-west India. Thus the pressure gradient is directed from the sea to the land. Strong south-west winds blow over the Arabian Sea, less strong in the Bay of Bengal, carrying air masses loaded with water vapour resulting in the abundant summer rains of the Indian peninsula, Ceylon and all the region south of the Himalayas(Fig.1-9). During the southern winter the south-east Trades begin to blow around 25-30^{o}S. The lows disappear over Australia and South Africa. Therefore Trade winds become much stronger than in the summer (January),more regular and more constant in direction between 25^{o}S and 10^{o}S, from Australia to Madagascar. The system of south-west winds (monsoonal system) is found to be in continuity with the south-east and South south-west winds (Tchernia, 1980; Weser, 1974).

According to Weser (1974), the energy generated by the monsoons extends beyond its influence on the wind-driven circulation, as it is also translated into wave energy. This energy, when coupled with tidal currents, results in sediment transport at considerable water depths. Off the western

Fig.1-8. Winter monsoon. (From Schott., 1935)

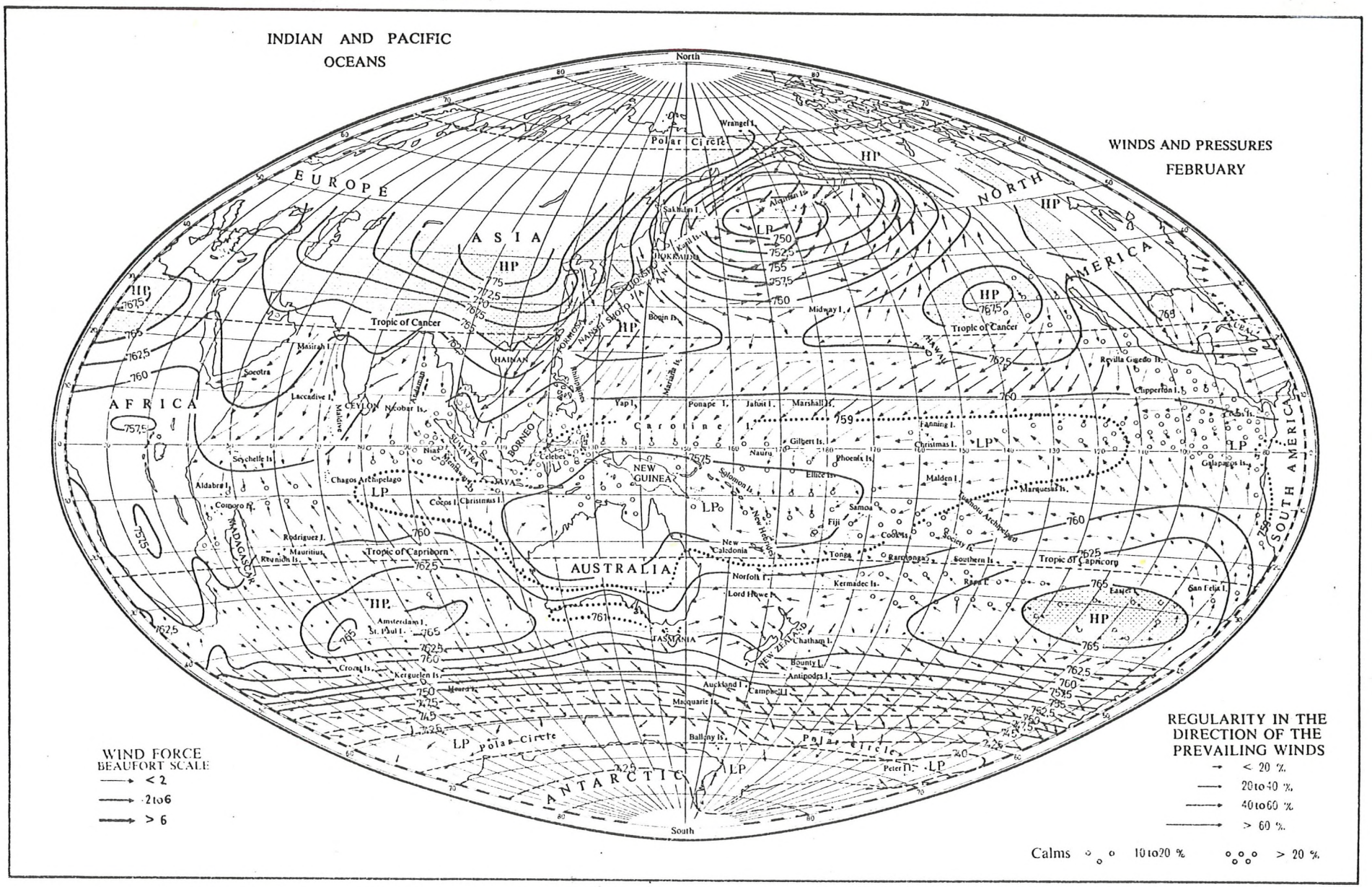

Fig.1-9.Summer monsoon.(From Schott.,1935)

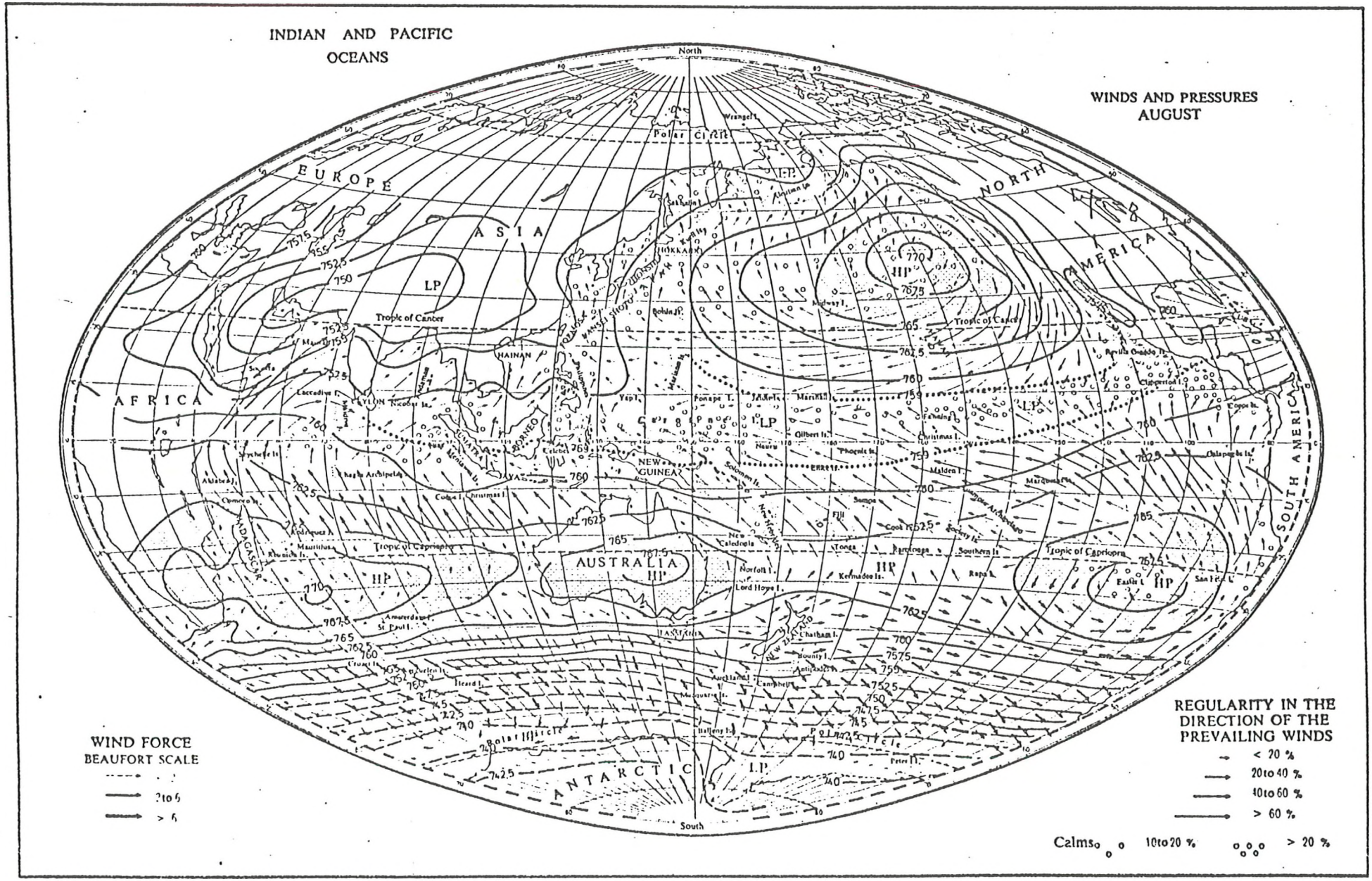

Adapted from O. SCHOTT (1935)

Indian coast, Düing (1970) noted their effect on sediments down to 400 metres. This indicates that suspended matter is made available to far-ranging shallow and intermediate depth water masses. As relating to sediment transport, the monsoonal winds are the prime factor in the considerable influence of aeolian sedimentation in the Arabian Sea. At times, exceptionally strong north-east winds blow dust from the Pakistani and north-western Indian deserts. During the south-west summer monsoon, dust-laden air is derived from the Arabian and African deserts. Stewart et al. (1965) mentioned that summer dust storms also occur along the Makran coast of Pakistan and Iran. The trade winds can also blow dust from Australia and South Africa, since the atmospheric highs appear on them during the southern winter.

b. Climate through time

An understanding of the climate of the surrounding area through time is necessary since the distribution of minerals in the surface layer of Indian Ocean sediments is affected by the climatic zoning of weathering processes and soil formation on the land.

i) Mesozoic

The whole of the Mesozoic Era represented a warm phase in the Earth's history. Glaciation was unknown, and the Polar regions were warm areas with a rich vegetation (Schwarzbach, 1963; Pearson, 1978).

In the late Cretaceous, in Africa deposits of gypsum and, in part, of salt were present along the northern margin of the Sahara, from Dakar on the west to the Red Sea on the east, occurring partly at the base of the Cenomanian in the Turonian (Algeria) and Santonian (Algeria) (Strakhov, 1967). According to Pearson (1978), material from Cretaceous horizons clearly established a temperature maximum in the Albian. This then declined during the Cenomanian, only to be followed by a further maximum in the Coniacian - Santonian interval. The Maasterichtian was then characterised by declining temperatures.

Throughout all of the Mesozoic strata of Australia, there is evidence of much more humid than of arid conditions (King, 1961; Schwarzbach, 1963). However, arid regions existed in the interior parts of Australia during the late Cretaceous (Schwarzbach, 1963).

ii) Tertiary

Schwarzbach (1963) and Strakhov (1967) have noticed widespread

salt deposits in North Africa and Asia, and suggested an arid condition for those areas in the Tertiary. However, along the eastern margin of the Arabian Sea the climate was humid, favouring intense chemical weathering and development of laterite profiles on the Deccan Traps. According to McGowran (1978), in the earliest Tertiary laterite developed in India. In the Eocene, abundant precipitation characterised the entire western margin of the Indopacific, and the wet belt probably extended to considerably higher latitudes than at present because surface waters in the oceans were warmer. Continental regions adjacent to and downwind from high surface-water temperatures were wet. Similarly, areas bordering on and upwind from cold currents are considered to be dry, as compared with the average conditions for that latitude. Monsoonal conditions must have existed in coastal regions facing the Equator, and within the range of the seasonally varying intertropical convergence zone (Frakes et al., 1972) (Fig.1-10). According to them, on the basis of the geological record available, the Oligocene climatic picture appears slightly cooler and drier than that of the Eocene (Fig.1-11).

In the Neogene in South Africa and in the interior of Australia, arid conditions prevailed in the same general areas as in modern geologic time.

Huge arid regions existed in North Africa. In the western part of Asia, a great belt of Miocene gypsum and, in part, halite deposits stretched from Syria through Iraq to the Persian Gulf. In the Pliocene, lateritic weathering crust developed widely in equatorial Africa, India and northern Australia (Strakhov, 1967). According to Gill (1961) lateritic 'duricrust' occurs widely, particularly in western Australia in the Miocene.

6. Evolution of the Indian Ocean

The Indian Ocean has gone under extensive tectonic activities at different times in the past. Reconstruction of the relative positions of India, Australia and Antarctica through time is shown in Figure 1-12. A brief summary of evolution of the Indian Ocean is given as follows:

a. Late Jurassic

The formation of the Indian Ocean was a complex process involving the movement of five lithospheric plates: Africa, Antarctica, Madagascar, India and Australia.

Continental dispersal began first off north-western Australia in the

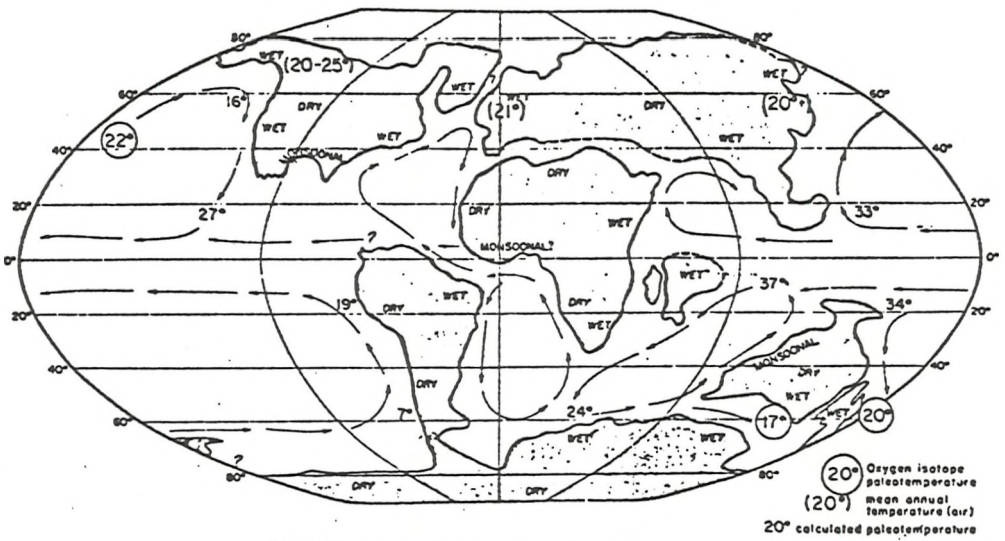

Fig-1-10 Reconstruction of weather patterns in Eocene.

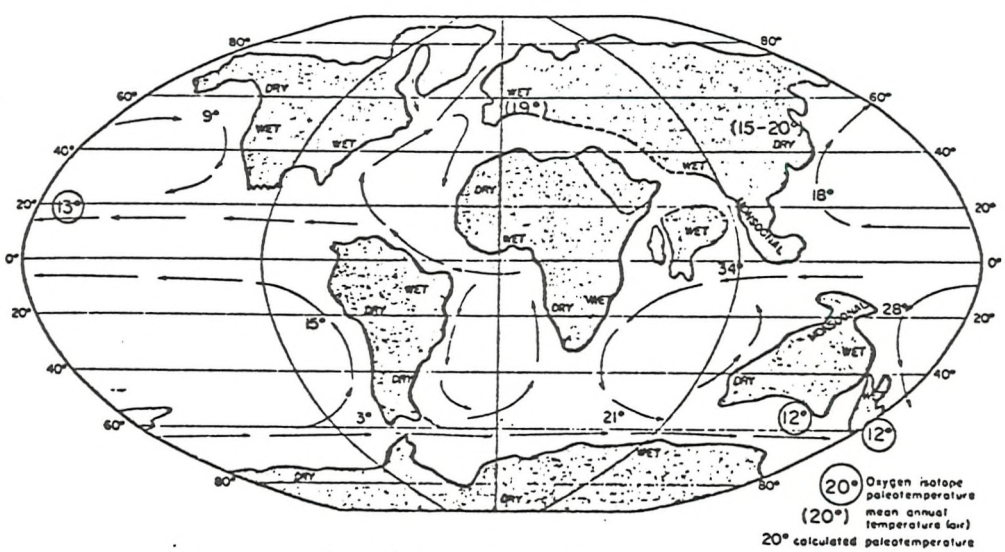

Fig-1-11 Mid-Oligocene weather patterns.

(Both figures from Frakes et al., 1972.)

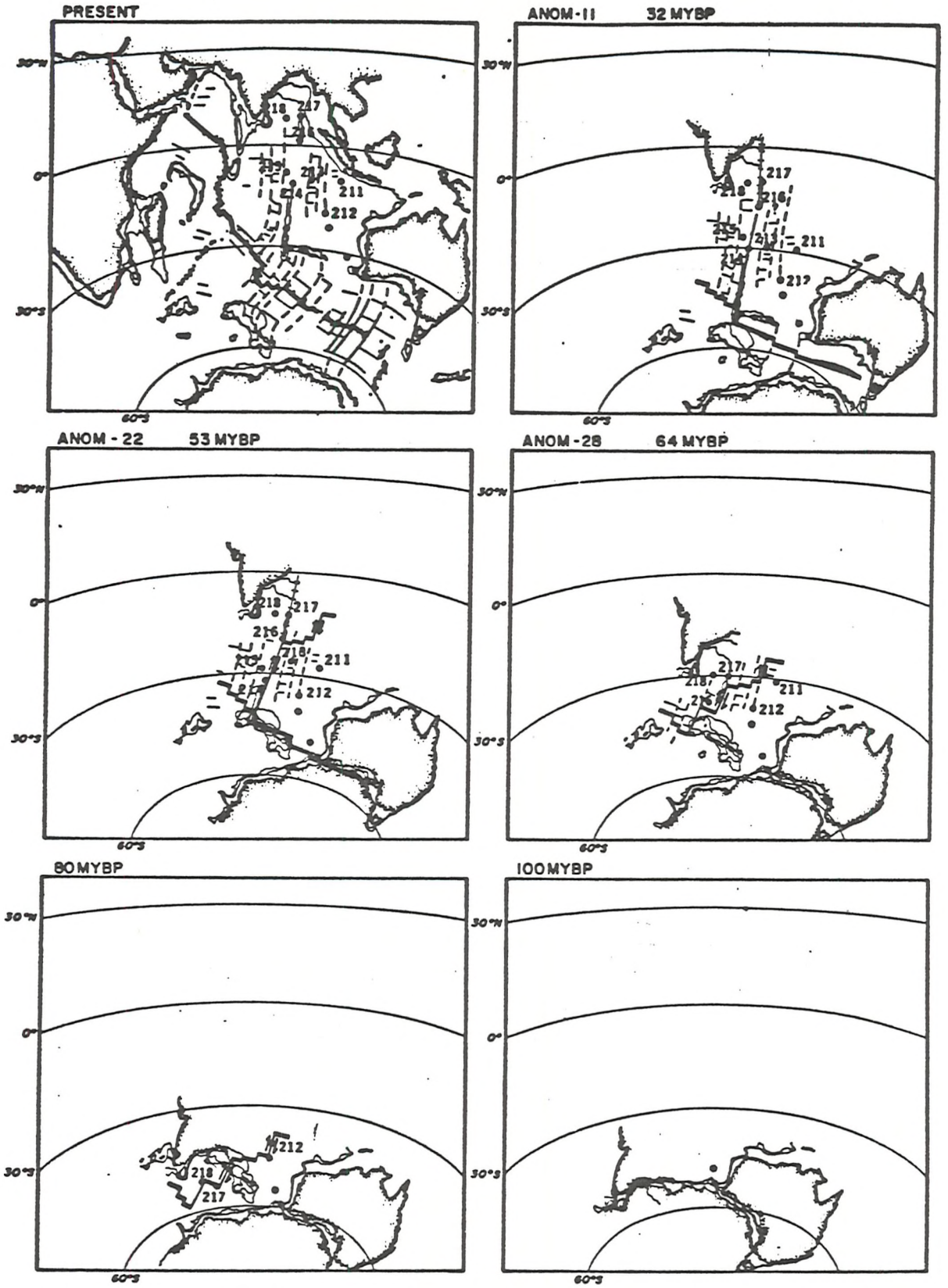

Fig.1-12. *Reconstruction of the relative position of India, Australia, and Antarctica, 32 m.y.B.P., 53 m.y.B.P., 64 m.y.B.P., 80 m.y.B.P., and 100 m.y.B.P. The heavy lines mark the active spreading centers. The thin continuous lines are known fracture zones; the dashed lines projected fracture zones. The horizontal lines represent identified magnetic anomalies* (after Sclater et al., 1974a)

Late Jurassic (Tarling, 1971; Larson, 1975; Markle, 1978). The sea floor to the north-west of Australia, that is in the Gascoyne and Argo Abyssal Plains, is late Jurassic, as shown by deep sea drilling (Site 261). The Argo and Gascoyne Abyssal Plains contain evidence of spreading in late Jurassic time (155 to 145 M.Y.B.P.; Falvey, 1972; amended by Larson, 1975; Veever and Heirtzler, 1974). This suggests a landmass was rifted away from north-western Australia about 155 m.y. ago (Larson, 1975).

b. Early Cretaceous

The separation of Africa from Antarctica commenced during or prior to, the Early Cretaceous (Sclater et al., 1974c; Johnson et al., 1976; McElhinny, 1970). By the mid-Cretaceous, both Antarctica and the India-Madagascar block were situated further south of Africa, so that although Antarctica and India were separating, this fragment of Gondwanaland had moved southward (McElhinny, 1970).

The SWB (south-west Branch) transform was uplifted and became a spreading centre (Luyendyk, 1974) and a new spreading centre was created between Madagascar and the Somali coast (Heirtzler & Burroughs, 1971).

c. Late Cretaceous and Palaeogene

The placing of the spreading ridge close to Madagascar at this time is supported by the richness in montmorillonite in the clays of the developing Madagascar Basin (Kidd et al., 1978; Leclair, 1974). By the close of the Mesozoic era, the opening between Antarctica and Africa was almost complete and the south - south-west part of the Indian Ocean had opened (McElhinny, 1970). During the Maastrichtian and Palaeocene spreading was very rapid, with India moving rapidly northward (Sclater et al., 1974c). The spreading between African and Antarctica had stopped with the SWB reverting to a transform fault (McKenzie & Sclater, 1971). Antarctica and Australia were still joined as one major landmass in the late Cretaceous, but the initiation of rifting had several results, including the formation of the Broken Ridge/Kergulen Plateau, Naturaliste Plateau and the northern portion of the Ninetyeast Ridge due to volcanic upwelling along the rift (Brown et al., 1968; Luyendyk & Davies, 1974).

Numerous models have been proposed for the formation of the Ninety-east Ridge (McElhinny, 1970; Sclater & Fisher, 1974c; Luyendyk & Davies, 1974). Most models involve leakage along a transform fault between the Indian and Australian plates from early Eocene until early Oligocene, when

two portions of the oceanic crust coalesced, India and Australia became part of the same plate, and motion on the Ninetyeast Ridge ceased (Luyendyk & Davies, 1974). Thus the ridge has a shallow-water volcanic origin; it ranges in age from the late Cretaceous to Oligocene. It is tectonically part of the Indian plate and has moved northward with that plate, which is why it is oldest in its northern portion and gets younger to the south (Sclater et al., 1974c). Therefore parts of the Ninetyeast Ridge were the scene of volcanic activity from Cretaceous to early Oligocene (Kidd et al., 1978, Davies et al., 1976).

Davies (1968) suggested that the Seychelles formed part of an India-Madagascar block. He believed that India and Seychelles parted company some time in the Palaeocene. This rupture was also accompanied by the rupture of India and Madagascar at 30^{o}S.

During the Early Tertiary, India, the Ninetyeast Ridge, the Broken Ridge and the Naturaliste Plateau formed a topographical barrier (Luyendyk, 1974; Davies et al., 1976; Kidd et al., 1978). Therefore the new Indian Ocean existed in two parts: a closed basin to the east and a western basin with open connections with the South Atlantic and the Tethys. Around the margins of the present-day Wharton Basin, the late Cretaceous is represented by detrital clays (Kidd & Davies, 1978), while in its central parts detrital clays give way to pelagic clays (Kidd & Davies,1978; Luyendyk, 1974). Carbonates were being deposited on the Naturaliste Plateau, Broken Ridge and the northern part of the Ninetyeast Ridge (Kidd & Davies, 1978). Volcanic activity was being recorded on other sections of the Ninetyeast Ridge and Naturaliste Plateau (Luyendyk, 1974).

In the Palaeocene, calcareous sediments were accumulating on ridges and plateaux, while basin sites contain pelagic clays (Kidd & Davies,1978; McGowran, 1978). By the Eocene, spreading had started between Antarctica and Australia along a ridge (Weissel & Hayes, 1971), resulting in the uplift of Broken Ridge above sea level and the development of an unconformity on it. The Ninetyeast Ridge had also been elevated so that by this time it was above the carbonate compensation depth (CCD) (McKenzie & Sclater, 1971). At this time (Eocene), the Wharton Basin, Central Indian Basin and the Madagascar and Mozambique Basins were still areas of very slow accumulation of deep sea clays, while calcareous sediments occurred at most other sites. Sediments at basin sites off Africa differ, however, in having a substantial silty terrigenous component and significant amounts of pyrite (Kidd &

Davies, 1978). Carbonate sediments were also accumulating at this time on the Chagos-Laccadive and Mascarene Plateaux, while great thicknesses of volcanic ash were being deposited at the southern end of Ninetyeast Ridge (von der Borch et al., 1974).

By the early Oligocene, the geography of the Indian Ocean region more closely resembled that of today. The mid-Ocean ridge system in its present configuration was becoming active. Volcanic activity, probably sub-aerial, was proceeding at the southern end of the Ninetyeast Ridge. The Oligocene sediments record is poorly represented because of the development of a regional hiatus. Pelagic carbonate sediments are recorded on the Ninetyeast Ridge, the Kerguelen Plateau and in the Chagos-Laccadive/ Mascarene area. Volcanic activity continued on the southern end of the Ninetyeast Ridge (Davies et al., 1974).

i) Unconformities

Deep Sea Drilling in the Indian Ocean has revealed unconformities of ocean-wide significance. The unconformities are of Oligocene, early Tertiary and late Cretaceous age, and can be explained as consequent variations in the circulation pattern of the whole Indian Ocean (Davies et al., 1975; Davies et al., 1976; Kidd et al., 1978; Pimm, 1974). Recognising the limited data available and the complexity of the problem, the above authors have limited their speculations to the Oligocene and early Tertiary hiatuses.

True unconformities are due to erosion or non-deposition caused by vigorous surface and/or deep ocean currents. The fact that the hiatuses in question cover a wide depth range indicates that both deep and surface circulation have been involved (Davies et al., 1975).

Bottom water in the Southern Hemisphere forms in the Antarctic Shelf regions, notably in the Ross and Weddell Seas. Weddell Sea water in part flows east into the south-western regions of the Indian Ocean where it behaves as western boundary undercurrent. Bottom water also drifts north through fracture zones in the south-east Indian Ridge, where it may be joined by Ross Sea water flowing west between Australia and Antarctica, to pass through the gap between Naturaliste Plateau and Broken Ridge into the Wharton Basin (Heezen & Holister, 1971). This pattern of circulation seems to mirror the regional development of the Oligocene hiatus and possibly the early Tertiary one as well, and would explain why the hiatuses

are more definitely expressed in the western ocean regions. Tectonic and climatic events in the Antarctic are therefore important (Davies et al., 1975; Davies et al., 1976).

An important event in the late Cretaceous was the rifting of New Zealand from Antarctica and the opening of the Ross Sea (Hayes et al., 1973). Shortly after this, in the early Eocene, climatic deterioration and glacial conditions occurred in Antarctica (Margolis et al., 1970). This combination of events may have led to the formation of substantial amounts of 'aggressive' erosive Antarctic bottom water, Weddell Sea water spreading eastwards between Africa and Antarctica into the western basins and through the gap between Broken Ridge and Naturaliste Plateau into the Wharton Basin. Surface circulation was intensified as a result of climatic cooling and perhaps increased storminess. This could explain the occurrence of well-defined unconformities at many of the shallow sites (Davies et al., 1975). Further climatic deterioration occurred in Antarctica in Oligocene times, and this led to late Oligocene glaciation (Margolis et al., 1970), which would have resulted in the formation of the Oligocene unconformity (Davies et al., 1975; Davies et al., 1976). The Oligocene hiatus was brought to a close by the gradual establishment of the present pattern of circum-Antarctic flow toward the end of the Oligocene (Kennett et al., 1974), which was associated with final rifting south of the Tasmania Rise (Kennett et al 1975a). Formation (or reactivation) of SWB in the late Oligocene-early Miocene has also deflected and weakened the aggressive Antarctic bottom water (Lepichon, 1960).

d. Neogene to Recent

By the Miocene, the movement of India north of the Equator (McElhinny, 1970) permitted the onset of the surface equatorial monsoonal pattern (Leclair, 1974). Increasing productivity as a result of this circulation was reflected in the development of a band of siliceous sediments in equatorial regions below the CCD.

On the Bengal Fan, the influence of the Ganges-Brahmaputra system was, by the middle Miocene, dominant. Miocene to Recent subduction of India under the Eurasian Plate created the Sunda Java Trench. The associated development of the Indonesian volcanic arc caused an extensive build-up of volcanogenic sediments in this region in Pliocene to Recent times (Kidd et al., 1978).

C. The Minerals

1. Palygorskite (Paly)

a. Chemistry

Palygorskite (also called attapulgite, pilolite, lassolite, mountain leather, etc.) was first recognised, many believe, as a distinct mineral species by De Lapparent (1935), who determined its chemical composition from samples obtained from the Georgia-Florida deposits and those at Mormoiron, France. Ovcharenko et al. (1964) reported that Fersman (1913) was actually the first to describe in detail both palygorskite and sepiolite, and did so for samples obtained from the Palygorsk Range on the Popova River (U.S.S.R.), where the mineral palygorskite has been known since 1861.

Palygorskite is a hydrous Mg-Al silicate. It has a fibrous texture and a chain structure. The chemical formula proposed by Bradley (1940) is: 5 MgO, 8 SiO_2, 9 H_2O. The structure proposed by Bradley (1940) is that of a 2:1 layer structure with five octahedral positions (four filled); four Si tetrahedra occur on either side of the octahedral sheet. These units alternate in a checkboard pattern, leaving a series of channels between the structural units. These channels contain water molecules.

Three forms of water exist:

a zeolitic water, bound water (at the edges of the octahedral sheet), and structural hydroxyls. Nathan et al. (1970) have suggested that hydrothermal palygorskite is monoclinic and sedimentary palygorskite is orthorhombic. Christ et al. (1969) found that X-ray diffraction powder data for palygorskite samples show both orthorhombic and monoclinic structures and suggested that the variations in symmetry reflected variations in chemical composition. Weaver & Pollard (1973) believed that the present data suggest the most likely difference is octahedral Fe.

b. Origin

Palygorskite occurs in a great variety of sedimentary environments: continental, continental lacustrine and marine. It has been reported as forming in normal marine waters, marine and non-marine hyper-saline waters, and in freshwater lakes. Palygorskite may be detrital or diagenetic (formed by precipitation from solution). The requirements for palygorskite formation can be specified: alkaline pH, high Si and Mg and low Al

activities (Singer, A.,1979; Couture, 1977a).

i. Continental occurrences

In continents it has been obtained from hydrothermal alteration products of igneous rocks, where palygorskite forms pseudomorphically; and from soils and palaeosols, where palygorskite precipitates from solution.

Furbish and Sand (1976) have described palygorskite, associated with aragonite, as a fracture filling in a dunite body that has been intruded by felsic pegmatites. The palygorskite formed by direct precipitation from solutions given off by the pegmatite solutions,while Mg^{2+} was derived from the serpentinization of the dunite along the host fractures. Palygorskite is reported in soils from several parts of the world: Australia, North Africa, Saudi Arabia, Iraq, Iran, south of France, western Texas, Scotland and Cyprus. Since this study is concerned with the palygorskite formation in the Indian Ocean, only a review of occurrences of palygorskite in the continents surrounding the Indian Ocean is discussed.

Palygorskite in soils

Most examples of reported palygorskite occurrences are from semi-arid or arid environments. Paquet and Millot (1972) have stated that palygorskite in soils is unstable and weathers to smectite when the mean annual rainfall exceeds 300 mm. Eswaran et al. (1974) have studied palygorskite in soils of Iraq. They have stated that rainfall of 100-400 mm and a pH of 7·9 are favourable for palygorskite formation.

Micromorphological studies have indicated that gypsum is a secondary formation in these soils and, as palygorskite is frequently observed as coating on the gypsum grains, it has been concluded that palygorskite has been formed after the crystallization of gypsum.

Millot et al. (1969) found palygorskite strongly associated with calcic soil horizons in Morocco and argued a pedogenic origin. Muir (1951) reported the presence of palygorskite in brown calcareous desert soil from Syria. Yaalon et al.(1976) described palygorskite in carbonate nodules from a loess in semi-arid southern Israel, and suggested the formation of palygorskite at the expense of montmorillonite, with the additional Mg supplied by release from Mg-calcite. Elprince et al.(1979) have described palygorskite

in soils of Saudi Arabia. Since it was not found in parent material of Miocene or Pliocene age, they believed that it was of pedogenic origin and formed at the expense of smectite.

Hassouba et al. (1980) studied palygorskite in soils of Egypt. They suggested an authigenic formation, the necessary Mg for palygorskite formation coming from high Mg calcite and aragonite conversion to low Mg calcite during caliche formation. Singer et al. (1974) found palygorskite in southern Australia and suggested that it was of pedogenic origin since it was found coating the soil aggregate but was absent from the soil material. They also could not find a precursor mineral or volcanic glass.

ii. Continental lacustrine

Palygorskite has been reported in Recent lacustrine sediments, as of detrital, neoformed and diagenetic origins. From Southern Australia, Callen (1977) describes palygorskite occurrences in association with dolomite in late Cainozoic alkaline lake sediments. The author proposed neoformation of this mineral since no palygorskite is known from pre-existing sediments. Palygorskite identified in amounts of up to 15% in the recently deposited clays of lake Kinneret, Israel, were derived from adjacent Neogene marly rocks, and therefore is of detrital origin (Singer et al., 1972).

iii. Marine occurrences

Because of their delicate nature, palygorskite fibres were not thought to be capable of surviving prolonged transport. A detrital origin was therefore excluded for this mineral until recently. Evidence has accumulated meanwhile, however, that many occurrences of marine palygorskite are of detrital origin. In the following sections the occurrence of palygorskite is discussed in three oceans. Figure 1-13 shows the deep sea drilling sites where palygorskite has been found.

The Atlantic Ocean

Bonatti et al. (1968) have found palygorskite, from the Barracuda Escarpment in the western Atlantic, in association with clinoptilolite, serpentine, smectite, sepiolite and quartz. Volcanic glass was not observed, but the presence of abundant smectite throughout the core suggested that volcanic glass was originally present in the sediments. They suggested that palygorskite was formed by Mg-rich solutions, possibly hydrothermal acting on montmorillonite group clays. Sabatier (1969) has

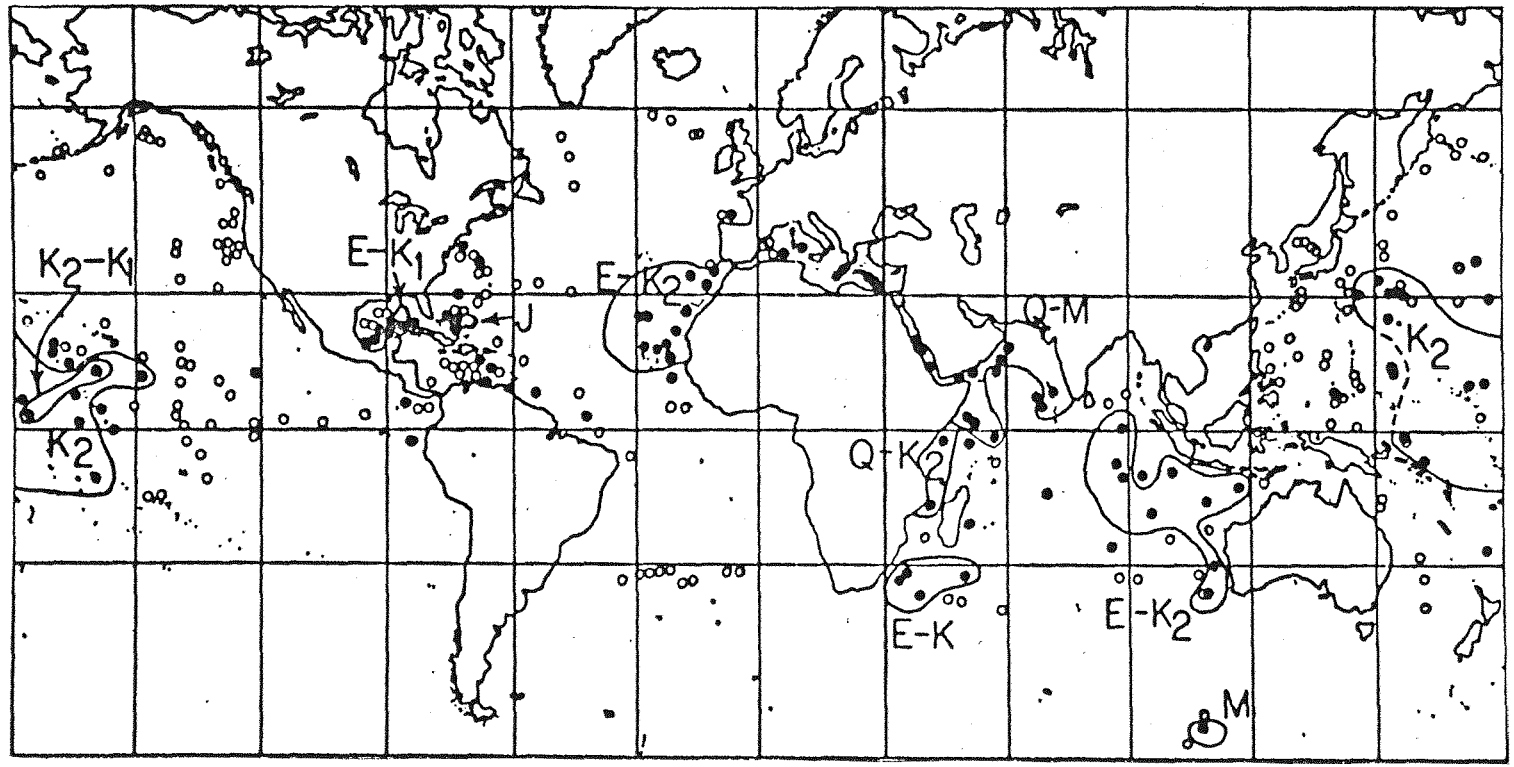

Fig.1-13.Deep Sea Drilling Sites where paly has been found(closed circles). Open circles show sites where no paly has been found.Areas with the greatest concentrations of paly are circled,and the ages are shown: J-Jurassic;K1-early Cretaceous;K2-late Cretaceous;P-Paleocene;E-Eocene;M-Miocene;Q-Quaternary (after Couture,1977a).

suggested that the palygorskite found by Bonatti and Joensuu might have been derived from deposits rich in this mineral occurring on adjacent land masses.

Bowles et al. (1971) have described palygorskite in the Atlantic Ocean from a scarp on the Bermuda Rise and in fracture zones and on sea-mounts. The associated minerals were quartz, calcite and dolomite. No smectite or volcanic ash were found. They believed that the vertical orientation and curved nature of many of the crystals strongly suggested crystal growth from a saturated solution. Therefore, they suggested that the palygorskite was the result of chemical precipitation brought about by the reaction of hydrothermal solutions with sea water. A high percentage of palygorskite occurs in the eastern Atlantic. In some samples it constitutes nearly all of the clay fraction. Couture (1977a) believed that at most sites in the eastern Atlantic, the presence of dolomite, gypsum and high salinity in interstitial waters suggested that palygorskite and sepiolite might have been produced by the reaction of hypersaline brine with detrital clay and radiolaria. Weaver et al. (1977) suggested that palygorskite and dolomite might have been either transported from coastal areas into deep marine environments, or the continental rise and abyssal plain could have been areas of brackish, shallow water sedimentation during the Cretaceous and Palaeogene. Interstitial water studies showed that evaporite deposits existed at depth (Waterman et al., 1972). Therefore Weaver et al. (1977) concluded that shallow water conditions probably existed in this area immediately prior to the deposition of the upper Cretaceous palygorskite-sepiolite. von Rad et al. (1972) studied nine drilling sites of Leg 14 located off north-western Africa and north-eastern South America. Palygorskite was the dominant or second most abundant constituent in several samples from this Leg. Most samples were of latest Cretaceous to Palaeogene age deposited at low sedimentation rates. It usually occurred in a) volcanogenic glass associated with clinoptilolite and montmorillonite at site 136; b) carbonaceous clays (Site 135); c) dolomitic siliceous muds and palygorskite-lussatite cherts (Sites 135, 137, 138, 141 and 144). The association of montmorillonite, clinoptilolite and residual volcanic glass suggested alteration products of volcanic ashes for palygorskite formation. As the distance from the African continent increased between Sites 139 - 140 - 138 - 137, kaolinite appeared to give way to palygorskite. In many samples of pelagic and hemipelagic clays (for example Sites 137, 140 and 141) palygorskite was associated with montmorillonite, kaolinite and quartz. It

was possible that much of the palygorskite originated from the slow diagenetic degradation of montmorillonite with silica as by-product. The palygorskite of the pelagic brown clays, siliceous muds, and of the white palygorskite-lussatite cherts (Sites 140-3, 140-6-2) might have a different origin. They believed that, in the case of these sediments, it was easier to derive the excess silica from the partial dissolution of opaline fossil tests. A detrital origin for the palygorskite was unlikely, since its proportion did not increase toward the continents. The restriction of palygorskite and sepiolite to late Cretaceous and Palaeogene sediments, and its common paragenesis with slowly deposited montmorillonite clay and authigenic clinoptilolite clearly suggested a diagenetic origin.

The Pacific Ocean

Stonecipher (1978) has studied Site 163 in an abyssal hill region of the central equatorial Pacific. In this site, palygorskite is present in companion with nannofossil chalks interbedded with cherts. The associated minerals are: quartz, mixed layer illite-smectite (S/I), K-feldspar, plagioclase and illite. Stonecipher then refers to the following diagenetic trend based on observed mineralogic association from many sites.

$$\begin{aligned} \text{S/I + Opal - A} &= \text{A} \\ &\downarrow \\ \text{S/I + Opal - CT + Clin} &= \text{B} \\ &\downarrow \\ \text{S/I + Opal - CT + Clin + I} &= \text{C} \\ &\downarrow \\ \text{S/I + Opal - CT + Clin + I + K-feld + Paly} &= \text{D} \\ &\downarrow \\ \text{Qtz + I + K-feld + Paly} &= \text{E} \end{aligned}$$

where, Opal - A = amorphous silica, Opal - CT = disordered α-cristobalite - α - tridymite, I = illite, Paly = palygorskite and clin = clinoptilolite. Couture (1977b) has studied Site 164 located near Hawaii Island and Site 194 located in the far western Pacific on the abyssal sea floor east of the Izu-Bonin Trench. The sediments are from Cretaceous to Quaternary in age. He found phillipsite - montmorillonite - radiolarian assemblage in the Tertiary and clin + paly + chert assemblage in Cretaceous sediments. He believes that the presence of palygorskite is related to the state of preservation of radiolarians and where radiolarians have dissolved and been converted to chert, silica has been mobilized. Couture, by presenting

these pieces of evidence, suggested that the palygorskite-clinoptilolite assemblage might form in three ways:

a) it could have formed from silicic or intermediate glass;

b) it could have formed from basaltic debris with subsequent redistribution;

c) it could have formed from redistributed oceanic smectite and phillipsite by reaction with biogenic silica and interstitial water.

He also believes that high temperature favours precipitation of palygorskite since, until the late Eocene, the ocean was probably 10-15°C warmer than today, and palygorskite is most common in Eocene or older sediments in the Pacific Ocean.

From the minor and isotopic chemistry of the palygorskite-smectite fractions from a mid-Pacific sediment core, Church et al. (1979) deduced that these minerals were formed, at least in part, from precursor detrital minerals, rather than just dissolved sea water ionic species. The formation reaction appeared to have taken place at temperatures higher than those of the normal deep sea.

The Indian Ocean

Muller (1961) and Wiersma (1970) observed a trend in the Miocene sediments of the north-western Indian Ocean. The palygorskite content increases systematically from approximately 10% in the vicinity of Madagascar to 40-60% near the southern coast of Arabia. Therefore, they suggested a detrital source from Arabia where paly is abundant. Goldberg et al. (1970) also observed a similar increase in paly towards the coast of Arabia during the bottom sediments study. They believe that the distribution indicates an aeolian contribution from the African continent. Kolla et al. (1981) have studied mineral distribution in surface sediments of the Arabian Sea and suggested that paly clays from the arid regions of Arabia-Somalia appear to have been transported by winds eastward to as far as the Indian continental margin.

Paly is relatively abundant (30-50%) in Palaeocene and Eocene clayey sediments in the vicinity of the Island of Madagascar. Weaver et al. (1977) concluded that the paly is detrital, since quartz, illite, kaolinite and some of the montmorillonite are detrital too. Gieskes et al. (1975) have observed paly, clino and mont assemblage in the Eocene nanno oozes and chalks of the south-west Indian Ocean at

Site 245. Since detrital components are small, a diagenetic transformation of volcanic glass into paly was proposed.

Paly is abundant in Eocene through to Palaeocene sediments in the Eastern Indian Ocean. It appears at Sites 259 and 260 only in Quaternary sediments. The high concentration of the palygorskite at Sites 214, 215 and 216 on the Ninety-east Ridge makes a detrital origin very doubtful. Couture (1977a) has found quartz, amorphous material, associated with palygorskite, at Site 215. Kolla (1974) reported palagonite and volcanic rock fragments at Site 215. Therefore Kolla and Couture both suggested a volcanic origin. Paly at Site 211 (south of Java Trench) is situated in sediments between two basalt horizons. It is associated with quartz, K-feldspar, and calcite or dolomite. Since Ti/Al and Fe/Al ratios of the paly resemble those of tholeiitic basalt, Couture suggested that it is the result of the reaction of interstitial water with basaltic volcaniclastic material and biogenic silica and calcite.

2. Zeolites

A zeolite is an alumino-silicate, whose framework structure of $(Si, Al)O_4$ tetrahedra contains pores field with water molecules and exchangeable cations (Hay, 1966; Gottardi, 1978; Hurlbut et al.,1977).

The general formula for zeolites is Xu Yv Zn O_{2n}. m H_2O where X represents Na and K, Y represents Ca and also Sr, Ba and Mg; Z represents Al and Si. Na + K + (2Σ divalent cations) = Al, and (Si + Al): O = 1:2 (Kastner, 1979; Gottardi, 1978). They average between 3½ and 5½ in hardness (Hurlbut et al., 1977). Specific gravities of zeolites are low (generally 2·00 - 2·40) because of their open structures (Hay, 1966; Hurlbut et al.,1977). Refractive indices are correspondingly low (generally 1·44 - 1·52) (Hurlbut et al., 1977). A zeolite boils at about 200°C giving off water which is readily re-adsorbed at room temperature.

The formation of zeolites depends on the physical environment and the activities of dissolved species such as H^+, alkali and alkali-earth ions, H_4SiO_4 and $Al(OH_4)$. The content of dissolved silica bears a variable but significant relation to the nature of zeolites (Hay, 1978). The chemical composition of the various zeolites depends primarily on the following factors: 1) composition of precursors; 2) composition of host sediments and

interstitial waters; 3) pH; 4) temperature; 5) thermodynamic stability; 6) hydrodynamics of the system; 7) time; and 8) age (Hay, 1966, 1978; Kastner et al., 1978; Riech, 1979).

Phillipsite and clinoptilolite are the most common zeolites in deep sea sediments. Other zeolites such as erionite, gmelinite, natrolite, thomsonite, chabazite, laumontite and thaumasite do occur in deep sea sediments, but they are quantitatively not important.

Phillipsite crystallizes in monoclinic systems (P_{2i}/m) (Rinaldi et al., 1974; Gottardi, 1978). It occurs as colourless to yellowish stout prisms and stubby laths, 8 - 250 μm in length and 0·3 - 3 μm thick, and complex sector-twinned crystals (Murray & Renard, 1891; Sheppard et al.,1970; Mumpton & Ormsby, 1978). A common characteristic of many phillipsites is a cracking along cleavage surfaces parallel to the axis of elongation, breaking the crystal into smaller sections (Mumpton & Ormsby, 1978). They often contain numerous inclusions, indicating rapid growth; the yellowish colour of some phillipsite crystals is mainly due to Fe-oxide or hydroxide inclusions (Stonecipher, 1978).

An average representative formula of marine phillipsite is: $K_{2.8}Na_{1.6}Al_{4.4}Si_{11.6}O_{32}$. 10 H_2O (Kastner, 1979). The Si/Al ratio is between 2·3 and 2·8 (Stonecipher, 1978). Sedimentary phillipsites which have been analysed are more siliceous than non-sedimentary phillipsite (Hay, 1966). Phillipsite (phill) is more abundant in areas of slow sedimentation such as the Pacific (Hay, 1966). Chemical analyses of deep-sea phill by Murray & Renard (1891), Goldberg (1961), Rex (1967), Sheppard et al. (1970) and Stonecipher (1976) show that they are intermediate in their Si/Al ratio between phill in mafic igneous rocks and phill from silicic tuffs in saline lacustrine deposits, and have high alkali/alkali-earth ratios. Generally K > Na >> Ca (Stonecipher, 1978; Sheppard et al., 1970). Phill is more abundant in the Pacific and Indian Oceans than in the Atlantic Ocean (Murray & Renard, 1891; Kolla & Biscaye, 1973b; Stonecipher, 1976). Phill has been reported to occur as cement in palagonite (Morgenstein, 1967; Honnorez, 1978) as fracture filling in drilled and dredged basalts (Bass et al., 1973; Garrison et al., 1973), and as cavity fillings in marine tuffs (Rex, 1967). Bass et al. (1973) described replacement of plagioclase by phill. Murray and Renard (1891), Bonatti (1963) and Bonatti and Nayudu (1965) report phill in the interior of Mn nodules.

Riech (1979) has observed that phillipsites replace the calcareous-clayey matrix or grow in open foraminiferal chambers. In coarse-grained rocks with intraparticle pores, a distinct cavity-lining 'rim cement' of phill is developed. Statistical analysis of phill distribution patterns (Kolla & Biscaye, 1973b; Stonecipher, 1976, 1978; Kastner & Stonecipher, 1978; Iijima, 1978) indicate a trend to phill occurrences as a function of phill in each lithology as follows:

clay-rich > volcanic > calcareous > siliceous.

This would imply a negative correlation between phill abundance and sedimentation rates (Stonecipher, 1977, 1978; Kastner & Stonecipher, 1978). Phill occurs mainly in Miocene sediments and younger ones (Peterson et al., 1970; Kolla & Biscaye, 1973b; Stonecipher, 1976). The presence of basaltic volcanic materials seems to be essential for the formation of phill, since basaltic glass and/or palagonite has been observed in association with phill (Murray & Renard, 1891; Bonatti, 1965; Rex, 1967; Sheppard et al., 1970; Kolla & Biscaye, 1973b; Stonecipher, 1978). Stonecipher (1978) showed that even in the absence of visible basaltic material, the Ti/Al ratios of phill-bearing clays suggest that there was originally a basaltic component contribution to the sediment. Many authors have suggested three alternatives as precursors of phill. The first is fresh anhydrous glass, the second palagonite and finally an intermediary reaction product such as a smectite derived from basaltic glass and/or palagonite. Murray and Renard (1891), Sheppard et al. (1970), Honnerez (1978); Iijima (1978), Kastner and Stonecipher (1978) have suggested that palagonite is the precursor. Iijima (1978) believes that since a favourable chemical environment for phill formation is one with a lower activity of silica and higher activities of alumina and potassium, the palagonitization of mafic glass could provide the necessary alumina. Moore (1966) examined the Na/K ratios of basaltic glass (2-3) and palagonite ($\sim$ 0·3), and concluded that because deep sea phill is predominately potassic, alteration of fresh glass to palagonite prior to phill formation would be more likely than direct formation of phill from basaltic glass. Honnerez (1978) has suggested three stages of palagonitization for phill formation. The initial stage of palagonitization results in an intergranular Na > K phill with low Ca and a probably K-rich saponite. Phill, and to a lesser degree smectite, probably accumulated K and Na from sea water during palagonitization. At this stage the bulk rock has been enriched in K, Na and Mg and depleted in Ca, whereas the other elemental concentrations did not change. At the mature stage palagonitized

glass granules are replaced *in situ* by intergranular phill and possibly minor Fe-rich saponite or Mg-bearing nontronite. At this stage, the phill exchanges its Na ions for K. At the final stage of palagonitization, the hyaloclastite has been completely replaced by an intimate mixture of authigenic K > Na phill with almost no Ca and smectite, and Fe-Mn oxides. Hay (1966) believed that the alteration of glass to montmorillonite is an important factor in providing the chemical environments for phill formation.

Clinoptilolite (clino) crystallizes in monoclinic systems (Merkle & Slaughter, 1968). It usually occurs as euhedral plates and laths (Mumpton *et al.*, 1978; Boles *et al.*, 1978; Stonecipher, 1978), less than 45 μm (Stonecipher, 1976). Inclusions are much less common than in phill, indicating slow growth rates (Stonecipher, 1978). An average representative formula of marine clino is $K_{2.3}Na_{0.8}Al_{3.1}Si_{14.9}O_{36} \cdot 12\ H_2O$ (Kastner, 1979). The Si/Al ratio of clino can vary between 4.0 and 5.25 (Stonecipher, 1978). Alkalis are in excess of alkali-earth cations and in most samples K > Na (Stonecipher, 1978; Boles *et al.*, 1978). Clino from carbonate-rich horizons is somewhat enriched in Ca (Stonecipher, 1978). In most sedimentary clino, Na predominates (Sheppard *et al.*, 1970). Clino casts of radiolarians and forams have been widely noted in non-tuffaceous sediments (von Rad & Rosch , 1972). Clino is the most abundant zeolite in the Atlantic Ocean, but it is also common in the Pacific and Indian Oceans (Biscaye, 1965; Turekian,1965; Kolla & Biscaye, 1973b; Stonecipher, 1976, 1978; Iijima, 1978).

Clino abundance is a function of lithology such that:

calcareous > clayey > volcanic > siliceous (Stonecipher, 1976, 1978).

This sequence suggests a positive correlation between sedimentation rates and clino abundance (Stonecipher, 1976). Stonecipher's (1976) statistical analysis shows that clino occurs in sediments of Cretaceous to Miocene age, with a steady increase in abundance from Miocene to Cretaceous. Clino is least common in sediments of less than 100m depth, and is rather abundant between 900 and 1200m (Stonecipher, 1978). In the Indian Ocean, Kolla and Biscaye (1973b) observed that clino is restricted to Cretaceous to Eocene sediments close to continental land masses and that it is more abundant in indurated chalks. It is also commonly associated with chert and/or opal. Clino seems to be able to form from both volcanic and non-volcanic

precursors (Kastner & Stonecipher, 1978; Stonecipher, 1978). Stonecipher (1978) has suggested a volcanic origin for most of the Cretaceous clays since detrital clays are absent and structural characteristics such as numerous thin, sharply defined ungraded beds, which seem to be altered ash beds, are present. She believes that volcanic material was not basaltic, since the abundant plagioclase material was absent and the bulk chemical analyses show the high Si/Al ratios and low Ti/Al ratios. Cook and Zemmels (1972) reported an occurrence of clino associated with rhyolitic glass at Site 84, Leg 9, DSDP. Clino has been observed in smectite-rich sediments by Bramelette and Pasjak (1933). Iijima (1978) has suggested that clino forms by dissolution of silicic glass. He believes that palagonitization of mafic glass may be favoured if excess soluble silica is supplied from other sources, e.g. dissolution of biogenic silica or amorphous silica from weathering. Hay (1966) suggested that rhyolitic glass in marine environments is responsible for clino formation. Bonatti and Joensuu (1968) suggested that clino formed by reaction of smectite derived from alteration of volcanic material with silica derived from devitrification of silicic glass.

The following possible reactions for clino formation were also suggested:

a) Basaltic glass + silica (mainly biogenic) → clino (Weaver, 1968; Berger and von Rad, 1972; Cook & Zemmeles, 1972; Hathaway & Sachs, 1965).

b) Rhyolitic to andesitic glass; basaltic glass + silica (Kastner & Stonecipher, 1978).

c) Smectite + phill + biogenic silica → clino + paly (Berger and von Rad, 1972; Couture, 1977b).

d) Smectite + biogenic silica → clino (Kastner and Stonecipher, 1978).

e) Biogenic silica + Al + K → clino (Kastner & Stonecipher, 1978).

Boles and Wise (1978) have suggested that phill forms as a metastable silica-deficient phase in marine pore fluids and that it is eventually replaced by clino since 1) clino becomes progressively more abundant in older sediments, whereas phill becomes less common; 2) they both occur in similar compositions in deep-sea sediments. Couture (1977b) also suggested phill

as occurring in clino conversion.

Lisitzina et al. (1982) believe that different facies associated with phill and clino throughout the sedimentary mantle of the ocean from the Cretaceous to the Holocene, different sedimentation rates, different sources of primary material and regular change of zeolization in time show that phill into clino transformation does not appear to be able to explain the vertical stratification of oceanic zeolites. They suggested that the most probable reasons for vertical stratification of oceanic zeolites of global significance are changes of the character of volcanism in time and general evolution of sedimentation in the world oceans.

3. Smectite

The smectite structure was first determined by Hofmann et al. (1933) with further refinements by Marshall (1935) and Hendricks (1942). It has layers consisting of one aluminium hydroxyl unit sandwiched between two Si_4O_{10} sheets. These layers are stacked one above the other in the C direction with water molecules between them. Cationic substitution occurs in octahedral or tetrahedral sheets, and the corresponding differences in properties and chemical composition are used to classify the smectites (Mason, 1966).

Smectite is either a main alteration product of volcanic glass in deep sea sediments (Lisitzin ,1972; von Rad & Rosch, 1972 ; Hein et al., 1978) or derived from continents, either by rivers draining degraded volcanic formations and arid desert soils, such as the Amazon River with 30% montmorillonite (Gibb, 1967) and the Nile River (Rateeve et al., 1966), or by suspended transport from volcanic islands such as Maderia and the Cape Verde Islands (Correns, 1937). Montmorillonite can also be derived from degraded illite (loss of K^+) (von Rad & Rosch, 1972). Weaver & Pollard (1973) believe that the high Mg, low Al montmorillonite are most likely to have formed by the alteration of volcanic material and high - Al beidellite type to have been of hydrothermal origin or to have been formed as soil clay. According to Mackenzie et al. (1966), some of the nontronite in deep sea sediments may have been formed during the interaction between hot submarine volcanic lavas and sea water, and could be unstable with respect to a Fe-poor montmorillonite at the temperature of deep ocean water. Ross and Hendriks (1945), Grim (1953) and Harder (1972) believe that Mg is important for the formation of smectite. Weaver & Pollard (1973)

believe that its major contribution may be in enabling Al to take six-fold coordination under basic conditions. At low temperature Al tends to take six-fold coordination in an acid environment and four-fold in a basic environment (De Kimpe et al., 1961). Mg takes only the six-fold coordination. In the basic environment in which montmorillonite forms, it is likely that Al tends to resist six-fold coordination and Mg may be necessary to nucleate the octahedral coordination. Hawkins and Roy (1963) believe that the role of Mg is also to precipitate Si. Hawkins et al. (1963) and Weaver et al. (1973) have noted that the formation of smectite through basalt with sea-water interaction is possible when the Mg concentration is high enough. According to Bischoff et al. (1975), during high temperature alteration, Mg is available in the solutions from which smectite will be crystallized. Mg will be incorporated into smectite and is probably accompanied by $O\bar{H}$ from sea-water to keep electrical neutrality. This will cause a decrease of the pH, which will accelerate the alteration process. Increase of pH slows the rate of smectite formation. They proposed the following general reaction for smectite formation during hydrothermal alteration:

$$\text{glass} + \underset{\text{sea-water}}{Mg^{2+}} + H_2O \rightleftharpoons \text{smectite} + Ca^{2+} + K^{+} + H_4SiO_4 + H^{+} + Fe + Mn^{2+}.$$

4. Relation of Zeolites with Palygorskite and Smectite

Clinoptilolite, phillipsite, palygorskite and smectite are common minerals in the Indian Ocean sediments. Generally the formation of these minerals requires high pH. The formation and persistence of palygorskite would be encouraged by high pH (> 8–10), high activities of Si and Mg and low Al activity. Mg is also essential for smectite formation. Mariner & Surdam (1970) pointed out that pH could be a controlling factor in deep-sea zeolite formation. At high pH (9 plus), the dissolution of alumina species is rapid, causing a decrease in the Si/Al ratio and hence favouring the formation of a zeolite with lower Si/Al ratio in its lattice, i.e. phillipsite. However, in interstitial waters, the pH is at or a little above 7, and further, with the measured Na^{+} and K^{+} concentrations, gives compositional fields in which phillipsite is unstable. Elderfield (1976) pointed out that clinoptilolite should be the stable zeolite at the normal pH of sea-water on the basis that the Si/Al ratio is fairly high. Smectite is usually associated with clinoptilolite, phillipsite and palygorskite.

Several reactions have been suggested for the formation of the above minerals from smectite. Weaver & Pollard (1973) have suggested the following reaction for palygorskite formation:

$$3{\cdot}43 \text{ paly} + 34{\cdot}13\ H_2O(L) + 17{\cdot}9\ H^+(aq) \rightleftharpoons \text{Smec} + 1{\cdot}2\ Fe(OH)_{3(am)} + 19{\cdot}64\ H_4SiO_4(aq)$$

According to the above reaction, palygorskite (paly) is stable under high activities of Mg and H_4SiO_4 with respect to smectite. According to the following reaction, Cosgrove et al. (1979) showed that smectite into clinoptilolite transformation is thermodynamically possible and clinoptilolite is stable with respect to smectite under high activities of Na or K and H_4SiO_4.

$$0.7725 \text{ smectite} + 3.09(Na^+, K^+) + 8{\cdot}73\ H_4SiO_4 \longrightarrow 3{\cdot}09(H^+) + 8{\cdot}66\ H_2O + \text{clinoptilolite}$$

Hess (1966) has also suggested a reaction for smectite to phillipsite transformation as follows:

$$3 \text{ montmorillonite} + 2{\cdot}5\ Na^+ + 3{\cdot}5\ K^+ + 10\ SiO_2 + 7H_2O = 7\ \text{Phill} + 6H^+.$$

As shown by the above reaction, in the presence of alkali cations and silica, smectite can be transformed into phillipsite at high pH.

There is good correlation between clinoptilolite and paly abundance in late Cretaceous through Eocene sediments on a world-wide basis (Couture, 1977a). Paly is favoured over clinoptilolite in high pH, very high $[H_4SiO_4]$ and high ratio $[Mg^{2+}]/[Na^+]^6$ according to the following equation proposed by Weaver & Beck (1977).

$$4\ \text{Paly} + 6\ Na^+ + 16\ H^+ + \text{water} = 3\ \text{clino} + 6{\cdot}5\ H_4SiO_4 + 11\ Mg^{2+}$$

The association of paly with phill is rare. Kastner & Stonecipher (1978), Boles & Wise (1978) and Couture (1977a & b) all believe that clinoptilolite probably can be formed from phill by reaction with opaline silica or interstitial waters rich in H_4SiO_4. On the other hand, Petzing and Chester (1978, 1979), basing their arguments on experimental work, believe that such a reaction is not realistic and that, in general, the appearance of clino in older sediments, as compared with phill in younger material reflects a change in magma composition with time associated with change

in basin shape and sea floor spreading. Lisitzina et al. (1982) also supported the suggestion made by Petzing & Chester (1978, 1979), and reject phillipsite into clinoptinolite transformation.

TABLE 1-1: Summary of the Main Sedimentological Characteristics

Sample Number	Location	Lithology	Depth below Sea Floor (m)	Interval (cm)	Water Depth (m)	Age
211/6/2	South of the Java Trench	Rad-rich clay	182·5-184	48 - 52	5535	Pliocene
211/13/1	"	Clay	418·5-420	88 - 92	"	Early to Middle Companian
211/14/1	"	Clay-rich nanno ooze and nanno clay laminated	428 -429·5	22 - 24	"	
212/15/2	Wharton Basin	Brown zeolitic clay stone	289·5-291	48 - 52	6243	M.Miocene
212/15/3	"	"	291·0-292·5	98 - 102	"	?
212/16/1	"	"	297·5-299·0	59 - 63	"	?
212/16/2	"	"	299·0-300·5	65 - 69	"	?
212/17cc	"	"	309	-	"	?
212/18/1	"	"	316·5-318·0	102 - 105	"	L.M. Eocene
212/18/2	"	"	318·0-319·5	122 - 125	"	?
212/23/5	"	"	370·0-371·5	98 - 100	"	Late Middle Eocene
212/27/1	"	Nanno chalk - brown zeolitic clay stone	402·0-403·5	118 - 122	"	?
212/27/5	"	Brown zeolitic clay stone	408·0-409·5	65 - 69	"	?
212/28/2	"	"	413·0-414·5	78 - 82	"	?
212/29/1	"	"	421.0-422.5	52 - 55	"	Late Cretaceous
212/35cc	"	Iron oxide rich claystone	485·5-	-		?
212/36cc	"	Zeolitic clay stone	489.0-	-	"	?

/contd.over

TABLE 1-1 contd.

Sample Number	Location	Lithology	Depth below Sea floor(m)	Interval (cm)	Water Depth(m)	Age
212/37/1	Wharton Basin	Brown zeolitic clay stone	497.0-498.5	42 - 46	6243	?
212/37cc	"	"	498.5	-	"	
212/38/1	"	"	506.5-508.0	113 - 117	"	?
213/ 8/5	East side of Ninety-east Ridge	Rad-diatom ooze with varying clay	72.0-73.5	70 - 74	5611	Quaternary Upper Miocene
213/ 9/4	"	Zeolitic clay	80.0-81.5	128 - 132	"	Late Miocene
213/ 9cc	"	"	84.5-	-	"	"
213/10/3	"	"	88 -89.5	146 - 150	"	Middle Miocene
213/11/2	"	"	96 -97.5	94 - 98	"	?
213/11/5	"	"	100.5-102	98 - 102	"	?
213/12/5	"	"	110.0-111.5	68 - 72	"	?
213/13/2	"	"	115.0-116.5	8 - 12	"	?
213/13/5	"	"	119.5-121.0	38 - 42	"	?
213/14/3	"	"	127.5-129.0	51 - 55	"	E. Eocene
213/15/2	"	"	134.0-135.5	38 - 42	"	E. Eocene
215/ 8/2	West of Ninetyeast Ridge	Clay zeolitic in part	66.0-67.5	67 - 71	5319	Late Miocene
215/ 9/2	"	"	75.5-77.0	96 - 100	"	E. Eocene

/contd.over

TABLE 1-1 contd.

Sample Number	Location	Lithology	Depth below Sea Floor(m)	Interval (cm)	Water Depth(m)	Age
216/24/4	Crest of Ninetyeast Ridge	Clay-rich Micarb. chalk	342·5-344	19 - 23	2247	Late Maastrichtian
216/25/3	"	Volcanic clay Micarb.chalk	351·5-353	42 - 46	"	"
216/30/3	"	"	399·0-400·5	138 - 142	"	"
216/32/3	"	"	418·0-419·5	76 - 80	"	"
216/34/1	"	"	434·0-435·5	139 - 143	"	"
221/14/2	Arabian Abyssal Plain	Brown clay	137·5-139·0	98 - 102	4650	Miocene - Pliocene
221/14/5	"	"	142·0-143·5	47 - 51	"	"
221/15/2	"	"	146·5-148·0	17 - 21	"	"
221/15/4	"	"	149·5-151·0	94 - 98	"	"
221/16/2	"	"	168·5-170·0	14 - 18	"	Late Oligocene
235/ 9/6	Somali Abyssal Plain	Nanno clay	178·5-180·0	18 - 22	5130	Early Pliocene
236/16/5	North-east of the Seychelles Islands	Brown clay	145·5-147·0	98 - 102	4487	?
236/18/3	"	"	161·5-163·0	54 - 58	"	Early Miocene
236/19/2	"	"	169·5-171·0	27 - 31	"	"

/contd.over

TABLE 1-1 contd.

Sample Number	Location	Lithology	Depth below Sea Floor(m)	Interval (cm)	Water Depth(m)	Age
239/1/1	Mascarene Basin	Clay nanno ooze	0 - 1·5	87 - 91	4971	Pleistocene
239/4/3	"	"	70·5-72	15 - 20	"	Late Miocene
239/9/3	"	Clay/carbonate rich nanno ooze	143·0-144·5	9 - 14	"	Early Miocene
239/11/3	"	Brown silty clay	161·0-162·5	48 - 52	"	?
239/13/4	"	"	219·5-221·0	58 - 62	"	Late Oligocene
239/16/3	"	"	284·0-285·5	68 - 72	"	Late Palaeocene
239/18/2	"	"	301·5-303·0	79 - 83	"	Early Palaeocene
240A/2/1	Somali Basin	Clayey silt and silty clay	177·0-178·5	136 - 140	5082	Early Miocene - Early Pliocene
240/3/3	"	"	76·0-77·5	62 - 66	"	Pliocene
240/5/1	"	Silty clay, sandy silt and sand	163·0-164·5	81 - 85	"	Miocene
245/1/3	Southern Madagascar Basin	Brown clay	10·0-11·5	121 - 126	4857	?
245/5/3	"	Nanno chalk and chert	210·0-211·5	72 - 76	"	Early Eocene
245A/2/6	"	Brown clay	61·5-63·0	10 - 14	"	Late Eocene
245A/6/2	"	Silt-bearing brown clay	101·5-103	95 - 100	"	Middle Eocene
246/10/2	Madagascar Ridge	Clay and limestone	177·5-179·0	26 - 30	1030	Early Eocene

/contd.over

TABLE 1-1 contd.

Sample Number	Location	Lithology	Depth below Sea floor(m)	Interval (cm)	Water Depth(m)	Age
248/10/2	Mozambique Basin	Volcanic silty clay	313·5-315·0	140 - 144	4994	Late Early Eocene - Early Miocene
248/11cc	"	"	364·5-366·0	-	"	Late - Early Eocene
248/12/3	"	"	392·0-393·5	133 - 137	"	
248/14/1	"	Brown clay	407·0-408·5	68 - 72	"	Palaeocene or Early Eocene
248/14/6	"	"	414·5-416	138 - 142	"	"
250A/3/1	South-east corner of Mozambique Basin	Clay	55·5-57	47 - 51	5119	Quaternary
250A/6/3	"	"	190·5-192·0	20 - 24	"	?
250A/11/2	"	"	464·5-466·0	68 - 72	"	Lower to Middle Miocene
250A/15cc	"	"	630	-		?
250A/22/3	"	"	694·0-695·5	12 - 14	"	Conician
254/25/2	South end of Ninety-east Ridge	Brown sandy and silty clay	220·5-222·0	92 - 96	1253	Middle Tertiary
254/26cc	"	"	230·0-231·5	-	"	"
254/27/3	"	"	241·0-242·5	49 - 52	"	"
254/28cc	"	"	249·0	-	"	"

/contd.over

TABLE 1-1 contd.

Sample Number	Location	Lithology	Depth below Sea Floor(m)	Interval (cm)	Water Depth(m)	Age
256/2/3	South of Wharton Basin	Zeolitic brown clay	12·5-14	118 - 123	5361	Quaternary
256/4/5	"	"	91·5-93	8 - 12	"	?
256/6/3	"	"	183·5-185	67 - 72	"	Upper Cretaceous
256/7cc	"	"	213·5	-	"	Upper Cretaceous
256/8/4	"	"	242·0-243·5	67 - 72	"	Upper Albian
257/2cc	Wharton Basin	Detrital clay	15·5-17	-	5278	?
257/4/3	"	"	88·5-90	50 - 54	"	Cretaceous
257/5/2	"	"	125·0-126·5	16 - 20	"	Upper Cretaceous
258/14/1	Northern flank of Naturaliste Plateau	Zeolitic-rich clay	263·0-264·5	12 - 14	2793	Cenomanian
258/15/1	"	"	282·0-283·5	123 - 127	"	Late Albian
258/16cc	"	Brown-black ferruginous detrital clay	310·0-311·5	-		"
258/17/2	"	Zeolitic-rich clay	321·5-323	52 - 56	"	"
258/22/4	"	"	439.5-441.0	73 - 78	"	Middle Albian
258/25cc	"	"	525·5	-	"	?

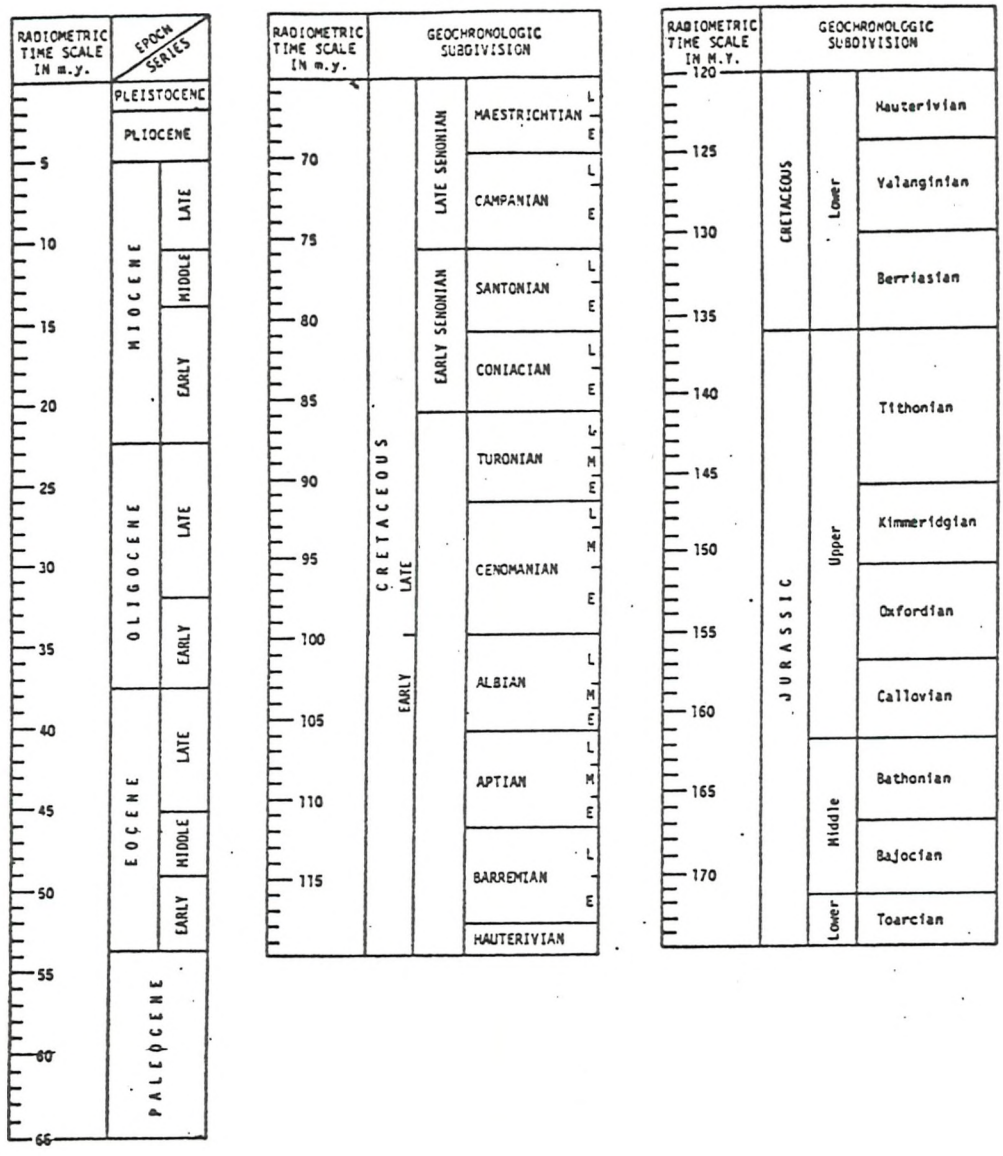

Table.1-2. Geological time scale used in the present study.

CHAPTER II

TECHNIQUES

A. Sample Preparation

1. Sample washing

In the early stages of the investigation, samples were washed with triple distilled water in order to remove salt resulting from contamination with sea-water at the time of drilling. Samples, previously disaggregated by hand, were placed on a filter paper with 0·7 μm retention and washed repeatedly with triple distilled water. Since the samples contained some very fine material (subsequently found to be grains less than 0·08 μm in size) a proportion was found to pass through the filter paper. A micropore filter with 0.45 μm retention was then used, but a part of the sample still passed through the filter paper. Because of this loss of material, it was decided not to wash the samples.

2. Grain size separation

10g of oven dried sample was weighed accurately and dispersed in triple distilled water ultrasonically until no aggregate was visible on the bottom of the beaker. The sand fraction (greater than 63 μm) was removed from suspension using a nylon bolting cloth sieve with 63 μm size mesh. The sand fraction was washed several times with triple distilled water and finally was transferred to an evaporating basin. It was dried at 110°C in an oven and then, if sufficient in quantity, was subjected to mineralogical examination using an X-ray diffractometer (X-R-D/see B.1); otherwise an optical microscope or electron microscope was used. A centrifuge (MSE.GF-8) was employed to speed up the separation of the clay from the silt fraction. The suspension was transferred to a 1000 ml plastic bottle. One ml of 20 N ammonia solution per 1000 ml was added to prevent flocculation. The plastic bottle was shaken by hand and placed in the centrifuge. The time needed for sedimentation under centrifugal acceleration for the separation of less than 2 μm size was calculated by means of Stoke's Law as follows:

$$t = \frac{n \log_{10} \left(\frac{R_2}{R_1}\right)}{3{\cdot}81\, N^2 r^2 (P - Po)}$$

in which t = sedimentation time in seconds;

n = viscosity in poises at the prevailing temperature;

R_2 = final distance of the particle from axis of rotation (cm);

R_1 = initial distance of the particle from axis of rotation (cm);

N = the angular velocity in revolutions/sec (rps);

r = the radius of the particle (cm);

P = the density of the particle (grams/cm^3);

Po = the density of the medium (grams/cm^3).

After operation of the centrifuge, the upper liquid was siphoned off. The process was repeated until approximately 50% of the clay fraction was removed. Complete removal of the clay fraction would take too long. The removal of 50% clay was determined by Coulter Counter.

The Coulter Counter consists of a glassware stand in an electronic processor. A suspended sample is passed through an orifice in the tube. The particles momentarily reduce the strength of an electric current passing through the orifice, and are thus counted. Where a known volume is sampled, data in terms of particles per volume can be gained. Known amounts of clay and silt-suspended material of a few samples were run on the Coulter Counter. The results showed that after extraction of 8 litres of suspensions, 50% of the < 2 μm fraction was removed and the remainder contained the other 50% of the < 2 μm fraction plus silt fraction. The < 2 μm fraction (separated) and the silt + clay fraction (remaining) were dried in an oven and weighed. The weight of sand, silt and clay was re-calculated to 100% based on the original weight of sample, and considering that the silt fraction contained 50% clay size particles. Bulk silt and < 2 μm fractions were run on X R D.

A suspension of the < 2 μm fraction was fractionated into 2 - 0·2 μm, 0·2 - 0·08 μm and $<$ 0·08 μm using a supercentrifuge (Sharples Laboratory Supercentrifuge).

A charge is fed through a glass funnel and plastic tube into a hollow cylinder called a 'bowl', which is rotated at high speed. Finer fractions separate out on the liner of the bowl at higher levels; the suspension of finer fraction (largely colloidal) flows out of the cylinder at the top (Fig.2.1). The speed for operation was selected at 24000 rpm, and kept the same throughout the separation of different fractions, but the flow rate was adjusted each time to obtain a particular grain size (Fig.2.2). Details concerning the centrifugal force gradient and flow rate

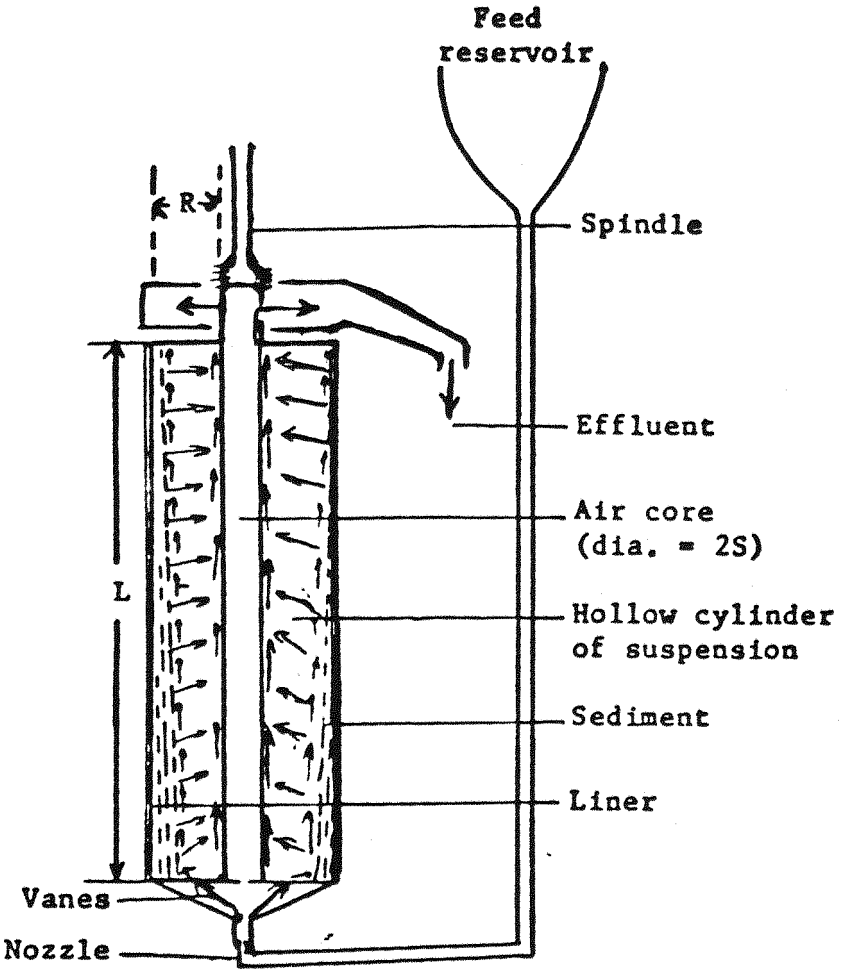

Fig.2.1. Flow of suspension along margin of sediment on liner of supercentrifuge bowl (after Jackson 1956).

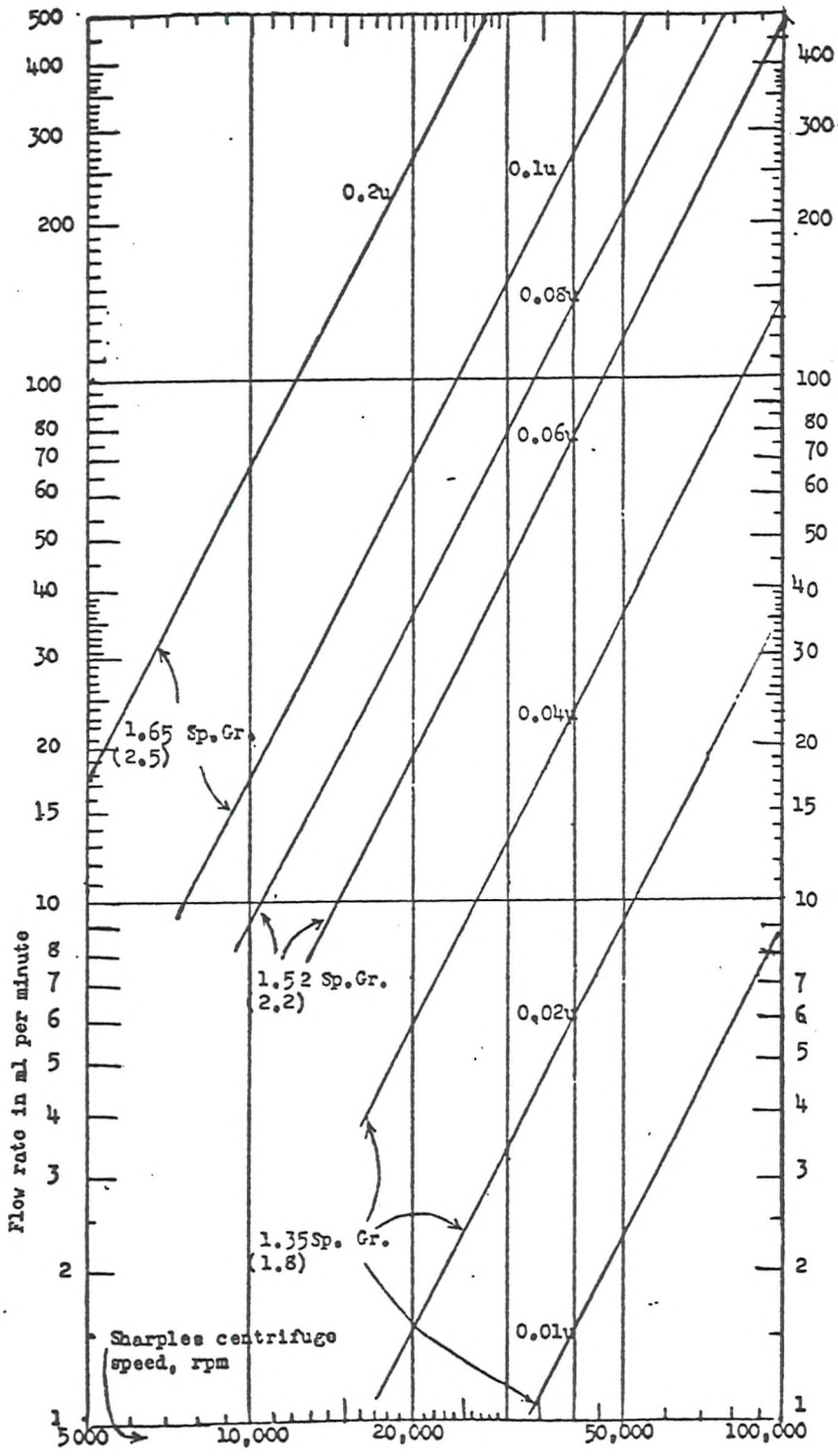

Fig. 2.2 --Nomograph of suspension flow rates through Sharples Laboratory Model supercentrifuge at 25°C as a function of soil particle diameter, particle specific gravity, and centrifuge speed. (after Jackson, 1956)

are obtained from Jackson (1956).

The suspension of the < 2 μm fraction was stirred and placed in the feed reservoir (funnel) of the supercentrifuge, an acetate liner being placed in the bowl earlier. In checking the velocity of the centrifuge, the tachometer is engaged in the thread of the bowl connector nut. The number of tachometer revolutions in 30 seconds equals the bowl velocity in thousands of rpm. The flow rate in ml per 30 seconds was checked after the feed nozzle of the centrifuge was placed at the bottom of the centrifuge. The flow rate was checked by collection of the first effluent in a 500 ml graduated cylinder for 30 seconds. The effluent was then collected in a beaker. An adjustment of flow rate is possible by change in the nozzle or the height of the reservoir. When the suspension was processed, 300 ml of water was poured into the feed to wash down the reservoir. The clay fraction between 2 to 0·2 μm was collected on the liner of the supercentrifuge bowl, and the 0·2 - 0·08 μm was collected in the beaker. The 2 - 0·2 μm fraction was transferred by means of a spatula. This fraction was re-suspended and centrifuged in small tubes. The cake formed at the bottom of the tube was removed and smeared on a glass slide by means of a spatula, in order to prepare oriented aggregates of clay flakes. These slides were run by X-R-D.

The separation of the $<$ 0·08 μm fraction from the effluent containing 0·2 - 0·08 and $<$ 0·08 μm was achieved in the same way as before, using the appropriate flow rate. The final suspension, which contained $<$ 0·08 μm fraction, was flocculated by addition of a few drops of 2 M ammonium chloride.

3. Heavy mineral separation

The heavy liquid specific gravity separation of minerals by the 'sink or float' technique is based on the fact that each mineral species tends to have a different density. In a heavy liquid of a known density, the minerals of less density float and the minerals of greater density sink. The object of heavy liquid separation was to increase the concentration of zeolite minerals (clinoptilolite and phillipsite) and purify them by removal of minerals of different specific gravity. Since the zeolites were present in the silt fraction, a centrifuge method was used. A mixture of Bromoform and Acetone was used as the heavy liquid. Acetone was used as the diluent

for Bromoform.

Standard cubes with known specific gravity were used for the determination of the specific gravity of the heavy liquid. The specific gravity of the zeolites falls between 2·20 and 2·18. 3 to 4g of the silt fraction was placed in a centrifuge tube which was half filled with heavy liquid of known specific gravity. Balance tubes were then placed in the centrifuge and spun at 900 rpm for 10 minutes. All of the heavy minerals did not come down with the first spin, so the tubes were removed from the centrifuge, the floating cake was stirred up with the liquid, and the tubes were spun again using the same conditions as before. The zeolite minerals at the top were decanted with the liquid onto a filter. The light fraction (zeolite)was then washed with acetone removing all the heavy liquid from the grains; the zeolites were dried in an oven at 110^{o} and mounted in a powder holder for examination by X-R-D. The X-ray trace usually showed the presence of small amounts of opal-CT, quartz and clay with the zeolite. The opal-CT was removed by sedimentation. The suspension of the zeolite and opal-CT was stirred and then allowed to stand quietly for five minutes for each 10 cm of beaker (Jackson, 1956). The supernatant liquid was then decanted into another beaker. This procedure was repeated several times. The sedimented portion was then dried and examined on the X-R-D. No opal-CT peak was observed, but a small amount of clay was still present. Only one of the samples of clinoptilolite did not show any impurity on the X R D and SEM. Therefore, that sample was later used as a standard in the study of the minerals by Energy Dispersive X-Ray. The amount of purified phillipsite was not enough for chemical analysis.

B. Mineral Analysis

1. X-Ray diffractometry

For X-Ray Diffraction the Bragg relationship $n\lambda = 2d \sin \theta$ is applied, where d is the spacing of atomic planes in the crystal, λ is the diffracted X-ray wavelength, n the order of the diffraction, and θ is the angle of incidence of the X-rays on the atomic planes of the crystal. A beam of X-rays of known wavelength is directed onto the crystal under investigation. The beam is split up by the crystal into many beams, each the result of diffraction by a plane of atoms in the crystal. For a particular X-ray beam, the angle of diffraction θ is related to an atomic spacing d within the crystal. By recording the diffraction angles, it is possible to determine the atomic plane spacings within the mineral concerned

and thus build up a picture of its atomic structure. In the present study, X-ray diffractograms were made for all samples using a Philips (PW1010) X-Ray Diffractometer (X-R-D) with Ni-filtered, Cu/Kα radiation generated at 36 KV and 24 mA, with 0·2 inch detector slit.

a. Bulk mineralogy

A semi-quantitative method described by Melieres (1978) was used. Samples and an internal standard were ground in an agate mortar after drying in an oven at 110°C. Sodium fluoride was used as the internal standard. The sample and internal standard were weighed in the ratio of 5 to 1. They were mixed and ground by a mechanical steel mortar for 10 minutes. The mixture was mounted in an aluminium powder holder after passing through a 230 mesh sieve (63 μm). The mixture was then run on the X-R-D from 2° to 75° 2θ at 1° 2θ/min. A semi-quantitative estimation was carried out using calibration curves previously prepared using mixtures of pure minerals with the internal standard. Calibration curves of quartz, feldspar, calcite, dolomite, halite and clay minerals were prepared using standard pure minerals available in the Geology Department. A sample of clinoptilolite from Hectorite in the U.S.A. was used for calibration since it was not possible to obtain enough pure clinoptilolite from the samples under study. However, one of the samples rich in phillipsite from Site 213 was used as the phillipsite standard after purification. Clinoptilolite and phillipsite standards had small amounts of quartz and clay impurities which it was not possible to separate. Therefore, the amount of quartz and clay impurities were estimated using the appropriate calibration curves and then the phillipsite and clinoptilolite percentages were estimated by subtracting the impurities percentages from 100. The peak height of the strongest peak was used for the estimation of all minerals except pyrite and quartz. The strongest pyrite peak overlaps with that of the internal standard; therefore the peak at 2·72 Å was used for calibration. The effect of the main pyrite peak on the internal standard peak height is small, since the pyrite percentage is low in the samples. The quartz main peak overlaps with illite; therefore the peak at 4·24Å was used. Halite does not exist in the sediment as a mineral, but results from the evaporation of the interstitial water when the samples are oven-dried. But as it is mentioned by Melieres, halite constitutes a part of the mass of the samples, and it is necessary to add it to the other crystallized constituents in order to obtain the total crystallized minerals.

Since the clay fraction is rich in smectite, 50% smectite standard

was mixed with other clay minerals such as kaolinite, illite and palygorskite for the clay standard.

Calibration curves were prepared using intensity ratios of mineral to internal standard versus percentage of mineral. The amorphous material was obtained by subtraction of the total crystallized constituents from 100. There are several sources of error in this method. For example, the standard pure minerals may have different chemical composition from those in the samples, since the standards are not all from deep sea sediment. This can give rise to different peak intensities due to chemical differences. Further, some error would result from ignoring the mass absorption of the various calibration standards and unknown samples, but this is compensated to some extent by using an internal standard.

The confidence interval was calculated for each mineral using the following equation:

$$CI = \bar{Y} \pm t\ Se$$

where CI = confidence interval;

$\bar{Y}$ = the mean of percentage;

t = student t test

Se = standard error of estimate.

The confidence interval for each mineral is as follows:

	CI (%)
Quartz	± 9
K-feldspar	± 8
Plagioclase	± 6
Clinoptilolite	± 8
Phillipsite	± 5
Clay	± 9
Calcite	± 7
Dolomite	± 5
Pyrite	± 1
Halite	± 3

The calibration curves are shown in Figures 2-3 to 2-12. CaO calculated from the calibration of calcite shows very strong correlation with CO_2 carbonate (determined on an infrared gas analyser) highly significant at 0·05% (Fig.2-13).

b. Clay mineralogy

As previously mentioned, the < 2 μm fraction was fractionated using a supercentrifuge. It was split into three fractions, and three oriented slides of each fraction were run from 2° to 30° 2θ at 2° 2θ/min and ¼ degree divergence and scatter slits on the X-R-D. The three slides were prepared as follows:

1) dried at room temperature; 2) glycolated at 60°C for a day;
3) heated at 550°C for two hours.

The semi-quantitative estimation was carried out using Matter's method (1974). The areas under the peaks at 17Å (mixed layer illite/smectite; I/S), 10Å (illite), 10·5Å (palygorskite) and 7Å (kaolinite and chlorite) were measured. The 7Å peak was divided between chlorite and kaolinite according to the peak height ratio at 3·55 and 3·57Å, respectively (Biscaye, 1964). The relative abundances of these clay minerals were calculated by adding 1/3 I/S, 1/1 illite, 1/2 kaolinite, 1/2 chlorite, and 1/2 palygorskite and normalizing to 100%.

C. Chemical Analysis

1. X-Ray spectrometry

If one of the orbital electrons is in some way removed from its normal energy level, and perhaps ejected from the atom altogether, the atom is then in an excited state and is said to be ionised. In order to stabilise the atom, an electron from a higher energy orbit falls immediately into this gap and its excess energy is emitted as an X-ray photon. This X-ray energy is the potential energy difference between the two shells. X-ray spectroscopy is dependent on the excitation of these electrons to produce an emitted X-ray spectrum characteristic of the element concerned. In Energy Dispersive X-ray analysis and the β-probe, this excitation is caused by a primary electron beam which must have sufficient energy to remove an electron from one of the inner shells of the atom concerned. For a given element, the intensity of X-ray emission is related to the

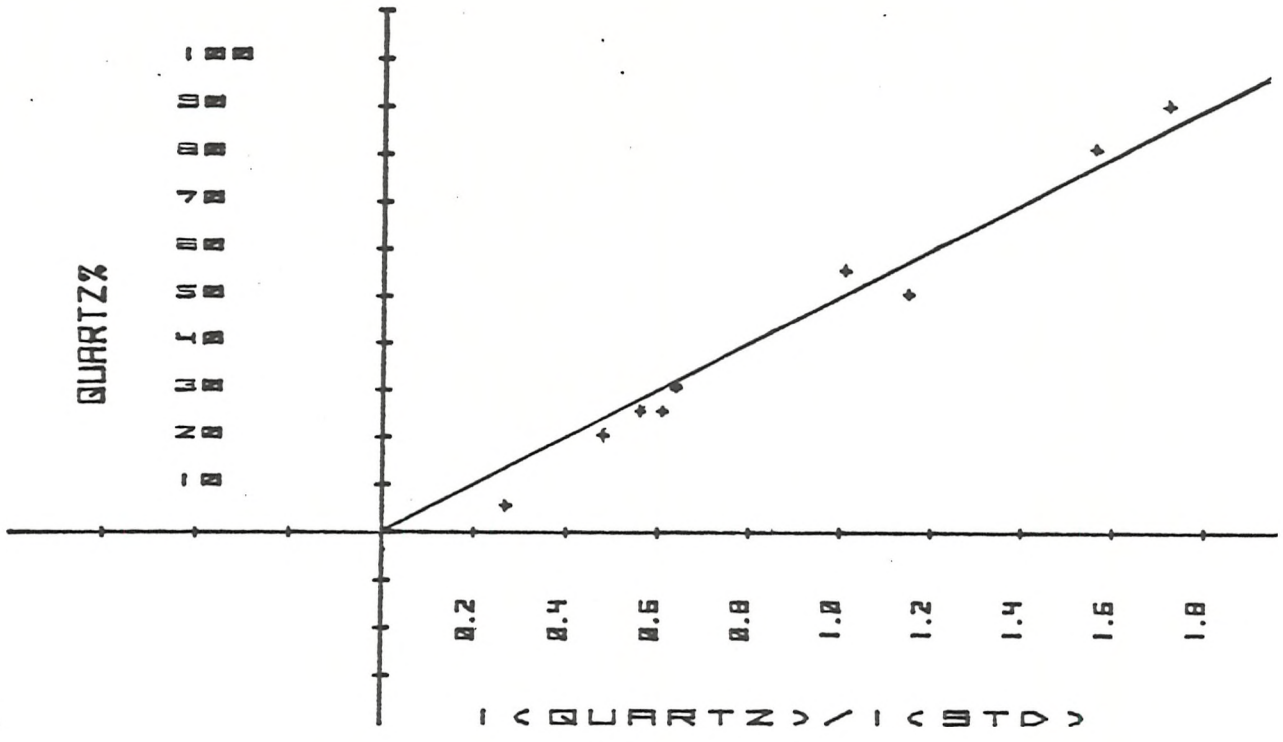
QUARTZ%
0.2
0.4
0.6
0.8
1.0
1.2
1.4
1.6
1.8
I<QUARTZ>/I<STD>

Fig.2-3

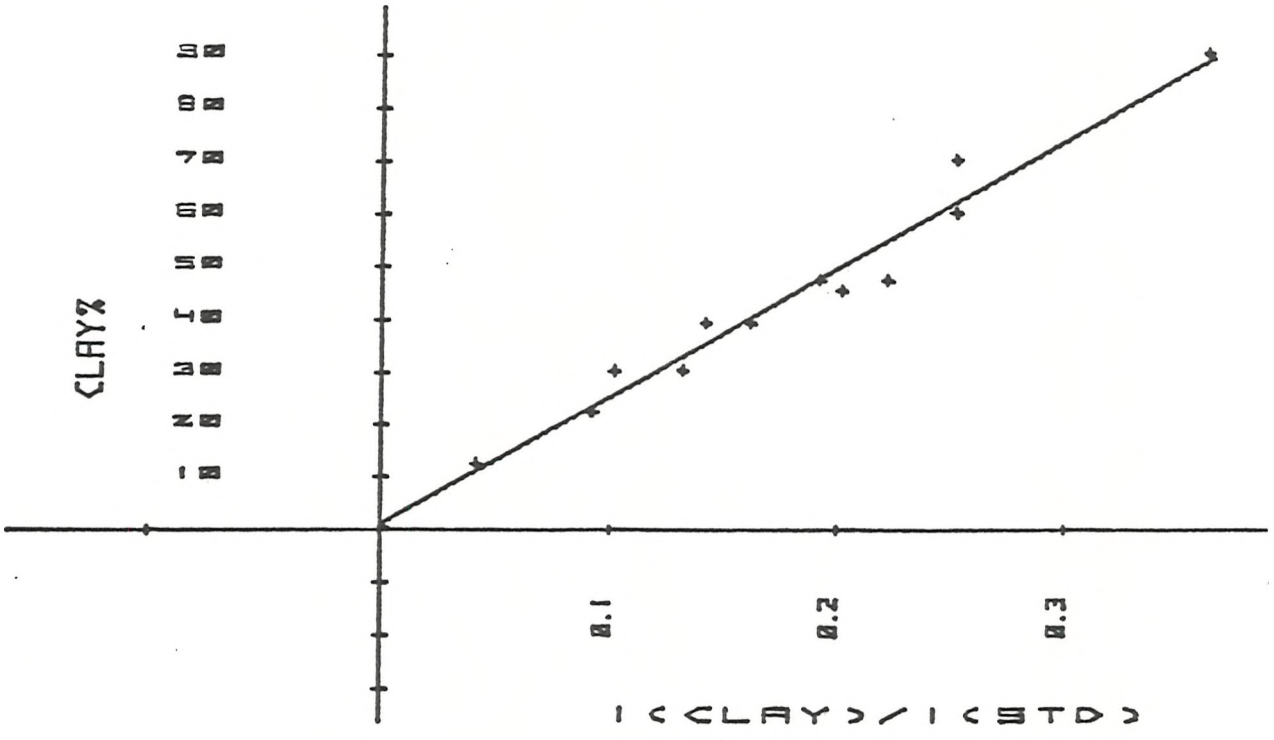
CLAY%
0.1
0.2
0.3
I<CLAY>/I<STD>

Fig. 2-4

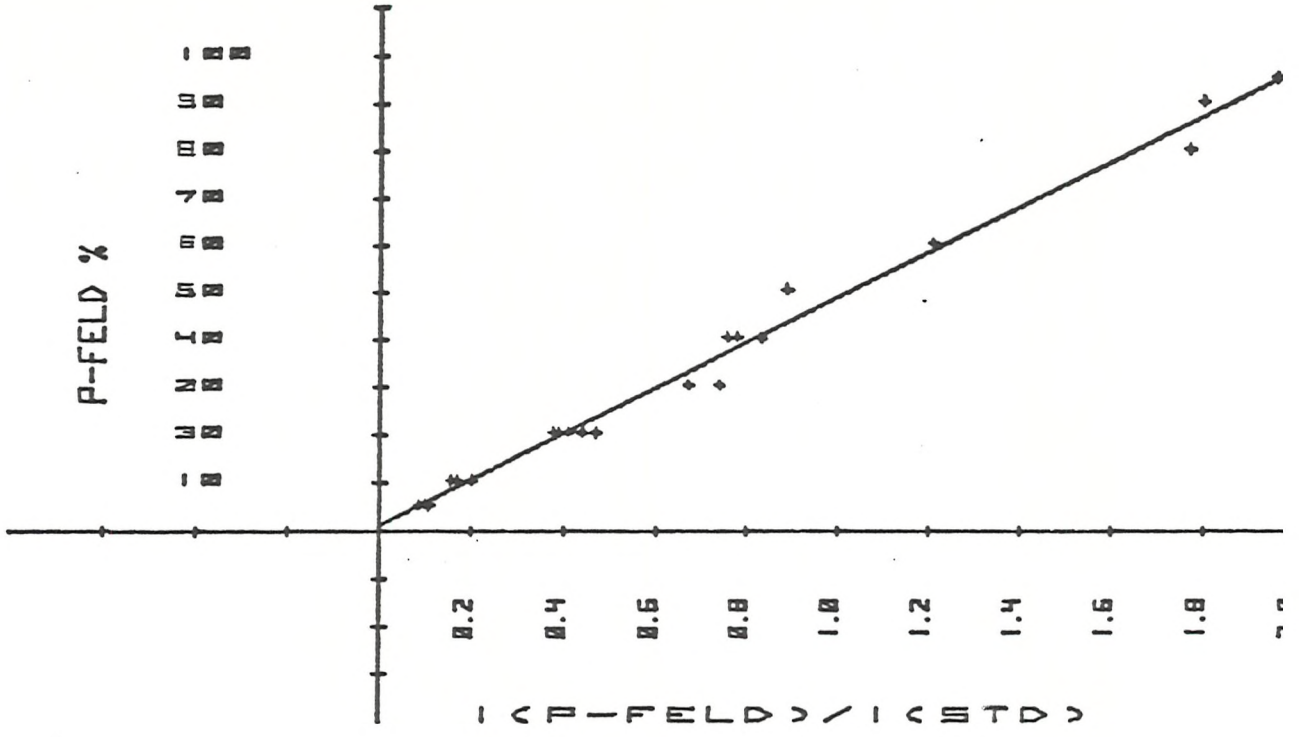
P-FELD %
0.2
0.4
0.6
0.8
1.0
1.2
1.4
1.6
1.8
I<P-FELD>/I<STD>

Fig.2-5

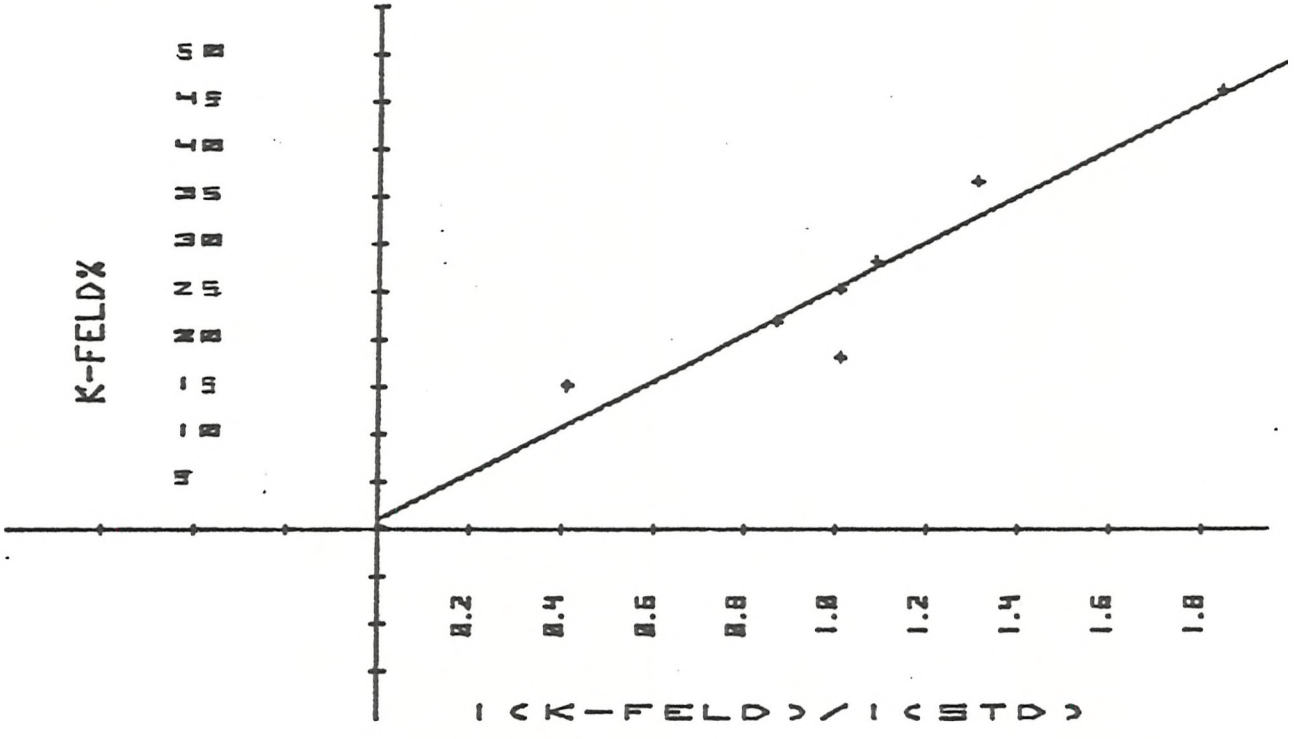
K-FELD%
0.2
0.4
0.6
0.8
1.0
1.2
1.4
1.6
1.8
I<K-FELD>/I<STD>

Fig. 2-6

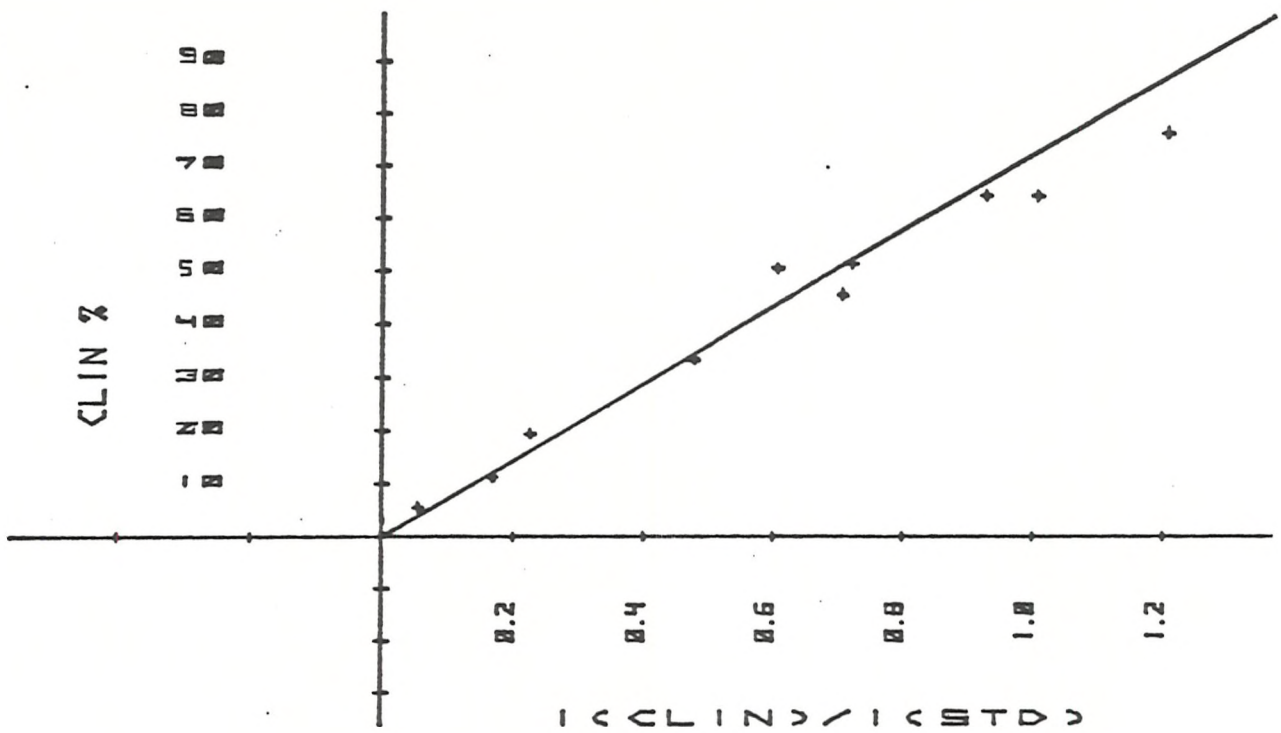

Fig. 2-7

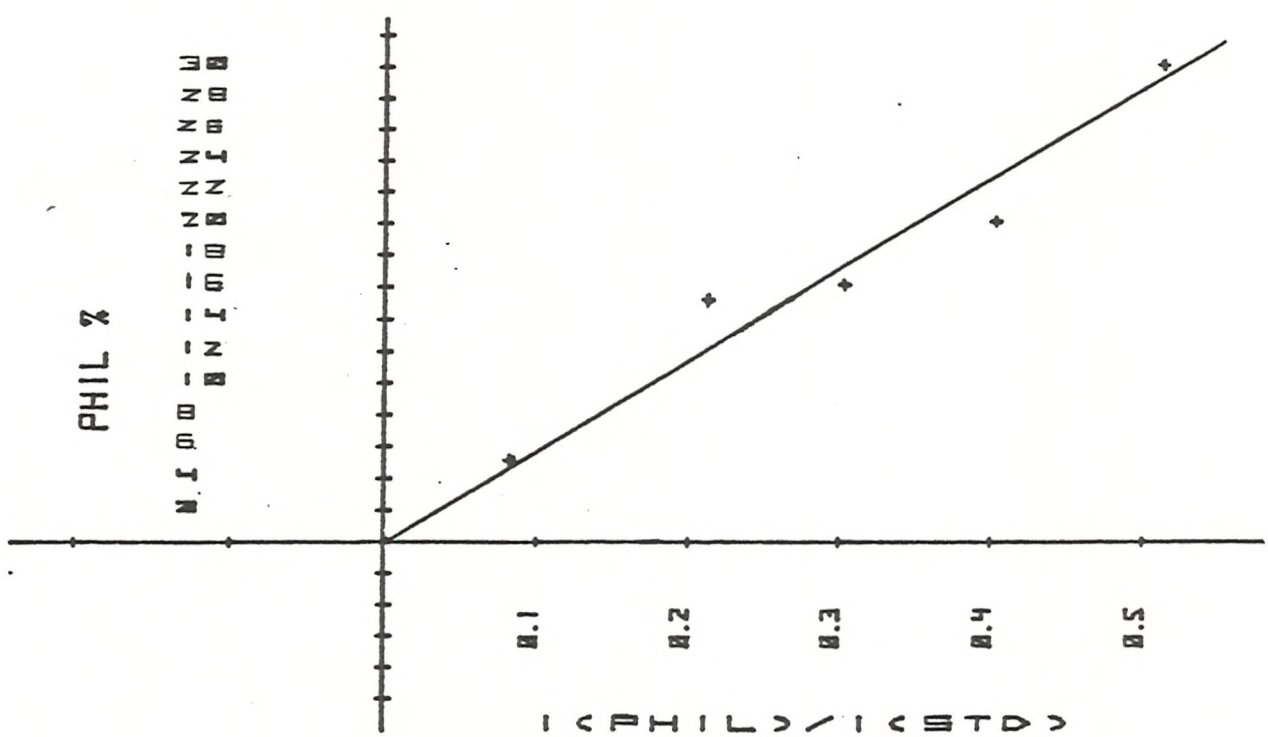

Fig. 2-8

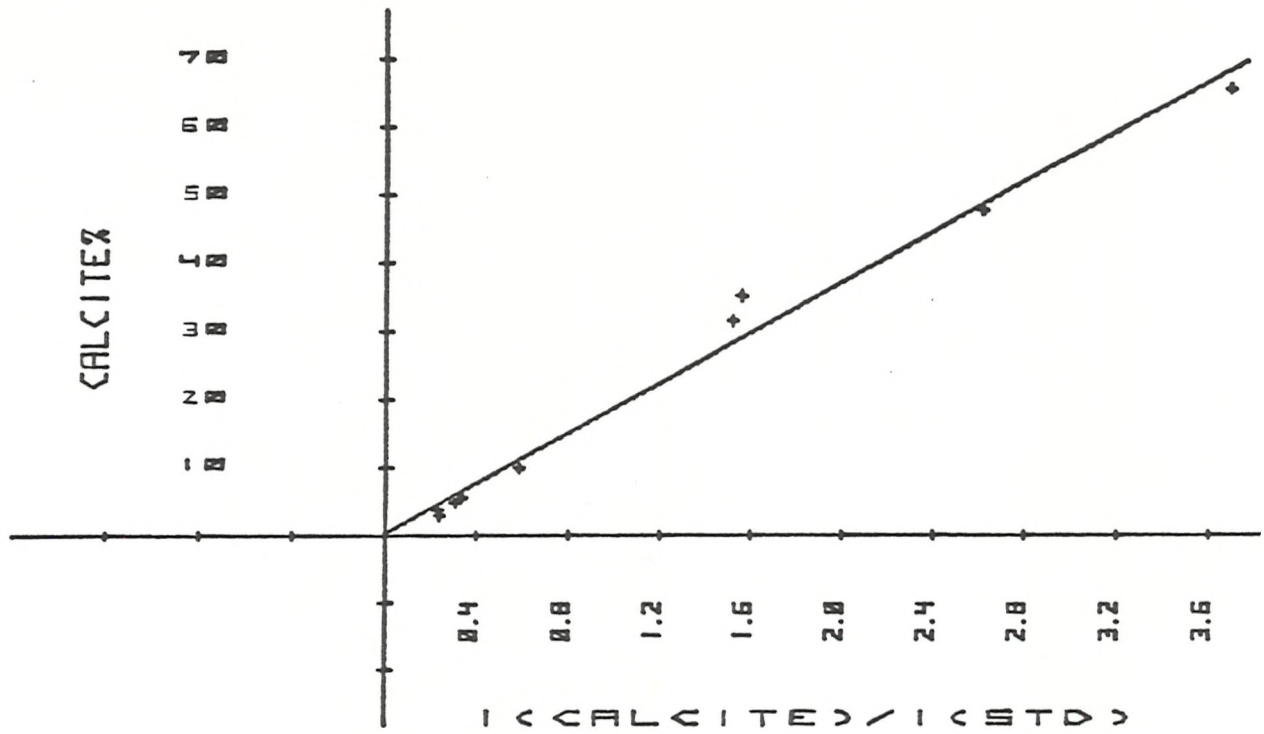

Fig. 2_9

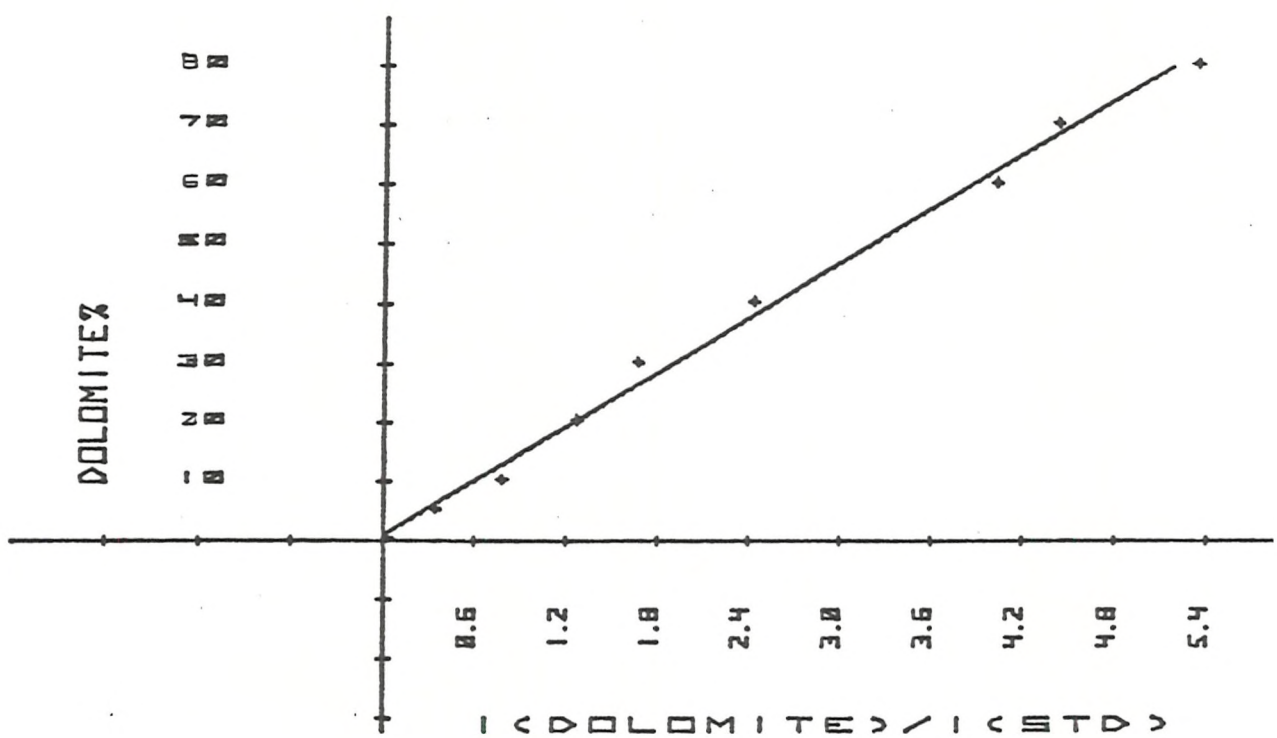

Fig. 2_10

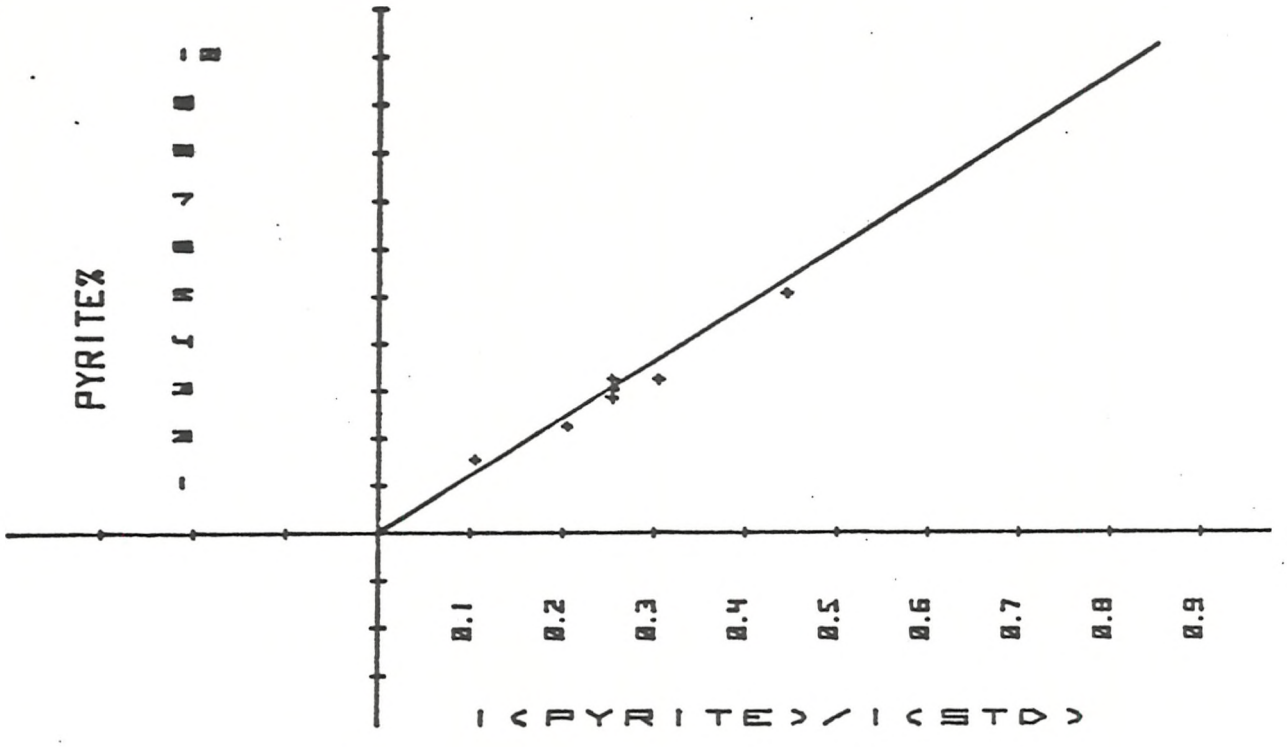

Fig. 2.11

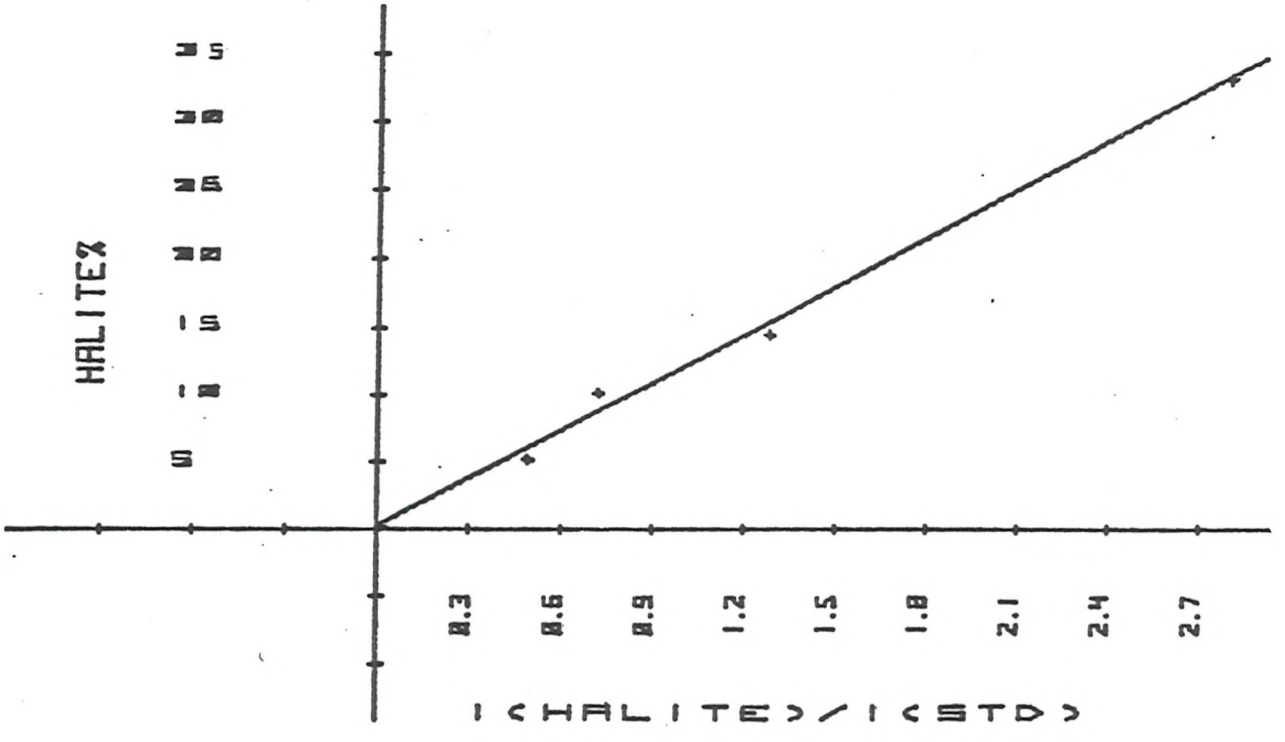

Fig. 2.12

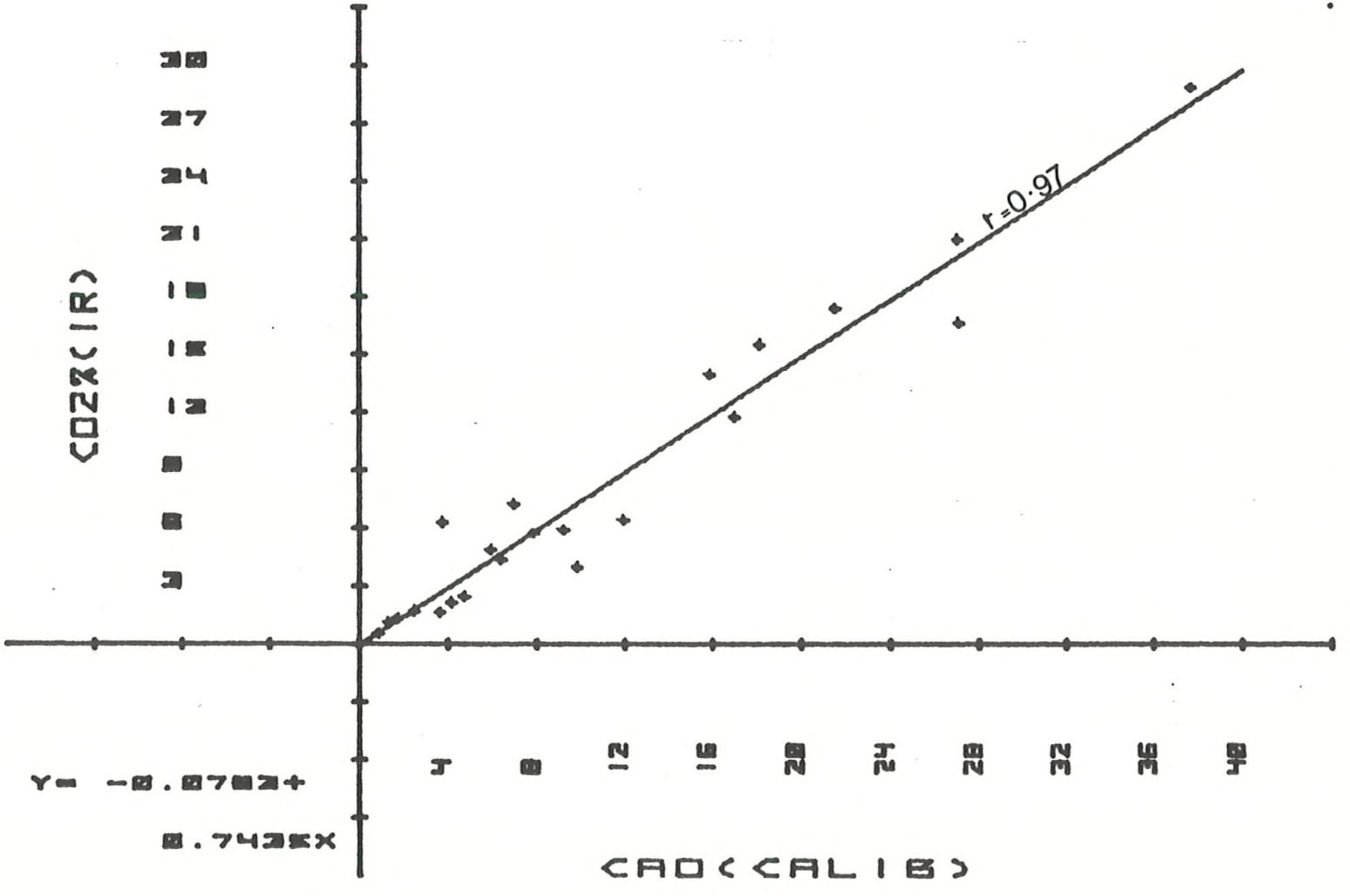

Fig. 2-13

concentration of the element being excited.

a. Beta probe

The basis of this equipment is that the sample is excited by a beam of high energy electrons or photons, so that the individual elements in the sample emit their characteristic X-radiation. A quantitative analysis of the elements present can be made by recording the X-ray wavelengths which are present in pre-set channels by crystal dispersion. A quantitative analysis can be made by accurately measuring the intensities at the wavelengths characteristic of the elements being analysed, and comparing these with intensities from a set of standard samples. In this case, the instrument was calibrated for the analysis of Si, Ti, Al, Fe, Mg, Ca, K, Na and P in a range of rock matrices. The particular attraction of this equipment is that the determination of all elements is simultaneous. In the present study, a Telsec B-300 Beta-probe was used. Since the sample was rich in clay and could absorb water easily, it was decided to prepare beads. The method consists of fusing the sample with lithium metaborate in a crucible of platinum + 10% gold. The sample was dried in an oven at 110°C for two days. Lithium metaborate was dried in a furnace at 600°C overnight. Then powder sample and lithium metaborate were weighed in the ratio of 1 to 5 into a crucible and fused over a Meker burner until the whole sample was melted and thoroughly mixed with flux. The mixture was then cooled in a desiccator and weighed again. The difference between the weight before and after heating was recorded as loss on ignition (L.O.I.). Li metaborate was added to the crucible to make up the weight of the mixture to its original value (before heating) and the material was fused again until mixed. It was then allowed to cool to a glass bead. Oven-dried graphite was then added to the glass bead formed by fusion (as much as 10% of the weight of bead) and ground-mixed in a 100 cc-barrel Tema disc mill for 15 minutes. The mixture of bead with graphite was pressed in a lead disc and run on the Beta-probe for the elements listed above against bead standards.

The calibration statistics of this method are shown in Table 2-1.

TABLE 2-1: Element Calibration Statistics for Bead Silicates

	No.of Stds.	Mean (%)	Range (%)	Standard Error of Estimate (SEE) (%)	SEE as % of Mean
SiO_2	30	55·03	28·29-76·20	0·704	1·28
TiO_2	31	0·67	0·038-2·72	0·033	4·82
Al_2O_3	32	13·73	0·44-23·58	0·387	2·82
Fe_2O_3	30	7·26	1.40-16·97	0·319	4·39
MgO	32	5·55	0·03-43·30	0·235	4·23
CaO	32	4·71	0·31-13·30	0·130	2·76
Na_2O	30	2·68	0·04- 8·92	0·135	5·02
K_2O	33	3·17	0·01-15·34	0·086	2·83
S	Not calibrated				
P_2O_5	32	0·188	0·01- 0·94	0·020	10.69
F	Not calibrated				

$$\text{SE of E (x)} = \text{SD(x)} \sqrt{1 - r^2}$$

where r = correlation coefficient

SD(x) = standard deviation of element concentration values.

b. X-ray fluorescence

The principle is similar to Beta-probe and Energy Dispersive Spectrometer attached to Scanning Electron Microscope but, in this case, the atoms are excited by a primary X-ray beam rather than by electron beam. X-rays produced by high voltages in the generator are directed onto the sample, exciting the elements in it. Since many elements are present, the secondary (or fluorescent) X-rays so produced have many different wavelengths. These are differentiated by an analysing crystal which diffracts the X-rays according to the Bragg equation (B.1).

In the present study the minor elements (Rb, Sr, Ba, Zr, V, Nb, Y, Cr, Mn, Ni, Cu, Zn, Mo, Pb, As, Ce and La) were determined by an X-ray fluorescence spectrometer (Philips PW1212).

3 to 4g of powder sample was mixed with 2-3 drops of a binder (2% aqueous solution of poly-vinyl pyrrolidine). As well as having good

self-binding properties, the binder must be free from significant contaminant elements and must have low absorption. A pellet was made of wetted sample with binder and boric acid. Boric acid was used as a backing for the sample to give it extra strength. Details concerning the calibration processes, lower limits of detection, precision and accuracy for each element are given in Cosgrove (1972) (see also Suliman, 1972; Baqri, 1976; El-Shahat, 1977; Baig, 1982). The operational conditions for the X-ray fluorescence determinations are summarised in Papavasiliou (1979) and Baig (1982).

c. SEM and EDX

The morphological characteristics of the minerals present in the samples were studied by ISI-60 Scanning Electron Microscope (SEM) and chemical analyses were made using a PGT system III Energy Dispersive X-ray spectrometer (EDX) attached to the SEM.

Samples were broken to expose fresh surfaces,and chips about 10 mm in size were cemented with carbon cement to half-inch diameter aluminium discs. Silt and clay-size materials were suspended in distilled water. A drop of suspension was placed on a carbon stub and dried at room temperature. Chips, clay and silt samples were then coated with a composite film of carbon in order to reduce damage to thick specimens during electron bombardments and to allow the heat and electrostatic charge generated in the specimen to be conducted safely away. Selected areas were examined by energy dispersive X-ray spectroscopy to obtain qualitative and quantitative elemental analysis of individual crystals. The data collection and processing programmes for the element analysis are held on disc.

The heart of an energy dispersive system is a Si(Li) (lithium drifted silicon) detector, where X-rays are converted into electrical pulses proportional to their different energies. A low temperature is required at all times to limit lithium diffusion in the silicon crystal. Consequently, the detector is connected through an efficient heat conductor to a liquid nitrogen dewar (Barbi, N.C., 1981). When a fluorescent X-ray penetrates a detector, it produces atomic collisions inside the detector crystal. Electrons released by these collisions are collected at the detector output by means of an electric field introduced into the crystal

from a bias supply. These collected electrons form a pulse, the intensity of which is proportional to the energy of the incident X-ray. This process is the basis of modern pulse height analysis (P.G.T. manual, internal publication, 1981). Here it must be emphasized that the SEM with the EDX attachment were newly available in the Department, and were used for the first time by the writer in the present study.

i. Quantitative Analysis

The data collection and processing programmes are held on disc. The background subtraction and overlap correction programmes were used in the analysis. The standards used were mainly extracted from the samples under study, as previously explained. Analyses were made using 8, 14 and 20 Kv accelerating voltages. Since the peak to background ratios did not show a significant difference between the analyses by different Kv's, a compromise was made and 14 Kv analyses were chosen. All measurements and the data collection were standardized by keeping the total count rate to a specific range for all minerals; that is, keeping specimen current constant. All measurements were made using a live time of 100 seconds, 10° tilt and working distance of 28 mm. The collected spectra were then subjected to background subtraction and overlap correction. Figure 2-14 shows the characteristics of the collected spectra.

The characteristic X-ray radiation occurs when primary electrons interact with orbital electrons of the atom. Another type of radiation occurs when the primary electron beam interacts with the nucleus of an atom. This radiation is called 'white radiation' or 'continuum'. The white radiation forms the major part of the X-ray background upon which the characteristic lines are superimposed. As mentioned previously, background subtraction is done by using a programme. In this programme a theoretical model for the continuum intensity, as a function of energy, is utilized. The shape of the background that is generated from the sample follows a hyperbola, with increasing intensity as energy approaches zero. The calculated shape available in the programme is scaled to the working spectrum by fitting points in appropriate places. With this approach to background subtraction, a very accurate background shape can be calculated for any given sample. Overlap correction was then applied when necessary. A number of peaks occur in the same energy region, such that overlap occurs;

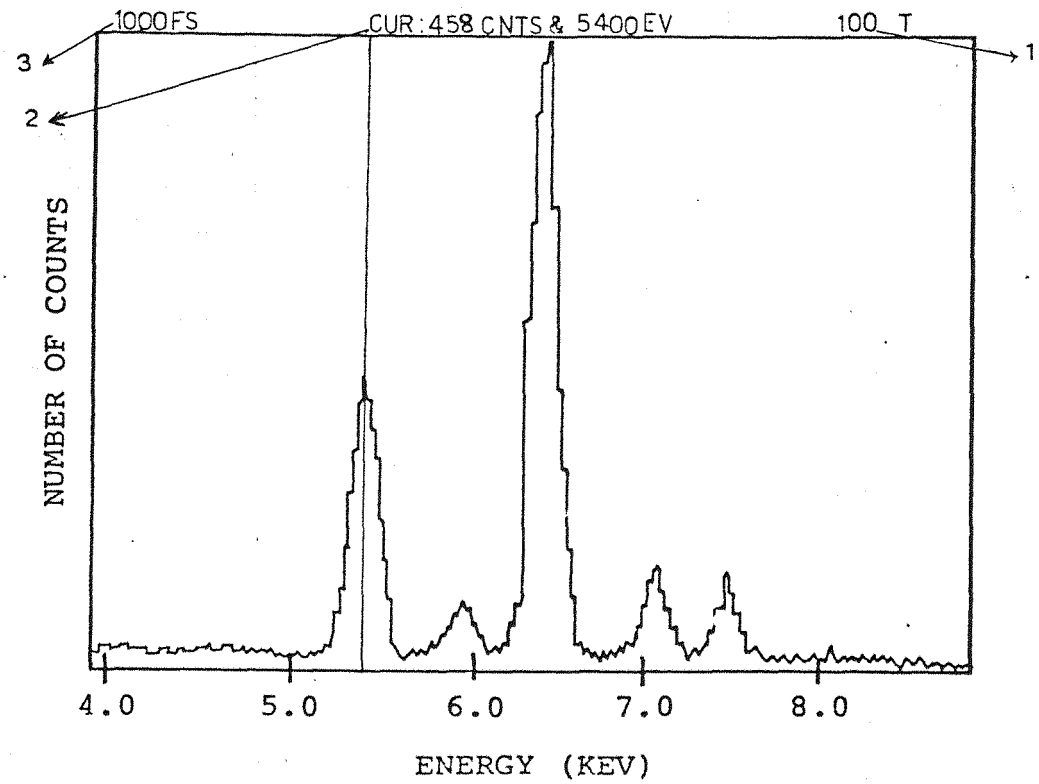

Fig.2-14 . Spectrum obtained by scanning .
(1)=spectrum run time;(2)=cursor data-include the number of counts at the cursor energy and the location of the cursor in eV;(3)=full scale intensity.

It is impossible to tell initially what individual peaks are present. This situation is potentially serious for $K_{K\beta}$ - $Ca_{K\alpha}$, $Ti_{K\alpha}$ - $Ba_{L\alpha}$, $Ti_{K\beta}$ - $V_{K\alpha}$, $Cr_{K\beta}$ - $Mn_{K\alpha}$, $Mn_{K\beta}$ - $Fe_{K\alpha}$ and $Fe_{K\beta}$ - $Co_{K\alpha}$. Overlap correction can be achieved in a number of ways, one being peak stripping. In this method, a spectrum is collected from the known constituent of the overlap. If, for example, the chromium K peak conceals another underlying peak, a spectrum from a sample containing non-overlapped chromium peak is collected. After background subtraction, the element spectrum is subtracted from the overlapped spectrum. In the example used here, the chromium $K\alpha$ and K_β would be stripped from the spectrum, revealing the manganese $K\alpha$ peak, which could then be identified as the unknown constituent of the overlap. A pure manganese standard is then collected. The standard spectrum with the stripped spectrum are displayed. By a simple ratio, an estimate of the manganese weight fraction is possible.

Estimation of concentration

As previously mentioned, the clay standards were prepared using pure minerals extracted from the present study samples (Table 5-2) and clinoptilolite from Sample 256/7cc (Table 5-6a) as standard for zeolites. The percentages of the elements in the standard were determined by Beta-probe. The standards were then mounted on a carbon stub and run on the SEM under the conditions previously mentioned. The ratio method was used for zeolites since there were not many standards available and also there is not very much variation in the chemistry of zeolites. Calibration curves of the intensity against percentage were prepared for clay samples. In both cases peak to background ratios were used. According to Statham (1979), the ratio of intensities of characteristic radiation and continuum of the same wavelength is approximately independent of absorption and back-scatter effects; the peak to local-background ratio (P/B) serves as a measure of composition which is essentially unaffected by changes in specimen geometry or sample thickness. Methods are described for quantification by (P/B) values in the analysis of bulk specimens, thin films and small particles. According to him, the P/B value is not only independent of the resolution

and efficiency of the spectrometer, but is also independent of spectrum scale, so fluctuations in beam current are of no consequence. Statistical errors can be a problem with low background levels and all sources of stray background have to be eliminated, but absorption and back-scatter corrections are always close to unity (Statham, P.J., 1979).

Ratio method

After background has been subtracted and overlap corrections applied, the peak to background ratios of interest are obtained. By comparison with the intensity from a standard, a K-ratio is determined for each element. The concentration of each element is then calculated as follows:

$$C^{\ell} = KC$$

where C^{ℓ} is concentration of element in sample, C is concentration of the same element in the standard, and

$$K = \frac{I}{I^{\ell}}$$

where I is the intensity of element in the standard and I^{ℓ} is the intensity of element in the sample. Since standards resemble the unknown in chemical composition and physical properties, and a ratio method is used, no ZAF (Z = atomic number correction, A = absorption effect, and F = fluorescence effect) correction was made.

Calibration curve preparation

The calculation of the element concentration from its line intensity was done using a calibration graph. This was constructed by plotting the intensities (measured relative to the background) of a set of samples with known concentrations (Fig.2-15 to 2-21).

The calibration statistics are shown in Table 2-2. The advantages of using EDX are:

1. A small sample is sufficient for analysis of all elements.
2. The determination of all elements is simultaneous.
3. The time required for analysis is short.
4. Easy to operate.

Fig. 2.15

Fig. 2.16

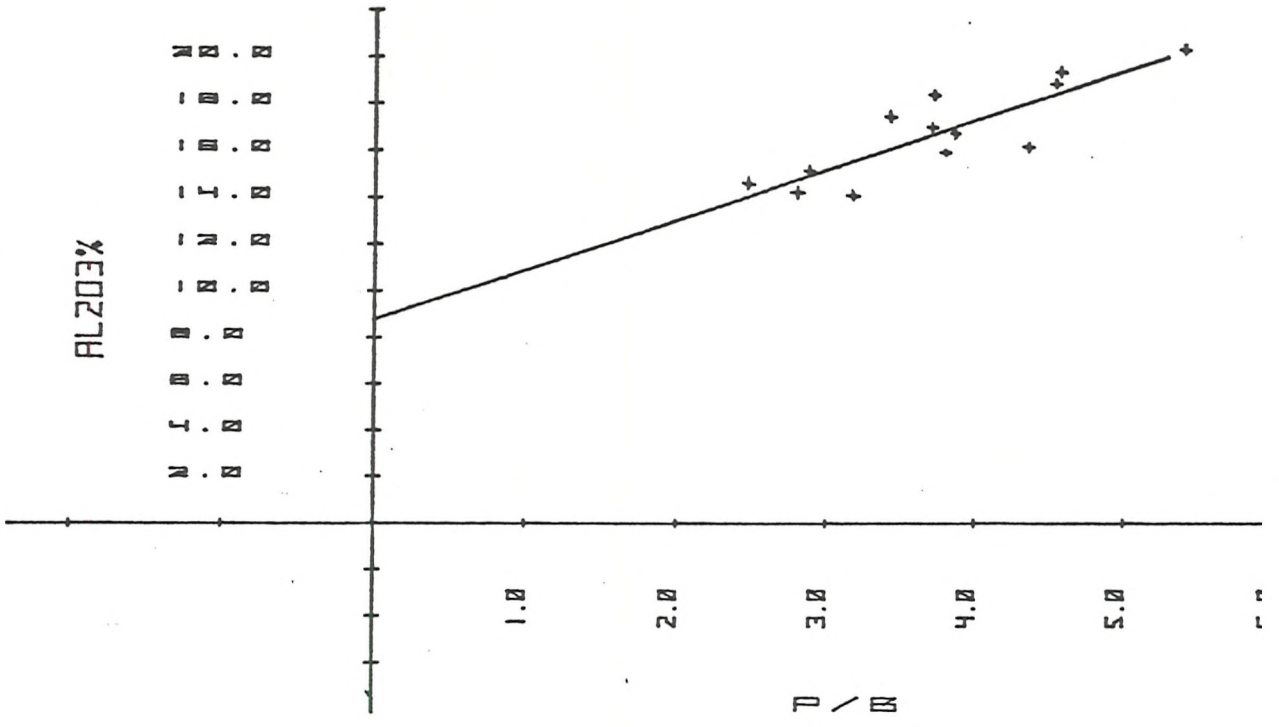

Fig. 2_17

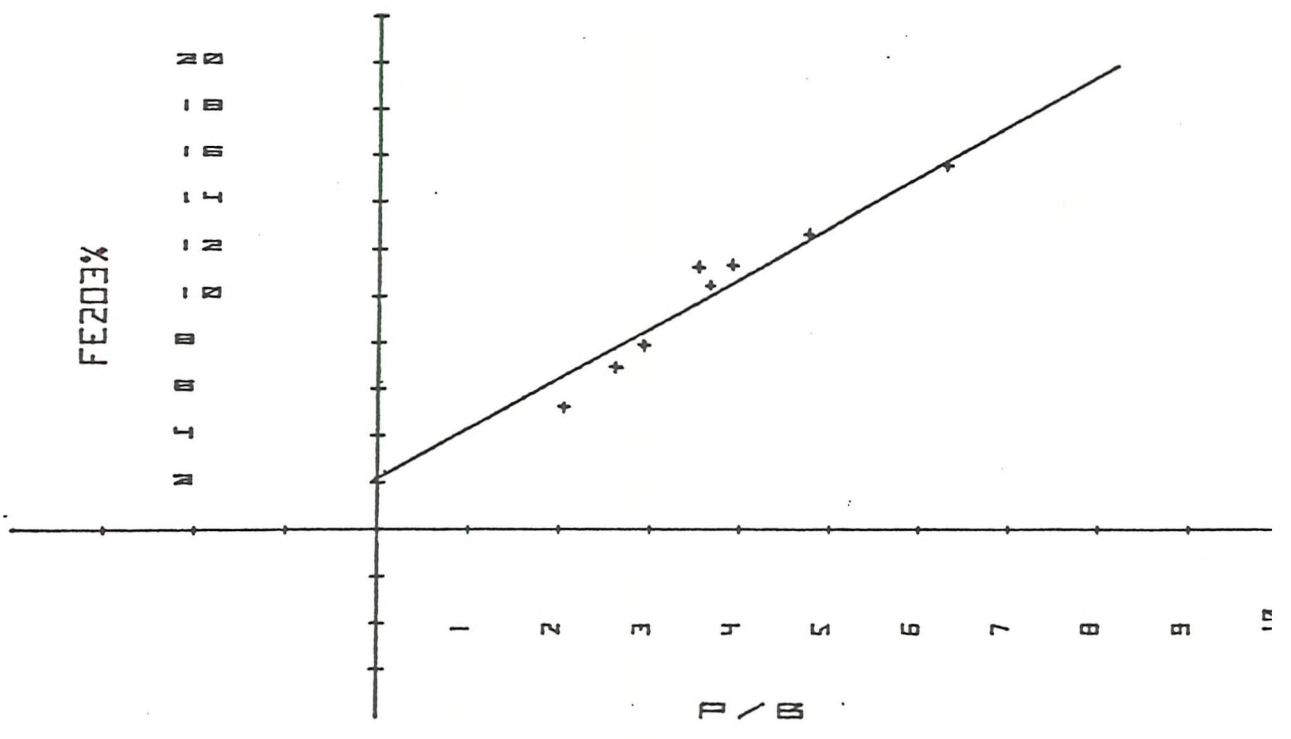

Fig. 2_18

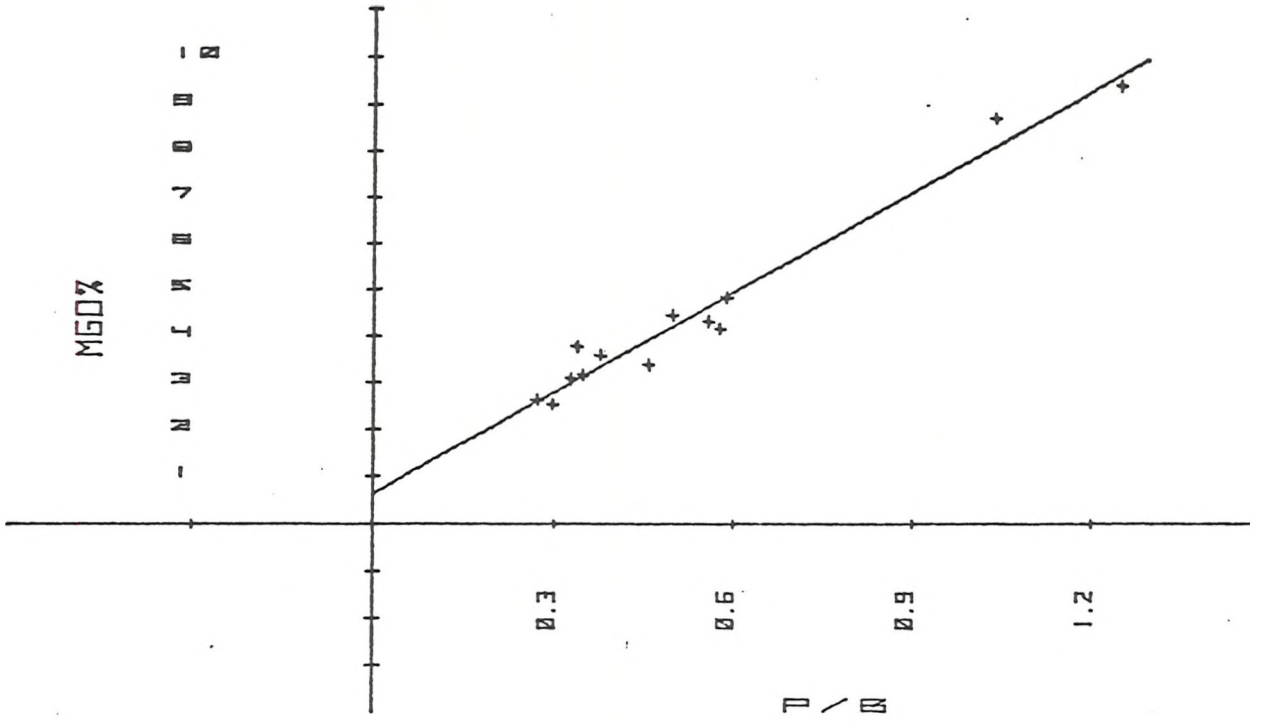

Fig. 2_19

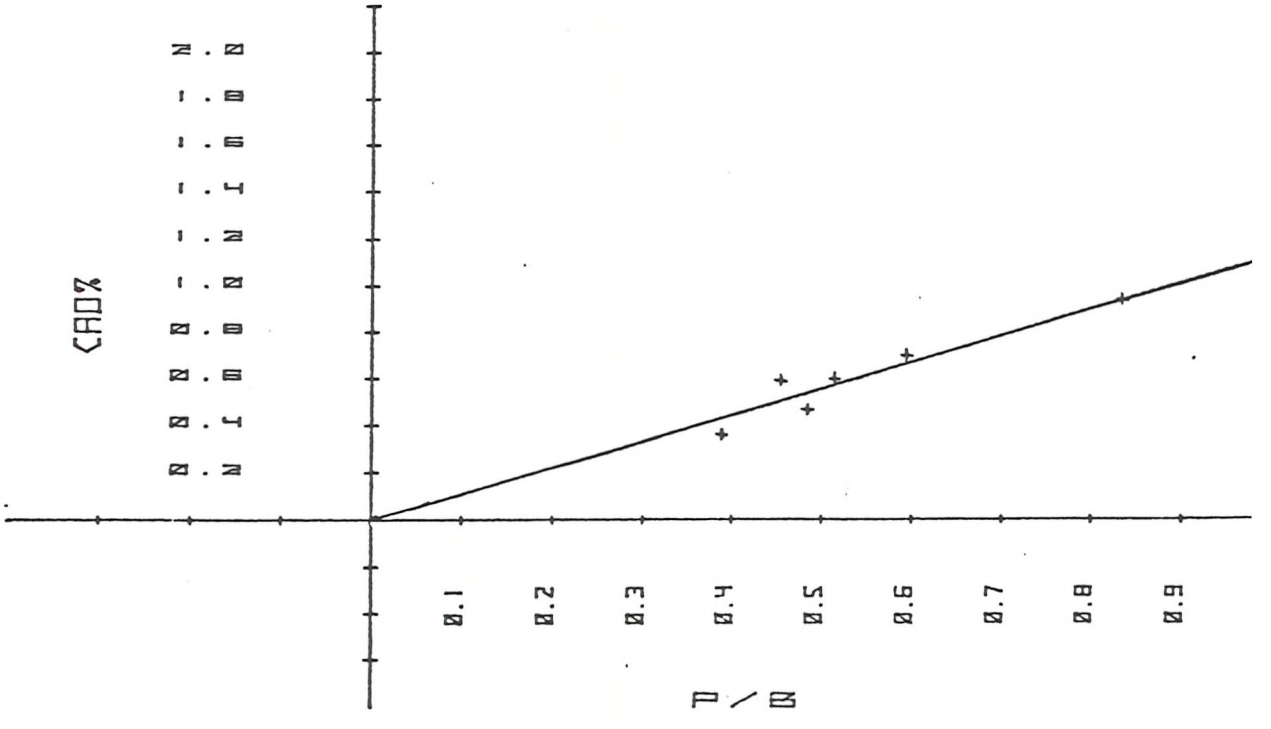

Fig. 2_20

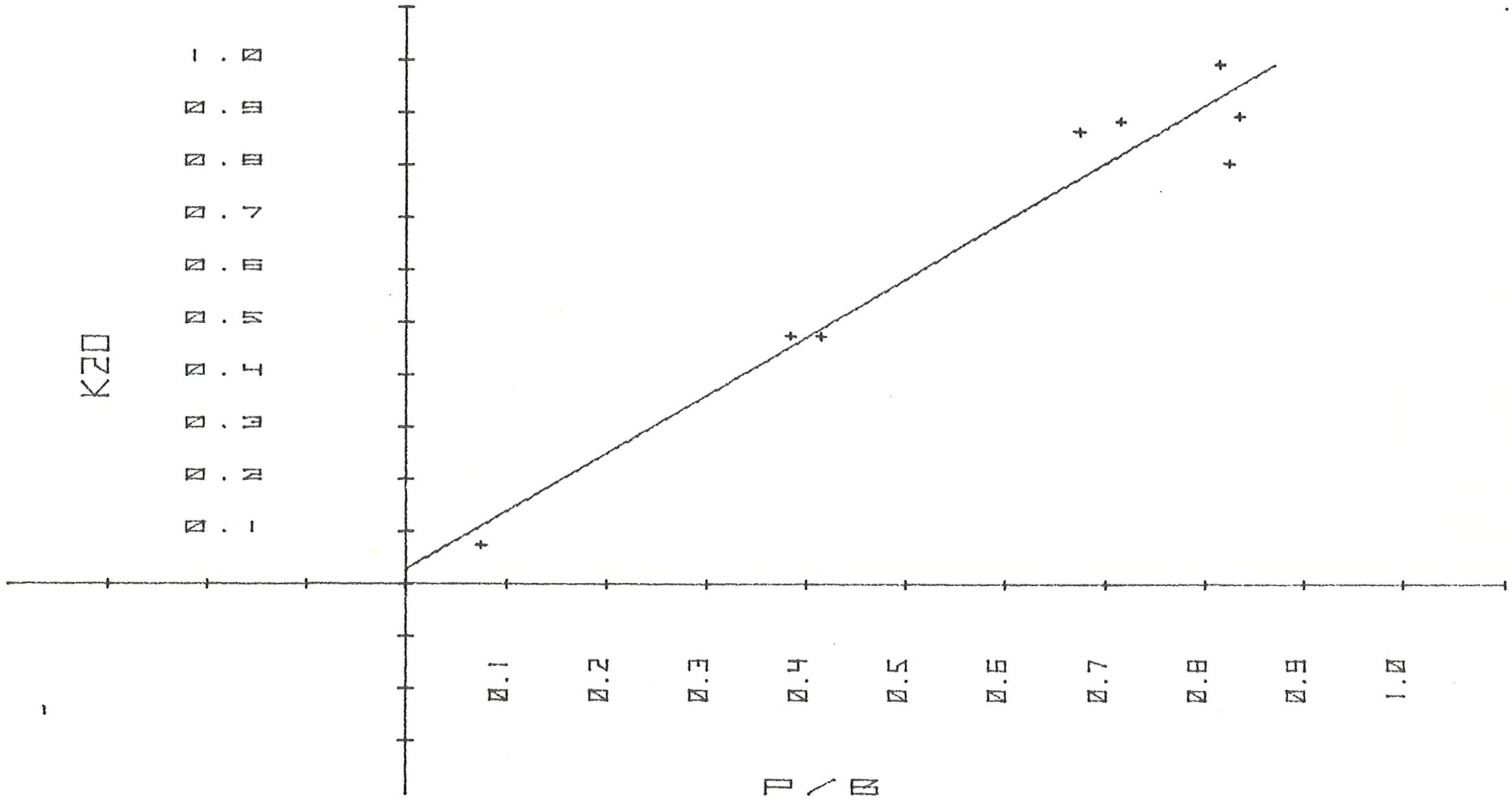
K20
1.00
0.90
0.80
0.70
0.60
0.50
0.40
0.30
0.20
0.10
0.1
0.2
0.3
0.4
0.5
0.6
0.7
0.8
0.9
1.0
T / TN

Fig.2_21

TABLE 2-2: Element Calibration Statistics of EDX

	No.of Stds.	Mean (%)	Range (%)	Standard Error of Estimate (SEE)	SEE as % of Mean
				%	
SiO_2	13	52·13	44·23-58·68	2·49	4·77
TiO_2	10	0·54	0·13- 2·29	0·068	12·45
Al_2O_3	13	16·68	13·98-20·22	1·04	6·23
Fe_2O_3	8	10·81	5·15-16·31	0·92	9·00
MgO	13	4·42	2·57- 9·38	0·39	8·99
CaO	7	0·51	0·00- 0·93	0·06	11·07
K_2O	8	0·67	0·07- 0·99	0·076	11·27
P_2O_5		Not calibrated			

---

2. Free Iron Removal

The presence of iron-bearing inclusions in the zeolite has been reported by many workers (Stonecipher, 1978; Sheppard et al.,1970; Boles et al., 1978). The analysis of the pure mineral showed the presence of iron. Therefore, in order to determine whether the reported iron in the composition of the pure mineral was iron in an inclusion or structural iron, the method suggested by Mackenzie (1954) was used. 40 mg of air-dried concentrated zeolite mineral was weighed into a centrifuge tube and wetted with distilled water thoroughly and immersed in water at 40°-45°C. 0·4g of $Na_2S_2O_4$(sodium dithionite) was weighed into a 100 ml measuring cylinder and dissolved in 10 ml 0·3% NaOH by shaking. The above solution was immediately added to the mineral, and the centrifuge tube was immersed in water at 40°-45°C for 5 minutes with occasional shaking. The suspension was then centrifuged and the supernatant liquid collected in a 250 ml beaker. 10 mls of 0·05 N HCl were then added to the centrifuge tube and left at 40°C in water for 3 minutes, after which this liquid was poured into a different 100 ml beaker. These processes were repeated three times. According to Mackenzie (1954) preliminary tests with clays and soils indicated that while two treatments with sodium hydrosulphite solution were necessary for reasonably complete removal of all the free iron oxide, a third treatment removed very little. After bleaching, in order to remove soluble iron salts retained in the sample, two washings were given with 1 N NaCl. These washings were added to the HCl

extract. The beakers were covered and heated on steam, both for 20-30 minutes. 10 ml and 5 ml of 20 mol H_2O_2 were added to the $Na_2S_2O_4$ washing and HCl extract respectively. The solutions were re-heated and after effervescence finished, combined, filtered and made up to 100 ml. Iron was then determined by Atomic Absorption.

3. H_2O Determination

The Du Pont 951 thermogravimetric analyzer (TGA) is a plug-in module for the 990 thermal analyzer. It measures the weight and rate of weight change of a material continuously, as a function of increasing temperature; thus heating the sample would result in the loss of absorbed moisture, lattice-held water, CO_2 and S. Small sample size and fast-heating rate allow a rapid analysis.

In the present study a combined sample and pan weight of 20 mg was used for making a plot between loss and temperature. The plot was made during raising the temperature to 1000°C. Subtracting the CO_2 content from the total weight loss would yield the water content of the sample. Some CO_2 and S (as SO_2) can be lost up to 650°C, the bulk of the CO_2 will be lost above 650°C. The precision of the method is given in Papavasiliou (1979).

4. Total CO_2 Determination (carbonate and organic carbon)

The basis of the determination of CO_2 was its detection and measurement by infrared absorption, using a BINOS 1 (Ley bold - Heraeus)infra-red photometer set to the appropriate wavelength.

In the present study 0·02g of 100% pure $CaCO_3$ was used as a standard. It was weighed in a silica boat and heated in a tube furnace to 860°C in a stream of oxygen. Inert gases and equiatomic gases, such as N_2, O_2 and H_2 are not infrared-active; therefore O_2 was used to:

a) flush away the remaining CO_2 from the previous runs or air;

b) oxidise the organic carbon.

The resulting CO_2 from the decomposition of carbonates and the oxidation of organic matter was collected in a 1 litre volumeter. The CO_2 and O_2 mixture was expelled through the infrared analyzer (IR), and the output was visually

displayed by meter and displayed on a chart recorder. 0·02g of sample was weighed and processed in the same way as the standard. Since $CaCO_3$ contains 43·97% CO_2, the total CO_2 percentage in the sample can be calculated as follows:

$$\frac{\text{Peak height (sample)}}{\text{Peak height (standard)}} \times 43{\cdot}97\% \qquad (1)$$

Peak height was measured from the recorder trace. In order to determine carbonate CO_2, 0·02g of standard was weighed in a glass boat and placed in a glass tube to which a pipette containing warm phosphoric acid was connected. A few drops of warm acid were added to the standard in the boat. The CO_2 thus derived was collected in the volumeter and determined by IR as described earlier. Samples were run in the same way as the standard and the percentage of CO_2 was calculated using equation (1). The CO_2 resulting from organic matter was calculated by subtraction of carbonate CO_2 from total CO_2.

There are several factors that affect the reproducibility of the analyses. They include machine fluctuation and weighing. In order to indicate the importance of the above factors, a coefficient of variation (cv) was calculated. Five samples were selected containing variable percentages of CO_2 between 1 and 30%. Each sample was run through the system five times. The mean percentages of the samples were then plotted against their cv. (Fig.2-22). If the CO_2% is more than 10, each one of the five determinations will be within 2 per cent of the mean. The reproducibility is less for amounts less than 10%. For example, for 1·5% CO_2, the single determination will be within 12% of the mean.

5. Ferrous Iron Determination

The method proposed by French and Adams (1972) was used. 0·25g of a sample was placed in a polyethylene bottle. 5 ml of 40% HF was mixed with 5 ml concentrated H_2SO_4 and the mixture was added to the sample. The sealed plastic bottle was placed in a hot water bath for 15 minutes. The decomposed sample was then transferred to a 250 ml beaker and made up to 200 ml by addition of saturated boric acid solution. Iron was determined titrimetrically with $Ce(SO_4)_2$ after the addition of a few drops of indicator (N-phenylanthronolic acid).

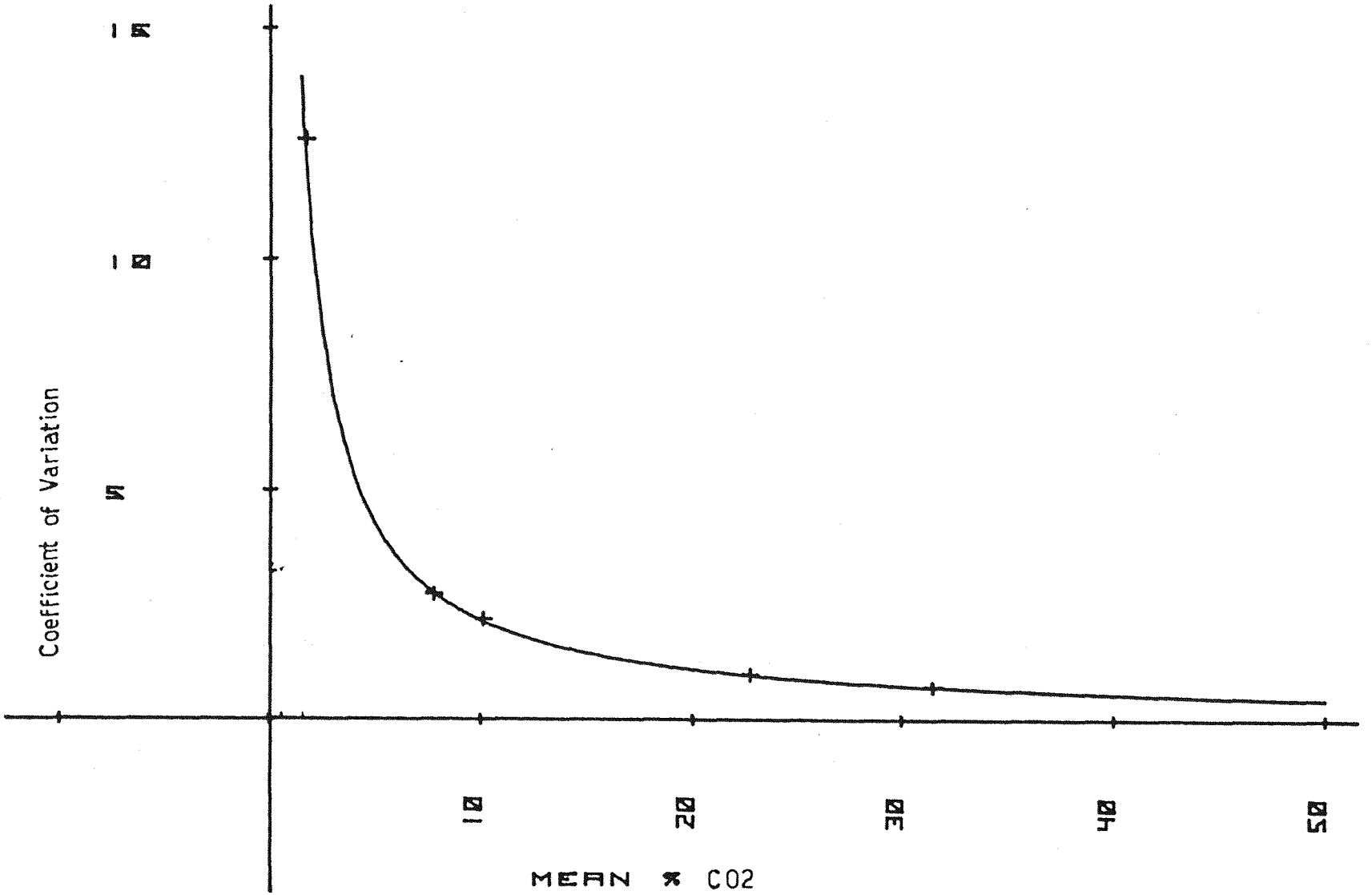

Fig 2-22

CHAPTER III

MINERALOGY

A. Bulk Mineralogy

Semi-quantitative mineral analysis was undertaken on a 'whole rock basis' on 90 samples by X-ray diffraction. Results are shown in Table 3.1.

Minerals were identified by their characteristic basal peak except in the case of pyrite, when the peak at 2·7Å was used. Details of sampling procedures, sample preparation, X-ray diffraction techniques, mineral identification procedures and quantitative methods are given in Chapter II.

The main identified constituents are quartz, feldspars (both K-feldspar and plagioclase), clinoptilolite, phillipsite, clay minerals, calcite, dolomite, pyrite and opal-CT (irregular structural inter-stratification of cristobalite and tridymite layers). The clay mineral groups observed in this study are mixed layer illite/smectite (MLIS), illite, kaolinite, palygorskite and chlorite. In addition to the above minerals, which constitute the bulk of the samples, several other minerals were identified. These include gibbsite, goethite, gypsum, ilmenite, anatase, apatite, garnet, zircon. Semi-quantitative estimation was not done for the above minerals since they were present in traces.

1. Quartz

The occurrence of quartz as a primary mineral in igneous rocks, especially those on the continents, and its resistance to chemical and mechanical weathering, account for its presence in marine sediments. Almost all of that found in deep sea sediments is detrital and originates from terrestrial weathering, or is formed during sub-aerial or submarine volcanic processes (Windom, 1976; Chester et al., 1976; Peterson et al., 1962).

The principal transport processes responsible for the distributions of quartz in marine sediments include wind transport, river discharge and ice-rafting (Goldberg et al., 1970; Chester et al., 1976; Windom, 1976; Aston et al., 1973, Beltagy et al., 1972).

Quartz is common in all samples of the present study. The amount of quartz varies from 75% at Site 240 in the Somali Basin to mere traces

at Site 216 on the Ninetyeast Ridge. It is usually concentrated in the > 2 μm fractions of the sediments. Quartz usually occurs as angular grains in most of the sediments, suggesting that they did not travel long distances, while rounded quartz grains at Sites 240 and 239 indicate long distance transport (Plate 3.1).

At Site 212 zeolitic clay samples show a decrease in the amount of quartz in comparison with adjacent non-zeolitic clay samples in the upper and lower parts of the hole; this distribution of quartz may be related to a very low sedimentation rate in the case of zeolitic clay. The increase in quartz percentages in samples 36cc and 37/1 is probably due to the increase in sedimentation rate and detrital input. There is a downward decrease in quartz percentages at Sites 211, 221 and 236, which again suggests increase in detrital input in younger sediments. There are no specific patterns in the distribution of quartz in the rest of the samples. This is probably due to the quartz being brought into the area by a variety of transport mechanisms.

2. Feldspars

Feldspars are ubiquitous in the sediments of the world oceans. The feldspars in marine sediments originate from both marine volcanism and continental weathering (Windom, 1976). The distribution of feldspars in the sediments of the world oceans therefore reflects not only the continental weathering and transport regimes, but also marine volcanic activity.

Feldspars are found in all samples of the present study, and the amount varies from traces up to 47%. It is concentrated in the > 2 μm fractions. From the preliminary examination by X-ray diffraction, it was found that plagioclase with the main reflection at 3·19Å dominates over K-feldspar with the main reflection at 3·24Å. Subsequent Energy Dispersive X-ray analysis confirmed these identifications. There is no specific pattern in the distribution of feldspars in the samples. SEM studies of feldspar grains revealed the presence of angular and rounded grains (Plate 3.2). These features suggest a detrital origin. There is no evidence of secondary (authigenic) feldspar.

3. Zeolites

Phillipsite and clinoptilolite were the two common zeolites found

PLATE 3-1

a. quartz grain in Sample 211/14/1

b. " " " Sample 212/38/1

c. " " " Sample 213/15/2

d. " " " Sample 216/32/3

e. " " " Sample 239/16/3

f. " " " Sample 240/5/1

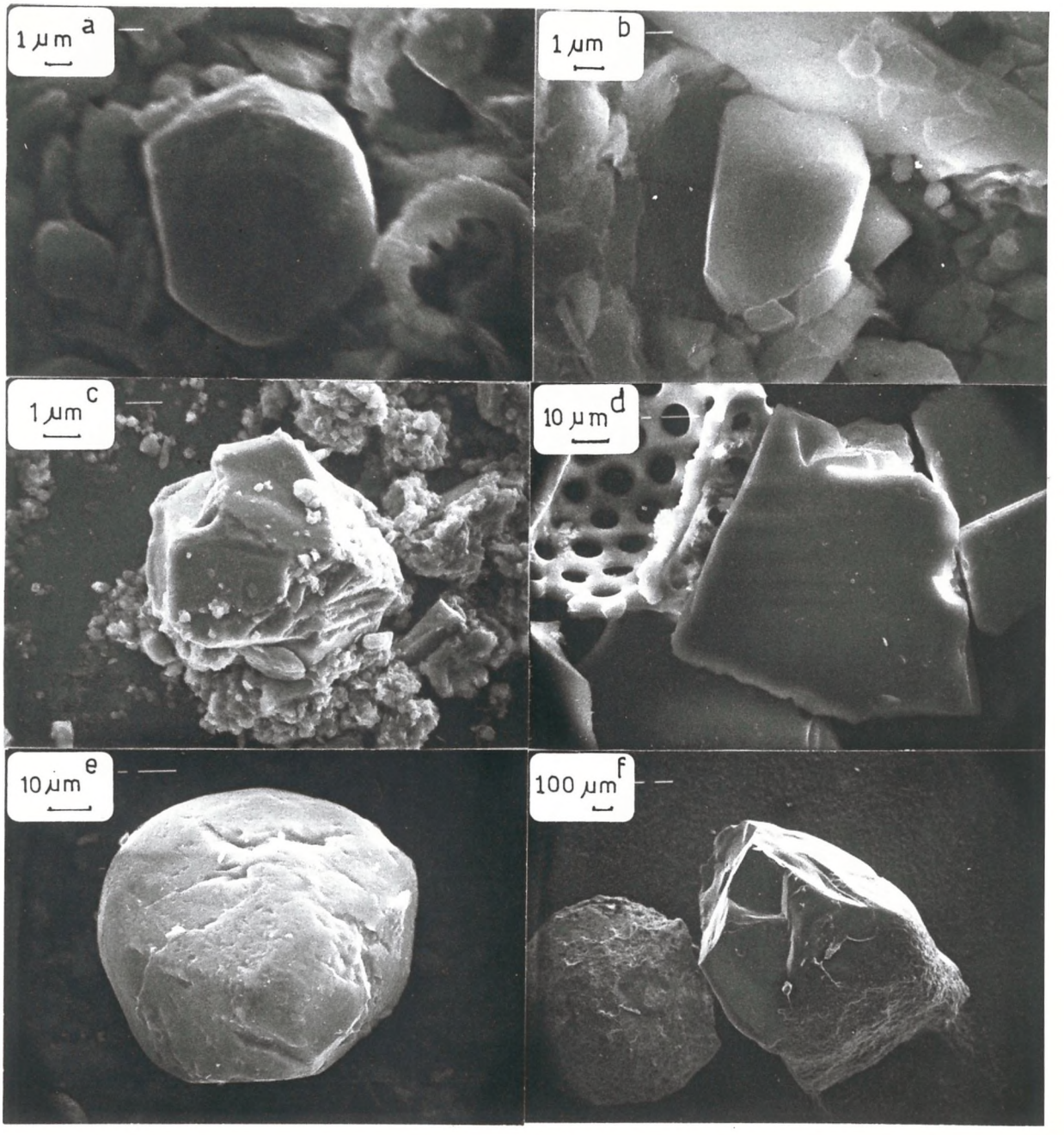

PLATE-3-1

PLATE 3-2

a. feldspar grain in Sample 212/38/1

b. " " " Sample 216/25/3

c. " " " Sample 239/1/1

d. " " " Sample 240A/2/1

e. " " " Sample 245A/6/2

f. " " " Sample 250A/22/3

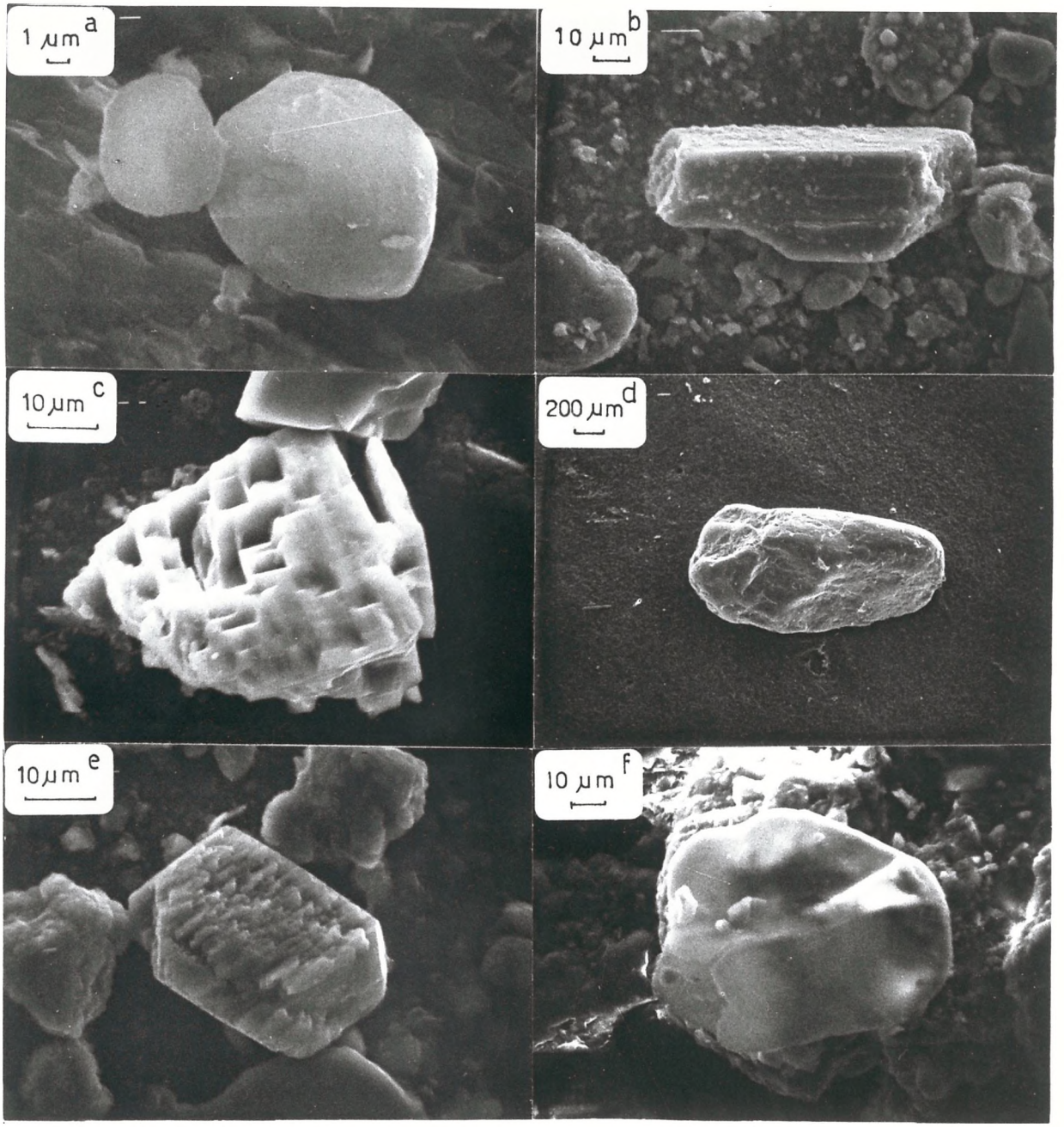

PLATE·3-2

in the >20 μm size fractions. They were identified by their characteristic basal peaks (Figs. 3-1 & 2). Their morphology and chemistry were studied by Scanning Electron Microscope (SEM) and Energy Dispersive X-ray (EDX).

a. Clinoptilolite

The amount of clinoptilolite varies between 5% up to 67%. It is usually associated with disordered tridymite/cristobalite (opal-CT) and mixed layer illite/smectite. It occurs as discrete euhedral crystals (Plate 3-3, a-c), twinned crystals (Plate 3-4a) and as spherical aggregates (Plate 3-4,b-d). It usually appears in the pore spaces (Plate 3-5, a-d).

Other workers (Mumpton et al., 1976; Kastner et al., 1978; Boles et al., 1978) have studied clinoptilolite under SEM. There are many similarities between the clinoptilolite of the present study and that described by the above authors.

Kastner et al. (1978) and Stonecipher (1976) observed that clinoptilolite predominates in calcareous and clayey sediments of Miocene to Cretaceous age. It persists even below 850m depth.

In the case of the present study, the relation between the distribution of clinoptilolite and the various lithologies, age and depth showed that it was more common in brown clay (Fig.3-3) and sediments of Miocene to Cretaceous age (Fig.3-4). It also showed persistence up to 700m depth, but its highest abundances occurred between 200-250 and 500-550 metres (Fig.3-5).

b. Phillipsite

In the present study phillipsite percentage varied between 3% and 27%. It was associated with mixed layer illite/smectite and Mn micro-nodules.

SEM studies of phillipsite crystals showed many similarities with those of Mumpton et al. (1978) and Stonecipher (1976). It occurred as elongated crystals (Plate 3-6,a-b) and complex sector-twinned crystals (Plate 3-6, c-d). A common characteristic of phillipsites is a 'cracking' along cleavage surfaces parallel to the axis of elongation, breaking the crystal into smaller sections (Mumpton et al., 1976). This was observed

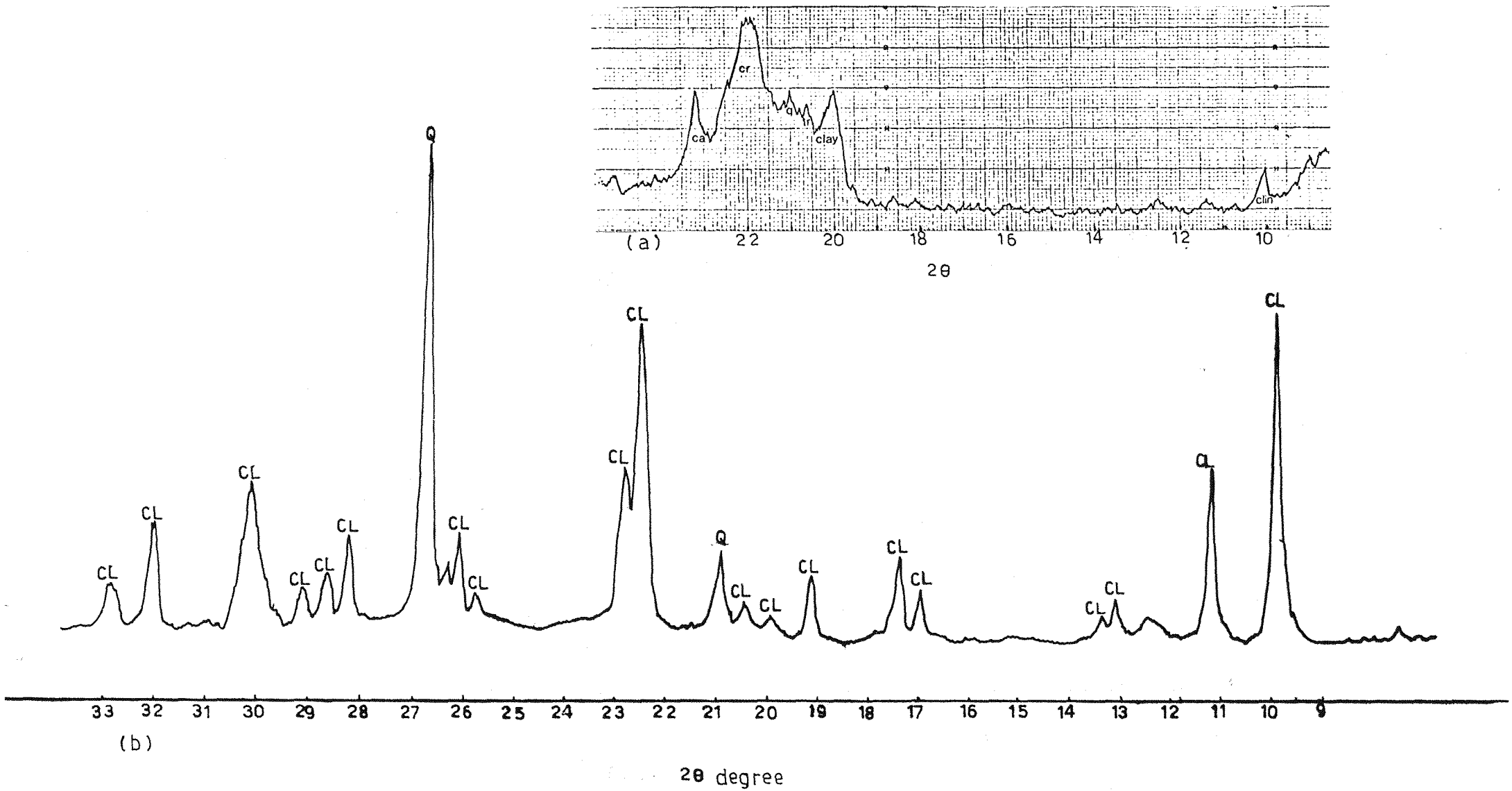

Fig.3-1.Diffraction patterns of opal-CT(a) and clin(b) from site 258(cores 15/1 and17/2, respectively).tr=tridymite,cr=cristobalite,q and Q=quartz,ca=calcite,CL=clin.

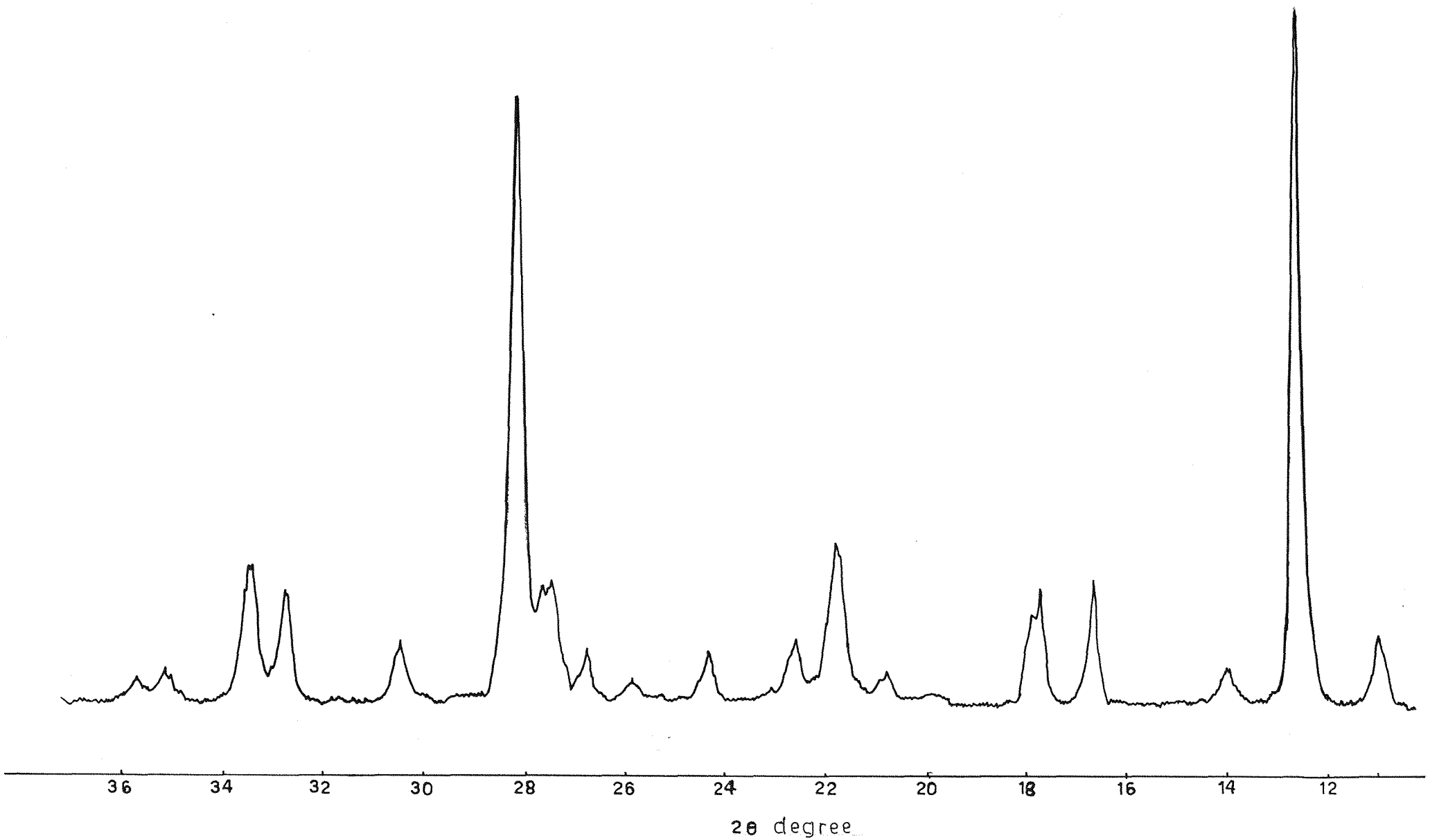

Fig.3-2.Diffraction pattern of phillipsite from sample 213/13/5.

PLATE 3-3

a & b = Euhedral crystal of clinoptilolite in Sample 258/17/2

c & d = Euhedral crystal of clinoptilolite in Sample 258/25cc

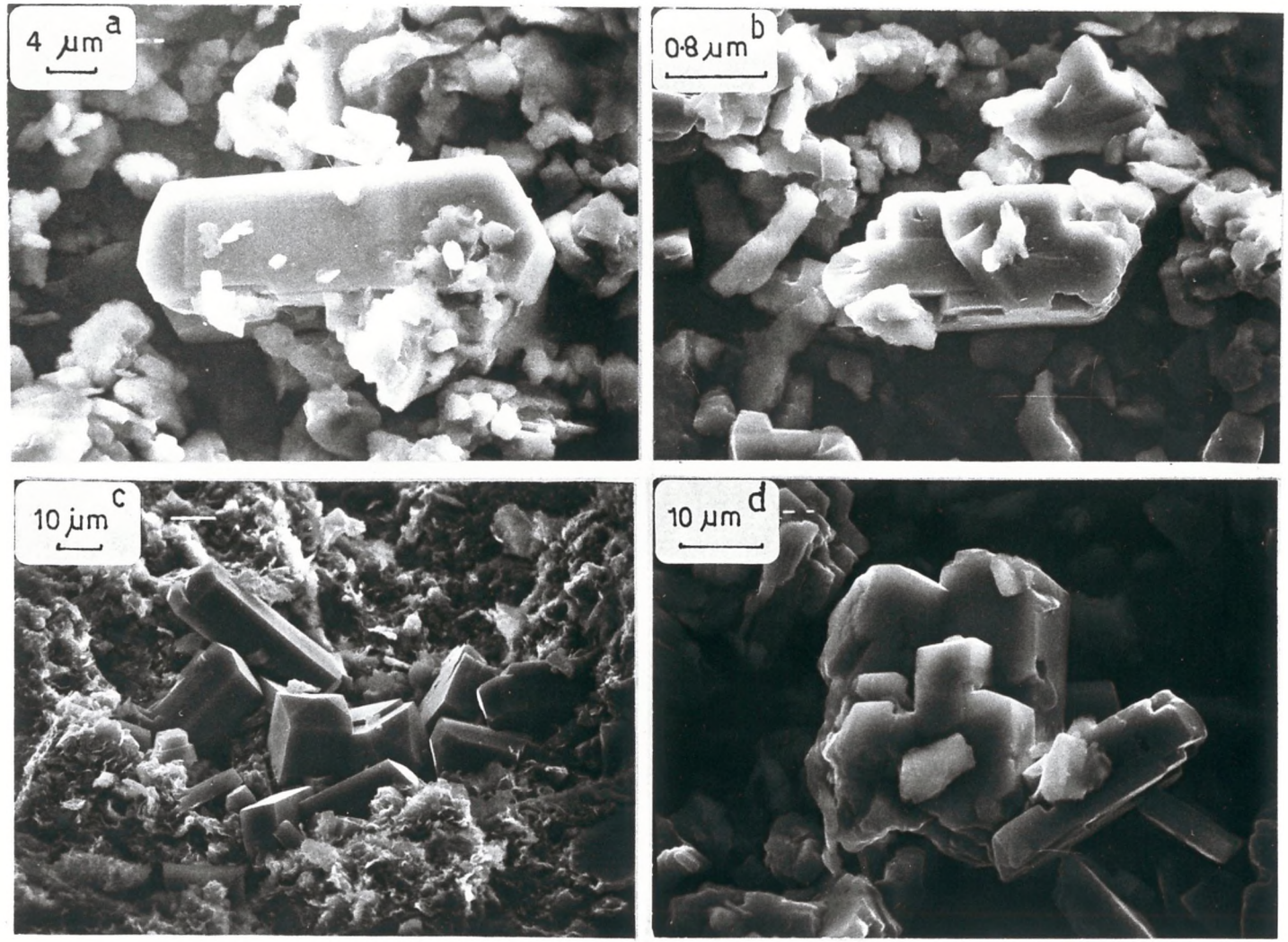

PLATE · 3-3

PLATE 3-4

a. Twinned crystal of clin in Sample 258/17/2

b. Spherical aggregate of clin in Sample 258/25cc

c & d. High magnification of Figure b.

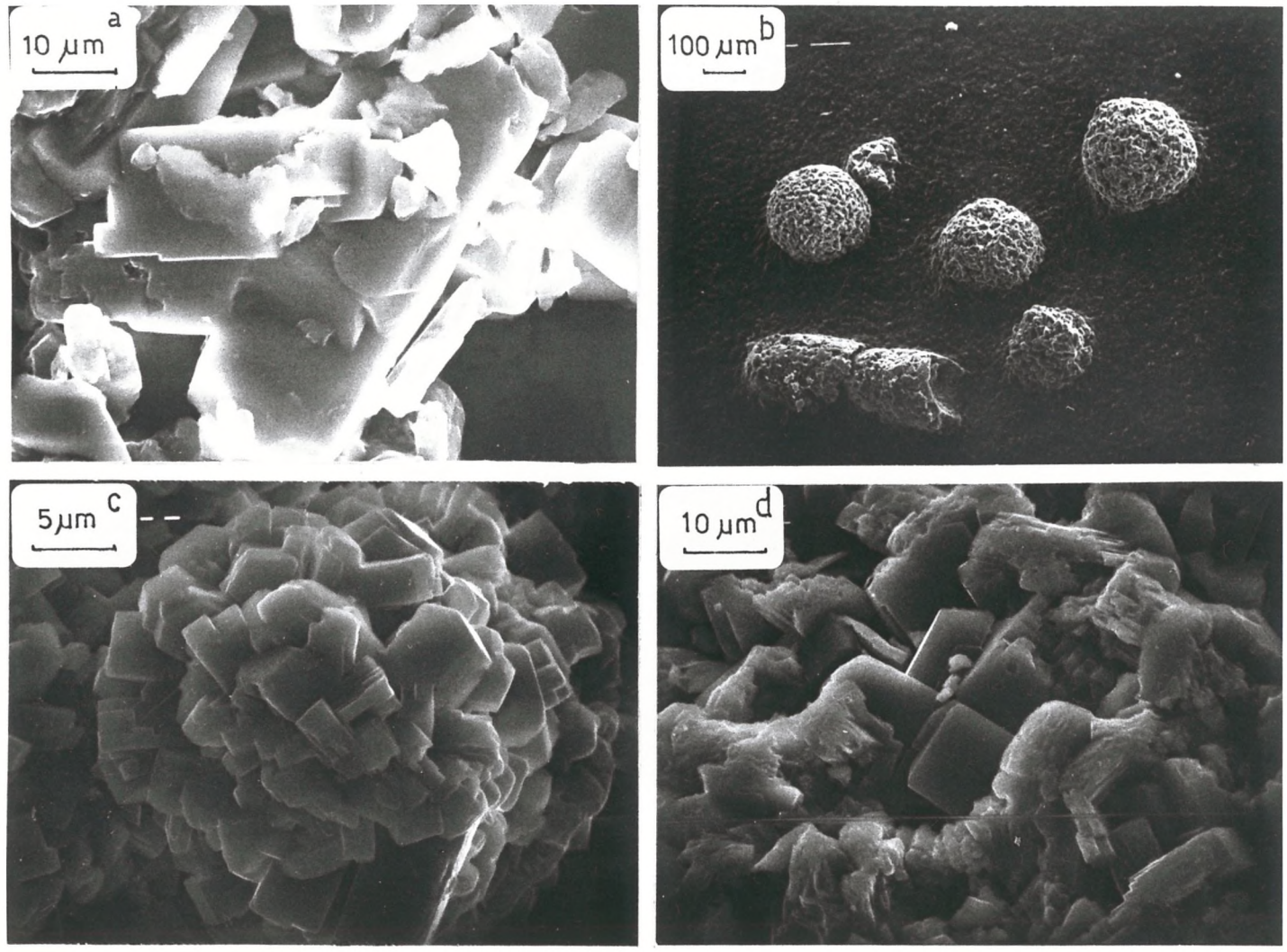

PLATE·3-4

PLATE 3-5

a. Clinoptilolite crystals in association with Opal-CT in the pore space in Sample 258/14/1.

b. Clinoptilolite crystals in association with Opal-CT in the pore space in Sample 258/25cc.

c.& d. Clinoptilolite crystals in the pore space in Sample 258/25cc.

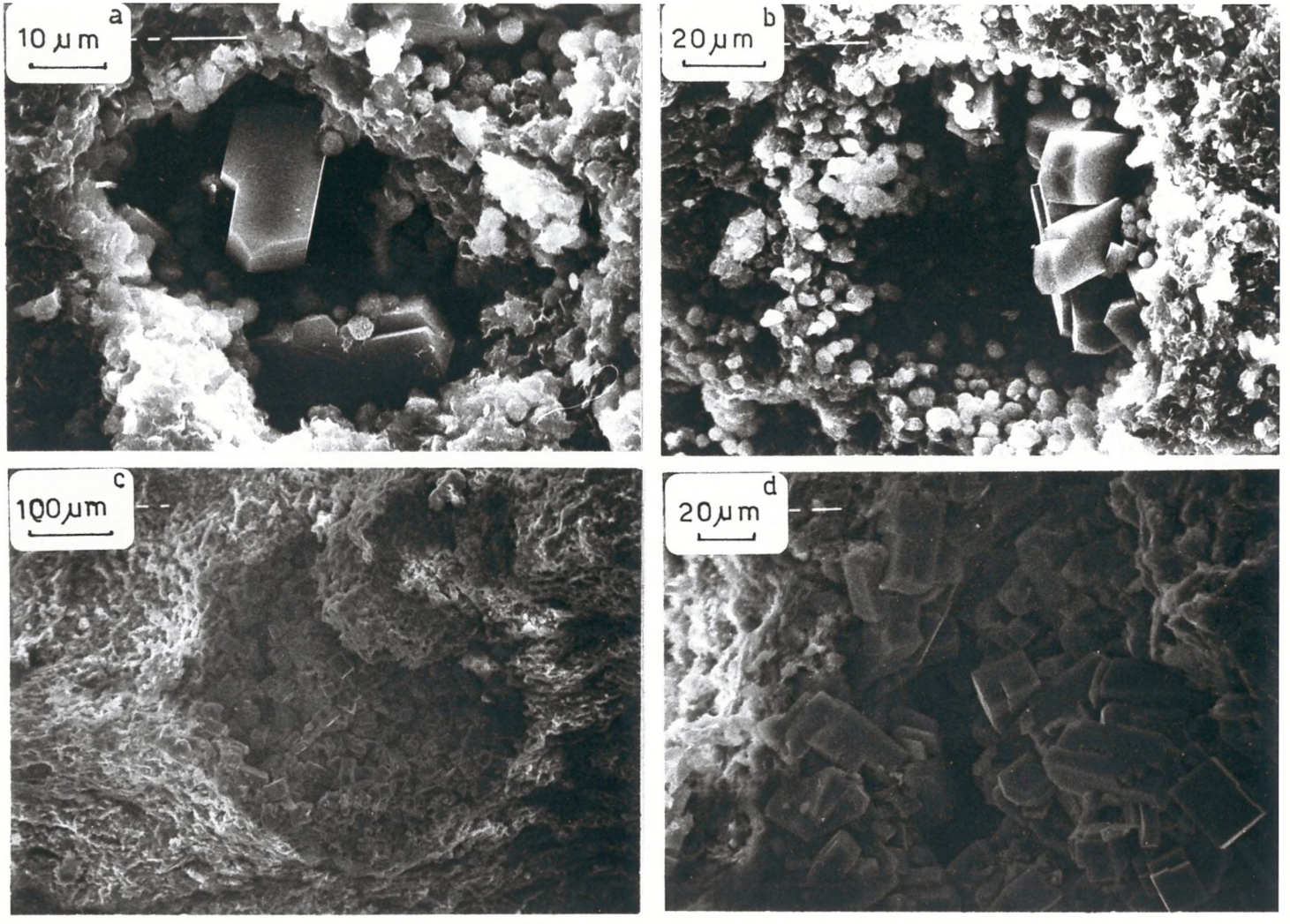

PLATE · 3-5

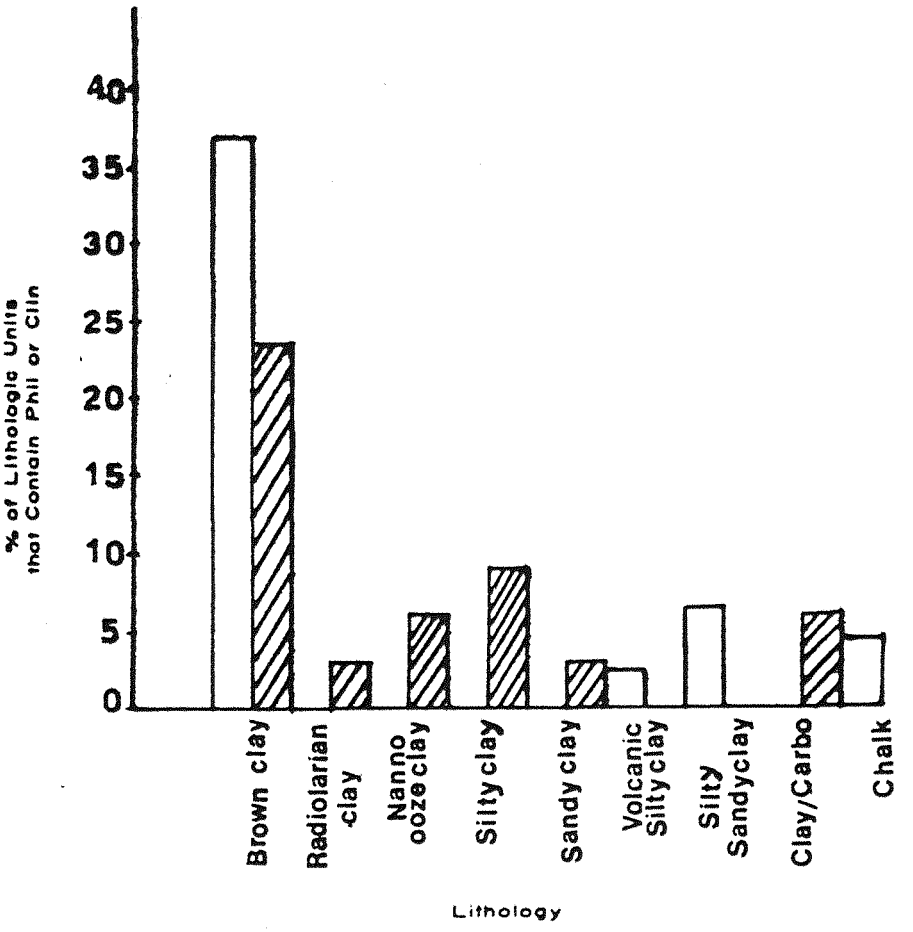

Fig. 3-3. Frequency of occurrence of phillipsite ▨ and clinoptilolite □ in various lithologies.

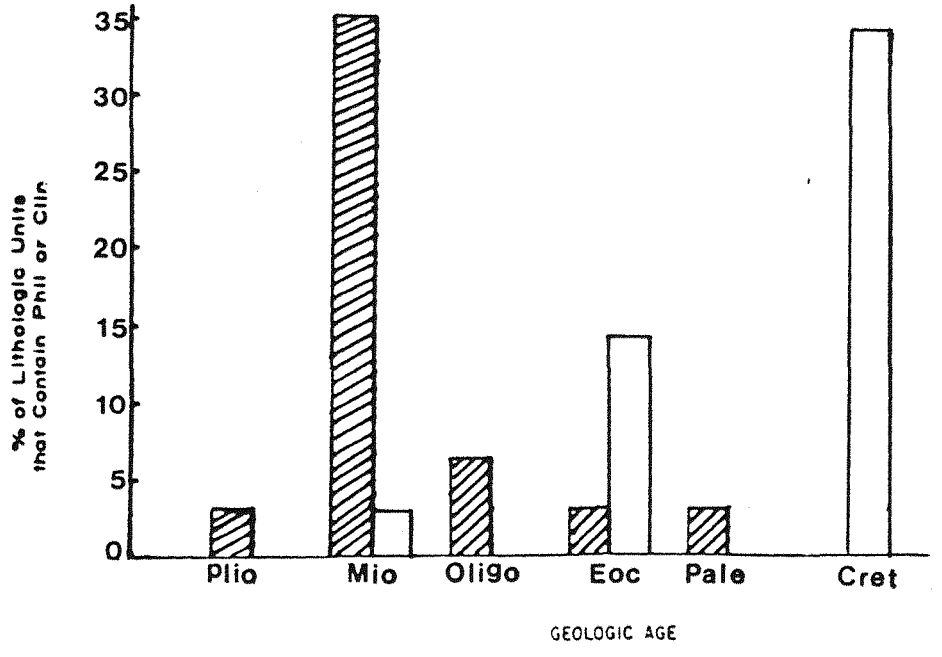

Fig. 3-4. Frequency of occurrence of phillipsite ▨ and clinoptilolite □ in sediments of various geologic ages.

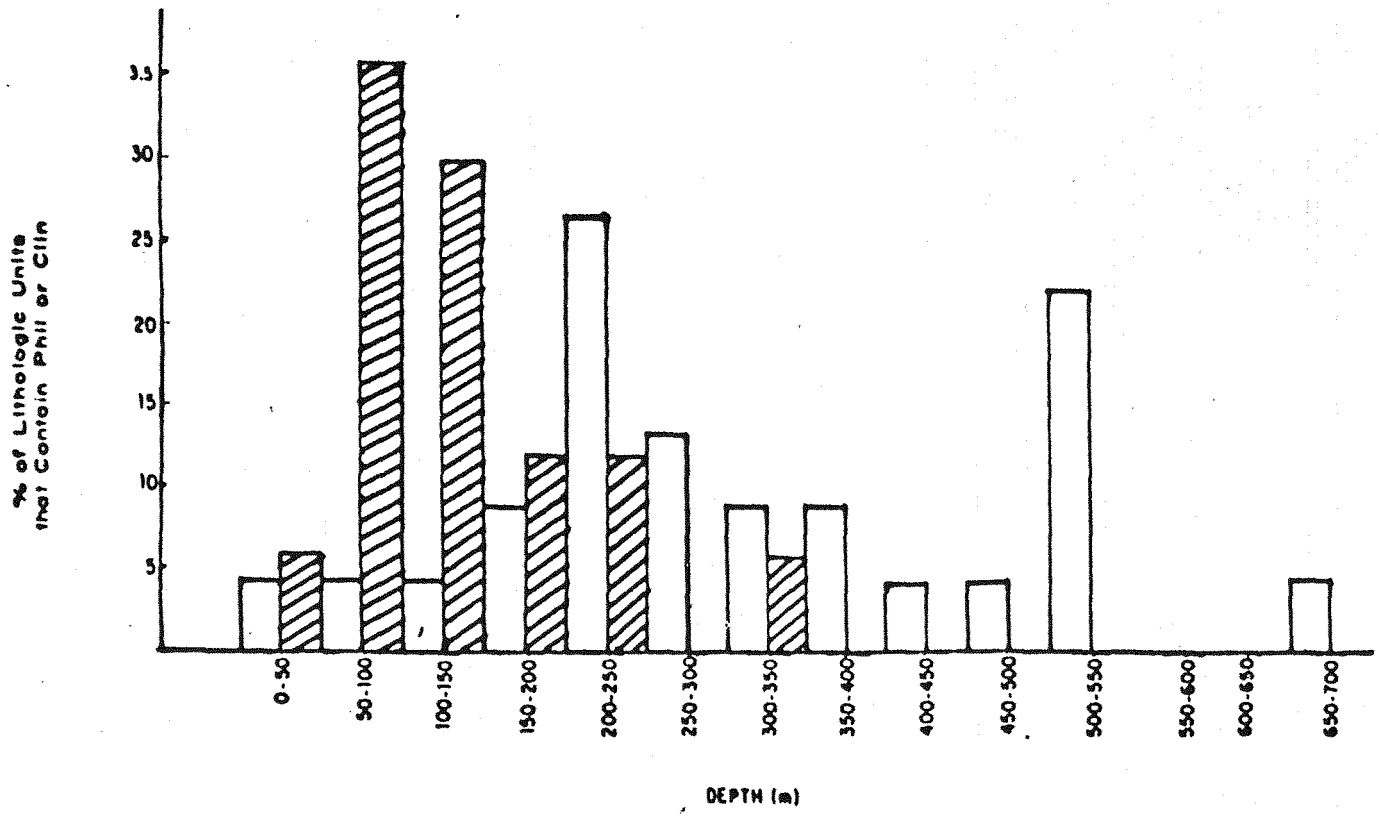

Fig.3-5. Distribution of phillipsite ▨ and clinoptilolite □ with respect to depth from the sediment/water interface.

PLATE 3-6

a & b. Elongated phillipsite crystals in Sample 213/11/2

c & d. Twinned phillipsite crystals in Sample 213/11/5

e & f. Phillipsite crystal with cleavage and etched surface in Sample 213/11/2

g. Volcanic glass in Sample 254/25/2

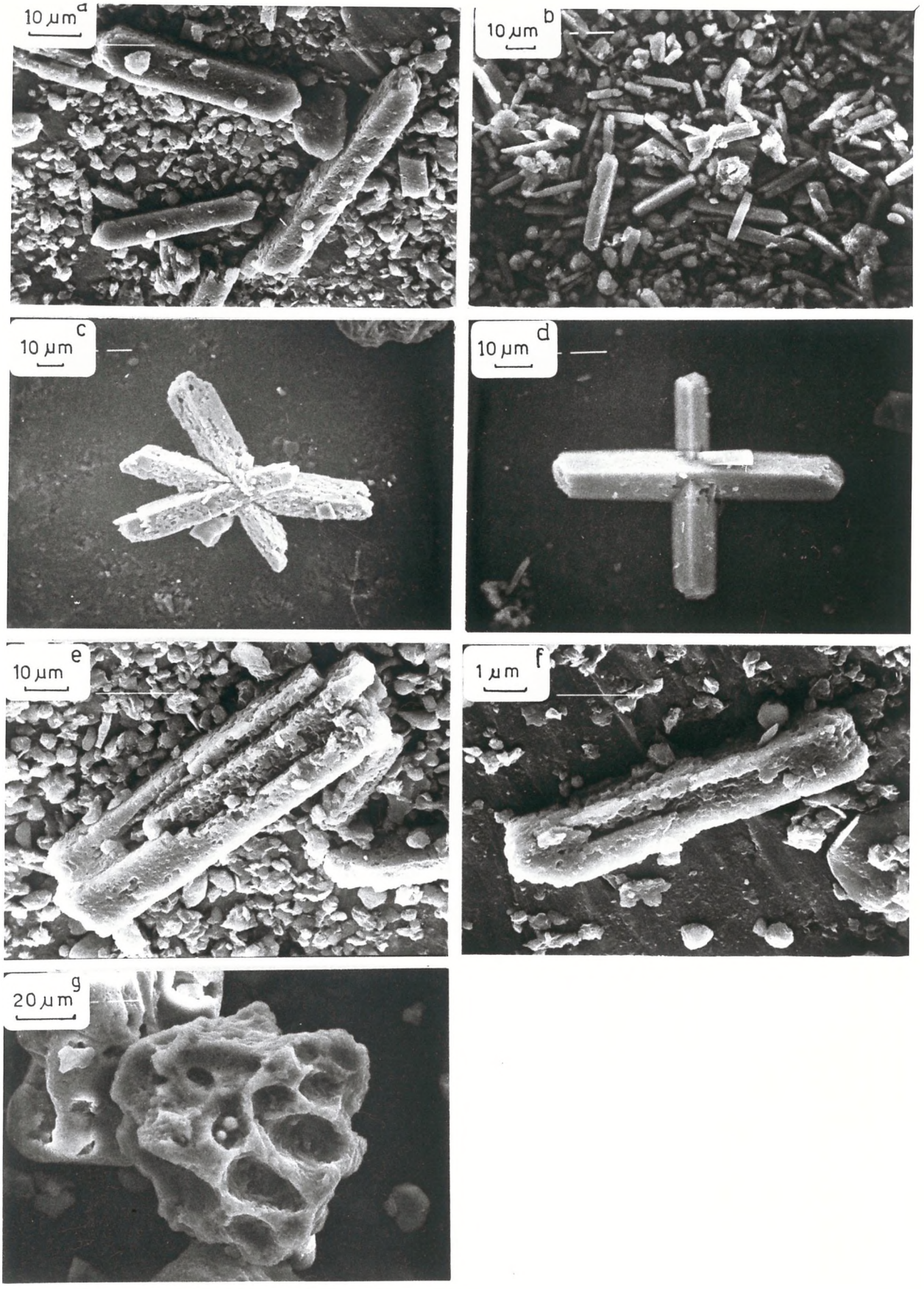

PLATE·3-6

in the present study phillipsites (Plate 3-6,e). Some crystals showed etched surfaces due to dissolution (Plate 3-6, e & f).

According to Kastner et al.,(1978) and Stonecipher (1976), phillipsite predominates in volcanogenic and clayey sediments of Recent to Eocene age. It is not usually found in great abundance below 150m depth; below about 500m depth it is rarely present. In the case of the present study, phillipsite showed a predominance in brown clay (Fig.3-3) and Miocene age (Fig.3-4). It was common in Tertiary sediments and was found in great abundance between 50 and 150 metres, and was not present below 350 metre depth (Fig.3-5).

c. Origin

According to many authors (e.g. Murray et al., 1891; Bonatti, 1965; Rex, 1967; Sheppard et al., 1970; Kolla et al., 1973b; Stonecipher, 1978) basaltic volcanic materials are essential for the formation of phillipsite, since basaltic glass and/or palagonite has been observed in association with phillipsite. However, clinoptilolite could have a volcanic and/or non-volcanic origin. The suggested precursors for clinoptilolite are: basaltic glass + biogenic silica; rhyolitic to silicic glass; smectite + phillipsite + biogenic silica; smectite + biogenic silica and biogenic silica + Al + K (Weaver, 1968; Berger et al., 1972; Cook et al., 1972; Kastner et al., 1978).

In the present study, volcanic material associated with sediments rich in phillipsite was observed at Sites 239, 246 and 254 under SEM (Plates 3-6g, 3-13 and 3-14). No visible volcanic material was observed at Site 213, but bulk chemistry element comparisons (i.e. Fe/Ti vs Al/(Al+Fe+Mn), Ti vs Al and Cr vs TiO_2 plots) indicated the presence of both silicic and/or basaltic volcanic material in the sediments, which suggests volcanic material (basaltic or/and silicic) as the phillipsite precursor.

Clinoptilolite was associated with high %E MLIS, biogenic silica and opal-CT in most sites. It was also observed in association with phillipsite in two samples (246/10/2 and 254/25/2) and in co-existence with low %E MLIS and palygorskite in five samples, of which four are Cretaceous. It also showed association with both silicic and/or basaltic debris and negative correlation with total clay and mixed layer illite/smectite. Therefore, on the basis of negative correlation with MLIS,

and association with biogenic silica, a MLIS + biogenic silica and/or silicic volcanic glass into clinoptilolite transformation is suggested.

4. Calcite

The amount of calcite varies from 1% to 67% and is composed of zooplankton (principally foraminifera) (Plate 3-7 a-c) and phytoplankton (coccolith and discoaster) (Plates 3-7 d, and 3-8 a-d).

According to Milliman (1974) deep-sea carbonates are thought to be organically derived. He believes, however, that inorganic precipitation of calcium carbonate can occur in the deep sea. Krauskopf (1979) believes that the precipitation of $CaCO_3$(calcite or aragonite) may occur either inorganically or through the agency of organisms; organisms may accomplish the precipitation either in the building of their shells, or incidentally as they remove CO_2 from the water, or during decay if they supply alkaline materials to the water. Chester and Aston (1976) found that biogenous carbonates (chiefly calcite and aragonite) constitute $>$ 90% of some of the deep sea sediments. According to them, carbonate oozes, which contain $>$ 30% of skeletal carbonates, cover almost half of the deep ocean floor, and are quantitatively the most important type of deep-sea sediment. Calcareous nannofossils and foraminiferal tests, which comprise most pelagic carbonates, originate in the euphotic zone (Matter, 1974). The tests of dead planktonic foraminifera are then transported from the photic zone by ocean currents and gravity (Davies et al., 1976). While settling through the water column and accumulating on the sea floor, they are differentially dissolved according to their resistivity to solution. This accounts for the observation that in pelagic carbonates well-preserved and corroded species occur together with the most solution-prone forms being completely absent. Dissolution causes disintegration of coccoliths into isolated shields, and further into individual segments or elements which are found as micro-crystalline particles, called 'micarb' in the sediment (Matter, 1974). According to Milliman (1974) the most critical factor controlling carbonate content in deep-sea sediment is the degree of carbonate saturation in the ambient and overlying waters. Only the surficial layers of the world oceans are supersaturated with respect to both aragonite and calcite (Wattenberg et al., 1936). The underlying waters are either saturated or under-saturated. At some depth in the water column, termed the 'compensation depth', the rate of carbonate

PLATE 3-7

a & b. Foraminifera in Sample 216/32/3

c. " " Sample 216/25/3

d. Coccoliths " Sample 212/15/3

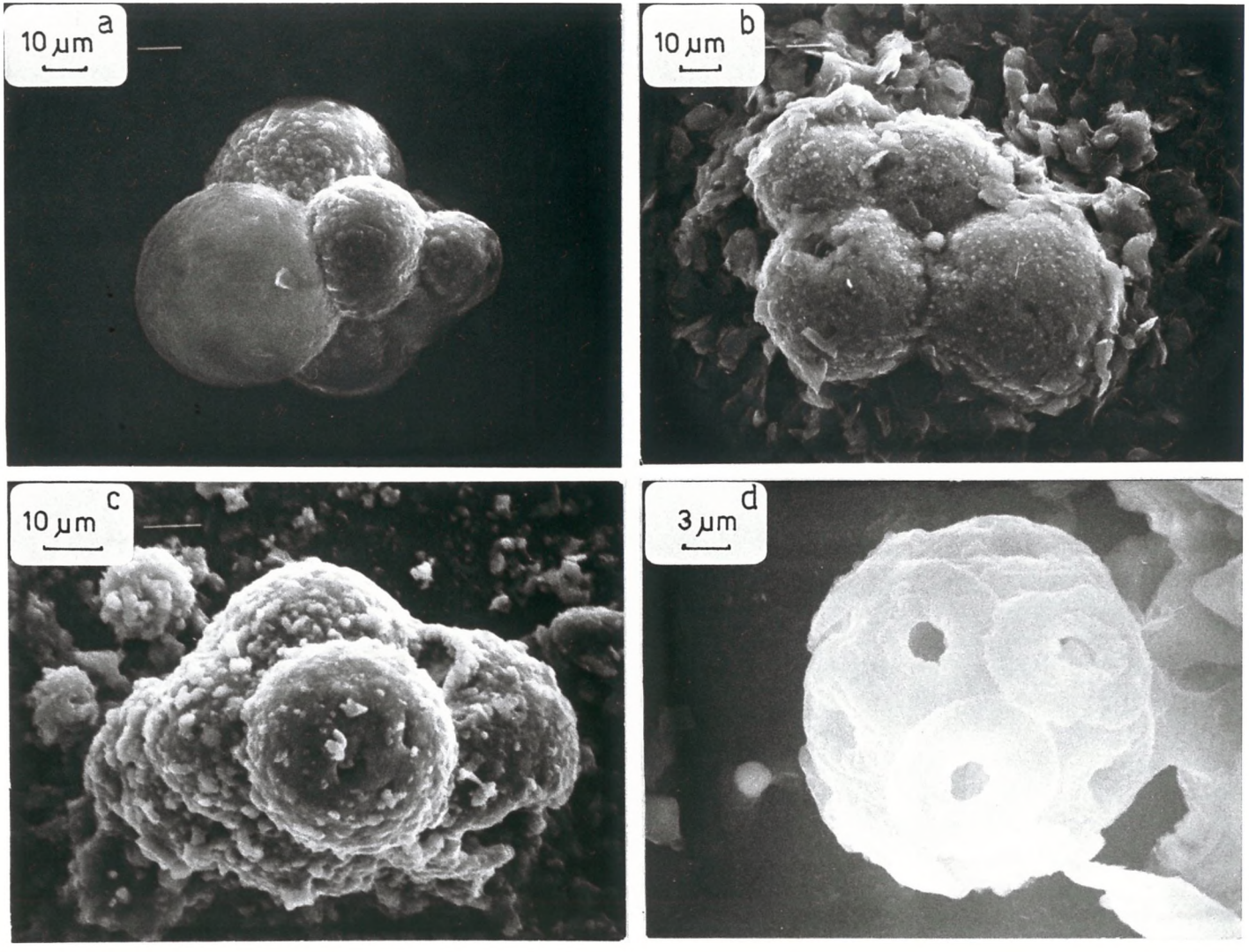

PLATE-3-7

PLATE 3-8

a-d Discoaster in
Sample 213/15/2

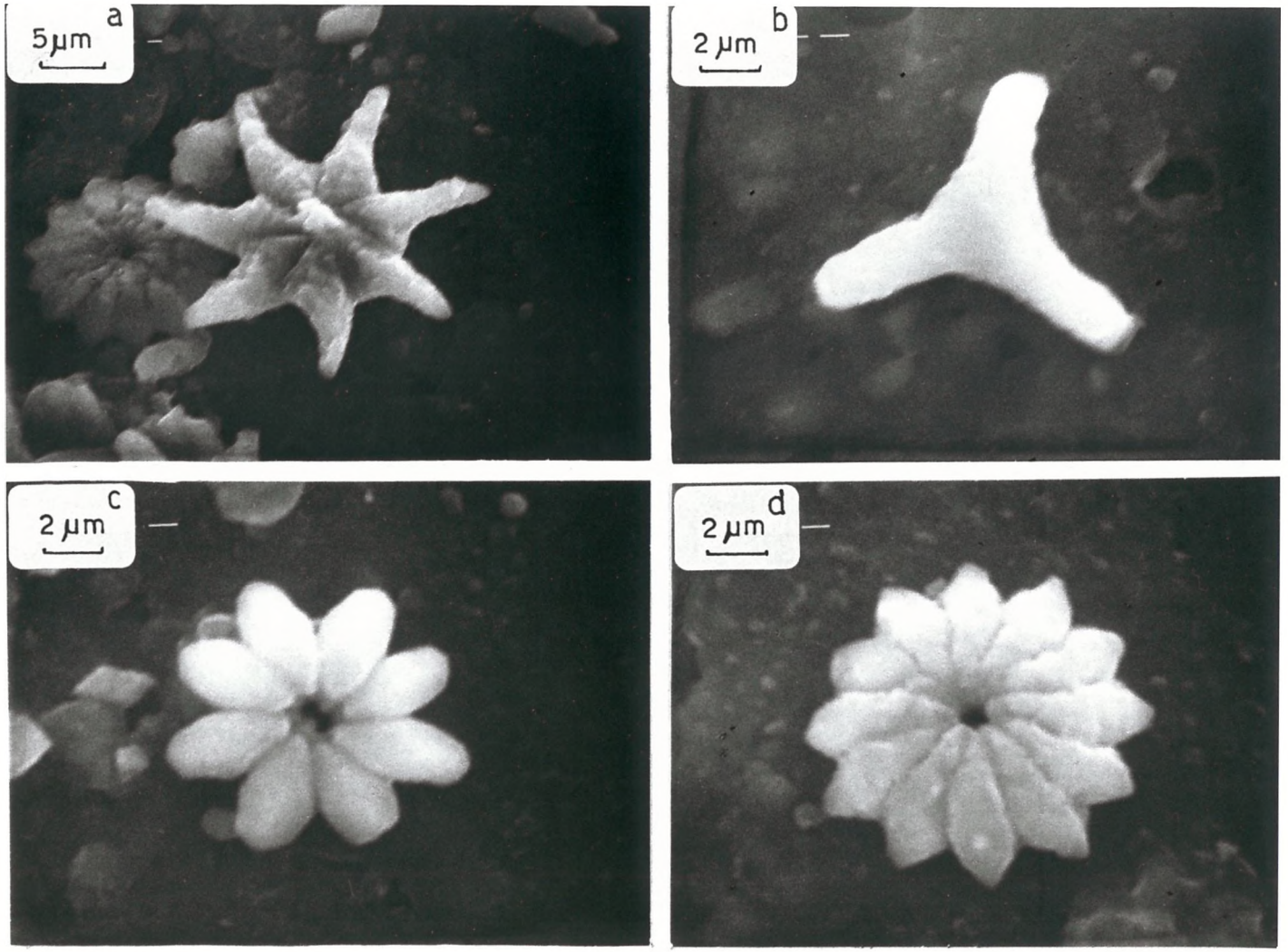

PLATE-3-8

dissolution equals the rate of carbonate deposition (Pytokowicz, 1970). Therefore, calcium carbonate can dissolve in environments which are under-saturated with respect to it.

At Site 211, disintegrated coccoliths and foraminifera chambers (filled with calcite crystals) were observed (Plate 3-9, a-d). Disintegration of coccoliths into isolated shields has taken place either during settling through the water column, or after burial. If dissolution of coccoliths has happened during settling (in the former case), the site has probably been below 'compensation depth', whereas in the latter case the environmental parameters conducive to under-saturation, i.e. low temperature, high partial pressures of CO_2(low pH) and increased hydrostatic pressure (Milliman, 1974) have been achieved in the sediments. Consequently, dissolved $CaCO_3$, which is gained from the dissolution of the coccoliths and foraminifera micarb, is deposited in void spaces (foraminifera chambers) (Plate 3-9 c-f). The same situation has probably happened at Site 258. The rest of the calcite-bearing samples showed well preserved to disintegrated fossil particles.

5. Dolomite

Dolomite is present in small amounts in a few samples (Table 3-1). According to Manheim (1976), small amounts of dolomite are widespread in deep-sea sediment cores.

Samples 211/13/1, 211/14/1 and 213/15/2 were studied under SEM. The dolomites occur as individual crystals and tend to be large and well formed (Plate 3-9 a-b).

Milliman *et al.* (1973) have studied deep-sea dolomite and suggested an authigenic origin for their dolomites, since they occur as well-formed and large crystals (coarser than 6 μm). Füchtbauer and Müller (1970) have suggested that such 'large' crystals infer a slow nucleation and crystallization rate. According to Irwin (1980) and Milliman (1974), dolomite may form by direct precipitation or by replacement of a calcium carbonate precursor. Sea water is supersaturated for dolomite and theoretically should dolomitize calcium carbonate, since mMg^{2+}/mCa^{2+} is greater than unity (Hanshaw, Back & Deike, 1971). However, Sass (1965) found experimentally that sea water in contact with calcite is under-saturated with respect to dolomite, and saturation is brought about by raising the temperature and/or increasing the Mg^{2+}/Ca^{2+} ratio

PLATE 3-9

a & b. Disintegrated coccoliths in association with dolomite rhombs in Sample 211/14/1

c. Foraminifera chamber filled with calcite crystals in Sample 211/13/1

d. High magnification of Figure c.

e. Fragment of a foraminifera, showing granular surface due to dissolution and probably new calcite crystals are developing along the edges in Sample 258/25cc.

f. High magnification of Figure e.

g. Dolomite rhomb growing around a coccolith in Sample 211/14/1.

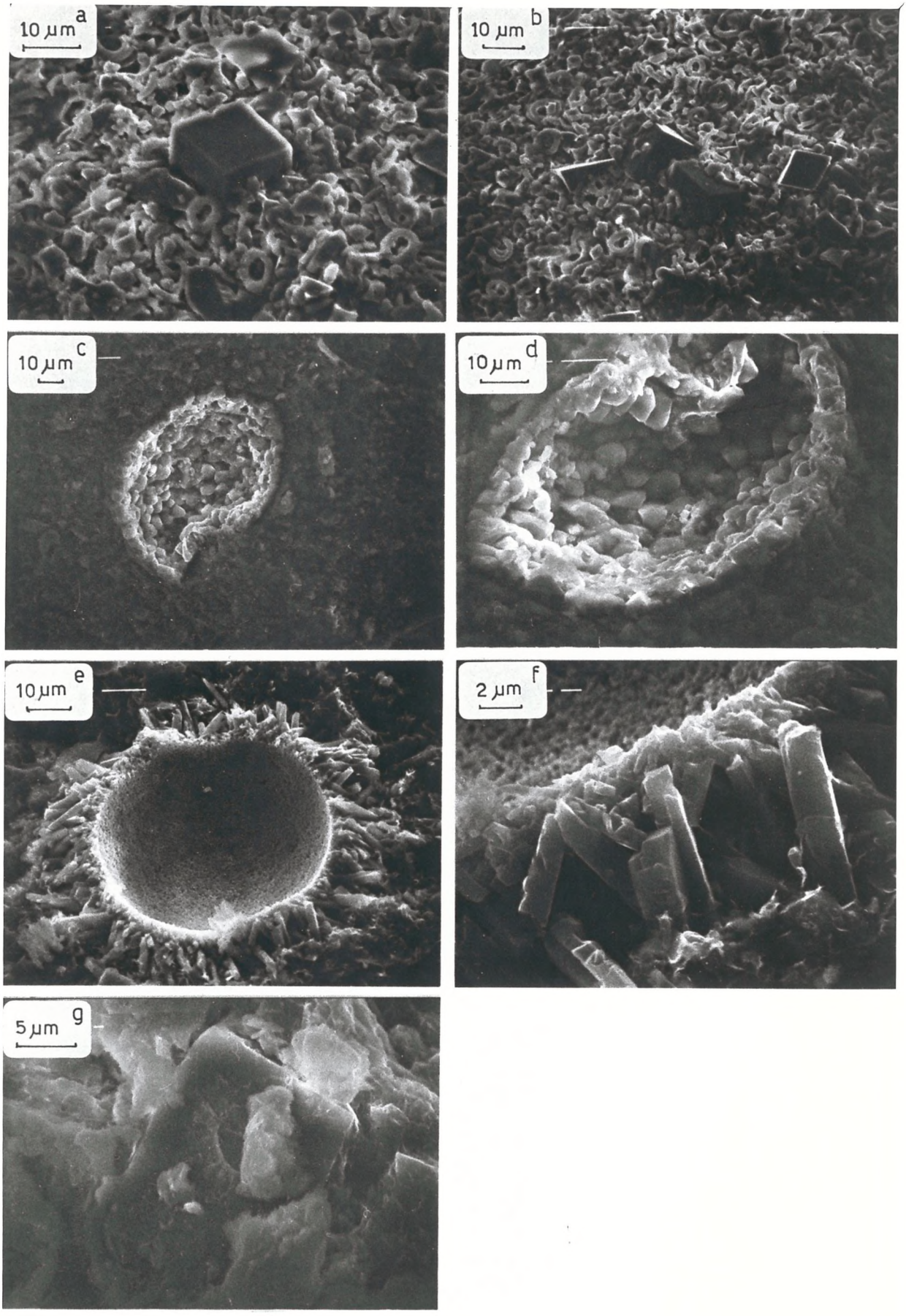

PLATE 3_9

or salinity. There are two requirements for dolomite formation: a high enough Mg^{2+}/Ca^{2+} ratio and sufficient time (Irwin, 1980; Milliman, 1974).

At Site 211, as the dolomite percentage increases, calcite and organic carbon percentages decrease. In Sample 211/14/1 a dolomite crystal contains a structure which might have been a coccolith (Plate 3-9g). Krauskopf (1979) has suggested a reaction between Mg^{2+} and the $CaCO_3$ of fossils to produce dolomite. This process could well be responsible for the dolomite crystals discussed above (at Site 211). As previously mentioned, disintegration of coccolith fossils was caused by dissolution, and dissolved $CaCO_3$ was used up in the formation of calcite crystals filling foraminifera chambers; when the Mg^{+2}/Ca^{+2} ratio reaches high levels, dolomite diagenetically replaces the carbonate fossil. The Mg^{2+} may come from either sea-water trapped in the pores or from volcanic sources. Manheim and Sayles (1974) have pointed out that even if Mg^{2+} had diffused continuously from the overlying sea-water, it would be unlikely that the sediments could accumulate more than about 1% of dolomite through interstitial water reaction, unless additional sources of Mg^{2+} were available. Davies et al. (1973) believe that Mg^{2+} may have come from volcanic sources, since the cyclic sequence sediment under this study is intruded by a 50 cm thick basalt sill and contained two thin ash layers.

In the case of Site 211, samples containing dolomite are bounded between a basaltic basement and an andesitic diabase sill. No ash was observed. However, Ti/Al, Cr/TiO_2 and Fe/Ti versus Al/(Al+Fe+Mn) plots (Figs.4-1,2 & 3) indicated a basaltic contribution to these sediments, and thus Mg^{2+} may well have been derived from the alteration of basaltic material.

Dolomite at the rest of the sites was not studied under SEM, but from its positive correlation with plagioclase and K-feldspar, a detrital origin is suggested for them.

6. Pyrite

Thermodynamic calculations (Garrels and Christ, 1965; Berner, 1964b) indicate that pyrite is stable only in the absence of air and in the presence of dissolved sulphide. Garrels and Christ (1965) reported the necessary range of Eh ($\leq$ -0·2) and pH (7-8) for the stability of

pyrite in an anoxic environment. According to Krauskopf (1979), pyrite can form only at Eh values below about +0·2 volt in acid solutions and -0·2 volt in basic solution.

Pyrite is almost always present in organic-rich marine sediments (Elderfield, 1976; Berner, 1970). Studies of early diagenetic pyrite in Recent sediments (Ostroumov, 1953; Vanstraaten, 1954; Volkov, 1961; Kaplan et al., 1963) and experimental work (Berner, 1964a; Rickard, 1969) are well established. They all have come to the same conclusions on the fundamental stages in pyrite formation. The stages are: bacterial sulphate reduction, reaction of H_2S with iron minerals, and transformation of black iron monosulphides to pyrite.

The two principal sources of H_2S for pyrite formation are the bacterial reduction of dissolved sulphate and the decomposition of organic sulphur compounds. It has been shown that the organic fraction of sediments is an inadequate source of sulphur for pyrite formation, and that the single most important source is the reduction of sulphates from the overlying sea-water (Kaplan et al., 1963).

Berner (1970) believes that simple burial of sea-water and reduction of all included sulphate can provide only about 0·3 per cent pyrite sulphur; diffusion into the sediment is therefore necessary. He believes that continuous sulphate reduction brings down the concentration of sulphate in the sediment pore water, and additional sulphate is made available for reduction by diffusion down the concentration gradient from the overlying water. According to Krauskopf (1979), the reduction of sulphate to sulphide takes place where sulphate comes in contact with organic matter. A special type of bacteria (anaerobic) use this reduction process as both a source of energy and a source of oxygen. Therefore, H_2S is formed at the expense of bacterial sulphate reduction. He has proposed the following reaction for sulphate reduction:

$$2H^{+} + SO_4^{=} + CH_4 \longrightarrow H_2S + CO_2 + 2H_2O.$$

The CO_2 and H_2O are the same as the products of respiration in aerobic organisms. He has mentioned that the above reaction has not been demonstrated to take place in the laboratory with methane, but with more complex organic materials. Berner (1970) showed the essential requirements for the production of microcrystalline pyrite in normal marine waters are that there is (a) organic matter for the metabolism of sulphate-reducing

bacteria; (b) diffusion, and the establishment of a diffusion gradient of sulphate in the sediment; and (c) sufficient reactive iron. Iron monosulphide (mackinawite and/or greigite) is first formed by the reaction of hydrogen sulphide with iron (Polushkina et al., 1963; Jedwab, 1967). Hydrogen sulphide is oxidised to give elemental sulphur, which slowly reacts with the iron sulphide to form pyrite (Volkov, 1961; Berner, 1970), e.g.

$$FeS + S^{o} \longrightarrow FeS_2$$

Oxidation is accomplished either inorganically or by sulphur oxidising bacteria. If no active oxidising agent is present in a sediment, even though there may be a high concentration of H_2S, no pyrite can form. Under aerobic bottom conditions, considerable elemental sulphur is formed by the reaction of FeS and H_2S with dissolved oxygen, which is stirred into the sediment from the overlying water by burrowing organisms or by storm waves and currents. Part of the elemental sulphur is subsequently oxidised to dissolved sulphate. The remaining elemental sulphur slowly reacts with FeS to form pyrite (Berner, 1970).

In the case of the present study, pyrite is present in samples from Sites 216, 248, 254 and 258. The amount of pyrite varies between traces up to 4%. Organic carbon also varies between 0·3 and 1·3%. Pyrite was examined by SEM (Plate 3-10). It occurs as collections of octahedral microcrystals (Plate 3-10a) and as framboids, which are aggregates of microspheres, whose surface texture indicates that they are comprised of aggregates of even smaller pyrite crystals (Plate 3-10 b & c). Microcrystals are ordered in a regular system, and the size of the microcrystals is uniform throughout the framboid. Two types of framboidal pyrite are distinguished. Framboids with a matrix between the microcrystals (Plate 3-10b), whereas the second type lack a matrix (Plate 3-10d). Berner (1970) has shown experimentally that pyrite is formed as small framboidal microspheres averaging about 1 μm in diameter and embedded in the surface of much larger grains of elemental sulphur.

According to Davies et al. (1974), the poor sorting, lack of traction-current features and substantiated intraformational breccias, indicate rapid deposition in quiet water at Site 254. They also reported a sedimentation rate at least as high as 45m (m.y.) in the Early Cretaceous at Site 258. High sand and silt percentages at Sites 216, 248 and 254

PLATE 3-10

a. Octahedral microcrystalline pyrite in Sample 254/26cc.

b. Framboidal pyrite (aggregates of microspheres, whose surface texture indicates smaller aggregate) in Sample 254/26cc.

c. Framboidal pyrite in Sample 254/25/2.

d. Framboidal pyrite without matrix in Sample 258/25cc.

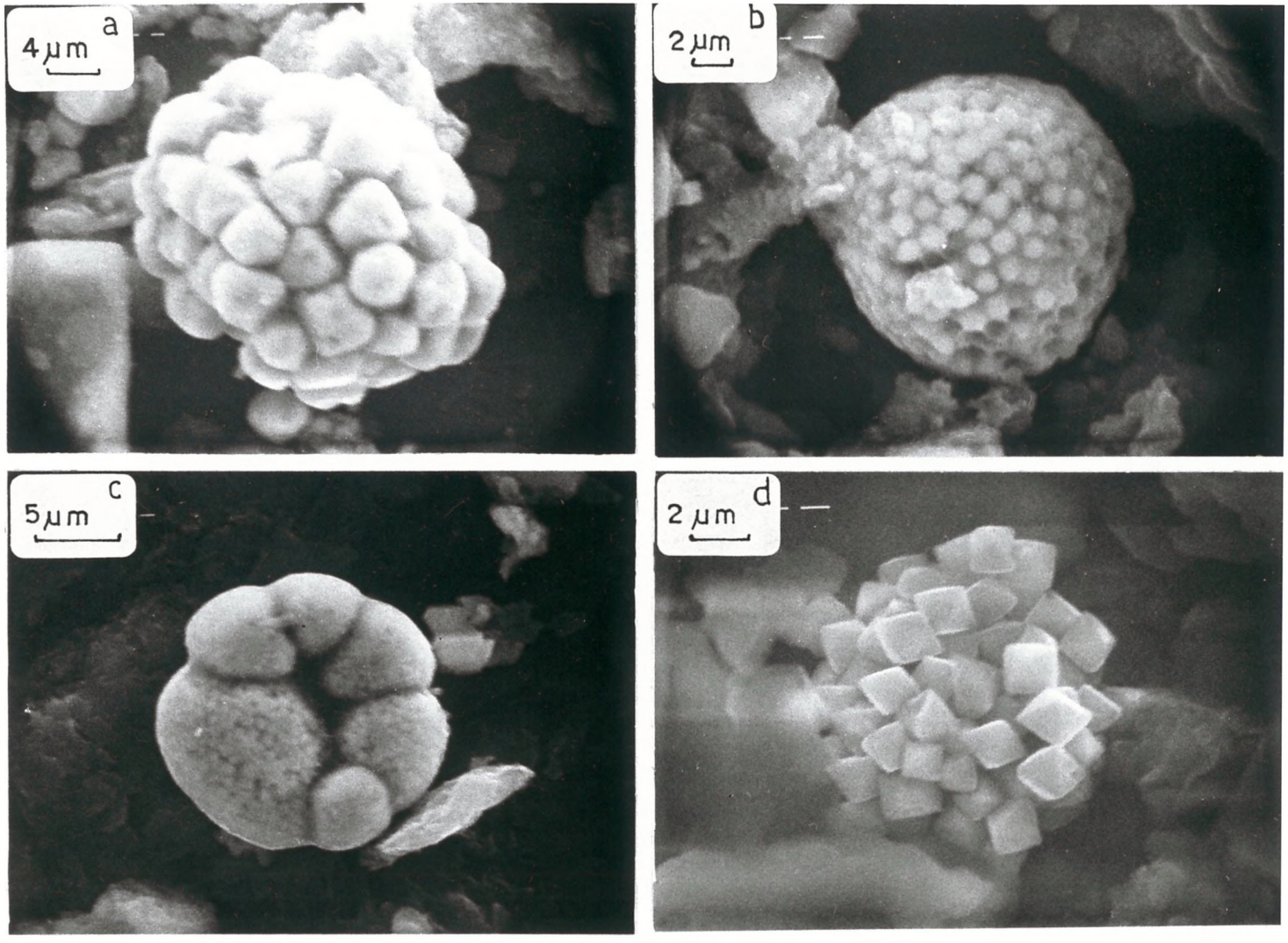

PLATE-3-10

also suggest high sedimentation rates. Consequently, high accumulation rates cause the deposited organic matter to bury rapidly and thus be preserved. An important outcome of rapid accumulation rates of biogenous sediments is the establishment of anoxic conditions below the surface layers. Therefore, at the mentioned sites a reducing environment existed at the sediment water interface. This is further supported by the positive correlation between pyrite and organic carbon (Fig.3-6). The necessary sulphur for pyrite production was supplied by the diffusion gradient from the overlying water. The last requirement for pyrite formation is iron, which could become available from ilmenite, goethite, clay minerals and volcanic glass. Berner (1970) suggested iron contained within or adsorbed upon fine-grained detrital material as a source. Carroll (1958) proposed clay minerals and Criddle (1974) believed that nannoplankton could be the source.

7. Gibbsite

Aluminium hydroxide ($Al(OH)_3$ or $Al_2O_3.3H_2O$) is rare and virtually unknown as a constituent of sedimentary rocks. It may occur as an important constituent of some soils, notably the laterites (Pettijohn, 1957).

Biscaye (1965) found a very strong association between kaolinite and gibbsite in the deep-sea sediments of the Atlantic Ocean, and both minerals were found to be the most abundant in sediments of the tropical Atlantic Ocean. He suggested a continental origin for both minerals, since both occur in weathering profiles of tropical land areas.

In the present study gibbsite was identified on the basis of its reflections at 4.85Å and 4.34Å. No quantitative estimation was performed, since only small amounts were present in the samples. It was always associated with kaolinite. There are some mineralogical similarities of the sediments at these sites to the surrounding lands. According to Griffin et al. (1968), deserts of Australia contain relatively high contents of kaolinite. According to Fitzpatrick (1971), Krasnoz soil, which is composed of kaolinite, goethite, gibbsite and the resistant residue, has formed in Australia and Pleistocene and Holocene climatic changes have caused some of these soils to occur outside their normal climatic range in western Australia. Mohr et al. (1954) have noted the gibbsitic character of Madagascar laterites, and this is reflected in the extremely high ratios of gibbsite relative to either chlorite (Biscaye,

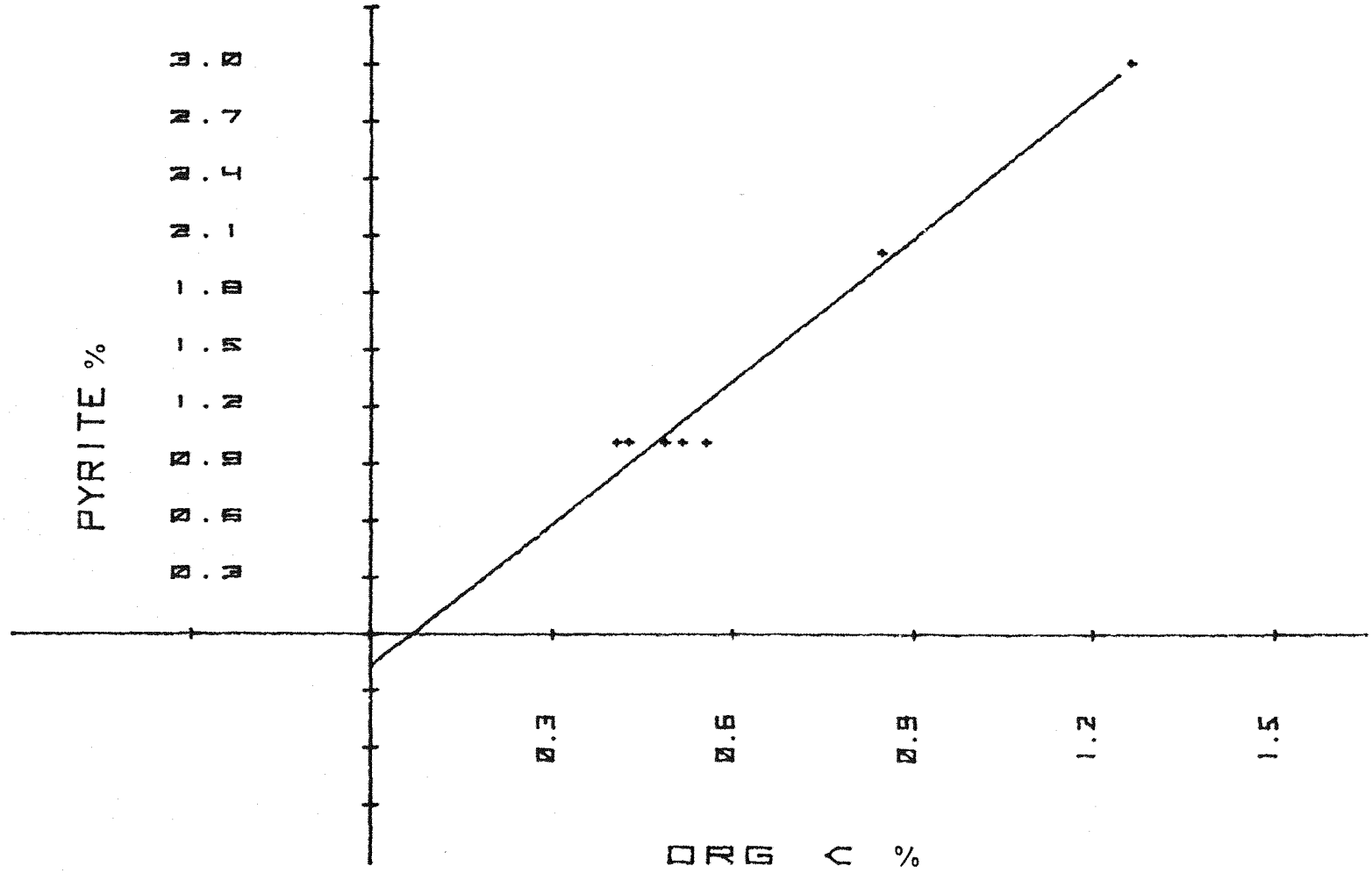

Fig.3-6.Correlation between organic carbon and pyrite.r=0.98

1964, quoted by Biscaye, 1965) or illite near that island. Biscaye (1965) has proposed a land-derived origin for kaolinite and gibbsite in the south-western Indian Ocean, referring to observations of Mohr et al. (1954) and Biscaye (1964) on Madagascar. According to Strakhov (1967) and McGowran (1978), along the Arabian Sea and the Deccan Traps, lateritic profiles were developing during the Tertiary period. Therefore, a continental origin is suggested for kaolinite and gibbsite.

8. Apatite

According to Elderfield (1976), most of the phosphate in marine sediments occurs as discrete nodules, concretions or phosphorite rock, in which it is present as carbonate fluorapatite. In addition, phosphate may be found as a sorbed phase, particularly on iron-rich sediment.

Tooms et al. (1969) have discussed the mechanisms of phosphate formation in terms of (a) chemical precipitation, (b) inorganic replacement, and (c) organic activity. To these mechanisms some authors (Mansfield, 1940) also add volcanism, which they think may assist apatite precipitation.

In the present study, the morphology of the apatite grains tend to suggest a detrital origin for them. SEM studies show angular and nodular grains (Plate 3-11. a-b). Correlation programme (Table 4-5) also shows P_2O_5 association with Fe-Mn oxides/hydroxides.

9. Minor Minerals

Numerous minerals beside gibbsite and apatite have been observed in minor amounts. These include ilmenite, anatase, zircon, garnet, hematite, barite, goethite, glauconite, serpentine and gypsum. Photographs of some of them are shown in Plate 3-11, c-g). The morphology of their grains suggests a detrital origin.

Windom (1976) believes that because of their low abundance in continental rocks, and/or their relative instability in the marine environment, these minerals are not common in deep-sea sediments. He mentioned that many of them are found in minor amounts in the sediments near their source (e.g. on continental shelves and in the vicinity of oceanic ridges or volcanic areas).

PLATE 3-11

a. Angular apatite in Sample 212/15/3

b. Nodular apatite in Sample 213/11/5

c. Ilmenite in Sample 211/14/1

d. Anatase in Sample 258/25cc

e. Goethite in Sample 212/35cc

f. High magnification of Figure e

g. Barite in Sample 245A/6/2.

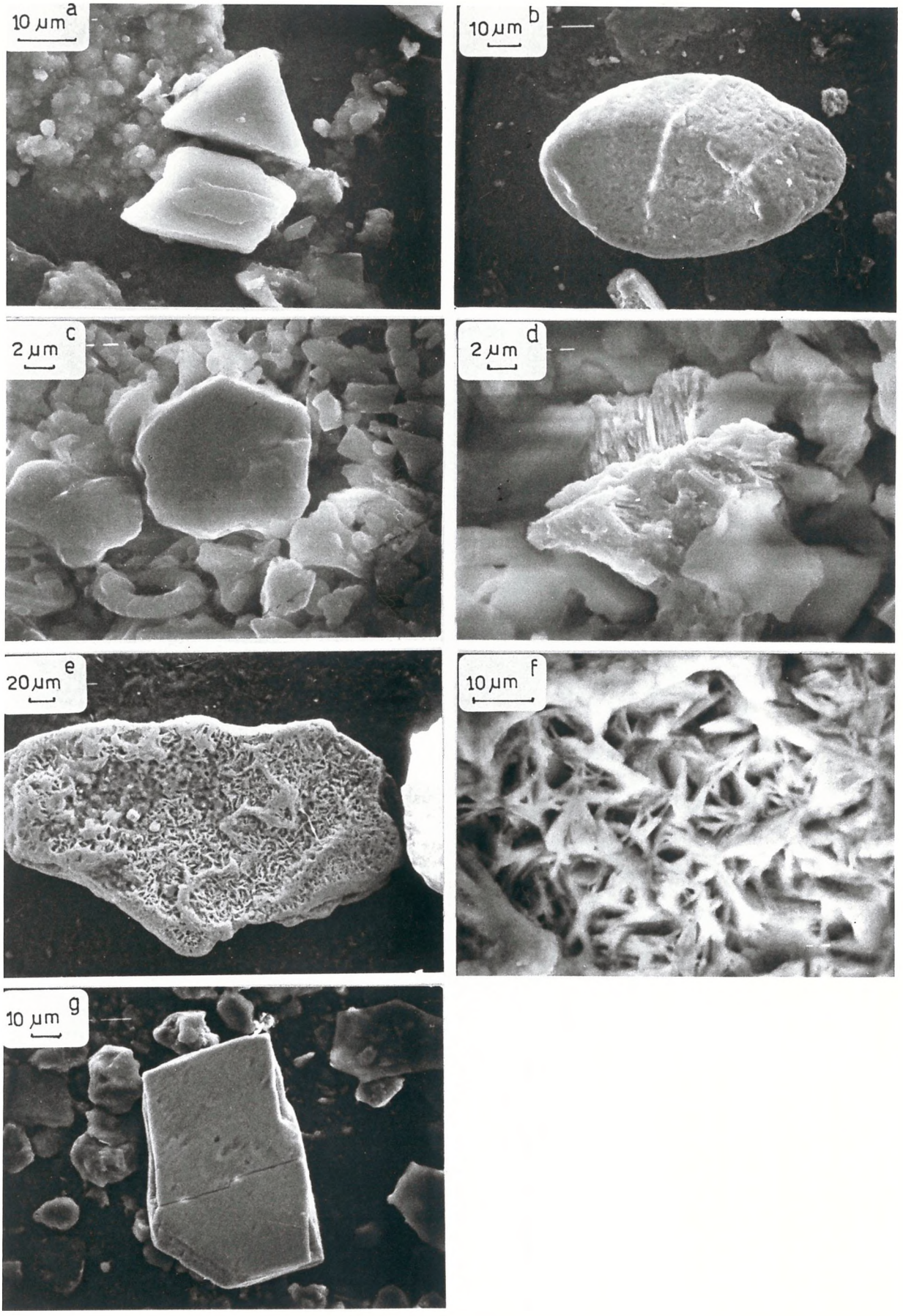

PLATE-3_11

10. Correlations

The correlation coefficient matrix is shown in Table 4-5, and the summaries of statistics in Table 4-6.

a) The strong positive correlation of quartz - K-feldspar (at 99%), K-feldspar - plagioclase and plagioclase - dolomite (significant at 99.99%), K-feldspar - dolomite (significant at 99%), quartz - plagioclase (significant at 95%), and negative correlations of quartz-B (biogenic silica, opal-CT, volcanic glass and minor minerals), and K-feldspar - B (significant at 99%) suggest a detrital origin for quartz, plagioclase, K-feldspar and dolomite. However, dolomite has an authigenic origin at Site 211.

b) The positive correlation of pyrite-organic carbon (significant at 90%) indicates a diagenetic relation between them. A high sedimentation rate, that is common in pyrite-containing sediments, caused rapid burial of deposited organic matter, resulting in its preservation and establishment of anoxic conditions below the surface sediment, which is one of the main conditions for pyrite formation.

c) Clinoptilolite shows negative correlation with clay (at 99.99%) (Fig.3-7), plagioclase and K-feldspar (at 99%) and B (at 90%). The negative correlation with plagioclase is expected, since plagioclase is of detrital origin. Stonecipher (1978) and Cosgrove et al. (1979) suggested that clinoptilolite might form as a result of the reaction of smectite with biogenic silica and interstitial water. Negative correlation of clinoptilolite with total clay and B tends to support the above suggestion.

d) Clay is negatively correlated with calcite (Fig.3-8) (significant at 99.99%).

e) Depth showed a strong negative correlation with phillipsite (at 99%), negative correlation with B (at 98%), and weak positive correlation with clinoptilolite (significant at 90%). This depth correlation with the zeolites seems to agree with the findings of Stonecipher (1976, 1977), i.e. phill usually occurs at shallower depth, while clinoptilolite is deeper. According to Calvert (1974), in relatively long sediment cores, silicon concentrations are observed to decrease with depth from a maximum

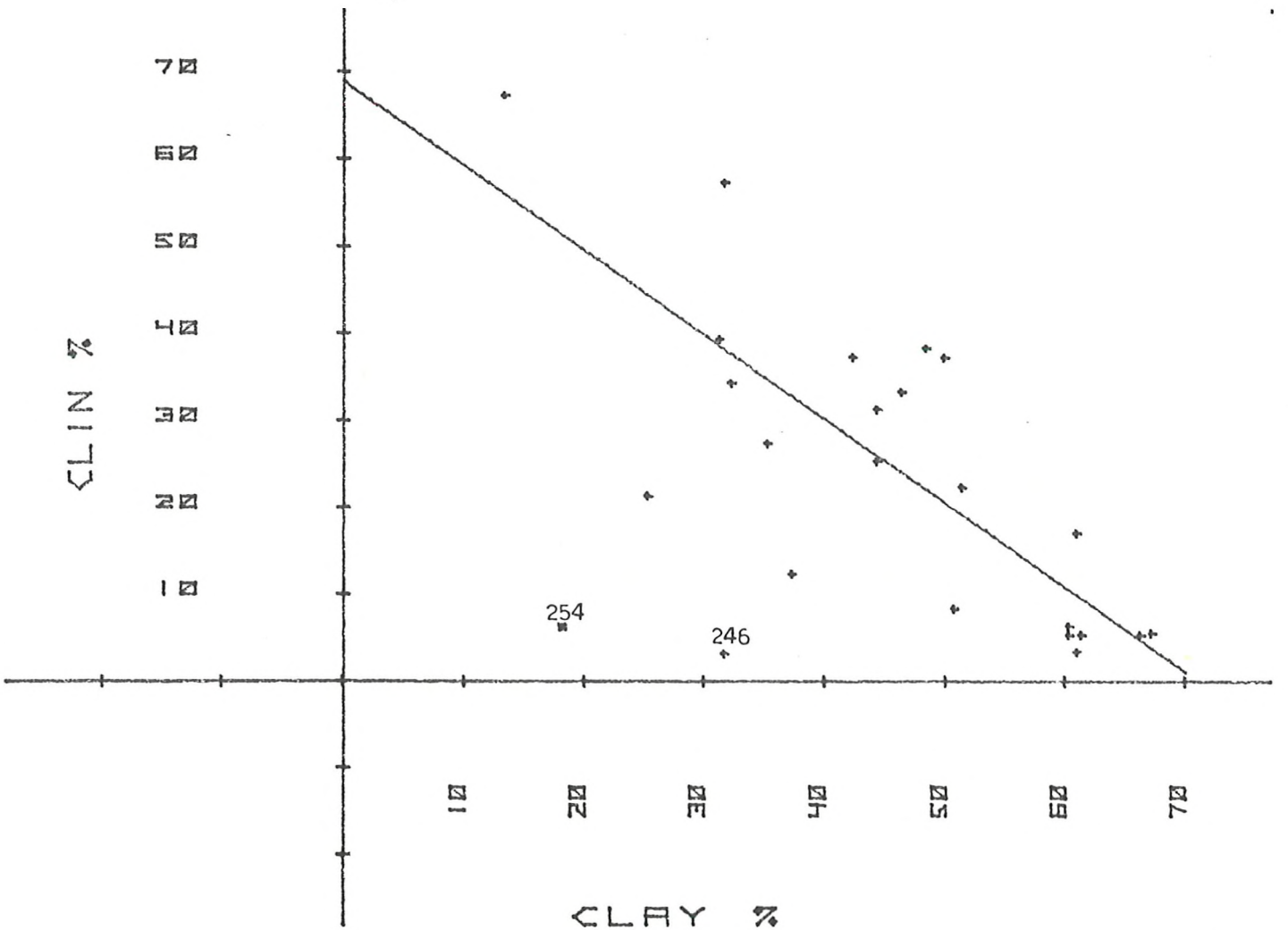

Fig.3-7. Correlation between clay and clin in zeolite-bearing samples. (246) and (254) indicate samples with clin + phil in association.

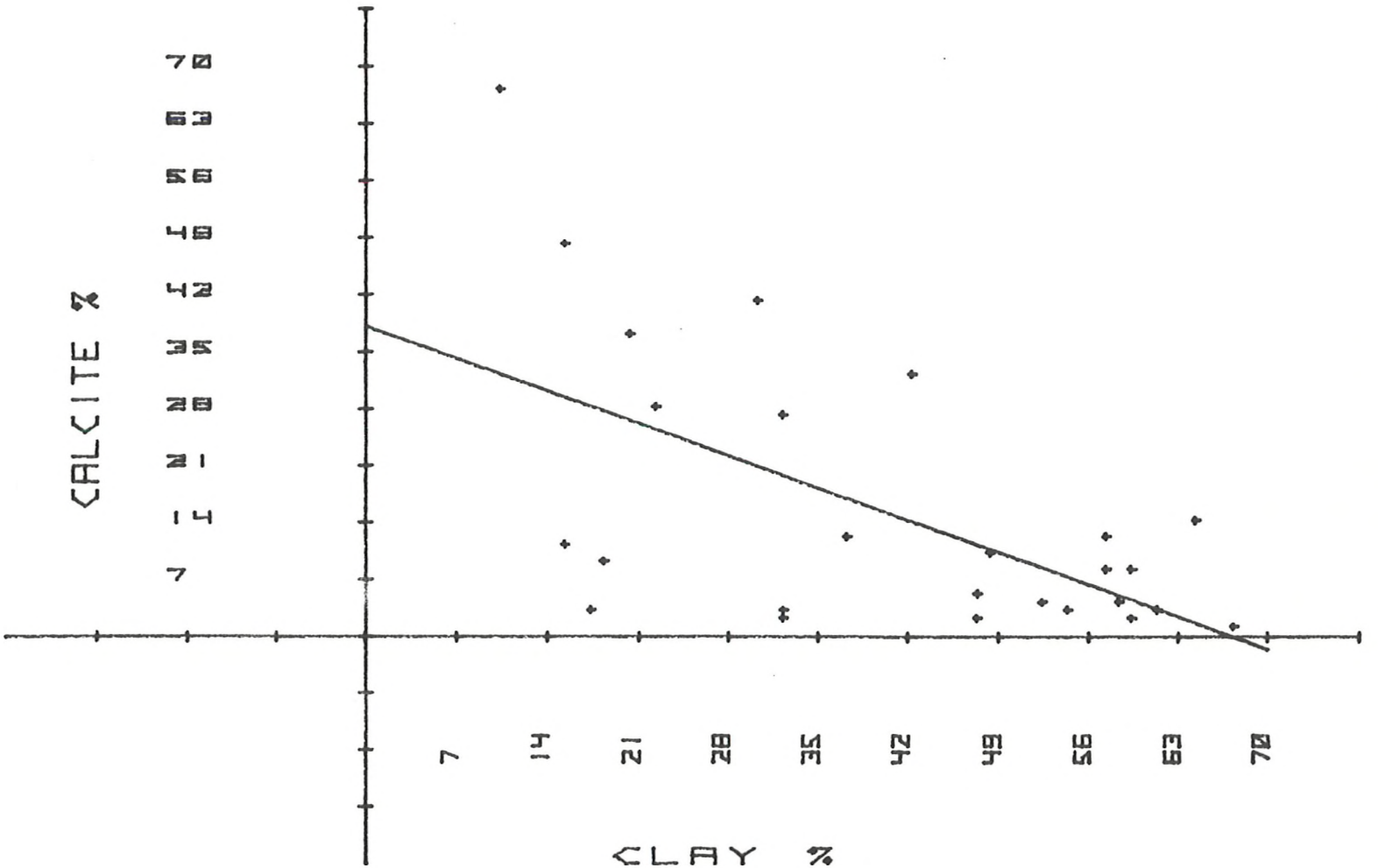

Fig 3-8. The antipathetic relationship between clay% and calcite%. r=-0.59, p=0.01

to a relatively constant value. Hurd (1973) believes that the uptake of dissolved silicon released from the solution of biogenous opal by the formation of authigenic silicate mineral is a possibility. Therefore, the negative correlation of B with depth and clinoptilolite could suggest the uptake of B by clinoptilolite, as previously mentioned.

11. Conclusions

The mineralogical analysis by X-ray diffraction and SEM of bulk samples showed that:

a) The detrital group of minerals consists of quartz, K-feldspar, plagioclase and some dolomite.

b) Biogenic calcite mostly consists of coccoliths and foraminifera.

c) The authigenic group of minerals consists of clinoptilolite, opal-CT, phillipsite, pyrite and some calcite and dolomite (Sites 211 and 258):

i) phillipsite was dominant in brown clay, Miocene sediments and shallow depth (50-150m), whereas clinoptilolite was dominant in brown clay, Cretaceous sediments and in 200-250m and 500-550m sediment depth.

ii) clinoptilolite association with biogenic silica and opal-CT and its negative correlation with clay suggested its formation via the reaction of clay with biogenic silica.

iii) pyrite formed authigenically in the reducing conditions provided by the burial of organic matter. The necessary iron was probably provided from clay minerals, volcanics, goethite or ilmenite.

iv) authigenic dolomite gained its Ca^{2+} from the biogenic calcite, whereas its necessary Mg^{2+} could come from the alteration of basaltic rocks.

B. Clay Mineralogy

The results of the relative abundance determination of the clay minerals of the analysed samples are shown in Table 3-2. The variation of the clays in relation to depth is shown in Figure 3-9a-d . The investigation of the $< 2\ \mu m$ size fraction of samples collected during Legs 22, 23, 24, 25 and 26 of the Deep Sea Drilling Project in the Indian Ocean was carried out mainly by means of X-ray diffraction analysis.

An oriented paste-on-glass slide of the $< 2\ \mu m$ particles of each sample was dried in air, and the X-ray diffraction patterns were obtained.

Three slides for each sample were prepared as follows: (a) untreated, (b) treated with ethylene glycol for a day at 60°C, and (c) heated for two hours at 550°C. X-ray examination was performed at room temperature immediately upon cooling. The semi-quantitative estimation suggested by Matter (1974) was applied. In this method the areas under basal peaks were taken into account. Details of this technique are given in Chapter II.

X-ray diffractograms show that the clay fractions consist mainly of a mixture of mixed layer illite/smectite (MLIS), illite, kaolinite, chlorite and palygorskite (Fig.3-10a-b). Detail concerning mineral identification is summarized in Table 3-3.

Kaolinite 001 peak coincides with 002 peak of chlorite at 7Å. The presence of kaolinite in addition to chlorite is identified at 3·57 to 3·60Å and 3·53 to 3·55Å, respectively. Biscaye (1964) and Matter (1974) suggested that the 7Å peak can be divided between kaolinite and chlorite according to the peak height ratio at 3.57-3.60Å and 3·53-3·55Å, respectively.

Material which expands to a 17Å (001) peak upon glycolation is assigned to mixed layer illite/smectite (MLIS). Eslinger et al. (1976) and Papavasiliou (1979) also interpreted 17Å peak as mixed layer illite/smectite. Reynolds and Hower (1970) showed that pure montmorillonite with no mixed layering has a 17Å peak, but so does mixed-layer mica-montmorillonite, with up to 50 or 60 per cent non-expandable mica layers. Therefore,

Fig.3-9 (a-d): Depth (m) versus percentage of MLIS (mixed layer illite/smectite), ILL (illite), KAO (kaolinite), CHL (chlorite) and PALY (palygorskite) at Legs 22, 23, 24, 25 and 26. 1-3 = Site 211; 4-7 = Site 212; 8-12 = Site 213; 13-17 = Site 215; 18= Site 216; 19-22 = Site 221; 23-26 = Site 236; 27-29 = Site 239; 30-32 = Site 240; 33-37 = Site 245; 38-41 = Site 248; 42-45 = Site 250; 46 = Site 254; 47-50 = Site 257; 51-53 = Site 257; 54-57 = Site 258.

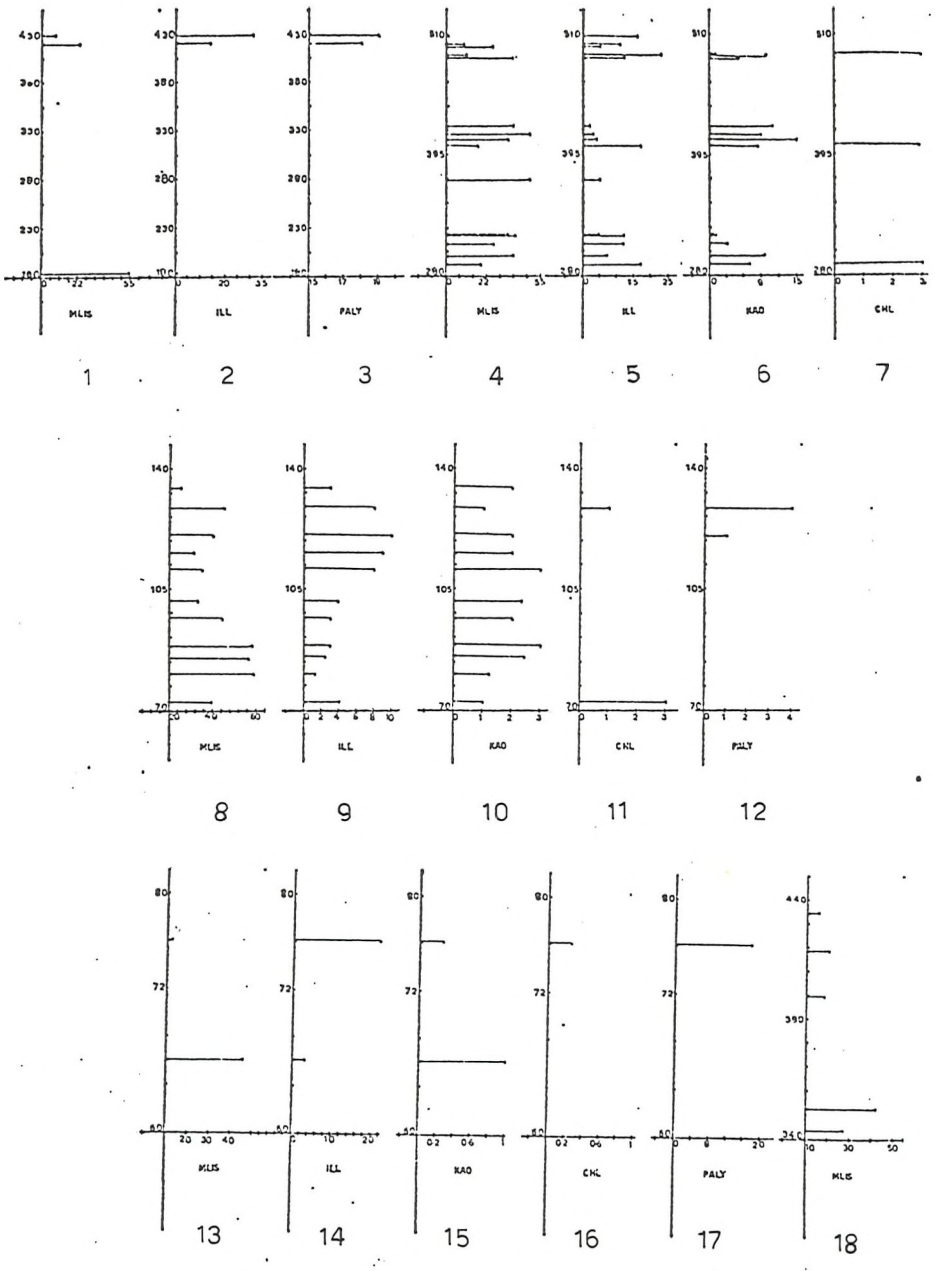

Leg 22

Fig. 3-9a

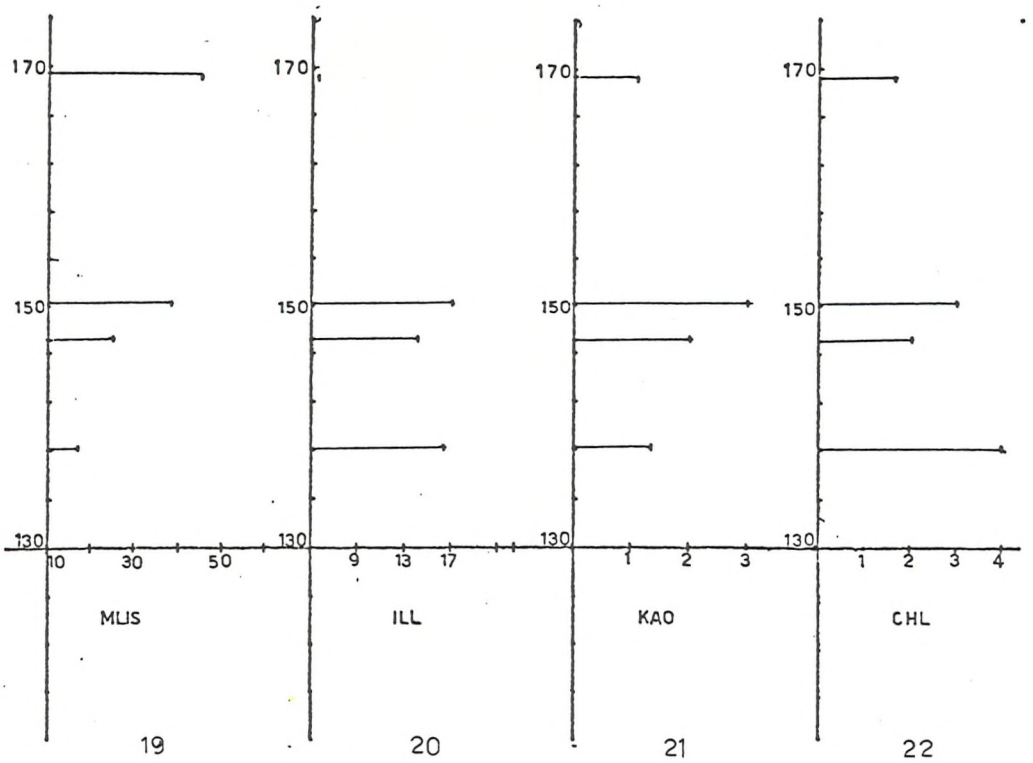

Leg 23

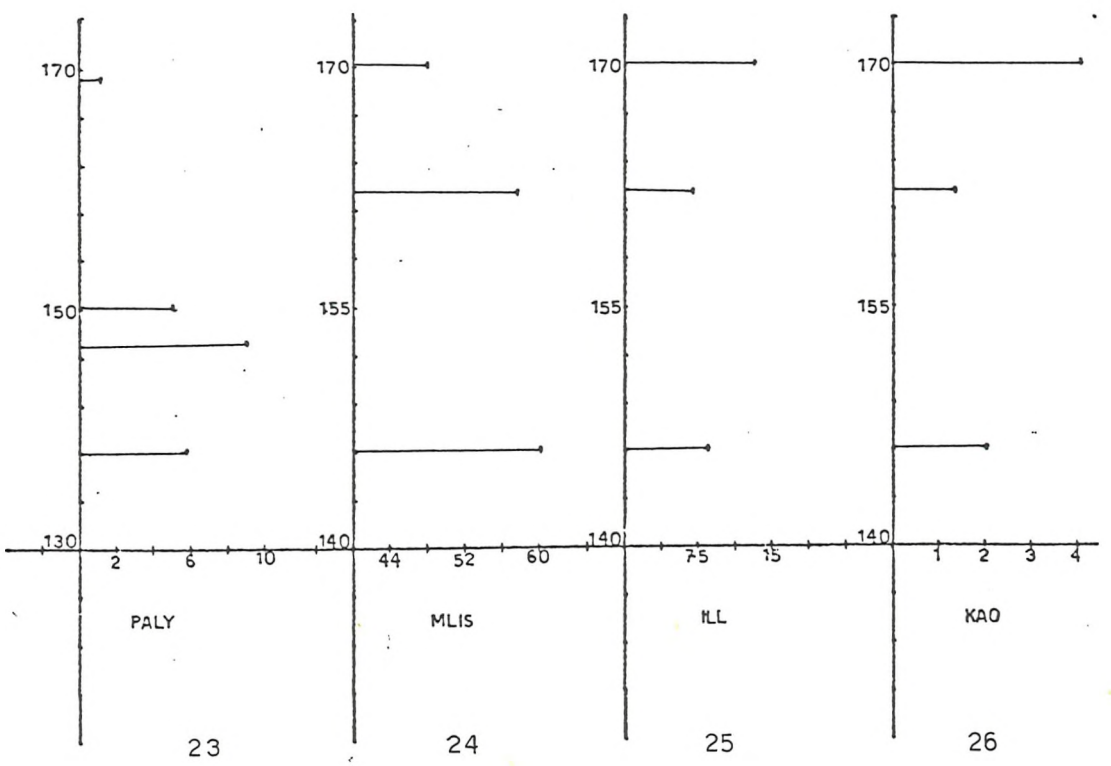

Leg 24

Fig. 3-9 b

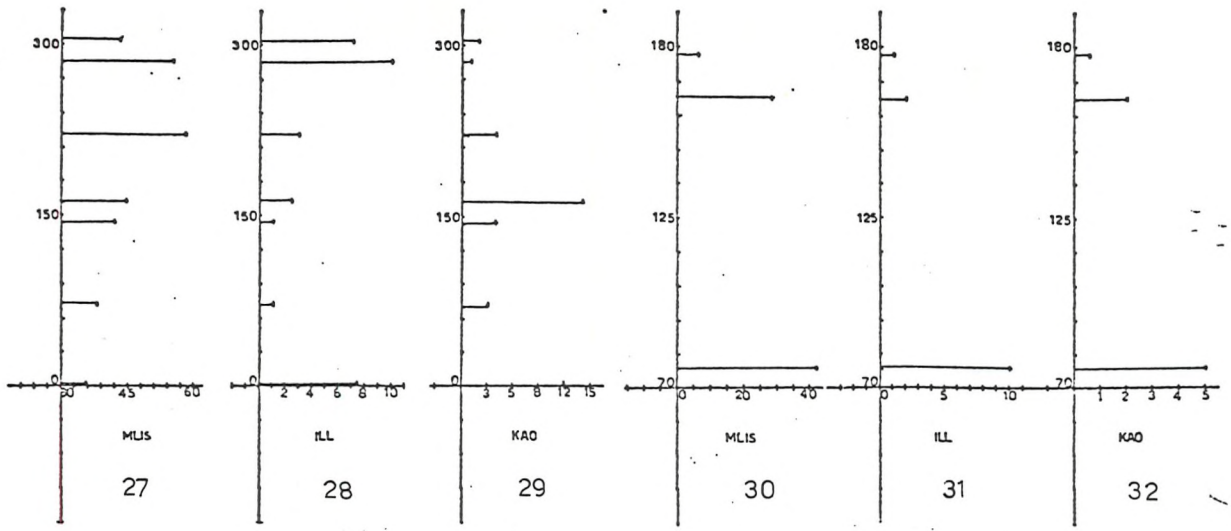

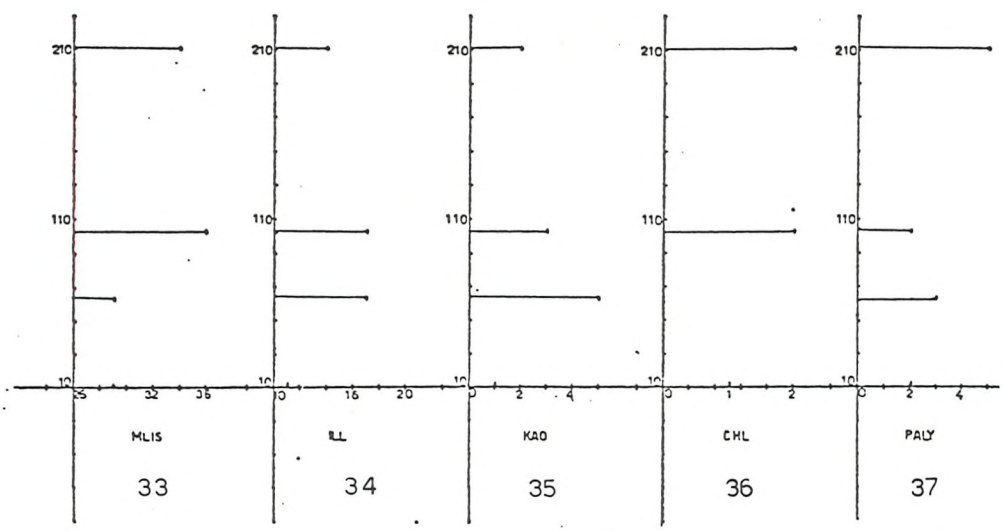

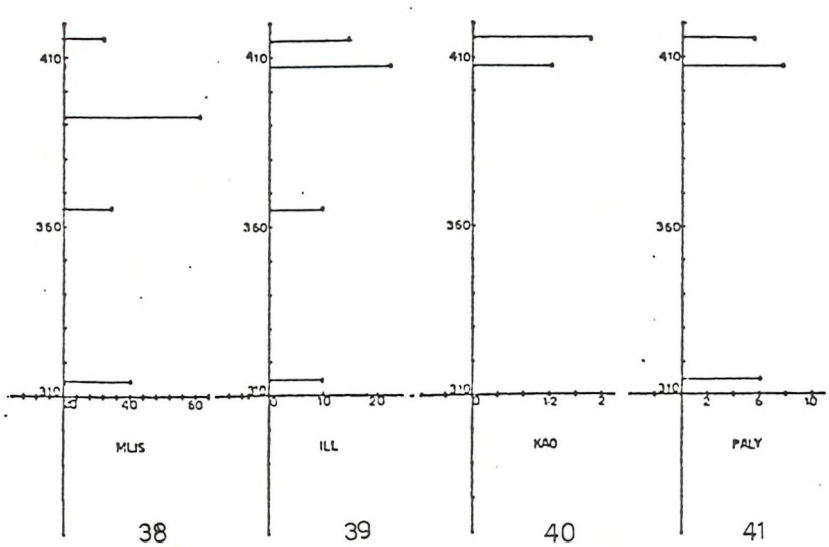

Leg 25

Fig. 3-9C

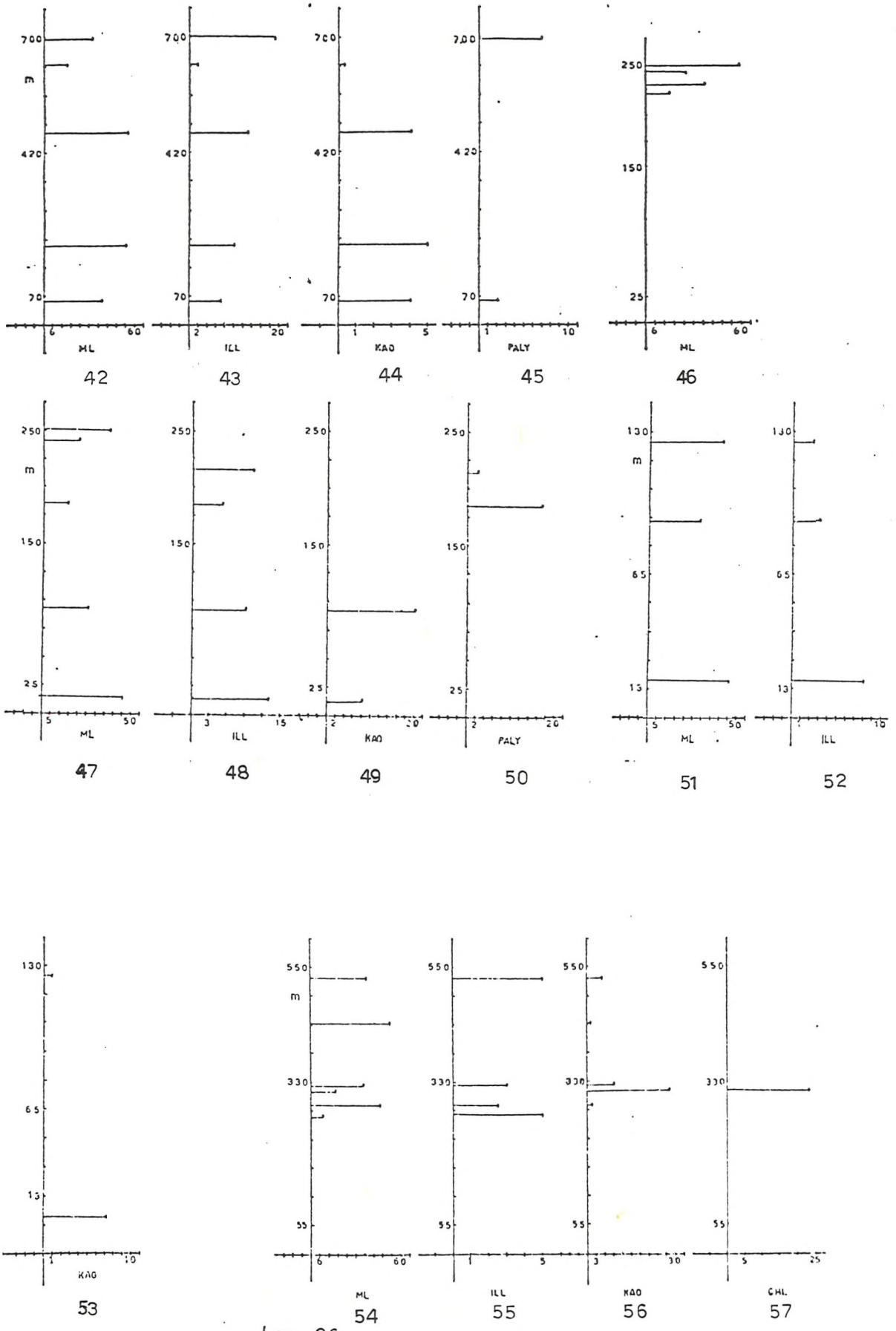

Leg 26

Fig - 3-9d

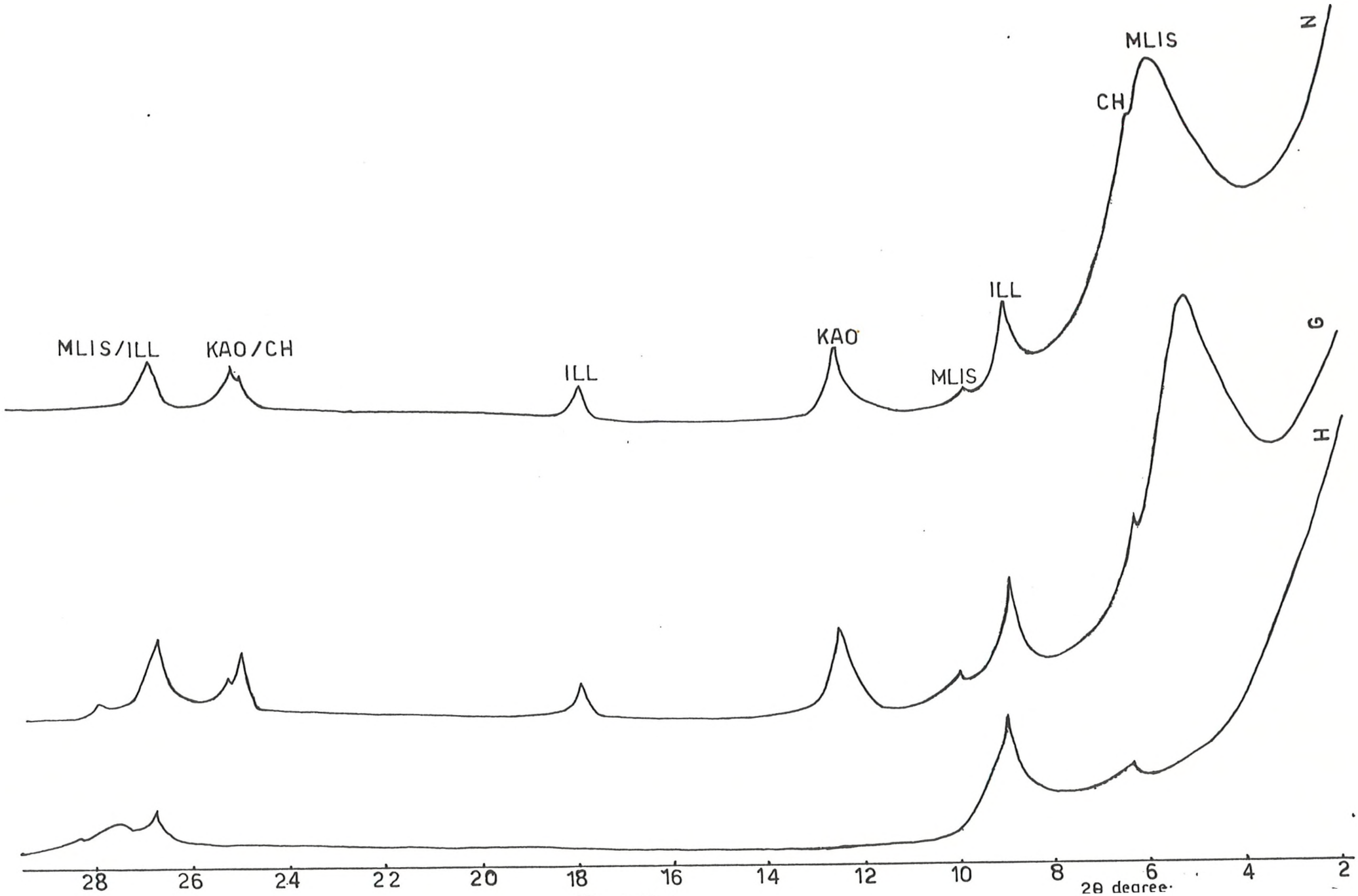
MLIS/ILL
KAO/CH
ILL
KAO
MLIS
ILL
CH
MLIS
N
G
H
28
26
24
22
20
18
16
14
12
10
8
6
4
2
2θ degree

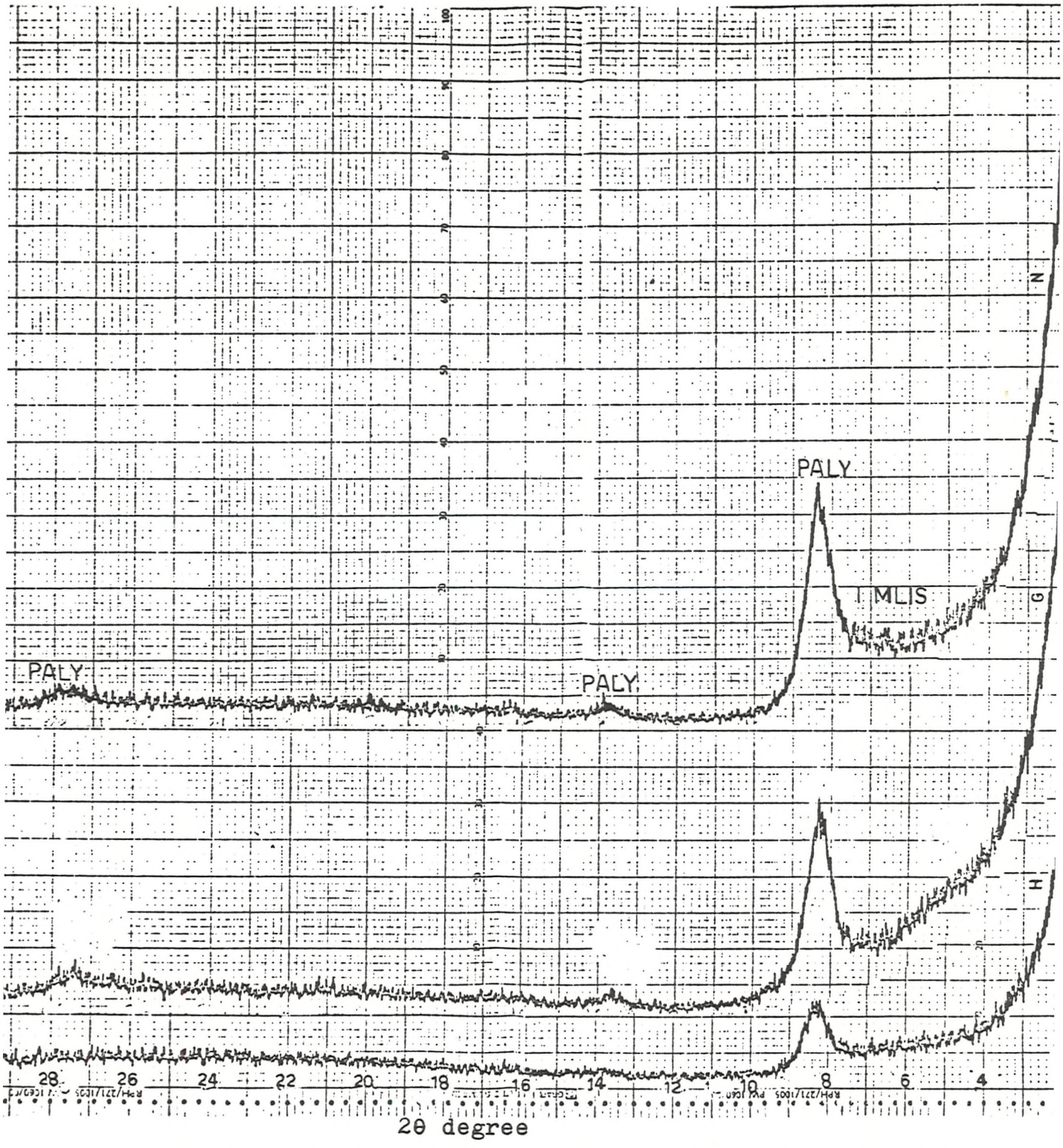

Fig.3-10b.Diffraction pattern of paly (sample 215/9/2).

TABLE 3-3: Peak Positions of the Clay Minerals on the X.R.D. Diffractograms after Certain Treatments

Basal diffraction spacing (Å) various treatments			Mineral
Normal (N) (Air Dried)	Glycolated 60°C	Heated (H) 550°C	
7	7	Destroyed	Kaolinite
12.2-15.5	17	9.9	Mixed layer illite/smectite
9.9	9.9	9.9	Illite
14.24	14.24	13.80	Chlorite
10.5	10.5	10.5	Paly

according to Hayes (1973) 17Å clay is not necessarily pure montmorillonite.

The expandability or percentage of smectite layers of the MLIS component is very important, since it can be related to the origin of the clay. Reynolds et al. (1970) proposed a method for the determination of expandable layers based on the fact that the d-values of $(001)_{10}$ illite/$(002)_{17}$ smectite and $(002)_{10}$ illite/$(003)_{17}$ smectite (in glycolated samples) vary according to layer composition. In the present study, those particular peaks are not sufficiently individualized in the diffractograms. Therefore the method suggested by Eslinger et al. (1976) was applied. They suggested that the nature of the 17Å MLIS peak could help to estimate the percentage of expandable layer (E%). They used the parameter v/h, where 'v' is the peak-to-trough distance on the low angle side of the 17Å peak, and 'h' is the peak-to-trough distance on the high angle side of the peak; the parameter v/h increases as the expandability of the mixed-layer phase increases (Fig. 3-11). According to Eslinger et al. (1976) the calculated diffraction profiles of Reynolds et al. (1970) indicate that v/h values of 0.39 and 0.77 correspond to 60% and 80% expandable layers respectively. Percentages of expandable layers in the MLIS were estimated using a graph based on the above values (Fig. 3-12). However, chemistry of individual MLIS phases (Ch.V) suggest that the %E values obtained by this method are much too low for most of the samples. It seems likely that much of the apparent variation in %E can be explained in terms of crystallinity differences (Hein et al. 1978).

1. Present-day distribution and sedimentation of clay minerals

The clay mineralogy of the surface sediments in the Indian Ocean has been investigated by many authors. Stewart et al. (1965), Gorbunova (1966) and Kolla et al. (1981) have studied clay mineral distribution in the Arabian Sea. Goldberg et al. (1970) have investigated the northern Indian Ocean clay minerals. Kolla et al. (1973a, 1974) made an extensive study of the clay minerals from the eastern and western sides of the Indian Ocean. They have distinguished several provinces in the Indian Ocean based on fine sediment (< 2 μm size) mineralogy (Figs.3-13 and 3-14).

a. Smectite

Kolla et al. (1973a) distinguished two Quaternary smectite-rich provinces in the eastern Indian Ocean as follows:

(1) the Deccan province in the western Bay of Bengal. The sediment dispersal in the province is by surface water circulation and

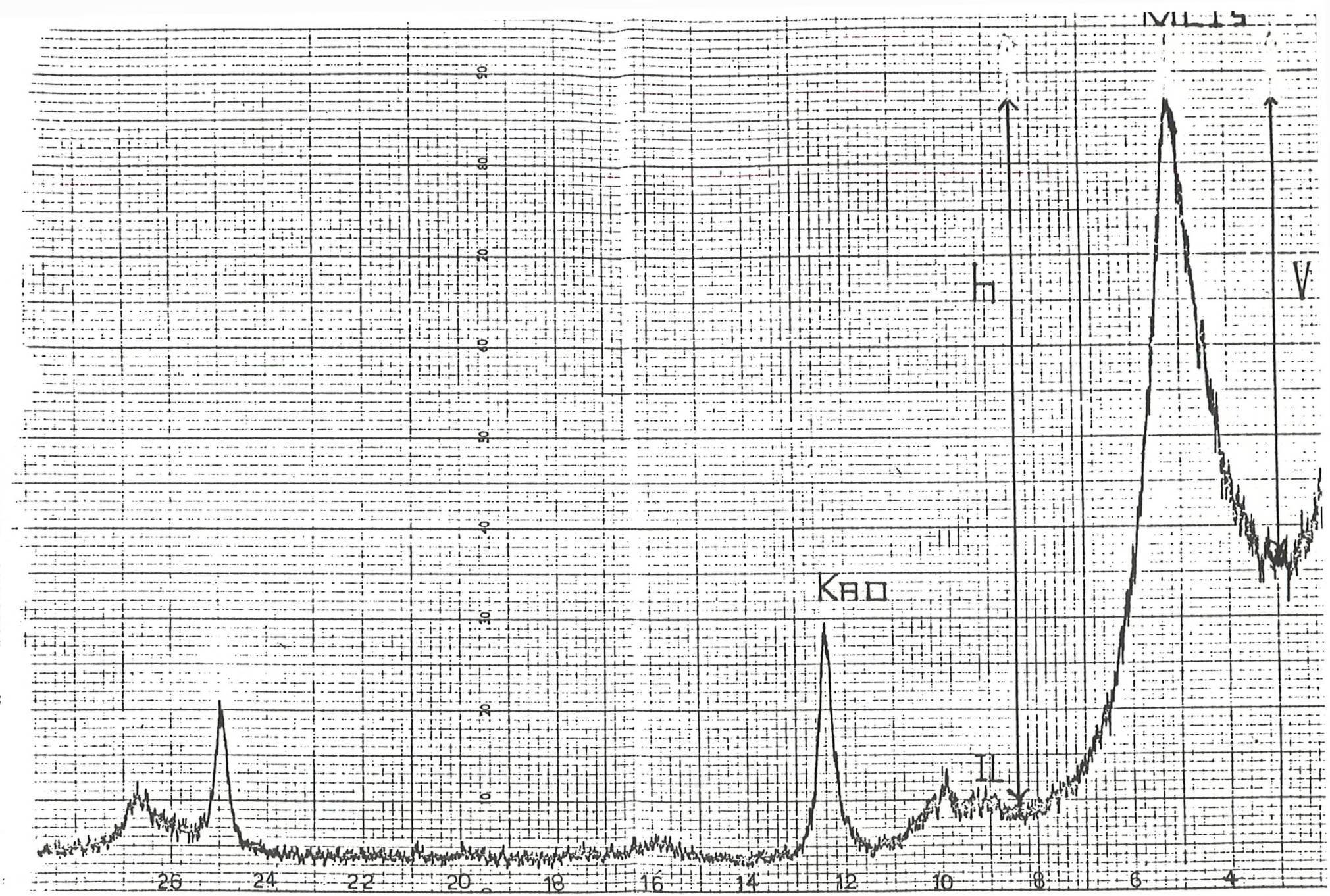

Fig.3-11

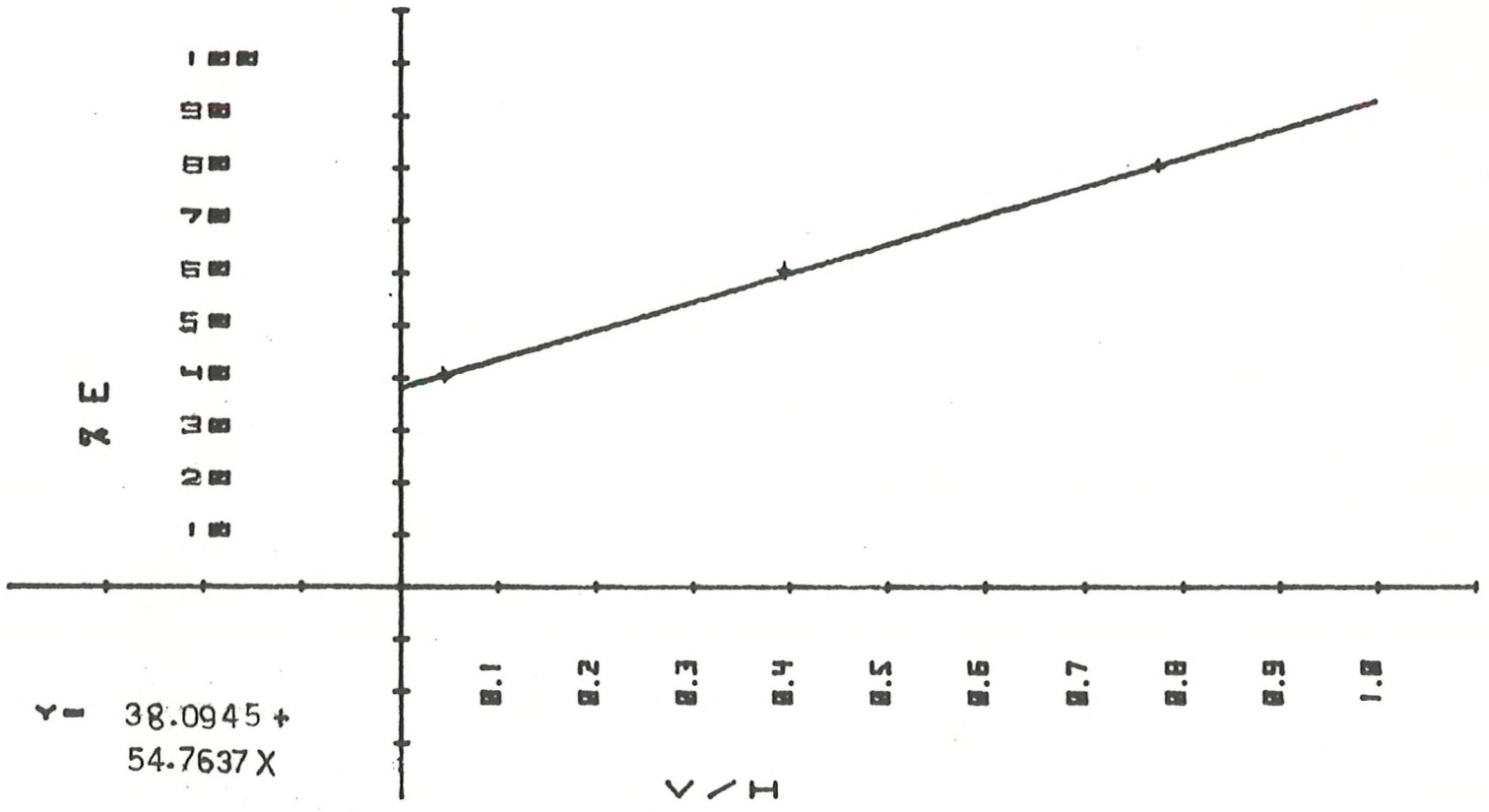

Fig.3-12

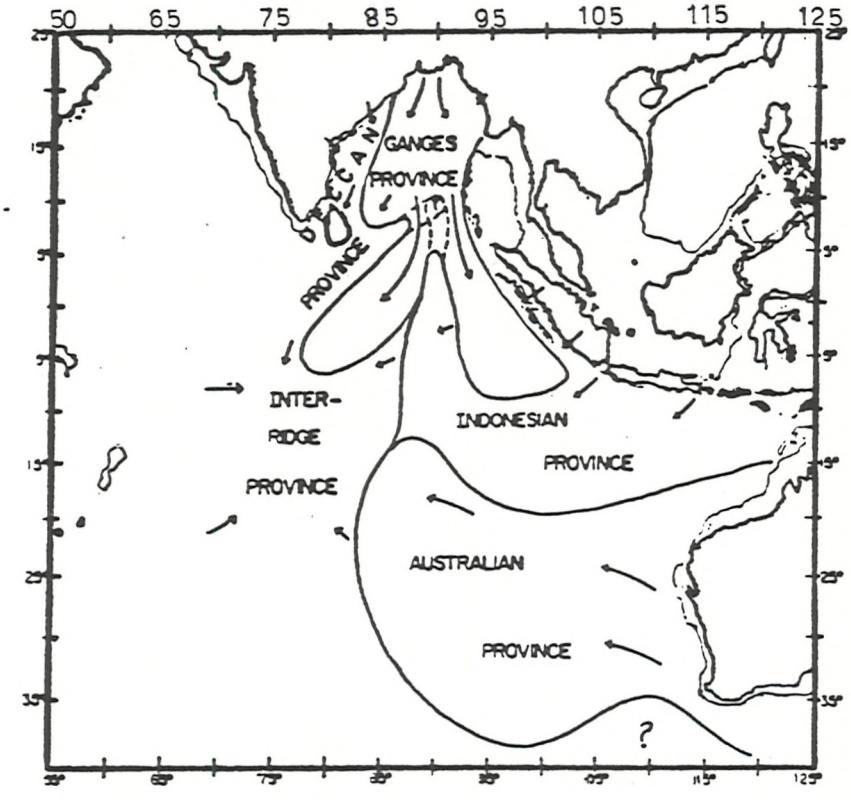

FIG. 3.13 Clay mineral provinces and dispersal paths of sediments in the eastern Indian Ocean. (after Kolla et al., 1973a).

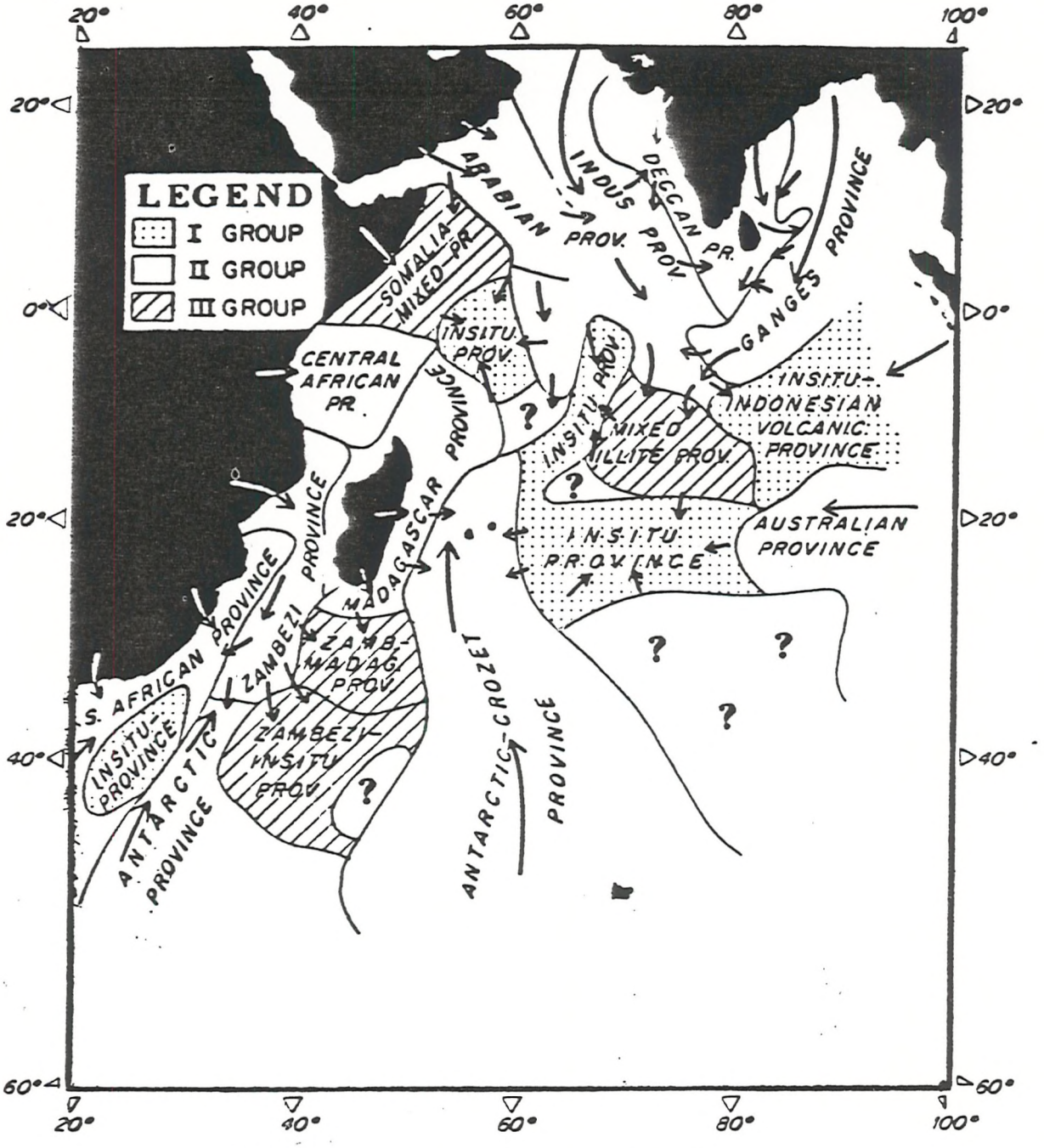

Fig. 3-14. Mineral provinces in the western Indian Ocean.

I Group. Provinces rich in smectite derived from the alteration of *in situ* submarine basalts and with little or no effects of long-distance sediment transport.

II Group. Provinces rich in different minerals derived from continents or southern ocean volcanic areas and with significant effects of several modes of long-distance sediment transport.

III Group. Mixed type provinces with no minerals in characteristically high amounts.

The sources of sediments for areas with question marks are not known.

(after Kolla et al., 1976).

turbidity currents. These sediments are derived from the Deccan Trap basalt.

(2) the Indonesian province with high smectite adjacent to the Indonesian Islands, on the Cocos-Roo Rises, and on the Ninety-east Ridge between 5°N and 14°S. This province is influenced by aeolian transport of silicic volcanic ash from the Indonesian island arc.

In the Arabian Sea, smectite-rich sediments occurring along the Indian margin have been derived from the western region of peninsular India (Kolla et al., 1976, 1981; Goldberg et al., 1970). Kolla et al. 1976, 1981) believe that smectite clays have been supplied by the Narmada and Tapti Rivers that drain the soils developed on the Deccan Trap basalts and have been subsequently dispersed by prevailing southerly, and to some extent northerly surface currents. The content of smectite along the Indian margin, derived from the Narmada and Tapti Rivers, decreases from north to south (Kolla et al., 1981; Goldberg et al., 1970). Near the southern tip of India, the smectite percentage increases significantly. Kolla et al. (1981) believe that the sediments are carried around the tip by Bay of Bengal surface water currents (Wyrtki, 1971). Matter (1974) suggested that the high amounts of smectite at Site 221 at the foot of Carlsberg Ridge is obviously a turbidity current deposit and probably originates on the Indian shelf or upper slope.

High concentrations of smectite are located over parts of the Carlsberg Ridge (Goldberg et al., 1970; Kolla et al., 1981). The high montmorillonite concentrations outlining the ridge areas in the equatorial and southern Indian Ocean below the Arabian Sea most probably result from the alteration of volcanic debris (Goldberg et al., 1970). In the central Indian Ocean, smectite-rich clays appear to be derived mainly from the alteration of in situ submarine basalts and the associated volcanic products (Griffin et al., 1968; Kolla et al., 1976).

Kolla et al. (1976) have recognised smectite-rich areas occupying the north-easternmost region of the Indian-Antarctic and Crozet Basins, part of the Mid-Indian Ridge (50° to 63°E and 30° to 25°S) and the eastern sections of the Madagascar and Mascarene Basins. They pointed out that this province is influenced mainly by the Antarctic bottom water current

(AABW) transport of smectite-rich clay from the areas of southern ocean volcanism - the Crozet plateau - Island and Kerguelen plateau regions. The altered products of the Mid-Indian Ridge volcanics and the sediments from the Madagascar Province could also locally influence the Antarctic-Crozet province.

b. Kaolinite

Gorbunova (1966) found maxima in the sediments, near Madagascar and in a belt extending south-west from Java. She found kaolinite concentrations particularly low in sediments of the Arabian Sea and west of the Bay of Bengal. Goldberg et al. (1970) also confirmed the low kaolinite content of the Arabian Sea when compared with the equatorial region. Griffin et al. (1968) suggested that kaolinite near Madagascar probably results from run off weathering products of this tropical environment, or it may perhaps be an extension of the input from the south-easterly winds operating to transfer lateritic material from the western part of Australia. Matter (1974) suggested the Indus River as the source of kaolinite, since this mineral has a strong positive correlation with chlorite at Site 222. Kolla et al. (1981) propose that, in the southernmost areas where kaolinite is very high in comparison with the other areas, the mineral is probably derived from tropical soils of Africa, Madagascar and southern India, and is then dispersed in the area by equatorial circulation prevailing north of the equator. The high concentration of kaolinite off the coast of western Australia, southern Wharton Basin and on the Ninetyeast Ridge south of 15°S, has an aeolian origin from western Australia (Griffin et al., 1968; Kolla et al., 1981).

c. Illite/Chlorite

Illite is the dominant clay mineral in most of the sediments of the Indus Fan and the Western Arabian Sea, including the Gulf of Oman and Murray Ridge off the Iran-Makran region. Kolla et al. (1981) have identified several sources for illite-rich sediments in areas proximal to land: Indus River source, high percentage illite plus chlorite; Iran-Makran source, high in illite with maximum amounts of chlorite; Arabian source with high amounts of palygorskite, illite and chlorite; Somalia source, with high palygorskite and smectite (although illite is moderately high, this mineral and chlorite are less in this source than in the Arabian source).

According to Griffin et al. (1968), data of Gorbunova (1966)

indicate three sources of illite: (1) from the Antarctic continent feeding into the southern Indian Ocean; (2) from the north-west tip of Australia; and (3) from the rivers draining into the Bay of Bengal and the Arabian Sea. Griffin et al. (1968) have suggested aeolian transport of illite from the Arabian Desert to the Carlsberg Ridge. High values off the South African coast are a part of the lobe of illite-rich sediments extending into the South Atlantic and Antarctic Oceans. This area coincides with the high illite soils of the south tip of Africa (van der Merwe et al., 1956). Griffin et al. (1968) postulate glacial transport in this region. The region between Madagascar and Africa, the Mozambique Basin, and to some extent the Madagascar Ridge, where it is diluted by Madagascar province clays, receives its illite from the Zambezi River. The Agulhas surface and turbidity currents, the AABW and North Atlantic deep water play important roles in the transport of Quaternary Zambezi sediment or the re-distribution of it (Kolla et al., 1976).

d. Palygorskite

Palygorskite (paly) minerals are characteristic of the weathering of the crust in an arid climate. According to Gorbunova (1966), they are carried from the Arabian Peninsula to the Arabian Sea. Goldberg et al. (1970) showed an eastward decrease towards the tip of India in palygorskite percentage in the Arabian Sea just north of the Equator. They suggested an aeolian contribution to the Arabian Sea from the African continents for paly. Heezen et al. (1965) found paly increases in abundance going from the Red Sea through the Gulf of Aden into the Arabian Sea. Kolla et al. (1981) suggested aeolian transport of this mineral from both the arid regions of the Arabian Peninsula and Somalia (Horn of Africa). According to them, this mineral has been transported by winds eastward to as far as the Indian continental margin. However, Matter (1974) suggested an authigenic origin for paly resulting from the alteration of volcanic glass in the Arabian Sea. He believes that paly is diluted by the detrital sediment input from the Indus, and that is the reason for high paly/illite ratio on the distal Indus Cone.

2. Clay mineralogy from Legs 22, 23, 24, 25 and 26 and their provenances

As previously mentioned, the clay minerals of the $< 2\ \mu m$ fraction from 86 samples were investigated (Table 3-2). The present clay minerals were MLIS, illite, kaolinite, chlorite and palygorskite. The mean relative

abundance of each mineral is shown in Table 4-6. MLIS was the dominant clay mineral. The v/h parameter of Eslinger et al. (1976) was used as an indicator of its origin.

According to Eslinger et al. (1976) as v/h ratio increases, the percentage of expandable layer (E) increases. They believe that illite/smectite mixed layers having a lower percentage of expandable layer are mainly of detrital origin, which co-exist with significant amounts of mica (illite), chlorite, kaolinite and quartz. On the other hand, random mixed-layers are mainly of authigenic origin (typically called authigenic smectite) and that they co-exist with zeolites and low contents of detrital mica(illite), chlorite, kaolinite, feldspar and quartz (Gieskes and Kastner, 1975; Eslinger et al., 1976). According to Vallier (quoted by Hein et al., 1978), if the percentage of smectite in the total clay fraction ($< 2\,\mu m$) is greater than 90%, then that size fraction is thought to be of volcanic origin. If the percentage is greater than 75% but less than 90%, the clay fraction is mostly of volcanic origin; if it is between 50% and 75%, some volcanic input is suspected. Hein et al. (1978) also noticed that sediments from the Bering Sea containing about 75% or greater smectite (in the $< 2\mu m$ fraction) show less than 20% illite interlayered with smectite, and the terrigenous deposits in the southern Bering Sea show 45% to 55% illite interlayered. Perry et al. (1976b) reported terrigenous debris at DSDP Site 149 (Caribbean Sea) has 60% expansible layers.

In the present study, the amount of MLIS was not used as a criteria for being volcanic (authigenic), since MLIS is involved in the authigenic reactions (e.g. zeolite or paly forming reactions) and is used up in such reactions, which causes a decrease in the MLIS percentage and increase in other clay minerals. Therefore, the percentage of expandable layer was used in the same manner as by Eslinger et al. (1976). It is therefore suggested that MLIS with a percentage of expandable layer higher than 60% is of authigenic origin, and those with less than 60% expandable layer are of detrital origin.

As discussed in the Chapter on bulk chemistry (Chapter IV), the Fe/Ti vs Al/(Al+Fe+Mn), Ti vs Al and Cr vs TiO_2 plots (Figs. 4-1,2 & 3) indicate the contribution of volcanic fragments/glass (basaltic and/or granitic) and shale to the sediments from the surrounding lands. The

volcanic material was probably brought to the site of deposition at the same time as volcanism was occurring on the continents and islands, or sometimes later. The alteration of such volcanics probably resulted in authigenic MLIS.

a. Eastern sites

i) South-eastern sites of the Indian Ocean (212, 256, 257 and 258)

The bulk chemistry shows basalt, granite and shale contribution to the sediment from the surrounding lands. Some of the samples also show tholeiitic basalt contribution from the basement (Samples 256/7cc and 256/8/4).

Kaolinite, illite and detrital MLIS are probably brought from Australia, Antarctica and India. Griffin et al. (1968) and Kolla et al. (1981) suggested that the high concentration of kaolinite off the coast of western Australia, southern Wharton Basin and on the Ninety-east Ridge south of 15°S, has an aeolian origin from western Australia. Kolla et al. (1973a) also suggested that the formation of kaolinite soils was probably at a maximum in the Miocene, since high temperature and humidity prevailed. Therefore, the Miocene to Recent sediments at the above-mentioned sites (212/17cc upwards and 256/2/3) probably received kaolinite from western Australia.

High percentage expandable MLIS, which is of the authigenic origin and results from the alteration of volcanic glass, is common in the sediment, and could indicate the volcanic activity on the surrounding land. For example, the high percentage expandable MLIS in Samples 212/23/5 and 212/18/1 indicates the separation of Australia from Antarctica in the Eocene. During the Cretaceous, also, volcanic activity occurred on the lands (rifting between Australia and Antarctica and volcanic activity in India), and contributed volcanic material to the sediments.

Palygorskite is associated with low %E MLIS, even in the presence of clinoptilolite (Sites 256 and 212) (Plate 3-12). Samples at Sites 212 (cores 37cc and 38/1) and 256 (cores 6/3 and 7cc) show a decrease in MLIS and clinoptilolite and increase in palygorskite. However, clinoptilolite is associated with high %E MLIS in the absence of palygorskite at all sites, and shows negative correlation with MLIS.

PLATE 3-12

a-c. Palygorskite in Sample 215/9/2

d. Palygorskite-clinoptilolite and opal-CT association in Sample 256/7cc.

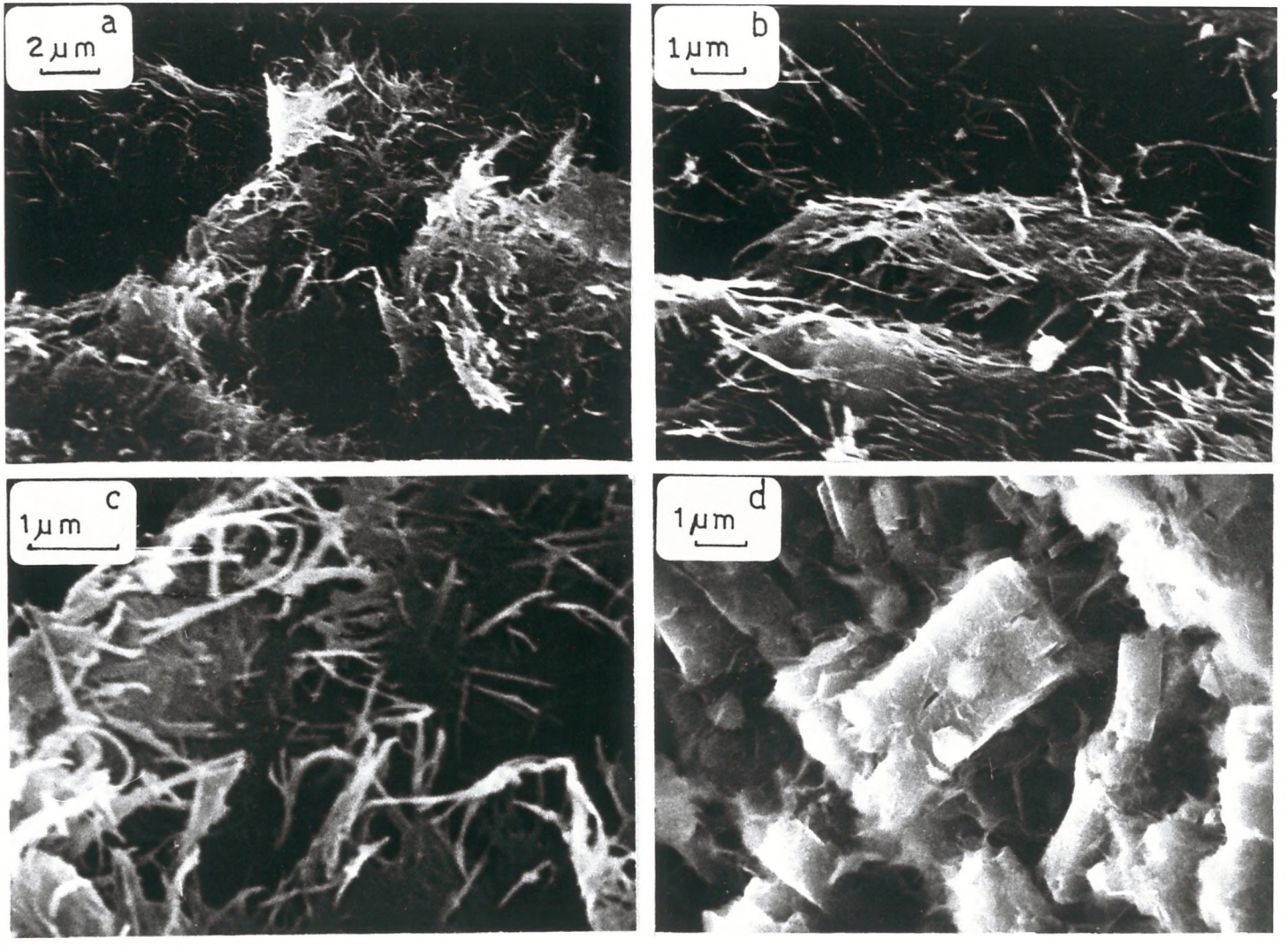

PLATE·3-12

ii) Site 211

One sample from the Pliocene (core 6/2) and two from Cretaceous sediments (cores 13/1 and 14/1) were studied.

This site is situated in the Indonesian province. Kolla (1974) has observed a mineralogical change in the sediments of the early Pliocene (cores 4, 6 and 9). According to him, these sediments have high amounts of illite and chlorite in the $< 2\ \mu m$ size fraction (Table 3-4) and abundant quartz, amphibole and epidote. Turbidities are also frequently present in these Pliocene sediments, but sediments of the late Pliocene show high smectite percentages. Therefore, he suggested that in the early Pliocene, the Ganges-Brahmaputra River sediments, rich in illite, and the other minerals described, were transported to the area of Site 211 by turbidity currents similar to the adjacent Quaternary Ganges province. This source was then replaced in the late Pliocene by smectite derived from silicic volcanic ash of the Indonesian arc.

In the present study, Pliocene sediment (core 6) is rich in MLIS with high %E. Small amounts of kaolinite and illite are also present (1% in the $< 2\ \mu m$ fraction). Matti et al. (1974) reported no chlorite in core 6 and less than 10% illite in cores 4, 5 and 6, which means less than the amount found in Quaternary sediment (20%) (Table 3-5). They reported a high percentage of kaolinite and mica in core 10 ($> 10\%$). MLIS is dominant in all cores.

The above results plus the X-ray analysis of the present study of core 6 suggest that core 10 probably indicates the activity of Ganges-Brahamaputra Rivers, and this source was probably replaced by silicic volcanic ash of the Indonesian arc earlier than the late Pliocene.

Samples of the Cretaceous are bounded between the basaltic basement and an andesitic sill on the top. The bulk chemistry element comparison shows tholeiitic basalt contribution to the sediments. The percentage of expandable layer was found to be low, suggesting a detrital origin for MLIS. Percentage of MLIS and expandable layer decreases with depth, whereas illite increases. Palygorskite also shows a slight increase. These variations could suggest an authigenic origin for both illite and paly, i.e. MLIS into illite and paly transformation.

TABLE 3-4: Clay Mineral Composition of < 2 μm size fraction (after Kolla, 1974)

Sample	Interval (cm)	Smectite %	V/P Ratio smectite	Illite %	Kaolinite %	Chlorite %	Age
211/1/3	0 - 10	76	0·53	10	11	2	Quat.
211/2/3	"	83	0·71	8	8	2	"
211/3/4	"	77	0·60	11	10	2	Lt.Plio.
211/4/3	"	66	0·72	22	4	7	Plio.
211/6/5	"	51	0·69	35	5	7	Plio.
211/9/3	"	22	0·43	57	7	14	Plio.
211/12cc	8 - 10	17	0·02	69(?)	11	2	Camp.
211/14/1	12 - 19	14	0·00	83(?)	3	3	-

TABLE 3-5: Clay Mineralogy of $< 2\mu$ fraction (after Matti et al., 1974)

Sample	Sample depth below sea floor (m)	Mont	Mica	KaO	Chlo	Paly
211/1	0·0 - 9·0	43·4	20·7	17·8	1·6	
211/3	57·0 -66·0	47·1	17·3	15	1·5	
211/4	95 -104·5	81·9	5·3	2·3	1·7	
211/5	133 -142·5	67·2	6·6	10	-	
211/6	180·5-190·5	73·1	4·1	7·7	-	
211/10	342 -351	50·3	10·7	21·8	-	
211/11	389·5-398	43·5	-	-	-	14·5
211/12	409 -418·5	11·9	4·9	1·9	1·3	63·5
211/13	418·5-428	35·1	13·3	0·6	1·7	31·4
211/14	428 -437·5	2·4	4·4	-	-	62·8

Couture (1977a) and Kolla (1974) also investigated samples from this part of Site 211 (cores between basement and sill). Couture (1977a) compared the whole rock chemistry with the chemistry of basalt, and noticed that the sample resembles tholeiitic basalt in its Ti/Al and Fe/Al ratios, but has slightly low Mg/Al and higher Si/Al and K/Al ratios. He believes that the reaction with interstitial water has apparently added K and removed Mg, but it is not clear for him whether the paly was formed by hydrothermal activity or by diagenesis. Kolla (1974) also found palagonite in this part, and suggested that in situ alteration of volcanics resulted in upper Cretaceous sediments rich in palygorskite.

iii) Site 213

Eleven samples from the Miocene were investigated. They showed high percentages of MLIS in association with illite and kaolinite. Chlorite is present only in one sample (core 8/5) and paly is present in the bottom samples. No specific relation among clay minerals is observed. MLIS with high as well as low percentages of expandable layer is present. The bulk chemistry shows silicic volcanic glass contribution to samples 213/11/5 upwards, and basaltic + silicic volcanics to samples 213/11/5 downward. This evidence tends to support the suggestion made by Kolla (1974). He believes that since the late Miocene, wind systems have transported silicic volcanic glass to this area from silicic Indonesian volcanics, while in pre-middle Miocene times basaltic volcanics were the main source of the sediments. Illite and kaolinite are probably transported to this region from the Indonesian arc.

iv) Sites 216 and 254

These sites are situated on the Ninetyeast Ridge. MLIS, with a high percentage of expandable layer, is the only clay mineral present at these sites. Abundant volcanic glass is also observed (Plate 3-13). The bulk chemistry indicates a high amount of tholeiitic basalt and low percentage of terrigenous material contribution to sediments at Site 216 (cores 24/4, 25/3 and 34/1) and a high percentage of alkali basalt + low amount of tholeiitic basalt to sediments at Site 216 (cores 30/3 and 32/3) and 254 (25cc, 36cc, 37/3 and 28cc). Samples at Site 216 are of the late Cretaceous, whereas at Site 254 they are of the mid-Tertiary.

The Ninetyeast Ridge formed during the Cretaceous to early Oligocene. Therefore parts of it were the scene of volcanic activity

PLATE 3-13

a. Volcanic glass in Sample 254/25/2

b. " " " Sample 216/30/3

c. " " " Sample 254/25/2

d. " " " Sample 254/28cc

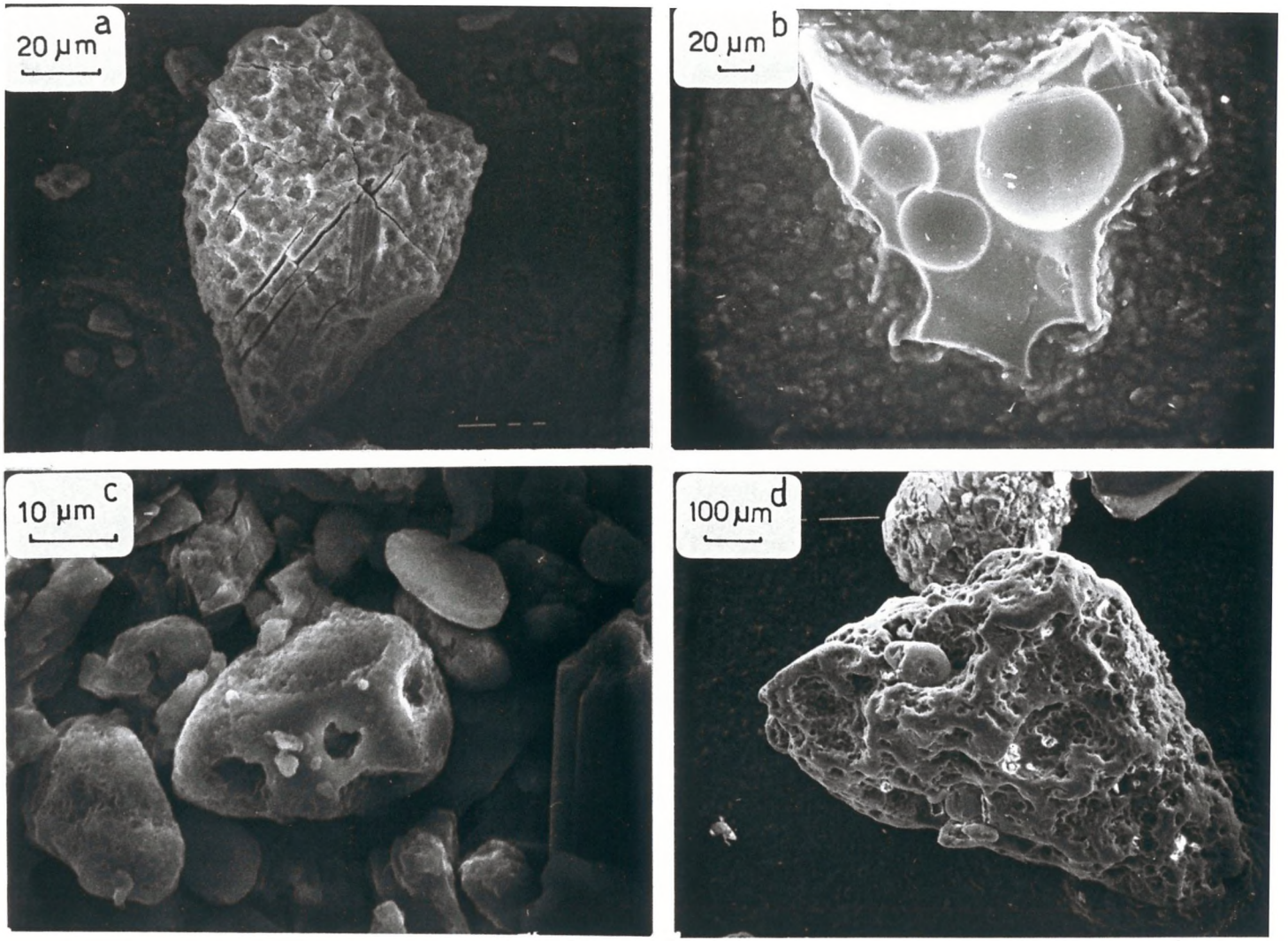

PLATE-3-13

from the Cretaceous to early Oligocene (Kidd et al., 1978). According to Davies et al. (1974), the sediments of Site 254 (cores 25-28) indicate the weathering and erosion of a basaltic terrain adjacent to and composed of the same type of volcanic rocks as those of underlying layers. Thus the high percentage of expandable layer and presence of volcanic material suggest the formation of MLIS via in situ alteration of volcanic material.

v) Site 215

Two samples from the Eocene (215/9/2) and Miocene (215/8/2) were studied. The bulk chemistry showed silicic volcanic glass contribution to Sample 215/8/2 and basaltic + granitic contribution to Sample 215/9/2. Kolla (1974) also suggested a volcanic influence on these sediments. MLIS, illite, kaolinite, chlorite and palygorskite were present. Sample 215/9/2 showed the presence of the highest amount of palygorskite in the present study (Plate 3-12a-c). Both authigenic and detrital MLIS are present in Samples 215/8/2 and 215/9/2 respectively. There is a downward decrease in the percentage of expandable layer and MLIS, and an increase in illite and palygorskite. These variations cannot be attributed to burial diagenesis, since these sediments are from a shallow depth between 66 to 77 metres. The high abundance of palygorskite and its remoteness from palygorskite-rich areas makes its detrital origin unlikely.

b. Western sites

i) Site 221

Four samples from the late Oligocene to Miocene were analysed for clay mineralogy. MLIS, illite, kaolinite, chlorite and paly are present. None of the clay minerals show a consistent trend of variation. Activity of the Indus, Narmada and Tapti Rivers, and the wind system in this area, suggest a high detrital input. Matter (1974) believes that the high detrital montmorillonite at Site 221 is obviously a turbidity current deposit and probably originated on the Indian Shelf or upper slope. According to him, illite is distributed from the Indus mouth as far as the foot of the Carlsberg Ridge by density currents which, at least partly, follow the distributive deep-sea fan channels. He found positive correlation between chlorite and kaolinite. Thus, he suggested the Indus River as a source of chlorite and kaolinite. Griffin et al. (1968) and Gorbunova

(1966) found a low concentration of kaolinite in the Arabian Sea. Kolla et al. (1981) believe that in the southernmost areas, where kaolinite is very high in comparison with the other areas, the mineral is probably derived from tropical soils of Africa-Madagascar and southern India, and then is dispersed in the area by equatorial circulation prevailing north of the Equator.

In the present study, low percentages of expandable MLIS, illite, kaolinite, chlorite and palygorskite are present. Chlorite shows very weak positive correlation with quartz (at 90%) and K-feldspar (at 80%). This could suggest a common source for chlorite, quartz and K-feldspar. According to Kolla et al. (1981) the north-west - south-east orientation of a high quartz band in the northern Arabian Sea, far from the Indus River mouth and the continental slope, may be due to aeolian transport of the mineral from the Iran-Makran region. Furthermore, he suggested a source high in illite plus maximum amounts of chlorite from the Iran-Makran region. The results of this study are thus in sympathy with Kolla's views, although the above-mentioned correlations are very weak, which could be due to the scarcity of the number of samples available. No other trend of variation was observed among clays. The chemistry showed the presence of volcanic material (basaltic + granitic) in the sediments. However, the proximity of this site to areas rich in palygorskite and the absence of any relation with MLIS and illite, make a detrital origin likely. Kolla et al. (1981) suggested aeolian transport of palygorskite and illite from an Arabian source. Elprince et al. (1979) observed palygorskite in the soil of Saudi Arabia.

ii) Site 236

This site is situated south-west of the Carlsberg Ridge and about 270 km north-east of Seychelles Bank. MLIS, with low percentages of expandable layer, illite, kaolinite and trace amount of palygorskite of the Miocene and younger are present. As MLIS decreases downward, illite increases. The bulk chemistry also shows the volcanic fragment contribution to the sediments.

iii) Site 239

It is situated in the Mascanene Basin. MLIS, kaolinite, illite, and trace amounts of palygorskite of early Palaeocene to Quaternary are

present. None of the clay minerals show any variation through time. According to the classification by Kolla et al. (1976), it is situated in Madagascar Province, and receives smectite and kaolinite from Madagascar. Illite also could reach to this site from Antarctica Crozet province. The presence of volcanic material, which is confirmed by both bulk chemistry and SEM studies, is probably responsible for the presence of authigenic MLIS. According to Vallier (1974), it is probable that volcanic materials in Cretaceous-middle Miocene sediments are associated with volcanism, which accompanied the formation of the Central Indian Ridge and/or the development of the 'Chagos Fracture Zone'. He believes that volcanic contributions in the middle Miocene-Quaternary are most likely related to the volcanism on nearby seamounts and islands in the Mascarene Island Group.

iv) Site 240

This site is situated in the eastern part of Somali Basin. MLIS, illite, kaolinite and a trace amount of palygorskite of the Miocene and Pliocene are present. None of the clay minerals show any trend of variation through time. Kolla et al. (1976) have classified this area within the central Africa province, where it receives high amounts of kaolinite from African soils. Illite may have also been derived from African soils. However, MLIS with high to medium percentage of expandable layer probably resulted from in situ alteration of volcanic material. According to Vallier (1974), Miocene to Recent volcanic contributions can be related to volcanism on Madagascar and the Comoro Islands and to erosion of the East Africa rift valley volcanics. The bulk chemistry of the present study samples shows the presence of volcanic material (basaltic + granitic).

v) Site 245

Eocene sediment of this site was studied. MLIS, with a low percentage of expandable layer, is associated with illite, kaolinite, chlorite and palygorskite.

According to classification by Kolla et al. (1976), this area is situated in the Antarctic-Crozet province. This province occupies the eastern sections of the Madagascar and Mascarene Basins. They believe that the Antarctic-Crozet province is influenced mainly by the Antarctic bottom water transport of smectite-rich clays from the areas of southern

ocean volcanism - the Crozet Plateau Island and Kergulen Plateau regions. He further mentioned that altered products of the mid-Indian Ridge volcanics and the sediments from the Madagascar province could also locally influence the Antarctic-Crozet province. He thought that thick sediments (300-500m) above the basement suggested that the Antarctic bottom water has been active in the Crozet Basin since pre-Quaternary times.

Gieskes et al. (1975) have studied this site. They believe that alteration of volcanogenic and basaltic material has led to the formation of several authigenic minerals: montmorillonite in the bottom portion of the basal sediments, montmorillonite and clin in the upper portion of the basal sediments, and montmorillonite, paly and clin in the Eocene nanno oozes and chalks overlying these deposits.

In the present study no clinoptilolite was observed. The bulk chemistry suggested the presence of volcanic material (basaltic + granitic). Volcanic glass was also observed at this site (Plate 3-14). No relation exists between MLIS and paly. The aeolian transport of paly in this area is unlikely since lands rich in paly are far from this area. Therefore, on the basis of the remoteness of the site from the land rich in palygorskite and the presence of volcanic fragments, an authigenic origin is suggested for palygorskite.

vi) Site 246

This site is situated on the Madagascar Ridge. One sample of the Eocene was studied. A high percentage of highly expandable layer with a very low percentage of kaolinite and illite are present. Volcanic material was observed under SEM (Plate 3-14). The volcanic material appears to be derived during periods of high volcanic activity, probably from Madagascar, the Madagascar Ridge or nearby volcanic islands. However, a high percentage of expandable layer and the existence of volcanic material suggest the formation of MLIS via in situ alteration of volcanic material.

vii) Site 248

This site is situated on the Mozambique Basin. Sediments of the Eocene containing MLIS, illite, kaolinite, chlorite and palygorskite were studied. The bulk chemistry showed volcanic material (basaltic + granitic) contribution to the sediments from the surrounding lands. The percentage of expandable layer is high ($>$ 60%) in the three topmost

PLATE 3-14

a. Volcanic glass in Sample 246/10/2

b. " " " Sample 245A/6/2

c. " " " Sample 239/16/3

d. " " " Sample 248/14/6

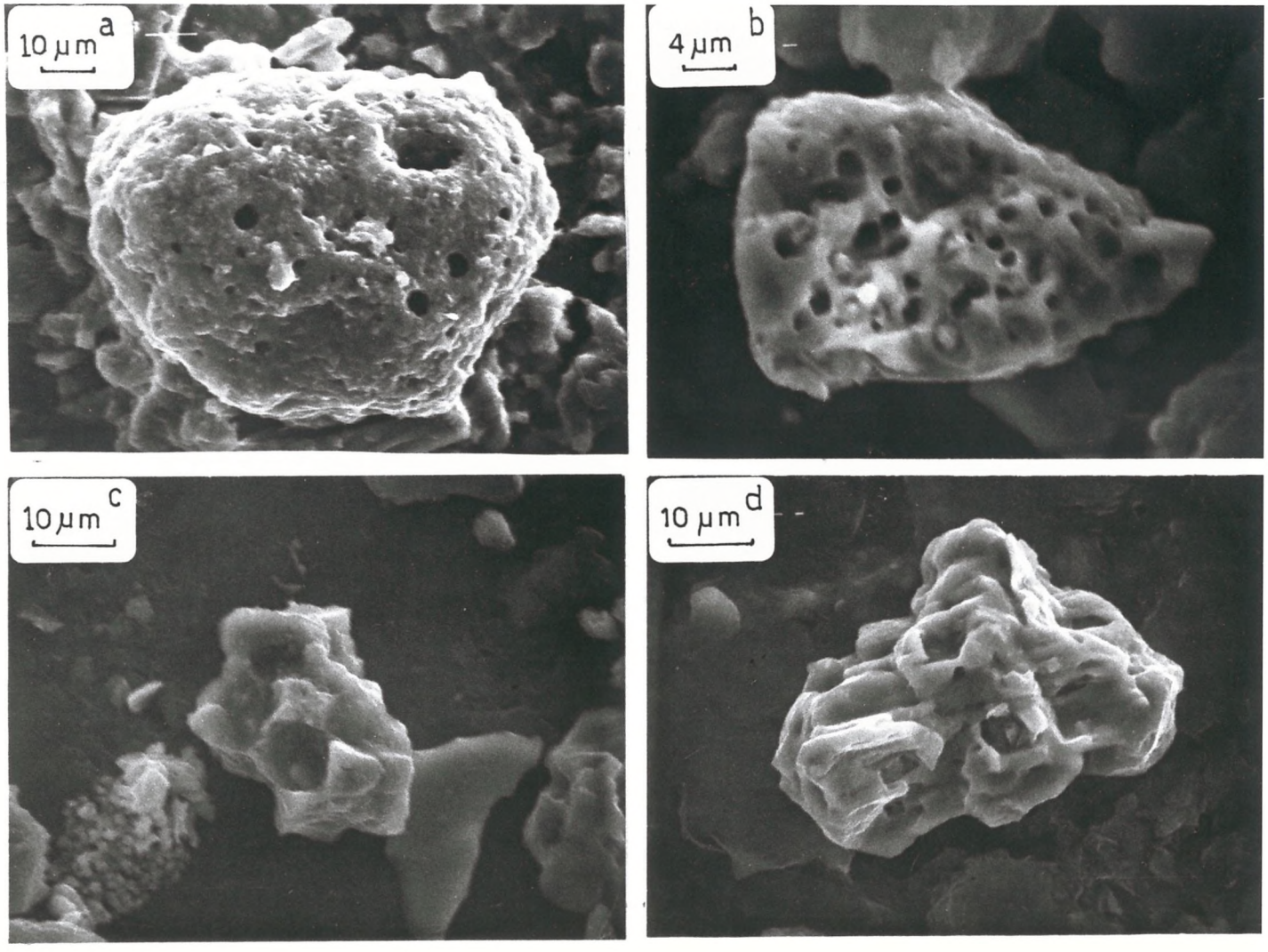

PLATE · 3-14

samples, whereas it decreases in the bottom-most sediments. MLIS with a low percentage of expandable layer decreases as palygorskite and illite increase. MLIS with a high percentage of expandable layer is the only clay mineral associated with clinoptilolite (core 12/3). The volcanic contribution to the sediments was possible from Madagascar Island by wind, since volcanic activity was reported in the northern part of Madagascar in the Eocene (Vallier, 1974). Kaolinite and detrital MLIS could also reach this area by wind from South Africa and Madagascar.

On the basis of the presence of volcanic fragments, negative relation of MLIS with illite and palygorskite and remoteness from the land rich in palygorskite, a MLIS into palygorskite and probably illite is suggested.

viii) Site 250

This site is situated on the Mozambique Basin. One sample from Cretaceous age containing MLIS, illite and paly, and four samples from Miocene to Quaternary containing MLIS with illite, were studied. Kolla et al. (1981) have classified this site within Zambezi province, where it receives high amounts of kaolinite in addition to illite from the Zambezi River. Davies et al. (1974) also believe that much of the sediment is derived from the Zambezi canyon and fan system, which transports sediments from East Africa and Madagascar south to the Mozambique Basin. According to them the sediments were re-distributed in the basin by bottom current. Therefore, kaolinite, illite and MLIS may have derived from East Africa and Madagascar. Sedimentation at this site has been under the control of active bottom current circulation, since some time in the Miocene. Sedimentation was much gentler from the late Cretaceous until Miocene. This is evident by the thinness of the section. The present study bulk chemistry showed the presence of volcanic material (i.e. basaltic + granitic) contribution from the surrounding land. This site could receive volcanic material from southern and western parts of Madagascar since volcanic activity was occurring at this time (Cretaceous) in Madagascar (Vallier, 1974). Palygorskite, in association with a low percentage of expandable MLIS, illite and clinoptilolite, was observed in Cretaceous sediments.

3. Correlations

The correlation matrix for 84 samples and the following variables -

MLIS, illite, kaolinite, chlorite and palygorskite, is presented in Table 4-5.

MLIS of detrital origin is negatively correlated with palygorskite and illite (significant at 99·99%). Palygorskite shows a positive correlation with illite (significant 99·99%).

In the absence of palygorskite, illite shows a strong positive correlation with quartz (Fig.3-15). As previously mentioned, quartz is thought to be of detrital origin (mostly wind borne). Therefore, illite is partly of the same origin as quartz in these sediments. In paly-bearing samples, illite does not show any correlation with quartz, which suggests a different origin for illite as well as palygorskite.

MLIS of authigenic origin shows negative correlation with clinoptilolite (significant at 99·99%) (Fig.3-16).

These correlations suggest a different origin for ML and probably a ML into illite and palygorskite transformation. Elprince et al. (1979) have suggested that paly could form at the expense of smectite in soils. Bonatti et al. (1968) and von Rad et al. (1972) have studied samples from the Deep Sea and suggested a montmorillonite into paly transformation.

As previously mentioned, the negative correlation between MLIS and illite suggests a MLIS into illite transformation. Burst (1969), in studying Gulf Coast sediments, noted a progressive modification in the structure of montmorillonite and its eventual disappearance with increasing burial depth. Powers (1967) considered the loss of montmorillonite with depth in Gulf Coast sediments as a conversion to illite by the substitution of Mg^{+2} for Al^{+3} in the silicate structure, with the consequent fixation of interlayer potassium. Perry et al. (1970) showed that the diagenetic reaction by which highly expandable illite/mont is transformed into illite/montmorillonite of lower expandability takes place by adsorption of potassium. Matter (1974) also suggested illite/montmorillonite into illite transformation since he observed a decrease in amounts of illite with concomitant increase of illite/montmorillonite and narrower illite peak width.

4. Origin of paly

Although a detrital origin is not unlikely for palygorskite,

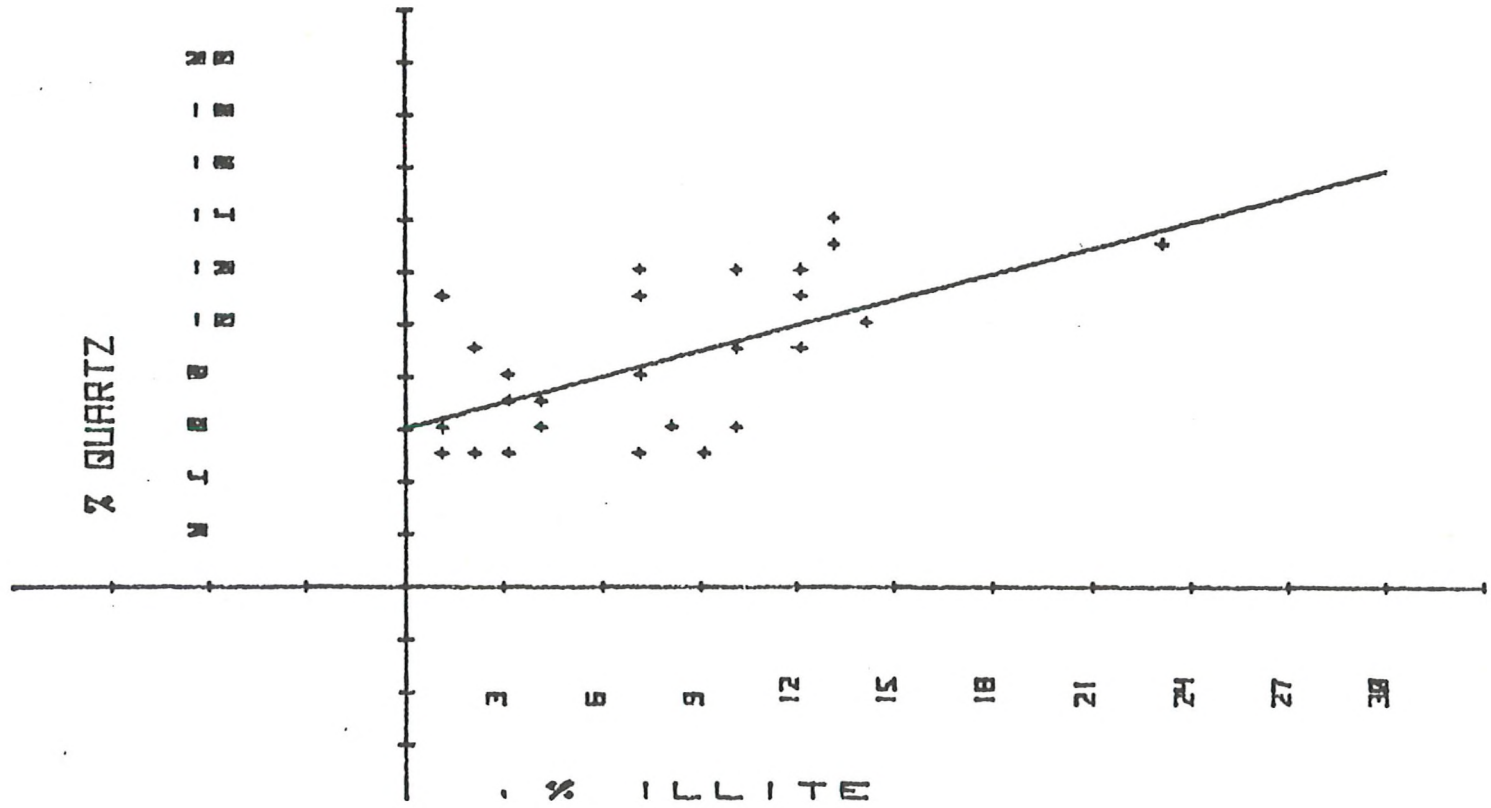

Fig.3-15. Correlation between quartz and illite in samples with no paly.

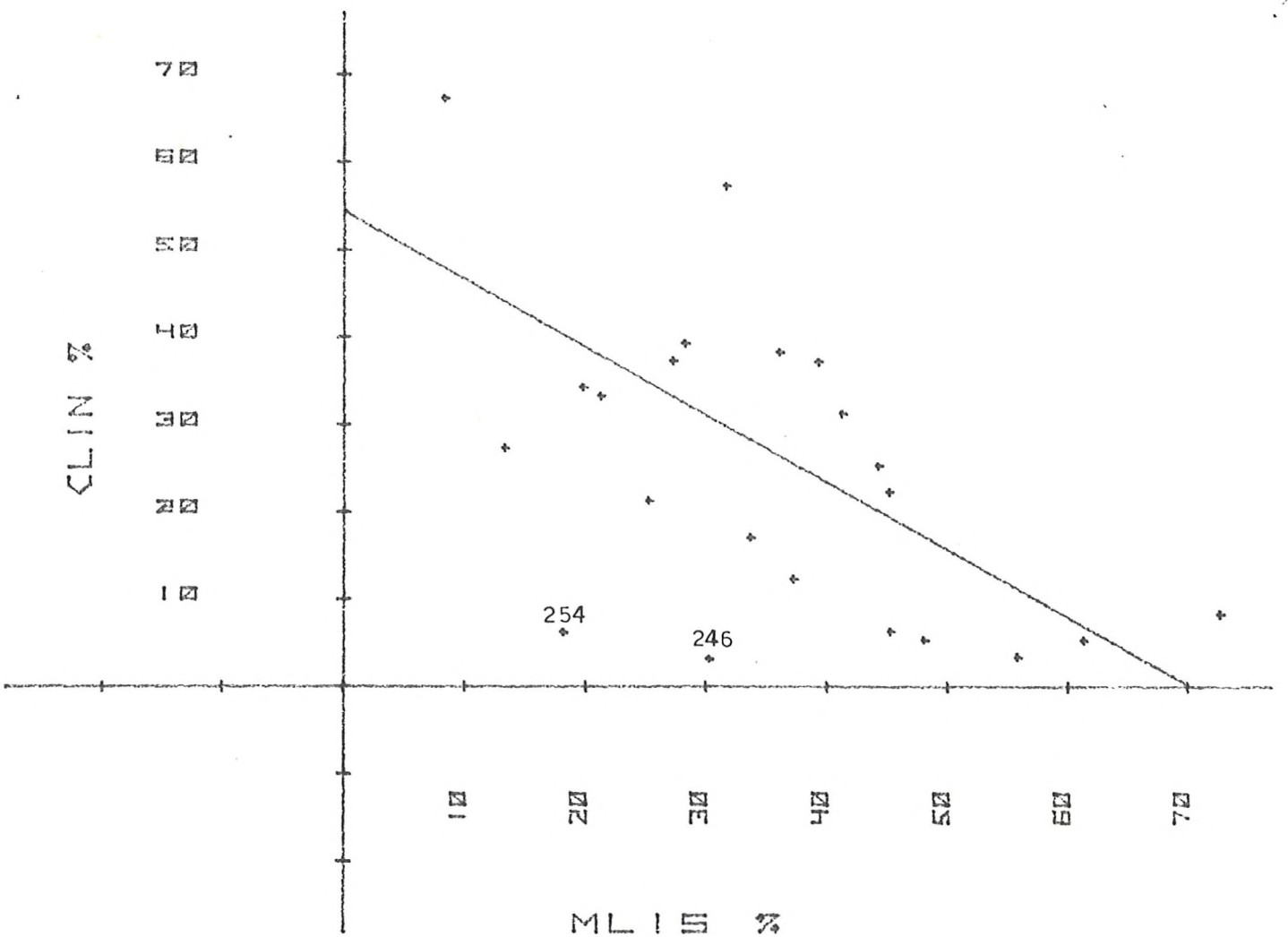

Fig 3-16. Correlation between MLIS and CLIN in zeolite-bearing samples.246 and 254 indicate samples with clin+phil in association.

several pieces of evidence indicate its authigenic origin in late Cretaceous to Eocene sediments:

a) remoteness of the sites of study from the lands rich in palygorskite;

b) presence of volcanic material and Mg-bearing minerals;

c) presence of hiatuses and/or slow sedimentation rates;

d) negative correlation with MLIS of detrital origin; and

e) negative relation with clinoptilolite.

The above evidence is observed at Sites 211, 212, 213, 215, 245, 248, 250 and 256, and thus a MLIS into palygorskite and palygorskite into clinoptilolite transformation is suggested. However, the remoteness from the land rich in palygorskite, and the existence of an hiatus seem to be the most important factors. Thus, since these factors were not observed at Site 221, a detrital origin was proposed for palygorskite at this site. The studied sediments from this site are of Miocene age, close to lands rich in palygorskite and no hiatuses exist in these sediments. Couture (1977a) and Donnelly et al. (quoted by Couture, 1977a) believe that the necessary Mg for palygorskite formation is derived from sea water during a sedimentary hiatus.

TABLE 3-1: Bulk Mineralogy

S.No.	Quartz	K-Feld	Plag	Clino	Phill	Clay	Calc	Dolo	Hali	Pyrite	Org C	B	Minor * Minerals
211/6/2	17	6	14			55			3		0·51	4·41	Ilm
211/13/1	11	2	6			57	12	1			0·70	10·3	Bar
211/14/1	9	3	12			59	8	3			0·24	5·76	Bar
212/15/2	10	2	9			62					0·36	16·64	Apa, Gib, Op-CT
212/15/3	9	3	7	5		52	4				0·08	19·92	Apa, Gib, Op-CT, Ilm
212/16/1	8	2	7			64					0·23	18·77	Gib Op-CT
212/16/2	9	1	5			66					0·31	18·69	Bar
212/17cc	12	3	5			54						26	
212/18/1	9		7			61						23	
212/18/2	5	1	5	22		51			1			15	Ilm, Hem, Op-CT
212/23/5	3	1	6	5		59	2				0·45	23·55	Go, Op-CT
212/27/1	7	1	6			64					0·21	21·79	Go, Gib, Op-CT, Ilm
212/27/5	7	2	6			64					0·22	20·80	
212/28/2	8	1	4			66					0·58	20·42	Go, Gib

Ilm = Ilmenite
Go = Goethite
Gib = Gibbsite
Bar = Barite
Op-CT = Opal-CT
Apa = Apatite
Hem = Hematite
Zir = Zircon
Gar = Garnet

B = 100 -(Qtz + Kf + Pf + Clin + Phill + Clay + Calc + Dolo + Halite + Pyrite + Org C)

B = amorphous material (biogenic silica, volcanic glass) + minor minerals + Opal-CT

* minor minerals were identified by SEM and/or XRD.

TABLE 3-1 contd.

S.No.	Quartz	K-Feld	Plag	Clino	Phill	Clay	Calc	Dolo	Hali	Pyrite	Org C	B	Minor Minerals
212/29/1	6	1	4	5		60					0·21	23·79	Go, Gib, Op-CT
212/35cc	9	2	3			64	14				0·32	7.68	Go, Gib, Apa
212/36cc	13	4	12			64					0·55	6·45	Go, Gib, Hem
212/37/1	14	3	10			47					0·16	25·84	
212/37cc	8	3	7	37		42					0·43	2·57	
212/38/1	7	1	6	33		46			1		0·09	5·91	Op-CT, Go, Hem
213/8/5	7		4		7	47			6		0·21	28·79	
213/9/4	5	3	7		7	57			5		0·25	15·75	
213/9cc	3	3			9	58			5		0·25	21·75	
213/10/3	5	3			12	64			6		0·25	9·75	
213/11/2	3	7			27	49			3		0·68	10·32	
213/11/5	6	5	9		15	46			2		1.24	15.76	Gib, Ilm, Apa, Hem
213/12/5	6	5	8		12	46			5		0·33	17·67	Apa, Bar, Gib
213/13/2	5	5	11		9	42			3		0·51	24·49	Bar, Hem, Apa

/contd.over

TABLE 3-1 contd.

S.No.	Quartz	K-Feld	Plag	Clino	Phill	Clay	Calc	Dolo	Hali	Pyrite	Org C	B	Minor Minerals
213/13/5	6	4	8		6	52			3		0·65	20·35	Hem, Gib, Apa,
213/14/3	5	6	11			59					0·48	18·52	
213/15/2	7	2	3			30	41	1	2		0·60	13·4	Apa
215/8/2	6	2	8			49			7		0·30	27·7	Apa
215/9/2	8					46			6		0·76	39·24	
216/24/4		2	3			10	67				0·78	17·22	
216/25/3	2	1	12			42	32				0·15	10·85	
216/30/3	2	3	18			18	9	3	2		1·08	43·92	Ilm, Apa, Gypsum
216/32/3	3	1	11			20	37	1	5		0·30	21·70	Ilm,
216/34/1				27		15	48		1	1	0.56	7·44	Go, Gypsum
221/14/2	18		9			38			1		0·46	33·54	
221/14/5	15	3	11			50		1	1		0·45	18·55	Gib, Ilm

/contd.over

TABLE 3-1 contd.

S.No.	Quartz	K-Feld	Plag	Clino	Phill	Clay	Calc	Dolo	Hali	Pyrite	Org C	B	Minor Minerals
221/15/2	11		12			52					0·47	24·53	
221/15/4	11	1	10			66					0·41	11·59	Apa, Gib
221/16/2	4	1	7			32	2		1		0·14	52·86	
235/9/6	6	2	8			61	3	1			1·12	17·88	Hem
236/16/5	4	2	8			72					0·45	13·55	
236/18/3	5	2	9			67	1	1	1		0·19	13·81	Go
236/19/2	5	2	6	5		50			2		0·35	29·65	Gib, Hem
239/1/1	11	3	12		6	48	10	2	5		0·58	2·42	Zir, Bar
239/4/3	11	5	14		7	42		2	4		0·85	14·15	Bar, Zir, Gib
239/9/3	6	3	10		4	48			2		0·34	26·66	Go, Gib
239/11/3	9	3	10		11	53		2				12	Go
239/13/4	8	4	7		5	65			1		0·30	9·7	Zir, Bar,

/contd.over

TABLE 3-1 contd.

S.No.	Quartz	K-Feld	Plag	Clino	Phill	Clay	Calc	Dolo	Hali	Pyrite	Org C	B	Minor Minerals
239/16/3	9	4	9			66					0·25	11·75	Zir, Gib
239/18/2	12	4	10		3	52		1			0.37	17.63	Go
240A/2/1	75	7	9			8					0·33	0·67	Gar
240/3/3	6	4	9			57			2		0·45	21·55	Ilm, Gib, Go
240/5/1	43	7	11			32	3		1		0·32	2·68	
245/1/3	8	2	10			44			5			31	Gib, Go, Hem
245/5/3	11	3	9			57	8		2		0·47	9·53	Ilm, Gib
245A/2/6	12	2	9			54			2		0·30	20·70	Gib, Hem
245A/6/2	12	4	8			60			1		0·33	14·67	Bar, Apa, Hem, Go, Gib
246/10/2	4	11	15	2	9	22	28		2		0·29	6·71	
248/10/2	10	3	11			56					0·52	19.48	Op-CT

/contd.over

TABLE 3-1 contd.

S.No.	Quartz	K-Feld	Plag	Clino	Phill	Clay	Calc	Dolo	Hali	Pyrite	Org C	B	Minor Minerals
248/11cc	12	2	10			44				1	0·42	30.58	Op-CT, Gib, Ilm
248/12/3	13	3	5	5		61			1	1	0.40	10.60	Op-CT
248/14/1	12	4	11			52					0·22	20·78	Ilm, Zir, Bar, Op-CT
248/14/6	9	3	9			60					0·42	18·58	Gib
250A/3/1	14	2	7			51			3		1·02	21·98	Go
250A/6/3	12	2	9			69			2		0·43	5·57	Op-CT
250A/11/2	14	1	7			72					0·55	5·45	
250A/15cc	17	9	47			17	3	7			0·31	-	
250A/22/3	7		8	16		58	4				1·28	5·72	
254/25/2	3	8	10	5	13	15	11		2	3	1·26	28·74	Bar, Gypsum, Gib, Ilm, Olivine
254/26CC	7	2	8	12		37		1	2	2	0·84	28·16	Gypsum, Gib, Ilm
254/27/3	5	1	7	21		25			2	1	0·48	37·52	Ilm, Anatase, Go
254/28cc	4	3	5			60				1	0·48	26·52	Apa, Gypsum, Ilm

/contd.over

TABLE 3-1 contd.

S.No.	Quartz	K-Feld	Plag	Clino	Phill	Clay	Calc	Dolo	Hali	Pyrite	Org C	B	Minor Minerals
256/2/3	11	3	9			45			3		0·43	28·57	
256/4/5	5		4			54			2		0·32	34·68	Go, Gib, Op-CT
256/6/3	7	2		27		35			1		0·24	27·76	Op-CT
256/7cc	8	1	3	34		43			1		0·32	9·68	Op-CT
256/8/4	3	5		21		37	12	1			0·54	20·46	Op-CT, Apa
257/2cc	10	2	5	6		60			5		0·35	11·65	Go, Op-CT
257/4/3	5	2	6	39		31			3		0·30	13·70	
257/5/2	7	2	6	31		44			2		0·15	11·85	Go, Op-CT
258/14/1	5			67		13					0·41	14·6	Op-CT
258/15/1	9			5		32	27				0·98	26·02	Op-CT
258/16cc	3	2	3			67				1	0·55	23·45	Op-CT, Gib
258/17/2	2	1	2	37		47	2				0·86	8·14	Op-CT
258/22/4	18	7	3			54	3				1·15	13·85	
258/25cc	7		2	35		47	5				1·15	2·85	Go, Gib, Apa, Op-CT, Ilm

TABLE 3-2: Clay Mineralogy

Sample No.	Percent.of expandable layer (E)	MLIS	Illite	Kaolinite	Chlorite	Palygorskite
211/6/2	70	98	1	1		
211/13/1	49	40	25	3		32
211/14/1	45	13	52	1		34
212/15/2	51	54	28	10	5	2
212/16/1	58	74	11	15		
212/17cc	43	73	22	5		
212/18/1	70	78	21	1		
212/18/2	57	88	9	1		2
212/23/5	70	91	9			
212/27/1	57	51	27	13	4	5
212/27/5	45	70	6	24		
212/28/2	60	82	5	13		
212/29/1	43	78	3	19		
212/35cc	76	73	19	8		
212/36cc	49	43	36	15	6	
212/37/1	51	83	10	3		4
212/37cc	39	65	27			8
212/38/1	45	45	35			20
213/8/5	49	83	8	3	5	
213/9/4	69	96	2	2		
213/9cc	64	92	4	4		
213/10/3	77	90	6	4		
213/11/2	69	89	6	5		
213/11/5	64	84	10	6		
213/12/5	43	77	18	5		
213/13/2	57	74	22	4		

/contd.over

TABLE 3-2 contd.

Sample No.	Percent.of expandable layer (E)	MLIS	Illite	Kaolinite	Chlorite	Palygorskite
213/13/5	53	74	20	4		2
213/14/3	61	77	14	2	2	5
213/15/2	59	83	11	6		
215/8/2	74	91	6	3		1
215/9/2	48	23	42			33
216/24/4	79	100				
216/25/3	87	100				
216/30/3	58	100				
216/32/3	69	100				
216/34/1	85	100				
221/14/2	41	38	37	3	9	13
221/15/2	41	49	27	4	4	16
221/15/4	43	58	25	4	4	9
221/16/2	55	83	10	2	3	2
236/16/5	56	83	13	3		1
236/18/3	59	87	11	2		
236/19/2	57	73	21	6		
239/1/1	48	74	10	16		
239/4/3	53	91	3	6		
239/9/3	64	88	2	9		1
239/11/3	57	73	4	23		
239/13/4	68	89	4	7		
239/16/3	76	83	15	2		
239/18/2	50	82	13	4		1

/contd.over

TABLE 3-2 contd.

Sample No.	Percent.of expandable layer (E)	MLIS	Illite	Kaolinite	Chlorite	Palygorskite
240A/2/1	62	79	14	7		
240/3/3	49	73	17	10		1
240/5/1	64	87	5	7		
245/1/3	49	67	24	2	2	5
245/5/3	41	60	25	3	3	9
245A/2/6	40	54	31	9		6
245A/6/2	39	60	28	4	3	5
246/10/2	69	96	1	3		
248/10/2	70	72	18			10
248/11cc	64	76	24			
248/12/3	65	100				
248/14/1	43	38	44	3		15
248/14/6	49	57	27	3	3	10
250A/3/1	53	75	14	8		3
250A/6/3	49	78	15	7		
250A/11/2	50	76	19	5		
250A/15cc	67	88	10	2		
250A/22/3	39	55	32			13
254/25/2	85	100				
254/26cc	82	100				
254/27/3	86	100				
254/28cc	70	98		2		
256/2/3	62	69	19	12		
256/4/5	40	47	16	37		

/contd.over

TABLE 3-2 contd.

Sample No.	Percent.of expandable layer (E)	MLIS	Illite	Kaolinite	Chlorite	Palygorskite
256/6/3	45	38	14			48
256/7cc	42	61	32			7
256/8/4	74	100	Tr			
257/2cc	63	74	13	13		
257/4/3	70	89	11			
257/5/2	70	93	5	2		
258/14/1	65	58	42			
258/15/1	84	92	5	3		
258/16cc	42	24		42	34	
258/17/2	72	74	6	20		
258/22/4	93	98		2		
258/25cc	73	78	11	11		

CHAPTER IV

GEOCHEMICAL STUDIES OF THE WHOLE ROCK

General Introduction

Table 4-1 presents the elemental contents of each sample on an absolute basis. The values given for trace element concentrations have been rounded off to a whole number.

Ninety samples representing the sediments cored at the eighteen sites of Legs 22, 23, 24, 25 and 26 were analysed for 28 elements (major and trace). The purpose of this study was to clarify the probable origins of the elements and thereby the origin of the sediments.

Al, Ti, Fe, Mn and Cr are of significant importance in the identification of the sediment source. Al has usually been used as an indicator of the amount of terrigenous debris in the sediments, since it is largely located in detrital minerals in deep sea sediments (Arrhenius, 1952; Landergren, 1964). Goldberg et al.(1958) have pointed out that in those sediments containing relatively high contents of titanium (i.e. > 0•7% Ti) and Cr (i.e.> 100 ppm), Ti is almost invariably associated with basaltic debris. Bostrom et al. (1969, 1972) and Bostrom (1970) have found that metalliferous sediments at some active centres of sea floor spreading are abnormally poor in aluminium and titanium, and rich in iron and manganese. Thus, to identify the origin of the elements plots of Fe/Ti vs Al/(Al+Fe+Mn) (Fig.4-1 a-e) (Bostrom et al., 1969, 1970, 1972), Cr vs TiO_2 (Fig.4-2) (Couture, 1977b) and Ti vs Al (Fig.4-3) (Stonecipher, 1978; Bostrom et al., 1972) were used.

There are weak points in using the Fe/Ti vs Al/(Al+Fe+Mn) and Ti vs Al plots. For example, the presence of Al and Fe in hydroxide forms (gibbsite and goethite) instead of alumino-silicate can result in wrong mixing composition, as can be observed at Site 212 (212/23/5, 35cc and 36cc). However, these models have been used successfully in combination with Cr/TiO_2 plot in the present study.

A. Origin of Al, Ti, Fe and Mn

The relationship Fe/Ti versus Al/(Al+Fe+Mn)(Fig.4-1,a-e) has been used to detect whether the sediments contain much continental or oceanic detritus, or whether it is largely of submarine exhalative origin (Bostrom, 1970; Bostrom et al., 1972).

Fig.4-1a-e: Relationships between Fe/Ti versus Al/(Al+Fe+Mn). The curves were produced when an extremely active ridge sediment (VM) was mixed at different proportions with terrigenous matter, tholeiitic and alkali basalts.

X = samples from Site 211
\+ = " " Site 212
✳ = " " Site 213
⁜ = " " Site 215
○ = " " Site 221
⌀ = " " Site 235
⊙ = " " Site 236
■ = " " Site 239
△ = " " Site 240
◇ = " " Site 245
▨ = " " Site 246
□ = " " Site 248
◪ = " " Site 250
● = " " Site 254
⅄ = " " Site 256
▲ = " " Site 257
★ = " " Site 258
• = " " Site 216

ΘI = 25% shale + 75% c.c (100% granite)

ΘII = 50% shale + 50% c.c (80% granite + 20% basalt)

ΘIII = 50% shale + 50% c.c (50% granite + 50% basalt)

ΘIV = 80% tholeiitic basalt + 20% TM [20% shale + 80% c.c (80% basalt + 20% granite)]

ΘV = 80% alkali basalt + 20% tholeiitic basalt.

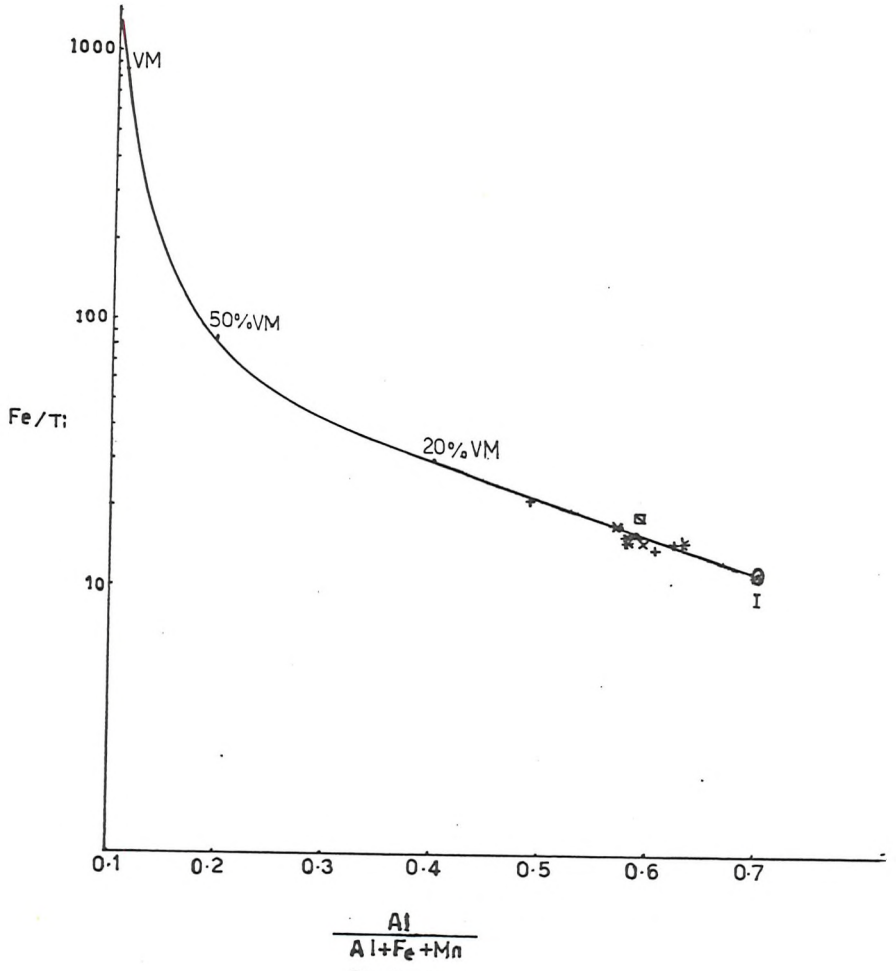

Fig.4-1a

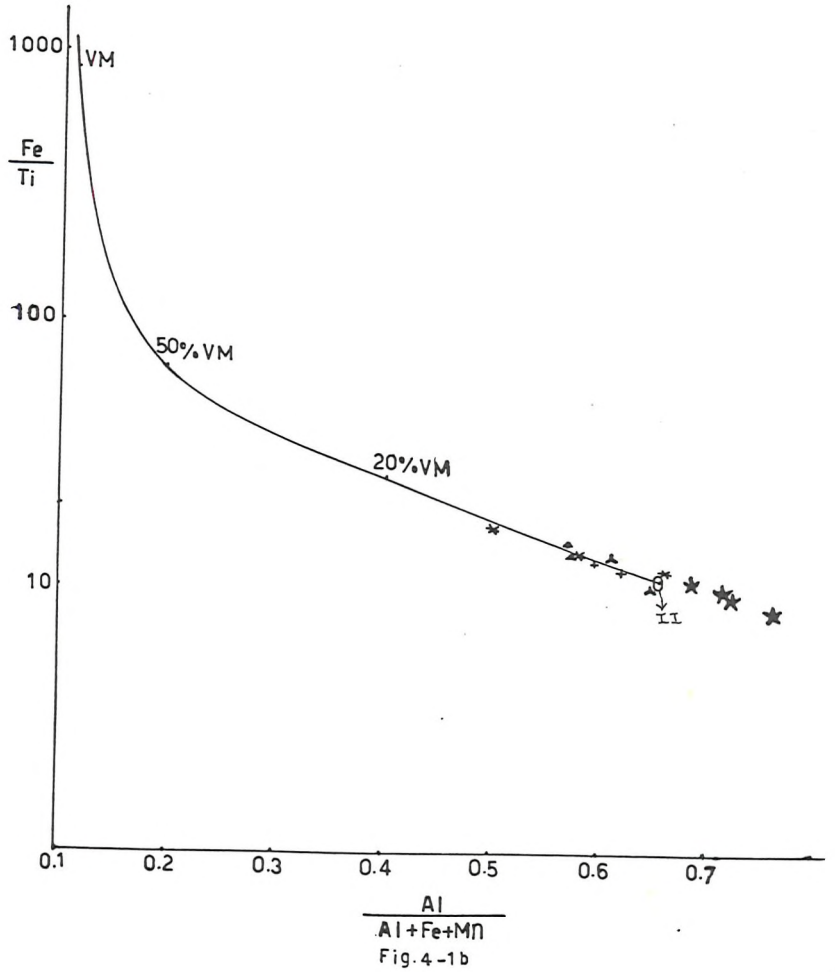

Fig.4-1b

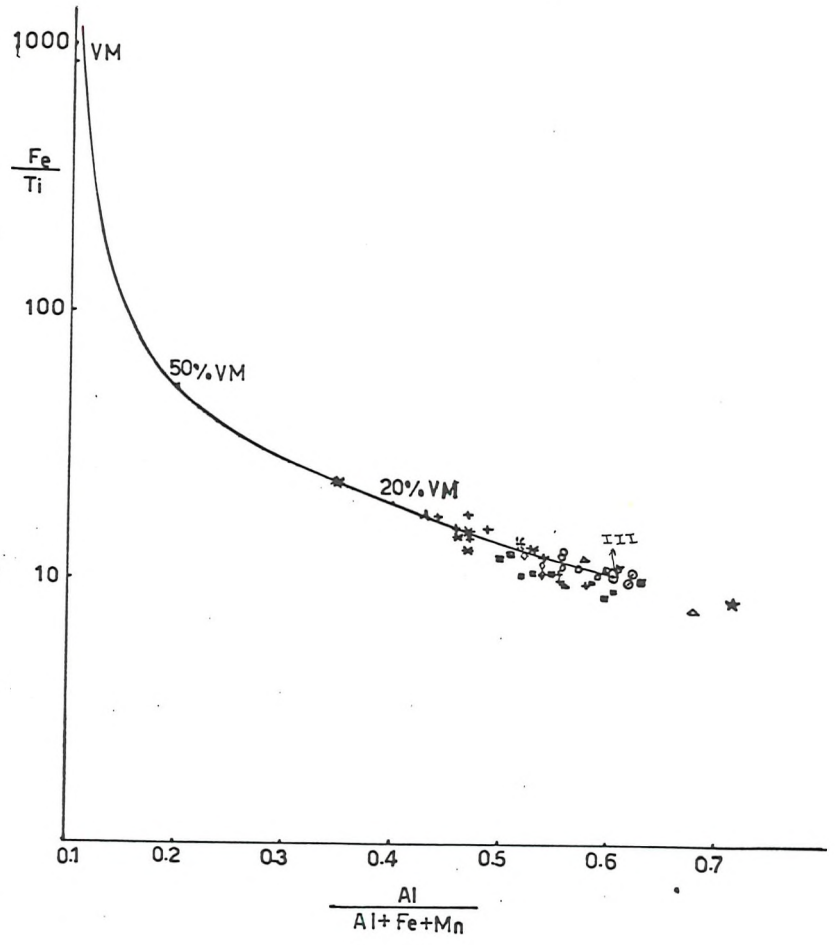

Fig. 4-1c

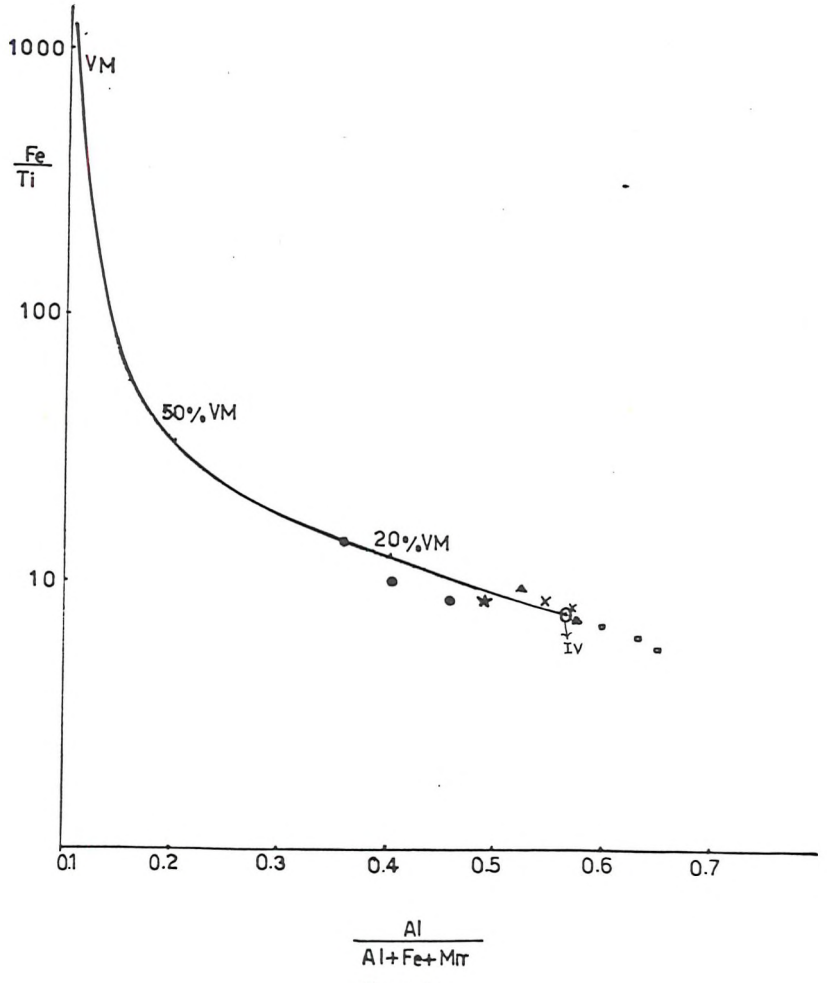

Fig. 4-1d

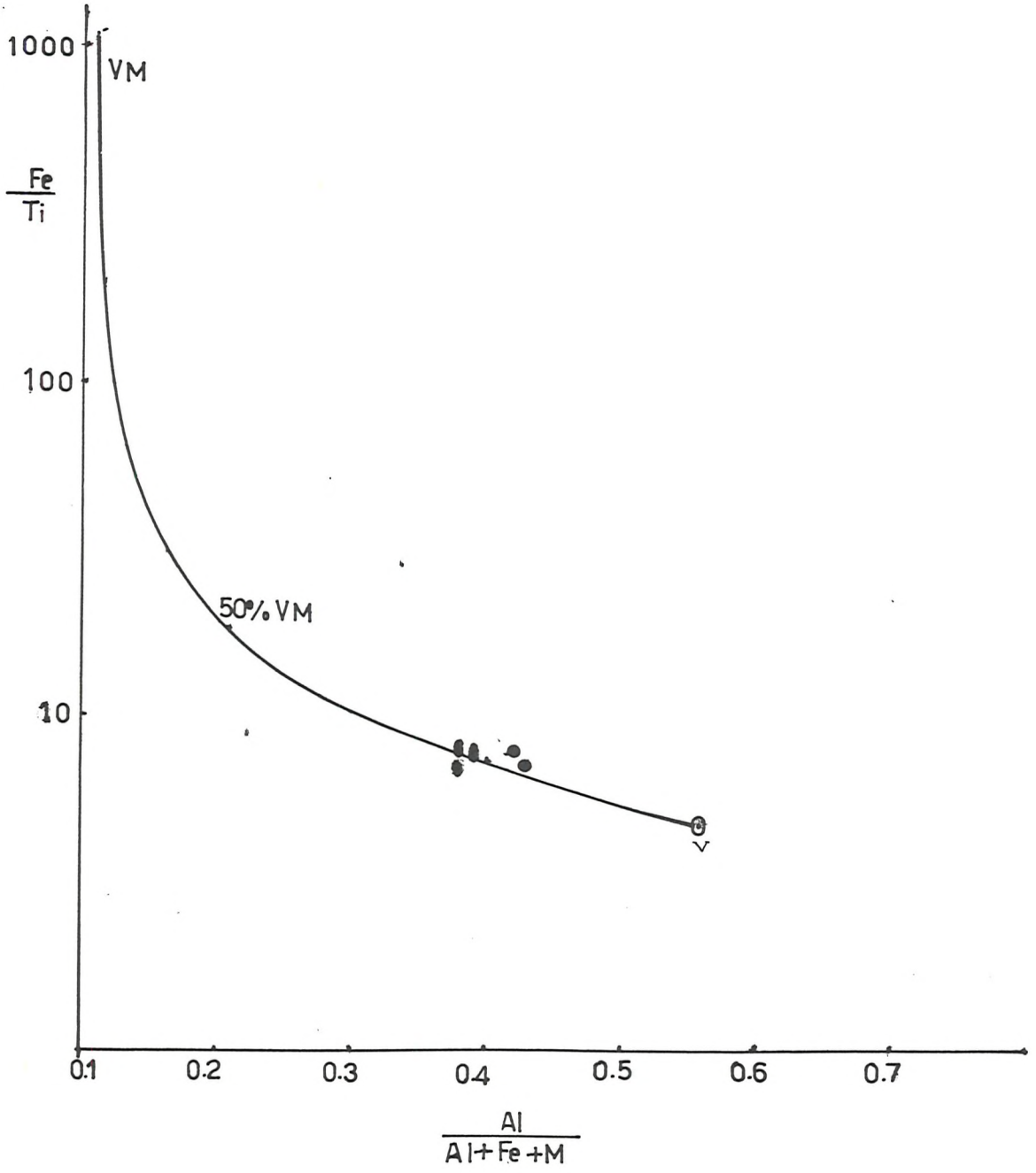

Fig. 4-1e

Fig.4-2: Plot of Cr (ppm) vs. TiO_2 % for bulk samples. The following signs represent average Cr/TiO_2 ratios for various igneous and sedimentary rock types.

⊕ = shale and normal terrigenous matter

◊ = granite

⊖ = alkali basalt

◒ = basalt

⊙ = tholeiitic basalt

● = volcanic matter (VM)

The rest of the symbols same as in Figure 4-1.

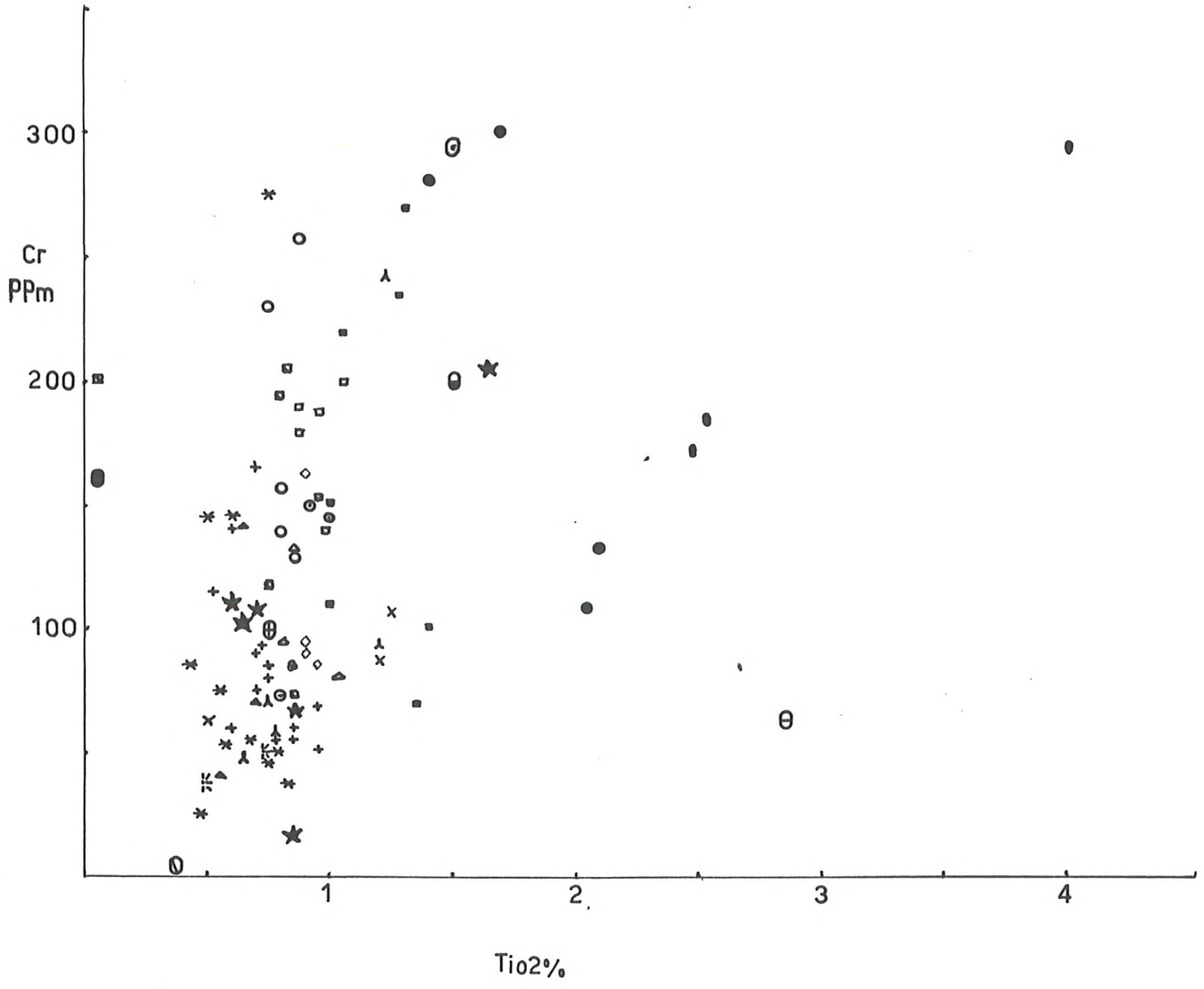
300
200
100
Cr
PPm
1
2
3
4
Tio2%

Fig.4-3: Plot of Ti vs. Al (weight % of the elements) for bulk samples. The plotted curves represent Ti/Al ratios for various average igneous and sedimentary rock types. Average alkali and tholeiite basalt - Engel et al. (1965); rhyodacite - Mauna Kea - Engel and Engel (1970); average shale - Clark (1924); average rhyolite - Clark (1966). The signs are the same as in Figure 4-1.

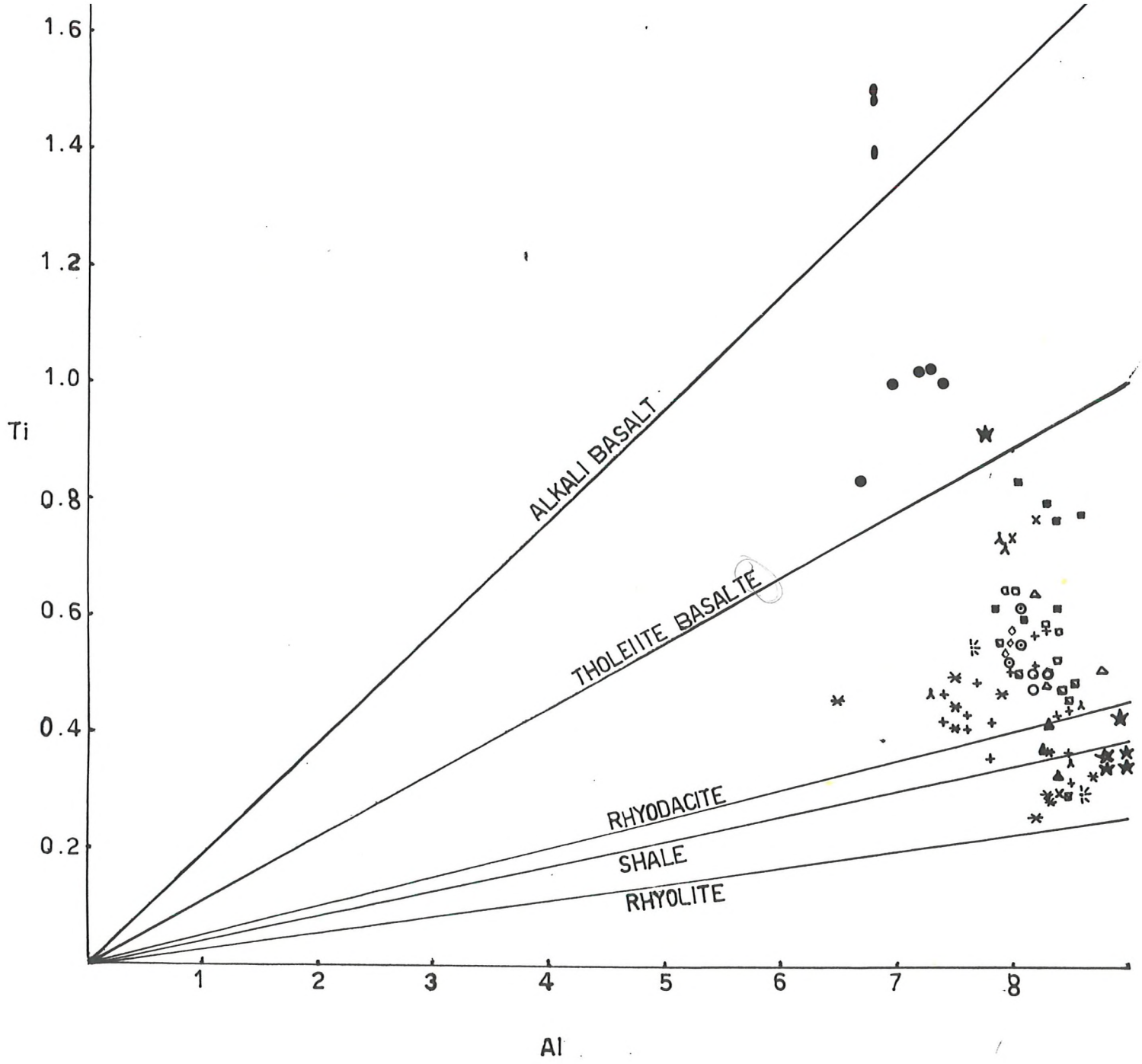
1.6
1.4
1.2
1.0
0.8
0.6
0.4
0.2
Ti
ALKALI BASALT
THOLEIITE BASALTE
RHYODACITE
SHALE
RHYOLITE
1
2
3
4
5
6
7
8
Al

Terrigenous and biogenous matter, as well as lithogenous constituents derived from basaltic debris, authigenic constituents formed from sea water and sediments derived from volcanic emanations occur in the sediments of the oceans. Bostrom et al. (1973) believe that sediments resulting from volcanic emanations form rapidly, and therefore must be of local origin. These sediments are found extensively on spreading ridges (Bostrom et al., 1969, 1971, 1972).

Using average values for Fe, Ti, Al and Mn in continental crust, oceanic crust and volcanic material (active ridge sediments mainly from the East Pacific Rise Deposits = VM) (Table 4-2), the above authors have derived a graph of the relation Fe/Ti versus Al/(Al+Fe+Mn) in any mixture of volcanic sediments with the above-mentioned sources.

Bostrom et al. (1976) have assumed that terrigenous matter (TM), which is weathered continental matter, consists of 75% average shale and 25% of average continental crust. The continental crust, according to Krauskopf (1967), consists of 50% average basalt + 50% average granite. These authors based their assumptions on the observation that usually the surface of the continents is covered up to 75% by sedimentary deposits having more or less the average shale composition.

In the present study, the plot of Fe/Ti vs. Al/(Al+Fe+Mn) showed five curves, which represented the existence of five types of sediment composition among 90 samples (Table 4-3a). Table 4-3b presents the set of samples which gather around five suggested curves. Each curve was generated by mixing volcanic matter with terrigenous matter in different proportions. Terrigenous matter composition differed from the assumed composition by Bostrom (op.cit.). The five recognised types are as follows:

1. Type I (Fig.4-1a)

This group was generated by the mixing of TM with volcanic matter in different proportions. TM consists of 25% shale + 75% continental crust (c.c), where c.c is of 100% granite. The composition of the mixture is presented in Table 4-3a. The samples belonging to this group show low Ti/Al ratios (Table 4-4) close to rhyolite or rhyodacite (Fig.4-3) except Sample 257/4/3, which is close to shale. However, Cr versus TiO_2 plot (Fig.4-2) shows its proximity to rhyolite. Since samples from Site 212 contain gibbsite, the Fe/Ti versus Al/(Al+Fe+Mn) is probably not

truly representative of these samples. This is also confirmed by Ti/Al and Cr/TiO_2 plots, which place them far from rhyolite and close to shale. Sediments from Sites 211, 215 and 213 are of the late Miocene or younger and, as previously mentioned, they receive their terrigenous input from the silicic Indonesian volcanics which may have been a source since the late Miocene (Kolla, 1974). Sample 213/10/3 is of middle Miocene age, and 213/11/2 is of unknown age, so the chemistry suggests that the silicic volcanic activity may have started earlier than the late Miocene.

Sample 246/10/2 could have received its TM from Madagascar, since granitic rocks have been observed in Madagascar (Besairie, 1972, quoted by Vallier, 1974), and also Eocene alkali intrusive volcanism of gabbro, syenite and granite occurred in northern Madagascar.

2. Type II (Fig.4-1b)

This group was generated by the mixing of TM with volcanic matter (VM) where TM was a mixture of 50% shale and 50% c.c., and c.c was of 80% granite + 20% basalt. The Ti/Al ratios were between 0·04 and 0·05 and most of the samples plotted close to either rhyodacite or shale. Cr/TiO_2 plot also shows that most of them are close to the average TM, shale or between shale and rhyolite. Therefore, all three figures suggest a composition of shale + granite with a small contribution of basalt.

The sediments are all from the eastern sites. Most of them are of Cretaceous age, except samples from Site 213, which are of the late Miocene. According to Luyendyk et al. (1974), much of the Albian and older sediments of Site 258 were apparently derived from the erosion of basaltic volcanic rocks. They believe that these volcanic sediments were the result of volcanic activity during the early Cretaceous along the zone of incipient rifting between Australia and Antarctica; they also could be derived from the Perth Basin. Basalts of early Cretaceous age are reported by Brown et al. (1968) from the Perth Basin. However, the above suggestion was made from the tectonic point of view for sediments of the Albian and older, whereas the chemistry of the sediments in the present study, which were of the middle Albian and younger, showed that granite + shale with small amount of basalt have contributed to Site 258, and this was also observed at Sites 256 and 257. Samples from Site 212

(cores 35cc and 36cc) contained gibbsite and goethite, which could mean that the suggested mixture is not their true chemistry. Therefore, it is likely that the sediments of Type II were derived from Australia, since granitic rocks of the Palaeozoic were reported from Australia by Brown et al. (1968). Kolla et al. (1973b) found that the clinoptilolite-rich areas are adjacent to both Africa and Australia, and suggested that the initial rifting may have produced a more silicic volcanism because of proximity to continental crust. According to them the circum-Pacific volcanism tends to be more silicic than that in the central basins. They further refer to Daly (1925) and Peterson et al. (1962), who have shown the possibility of local silicic volcanism in an otherwise dominantly silica-poor volcanic region. Therefore, they suggested that such a situation may have existed during the Cretaceous - Eocene times in the Indian Ocean, and silicic volcanic material may have been locally supplied to the Agulhas and Naturaliste Plateau areas. However, Samples 258/22/4 and 258/16cc showed a higher basic volcanic material contribution, which could mean that the rifting between Australia and Antarctica had an intermittent effect and the above samples could receive basaltic contribution from the surrounding lands.

Sediments of the late Miocene at Site 213 seem to have received lower amounts of silicic igneous rocks and more shale from the Indonesian island arc compared with the sediments of the earlier age at this site (i.e. those which fall in Type I). By the Oligocene, India and Australia became part of the same plate and moved northward with that plate. At this time, Site 213 became fused at latitude 30°S and moved northwards at roughly $0{\cdot}5^{\circ}$ per million years (Sclater et al., 1974a). Therefore, the influence of the Indonesian Island arc has probably decreased since the late Miocene, as this site was moving northward, increasing the distance from that source.

3. Type III (Fig.4-1c)

The terrigenous matter is a mixture of 50% shale + 50% c.c, where c.c is of normal composition as suggested by Krauskopf (1967) (i.e. 50% granite + 50% basalt). The Ti/Al diagram displays the sediments between rhyodacite and tholeiitic basalt but close to rhyodacite. In the Cr/TiO_2 plot, the sediments are situated between c.c (50% granite + 50% basalt), TM, shale and rhyolite, but closer to c.c.

Most of the sediments are of Eocene or younger, except samples from cores 37/1, 37cc and 38/1 of Site 212, which are of unknown age. However, these sediments could be of early or middle Cretaceous, since a) the overlying sediments (cores 35cc upwards) are of upper Cretaceous, and b) they show more basaltic contribution than the Cretaceous sediments of the other sites (258, 257 and 256), which are of mid-Albian to late Cretaceous. The volcanic episode in the Perth Basin occurred in the mid-Cretaceous and probably contributed to the above cores (37/1, 37cc and 38/1). These sediments (212/37/1 downward) could also have received their basaltic contribution from the basaltic basement. In the period between early Eocene and early-middle Miocene, before the activity of the Indonesian volcanics, the sediments from Site 212 (Samples 212/18/2 upwards), 213 (213/11/5 downward) and 215/9/2 received higher basaltic material compared with the time of activity of the Indonesian arc. Site 215 has probably received its contribution from India. India crossed the Equator in the Miocene, and so must have been close to Site 215 during the Eocene. The TM contribution from Australia is also possible to Sites 212 and 213. During the Eocene, the separation between Australia and Antarctica occurred, and thus Australia was probably closer to Sites 212 and 213.

The western sites received their TM from the surrounding lands; Sites 239, 245 and 246 from Madagascar. Sites 248 and 250 received their TM from Madagascar and south-east Africa. The Seychelles and East Africa have provided TM to Sites 240 and 236. Site 221 was under the control of India and north Africa. Matter (1974) and Girdley et al.(1974) suggested the above areas as the sources for TM based on proximity and physiographic conditions necessary for sediment transport to each site. Basaltic and granitic rocks have been observed in the above-mentioned provenances. McElhinny (1970) has observed two recorded major basaltic trap rock series in India, one of Albian age (the Rajmahal Trap Basalt) and the Deccan Trap Basalt of Palaeocene age.

In the extreme south of Madagascar, the massif Androy is made up of alternations of basalt and rhyolite. On the south-eastern coast, a wide band of basalt and glassy andesite, with some rhyolite and rhyodacite, crops out for a length of about 500 km (Besairie, 1972 and 1973, quoted by Vallier, 1974).

The larger islands of the Seychelles group are granitic. The granitic rocks contain olivine-bearing basaltic dykes and sills, as well as andalusite-bearing hornfels roof pendants (Girdley et al., 1974).

Flores (1970) has discovered basalt, rhyolites and tuffs of Jurassic age in south-eastern Africa. In East Africa, most of the rocks are metamorphic (Girdley et al., 1974).

4. Type IV (Fig.4-1d)

This type was generated by mixing 80% tholeiitic basalt and 20% TM, where TM consists of 20% shale and 80% c.c. C.c contains 80% basalt + 20% granite. Samples 211/13/1 and 211/14/1 are of the Campanian age. The Ti/Al plot places them close to tholeiitic basalt, although in the Cr/TiO_2 plot they are placed close to shale and TM. These samples overlie the basaltic basement and probably received a contribution from the basement. Samples 256/7cc and 256/8/4 are also of the Cretaceous and behave like samples at Site 211 (cores 13/1 and 14/1). They are placed close to tholeiitic basalt in the Ti/Al plot. These sediments could also receive their tholeiitic basalt contribution from the basement. Samples of Site 239 are of the Oligocene and younger age, and probably receive tholeiitic basalt from the Mid-Indian Ocean Ridge (MIOR). During the Oligocene, the MIOR was becoming active in its new configuration (Davies et al., 1976). Middle Miocene to Quaternary sediments at Sites 239 and 235 are related to volcanism on nearby seamounts and islands in the Mascarene Island Group.

Samples of Site 216 (cores 24/4, 25/3 and 34/1) are of Cretaceous (Maastrichtian) and could not receive their tholeiitic content from the basement of any place on the Ninetyeast Ridge, since the basaltic sediments of the Ninetyeast Ridge are of the St.Paul and Amsterdam Islands type (alkaline). These sediments could have received a contribution from somewhere near the Ridge, as the high sand and silt content suggests short distance transportation. This source could be the south-eastern branch of the MIOR.

5. Type V (Fig. 4.1e)

The curve is generated by mixing 80% alkali basalt and 20% tholeiitic basalt. Cr/TiO_2 and Ti/Al plots also display them close to

alkali and tholeiitic basalts. Sediments of Site 216 are of the Cretaceous, whereas those at Site 254 are of the mid-Tertiary age. According to Chester et al. (1976) oceanic basalts are divided into two principal groups or suites: the tholeiitic basalts and the alkali basalts. Both tholeiitic and alkali basalts are common on oceanic islands, but those dredged from the deep-sea floor are largely tholeiitic in character. von der Borch et al. (1974) and Subbarao et al. (1979) have observed a basaltic basement at Site 216, with a composition similar to the suite from St. Paul and New Amsterdam Islands, and significantly different from the MIOR basalts. The sediments of Sites 216 and 254 show a high amount of sand and silt, which suggests a short distance of transport. Therefore, the sediments of these sites were most probably derived from the Ridge itself.

6. Summary

The relationships Fe/Ti versus Al/(Al+Fe+Mn), Cr/TiO_2 and Ti/Al showed that:

a) there are tholeiitic and alkali basalts, terrigenous and volcanic matter contributions to the sediments;

b) most of the sediments show $< 20\%$ volcanic matter contribution;

c) the average composition of contributed TM differs from the suggested average value by Bostrom et al. (1976);

d) TM consists of basalt, granite and shale;

e) a basaltic and granitic contribution from the surrounding land is possible (India, Australia and eastern Africa).

In summary, early/middle Cretaceous sediments of Site 212 (37/1, 37cc and 38/1) received basaltic and granitic contributions from both the Perth Basin and Australia. Perth Basin volcanic activity was in the mid-Cretaceous. In the late Cretaceous, sediments from Sites 258 and 257 received more granitic and less basaltic (compared with the early/middle Cretaceous), which coincides with the initiation of the rift between Australia and Antarctica. The rifting had an intermittent effect on the sediments. Sediments of the late Cretaceous at Site 211 (cores 14/1 and 13/1) and Site 256 (cores 7cc and 8/4) have received a tholeiitic contribution from the basement. Eocene to mid-Miocene sediments of Sites 212 and 213 received a contribution from Australia, with

basalt becoming more dominant. Eocene is the time when Australia separated from Antarctica.

Samples 215/9/2 could receive TM from India, since India still had not crossed the Equator and so must have been close to this site. The sediments from the western sites of the Eocene to middle Miocene also received basaltic and granitic contributions from the surrounding lands. Vallier (1974) also believes that volcanogenic sediments from most sites in the western Indian Ocean are related to volcanism on land-masses, to volcanic activity on oceanic islands, and to major events in spreading histories. According to him, late Companian extrusive volcanism occurred in the eastern and southern part of Madagascar. In the extreme south, the massif at Androy is made up of alterations of basalt and rhyolite. On the south-eastern coast, a wide band of basalt, glassy andesite and rhyolite crops out. Volcanism also occurred in India (Raj mahal Traps, 100-105 m.y). Palaeocene volcanic activity occurred in India (Deccan Trap). Eocene alkali intrusives of gabbro, syenite and granite occurred in northern Madagascar. Late Eocene volcanism composed of syenites, quartz and microgranite occurred in islands north-west of the main island of Mahé (Seychelles Islands) (Upton, 1982). Middle Miocene to Quaternary volcanism occurred on sea-mounts and islands in the Mascarene Island Groups, Madagascar and the Comoro Islands (Vallier, 1974).

Girdley et al. (1974) examined the heavy and light minerals from Sites 239, 240, 246 and 248, and suggested that the heavy and light mineral suites were very indicative of complex provenances that include acidic plutonic, pegmatitic, metamorphic and volcanic pyroclastic or epiclastic contributions from East Africa and Madagascar.

Middle Miocene sediments of Sites 211 (core 6/2), 213 (cores 11/2, 10/2 and 9cc) and 215 (core 8/2) show silicic volcanic material due to Indonesian Island volcanic activity around this age. The sediments of the Miocene and Pliocene age of Sites 239 and 235 received tholeiitic basalt from nearby seamounts and islands.

Most of the sediments on the Ninetyeast Ridge from Sites 216 (Cretaceous) and 254 (mid-Tertiary) received contributions from the Ridge itself (alkali basalt). However, Samples 216/24/4, 216/25/3 and 216/34/1 received tholeiitic basalt from the surrounding area.

B. Origin of Trace Constituents and Some Major Elements

Log-log geochemical graphs, showing the relationships between the composition of sediment sources and the present study sediments, were used in order to explain the origin of trace elements and some major elements. This model was used by Bostrom et al. (1976). They found that neither biological matter (BM) nor terrigenous matter (TM) are sufficient sources of Mn, Fe, Ba, Ni, B and Cu. According to them, accumulation-rate data for Al, and Ti for the sediments from the spreading centres, demonstrate that TM must be a totally insufficient source for most trace constituents, since TM is poor in trace constituents. BM, on the other hand, is fairly rich in trace elements relative to Al and Ti. Therefore, they suggested a mixture of BM and volcanic matter (VM, which approaches the East Pacific Ridge, EPR , in composition). However, TM and BM are the most important sources for Si, Al, Ti, Zr, and Ca, and for most trace elements far from spreading centres. They also found that outside the emanation zone, dissolved matter and solutions play but a small role in the origin of deep-sea sediments.

Chester et al. (1976) have pointed out one important drawback to the acceptance of these models. They believe that little is known of the fate of elements once they have been brought to, and initially incorporated into, deep-sea sediments. For example, a very large proportion of the organic material brought to the sediment surface is lost by oxidation from slowly deposited deep-sea sediments. During and after this process, trace elements associated with the organic material may become available for incorporation into other sedimentary phases, e.g. ferro-manganese nodules. For some elements the marine biomass acts as an intermediate transport mechanism. These elements usually have a sea water, as opposed to a continental origin. However, these models have been successfully used by Bostrom et al. (1976) and Papavasiliou (1979).

1. Log-log diagrams

Log-log diagrams were used by Bostrom et al. (1976) to identify the origin of trace elements.

In the present study, using log-log diagrams, five groups were recognised. These groups showed the same composition as five types in Fe/Ti versus Al/(Al+Fe+Mn) plot (Fig.4-1 a-e). The addition of volcanic matter (VM) and biogenous matter (BM) was found necessary to produce a

better fit. VM refers to the sediments contribution from the spreading ridge, which are rich in Mn, Fe, Ba and some other elements. The chemical composition of the East Pacific Ridge (EPR) was used as standard VM.

Most of the groups show a good fit for Si, without the addition of any BM, although most of the samples contain BM. This is probably due to:

a) the SiO_2 concentration in the suggested average chemical model (TM = shale + basalt + granite; Table 4-3) is higher than it should be; or

b) since the average chemistry of a group of samples (i.e. samples with BM and/or without BM) was used, the effect of BM has probably decreased.

It is also apparent that, although sediments from Sites 216 and 254 show VM contribution in Figure 4-1 (Fe/Ti vs Al/(Al+Fe+Mn), the log-log diagram does not show such a contribution, which suggests that high amounts of BM probably have a diluting effect in the chemistry. However, this model gives an approximate source for some elements of the present study samples.

a. Group I

The same set of samples and chemical model as Type I form this group.

In Figure 4-4, the suggested chemical model of Type I (i.e. 75% granite and 25% shale) was plotted against the average chemistry of the sediments of Type I. It can be seen that the sediments of Type I are too rich in Mn, Cu, Cr and Ni to be formed mainly from TM. A sediment model rich in Mn, Cu, Ni and Cr is necessary to provide a better fit. The addition of 10% VM to TM (Fig.4-5) gives a better reproduction of the sediments of Type I. However, this plot shows a depletion of Ba in the sediments. Ba is mostly associated with opaline SiO_2 and opal-CT. Opaline SiO_2 and opal-CT are involved in the formation of zeolite and thus some Ba is lost to the interstitial water during such reactions.

Figs.4-4 - 4-15:

Geochemical graphs showing the relationships between the composition of the sediment sources and the sediments of the present study (on a carbonate free basis). All values represented in the logarithm for the concentration given in %. Input constituents are from Table 4-3.

SH = shale
c.c. = continental crust
G = granite
B = basalt
BM = biogenous matter
VM = volcanic matter
THB = tholeiitic basalt
ALB = alkali basalt

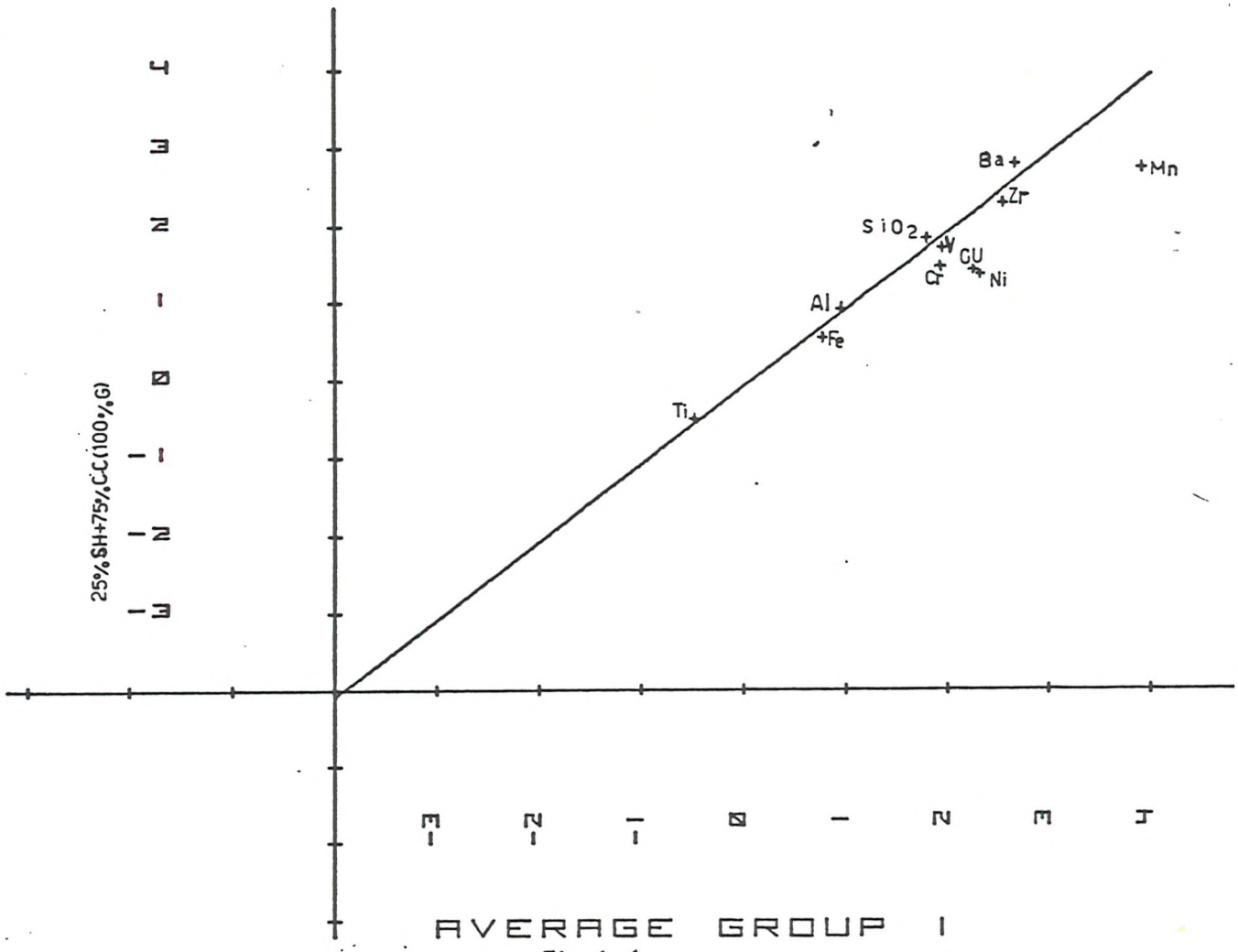

AVERAGE GROUP I

Fig.4-4

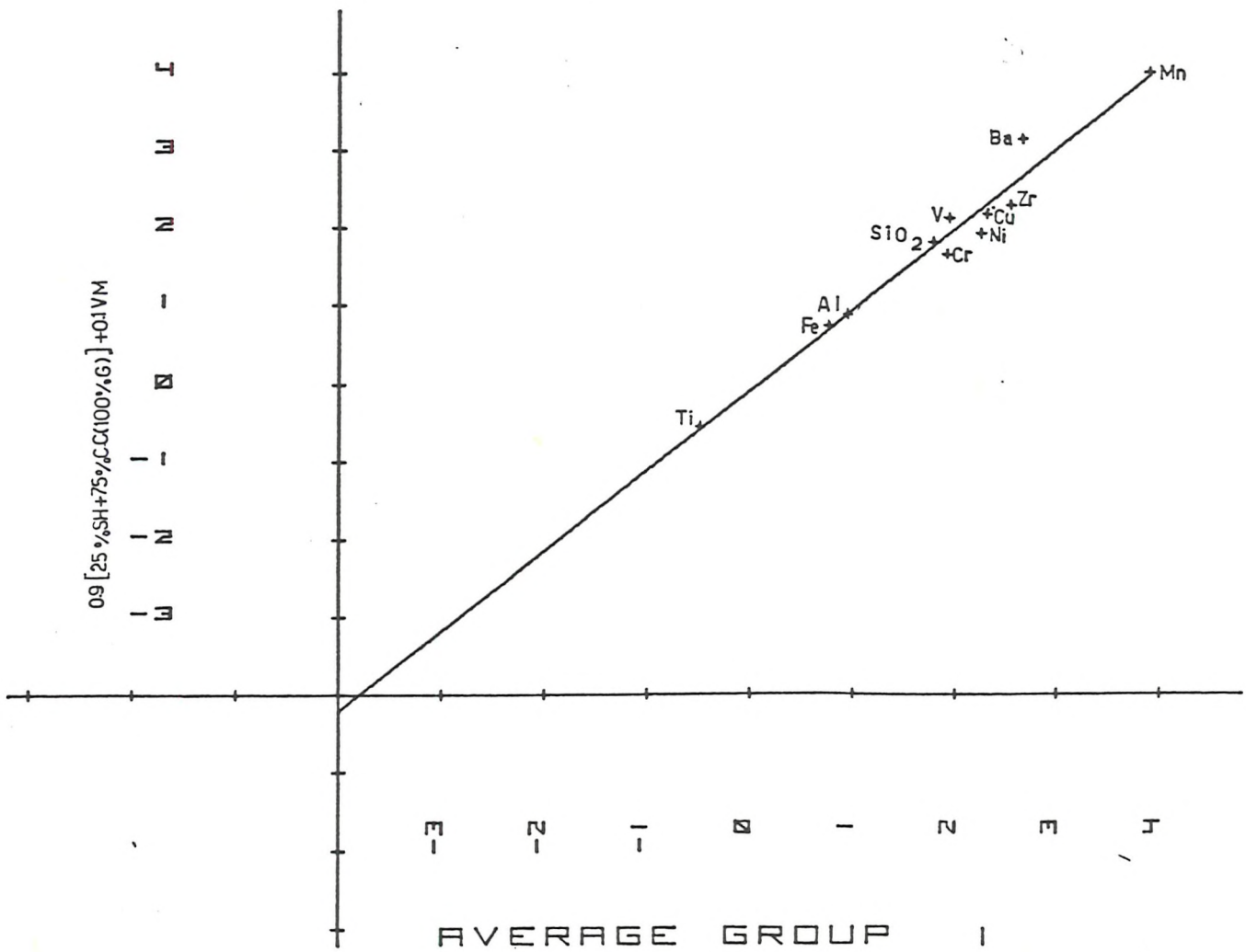

AVERAGE GROUP I

Fig. 4-5

b. Group II

The same set of samples and chemical model as Type II form this group. Two separate plots (Figs. 4-6 a,b and 4-7 a,b) were used, since samples from Site 258 (Fig.4-6a) indicate enrichment in Mn, Cu and Ni, whereas the rest of the sediments (Fig.4-7a) show enrichment in Ba and depletion in Mn and Zr. The addition of 5% BM and 5% VM produces a better fit (Figs.4-6b and 4-7b). However, Figure 4-7b (Site 258) still shows depletion in Mn and Zr.

c. Group III

This group is sub-divided into two sub-groups:IIIa with 5% BM and 5% VM, and sub-group IIIb with 15% VM.

i. Sub-group IIIa

This sub-group includes sediments from Sites 213 (core 14/3), 215(core 9/2), 221, 236, 239, 245, 248, 212 (core 37/1 downward) and 250.

Average TM of Type III was plotted against the average composition of the above sediments (Fig.4-8). There is an enrichment of Mn and Cu in the sediments. An addition of 5% VM and 5% BM produces a better fit (Fig. 4-8a).

ii. Sub-group IIIb

This sub-group includes Samples 212/18/2 upwards and 213/11/5 downwards (except 213/14/3).

The plot of Type III TM against the average composition of 212 +213 (Fig.4-9) shows enrichment in Mn, Cu, Ni, Fe and V in the sediments. The addition of 15% VM improves the fit (Fig.4-9a). The depletion in Ba can be explained in the same way as in Group I.

d. Group IV

Figure 4-10 displays the average composition of the sediments of Type IV against the suggested model for their sediment source (Table 4-3) (i.e., 20% TM + 80% tholeiite). This plot shows an enrichment in Ba. The addition of 5% VM and 5% BM provides a better fit (Fig.4-11), making a good correction for Ba.

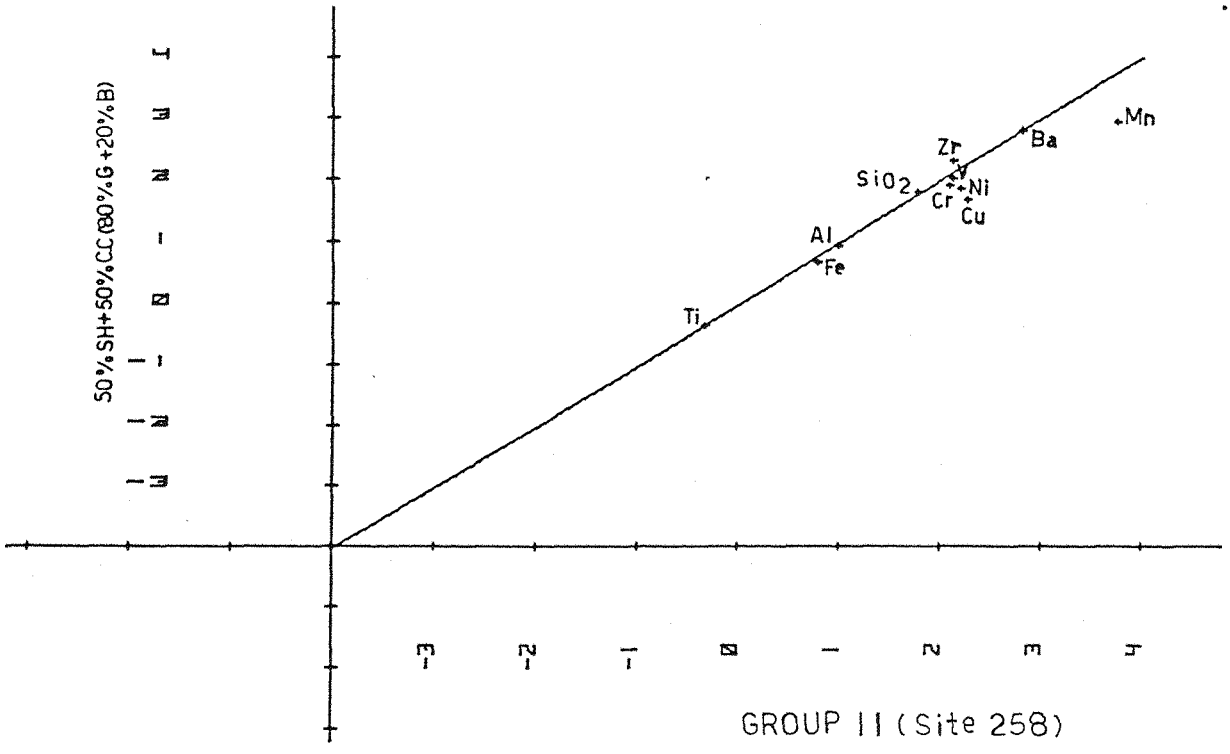

GROUP II (Site 258)

Fig.4-6a

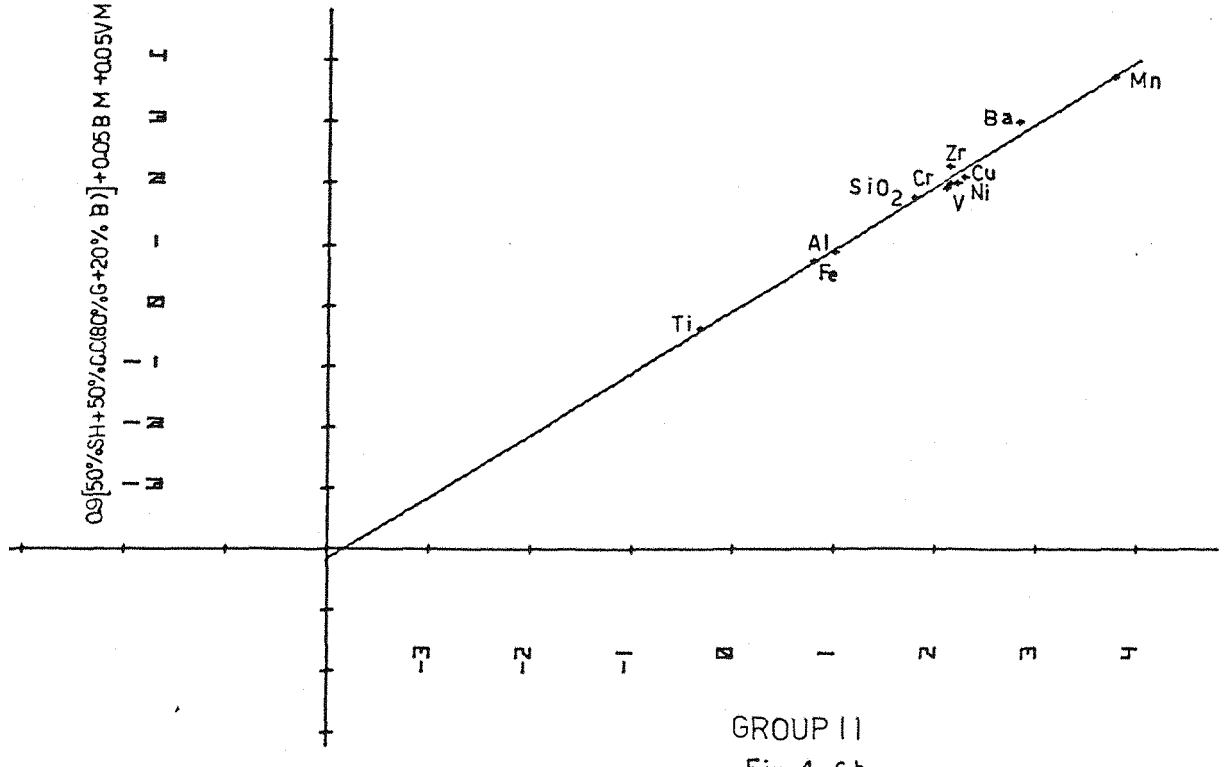

GROUP II

Fig.4-6b

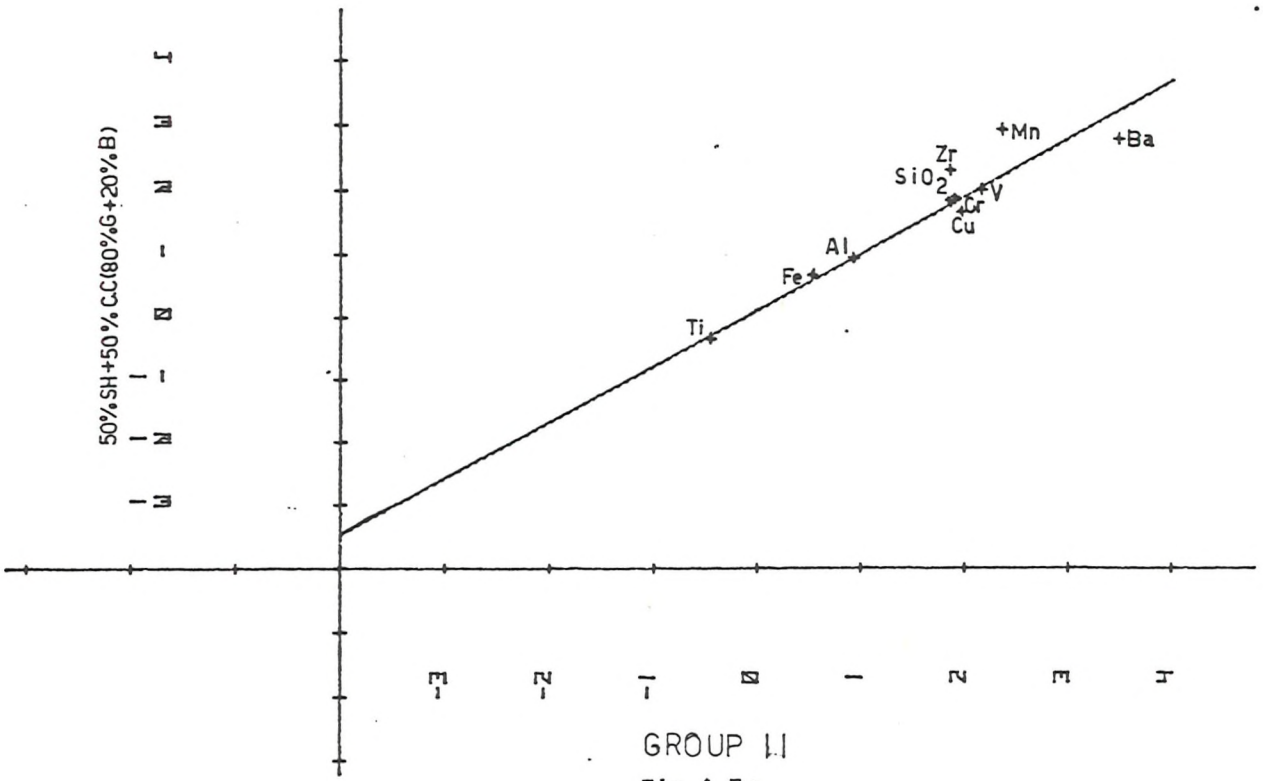

GROUP I.I

Fig.4-7a

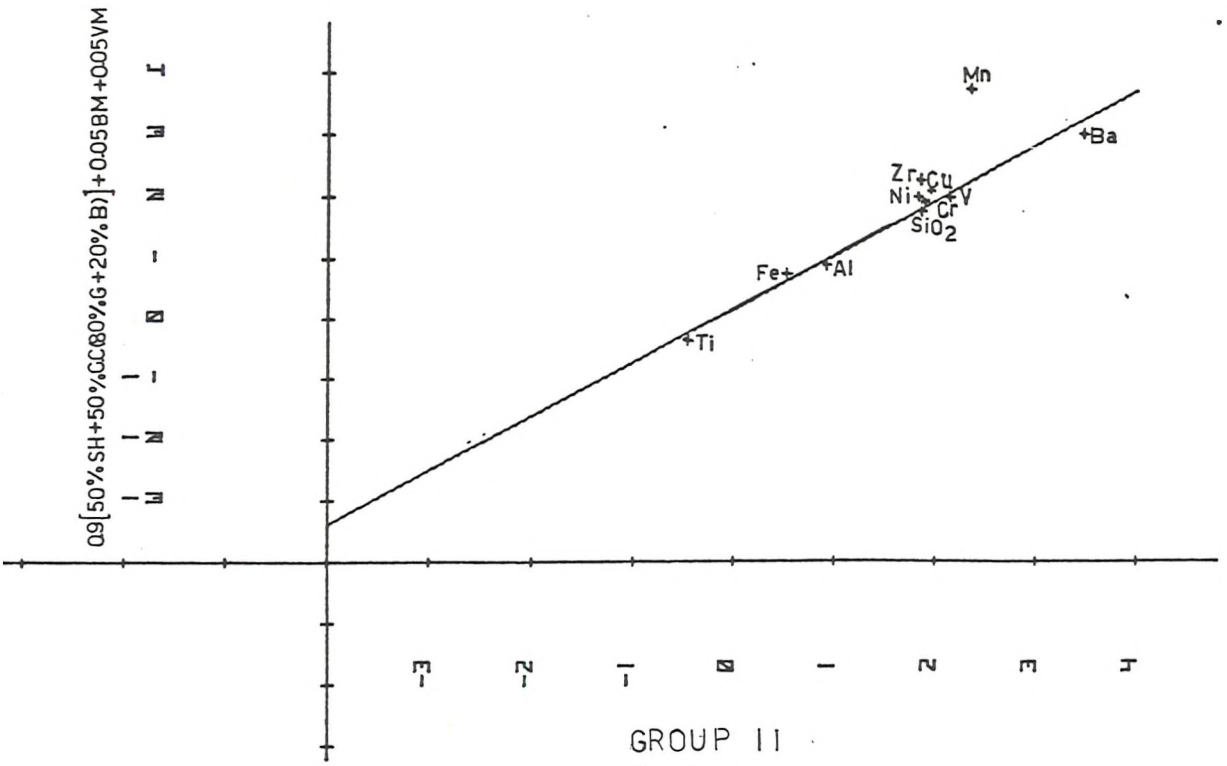

GROUP II

Fig.4-7b

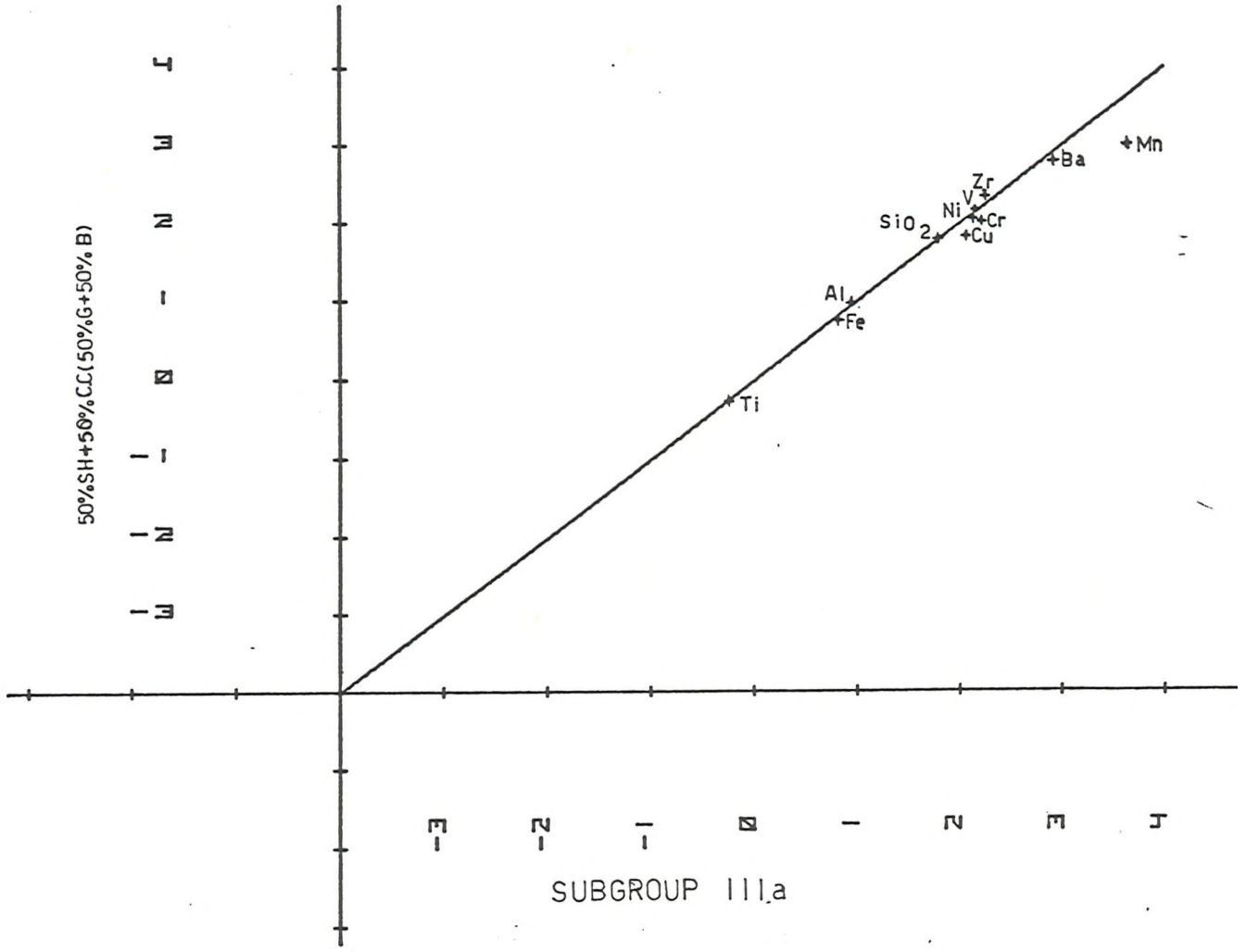

Fig.4-8 -

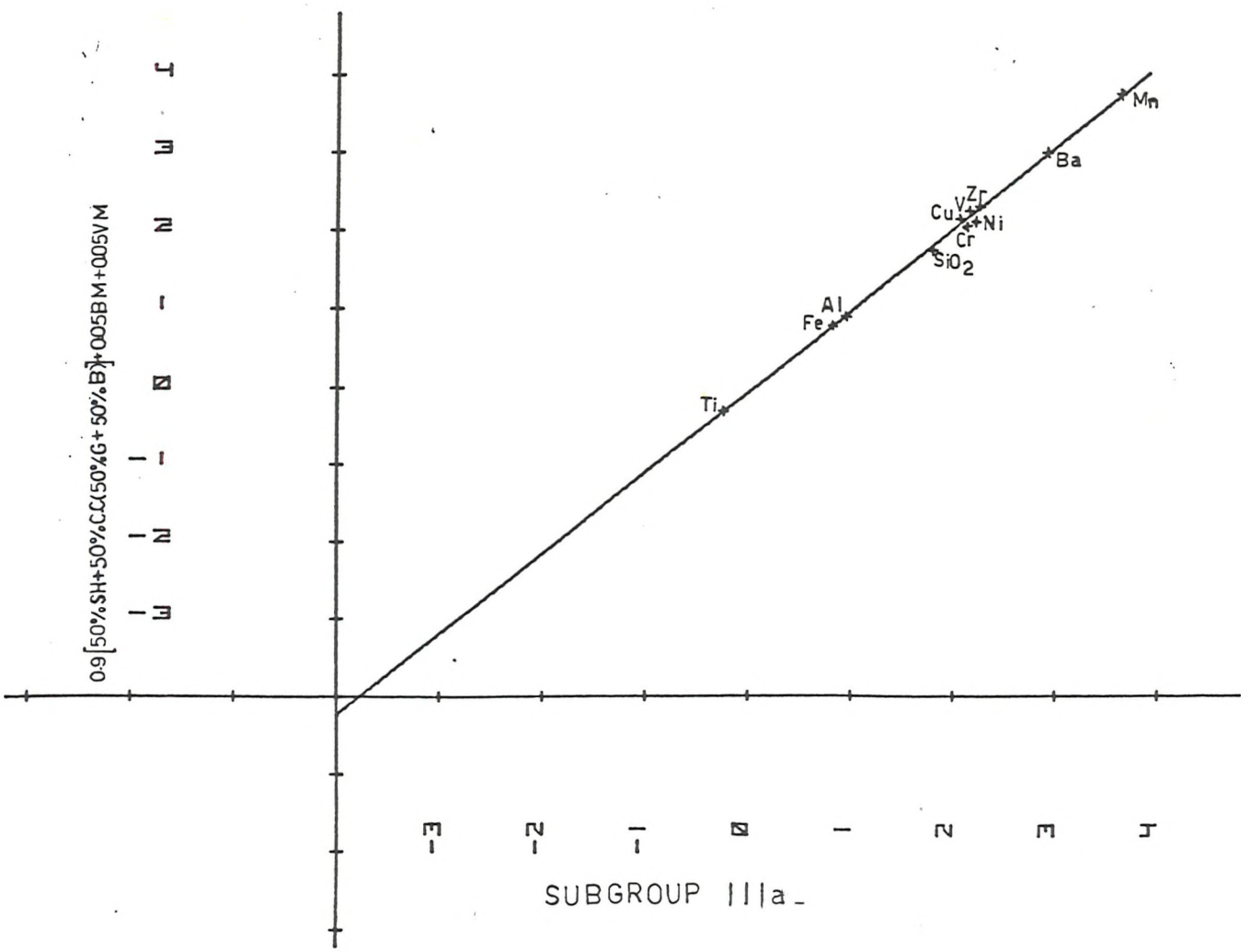

Fig.4-9 a

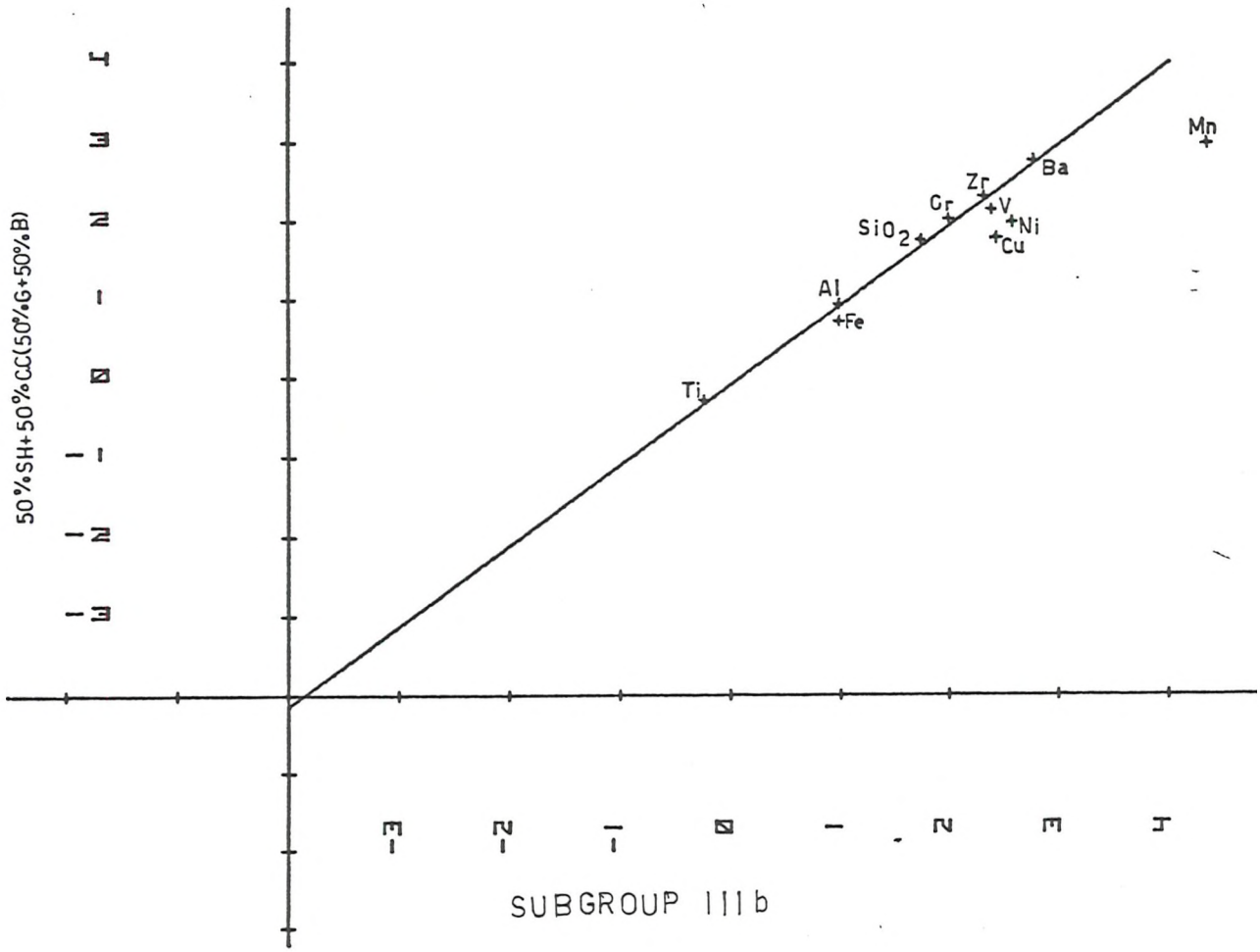
50%SH+50%CC(50%G+50%B)
Mn
Ba
Zr
Cr
V
Ni
Cu
SiO2
Al
Fe
Ti
SUBGROUP III b

Fig 4-9

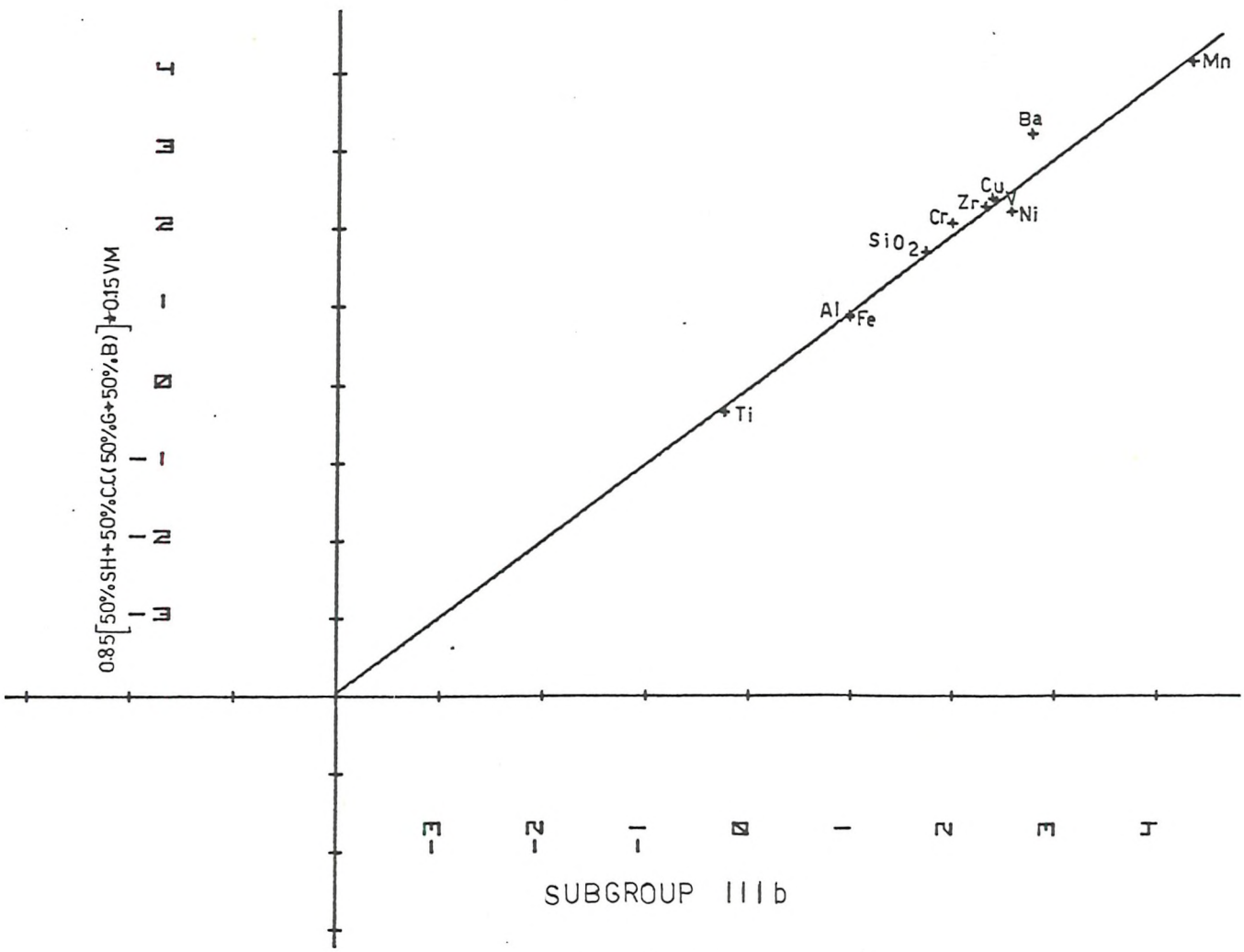
0.85[50%SH+50%CC(50%G+50%B)]+0.15VM
Mn
Ba
Cu
V
Zr
Cr
Ni
SiO2
Al
Fe
Ti
SUBGROUP III b

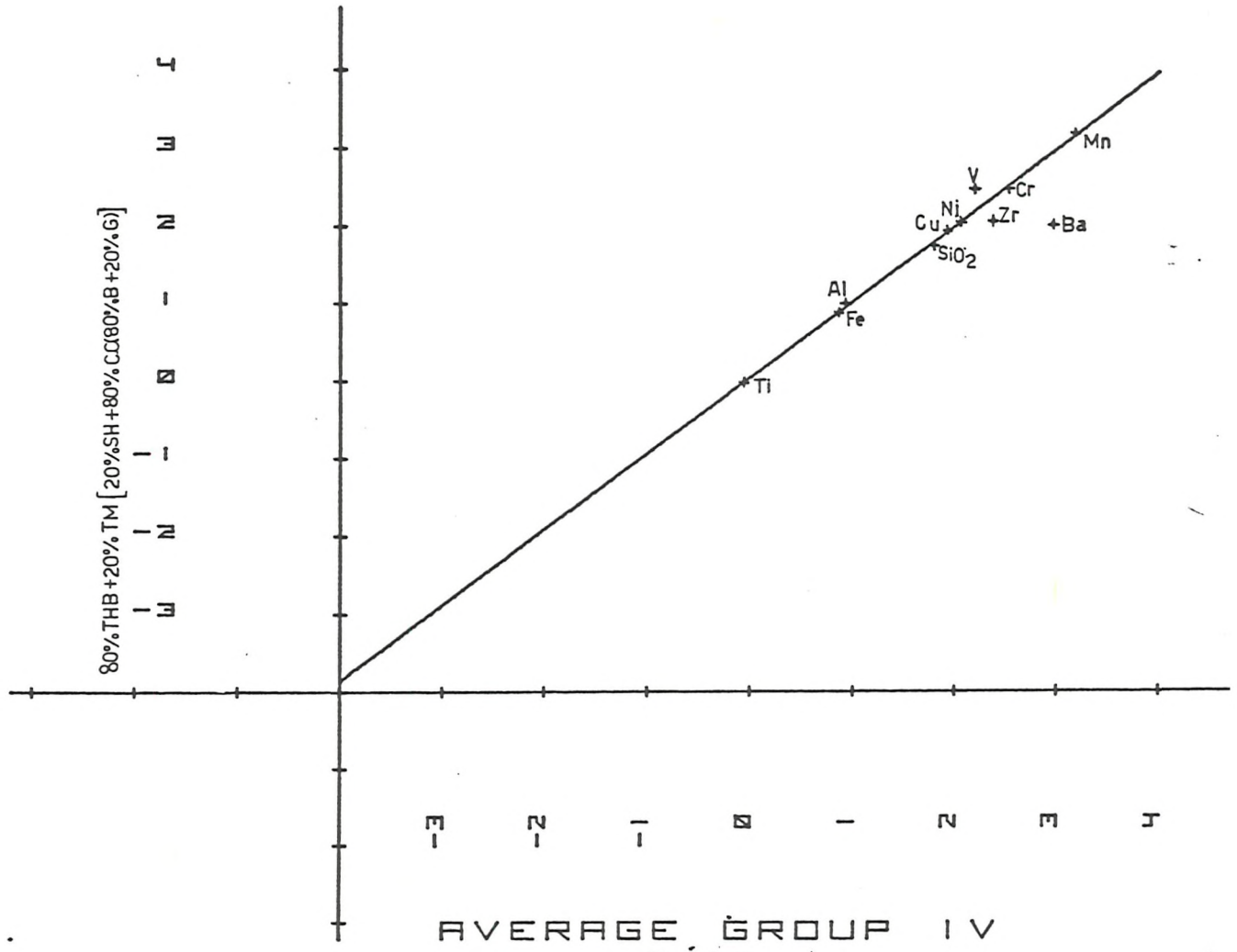

Fig. 4-10

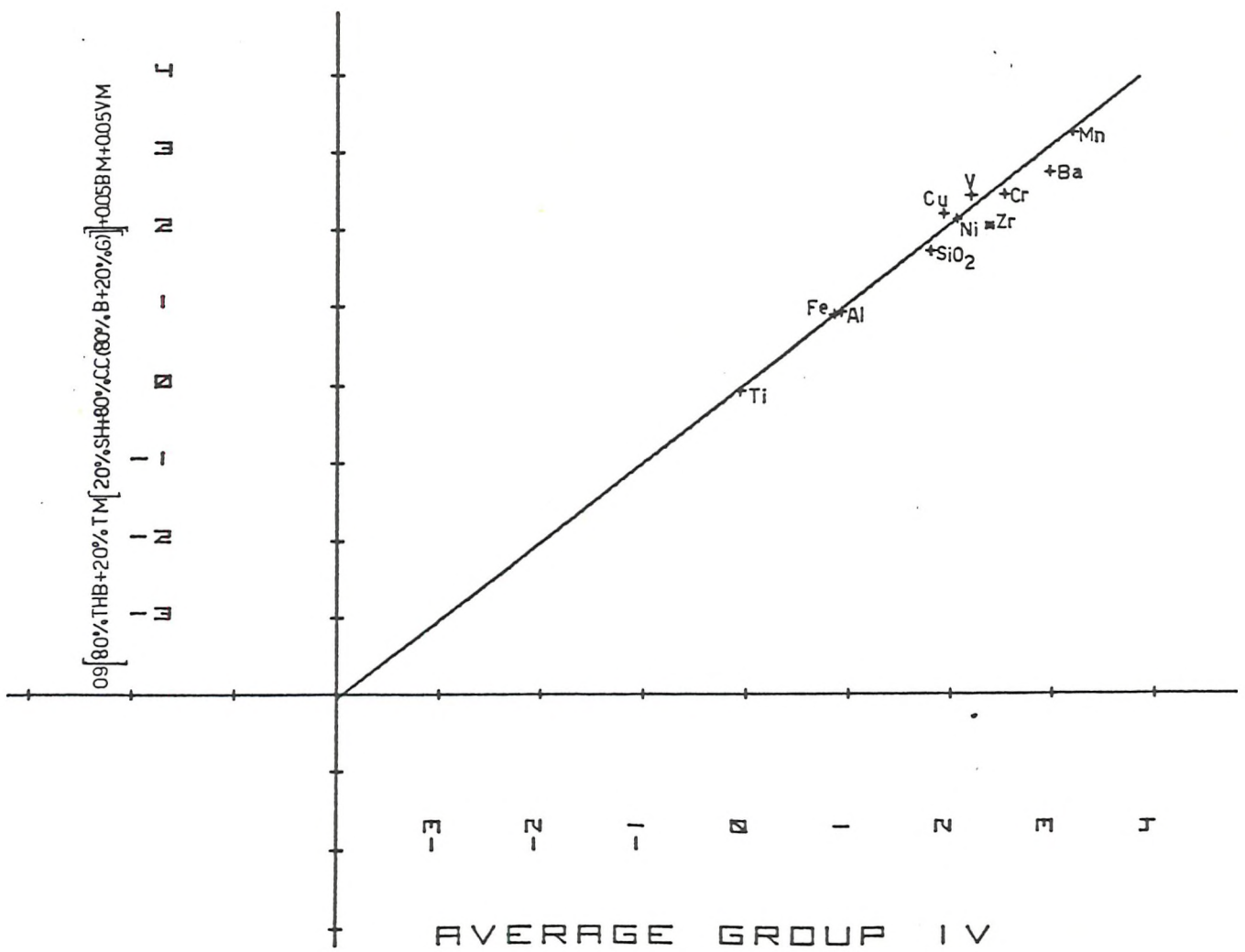

Fig. 4-11

e. Group V

The same set of samples and chemical model as Type V form this group. It was decided to show sediments of Sites 254 and 216 on two separate plots, since sediments of Site 254 show enricgment in Ba, whereas Site 216 shows enrichment in Zr.

In Figure 4-12, the average composition of samples from Site 216 (cores 30/3 amd 32/3) was plotted against the suggested chemical model of Type V (i.e. alkali basalt + 20% tholeiitic basalt). It can be seen that there is a small enrichment in Cu and depletion in Zr. An addition of biogenic matter seems to provide a better fit (Fig.4-13), except that it shows a depletion in Zr. The depletion could suggest the release of Zr into interstitial water after the basaltic material alteration. However, Zr, in sufficient concentration, could form its own silicate (zircon) (Krauskopf, 1979) since it is difficult to substitute for any ions in silicate minerals because of its small radius and high charge. Authigenic MLIS (i.e. MLIS with a high percentage of expandable layer), which is probably the alteration product of volcanic glass, was observed at this site. Volcanic glass was observed under SEM.

Figure 4-14 shows the average composition of samples from Site 254 against the suggested chemical model of Type V (i.e. 80% alkali basalt + 20% tholeiitic basalt). It is evident from this figure that a Ba enrichment in the sediments exists. An addition of 20% BM provides a better fit (Fig.4-15).

f. Conclusion

All groups in the log-log diagrams show the following patterns:

i) A source of VM was found necessary for Mn, Ni, Cu, Fe, Cr, Zn and V, and occasionally for Ba.

ii) The addition of BM provided better fits for Ba and occasionally for Cr, Cu and Ni. However, depletion of Ba was observed in Groups I and IIIb.

2. Origin of VM

The contribution of volcanic matter to the pelagic sediments of the Indian Ocean is expected since much volcanic activity and plate

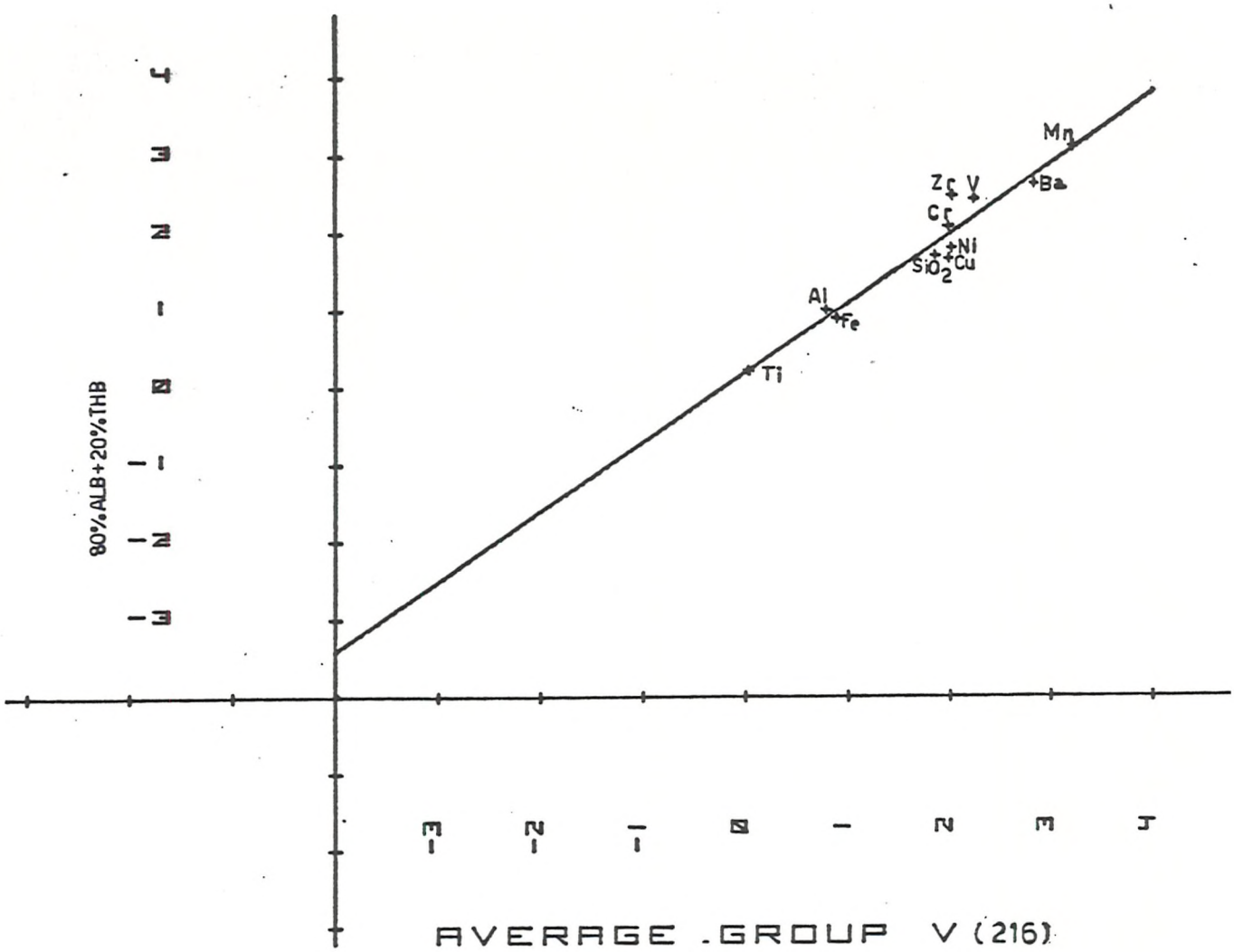
80%ALB+20%THB
Mn
Ba
Zr
V
Cr
Ni
Cu
SiO2
Al
Fe
Ti
AVERAGE .GROUP V (216)

Fig.4-12

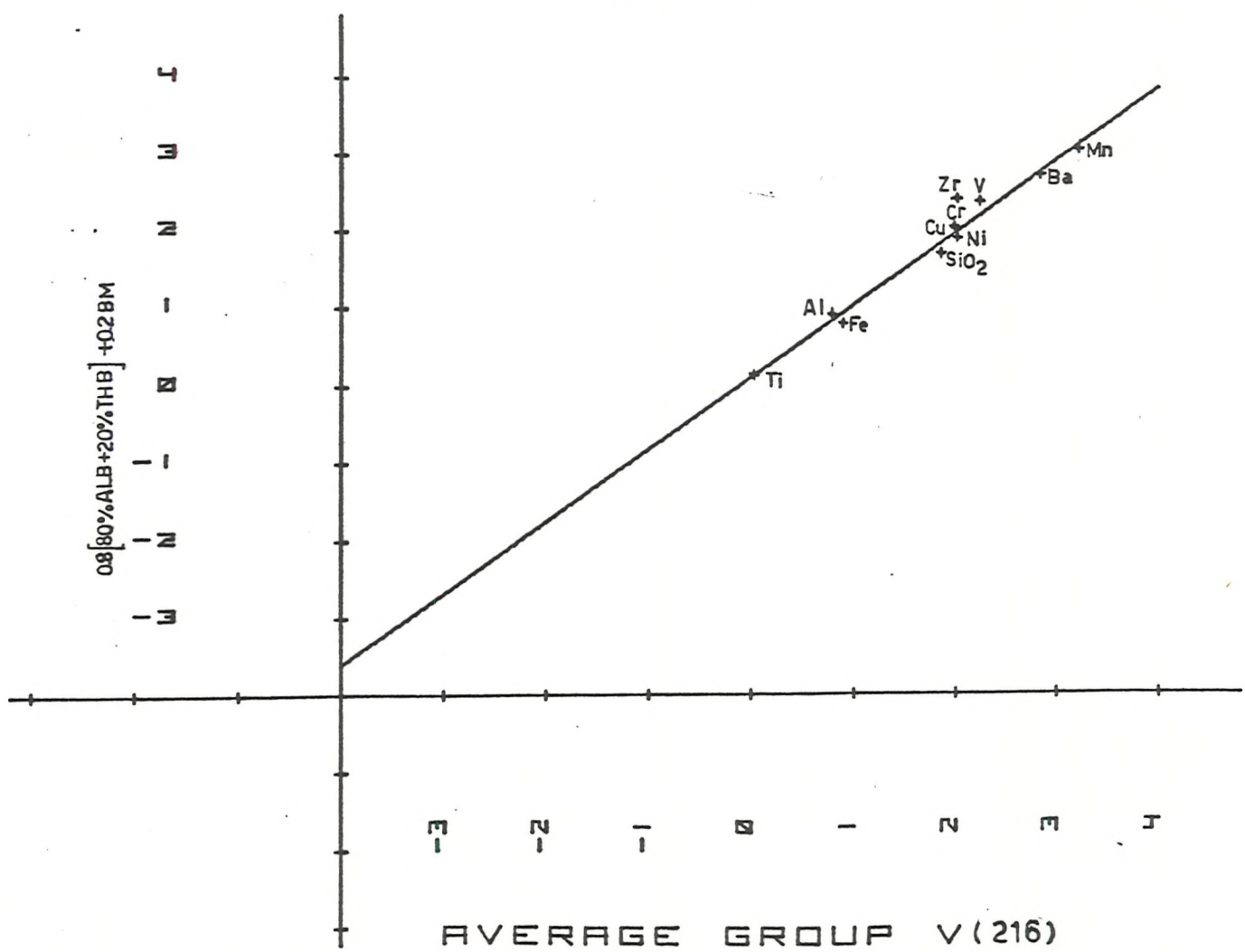
0.8[80%ALB+20%THB]+0.2BM
Mn
Ba
Zr
V
Cr
Cu
Ni
SiO2
Al
Fe
Ti
AVERAGE GROUP V (216)

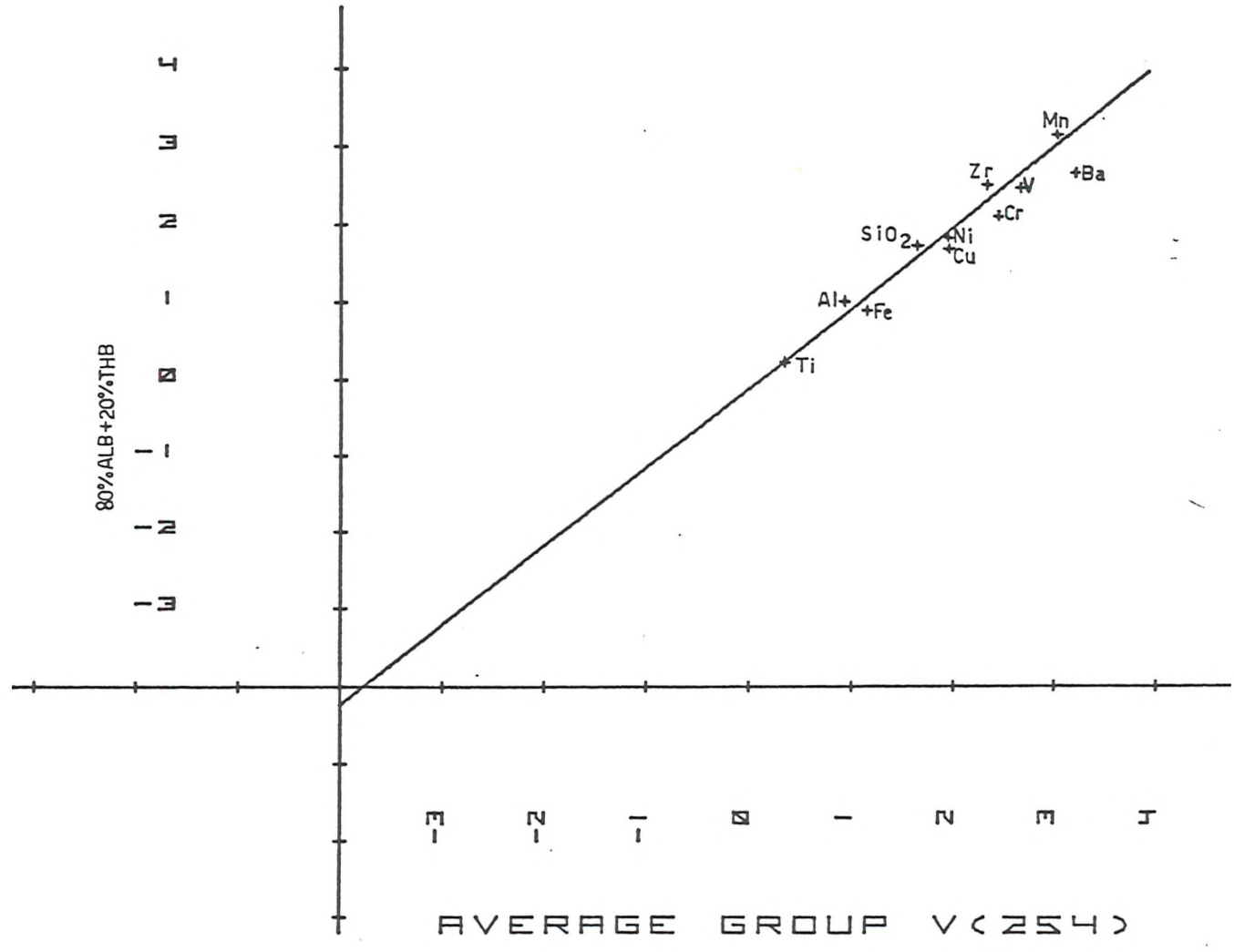

Fig.4-14

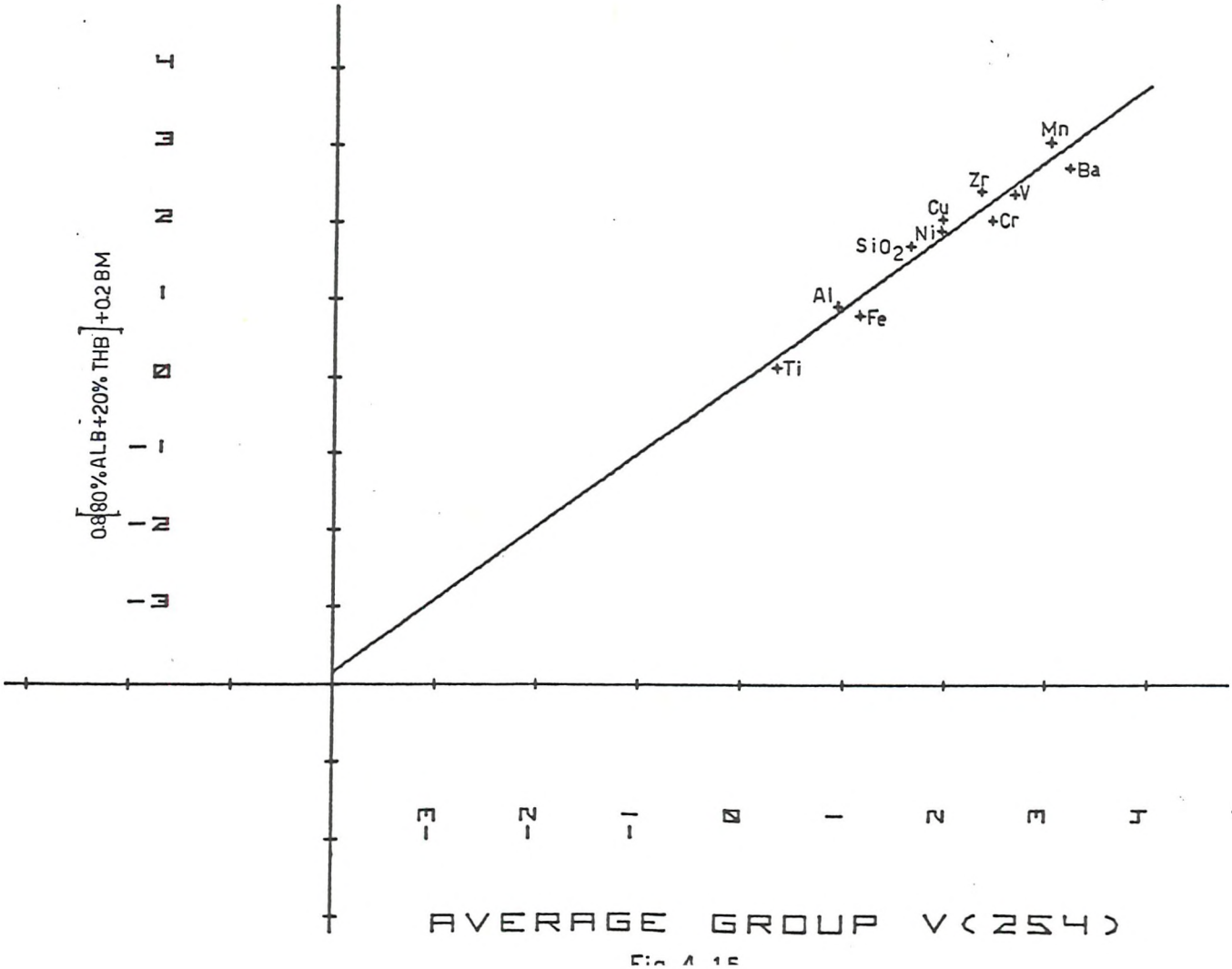

Fig.4-15

movement have occurred since the late Jurassic. According to Sclater et al. (1974a), India, Antarctica and Australia formed the eastern part of Gondwanaland.

Around 100-105 m.y.B.P. (Albian - Cenomanian) a spreading centre trending slightly south of east with transform faults trending just east of north became active in the Central India and Wharton Basins, and for the next 20 m.y.B.P. India moved north-northeasterly with respect to Antarctica. Therefore, the early Cretaceous sediments of the eastern sites (258, 257 and 212) probably received VM from this spreading centre. In the late Cretaceous (close to 80 m.y B.P.) there was a change in the direction of relative motion with India separating from the fixed Australia-Antarctica region in a more north-easterly direction. The pole of relative motion was close to 70° from the Ninetyeast transform fault. Thus, these spreading centres could still provide the VM input to late Cretaceous sediments of the eastern sites (in the case of the present study 212, 256, 216 and 211). In the Palaeocene (64 m.y.B.P.) the pole of relative motion moved to become almost 90° from the Ninetyeast transform fault. Between 64 m.y B.P. and 53 m.y.B.P. (Palaeocene to Eocene) the spreading centre just west of the Ninetyeast transform fault jumped 11° to the south. This spreading centre could have contributed sediments to Sites 254 and 215/9/2. Site 212 is located at the southern extremity of a fracture zone (Fig.4-16). According to von der Borch et al. (1974), basement sediments of Site 212 have suffered hydrothermal alteration, possibly due to the proximity of the Investigator Fracture Zone mentioned above. According to Curray et al. (1982), the Investigator Fracture Zone (I.F.Z.) is a transform fault of the late Cretaceous and early Tertiary. Therefore, high amounts of VM of Group IIIb could be related to this fracture zone. However, the Ninetyeast Ridge could also contribute sediments to this site, since it was still active. Miocene to Recent sediments of Sites 213, 212 and 211 could also have received their VM from the Java Trench. The western sites sediments of the present study are mainly of the Palaeocene or younger. Sites 239 and 245 have probably received VM from the MIOR. According to Vallier (1974), the volcanic matter in the Cretaceous, middle Miocene is associated with volcanism which accompanied the formation of the Central Indian Ridge and/or the development of the 'Chagos Fracture Zone'. The above author has related the volcanic contribution of the middle Miocene - Quaternary to the volcanism on nearby seamounts and

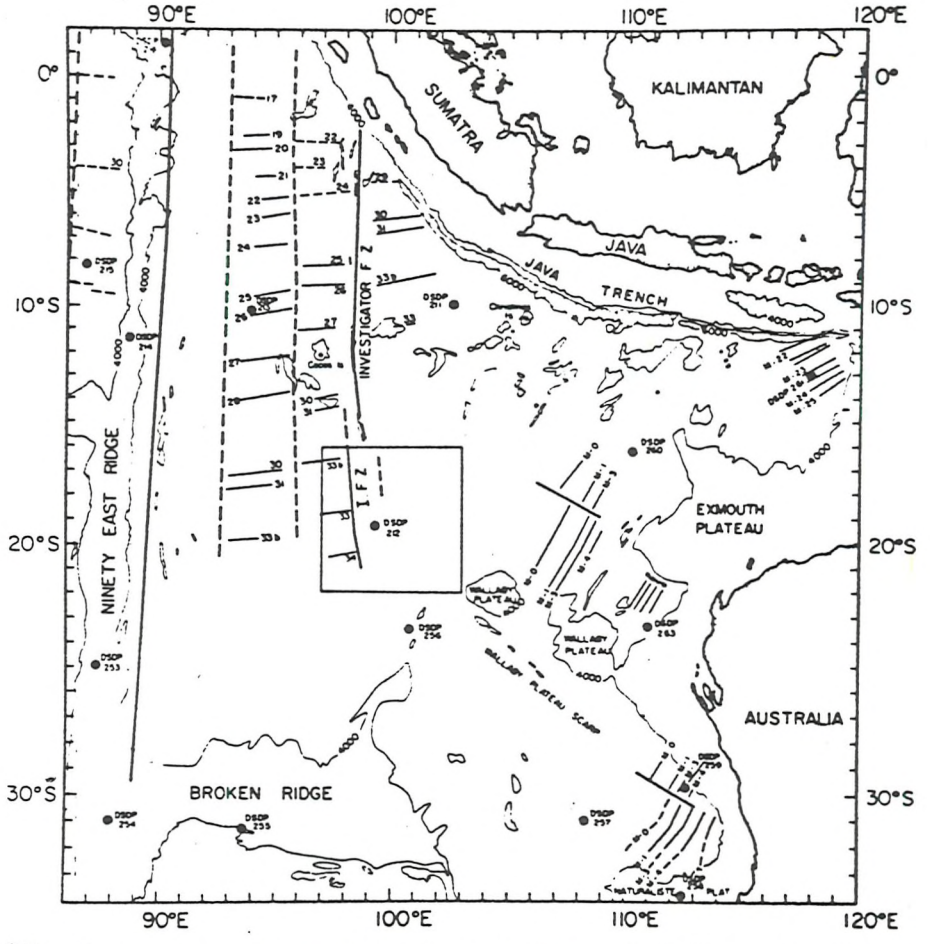

Fig. 4.16. Fracture zones and magnetic lineations in the Wharton Basin. The numbers follow the scheme proposed by Heirtzler *et al.* (1968) and Larson and Hilde (1975). DSDP sites are indicated by their numbers (after Larson *et al.*, 1978).
I.F.Z = Investigator Fracture Zone.

islands in the Mascarene Island Group. Sediments of Sites 221, 235, 236 and 240 could receive VM from MIOR, Carlsberg Ridge, Chagos Fracture Zone, Owen Fracture Zone and Davie Ridge, because of their proximity to these ridges and fracture zones.

3. Biogenous Matter (BM)

According to Leclaire (1974), increases in siliceous fossils, foraminifera and organic carbon contents in bottom deposits indicate increasing biogenic production of the overlying water masses. He pointed out that, presently, the equatorial zone is known to be one of the regions of high organic production which is related to upwelling induced by divergence. According to him, the onset of the equatorial circulation pattern was initiated as soon as India was sufficiently beyond the Equator. India is believed to have crossed the Equator in the Miocene (McElhinny, 1970). Therefore, sediments of Miocene age or younger could receive BM from this high productive circulation pattern (Sites 240, 236 and 235). However, according to Schlich et al. (1974), Upper Miocene to Recent sediments of Site 240 are mainly detrital material. They found that the sands and silts of Holocene to late Miocene age contain many displaced and/or re-worked benthonic foraminifera characteristic of a shallow nearshore shelf and reef environment.

Kidd et al. (1978) have linked the Eocene chert of sites in the Arabian Sea to the establishment of gyral circulation in the Arabian Sea at this time, which brought about upwelling off the Arabian and Indian coasts. They, on the other hand, believe that the distribution of the early Cretaceous cherts and sediments rich in radiolaria in the Wharton Basin drill sites and in land sections in northern Australia (Brown et al., 1968), when compared with the palaeogeography of the time, suggests that these were linked to open ocean conditions and productivity within Tethys.

von der Borch et al. (1974), on the basis of sedimentological and biostratigraphic evidence, suggested that calcareous units (of early - late Pliocene to late Miocene, early middle Miocene, Miocene, middle Eocene and Maastrichtian ages) had an exotic source, and the sediments were emplaced by a combination of turbidite and nepheloid layer transport. Schlich et al. (1974) have discovered extremely heavy

bioturbation throughout the chalk section of the late Palaeocene and part of the early Eocene at Site 245. They believe that the above observation indicates intense biological activity on the sea floor, and thus the favourable environmental conditions for the development of a flourishing benthonic fauna. Thick nannofossil deposits of early Eocene age suggested to them that a) the sediments were deposited well above the calcium carbonate compensation depth zone; and b) there was a fairly high productivity in the euphotic zone.

C. Geochemistry of the Major and Trace Elements

In this section, the distribution and origin of the elements among the most important minerals in the sediments are discussed with the aid of an inter-element plus mineral correlation programme. Table 4-5 shows the correlation matrix and Table 4-6 the summary statistics.

1. SiO_2

SiO_2 percentages vary from 17·66% at Site 216, to 80·51% at Site 240 (on an absolute basis). It occurs in aluminosilicates, biogenic silica, opal-CT and quartz. The present aluminosilicates are clay minerals, zeolites (clinoptilolite and phillipsite) and feldspars.

The X-ray diffraction pattern showed a combination of the broad d(111) - cristobalite peak between 21·7° and 21·9° 2θ, with a number of other cristobalite peaks and low temperature tridymite peak (e.g. at 20·6°, 23·3° and 36° 2θ) (Fig.3-1). This material, which was called 'opal-cristobalite' or 'low cristobalite' by von Rad et al. (1974),was observed under SEM as closely packed spherulites (Plate 4-1d). It was found that the pore spaces, which were left after the destruction of the soft parts of the micro-organisms, were filled with opal-CT (suggesting opal-CT formation from the skeletal opal dissolution) (Plate 4-1, a-c).

Flörke (1955), Ernst et al. (1969), Hathaway et al. (1970) and Heath et al. (1971) believe that the cristobalite is of low temperature diagenetic origin, originating from dissolved skeletal opal or devitrified volcanic glass, and terrigenous silt.

Bostrom et al.(1971) believe that the Si/Al ratio considerably exceeds 3·5(the approximate average ratio both in oceanic and continental crust)

PLATE 4-1

a. Radiolarian skeleton in Sample 258/17/2

b-d. Opal-CT (filling the pore space left after biogenic silica dissolution).

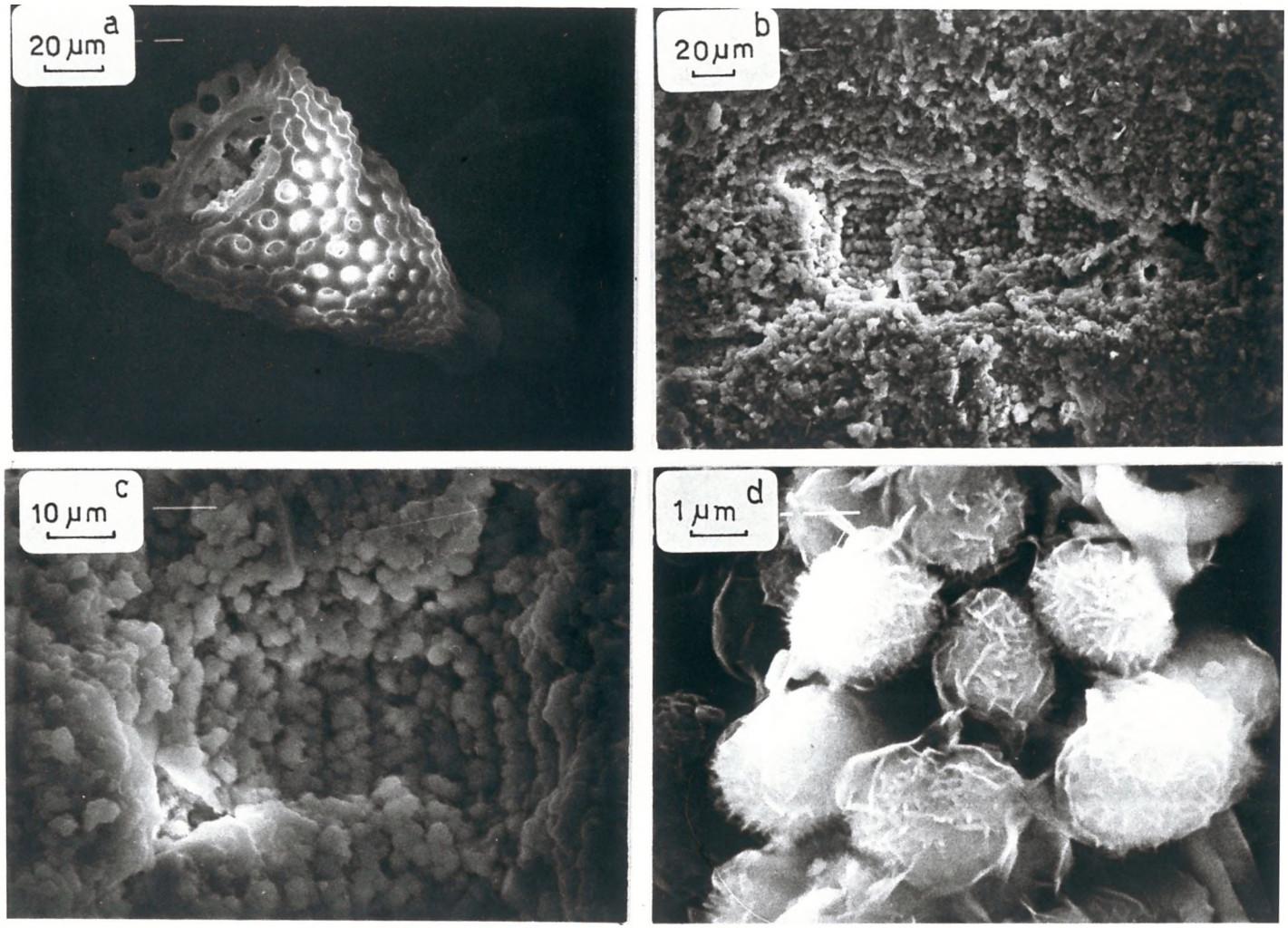

PLATE - 4_1

in sediments rich in opaline silica.

In the present study, a Si/Al ratio as low as 1·6 was observed at Sites 212, 256 and 258. The X-R-D studies confirmed the presence of both opal-CT and gibbsite in the above samples, and thus low Si/Al ratio was caused by the presence of minerals or volcanic glass rich in Al. However, Si/Al ratios exceeding 3·5 are rarely observed, even though most of the samples contain opaline silica (Plate 4-2, a-d). A high concentration of micro-organism skeletal remains was observed under SEM in Sample 213/8/5 with Si/Al ratio of 3·19. Therefore, low Si/Al ratios do not mean that opaline silica is absent. The highest Si/Al ratio (Si/Al = 10·58) belongs to Sample 240A/2/1, which is rich in quartz. The high Si/Al ratio in Sample 216/32/3 is caused by the amorphous silica of microfossils, as observed under SEM (Plate 4-2b). Sample 258/14/1, which is rich in opal-CT, shows a Si/Al ratio of 7·37. Figure 4-17, which displays the relation between SiO_2 and Al_2O_3, shows high SiO_2/Al_2O_3 for samples containing biogenic silica, opal-CT or quartz.

The correlation programme (Table 4-5) among 84 samples shows positive correlation of SiO_2 with quartz (significant at 99%), clinoptilolite and K_2O (at 99%) and Ba (at 98%). Most SiO_2 is either of biogenic silica or quartz. Therefore, its positive correlation with quartz and clinoptilolite is expected. Clinoptilolite is a high silica-bearing mineral and is usually associated with opaline SiO_2 and opal-CT. K_2O and Ba are important constituents of clinoptilolite and opal-CT.

SiO_2 also shows negative correlation with CaO and CO_2 (at 99%) and Sr (at 95%), which reflects its antipathetic relation with carbonate. According to Calvert (1976), calcitic sediments are sand-sized, whereas the organic and siliceous ones belong to the clay and silt-sized classes. Therefore, the negative correlation could either be the effect of grain size or the dilution effect of carbonate on clay and siliceous oozes.

Its negative correlation with TiO_2, V, Cr (at 99·99%), Fe_2O_3 (at 99%) and MgO (at 95%) suggests that these elements are partly not related to silicate and biogenic silica.

2. TiO_2

In the deep sea sediments titanium is usually present as a minor constituent in many aluminosilicates, e.g. the clays, feldspars, micas,

PLATE 4-2

a. Diatomaceous fossil in Sample 213/8/5

b. Tests of siliceous organisms in Sample 216/32/3

c & d. Radiolaria in Sample 216/32/3

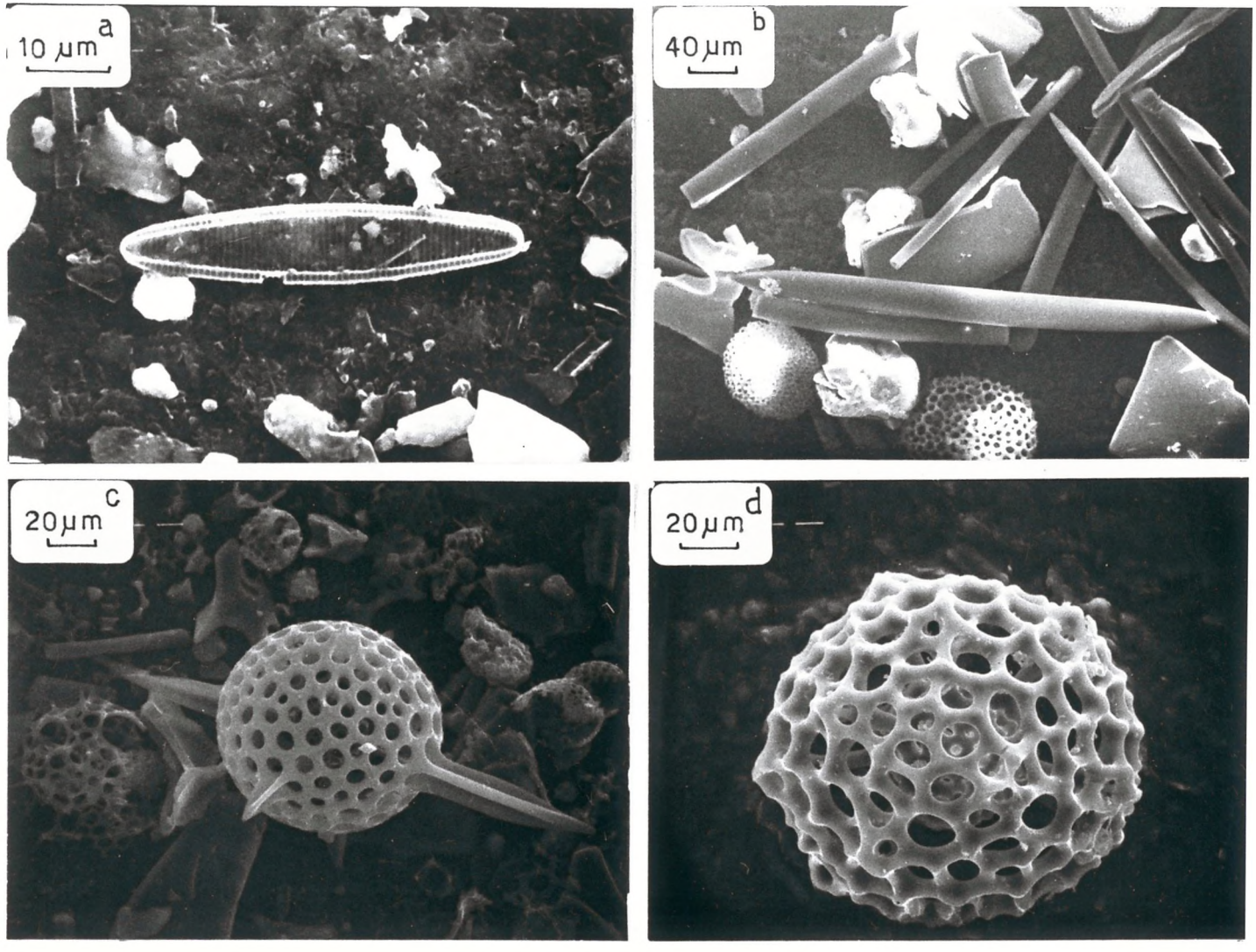

PLATE.4_2

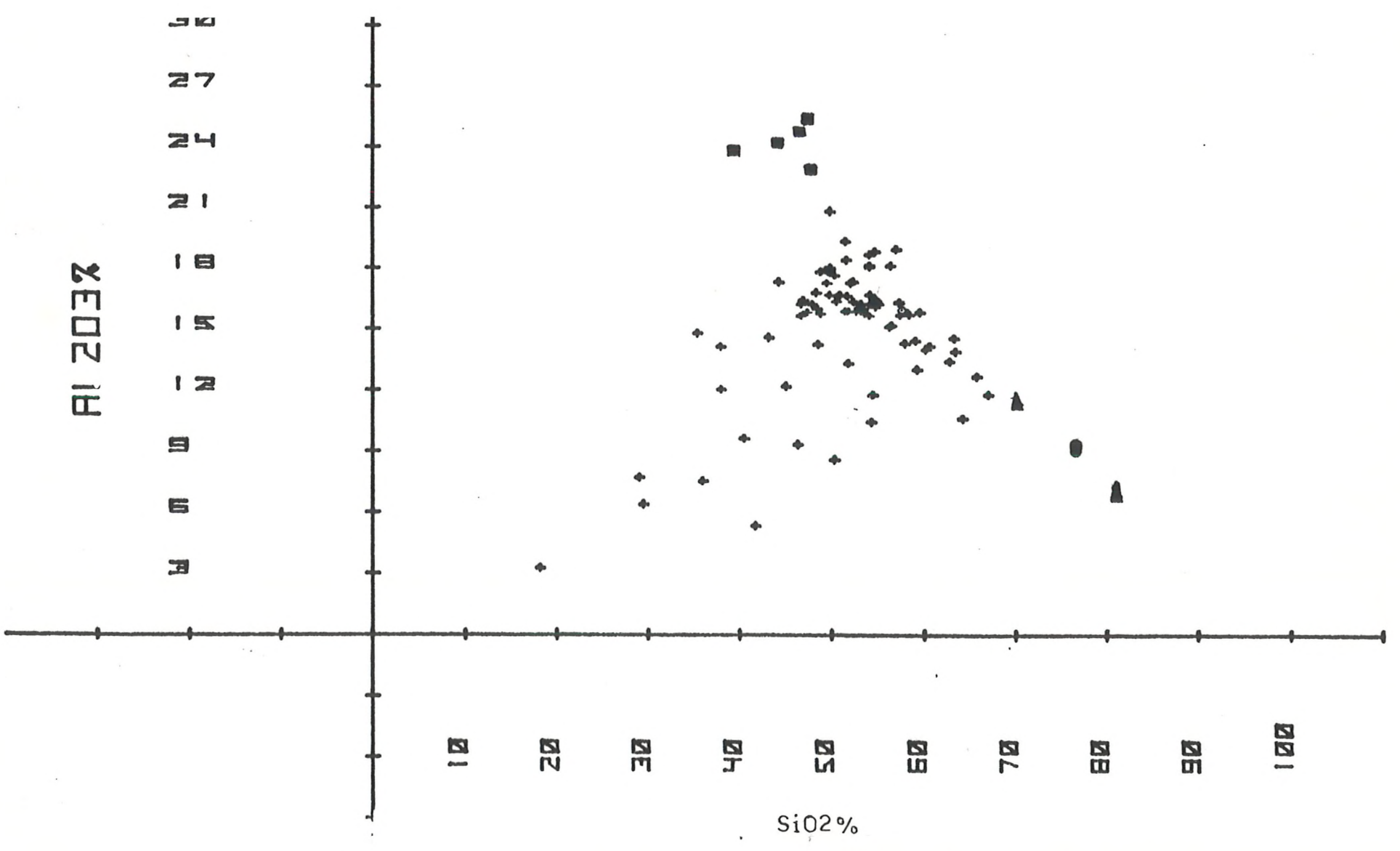

Fig.4-17.Correlation between Al203 and Si02. High Si02 is due to the presence of quartz and opal-CT in samples 240(▲) and 258(●).High Al203 indicates the presence of gibbsite in samples from sites 212,256 and 257(■).

etc., as well as in the form of its polymorphic oxides, anatase and rutile (Chester et al., 1976). Goldberg and Arrhenius (1958) have suggested that high Ti content of sediments is almost invariably indicative of basaltic debris contribution to the sediments. According to Bostrom (1970), Ti/Al ratios of $>$ 0·039 indicate basaltic volcanic contributions to the sediments. Donnelly et al. (1976), Donnelly (1977) and Couture (1977a) believe that Ti/Al is a good indicator of sediment source.

Titanium is also found in ferro manganese nodules (Chester, 1965) and marine organisms (Nicholls et al., 1959; Bostrom et al., 1974).

In the case of the present study, the titanium content (as TiO_2) of the samples on an absolute basis varies from 0·29 (258/15/1) on the Naturaliste Plateau, to 4·90 (254/28cc) on the Ninetyeast Ridge. The X-R-D studies showed the presence of ilmenite and anatase in a few samples at Sites 216 and 254. Ti/Al ratio was higher than 0·039 in most of the samples except Sample 211/6/2, Sample 213/11/2 upwards (at Site 213) and Sample 246/10/2 (Table 4-4). As previously mentioned, Sites 211 and 213 have been receiving silicic volcanic matter from silicic Indonesian volcanics since the mid-Miocene. Volcanic glass was also observed under SEM at Site 246. Indeed, the Ti/Al ratio of granite is in good agreement with the observed ratios at the above sites.

The correlation programme (Table 4-5) shows positive correlation of TiO_2 with pyrite, FeO, Fe_2O_3, organic C, Cr and V (significant at 99·99%) and MgO (at 98%). Negative correlation is shown with SiO_2 (at 99·99%), Pb (at 99%), V (at 95%), Rb and Mo (at 90%). TiO_2, MgO, Fe_2O_3, FeO, V and Cr could all be constituents of oxidised phases (e.g. ilmenite). According to Hart (1970), basalt, upon hydration by sea water, loses SiO_2, Mg and Ca and gains iron, sodium, phosphorous and titanium. He believes that titanium may go into the formation of ilmenite. The following positive correlations; pyrite - TiO_2, TiO_2 - FeO, and TiO_2 - OgC could suggest that the alteration of basaltic material takes place in a reducing environment. V and Cr could also have been lost during the alteration of basalt and then precipitated under reducing conditions. Vanadium is insoluble under reducing conditions (Calvert, 1976). According to Chester and Aston (1976), basaltic material loses some trace elements such as Cr under alteration.

The negative correlations suggest that TiO_2 is not an important constituent in free silica (amorphous SiO_2, quartz, opal-CT) and aluminosilicates.

3. Al_2O_3

It forms the main metallic constituent of aluminosilicates. Clay minerals, feldspars and zeolites are present in the samples. Other Al-bearing minerals such as gibbsite is also present in considerable amounts. Its abundance varies from 25·2 (212/28/2 in the Wharton Basin) to 3·14 (216/24/4 on the Ninetyeast Ridge) on an absolute basis. The average concentrations of Al_2O_3 are given in Table 4-7. Sediments rich in carbonate (Sites 216 and 246) and quartz sands (Site 240A)are poor in Al_2O_3 (average Al_2O_3 is about 6 - 9%), whereas the clayey sediments are relatively rich in this element (average = 16%). Al_2O_3 shows a strong positive correlation with clay (at 99·99%) since it is the main constituent of clay minerals. Figure 4-18 shows a plot of Al_2O_3 % against total clay %; the regression equation (Y = 2·61 + 0·257x) suggests that an average of 2·61% of Al_2O_3 is concentrated in the other aluminosilicates such as feldspars, zeolites and volcanic debris.

It has positive correlation with Fe_2O_3, Pb, As, Zn, Cu, Ce and La (significant at 99·99%); K_2O, V and Ni (significant at 99%); and Rb (significant at 95%). All these elements are present either in clay or zeolite and feldspar. It also shows strong negative correlation with calcite, CaO and CO_2 (at 99·99%) and clinoptilolite (at 95%), which once more confirms its association with clay, since clay and calcite plus clinoptilolite are antipathetically related. Al_2O_3 also shows positive correlation with MLIS and kaolinite (at 99·99%), chlorite (at 99%) and illite (at 95%).

4. Fe_2O_3 - FeO

Chester et al. (1976) believe that iron may have been transported to the oceans in association with terrigenous solids, particularly the clay minerals which form a large fraction of the land-derived material in deep-sea sediments. Iron may be associated with the clay minerals a) as an essential constituent within the crystal lattice; b) as a minor constituent within the crystal lattice; c) as iron oxide coatings on the surfaces of the clay particles (Carroll, 1958). It may have been deposited through the agency of a biological mechanism (Clarke et al., 1922; Bradley et al.,

TABLE 4-7: Average Al_2O_3

S.N.	Al_2O_3%	S.N.	Al_2O_3%	S.N.	Al_aO_3%
211	13•64	236	16•31	250	16•54
212	16•26	239	16•86	254	13•76
213	13•73	240A	6.72	256	11•99
216	6•24	245	15•27	257	15•49
221	16•30	246	9•50	258	13•42
235	15•75	248	14•45	240	14•62

S.N. = Site Number

Fig.4-18

1942; Elwakeel et al., 1961). The biologically derived iron occurs as coatings on skeletal parts (Elwakeel et al., 1961). It may also have been originated through processes involving the authigenic removal of iron from sea water.

In the present study, Fe_2O_3 is present in clay, ferromanganese nodules, volcanic debris and oxidised phases. Its abundance varies from 1·96% (258/15/1, on the Naturaliste Plateau) to 17·35% (254/28cc, on the Ninetyeast Ridge) on an absolute basis. FeO occurs in pyrite, goethite and amorphous oxides and hydroxides, ranging from zero to 5·2%. The highest abundances occur on the Ninetyeast Ridge at Sites 254 and 216, where considerable amounts of pyrite are present. The Fe^{3+}/Al ratio is higher than the average Fe^{3+}/Al ratio in terrigenous matter and the average shale (Tables 4-2 and 4-4). This could be due to the presence of volcanic material in the sediments.

The Fe^{3+}/Fe^{2+} ratio is used as an indication of the redox potential (Krauskopf, 1979). The higher the ratio, the more oxidizing is the environment. Honnorez et al. (1979) have used the following formula as a measure of the bulk rock oxidation ratio:

$$OX^{o} = \frac{Fe_2O_3/80}{Fe_2O_3/80 + FeO/72}$$

According to them, the completely oxidized rock has an oxidation ratio of 1.

The Fe_2O_3/FeO and oxidation ratios (OX^{o}) were calculated for the present study (Table 4-4). Both ratios show similar trends. The lowest ratios were observed at Sites 216, 254 (on the Ninetyeast Ridge), which is associated with high organic carbon and pyrite. At Site 258, low ratios are associated with pyrite, chamosite and high organic carbon. At Site 213, high ratio was due to the presence of phillipsite and Mn micro-nodules.

Correlation among 84 samples (Table 4-5) shows positive correlation of FeO with pyrite, organic C, TiO_2, V and chlorite (at 99·99%), Cr (at 99%), dolomite, and kaolinite (at 95%). The positive correlation of pyrite and organic C with FeO is expected, since organic C and FeO are the main requirements for pyrite formation. Dolomite also has FeO in its structure, as observed by X-R-D. The association of FeO with TiO_2 could reflect the association of both elements with oxidised phases (e.g. magnetite or ilmenite). The positive correlation of FeO with

chlorite suggests its existence in the chlorite structure. Chamosite was identified in Sample 258/16cc. Chamosite is considered to be an iron-rich septo-chlorite (Nelson and Roy, 1954). According to Calvert (op.cit.), the structure is similar to that of kaolinite, but with considerably more iron.

FeO also shows negative correlation with K_2O, Pb and La (significant at 99·99%), P_2O_5, Rb, Y, illite and SiO_2 (at 99%), clay, Cu, Ni, Mn and MLIS (at 95%). These negative correlations indicate that FeO probably does not occur in clay, Fe-Mn oxide/hydroxide and phosphorous phases. Fe-Mn oxide/hydroxide and phosphorous phases have low FeO content in deep sea sediments (Calvert et al., 1977) and form under oxidizing conditions (Price, 1976; Calvert, 1976).

Positive correlation of Fe_2O_3 with clay, TiO_2, Al_2O_3, MgO, V, As, Zn, Ce (at 99·99%), Ni, Pb, La, Is, kaolinite (at 99%), K_2O, Cu (at 98%) and P_2O_5 (at 95%) suggests the occurrence of Fe_2O_3 in the clay, especially in MLIS (it substitutes for Al^{3+} in octahedral positions, as observed in the study of pure MLIS) and in kaolinite (probably coating kaolinite as oxide or hydroxide). Fe_2O_3 also occurs in the phosphate phase, since Ni, Pb, Zn, Cu, La and As are associated with the phosphate phase. The correlation of Fe_2O_3 and FeO with V could suggest that this element is associated with dispersed oxide phases or volcanic debris. The negative correlation of Fe_2O_3 with calcite, CaO, CO_2 and SiO_2 (at 99%), quartz and clinoptilolite (at 95%) supports its association with clay.

5. MgO

MgO abundances on an absolute basis vary from 0·71% (Sample 240A/2/1, in the Somali Basin, poor in the clay) to 6·46% (Sample 215/9/2 on the flank of the Ninetyeast Ridge, rich in palygorskite). It occurs in clay minerals (palygorskite and mixed layer IS), zeolites, dolomite and volcanic matter.

Couture (1977b) has observed Mg/Al ratios of 0·26 and 0·34 for montmorillonite and zeolite-rich samples, and higher Mg/Al ratios of 0·34 and 0·40 for palygorskite-rich sediments. According to him, samples poor in palygorskite showed lower ratios of about 0·25.

In the present study, the highest ratio was about 0·633 (215/9/2)

but the ratio varies between 0·25 and 0·398 among palygorskite-bearing sediments at Sites 212, 213, 215, 221, 245, 248, 256 and 250 (Table 4-4). However, high Mg/Al ratios (0·26-0·9) were also observed at Sites 216, 246 and 254, which are due to the presence of volcanic matter and high Mg MLIS in the sediments. A small amount of dolomite is also present at Site 216.

Goldschmidt (1954) mentioned that high MgO (3 - 6%) is observed in the sediments when the original material of the sediments was derived from basic igneous rocks rich in Mg and especially when volcanic ash from basalts, andesites and related rocks was deposited with the residual and hydrolysate sediments.

The correlation programme (Table 4-5) shows positive correlation of MgO with Fe_2O_3 (at 99·99%), TiO_2 and V (at 98%) and palygorskite (at 95%), which suggests its occurrence in oxidised phases (magnetite or ilmenite) and clay.

6. CaO

It varies from 0·36% (250/15cc) to 40·08% (216/24/4) on an absolute basis. High amounts of CaO reflect abundant carbonates (especially calcite). This is evident from the strong positive correlation of CaO with CO_2 and calcite (at 99·99%) and Sr (at 99%). As previously discussed in Chapter III, calcite is mostly of biogenic origin. A small amount of CaO is present in zeolites (phillipsite and clinoptilolite), feldspars and the clay.

The average concentrations of CaO in non-carbonate sediments are less than in average shale and deep-sea clays (Table 4-1). It is less than one per cent in clinoptilolite-bearing sediments.

Its negative correlation with SiO_2, Al_2O_3, Ce, clay, K_2O (at 99·99%), Fe_2O_3, Na_2O, Pb, Zn, Cu, MLIS, illite (at 99%), Ni (at 98%) and Rb and La (at 95%) (Table 4-5) is expected, since those elements are the main constituents of clay.

7. Na_2O

Na_2O abundances vary from 0·26% (212/16/2 in the Wharton Basin) to 5·64% (215/8/2, on the flank of the Ninetyeast Ridge) on an absolute basis. Sample 215/9/2 was the only sample washed with distilled water, and therefore 0·21% Na_2O is not the original value.

It mostly occurs as halite resulting from the evaporation of the interstitial waters. The other sodium-bearing minerals present in the samples are feldspars, clay and zeolites. According to Chester and Austin (1976), the alkali elements may be associated with the clay minerals in two principal ways: in lattice structures and in surface and inter-sheet positions.

Geochemical partition studies for Site 223 have shown that an important proportion of Na is located in exchangeable positions of clay minerals (Papavasiliou, 1979). However, in the case of the present study, high Na_2O abundances were observed where high amounts of halite were present (213, 215 and 245). This is further confirmed by the strong positive correlation between Na_2O and halite (at 99·99%).

The positive correlation of Na_2O with phillipsite, Mn, Ni, Pb Cu, Y (at 99·99%), P_2O_5, Mo (at 99%), La, K-feldspar (at 98%) and MLIS (at 95%) indicates the association of Na_2O with phillipsite, phosphate, Fe-Mn oxide/hydroxide and clay (MLIS). This could be seen especially in samples from Site 213, where halite is associated with phillipsite, and Fe/Mn oxide/hydroxide.
The negative correlation with calcite, CaO and CO2 (at 99%) and Sr (at 98%) suggests its association with non-carbonate fraction.

8. K_2O

The abundance of K_2O varies from 0·3% (216/24/4, on the Ninetyeast Ridge) to 4·13% (248/14/1, in the Mozambique Basin) on an absolute basis. It occurs in the clay (especially illite - strong positive correlation of K_2O with illite, significant at 99·99%), feldspars and zeolites. K_2O is present in the lattice structures of all the above minerals. It also occurs in surface and inter-sheet positions of the clay. K_2O abundances increase with depth at Sites 211, 245 and 257, whereas it decreases with depth at Sites 221 and 236. It does not show any specific variation with depth at other sites.

The correlation programme among 84 samples (Table 4-5) shows positive correlations of K_2O with Rb, Zr, Zn, Ce and illite (at 99·99%), SiO_2, Al_2O_3, Mn, Ni, Pb, La, plagioclase, palygorskite and clay (at 99%), Fe_2O_3 (at 98%) and K-feldspar (at 95%), and negative correlation with calcite, CaO and CO_2 (at 99.99%). These strongly suggest the occurrence of K_2O in clay and zeolites. Its negative correlation with FeO (at

99·99%) and organic C (at 99%) may suggest the occurrence of illite in the oxic sediments.

9. P_2O_5

It varies from 0·03% to 1·31%. Its average concentration (0·27%) on an absolute basis is higher than the average TM, shale and deep-sea clay. Its highest concentration occurs with the highest concentration of Mn, Fe_2O_3, and most of the trace elements. A small amount of apatite and phosphorite nodules were observed under SEM in a few samples, whereas they were not observed by X-R-D because of their low concentration. However, it seems that P_2O_5 is mostly associated with Fe-Mn oxide/hydroxide and only a small amount of it is present as apatite, phosphorite nodules and in association with clays.

The correlation programme (Table 4-5) showed positive correlation of P_2O_5 with Mn, Y, Mo, Ni, Pb, As, Cu and La (at 99·99%) and Fe_2O_3(at 95%) which supports its association with Fe-Mn oxides/hydroxides. According to Calvert et al. (1970), P_2O_5 usually concentrates in Fe-Mn micronodules. Its positive correlation with Zn (significant at 99%) could suggest the occurrence of Zn in phosphorite nodules and apatite rather than Mn-micronodules, since there is no correlation between Zn and Mn. Further, the occurrence of Zn in phosphorite has been reported by Calvert (1976). The positive correlation of P_2O_5 with phillipsite and halite (at 99.99%) and Na_2O (at 99%) could indicate its occurrence in the shallow and oxic sediments.

10. Vanadium (V)

Its abundance varies between 19 ppm (Site 246) and 518 ppm (254/28cc) on an absolute basis.

The highest values are observed on the Ninetyeast Ridge (average 247 ppm), where there were high reducing conditions and a considerable amount of volcanic material which could be the main source for vanadium enrichment. The log-log diagram also showed VM could be a source for V. Bostrom and Fisher (1971) report values of 200 to 400 ppm vanadium (on a $CaCO_3$ + opaline silica-free basis) for hemipelagic sediments from the north-west of the Indian Ocean. They attributed these high vanadium values to high organic matter content and reducing conditions prevailing in these sediments. Vanadium content at Site 211 increases downward, which suggests the increasing effect of basaltic contribution to the

bottom sediment. At Site 212 V% is higher than the average TM and deep sea clay, but from Sample 212/27/1 this value gets closer to the above mentioned averages. The lowermost samples, which are rich in palygorskite and clinoptilolite, show values lower than the average TM. At this site vanadium increases as Fe_2O_3, P_2O_5, As, Y, Mo, Mn, Ni, Pb and clay increase, while clinoptilolite and K_2O decrease. Therefore, it could be suggested that this element is enriched in phosphorite and clay at this site. As previously mentioned, clay and clinoptilolite are negatively correlated; therefore, with a decrease in clay, there would be a decrease in vanadium and thus negative correlation with clinoptilolite results.

At Site 213, vanadium also shows an enrichment in Sample 213/11/5 downward, where the basaltic input increases. Its abundance increases as the amount of TiO_2, Fe_2O_3, P_2O_5, Mn, Pb, As, Zn, Ce and La increases, which could suggest its association with phosphorite. At Sites 215, 246 and 257 the average vanadium is lower than the average TM, which could indicate the effect of silicic rocks, as observed from the Al/(Al+Fe+Mn) versus Fe/Ti plot and tectonic history. Sites 236, 239 and 250 show an average close to TM, whereas Sites 221, 235, 248, 256 and 258 show higher vanadium than TM.

At Site 258, as kaolinite, chlorite, pyrite, Cu, Mn, Cr, Zr, FeO, Fe_2O_3 and TiO_2 increase vanadium increases too, which could suggest its association with chlorite and kaolinite, and probably a high sedimentation rate of detrital material (chlorite and kaolinite) has produced reducing conditions to bring about the development of pyrite.

The correlation programme (Table 4-5) shows positive correlation of vanadium with TiO_2, Fe_2O_3, FeO, As (at 99·99%), Al_2O_3, Cr, pyrite, organic C, chlorite (at 99%), MgO, kaolinite (at 98%) and Zn, Ba, Ce (at 95%). These correlations indicate vanadium association with clay and reducing conditions.

11. Chromium (Cr)

Its abundance varies from 10 ppm (Sample 258/14/1) to 360 ppm (Sample 254/28cc) on an absolute basis.

According to Goldberg et al. (1958), an excess of Cr above approximately 0·01% in pelagic sediments is a useful indication of the

presence of basaltic pyroclastics.

In the present study, the north-eastern sites (i.e. 211, 212, 213 and 215) show low Cr content in comparison with average TM, deep sea clays and basic igneous rocks. The north-eastern sediments younger than late Miocene have been under the influence of silicic volcanism from the Indonesian Island arc, and it is not surprising that they show $<$ 100 ppm Cr concentration. In the sediments older than Miocene, the Cr concentration is still lower than 100 ppm, although the influence of the basaltic material increases (Table 4-4). According to Fleet et al. (1974), basaltic material loses Cr during alteration.

The south-eastern sites (i.e. 256, 257 and 258) also show low Cr content in the upper part of the section, but as the depth increases the Cr increases to more than 100 ppm, which could indicate the increased influence of basalt to the sediments.

The western sites show the Cr content to be higher than 100 ppm, except for Sites 245, 246 and 240. The chemical model (Table 4-3) showed the high silicic rock contribution to Site 246. Sites 240 and 245 also receive a mixture of basaltic and granitic rocks. However, the bottom-most sediments of Sites 245 and 240 show high Cr content ($>$ 100 ppm), which could suggest a basaltic basement contribution to these sediments or volcanic matter input from the MIOR.

The correlation programme among 84 samples (Table 4-5) shows positive correlation of Cr with TiO_2 (at 99·99%), FeO, organic C, CaO, CO_2, calcite and V (at 99%), chlorite (at 98%) and pyrite (at 95%). The high positive correlation with TiO_2 could be related to its occurrence in basaltic material, whereas the correlation with FeO, organic C, CaO, CO_2, calcite and pyrite could suggest the occurrence of Cr under reducing conditions. (The organic tissue of calcareous fossils could provide the necessary organic matter for pyrite formation.) Under reducing conditions, Cr released from the alteration of basaltic material is insoluble and could exist as insoluble hydroxide or sulphide in the anoxic layer. Chester et al. (1976) believe that Cr and V are largely lithogenous in origin, i.e. they are transported from the continents in lattice positions within crustal minerals.

Its negative correlation with SiO_2 (at 99·99%) is expected since

a large amount of SiO_2 is of biogenic and detrital origin (quartz). Its negative correlation with Mn (at 99%), P_2O_5, Pb (at 98%), Na_2O, Y, Cu and La (at 95%) is expected, since Cr occurs in anoxic sediments, whereas all the above elements which refer to Mn-phosphorous phases indicate more oxic conditions.

12. Manganese (Mn)

Its abundance varies from 0·01% to 4·68% (on an absolute basis). The average Mn content, derived from Table 4-6, is 0·57%. This value compares favourably with other values for deep sea clays presented by other authors, e.g. 0·37% (Price, 1967), and 0·3 - 0·8% (Lynn and Bonatti, 1965).

It is present either as Fe-Mn oxide/hydroxide coating the clay and feldspars or as Mn micronodules. Its positive correlation (Table 4-5) with plagioclase (at 99·99%), dolomite (at 99%) and K-feldspar (at 98%) suggests its presence as Fe-Mn oxide/hydroxide coating the detrital grains. The Tertiary sediments of the eastern sites show high Mn content (1-2%). Mn micronodules were observed under SEM at Sites 213, 221 and 250 (Plate 4-3, a-c). The highest Mn% occurs with the highest amount of P_2O_5, Fe_2O_3 and most of the trace elements at some of the sites (e.g. 256 and 221), but it does not show any correlation with iron in some other sites (e.g. 216 and 254). The correlation programme among all 84 samples (Table 4-5) shows no correlation between Mn and Fe, whereas correlation studies between Mn and iron among the samples of each individual site show medium to weak correlation between the two elements at some sites (e.g. 212,239 and 256). Cronan et al. (1967) pointed out that iron is generally lower in abundance than Mn in abyssal Indian Ocean nodules, including those from most of the eastern portion of the basin, and is also relatively low in those from the depressions in the west.

The positive correlation of Mn with Y, Mo, Ni, Pb, As, Cu, La and P_2O_5 (at 99·99%) points to the well-known ability of both ferric and manganese oxides/hydroxides to efficiently co-precipitate cations and anions (Kurbatov et al., 1951; Burser & Grutter, 1956; Calvert & Price, 1977). Burser and Grutter (1956) based the presence of the high concentration of the accessory metals in manganese nodules on the existence of large surface areas in the nodule materials. According to Goldschmidt (1954) polyvalent ions with a high charge density, like copper, the rare

PLATE 4-3

a & b. Mn micronodule in Sample 213/11/2

c. " " " Sample 221/15/4.

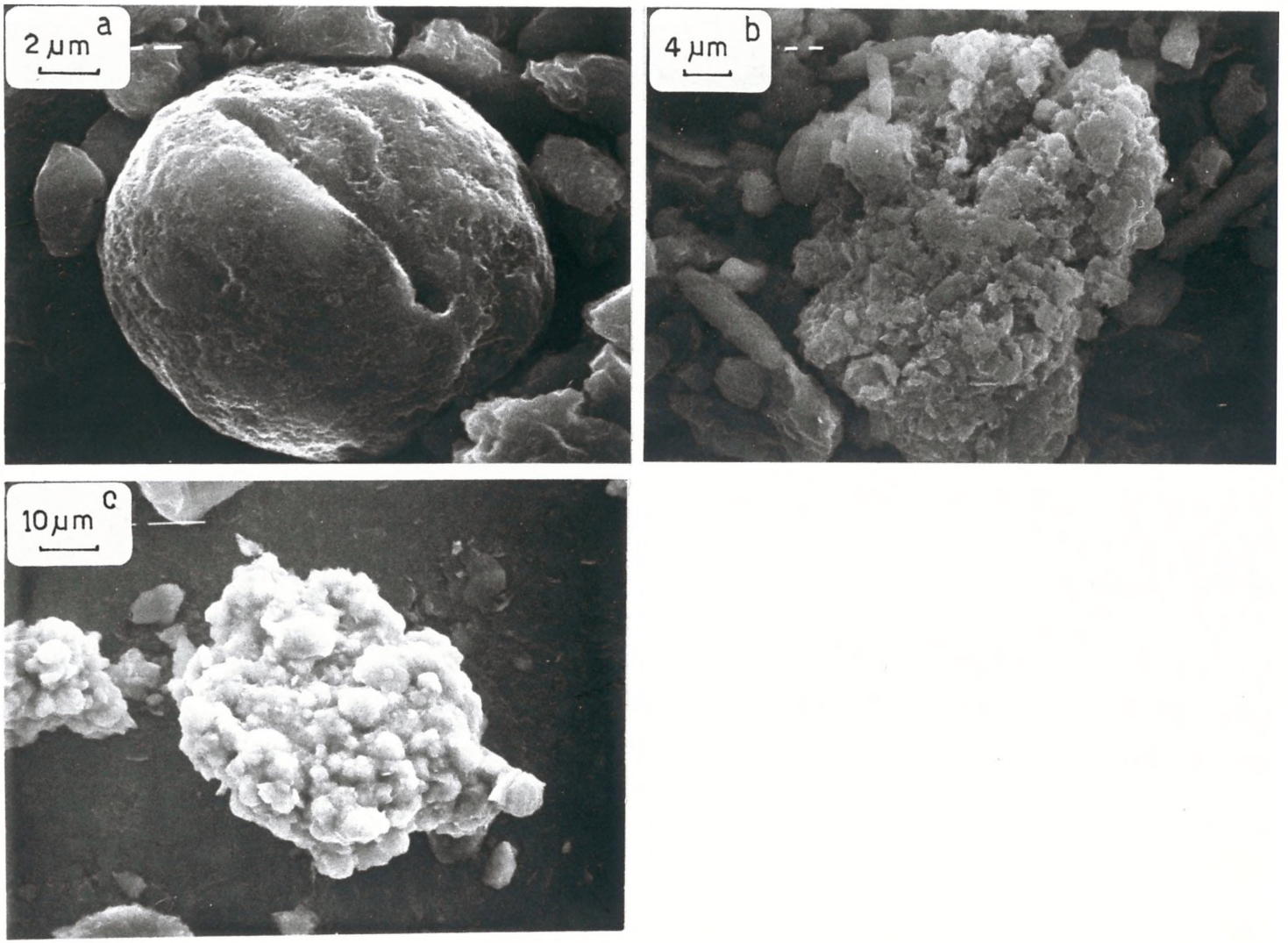

PLATE · 4_3

earths, zinc, lead, etc. more readily enter into sorption reactions than the alkali or alkali-earth metals.

Mn also shows positive correlation with Na_2O (at 99·99%) and phillipsite (at 99%), which could reflect the occurrence of Mn micro-nodules at shallow depth and in oxic sediments. It could also point to the low sedimentation rates of the sediments. The source and mechanism of accumulation of this element has been discussed by many authors. Murray and Renard (1891) suggested the crustal rocks of the continents as a source. Correns (1941) indicated the possibility of a biological extraction of Mn from the sea-water into foraminiferal tests. Bostrom et al. (1969) suggested submarine volcanism along active oceanic ridges (ridges with ocean floor spreading). According to Bostrom (1967), the more deeply buried strata of the pelagic sediments could be a source for Mn. He believed that Mn(III) and Mn(IV) - compounds are easily reduced to mobile Mn(II)- compounds due to reactions with reducing organic compounds, or magmatic gases. The Mn(II)-compounds formed are more soluble than co-existing iron compounds and migrate upwards as a disperse phase together with other products, primarily CO_2 and H_2O, of the redox reactions and dehydration processes going on at depth. This migration is favoured by tectonic processes and volcanic eruptions, which provide channels for the solutions on their way to the sediment-water interface. Many authors have reported the occurrence of the Mn nodules in areas marked by strong, sediment-eroding bottom currents or where the rate of sediment deposition is sufficiently low to ensure that accreting manganese does not become covered and removed from the sediment-water interface (Watkins and Kennett, 1971; Lonsdale et al., 1972; Kennett et al., 1975, 1976).

Kennett et al. (1976) have shown that the same factors account for the formation of the south-east Indian Ocean Mn pavement, but recently Watkins and Kennett (1977) have suggested that factors other than sediment erosion, such as the chemical environment and the proximity of element source (Mero, 1960), are also important in nodule growth. They suggested that the proximity of volcanically active sea floor, which acts as an element source, is a probable explanation of extensive manganese nodule growth in areas of erosion. They pointed out that the south-east Indian Ocean manganese pavement is adjacent to the Diamentina Fracture Zone, the western end of which intersects Ninetyeast Ridge, which is a major

transform fault according to McKenzie and Sclater (1971), and thus this fracture zone is the source of Mn nodules in this area. Summerhayes (1967, 1969) suggested that the availability of Mn from local volcanic sources was essential for Mn growth on the Campbell plateau in the vicinity of the Antipodes Islands. Goodel (1973) also suggested a close association between manganese nodule development, current activity and submarine volcanism of the mid-oceanic ridge system, and the Eltanin Fracture Zone.

In the present study, it seems that two conditions favouring Mn nodule development (i.e. active bottom current and local volcanic activity) are met in most of the sites. Sites 245 and 248 are of Eocene age, whereas Site 250 is of the late Cretaceous. These sites, as previously mentioned, could receive volcanic matter from MIOR and the Carlsberg Ridge. On the other hand, a widespread hiatus in the Oligocene sediment, which is attributed to the bottom water activity at that age,also exists.

The eastern sites are mostly of Eocene or younger age. As previously mentioned, fracture zones existed near Site 212 (von der Borch et al., 1974) and the Mn micronodules appear in the brown zeolitic clay, which could indicate a slow sedimentation rate. However, the occurrence of unconformity between the lower Eocene and middle Miocene sediments at Site 213 (Johnson, 1974) could indicate the activity of the Oligocene aggressive bottom water in this area.

13. Nickel (Ni)

It varies between 26 ppm (246/10/2) and 606 ppm (213/11/5) on an absolute basis. The average Ni concentration is 146 ppm. The log-log diagrams (Figs.4-4 to 4.15) suggested that Ni could be contributed by VM and BM to the sediments. Its highest percentages occur with the highest percentages of clay, Ce, La, Pb and Y at Sites 221, 236, 239 and 250, and with Mn, P_2O_5, La, Cu, Fe, Mo and Pb at Sites 256 (Core 2/3), 245 and 216. Therefore, it is probably associated with clay and Fe-Mn oxide/hydroxide. The enrichment of ferro-manganest nodules and clay in Ni has been reported by Chester and Aston (1976). Suliman (1972) has reported the occurrence of Ni in Fe-Mn oxides/hydroxides and clay.

Calvert (1976) also reported the presence of Ni in ferro-manganese

nodules and clays. The correlation programme (Table 4-5) also confirms the occurrence of Ni in clay and Mn phases. It showed positive correlation with Cu, Pb, As, Zn and La (at 99·99%), Ce and halite (at 99%), clay (at 98%) and MLIS (at 95%). Its negative correlation with clinoptilolite and calcite (at 99%) confirms its association with clay.

14. Copper (Cu)

It varies between 30 ppm (239/1/1) and 372 ppm (213/11/5) (on an absolute basis). It is higher than the average TM and shale in all sites, which could mean that the sediment source contributes more basic or biogenic matter to the sediments. The log-log diagram showed a source of VM and BM is possible for Cu. Krauskopf (1956) has shown that Cu is efficiently adsorbed by $Fe(OH)_3$, $Mn(OH)_3$ and clay minerals.

In the case of the present study, it is mostly associated with Fe-Mn oxide/hydroxide phase and clay minerals.

The correlation among 84 samples (Table 4-5) shows positive correlation of Cu with Al_2O_3, Na_2O, P_2O_5, Y, Mo, Mn, Ni, Pb, As, Zn, La, phillipsite, halite (at 99·99%), clay, MLIS, Ce (at 99%) and Fe_2O_3 (98%), which confirms its association with clay, Fe-Mn oxide/hydroxide and phosphorite phases.

15. Zinc (Zn)

Its abundance varies between 229 ppm (Sample 257/2cc) and 70 ppm (Sample 239/1/1) on an absolute basis.

It is mostly associated with clays. The correlation programme (Table 4-5) confirms the association of Zn with aluminosilicate (clay). There is positive correlation between Zn and Al_2O_3, Fe_2O_3, K_2O, Ni, Pb, As, Cu, Ce and La (at 99·99%), P_2O_5, Zr, Nb, clay and illite (at 99%) and Y (at 98%).

The positive correlation of clay with Zn is illustrated in Figure 4-19. The positive correlation which is significant at 99% has an intercept of 4·57 ppm. This means that 4·57 ppm is not associated with clay or that an average of about 119 ppm is associated with clay, which is 96% of the total Zn. Leaching studies by Papavasiliou (1979) showed that Zn was 69% 'lattice held'. Chester et al. (1976) also reported 66% 'lattice

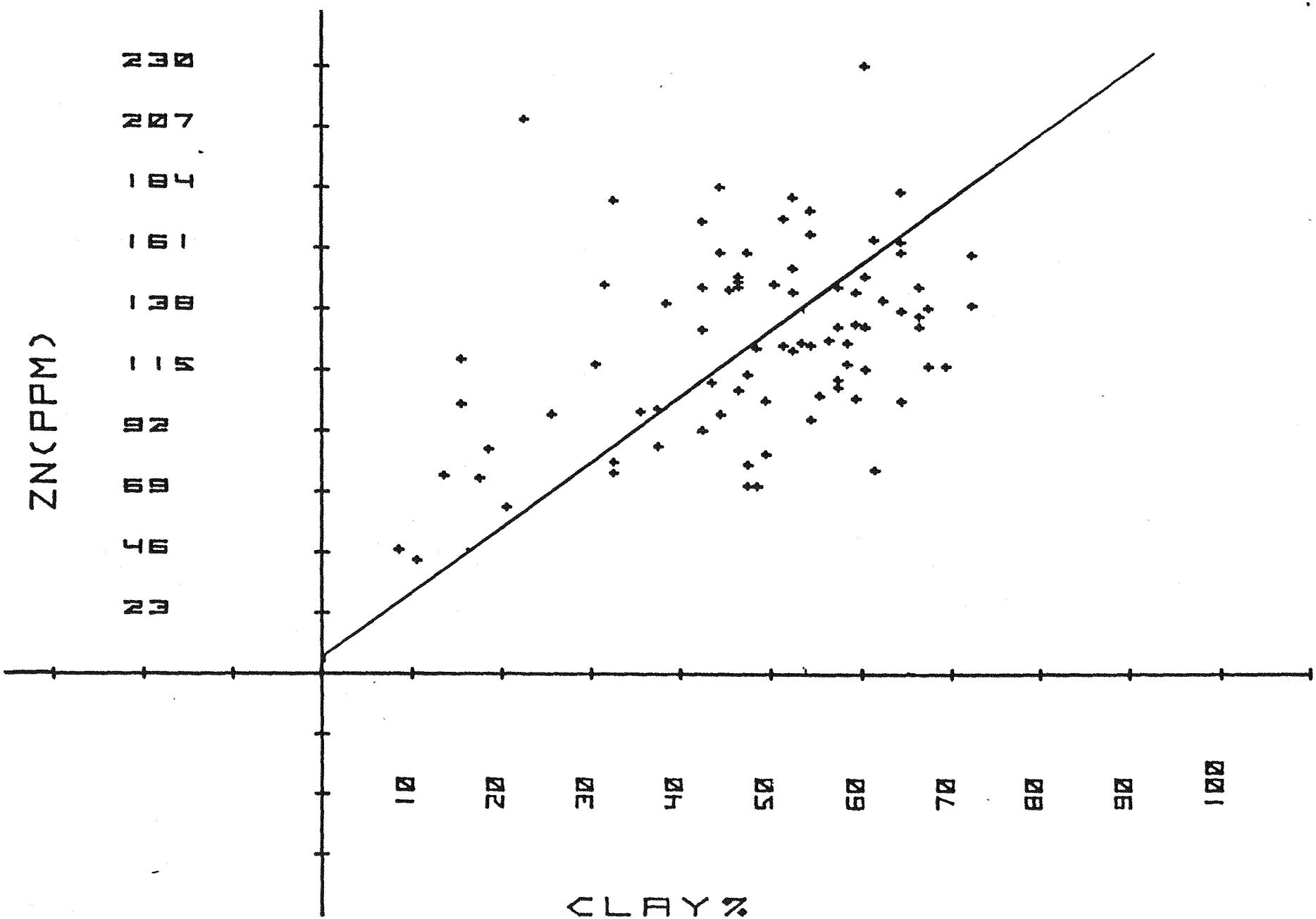
ZN(PPM)
230
207
184
161
138
115
92
69
46
23
10
20
30
40
50
60
70
80
90
100
CLAY%

Fig. 4-19

held' Zn. Papavasiliou (op.cit.) believed that Zn connected with the 'lattice held' is controlled mainly by the clay minerals. The present study suggests an even greater association of Zn with clay minerals, possibly 'lattice held' and surface adsorbed. However, the remaining 4-5% of total Zn is probably associated with phosphorite, as suggested by the correlation programme. Price (1976) and Calvert (1976) reported the occurrence of Zn in phosphorite. Price believes that this element seems to substitute for Ca^{2+} in the lattice.

16. Arsenic (As)

It varies between zero and 57 ppm (on an absolute basis). It is higher than the average TM, shale and deep-sea clay in the eastern sites sediments, whereas in the western sites sediments it is either absent or close to the average TM and shale.

It is absent at Site 216, except in Sample 216/25cc where the highest amount of MLIS is present. At Site 215 it increases as clay, P_2O_5 and Mn increase. The same trend was observed at Site 240. At Site 239, it increases as Mn increases, whereas at Site 212 it increases as Mn and P_2O_5 increase. Therefore, it seems that As is associated with three phases: clay, Fe-Mn oxides/hydroxides and phosphorites. Calvert and Price (1970) reported the occurrence of As in Mn nodules. Calvert (1976) pointed out the substitution of As as AsO_4^{3-} for PO_4^{-3}. Baig (1982) reported the occurrence of As in clay and Fe-Mn oxides/hydroxides.

The correlation programme (Table 4-5) confirms its relationship with phosphorites and Fe-Mn oxides/hydroxides and clay. It shows positive correlation with Al_2O_3, Fe_2O_3, La, Mo, Zn, Cu, P_2O_5, Mn, Ni, V and Pb (at 99.9%) and Y (at 99%).

17. Rubidium (Rb)

It varies between 158 ppm (250A/11/2) and 11 ppm (216/32/3) on an absolute basis. It is lower than average TM and shale in the eastern sites, whereas the western sites show an amount close to either average TM or shale. Both Rb and illite are either absent or present in low amounts at Sites 216, 254, 256, 257 and 258. According to Hirst (1962), Rb is present in the clay mineral and feldspars. Calvert (1976) believes that Rb occurs in the lattices of mica and chlorite. Goldschmidt (1954) and Krauskopf (1967) have suggested that Rb is able to

substitute for K^+ in potassium minerals because of similar ionic radii values (Rb^+: 1·47Å; K^+: 1·33Å).

The association of Rb with illite is also supported by the correlation programme (at 99·99%). The other significant correlations in this programme (Table 4-5) are the positive correlations of Rb with clay and K_2O (at 99·99%), Zr (at 99%), Al_2O_3, Zn and plagioclase (at 95%).

18. Strontium (Sr)

It varies between 62 ppm (Sample 256/8/4) and 613 ppm (216/24/4) on an absolute basis. It is present in the clay, zeolites, feldspars, ferro-manganese oxides and phosphorite. Calvert (1976) has discussed the occurrence of Sr in the above minerals.

In the case of the present study, it is mostly controlled by carbonates, particularly calcite in carbonate-rich sediments. This is confirmed by the positive correlation of Sr with CaO, CO_2 and calcite (at 99%). Calcite is mostly of biogenic origin in the present study. Chester (1965) stated that Sr is of biogenic origin and is supplied by the calcareous marine organisms. The association of Sr with biogenic carbonate has also been reported by Papavasiliou (1979), Turekian (1964), Bostrom et al. (1974) and Baig (1982). The size of the strontium ion indicates that it can proxy for Ca in Ca-bearing minerals (higher ionic radius, Sr = 1·12; Ca = 0·99) (Mason, 1966).

Figure 4-20 shows the positive correlation of Sr with $CaCO_3$ in carbonate-rich sediments. The regression intersecting the vertical axis at about 194 ppm suggests that this amount of Sr is not associated with $CaCO_3$. There are a few samples which plot away from the regression line. The samples below and away from the line probably suggest the existence of calcite with low Sr concentration. Manheim et al. (1971) have observed Sr enrichment of interstitial water in rapidly deposited carbonate-rich sediments. They have concluded that most Sr enrichments occur when coccolith-foram-calcite recrystallizes to a calcite which is poor in Sr. The points above the line tend to suggest the association of Sr with another phase besides calcite. In Sample 212/15/3 Sr is probably associated with Mn and phosphorite, since it is rich in those phases. Sample 250A/15cc contains high Mn and feldspar, whereas, in Samples 239/1/1 and 258/25cc, it is associated with zeolites (phillipsite and clinoptilolite, respectively).

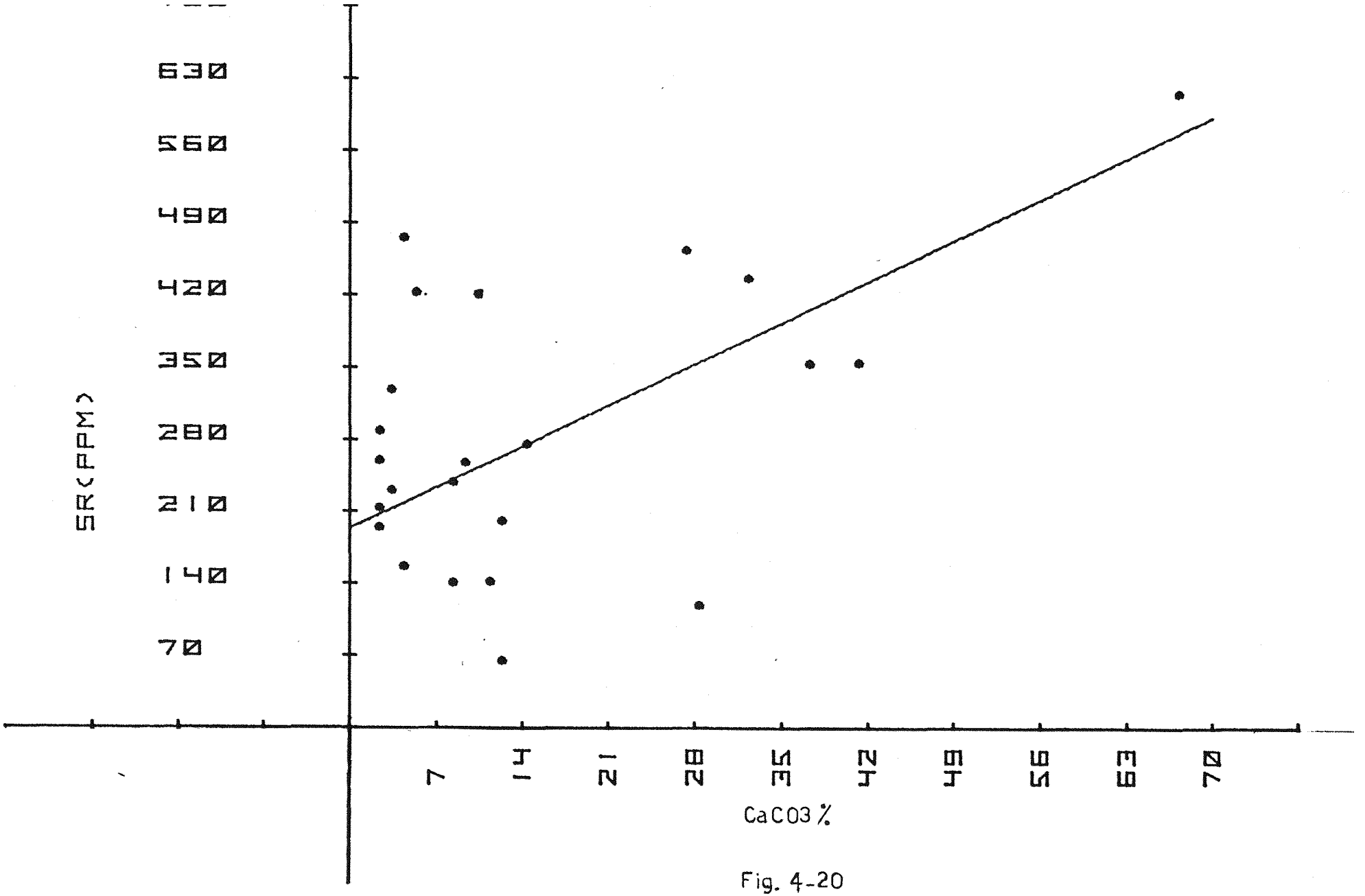
630
560
490
420
350
280
210
140
70
SR(PPM)
7
14
21
28
35
42
49
56
63
70
CaCO3 %

Fig. 4-20

19. Yttrium (Y)

It varies between 12 ppm (Sample 240A/2/1) and 273 ppm (Sample 256/8/4) on an absolute basis. Its average (62 ppm) is higher than the average TM, shale and igneous rocks. It increases as plagioclase, K-feldspar and dolomite increase at Sites 248, 250 and 254, which confirms its detrital origin. It probably occurs in the lattice of feldspars. At Site 212 it increases as P_2O_5, Mn, Fe_2O_3, Ni, Pb, As and Cu increase, which could suggest the occurrence of Y in phosphorite and Fe-Mn oxides/hydroxides.

The correlation programme among 84 samples shows positive correlation of Y with Na_2O, P_2O_5, Nb, Mn, Mo, Ni, Pb, Cu, halite (at 99·99%), phillipsite, La and Zn (at 99%). These correlations tend to confirm the occurrence of Y in phosphorite and Fe-Mn oxide/hydroxide. Chester and Aston (1976) have observed the occurrence of phosphorite in ferro-manganese nodules.

The positive correlation of Y with halite and phillipsite probably relates to the occurrence of Mn nodules at shallow depth, as was evident at Site 213.

20. Zirconium (Zr)

It varies between 34 ppm (Sample 257/5/2) and 705 ppm (Sample 246/10/2) on an absolute basis. It fits the suggested chemical model (Table 4-3 and Figs.4-4 to 4-15). However, a depletion is observed in Group V, which is assumed to have been released into the interstitial water after volcanic rock alteration.

The correlation programme (Table 4-5) shows positive correlation of Zr with K-feldspar and plagioclase (at 99·99%), K_2O, Rb, Zn and dolomite (at 99%). As previously mentioned, K-feldspar, plagioclase and dolomite are of detrital origin. Therefore, Zr could also be present as detrital zircon and thereby is of the same origin as the rest of the detrital phases. According to Krauskopf (1979), the rare metal zirconium cannot fit easily into common silicate structures, and even a very small amount of it goes into separate crystals of the accessory mineral zircon.

21. Niobium (Nb)

It varies between 6 ppm (258/25) and 203 ppm (256/8/4), on an absolute basis. Its average is lower than average TM, shale, granite,

mafic and ultra mafic igneous rocks and deep-sea clays in most of the sediments, except those of Sites 235, 236, 240, 246, 256 and 257 which are much higher.

The correlation programme shows positive correlation of Nb with Y (at 99·99%) and Zn (at 99%). Y is strongly connected with phosphorite. Therefore Nb may be present in phosphorite. According to Calvert (1976), Nb could be present as an impurity in phosphorite.

22. Barium (Ba)

It is either of biogenic or volcanogenic origin in deep-sea sediments (Bostrom et al., 1976).

In the case of the present study, it is hosted in clay, barite, feldspar, biogenic silica and zeolites, especially clinoptilolite. It varies between 240 ppm (213/9cc) and 4771 ppm (258/14/1) on an absolute basis.

Ba is present in high concentration in clinoptilolite-bearing sediments, which are also rich in biogenic silica and opal-CT. The correlation programme (Table 4-5) also shows positive correlation of Ba with clinoptilolite (at 99·99%). The observation of Goldberg et al. (1958) showed that the Ba is bonded in the opal or zeolite structure. The log-log diagrams also show the occurrence of Ba in BM and VM.

Ba positive correlation with SiO_2 (at 98%), V, TiO_2 and organic C (at 95%) and negative correlation with halite, Ce, Mo, P_2O_5, La (at 99%), Pb and Y (at 98%) indicate its association with biogenic silica, volcanic matter and reducing conditions.

23. Lanthanum and Cerium (La + Ce)

They both show a similar behaviour. The average abundance of Ce (111 ppm) is higher than the average TM and shale. La also shows a high average concentration (72 ppm). However, Sites 248, 250, 254, 257 and 258 are close to average TM and shale. The highest concentration of Ce is associated with the highest concentration of clay, and especially illite at Site 213. At Sites 212 and 257, it is associated with feldspars and quartz, whereas at Site 216 it is associated with P_2O_5 and Fe_2O_3.

The highest concentration of La is associated with the highest amount of clay, Mn, P_2O_5 and Fe_2O_3 at Site 212, and with clay, P_2O_5 and Fe_2O_3 at Site 257. At Site 213 it is associated with the highest P_2O_5, Org C, Mn, Fe_2O_3, plagioclase, quartz, kaolinite and MLIS. Therefore, it is suggested that Ce and La occur in feldspars, clay, Fe-Mn oxides/hydroxides and phosphorite.

Goldschmidt (1937), Hirst (1974), Stephens et al. (1975) have mentioned the strong relationship of 'REE' with clay. Chowdhury (1980) and Baig (1982) reported the association of Ce, La and Y with total clay, phosphorite and resistates. Calvert (1976) also believes that, in marine sediments, the 'REE' usually concentrate in association with phosphorite and iron oxide coatings on the surfaces of clay minerals. The association of Ce and La with clay, Fe-Mn oxide/hydroxide and phosphorite is also supported by the correlation programme (Table 4-5). This programme shows that Ce is positively correlated with Al_2O_3, Fe_2O_3, Pb, La and Zn (at 99·99%), illite, K_2O, Ba, As, Cu and Ni (at 99%), and Na_2O (at 98%), indicating the association of Ce with aluminosilicate. The aluminosilicate is clay since Ce shows a strong positive correlation with clay (at 99·99%). Its negative correlation with CaO, CO_2 and calcite (at 99.99%) is expected, since clay and carbonate are antipathetically related. The correlation programme (Table 4-5) shows positive correlation of La with Al_2O_3, P_2O_5, Mn, Cu, Ni, Pb, As, Ce and Zn (at 99·99%), Fe_2O_3, Y, phillipsite, clay and illite (at 99%), Na_2O (at 98%) and halite (95%), suggesting its association with clays.

The correlation of La with phillipsite, halite and Na_2O could suggest that the phosphorites and Fe-Mn oxide/hydroxide containing La occur at shallow depths, since this is the characteristic of phillipsite and halite in the present study. Negative correlation with FeO (at 99·99%), clinoptilolite (at 99%), CO_2, CaO, calcite, organic C and pyrite (at 95%) could indicate the detrital origin of La, since all the above minerals have either biogenic or authigenic origin. It could also indicate the occurrence of La in the oxic sediments.

24. Lead (Pb)

It varies between 5 ppm (254/27/3) and 7 ppm (212/15/2) on an absolute basis.

It is higher than average TM and shale in most samples. Sediments from Site 254 show Pb% close to mafic igneous rocks. A few samples (e.g. 213/15/2 or upper sediments of Site 212), which are rich in biogenic carbonate, show almost the same amount of Pb as that of biogenic matter. Pb increases as Mn, Cu, P_2O_5, and Mo increase at Site 212, whereas its increase is connected with Mn only at Site 213. As Pb increases, clay increases at Sites 248 and 254. Therefore, it is suggested that Pb is associated with Fe-Mn oxides/hydroxides, clay and phosphate phases.

The correlation programme among 84 samples showed positive correlation of Pb with Al_2O_3, La, P_2O_5, Y, Mo, Mn, Ni, As, Zn and Cu (at 99·99%), Fe_2O , K_2O, Na_2O, Ce, clay and MLIS (at 99%), which suggests the occurrence of Pb in clay (especially in mixed layer IS), Fe-Mn oxide/hydroxide and phosphate phases.

Its negative correlation with CaO, CO_2 and calcite (at 99%) reflects its association with clay. The negative correlation with FeO, organic carbon (at 99·99%) and pyrite (at 99%) confirms its occurrence in oxic sediments. Price and Calvert (1970) have proposed that metals which occur in open ocean nodules are largely precipitated from the overlying water onto oxidised surfaces.

D. Factor Analysis of Bulk Mineralogy and Chemistry

The principal aim of factor analysis is to reduce observed relationships among many variables to simpler relationships. The distribution of elements in sediments is characterised by the occurrence of groups of geochemically coherent elements; that is, groups of elements that under given circumstances behave in a similar way.

A programme by Mather (1970), modified by Clayton (1970) for the Southampton University Computer, was used. Mineralogical analysis has been included with the chemical data, since it shows reasonable correlation with the elements. The promax solution was run with $K_{min} = 4$. The factor pattern is shown in Table 4-8 and the factor scores in Table 4-9. Seven factors were extracted explaining a total of 68·85% of the variance.

TABLE 4-8: Promax Factor Pattern and Correlation Matrix

Factors	F1	F2	F3	F4	F5	F6	F7
Minerals	Pyrite	Calcite	Qtz	Plag-K-feld Dol - Qtz		Clay	Clino
positive loadings ↑ low					As Ce		La
			Y	Fe^{2+}	Ba, Rb	K, Zr, Cr	Ce
	Mg	Sr, Cr	K	Mn, K		Mg, La	Zn
	Nb		Si, Rb		Sr		Y
						Rb	
high		CaO, CO_2		Zr			Nb
high		Si	Ti, V				
	Mo	Al	Fe^{2+}		Na		
	As, Pb, Mn	K, Ce			P, Y	Ba	
	Cu, Ni	Ba	Fe^{3+}, Cr			Nb	Si, Mo
	Sr	Ti, Fe^{3+}			Cu, Ni, Mg	Si, Sr	Rb
negative loadings ↓	P	Rb, Na	Ba, Mg			Y	
	La						
	Fe^{3+}, Y, V						
low				Opal-CT, clay	K-feld, Phill.	Opal-CT	
Minerals	Phillipsite	Clay, Qtz	Org C, Pyrite	Clin	Halite	Clin	Qtz

Elements + minerals underlined indicate highest loading. Major inter-factor correlation shown by ⌊——⌋ (+ve & -ve). Only loadings > 0·2 listed.

1. Factor 1

This factor, which explains 21.26% of the variance, is governed by pyrite (representing low Eh) antipathetically related to phillipsite (representing high Eh).

There are high positive loadings for MgO, Nb and pyrite which are opposed by the negative loading among Fe_2O_3, P_2O_5, Sr, Y, Mo, Ni, Pb, As, La, Cu and phillipsite.

The negative loadings indicate the Fe-Mn oxide/hydroxide and phillipsite phases. Phillipsite usually forms in sediments with low sedimentation rate and shallow burial depths. Fe-Mn oxide/hydroxide (micronodules) also precipitates under oxidising conditions and low sedimentation rates. Therefore, this factor is controlled by authigenic phases and indicates the Eh of the environment.

2. Factor 2

This factor explains 11.82% of the total variance, and is determined by the biogenous fraction (calcite) against the clay fraction. Plotting the sample scores for this factor against calcite shows a good correlation (Fig.4-21) confirming its identification. Likewise, a plot of the same scores against total clays shows a similar, if less convincing, correlation (Fig.4-22).

There are positive loadings for CaO, CO_2, Sr and calcite which clearly indicate the carbonate. However, the positive loading of Cr indicates that carbonates are not the only phase present. Cr probably indicates the anoxic sediments. It is usually present in solution in the oxic layer, but is reduced to insoluble hydroxide or sulphide in the anoxic layer. These positive loadings are opposed by negative loadings for SiO_2, TiO_2, Al_2O_3, K_2O, Rb, Na_2O, Ba, Ce, quartz and clay.

3. Factor 3

This factor explains 10·52% of the total variance and is explained by a detrital fraction (quartz) against an authigenic phase (pyrite).

The negative loadings for TiO_2, Fe_2O_3, MgO, V, Cr, Ba, FeO, pyrite and organic carbon indicate reducing conditions and the occurrence

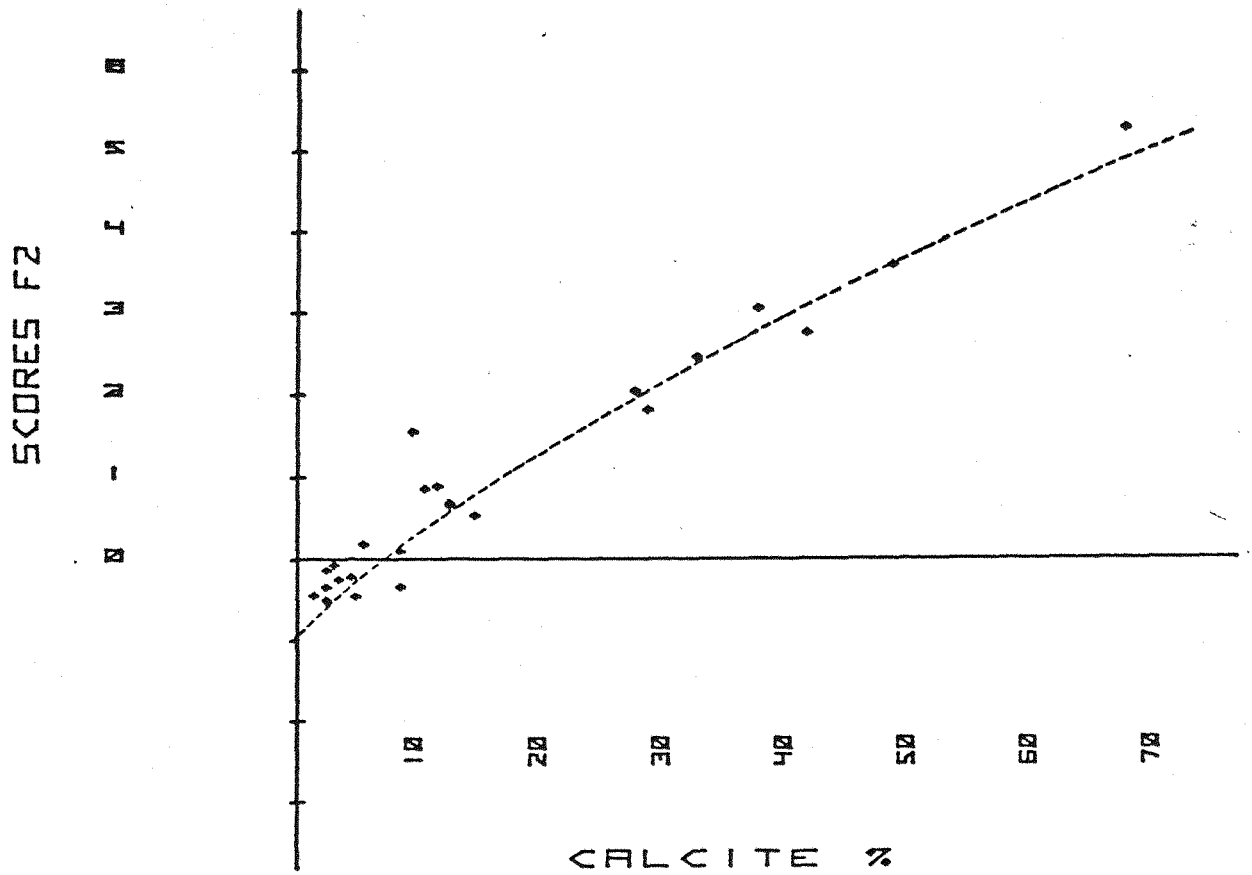

Fig. 4-21

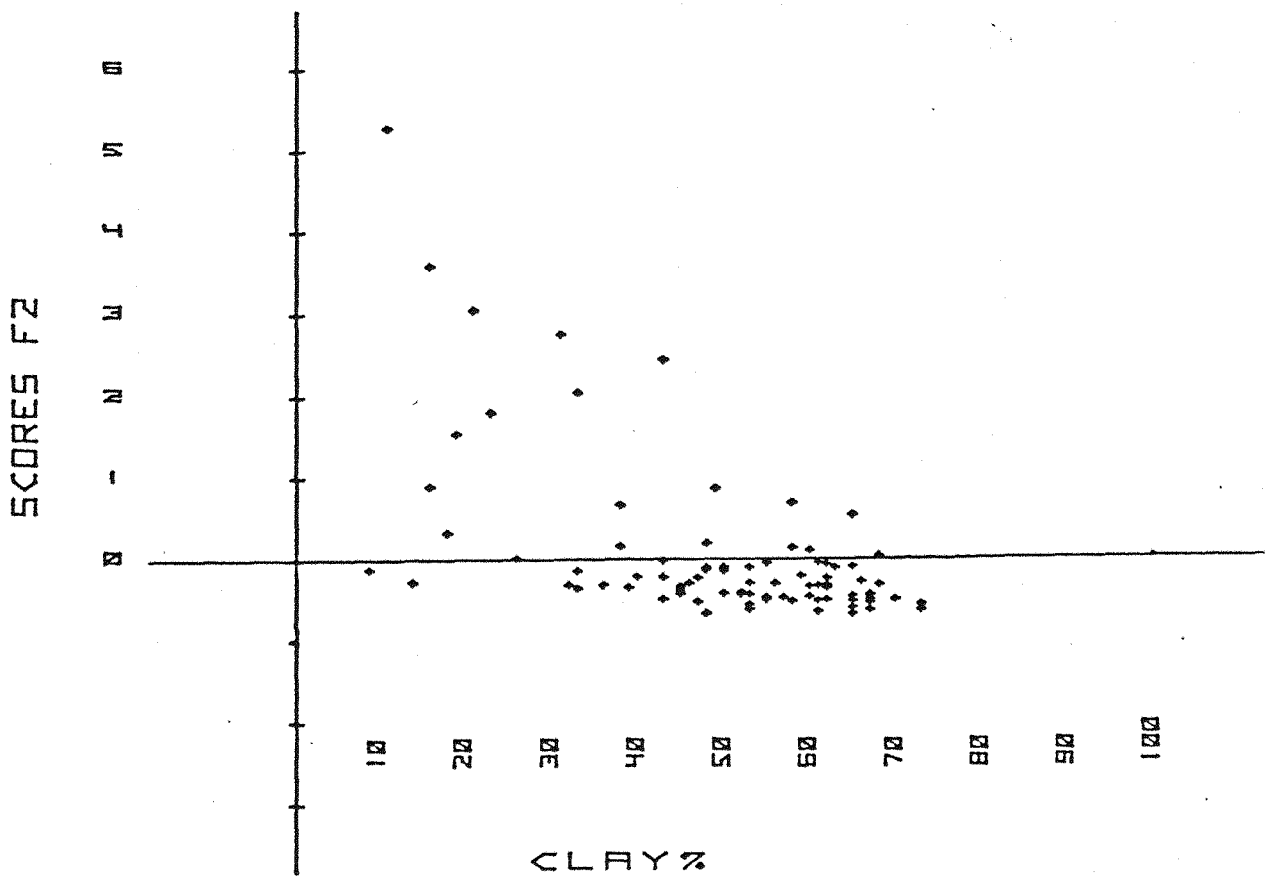

Fig. 4-22

of pyrite, ilmenite and/or magnetite (Fe^{3+}, Fe^{2+}, Ti and Mg). The precipitation of V and Cr under reducing conditions is also possible. Therefore, this factor is controlled by organic carbon.

4. Factor 4

This factor explains 8·28% of the total variance and is governed by detrital phases (quartz, feldspars and dolomite) as opposed to biogenic silica (clinoptilolite-opal CT). Figure 4-23 shows the sample scores against the sum of the Kf + Pf + Do percentages. There are positive loadings for K_2O, Zr, Mn, quartz, K-feldspar, plagioclase and dolomite, which indicate the detrital nature of these loadings. According to Chester et al. (1976), Mn could be associated with detrital minerals. Zr could also be present as the independent mineral zircon, or present in the lattice of feldspars. There are negative loadings for clinoptilolite, clay and opal-CT.

5. Factor 5

This factor explains 6·98% of the total variance. The positive loadings among Rb, Sr, As, Ba and Ce are opposed by the negative loadings for MgO, Na_2O, P_2O_5, Y, Ni, Cu, K-feldspar, phillipsite and halite. The negative loadings of the above elements also suggest the presence of Mn-Fe oxide/hydroxide.

This factor appears to be mainly controlled by phillipsite. Figure 4-24 indicates the sample scores against phillipsite.

6. Factor 6

This factor explains 2·13% of the total variance, which is governed by clay against clinoptilolite. Figure 4-25 shows a good correlation between the sample scores and clinoptilolite. It shows positive loadings for MgO, K_2O, Rb, Zr, Cr, La and clay, and negative loadings for clinoptilolite, SiO_2, Y, Nb, Sr and Ba.

Therefore this factor could be called the clinoptilolite and clay factor.

7. Factor 7

Positive loadings for Y, Nb, clinoptilolite, Zn, Ce and La are opposed by the negative loadings of quartz, SiO_2, Rb and Mo, which places

Fig 4-23

Fig. 4-24

Fig.4-25

an authigenic phase against a detrital phase, and could thus be designated the quartz factor.

TABLE 4-1: Chemistry of Bulk Samples (on an absolute basis)

(a) Major Elements

	SiO_2	TiO_2	Al_2O_3	Fe_2O_3	FeO	MgO	CaO	Na_2O	K_2O	P_2O_5	L.O.I.	$CO_2(T)$
211/6/2	59·09	0·50	15·70	6·17	0·32	3·39	1·43	1·00	2·06	0·43	9·53	2·25
211/13/1	44·53	0·97	12·05	7·26	0·03	2·72	11·72	-	3·79	0·11	16·15	9·63
211/14/1	51·31	1·09	13·18	7·22	0·03	3·81	5·94	-	4·03	0·17	12·25	5·58
212/15/2	47·71	0·89	17·08	11·75	-	3·25	1·11	2·31	2·69	0·42	9·48	1·31
212/15/3	46·16	0·81	16·10	12·39	-	2·94	2·56	2·03	2·58	0·36	9·58	2·30
212/16/1	49·18	0·97	17·68	12·24	-	2·91	1·04	0·46	2·63	0·35	10·65	1·64
212/16/2	48·88	0·84	17·78	11·18	0·04	2·64	0·94	0·26	2·31	0·26	13·92	1·90
212/17cc	49·24	0·92	16·55	13·44	-	2·86	1·15	1·60	3·08	0·49	8·58	0·90
212/18/1	49·34	0·85	17·87	12·93	-	2·97	0·86	1·98	2·40	0·33	8·5	0·66
212/18/2	55·98	0·85	15·05	9·23	0·04	3·38	0·86	2·32	3·09	0·17	7·5	1·02
212/23/5	57·44	0·58	14·16	10·76	0·11	4·29	0·93	2·59	2·29	0·15	7·00	2·33
212/27/1	45·78	0·94	24·38	11·50	0·07	2·11	0·85	1·77	2·27	0·38	9·03	0·78
212/27/5	47·22	0·86	22·74	10·56	0·03	2·38	0·66	0·25	2·22	0·18	12·47	1·21
212/28/2	46·92	0·84	25·2	10·96	0·06	2·19	0·83	1·64	1·94	0·34	10·00	2·12
212/29/1	46·01	0·90	24·61	11·14	0·16	2·21	0·93	1·57	2·17	0·39	10·40	1·51
212/35cc	46·38	0·74	16·28	7·94	0·12	2·76	7·86	1·80	2·77	0·20	12·55	7·43
212/36cc	54·13	0·86	18·70	8·20	0·32	2·70	0·65	0·90	3·64	0·20	7·88	2.50
212/37/1	57·90	0·96	15·59	8·08	0·06	3·50	0·70	1·52	3·50	0·17	7·23	0.60
212/37cc	59·73	0·77	13·86	7·06	-	3·25	0·92	2·24	3·13	0·26	7·78	2·27
212/38/1	58·54	0·88	14·29	7·60	0·03	3·24	0·89	2·03	3·24	0·24	7·83	1·04

$CO_2(T)$ = Total CO_2

/contd.over

TABLE 4-1 contd.

	SiO_2	TiO_2	Al_2O_3	Fe_2O_3	FeO	MgO	CaO	Na_2O	K_2O	P_2O_5	L.O.I.	CO_2(T)
213/8/5	57·15	0·53	15·83	5·26	0·03	2·09	0·85	4·40	2·38	0·17	9·18	0.76
213/9/4	51·77	0·68	17·22	7·74	-	3·54	1·38	4·52	1·95	0·38	8·75	0.90
213/9cc	52·10	0·50	15·73	6·61	-	3·66	1·39	4·64	1·72	0·60	10·20	0·90
213/10/3	52·40	0·49	15·92	6·29	-	3·61	1·36	4·23	1·75	0·58	9·43	0·90
213/11/2	51·08	0·46	16·53	6·68	-	3·07	1·34	4·74	3·25	0·63	8·68	2.51
213/11/5	47·78	0·65	16·67	9·06	-	2·96	1·57	3·62	2·92	0·83	9·63	4.55
213/12/5	46·70	0·84	15·71	10·62	-	3·12	2·21	4·35	3·10	1·01	9·55	1.21
213/13/2	47·34	0·78	16·10	10·21	-	3·08	2·64	3·70	3·27	1·27	8·60	1.87
213/13/5	47·86	0·94	15·89	10·63	-	3·43	2·35	3·10	2·93	1·07	8·93	2·37
213/14/3	51·29	0·83	15·76	9·25	-	4·28	1·95	2·48	3·40	0·91	8·28	1·77
213/15/2	28·51	0·47	7·58	9·59	-	2·28	23·38	1·64	2·35	0·76	22·18	18.65
215/8/2	52·82	0·47	15·83	6·21	0·03	3·77	0·79	5·64	1·75	0·16	10·30	1.11
215/9/2	53·92	0·60	11·63	7·02	0·04	6·46	2·56	0·21	2·17	1·31	13·12	2.79
216/24/4	17·66	0·40	3·14	3·39	0·07	1·31	40·08	-	0·30	0·10	33·80	31·54
216/25/3	35·50	0·81	7·40	8·99	0·76	6·00	19·68	0·73	0·90	0·17	19·15	15·35
216/30/3	45·80	1·38	9·19	3·44	5·20	3·74	16·50	2·14	0·45	0·09	11·18	10·10
216/32/3	41·21	0·80	5·21	2·64	2·05	2·40	22·57	1·00	0·34	0·09	20·18	18.33
216/34/1	28·98	0·76	6·27	4·65	0·76	5·05	28·51	1·10	0·52	0·16	25·10	22·84
221/14/2	53·67	0·90	16·12	7·09	1·26	4·85	1·13	1·90	3·00	0·12	8·03	2·27
221/14/5	54.16	0·86	15·97	7·15	1·35	5·05	1·18	1·96	3·09	0·12	8·55	2·42

/contd.over

TABLE 4-1 contd.

	SiO_2	TiO_2	Al_2O_3	Fe_2O_3	FeO	MgO	CaO	Na_2O	K_2O	P_2O_5	L.O.I.	CO_2 (T)
221/15/2	52·87	0·83	15·92	8·64	0·10	4·92	0·83	1·49	2·80	0·12	9·03	2·52
221/15/4	54·08	0·85	16·37	8·94	0·18	4·86	0·59	1·41	2·86	0·11	8·10	1·49
221/16/2	51·46	0·92	17·14	9·41	0·03	3·85	0·88	1·83	2·61	0·32	9·08	1·21
235/9/6	50·90	1·34	15·75	8·73	-	3·84	2·74	2·28	2·97	0·11	11·38	5·60
236/16/5	52·62	1·08	16·13	9·51	0·13	4·00	0·86	1·75	2·70	0·22	9·28	1·67
236/18/3	50·31	1·01	16·56	9·95	0·06	3·76	1·76	2·71	2·47	0·25	10·40	1·49
236/19/2	51·76	0·95	16·24	10·43	0·06	3·77	0·99	2·14	2·37	0·30	8·40	1·30
239/1/1	43·72	1·37	17·19	5·60	1·08	2·76	8·99	3·02	2·15	0·09	14·35	7·73
239/4/3	48·94	1·38	17·15	6·90	0·64	3·70	2·95	3·55	2·23	0·44	11·03	4·47
239/9/3	48·22	1·62	17·70	10·04	0·34	2·94	3·56	2·58	1·77	0·33	10·05	2·73
239/11/3	49·25	1·36	20·70	9·80	0·41	2·46	0·77	1·98	2·14	0·17	10·10	1·26
239/13/4	53·57	1·54	17·95	8·76	0·38	3·08	1·12	2·50	2·25	0·19	7·70	1·08
239/16/3	56·90	1·03	15·57	9·34	0·18	3·82	1·29	1·72	2·78	0·20	8·20	2·43
239/18/2	53·01	1·09	15·62	11·31	0·17	3·17	2·24	1·63	3·66	0·17	7·83	1·75
240A/2/1	80·51	0·34	6·72	3·21	0·40	0·71	1·17	1·53	1·97	0·03	2·8	1.21
240/3/3	53·55	1·25	18·03	9·97	0·41	3·30	0·38	2·50	2·72	0·15	9·15	1.66
240/5/1	69·58	0·58	11·21	3·47	0·38	1·44	2·29	2·07	2·16	0·08	4·7	1.97
245/1/3	48·21	1·00	15·64	9·14	0·06	3·24	1·50	5·02	2·71	0·42	8·48	1.80
245/5/3	47·96	0·84	14·11	9·21	-	3·64	4·78	1·92	3·13	0·26	11·90	4·78

/contd.over

TABLE 4-1 contd.

	SiO_2	TiO_2	Al_2O_3	Fe_2O_3	FeO	MgO	CaO	Na_2O	K_2O	P_2O_5	L.O.I.	CO_2(T)
245A/2/6	52·73	0·97	15·78	9·54	-	3·35	1·49	2·33	3·41	0·48	7·90	1·08
245A/6/2	53·51	0·94	15·55	9·54	0·03	3·70	0·77	2·31	3·48	0·19	9·13	1·22
246/10/2	39·95	0·30	9·50	4·70	0·14	2·86	17·90	3·44	2·72	0·03	18·63	14·86
248/10/2	62·85	0·84	13·77	6·10	0·50	3·45	0·79	1·48	2·70	0·10	6·78	1·89
248/11cc	65·16	0·70	12·54	6·02	0·45	2·85	0·55	1·70	2·25	0·05	3·20	1·53
248/12/3	62·20	0·83	13·28	6·79	0·23	3·18	0·89	2·16	2·32	0·15	7·00	2·33
248/14/1	53.60	1·19	16·56	10·63	0·03	3·94	0·49	1·49	4·13	0·08	6·93	0·81
248/14/6	54·48	1·15	16·11	10·13	0·06	3·15	0·60	1·42	3·97	0·06	7·38	1·54
250A/3/1	51·01	0·93	18·28	6·99	0·94	2·63	0·51	2·26	2·78	0·07	9·90	3·73
250A/6/3	53·54	0·94	18·55	7·89	0·94	2·88	0·58	2·24	3·06	0·09	9·13	1·58
250A/11/2	55·80	0·87	18·01	7·39	0·85	2·48	0·36	1·33	3·14	0·04	7·88	2·03
250A/15cc	55·68	0·85	14·99	2·39	0·81	1·40	4·68	3·04	3·66	0·15	8·85	7·26
250A/22/3	58·73	0·81	12·88	8·80	0·03	4·50	1·80	1·95	2·64	0·09	7·95	5·46
254/25/2	37·45	2·35	11·91	11·64	2·54	5·96	6·74	3·00	2·36	0·11	14·10	8·85
254/26cc	37·38	2·60	14·01	15·45	1·99	4·85	3·71	2·34	2·38	0·13	15·50	4·09
254/27/3	42·67	2·80	14·46	14·86	2·70	5·59	0·87	2·25	2·09	0·06	11·30	4·09
254/28cc	34·86	4·90	14·67	17·35	2·76	3·36	1·90	1·34	1·32	0·03	15·30	4·85
256/2/3	46·10	0·87	15·52	12·85	-	3·10	1·32	3·72	2·79	0·64	8·63	1·96
256/4/5	43·64	0·91	24·04	10·59	-	2·35	0·71	2·18	2·30	0·39	10·50	1·16

/contd.over

TABLE 4-1 contd.

	SiO_2	TiO_2	Al_2O_3	Fe_2O_3	FeO	MgO	CaO	Na_2O	K_2O	P_2O_5	L.O.I.	CO_2(T)
256/6/3	66·43	0·54	11·65	4·63	0·06	2·63	0·59	2·57	2·23	0·16	6·38	0·88
256/7cc	63·61	0·84	10·48	6·83	0·03	2·50	0·60	2·65	2·35	0·07	7·63	1·19
256/8/4	53·77	0·85	10·31	6·88	0·06	2·56	6·80	2·23	2·59	0·06	11·40	7·73
257/2cc	49·92	0·73	16·24	8·45	0·03	2·91	0·79	3·40	1·77	0·33	15·00	1·30
257/4/3	60·03	0·49	14·04	6·53	-	2·93	0·65	3·57	2·61	0·14	7·68	1·07
257/5/2	56·73	0·64	16·21	8·05	-	2·70	0·75	3·01	2·71	0·15	8·40	0·56
258/14/1	75·99	0·32	9·11	2·57	0·11	1·02	0·54	1·65	2·01	0·03	6·09	1·52
258/15/1	49·76	0·29	8·45	1·96	0·03	1·43	17·74	0·61	0·51	0·01	17·90	15·16
258/16cc	38·77	2·48	23·73	12·83	4·95	1·91	0·99	0·74	0·98	0·04	11·20	4·47
258/17/2	56·42	0·68	18·83	5·37	0·06	1·46	1·81	1·47	2·10	0·04	10.68	4.10
258/22/4	62·67	0·61	14·42	3·76	0·50	1·71	2·84	1·11	1·21	0·04	11·45	6.00
258/25cc	54·29	0·62	16·27	5·26	0·30	1·41	4·99	1·69	2·39	0·03	12·18	6·52

TABLE 4-1(b): Trace Elements in ppm, except Mn(%)

(Bd = below detection limits
Nd = not determined)

Sample No.	V	Cr	Mn	Ni	Cu	Zn	As	Rb	Sr	Y	Zr	Nb	Mo	Ba	La	Ce	Pb
211/6/2	96	64	1·06	176	257	104	9	107	113	64	150	11	Bd	362	57	67	36
211/13/1	126	69	0·22	77	59	107	9	116	198	36	308	40	7	703	62	126	16
211/14/1	122	91	0·22	90	66	103	Bd	122	138	48	259	19	Bd	813	96	134	18
212/15/2	212	97	2·30	372	294	140	41	95	425	92	210	20	76	680	93	143	78
212/15/3	211	85	2·26	365	291	131	40	90	473	84	190	17	74	529	88	122	71
212/16/1	225	87	1·87	337	240	162	35	98	418	82	185	15	19	684	129	137	56
212/16/2	244	200	1·84	311	254	142	47	99	425	84	193	14	46	565	100	155	62
212/17cc	281	65	1·92	239	193	174	57	97	553	82	184	12	59	792	76	153	64
212/18/1	260	59	1·69	204	188	163	56	79	403	69	186	10	45	595	115	127	56
212/18/2	129	60	0·40	92	113	123	23	82	545	44	139	11	5	741	44	126	33
212/23/5	162	133	0·16	103	55	131	Bd	82	257	40	109	10	Bd	348	74	92	16
212/27/1	186	93	0.23	91	161	181	42	90	197	73	159	11	13	688	119	161	48
212/28/2	224	178	0·51	144	112	145	39	77	200	62	154	17	29	519	116	174	40
212/35cc	141	94	0·17	89	151	136	12	90	273	45	122	9	21	622	42	126	34
212/36cc	132	118	0·12	122	102	158	17	131	147	53	174	14	9	723	76	144	38
212/37/1	103	69	0·35	91	187	145	Bd	116	155	45	199	14	7	638	101	174	50
212/37cc	77	48	0·70	117	129	158	9	96	329	60	147	8	Bd	701	65	136	34
212/38/1	86	48	0·50	84	157	149	7	97	316	58	169	10	4	916	68	155	37

/contd.over

TABLE 4-1(b) contd.

Sample No.	V	Cr	Mn	Ni	Cu	Zn	As	Rb	Sr	Y	Zr	Nb	Mo	Ba	La	Ce	Pb
213/8/5	73	72	0·62	206	182	70	11	81	108	59	136	6	16	324	55	48	31
213/9/4	124	159	1·10	244	291	110	15	83	143	110	174	9	28	599	101	119	43
213/9cc	74	145	1·30	277	329	116	17	64	175	152	154	9	49	240	99	63	43
213/10/3	96	26	1·60	320	346	102	13	55	151	129	138	Bd	32	384	86	95	44
213/11/2	93	91	1·94	418	335	102	15	73	129	121	133	11	44	326	88	119	45
213/11/5	147	59	2·35	606	372	147	29	83	178	155	169	15	67	426	129	146	55
213/12/5	162	52	2·17	462	244	145	31	75	197	172	188	15	40	458	161	141	49
213/13/2	175	61	2·32	479	280	170	33	77	196	229	191	13	41	397	126	131	49
213/13/5	188	43	2·16	416	234	179	30	Nd	Nd	Nd	Nd	Nd	Nd	538	169	157	52
213/14/3	121	53	0·82	229	134	143	7	88	144	117	163	15	19	513	141	152	40
213/15/2	137	170	0·81	131	125	116	43	47	352	82	107	16	21	324	102	77	44
215/8/2	78	37	0·62	158	220	82	Bd	68	109	59	122	6	Bd	617	72	67	44
215/9/2	73	41	0·89	167	89	106	7	72	132	151	106	7	9	390	148	67	23
216/24/4	50	636	0·003	30	12	42	Bd	18	613	19	59	Bd	24	299	40	Bd	18
216/25/3	179	162	0·06	56	56	91	9	20	434	18	47	Bd	26	519	14	16	29
216/30/3	237	72	0·10	62	91	84	Bd	Bd	255	16	73	Bd	28	600	Bd	35	12
216/32/3	106	50	0·09	44	35	62	Bd	11	351	25	53	6	Bd	263	26	7	9
216/34/1	143	140	0·10	48	45	101	Bd	143	Nd	Nd	Nd	Nd	Nd	323	26	27	Bd
221/14/2	180	266	0·39	232	104	139	13	116	144	43	174	16	10	1194	66	104	28
221/14/5	174	158	0·42	240	91	161	12	119	146	36	174	17	Bd	1262	78	110	36

/contd.over

TABLE 4-1(b) contd.

Sample No.	V	Cr	Mn	Ni	Cu	Zn	As	Rb	Sr	Y	Zr	Nb	Mo	Ba	La	Ce	Pb
221/15/2	158	237	0·48	261	145	152	11	105	133	47	171	16	4	1220	74	138	30
221/15/4	171	148	0·44	317	193	134	10	106	147	42	171	14	4	1493	97	160	45
221/16/2	162	141	0·60	202	313	178	12	90	192	58	341	35	7	1476	125	216	33
235/9/6	183	178	0·05	127	74	157	6	102	228	39	254	39	Bd	857	59	104	22
236/16/5	143	153	0·26	189	167	138	Bd	101	362	Bd	237	23	Bd	1359	85	169	27
236/18/3	124	161	0·24	145	191	137	7	82	335	Bd	202	16	4	735	81	107	27
236/19/2	132	78	0·33	156	208	146	10	103	398	60	244	36	5	1031	84	116	39
239/1/1	78	.284	0·04	89	30	70	Bd	61	418	33	295	23	Bd	400	46	59	19
239/4/3	180	252	0·04	110	96	129	8	68	356	55	216	20	Bd	816	77	121	37
239/9/3	198	111	0·16	122	94	122	16	64	313	55	176	19	Bd	811	94	127	31
239/11/3	181	288	0·15	138	90	124	13	82	209	35	214	23	7	608	76	131	28
239/13/4	91	80	0·11	79	55	113	Bd	66	213	48	452	63	7	851	151	199	25
239/16/3	185	152	0·09	132	98	130	Bd	124	120	33	165	10	Bd	743	57	79	31
239/18/3	122	114	0·13	118	98	143	14	151	144	47	177	17	Bd	737	68	163	34
240A/2/1	22	40	0·04	33	28	46	Bd	24	151	12	137	Bd	60	524	Bd	32	25
240/3/3	169	100	0·12	130	144	145	6	97	160	38	203	29	Bd	1368	55	168	18
240/5/1	62	89	0·04	44	55	75	Bd	64	211	34	268	18	Bd	670	50	78	17
245/1/3	142	88	0·60	175	179	183	17	93	186	95	172	17	19	835	125	153	43
245/5/3	131	90	0·40	133	90	130	11	101	236	49	137	16	4	580	81	71	33
245A/2/6	157	93	0·50	150	100	123	10	116	158	87	162	11	16	799	98	142	35

/contd.over

TABLE 4-1(b) contd.

Sample No.	V	Cr	Mn	Ni	Cu	Zn	As	Rb	Sr	Y	Zr	Nb	Mo	Ba	La	Ce	Pb
245A/6/2	130	168	0·27	138	84	114	13	113	125	45	161	15	Bd	734	70	112	27
246/10/2	19	38	0·06	26	Bd	209	Bd	39	116	62	705	81	4	192	119	121	18
248/10/2	141	162	0·05	80	79	125	Bd	131	99	29	143	9	4	782	47	77	21
248/11cc	126	151	0·04	86	77	97	12	109	83	28	134	7	4	658	43	69	15
248/12/3	99	118	0·05	68	33	76	Bd	118	112	32	137	10	Bd	487	42	57	22
248/14/1	170	98	0·44	126	76	121	Bd	127	90	23	166	15	7	1118	50	140	21
248/14/6	234	212	0·42	118	75	149	10	133	89	21	158	14	Bd	765	56	114	30
250A/3/1	137	232	0·06	101	109	171	11	131	133	28	133	17	5	845	63	100	35
250A /6/3	147	226	0·14	99	70	115	Bd	147	115	30	137	16	Bd	832	43	98	35
250A/11/2	165	130	0·04	103	63	157	8	158	111	27	149	15	Bd	770	52	114	24
250A/15cc	94	71	4·68	52	20	73	9	111	326	42	420	9	Bd	897	39	69	26
250A/22/3	104	130	0·32	109	85	124	Bd	100	154	27	114	6	Bd	962	56	88	12
254/25/2	375	173	0.16	60	84	118	13	17	139	32	132	8	5	1192	25	93	7
254/26cc	288	256	0·07	90	78	99	12	18	341	34	174	13	Bd	928	38	107	11
254/27/3	327	195	0·05	79	65	97	24	Bd	314	23	198	13	Bd	1213	37	101	5
254/28cc	518	360	0·06	82	89	130	15	Bd	134	27	253	19	Bd	2336	55	154	14
256/2/3	232	64	1·70	243	181	144	46	86	167	90	171	12	72	431	110	106	60
256/4/5	191	70	0·72	134	115	165	27	Nd	92	128	60	147	15	502	115	147	53
256/6/3	262	50	0·06	65	78	98	Bd	Nd	73	155	45	88	7	960	57	132	19
256/7cc	80	64	0·21	70	96	109	17	61	160	28	119	9	4	1034	36	103	26
256/8/4	98	167	0.14	60	57	85	Bd	Bd	62	273	27	139	12	584	47	64	21

/contd.over

TABLE 4-1(b) contd.

Sample No.	V	Cr	Mn	Ni	Cu	Zn	As	Rb	Sr	Y	Zr	Nb	Mo	Ba	La	Ce	Pb
257/2cc	131	68	0·26	81	117	229	23	Nd	74	108	60	155	13	389	53	73	35
257/4/3	80	34	0·54	65	143	146	12	Nd	69	169	42	86	8	776	40	124	29
257/5/2	108	146	0·74	104	128	158	15	Bd	98	236	34	84	8	772	38	142	57
258/14/1	111	10	0·01	30	59	74	Bd	20	451	22	36	Bd	Bd	4771	41	166	12
258/15/1	93	33	0·03	27	57	79	Bd	Bd	461	24	35	Bd	4	2162	27	71	19
258/16cc	357	334	0·04	78	144	115	Bd	Bd	71	25	198	Bd	5	1141	21	90	9
258/17/2	116	120	0·01	60	77	78	6	73	286	22	86	9	Bd	1142	43	92	23
258/22/4	112	92	0·009	59	60	95	7	59	192	27	137	10	4	1242	54	97	28
258/25cc	129	99	0·02	109	96	112	13	52	420	27	77	6	Bd	1683	31	93	28

TABLE 4-2 Average Chemical Composition of the Main Igneous Rocks and Sediments

	Average shale	Average granite	Average basalt	Average tholeiite	Average alkali basalt	Average ridge sediment	Average biological matter	Average terrigenous matter	Average deep sea clay
SiO_2	50·93	69·12	51·36	49·34	47·41	11·18	35·48	53·30	53·50
Ti	0·45	0·23	0·90	0·89	1·72	0·026	0·044	0·48	0·46
Al	8·00	7·70	8·80	9·02	9·54	0·25	0·24	8·10	8·40
Fe	4·70	2·70	8·60	6·69	7·42	22·12	0·44	4·90	6·50
Mn	0.085	0.04	0.20	0.13	0.12	8·36	0.016	0.088	0·67
Mg	1·34	0·16	4·50	4·34	2·89		10·00	1·58	2·10
Na	0·66	2·80	1·90	2·03	2·96			1·095	4·00
K	2·30	3·30	0·80	0·13	1-38			2·25	2·50
P	0·077	0·07	0·14	0·07	0·39			0·084	0·15
Rb	0·014	0·015	0·0045	0·001	0.0033			0·0128	0·011
Y	0·003	0·004	0·0025	0·0043	0·0054			0·0031	0·009
Zr	0·02	0·018	0·01	0·0095	0·0333	0·0112	0·002	0·019	0·015
Nb	0.002	0.002	0.002	0.0030	0·0072			0·002	0·0014
Mo	0·0002	0·0002	0·0001				0·0019	0·0002	0·0027
V	0·013	0·002	0·020	0·0292	0·0252	0·0758		0·013	0·012
Cr	0·010	0·0004	0·020	0·0297	0·0067	0·016	0·0048	0·01	0.009
Ni	0.0095	<0.0001	0.016	0.0097	0.0051	0.0515	0.012	0.009	0.0225
Pb	0.002	0.0020	0.0008				0.0065	0.0018	0.008
As	0.0006	0.00015	0.0002					0.0005	0.0013
Zn	0.008	0.004	0.013			0.0515	0.089	0.0078	0.0165

*/contd.over

TABLE 4-2 contd.

	Average shale	Average granite	Average basalt	Average tholeiite	Average alkali basalt	Average ridge sediment	Average biological matter	Average terrigenous matter	Average deep sea clay
Cu	0.0057	0.001	0.01	0.0077	0.0036	0.1152	0.033	0.0057	0.025
Ba	0.058	0.060	0.03	0.0014	0.0498	0.73	0.075	0.054	0.23
La	0.004	0.0040	0.001	0.008	0.009			0.0033	0.0115
Ce	0.005	0.0087	0.0048					0.0054	0.0345
Al/(Al+Fe+Mn)	0.625	0.738	0.50	0.569	0.558	0.00813		0.618	0.54
Fe/Ti	10.44	11.74	9.56	7.517	4.32	850.77		10.21	14.13
Ti/Al	0.056	0.0298	0.102	0.099	0.18	0.10	0.18	0.059	0.0548

Average shale from Krauskopf (1967).
Average granite " " "
Average basalt " " "
Average tholeiite from Engel et al. (1965)
Average alkali basalt " " "
Average volcanic material (VM) from Bostrom et al. (1976)
Average biological matter (BM) " " " "
Average terrigenous matter from Krauskopf (1967)
Average deep sea clay from Turekian & Wedepohl (1961).

TABLE 4-3a: Suggested Chemical Models of Terrigenous and Detrital Material as a Source of Sediments

	I = 25% shale + 75% c.c(100%g)	II = 50% shale + 50% c.c(80%g + 20%b)	III = 50% shale + 50% c.c (50%g + 50%b)	IV = 80% tho + 20% TM (20% shale + 80% c.c) c.c = 80b + 20g	V = 80% a-b + 20% tho
SiO_2	64.57	58.25	53.30	50.29	47.80
Ti	0.29	0.41	0.48	0.85	1.55
Al	7.78	7.96	8.09	8.9	9.44
Fe	3.21	4.29	4.89	6.73	7.27
Mn	0.0513	0.0785	0.088	0.1343	0.12
Mg	0.46	1.18	1.84	4.11	3.18
Na	2.27	1.64	1.51	1.98	2.77
K	3.05	2.55	2.18	0.40	1.13
P	0.07	0.08	0.09	0.08	0.33
Rb	0.015	0.013	0.012	0.0024	0.003
Y	0.0038	0.0034	0.003	0.004	0.005
Zr	0.0185	0.0182	0.019	0.0103	0.029
Nb	0.002	0.002	0.002	0.003	0.006
Mo	0.0002	0.00019	0.00018		
V	0.0048	0.0093	0.013	0.0265	0.026
Cr	0.0028	0.0072	0.0099	0.0268	0.011
Ni	0.0026	0.0065	0.0089	0.0102	0.006
Pb	0.002	0.0019	0.0017		
As	0.0003	0.0004	0.0004		

/contd.over

b = basalt
g = granite
tho = tholeiite
a-b = alkali basalt

TABLE 4-3a contd.

	I = 25% shale + 75% c.c (100%g)	II = 50% shale + 50% c.c(80%g + 20%b)	III = 50% shale + 50% c.c (50%g + 50%b)	IV = 80% tho + 20% thi (2P% shale + 80% c.c) c.c = 80b + 20g	V = 80% a-b + 20% tho
Zn	0.005	0.007	0.0083		
Cu	0·0022	0·0043	0·0057	0·0077	0.004
Ba	0·0595	0·056	0·054	0·0092	0.040
La	0·0004	0·0037	0·0033		0.009
Ce	0·0078	0·0065	0·0059		
Al/ Al+Fe+Mn)	0.705	0.646	0.619	0·565	0.560
Fe/Ti	11·069	10·46	10·19	7·92	4.69

TABLE 4-3b: Set of Sediments which gather around Five suggested Curves (Figs.4-1, a-e)

Type I:

211/6/2, 215/8/2, 213/9cc, 213/10/3, 213/11/2, 212/23/5, 212/27/1, 212/28/2, 246/10/2, 257/4/3.

Type II:

257/2cc, 257/5/2, 258/15/1, 258/17/2, 258/25cc, 258/14/1, 212/36cc, 212/35cc, 213/8/5, 213/9/4, 256/4/5, 256/6/3.

Type III:

239/11/3, 239/16/3, 239/18/3, 250A/3/1, 250A/6/3, 250A/11/2, 250A/22/3, 248/10cc, 248/11cc, 248/12/3, 248/14/1, 248/14/6, 245, 221, 236, 256/2/3, 240 , 213/11/5 downward, 212/37/1, 212/37cc, 212/38/1, 212/18/2 upward, 215/9/2, 258/22/4.

Type IV:

216/24/4, 216/25/3, 216/34/1, 211/13/1, 211/14/1, 239/1/1, 239/4/3, 239/9/3, 239/13/4, 256/7cc, 256/8/4, 258/16cc, 235/9/6.

Type V:

216/30/3, 216/32/3, 254.

TABLE 4-4: Some important Atomic Ratios and Other Ratios for the Major Elements
(* Palygorskite-rich sediments, $OX^{o} = \frac{Fe_2O_3/80}{Fe_2O_3/80 + FeO/72}$)

	Si/Al	Ti/Al	Fe^{+3}/Al	Mg/Al	Ca/Al	K/Al	Fe^{+3}/Ti	Al/(Al+Fe+Mn)	Fe_2O_3/FeO	OX^{o}
211/6/2	3·32	0·036	0·519	0·246	0·122	0·206	15·23	0·596	19·28	0·95
211/13/1	3·26	0.09	0·796	0·257*	1.31	0·493	8·77	0·545	242	0·995
211/14/1	3·44	0.09	0·724	0·33 *	0·609	0·479	7·76	0·568	241	0·995
212/15/2	2·47	0·06	0·91	0·196*	0·20	0·237	15·40	0·462	E	1
212/15/3	2·53	0·06	1·02	0·208	0·215	0·25	17·85	0·438	E	1
212/16/1	2·46	0·06	0·915	0·188	0·08	0·23	14·72	0·473	E	1
212/16/2	2·43	0·05	0·828	0·197	0·094	0·292	15·536	0·493	280	0·996
212/17cc	2·63	0·06	1·07	0·197	0·09	0·29	17·05	0·436	E	1
212/18/1	2·44	0·05	0·956	0·189	0·06	0·211	17·75	0·469	E	1
212/18/2	3·29	0·06	0·81	0·256*	0·08	0·32	12·73	0·537	231	0·995
212/23/5	3·58	0·05	1·004	0·345	0·09	0·25	21·89	0·491	98	0·989
212/27/1	1·66	0·04	0·623	0·099*	0·047	0·146	14·37	0·608	167	0·993
212/27/5	1·83	0·04	0.614	0.119	0·472	0·153			352	0·997
212/28/2	1·64	0·04	0·575	0·099	0·044	0·121	15·31	0·619	183	0·994
212/29/1	1·62	0·04	0·598	0·102	0·05	0·138			70	0·984
212/35cc	2·52	0·05	0·39	0·029	0·652	0·267	12·73	0·597	66	0·983
212/36cc	2·57	0·05	0·579	0·165	0·047	0·305	11·61	0·619	26	0·958
212/37/1	3·28	0·07	0·685	0·256	0·061	0·352	9·90	0·577	135	0·992
212/37cc	3·81	0·06	0·673	0·267*	0·089	0·354	10·69	0·566	E	1
212/38/1	3·62	0·07	0·703	0·258*	0·08	0·356	10·12	0·564	253	0·996

/contd.over

TABLE 4-4 contd.

	Si/Al	Ti/Al	Fe^{+3}/Al	Mg/Al	Ca/Al	K/Al	Fe^{+3}/Ti	Al/(Al+Fe+Mn)	Fe_2O_3/FeO	OX^{o}
213/8/5	3·19	0·04	0·439	0·150	0·073	0·236	11·65	0·659	175	0·994
213/9/4	2·66	0·04	0·594	0·234	0·108	0·178	13·28	0·583	E	1
213/9cc	2·93	0·036	0·555	0·265	0·119	0·172	15·42	0·584	E	1
213/10/3	2·91	0·035	0·52	0·258	0·115	0·172	14·98	0·584	E	1
213/11/2	2·73	0·032	0·534	0·212	0·109	0·308	16·94	0·569	E	1
213/11/5	2·53	0·04	0·718	0·202	0·127	0·275	16·26	0·504	E	1
213/12/5	2·63	0·06	0·893	0·226	0·189	0·309	14·75	0·464	E	1
213/13/2	2·59	0·06	0·838	0·218	0·221	0·319	15·27	0·474	E	1
213/13/5	2·66	0·067	0·884	0·246*	0·199	0·289	13·20	0·467	E	1
213/14/3	2·87	0·059	0·776	0·309*	0·167	0·338	13·00	0·534	E	1
213/15/2	3·32	0·07	1·67	0·343	4·165	0·486	23·81	0·348	E	1
215/8/2	2·95	0·034	0·516	0·271	0·067	0·173	15·43	0·628	207	0·995
215/9/2	4·09	0·058	0·79	0·633*	0·297	0·293	13·66	0·515	176	0·994
216/24/4	4·97	0·144	1·427	0·475	17·24	0·149	10·12	0·406	48·43	0·978
216/25/3	4·24	0·124	1·606	0·924	3·59	0·191	14·17	0·361	11·83	0·914
216/30/3	4·40	0·17	0·495	0·464	2·42	0·08	7·79	0·426	0·66	0·37
216/32/3	6·99	0·17	0·669	0·525	5·85	0·10	7·17	0·438	1·29	0·537
216/34/1	4·08	0·137	0·980	0·918	6·14	0·13	8·436	0·457	6·12	0·846
221/14/2	2·94	0·06	0·581	0·343*	0·095	0·292	11·007	0·574	5·63	0·835
221/14/5	2·99	0·06	0·592	0·36	0·099	0·304	11·737	0·566	5·30	0·827
221/15/2	2·93	0·06	0·616	0·352*	0·070	0·276	12·149	0·564	86·40	0·987

/contd.over

TABLE 4-4 contd.

	Si/Al	Ti/Al	Fe^{+3}/Al	Mg/Al	Ca/Al	K/Al	Fe^{+3}/Ti	Al/(Al+Fe+Mn)	Fe_2O_3/FeO	OX^{o}
221/15/4	2.92	0.06	0.721	0.338*	0.049	0.274	12.547	0.559	50	0.978
221/16/2	2.65	0.06	0.726	0.256*	0.07	0.239	11.977	0.558	314	0.996
235/9/6	2.85	0.096	0.733	0.278	0.235	0.296	7.602	0.575	E	1
236/16/5	2.88	0.076	0.768	0.283	0.072	0.263	10.279	0.552	73.15	0.985
236/18/3	2.68	0.069	0.794	0.267	0.144	0.234	11.572	0.547	166	0.993
236/19/2	2.81	0.066	0.849	0.265	0.082	0.229	12.893	0.528	174	0.994
239/1/1	2.25	0.09	0.43	0.183	0.706	0.196	5.792	0.655	5.19	0.82
239/4/3	2.52	0.09	0.53	0.246	0.232	0.204	6.436	0.629	10.78	0.907
239/9/3	2.41	0.104	0.75	0.189	0.272	0.157	7.504	0.557	29.53	0.964
239/11/3	2.10	0.074	0.63	0.135	0.050	0.162	8.799	0.599	23.90	0.956
239/13/4	2.64	0.097	0.645	0.196	0.084	0.197	6.957	0.593	23.05	0.954
239/16/3	3.23	0.075	0.793	0.279	0.112	0.280	10.81	0.549	52	0.979
239/18/3	2.99	0.079	0.957	0.231	0.194	0.368	12.31	0.503	66.53	0.984
240/2/1	10.58	0.058	0.63	0.120	0.235	0.459	12.289	0.578	8.03	0.878
240/3/3	2.62	0.079	0.731	0.209	0.066	0.237	9.732	0.563	24.32	0.956
240/5/1	2.48	0.059	0.409	0.146	0.276	0.302	7.831	0.682	9.13	0.8915
245/1/3	2.72	0.07	0.77	0.236*	0.129	0.272	10.473	0.540	152.33	0.993
245/5/3	3.00	0.07	0.863	0.294*	0.457	0.348	12.794	0.522	E	1
245A/2/6	2.95	0.07	0.799	0.256*	0.128	0.339	11.476	0.538	E	1
245A/6/2	3.04	0.07	0.811	0.271*	0.067	0.351	11.884	0.542	318	0.997

/contd.over

TABLE 4-4 contd.

	Si/Al	Ti/Al	Fe^{3}/Al	Mg/Al	Ca/Al	K/Al	Fe^{+3}/Ti	Al/(Al+Fe+Mn)	Fe_2O_3/FeO	OX^{o}
246/10/2	3·71	0·036	0·654	0·343	2·54	0·449	18·886	0·592	34	0·968
248/10cc	4·03	0·07	0·585	0·285*	0·077	0·308	9·245	0·607	12·2	0·917
248/11cc	4·59	0·06	0·634	0·259	0·059	0·281	10·868	0·591	13·40	0·923
248/12/3	4·14	0·07	0·676	0·273	0·091	0·274	9·905	0·586	29·52	0·964
248/14/1	2·86	0·08	0·848	0·271*	0·039	0·391	10·456	0·526	354	0·997
248/14/6	2·98	0·08	0·831	0·223*	0·05	0·387	10·346	0·530	169	0·993
250A/3/1	2·46	0·058	0·505	0·164*	0·038	0·239	10·081	0·630	7·44	0·87
250A/6/3	2·55	0·057	0·562	0·177	0·042	0·259	11·091	0·606	8·39	0·883
250A/11/2	2·74	0·055	0·542	0·157	0·027	0·273	11·178	0·619	8·69	0·887
250A/15cc	3·28	0·064	0·211	0·106	0·422	0·383	4·517	0·532	2·95	0·73
250A/22/3	4·03	0·07	0·903	0·398*	0·189	0·322	12·725	0·512	293	0·996
254/25/2	2·78	0·223	1·292	0·570	0·764	0·311	7·181	0·38	4·58	0·805
254/26cc	2·36	0·21	1·457	0·394	0·358	0·266			7·76	0·875
254/27/3	2·61	0·219	1·36	0·441	0·081	0·227	7·443	0·38	5·50	0·832
254/28cc	2·09	0·378	1·56	0·261	0·175	0·141	4·862	0·38	6·29	0·85
256/2/3	2·62	0·06	1·09	0·228	0·115	0·282	17·234	0·435	E	1
256/4/5	1·60	0·043	0·582	0·111	0·039	0·150	13·579	0·610	E	1
256/6/3	5·04	0·053	0·525	0·257*	0·068	0·300	10·149	0·649	77	0·986
256/7cc	5.36	0.091	0.861	0.272*	0.077	0.352	9.534	0.526	227.66	0.9951
256/8/4	4·61	0·09	0·882	0·283*	0·891	0·394	9·536	0·522	114·66	0.99

/contd.over

TABLE 4-4 contd.

	Si/Al	Ti/Al	Fe^{3}/Al	Mg/Al	Ca/Al	K/Al	Fe^{+3}/Ti	Al/(Al+Fe+Mn)	Fe_2O_3/FeO	OX^{o}
257/2cc	2·71	0·051	0·688	0·204	0·07	0·171	13·559	0·581	282	0·996
257/4/3	3·78	0·039	0·615	0·238	0·063	0·292	15·549	0·593	E	1
257/5/2	3·09	0·045	0·656	0·189	0·062	0·262	14·677	0·574	E	1
258/14/1	7·37	0·039	0·373	0·128	0·080	0·346	9·817	0·718	23·36	0·955
258/15/1	5·20	0·039	0·307	0·193	2·83	0·09	8·02	0·759	65·33	0·983
258/16cc	1·49	0·118	0·715	0·092	0·056	0·065	8·625	0·494	2·59	0·699
258/17/2	2·65	0·04	0·377	0·088	0·129	0·175	9·329	0·723	89·50	0·988
258/22/4	3·84	0·048	0·345	0·135	0·266	0·132	8·255	0·716	7·52	0·871
258/25cc	2·95	0·04	0·427	0·099	0·414	0·230	10·527	0·687	17·53	0·940

TABLE 4:5 : Correlation Coefficients Matrix of the Bulk Chemistry and Mineralogy.
CO_2 = carbonate CO_2; Clin = clinoptilolite; Phill = phillipsite;
K-feld = K-feldspar; P-Feld = plagioclase; Dolo = dolomite;
Ill = illite; Kao = kaolinite; Chlo = chlorite; Paly = Palygorskite.

	SiO_2	TiO_2	Al_2O_3	Fe_2O_3	FeO	MgO	CaO	K_2O	Na_2O	P_2O_5	CO_2	Rb	Sr	Y	Zr	Nb	Mo	V	Cr	Mn	Ni	Pb	As	In	Cu	Ba	Ce	La	Quartz	K-feld	P-feld	Clin	Phill	Clay	Calcite	Dolo	Halite	Pyrite	Organic Carbon	MLIS	Ill	Kao	Chlo	Paly	B	Depth
SiO_2	1.000																																														
TiO_2	-0.3613	1.0000																																													
Al_2O_3			1.0000																																												
Fe_2O_3	-0.3551	-0.6311	0.4943	1.0000																																											
FeO	-0.3019	0.6315			1.0000																																											
MgO	-0.2494	0.2768		0.3937		1.0000																																									
CaO	-0.6475		-0.6811	-0.3559			1.0000																																								
K_2O	0.3061		0.3513	0.2712	-0.4200		-0.5235	1.0000																																							
Na_2O			0.2049				-0.3084		1.0000																																						
P_2O_5				0.2396	-0.2939	0.2162			0.3194	1.0000																																						
CO_2	-0.6255		-0.6592	-0.3533			0.9771		-0.3228		1.0000																																					
Rb		-0.2157	0.2552		-0.3348		-0.2465	-0.4703				1.0000																																				
Sr	-0.2233		-0.2038				0.3248	0.5788	-0.2161		0.32		1.0000																																			
Y		-0.2338			-0.2987			-0.2101	0.4167	0.5295		-0.2040		1.0000																																		
Zr												0.2937			1.0000																															
Nb								0.3363				-0.3384	-0.2612	0.5312		1.0000																															
Mo		-0.2161							0.2911	0.4798				0.4198			1.0000																													
V	-0.3745	0.7935	0.2882	0.7214	0.5536	0.2711												1.0000																												
Cr	-0.4931	0.4259			0.3495		0.3189	-0.2521	-0.2738	-0.2819	0.3284			-0.2385				0.3029	1.0000																												
Mn					-0.2218			0.2894	0.3677	0.5851				0.3999		0.5389		-0.2977	1.0000																												
Ni			0.3120	0.3049	-0.2462		-0.2823	0.2878	0.4029	0.7147	-0.3069			0.4376		0.5846			0.6696	1.0000																											
Pb		-0.3077	0.4151	0.2875	-0.4644		-0.3141	0.3205	0.3363	0.5467	-0.3022			0.4731		0.6135		-0.2619	0.5987	0.6693	1.0000																										
As	-0.2476		0.3648	0.5614	-0.2026					0.4966			0.2200	0.3139		0.6063	0.5321		0.5321	0.5167	0.7028	1.0000																							
In			0.4419	0.4632	-0.2030		-0.3134	0.4014		0.2961	-0.2916	0.2488		0.2624	0.2848	0.3513				0.3616	0.5348	0.4902	1.0000																							
Cu			0.3645	0.2641	-0.2308		-0.3382		0.4795	0.5779	-0.3624			0.4381		0.5403	0.5653	-0.2437	0.5653	0.8278	0.6946	0.4695	0.3806	1.0000																					
Ba	0.2684							-0.3407				-0.265				-0.2949	0.2366				-0.2612				1.0000																				
Ce			0.5785	0.4767	-0.2605		-0.5457	0.5447			-0.5319				0.2244		0.2379			0.3066	0.3418	0.3241	0.5049	0.3218	0.3189	1.0000																			
La			0.3975	0.3543	-0.4419		-0.2549	0.3458	0.2691	0.7303	-0.2513			0.3499		0.2824		-0.2437	0.4424	0.6205	0.5252	0.4728	0.4298	0.4919	-0.2240	0.5771	1.0000																			
Quartz	0.5259			0.2436		-0.3179											-0.2437										1.0000																		
K-feld									0.2598						0.4680				0.2798						-0.2312			0.3134	1.0000																
P-feld								0.2776				0.2306			0.4931													0.2034		1.0000															
Clin	0.3103		-0.2256	-0.2299						-0.2510		-0.2605			-0.3232	0.2409			-0.2971						0.4939		-0.3361		-0.2849	-0.3140	1.0000															
Phill									0.3513	0.3964				0.2917		0.3339			0.3475	0.5385				0.4554	-0.2245		0.2920		0.4370			1.0000													
Clay			0.6941	0.4510	-0.2219		-0.5369	0.3542			-0.5129	0.4246								0.2784	0.3391		0.3388	0.2936		0.3951	0.3519			-0.344		1.0000												
Calcite	-0.6252		-0.6717	-0.3388			0.9788	-0.4965	-0.3232		0.9898	-0.2137	0.3041					0.3367		-0.2966	-0.3012		0.2902	-0.3373		-0.5277	-0.2481		0.2797				-0.5058	1.0000									
Dolo				0.2358	0.2373										0.3048				0.3308				-0.2412	-0.2425					0.7226			-0.2530		1.0000								
Halite									0.6741	0.4506				0.3623						0.2925				0.3672	-0.3269	-0.2241	0.2431				0.3912			1.0000								
Pyrite		0.4132		0.2353	0.3614									-0.2329			0.3215				-0.3162					-0.2344								1.0000							
Organic Carbon	-0.2638	0.4155			0.5288			-0.2898				-0.2615					0.3384	0.3252			-0.3591			0.2229		-0.2481									1.0000						
MLIS	-0.2187		0.3805	0.3104	-0.2223		0.3002		0.2503											0.2271	0.2845			0.3065						-0.2689		0.6513	0.2786	-0.2729			1.0000				
Ill			0.2190		-0.3229		-0.3096	0.6307	-0.2302		-0.2943	0.5459									0.2429		0.3483		0.3338	0.2875		-0.2358				0.4330	-0.2418				1.0000			
Kao			0.6377	0.2959	0.2213	-0.2879					-0.2837							0.2797														0.3731					1.0000			
Chlo		0.2331	0.3074		0.4782													0.2859	0.2665																		0.3287		0.6432	1.0000	
Paly						0.2437		0.3500	-0.3361			0.2015	-0.2183																									0.3874	0.5389		1.0000	
B																												-0.2951	-0.2893		-0.2062											1.0000	
Depth																															0.1886	-0.3453									-0.7619	1.0000

TABLE 4-6: Summary Statistics of Bulk Mineralogy and Chemistry

	Mean	S. Deviation+	S.E. of Mean*
SiO_2	51·34512	9·41974	1·02778
TiO_2	0·96175	0·63109	0·6886
Al_2O_3	14·96964	3·95797	0·43185
Fe_2O_3	8·24619	3·05868	0·33373
FeO	0·45869	0·94577	0·10319
MgO	3·19524	1·09823	0·11983
CaO	3·96643	7·00070	0·76384
K_2O	2·46952	0·82970	0·09053
Na_2O	2·21821	1·16952	0·12760
P_2O_5	0·26976	0·27889	0·03043
CO_2	2·27679	5·17543	0·56469
Re	73·61905	44·56994	4·86298
Sr	212·66667	134·19715	14·64211
Y	62·30952	54·48996	5·94534
Zr	156·78571	96·17467	10·49352
Nb	20·63095	30·00955	3·27431
Mo	12·60714	18·25589	1·99188
V	152·14286	78·71653	8·58868
Cr	124·77381	92·92403	10·13884
Mn	5715·51190	7907·20931	862·74727
Ni	145·94048	113·87336	12·42460
Pb	31·02381	15·26156	1·66517
As	12·82143	13·39768	1·46181
Zn	123·25000	38·01232	4·14748
Cu	128·64286	85·05273	9·28001
Ba	816·82143	585·92868	63·93006
Ce	110·58333	43·34846	4·72971
La	72·09524	37·11351	4·04942
Quartz	9·08333	9·14173	0·99744
K-Feld	2·75000	2·20008	0·24005
P-Feld	7·63095	5·84288	0·63751
Clin	5·85714	12·84115	1·40108

/contd.over

* standard error of mean

\+ standard deviation

TABLE 4-6 contd.

	Mean	S.Deviation	S.E.of Mean
Phil	1·92857	4·56753	0·49836
Clay	48·04762	15·38964	1·67915
Calcite	4·63095	11·80849	1·28841
Dolomite	0·30952	0·96912	0·10574
Halite	1·52381	1·86584	0·20358
Pyrite	0·20238	0·53278	0·05813
Organic C	0·48190	0·33209	0·03623
MLIS	35·13095	13·77599	1·50308
Illite	7·35714	6·72281	0·73352
Kaolinite	2·83333	4·30979	0·47024
Chlorite	0·63095	2·63333	0·28732
Palygorskite	1·76190	4·09413	0·44671
B	17·6638	10·2796	1·1085
Depth	248·9667	153·7944	16·2114

TABLE 4-9: Scores on Promax Factors

Sample No.	F1	F2	F3	F4	F5	F6	F7
211/6/2	0·058	-0·338	0·805	0·549	-0·612	0·265	-0·920
211/13/1	0·584	0·664	0·173	0·381	0·968	0·562	0·332
211/14/1	0·745	0·067	0·412	1·175	0·893	0·813	0·102
212/15/2	-2·446	-0·143	0·006	-0·076	0·704	0·152	0·448
212/15/3	-2·551	-0·482	0·019	-0·017	0·684	0·356	0·565
212/16/1	-1·683	-0·544	-0·101	-0·259	1·081	0·722	0·807
212/16/2	-1·989	-0·523	-0·156	-0·432	1·362	0·540	0·571
212/17cc	-2·269	-0·519	-0·204	-0·013	1·543	0·193	0·839
212/18/1	-1·866	-0·529	-0·207	-0·297	1·314	0·391	0·831
212/18/2	-0·056	-0·466	0·326	-0·429	0·802	-0·481	0·039
212/23/5	0·665	-0·373	0·129	-0·612	0·281	0·223	-0·162
212/27/1	-0·872	-0·623	-0·189	-0·681	1·076	0·890	1·362
212/28/2	-0·838	-0·566	-0·374	-0·728	1·013	0·742	1·000
212/35cc	-0·004	0·510	0·206	-0·545	0·773	0·520	0·158
212/36cc	0·099	-0·697	0·425	0·394	0·938	0·898	0·300
212/37/1	0·223	-0·696	0·681	0·412	0·668	0·609	0·227
212/37/cc	0·040	-0·524	0·919	0·026	0·400	-0·551	-0·103
212/38/1	0·206	-0·554	0·733	-0·264	0·497	-0·435	0·149
213/8/5	0·158	-0·174	0·713	-0·590	-1·643	-0·211	-0·942
213/9/4	-0·734	-0·263	0·344	-0·377	-1·506	0·351	0·010
213/9cc	-1·010	-0·104	0·606	-0·906	-2·217	0·111	-0·222
213/10/3	-0·995	-0·123	0·563	-0·925	-2·321	0·130	-0·371
213/11/2	-1·354	-0·133	0·584	-0·224	-2·637	0·207	-0·255

/contd.over

TABLE 4-9 contd.

Sample No.	F1	F2	F3	F4	F5	F6	F7
213/11/5	-2.402	-0.249	0.292	0.194	-1.741	0.600	0.286
213/12/5	-1.947	-0.259	0.216	0.204	-1.835	0.753	0.879
213/13/2	-2.148	-0.255	0.257	0.366	-1.674	0.527	0.953
213/13/5	-1.506	-0.324	-0.147	-0.328	-1.111	0.741	0.754
213/14/3	-0.465	-0.495	0.483	0.336	-0.485	1.007	0.702
213/15/2	-1.040	2.722	0.000	-0.342	0.370	0.349	0.759
215/8/2	0.170	-0.180	0.612	-0.365	-1.819	0.131	-0.530
215/9/2	0.091	-0.135	0.556	-1.106	-1.485	0.592	-0.139
216/24/4	0.561	5.249	-0.262	-0.512	0.680	-0.369	-1.002
216/25/3	0.237	2.420	-0.628	-0.292	0.706	-0.056	-0.623
216/30/3	0.941	1.518	-1.662	1.368	-1.066	-1.759	-2.148
216/32/3	1.180	3.016	-0.157	0.273	-0.679	-1.147	-1.592
216/34/1	1.230	3.553	-0.472	-1.139	0.095	0.250	-0.695
221/14/2	0.212	-0.377	-0.119	0.028	0.343	0.381	-0.336
221/14/5	0.178	-0.455	0.057	0.528	0.356	0.560	-0.115
221/15/2	0.097	-0.465	-0.009	0.043	0.514	0.655	-0.030
221/15/4	-0.268	-0.650	0.090	-0.368	0.682	0.929	0.140
221/16/2	-0.446	-0.531	0.169	-0.069	0.418	0.565	1.027
235/9/6	0.560	-0.271	-0.309	0.210	0.581	0.567	0.417
236/16/5	0.213	-0.598	-0.030	-0.191	0.825	0.831	0.242
236/18/3	0.148	-0.351	-0.087	-0.071	0.294	0.812	0.070
236/19/2	-0.161	-0.471	0.078	-0.344	0.242	0.438	0.438
239/1/1	0.863	0.833	-0.335	0.983	-0.728	0.078	-0.583
239/4/3	0.201	-0.066	-0.431	1.019	-0.655	0.073	0.005

/contd.over

TABLE 4-9 contd.

Sample No.	F1	F2	F3	F4	F5	F6	F7
239/9/3	0·056	-0·134	-0·720	0·016	0·032	0·255	0·314
239/11/3	0·131	-0·354	-0·451	0·574	0·337	0·485	0·288
239/13/4	1·210	-0·313	-0·361	-0·248	-0·480	0·058	-0·379
239/16/3	0·537	-0·467	0·099	0·046	0·536	0·745	-0·245
239/18/2	0·202	-0·589	0·230	0·535	0·828	0·943	0·422
240A/2/1	1·129	-0·154	1·733	1·380	-0·389	-2·643	-3·510
240/3/3	0·478	-0·547	-0·224	0·096	0·246	0·440	0·381
240/5/1	1·276	-0·176	1·225	1·244	-0·276	-1·206	-1·840
245/1/3	-0·553	-0·366	0·217	-0·028	-0·746	0·558	0·941
245/5/3	0·132	0·105	0·185	-0·086	0·164	0·670	0·154
245/2/6	-0·079	-0·518	0·245	0·019	0·150	0·737	0·321
245/6/2	0·369	-0·546	0·218	0·080	0·302	0·779	0·088
246/10/2	0·893	1·781	1·149	2·348	-0·832	0·329	1·394
248/10/2	0·964	-0·502	0·448	0·196	0·332	0·081	-0·919
248/11cc	1·016	-0·409	0·403	0·012	0·144	-0·378	-1·364
248/12/3	1·173	-0·387	0·350	-0·395	-0·144	0·009	-1·228
248/14/1	0·576	-0·641	-0·074	0·432	0·758	0·833	0·050
248/14/6	0·345	-0·670	-0·159	0·166	1·063	0·875	0·236
250A/3/1	0·401	-0·442	-0·023	-0·167	0·155	0·623	-0·035
250A/6/3	0·627	-0·526	0·059	-0·123	0·332	0·751	-0·244
250A/11/2	0·669	-0·661	0·180	-0·179	0·967	0·850	-0·131
250A/15cc	-0·022	0·296	1·048	6·573	0·095	-1·126	-1·497
250A/22/3	0·876	-0·239	0·245	-0·404	0·385	0·071	-0·591

/contd.over

TABLE 4-9 contd.

Sample No.	F1	F2	F3	F4	F5	F6	F7
254/25/2	0·550	0·865	-2·749	0·410	-0·826	-0·503	-0·068
254/26cc	0·387	0·118	-2·684	-0·154	0·162	-0·114	0·359
254/27/3	0·502	-0·014	-2·920	-0·331	0·279	-0·688	0·123
254/28cc	0·264	-0·080	-4·888	-0·486	1·114	-0·096	1·001
256/2/3	-1·911	-0·325	-0·185	0·079	-0·150	0·447	0·671
256/4/5	-0·667	-0·502	-0·085	-0·774	-0·177	-0·102	2·706
256/6/3	0·884	-0·349	0·496	-0·700	-0·592	-2·233	0·267
256/7cc	0·677	-0·387	0·668	-0·492	0·162	-1·209	-0·695
256/8/4	0·880	0·632	0·607	-0·226	-1·022	-1·844	1·219
257/2cc	0·128	-0·360	0·336	-0·622	-1·095	-0·580	2·046
257/4/3	0·482	-0·347	0·958	-0·253	-1·019	-1·768	0·844
257/5/2	-0·150	-0·458	0·815	-0·315	-0·516	-1·342	1·445
258/14/1	1·227	-0·308	1·025	-0·774	0·840	-4·019	-1·708
258/15/1	0·910	2·017	0·435	-0·918	0·449	-1·905	-1·518
258/16cc	0·715	0·005	-3·427	-0·815	0·264	0·100	-0·304
258/17/2	0·772	-0·156	0·287	-0·839	0·478	-1·105	-0·671
258/22/4	0·888	-0·089	0·540	0·005	0·110	-0·935	-1·334
258/25cc	0·447	0·156	0·178	-0·870	0·692	-1·353	-0·636

CHAPTER V

CHEMISTRY OF THE INDIVIDUAL MINERALS

A. Mixed Layer/Illite/Smectite (MLIS)

The $< 2\mu m$ fraction was separated into three size ranges: 2 - 0·2 μm, 0·2 - 0·08 μm and $< 0{\cdot}08\mu m$.

MLIS was the most abundant mineral in the $< 0{\cdot}08$ μm fraction (Fig.5-1). Table 5-1 lists the original mineralogy of the $< 0{\cdot}08$ μm size fraction of 21 samples used for chemical analysis. Samples for which more than 10% impurities were reported have been omitted. For smaller amounts of impurities, the original data have been corrected. The mixed layer illite/smectites were anlysed using the β-probe. The analyses are presented in Table 5-2. The 0·2 - 0·08 μm and $< 0{\cdot}08\mu m$ of sample 254/26cc were also analysed in order to find out if there was any variation in the chemistry of the same mineral in different size fractions. As seen in Table 5-2, there is no considerable difference in the chemistry of the two sizes. Hower and Mowat (1966) analysed three different size fractions of two illites and found that the compositions do not vary much over the different ranges of particle size. Roberson et al (1968) also found little variation in the composition of size fractions from the same montmorillonite.

1. Calculation of chemical formula

According to Hower and Mowat (1966) the most useful way of examining the chemical analysis of a mineral is to calculate first a structural formula.

Grim et al. (1978) did not include the dehydration loss in their calculation as they believed this would induce extra variance in the statistical analyses of the structural formula.

Hower et al. (1966) suggested that a single 'mean' structural formula should be written for mixed layer structures. In their structural formula TiO_2 was considered to be a separate phase and was excluded from the calculation. Grim et al. (1978) also did not include TiO_2 in their structural formula calculation since it was not certain whether it occurred in the smectite structure or as a separate phase in the sample. Grim (1953) has pointed out the presence of anatase as a minor component of kaolinites.

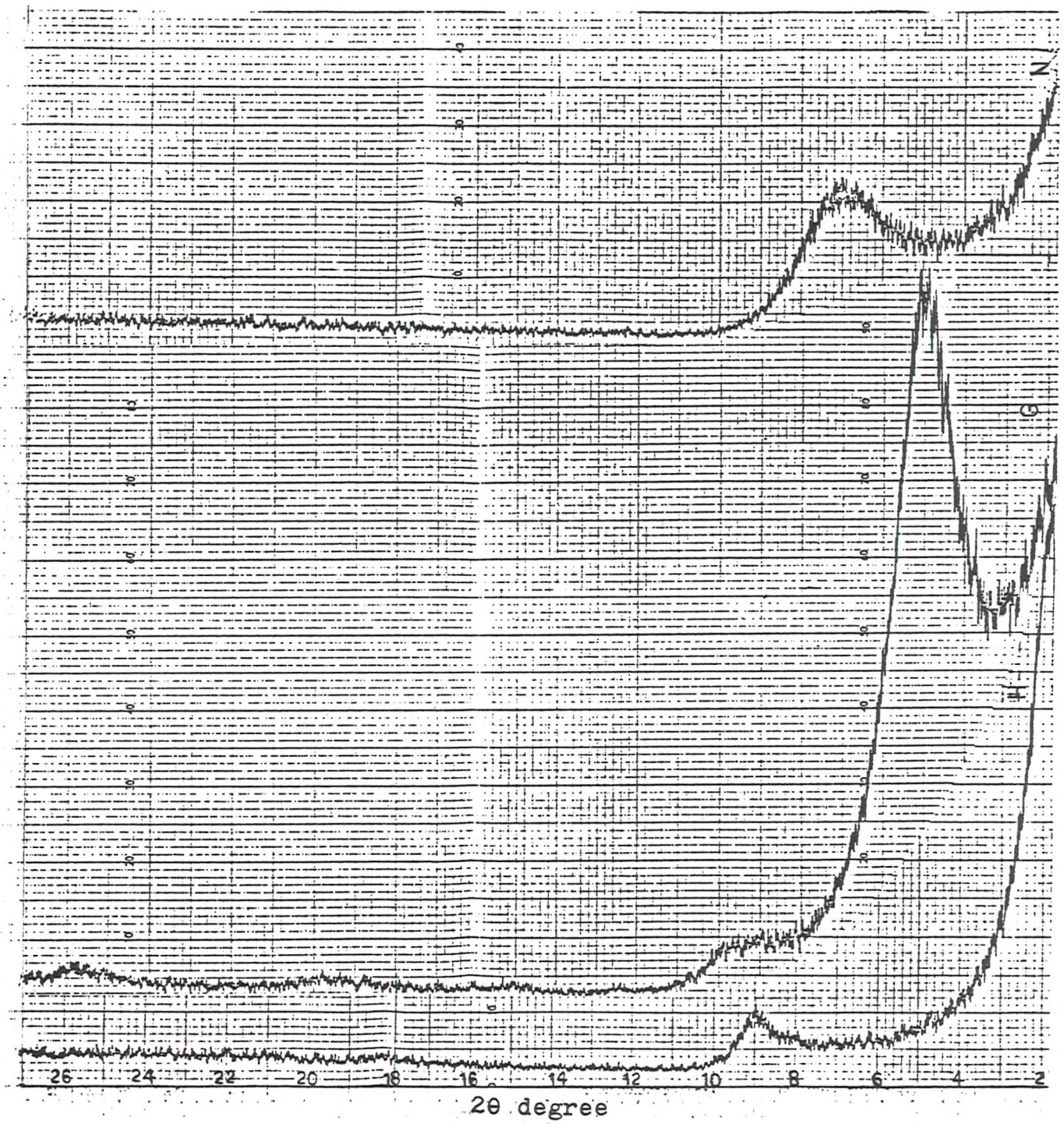

Fig.5-1.Diffraction pattern of MLIS(<0.08μm).

TABLE 5-1: Mineralogy of < 0·08 μm MLIS

	%E	MLIS	Illite	Kaolinite	Chlorite	Palygorskite
212/17cc	45	100				
212/18/1	71	100				
212/18/2	58	91		5 0		4
212/23/5	69	100				
212/27/1 (0·2-0·08)	57	95		5		
212/27/5 (<0·08)	45	100				
212/35cc	76	100				
213/11/5	52	94	6			
236/19/2	69	100	Tr	Tr		
246/10/2	67	100				
254/25/2 (<2μ)	85	100				
254/26cc (0·2-0·08)	81	100				
254/26cc (<0·08)	81	100				
254/27/3	84	100				
254/28cc	70	98		2		
256/8/4	68	100				
257/4/3	72	100				
257/5/2	67	100				
258/15/1	81	100	Tr			
258/17/2	72	95		5		
258/22/4	83	100				

In the present study, a single 'mean' structural formula was written for the pure mixed layer IS. Ilmenite and anatase were observed in a few samples by XRD and under SEM. The correlation programme of bulk samples (Table 4-5) also showed positive correlation among TiO_2, FeO, Fe_2O_3 and MgO, which suggested the presence of ilmenite. It also occurred in the basaltic volcanic glass. It was not clear whether P_2O_5 occurred in the structure, and it was not possible to check on the presence of either Ti or P with any sort of experimental work since there was insufficient sample available. Therefore, TiO_2 and P_2O_5 were omitted from the structural formula.

The formula was calculated on a unit cell consisting of 22 negative charges [i.e. $O_{10}(OH)_2$]. An example of the structural formula calculation is given in Table 5-3. A complete tetrahedral occupancy of 4 was assumed whereas an occupancy of 2 was assigned to the octahedral position. These assumptions lead to total layer charges between 0.2 - 1.51. Weaver and Pollard (1973) report values between 0.3 - 0.6 for mont, 0.7 or higher for beidellite and 0.88 for nontronite. The assumptions made in the calculations cannot be correct for samples from site 254 since they show impossibly high total charges (1.1 - 1.51). It is most likely that much of the Mg content assigned to interlayer position in reality occurs in octahedral positions. Therefore, it was decided for these samples, to assign values higher than 2 cations to the octahedral sites, such that the net charge deficiency on the octahedral sites became zero. This then gives a lower total charge (0.66 - 0.82). Although somewhat high, these fall within the ranges previously recorded for this type of mineral (Weaver and Pollard, 1973). Although the sum of octahedral ions show values as high as 2.35, Scheiedgger and Stakes (1977) report values as high as 2.38 for smectite with similar chemistry to the samples at site 254 (low Si and high Mg).

It is not known to what extent the other samples possess octahedral occupancy greater than 2. Separate determination of exchangeable cations would be necessary to determine this. If in fact this is the case, the layer charges presented will be somewhat high.

The method for charge distribution suggested by Tardy and Fritz (1981) was used. The theoretical cation exchange capacity was also calculated by the following method suggested by Gast (1977);

TABLE 5-3: Example of Structural Formula Calculation (Sample 212/17cc)

Oxides	Weight per cent	Molecular Proportion	Cation Proportion	Number of Oxygen	11 / 2·3694	Charge Distribution		
SiO_2	46·96	0·7816	0·7816	1·5632	3·63	Si 3·64 Al 0·36	}	tet = -0·36
TiO_2	0.38	0.0048	0.0048	0·0096	0·02			
Al_2O_3	15·76	0·1546	0·3092	0·4638	1·44	Al 1·08 Fe^{3+} 0·79 Mg 0·13	}	octahedral = -0·11
Fe_2O_3	13·50	0·0845	0·169	0·2535	0·78			
MgO	2·92	0·0724	0·0724	0·0724	0·34	Mg 0·21 K 0·06	}	Interlayer + 0·48
CaO		-	-	-	-			
Na_2O	-	-	-	-	-			
K_2O	0·65	0·007	0·0138	0·007	0·06			
P_2O_5	0.36	0.0025	0·005	-	-			
L.O.I.	19·70	-	-	-	-			
T.N.O.	-	-	-	2.3694	-			

L.O.I. = Loss on ignition.
T.N.O. = Total number of oxygen

CEC (meq/per 100g of clay) = (100/A) x charge deficit per unit cell

where

A = molecular weight per unit cell, not including the weight of the counter ions/1000.

The cation exchange capacities for 21 mixed layer IS are shown in Table 5-4. Most exchange sites are occupied by Mg^{2+}, and in fact charge deficiency is mostly controlled by Mg^{2+} (Fig.5-2), but some K^{+}, Na^{+} and Ca^{2+} are also present (Fig.5-3).

C.E.C. varies widely (between 29 and 200). The high values are due largely to a significant charge deficit in both the octahedral and tetrahedral layers. Weaver and Pollard (1973) observed Na^{+}, Ca^{2+}, Mg^{2+} and H^{+} as the most common interlayer cations. They reported C.E.C. values between 70 and 130 meq/100g for montmorillonite.

2. Structural and compositional relationships

Table 5-4 presents the structural formulae of the present study mixed layer IS.

All MLIS were of dioctahedral variety since trivalent cations such as Al^{3+} or Fe^{3+} were dominant and also the sum of the cations in the octahedral sites was 2, which means two of the three sites were filled. According to Weaver and Pollard (1973), the dioctahedral clays theoretically have 67% of their total octahedral positions filled.

Octahedral Mg^{2+}, Al^{3+} and Fe^{3+} for the dioctahedral clays were totalled and the relative proportion calculated (atomic per cent) (Fig. 5-4). As can be seen, Fe^{3+} and Al^{3+} are the dominant cations in the octahedral position. MLIS from the ridges (Sites 254 and 246) is rich in Mg^{2+} in comparison with the others. Mixed later IS from the Ninety-east Ridge (Site 254) is rich in Fe^{3+} and Mg^{2+}, whereas MLIS from the Madagascar Ridge (Site 246) is rich in Al^{3+} and Mg^{2+}.

In the tetrahedral sheet, the substitution of Al^{3+} for Si^{4+} appears to be limited to less than 10% (Table 5-4). However, samples from Site 254 are exceptional. They show between 15% and 20% substitution. The excess charge in the interlayer is balanced by deficiencies in both the tetrahedral and octahedral layers.

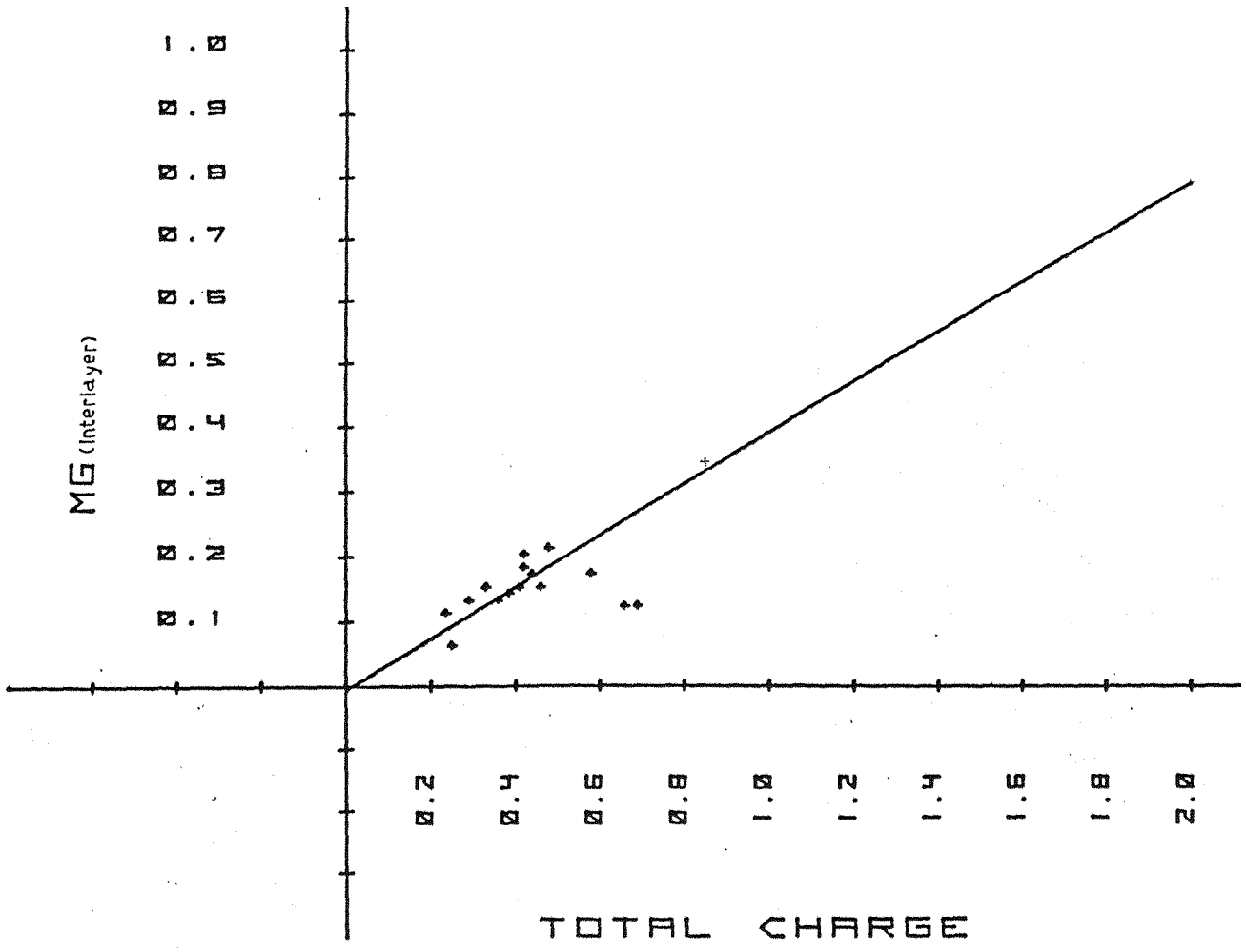
1.0
0.9
0.8
0.7
0.6
0.5
0.4
0.3
0.2
0.1
MG (Interlayer)
0.2
0.4
0.6
0.8
1.0
1.2
1.4
1.6
1.8
2.0
TOTAL CHARGE

Fig. 5-2

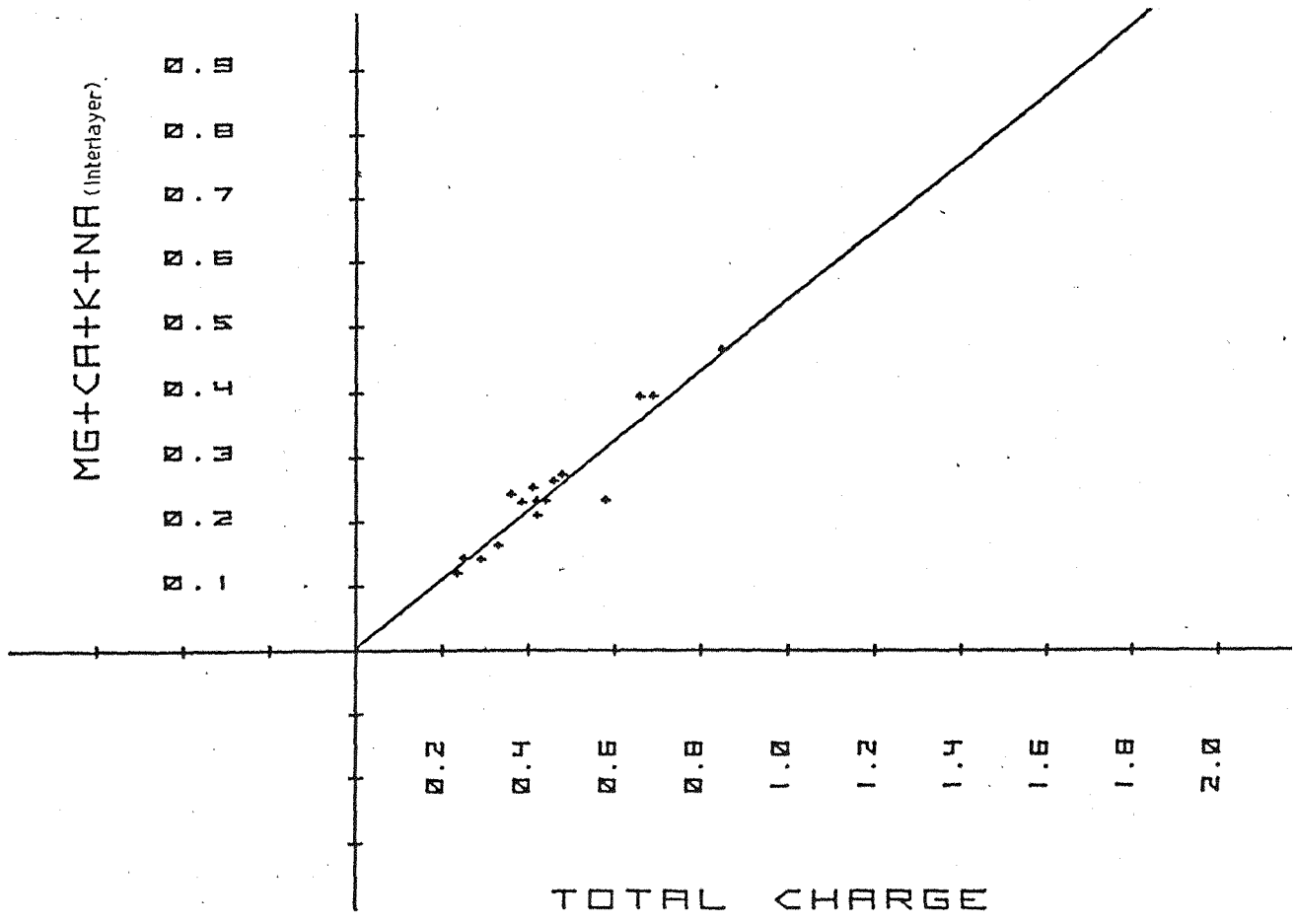
0.9
0.8
0.7
0.6
0.5
0.4
0.3
0.2
0.1
MG+CA+K+NA (Interlayer)
0.2
0.4
0.6
0.8
1.0
1.2
1.4
1.6
1.8
2.0
TOTAL CHARGE

Fig. 5-3

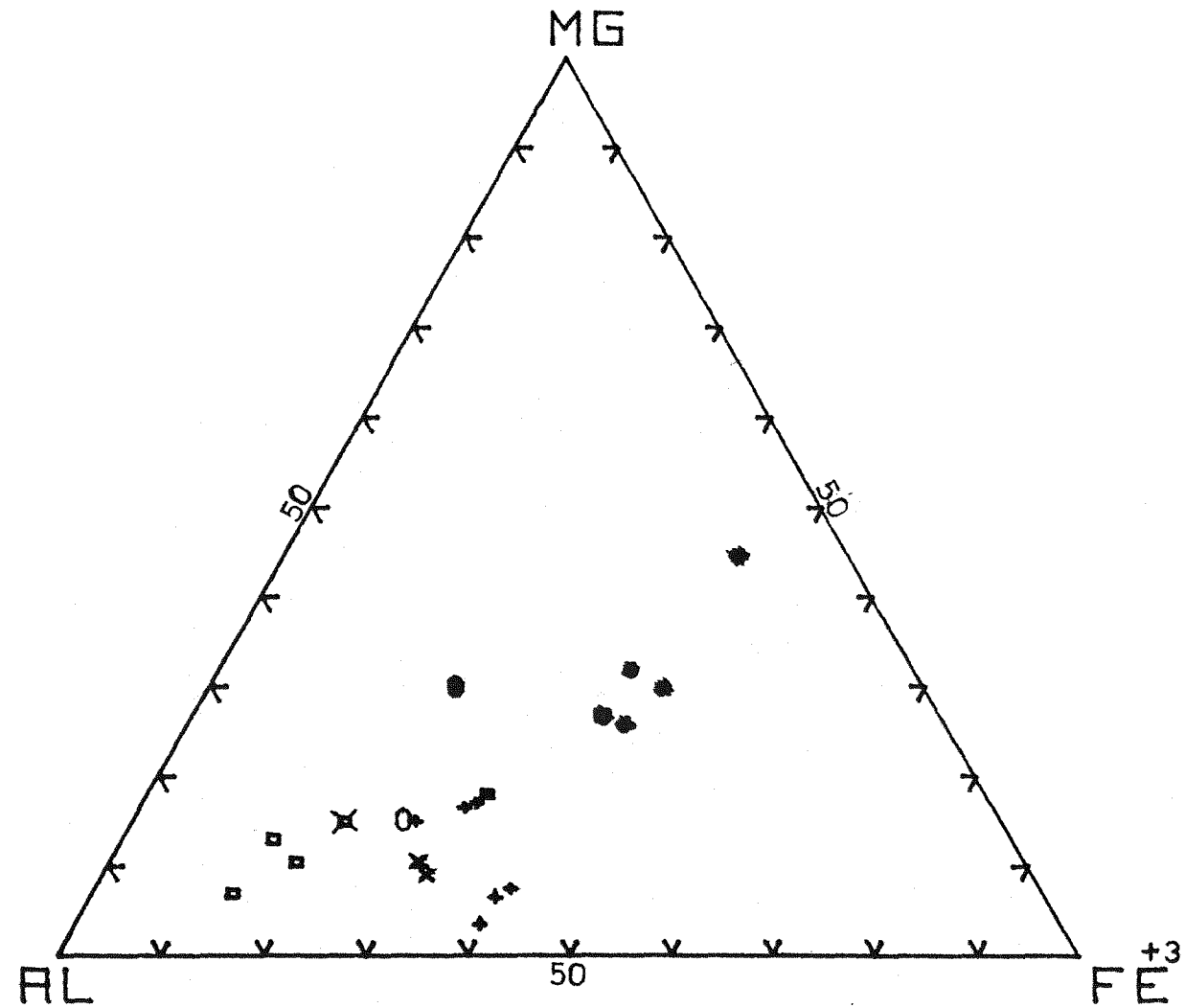

Fig.5-4. Al, Fe and Mg distribution in octahedral position. + site 212
■ site 213, ○ site 239, ● site 246, ● site 254, ⌑ site 256, × site 257
□ site 258.

Hower and Mowatt (1966) plotted the percentage of expandable layer against the number of fixed interlayer cations per structural unit. They showed that there was a negative relation between per cent expandable layers and the number of fixed interlayer cations (K + Na) per structural unit. This plot indicated a value of 0.8 equivalents of fixed interlayer cations for no expandable layers rather than 1 equivalent as in micas (Fig. 5-5).

The present study mixed-layer IS was plotted on this diagram. The %E determined by the v/h ratio method disagrees with the K%. One would expect much higher K% for the suggested values of %E. It seems likely that much of the variation in the v/h ratio is due to different crystallinity in the smectite. Poorly crystalline smectite would be interpreted as low %E MLIS using v/h ratio method. Using 0.8 formula units of K in the unit cell for 100% illite, the values of K obtained suggest expandable contents between 80 - 100% for these samples. It seems that the reported values for %E are in fact more representative of crystallinity differences than expandable layer content. However, only samples containing high amounts of MLIS were chemically analysed, and it is still probable that samples containing MLIS with low recorded values of expandable layer do contain a substantial illite content. Because of the difficulties in distinguishing between variation in crystallinity and variation in expandable layer by XRD, crystallinity variation should be considered wherever there is any mention of %E in the next chapters.

3. Octahedral-tetrahedral relations

Yoder and Eugster (1955) outlined the observed composition range of natural 2:1 clays in a triangular diagram in which two variables were tetrahedral R^{3+} and octahedral R^{3+} (Fig. 5-6). This, in effect, plots tetrahedral trivalent ions, ranging from zero of pyrophyllite and celadonite to two in muscovite, against octahedral trivalent ions ranging from four in pyrophyllite and muscovite to two in celadonite. These two variables fix the third parameter, namely the total of potassium, H_3O^+ cations, and exchangable cations. This plot was used in order to obtain some ideas about the relation between the chemistry and structure. All samples fall in either montmorillonite or MLIS fields. As the samples get further from the montmorillonite field, the %E does not decrease.

Three groups of MLIS are recognised on the basis of cation distribution in the octahedral sites (Table 5-5).

Group (1): MLIS of this group falls in the montmorillonite field. This group is rich in Al^{3+} (52% - 80%)

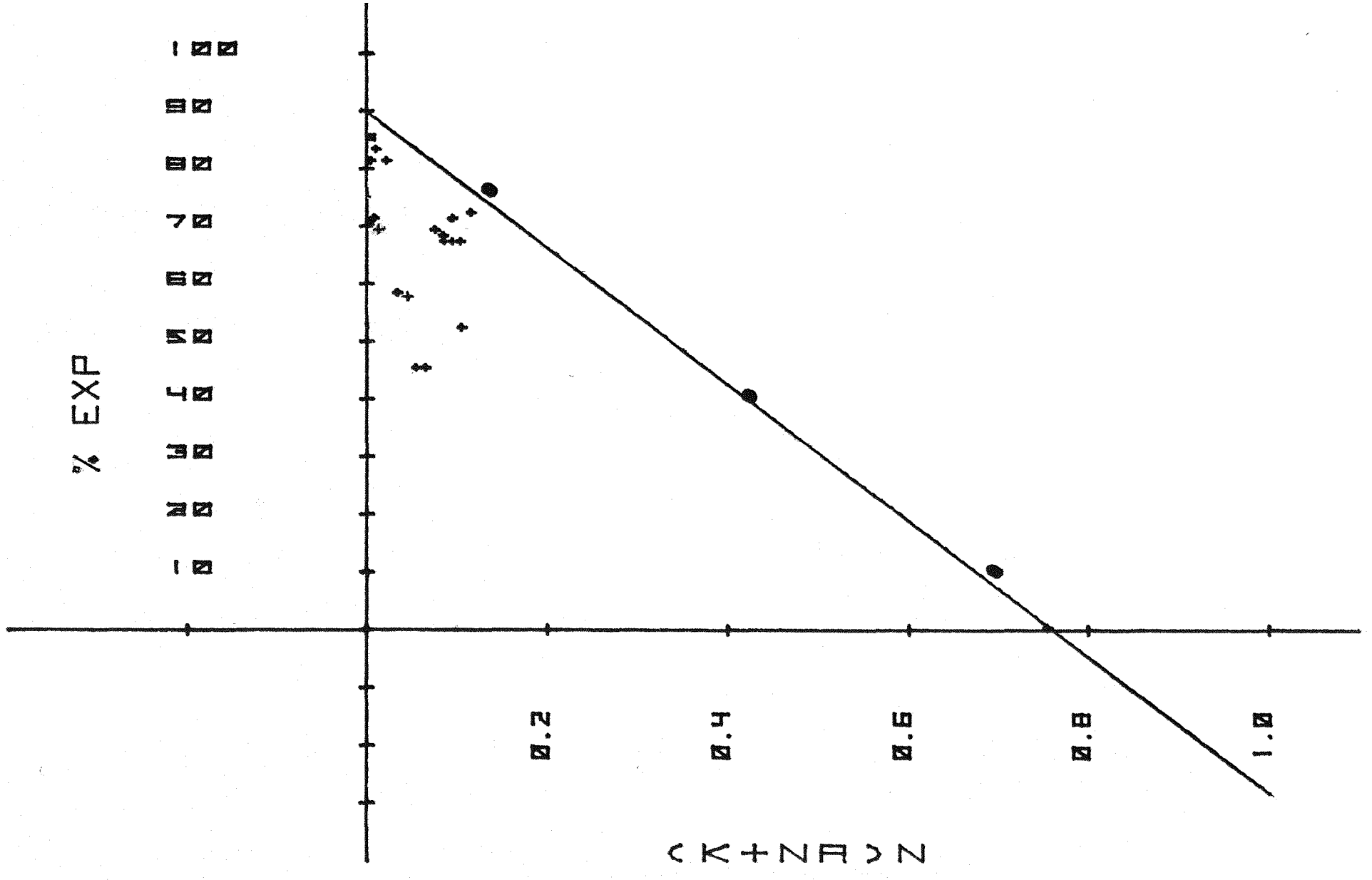

Fig.5-5.Percentage of expandable layer(% EXP) versus fixed interlayer cation(after Hower and Mowat,1966).Key: + from present study, ● from Hower and Mowat(1966).

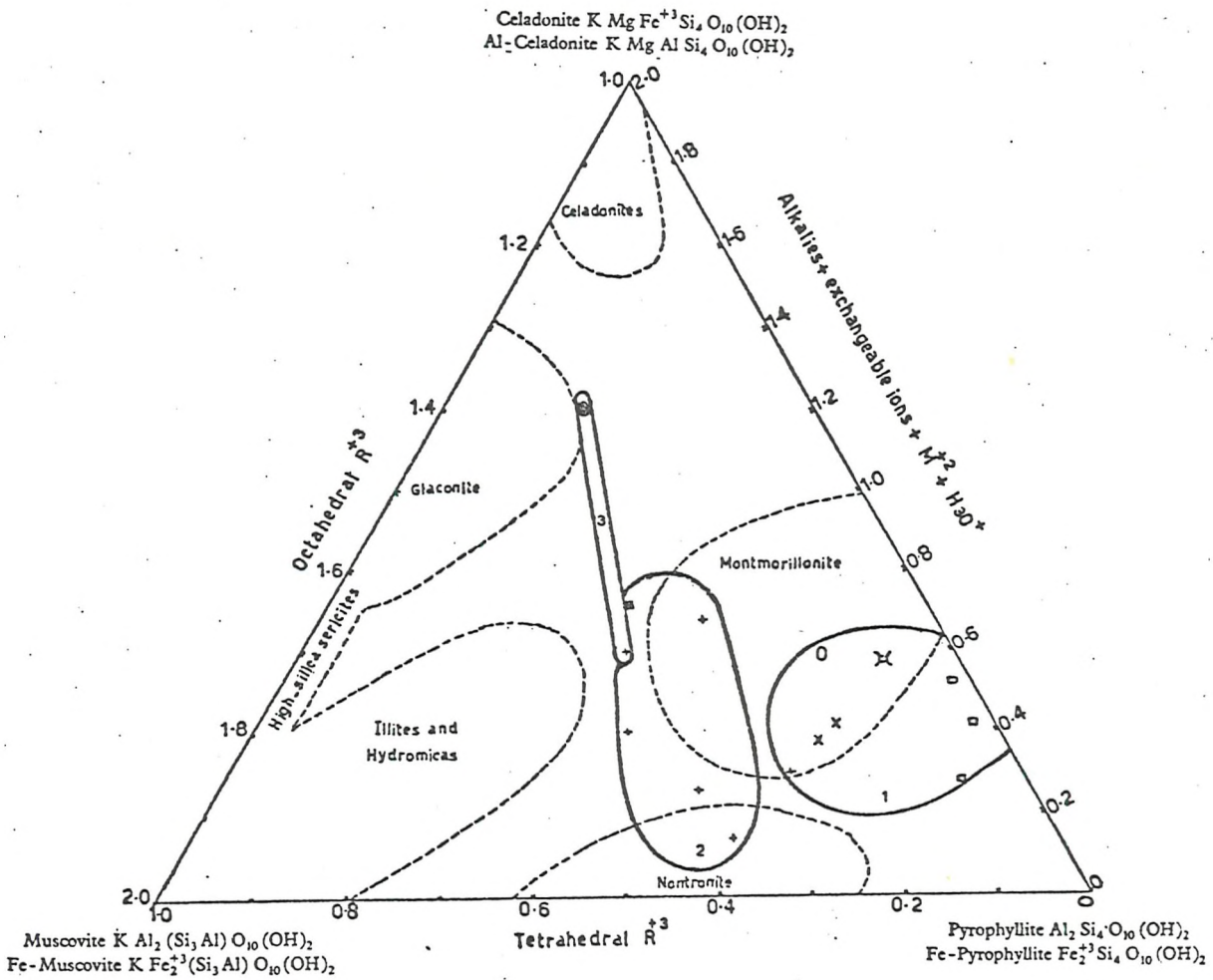

Fig.5-6.Plot of tetrahedral R and octahedral R(after Yoder and Eugster,1955).Key:——from present study,-----from Yoder and Eugster,1 indicating group I,2 indicating group II,3 indicating group III,+site 212,▪site 213,○site 239,●site 246,⌑site 256,xsite 257,□site 258.

Group (2): It shows lower %E in comparison with groups (1) and (3) and is intermediate in the chemistry (i.e. Al = 49% - 60%; Fe^{+3} = 31% - 40%; and Mg^{+2} = 4% - 18%).

Group (3): MLIS is rich in Mg^{2+} (15% - 30%) and shows similar %E to group (1). However, samples from Site 254 do not fit in such a composition triangle, since they have high tetrahedral (0·65-0·81) and octahedral (0·38-0·7) charges. According to Weaver et al. (1973) expanded dioctahedral smectites, which have a relatively high tetrahedral charge content (0·4), are called beidellites. These clays commonly have a total charge of 0·7 or higher.

4. Origin

As previously mentioned, three groups of MLIS are recognised. Groups 1 and 3 have MLIS with high %E (67% - 83%), whereas group 2 consists of low %E MLIS (45% - 58%). According to Perry et al.(1976a), Drever (1976), Perry et al.(1976b) and Eslinger et al.(1974), MLIS with high %E is of authigenic origin. Conversely, low %E MLIS is of detrital origin.

The authigenic MLIS could form via volcanic material alteration (basic and/or silicic) (Bonatti et al.,1968; Scheidegger et al., 1977; Hein et al., 1978; Papavasiliou et al.,1982).

In the present study, the bulk chemistry indicated a basaltic and/or silicic volcanic material contribution to the sediments. Thus the high %E MLIS probably resulted from the alteration of basaltic and/or silicic glass. All MLIS contain a considerable amount of Mg^{2+} in their structure and in the interlayer position, which could indicate that they are an important trap for Mg^{2+} from the interstitial water. According to Hein et al. (1978), volcanic rocks are 'weathered' or altered to release Ca and Mg, a process that elevates the alkalinity of pore water. Smectite forms as a weathering product that, in turn, depletes the alkaline pore waters in Mg and O^{18}, thereby lowering the alkalinity (Perry et al.,1976a, 1976b).

B. Chemical Characteristic of the Zeolites

Energy Dispersive X-ray techniques (EDX) were used to analyse individual zeolite crystals. The results are presented in Table 5-6a & b. Pure clinoptilolite from one of the samples (256/7cc) was analysed by β-probe and used as a standard. Most oxide analyses summed to between 70% and 89%. Steel et al.(1975) observed sums of 75% to 87%.

The structural formula was calculated on the basis of 72 and

32 oxygens for clinoptilolite and phillipsite, respectively (Table 5-7a & b). Kastner et al. (1978) reported the occurrence of Fe-oxide or hydroxide inclusions in phillipsite crystals and therefore subtracted it from analyses of clinoptilolite and phillipsite. Sheppard et al. (1970) also assumed that all Fe_2O_3 were impurities and subtracted it from the analyses.

In the present study, in order to check if Fe is in the structural positions of the zeolites, the method suggested by MacKenzie (1954) was used. The free iron oxide was removed using 4 per cent $Na_2S_2O_4$ (sodium hydrosulphite) with intermediate and final washing with 0.05N hydrochloric acid (full details of this technique are given in the Technique Chapter). Both the extraction (resulting from free iron removal) and pure zeolites were analysed by β-probe and atomic absorption (AA), and iron was measured (Table 5-8). As can be seen, the difference between the results from β-probe and AA is not considerable and is probably due to experimental error (such as weighing). Therefore, it was concluded that Fe was present as impurities (inclusion) in zeolites and thus could be subtracted from the chemistry. Variable results for Fe were also obtained as different points on one crystal were analysed during the analysis of zeolites by EDX. This suggests the presence of Fe as separate inclusions in the crystals.

Since it is difficult to assign a particular amount of water to zeolites and, also, as this water has no effect on the free energy calculation (to be discussed later), it was decided not to involve the water content of the minerals in the calculation of the structural formula. The problem of assigning water to the zeolite structure is discussed later.

Two checks were made on the corrections of the analysis. According to Steel et al. (1975), when the calculated formulae are considered, the number of Si + Al atoms must be half that of the number of oxygens. Figures 5-7a and b show this plot. Steel et al. (1975) also suggested a second check on charge balance; in this method the number of 2Ca + 2Mg + Na + K should equal the number of Al atoms (Figs.5-8 a & B). Passaglia (1970) defines a 'reliable' analysis as one with a balance error ($Eb = [(Al - \Sigma cat)/Al] \times 100$, where $\Sigma cat = [2(Ca + Mg) + K + Na]$ less than 10%. Stonecipher (1977) applied Passaglia's and Steel et al.'s criteria.

Fig.5-7a: Si vs. Al based on 72 (Ox) in clinoptilolite. Al + Si must equal 36·0 for zeolites (i.e. straight line). Deviation may be in part due to Sr influence on Si peak (Steel et al., 1975). Key: X data from Stonecipher (1978), ■ from Shepperd et al. (1970) and + data from present study.

Fig.5-7b: Si vs. Al based on 32 (Ox) in phillipsite. Symbols same as in Figure 5-7a.

Fig. 5_7a

Fig. 5_7b

Fig.5-8a: Plot for charge balance check in clinoptilolite. 2Mg + 2Ca + Na + K should equal Al (i.e. straight line). Deviation may be due to Sr and/or Ba, as pointed out by Steel et al. (1975). Key: • data from Stonecipher (1978), + data from present study.

Fig. 5-8b: Plot for charge balance check in phillipsite. Symbols same as in Fig. 5-8a.

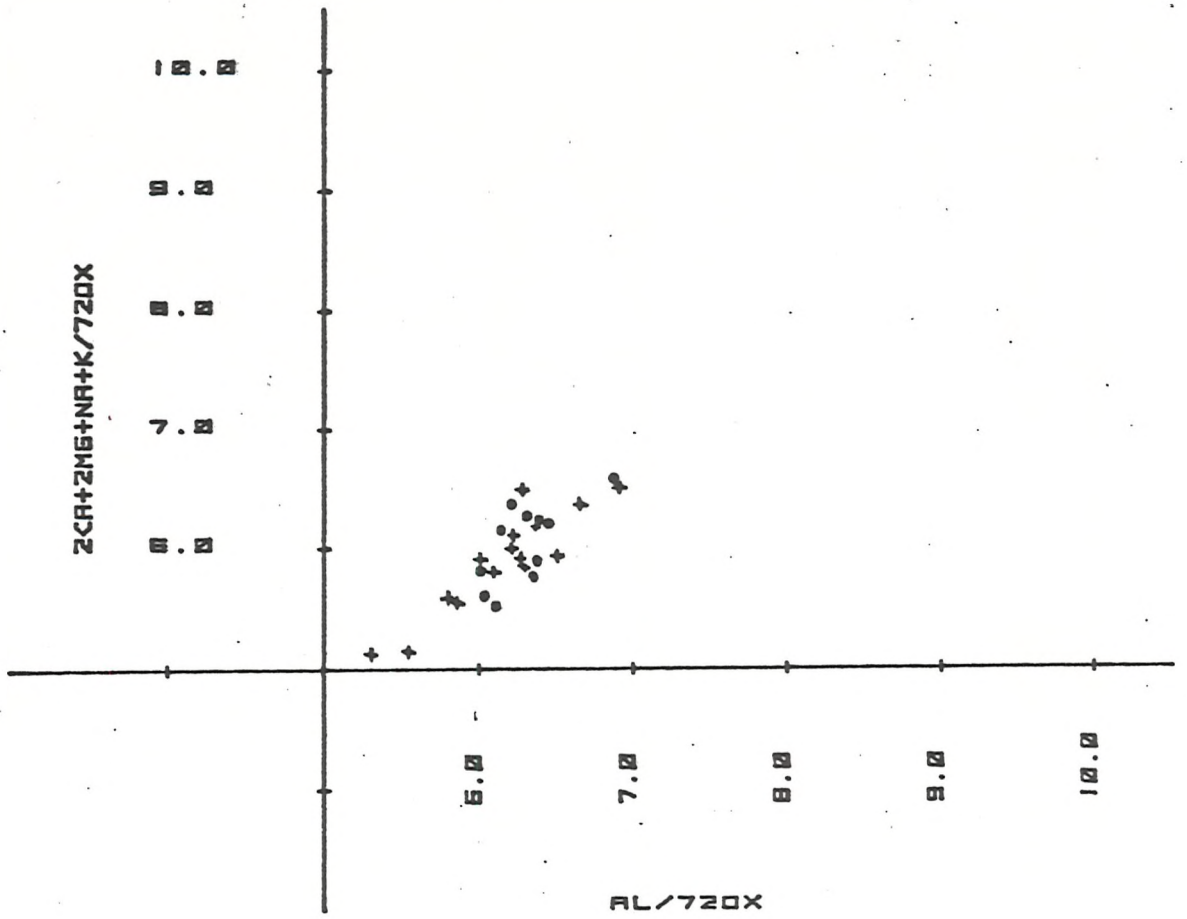

Fig. 5-8a

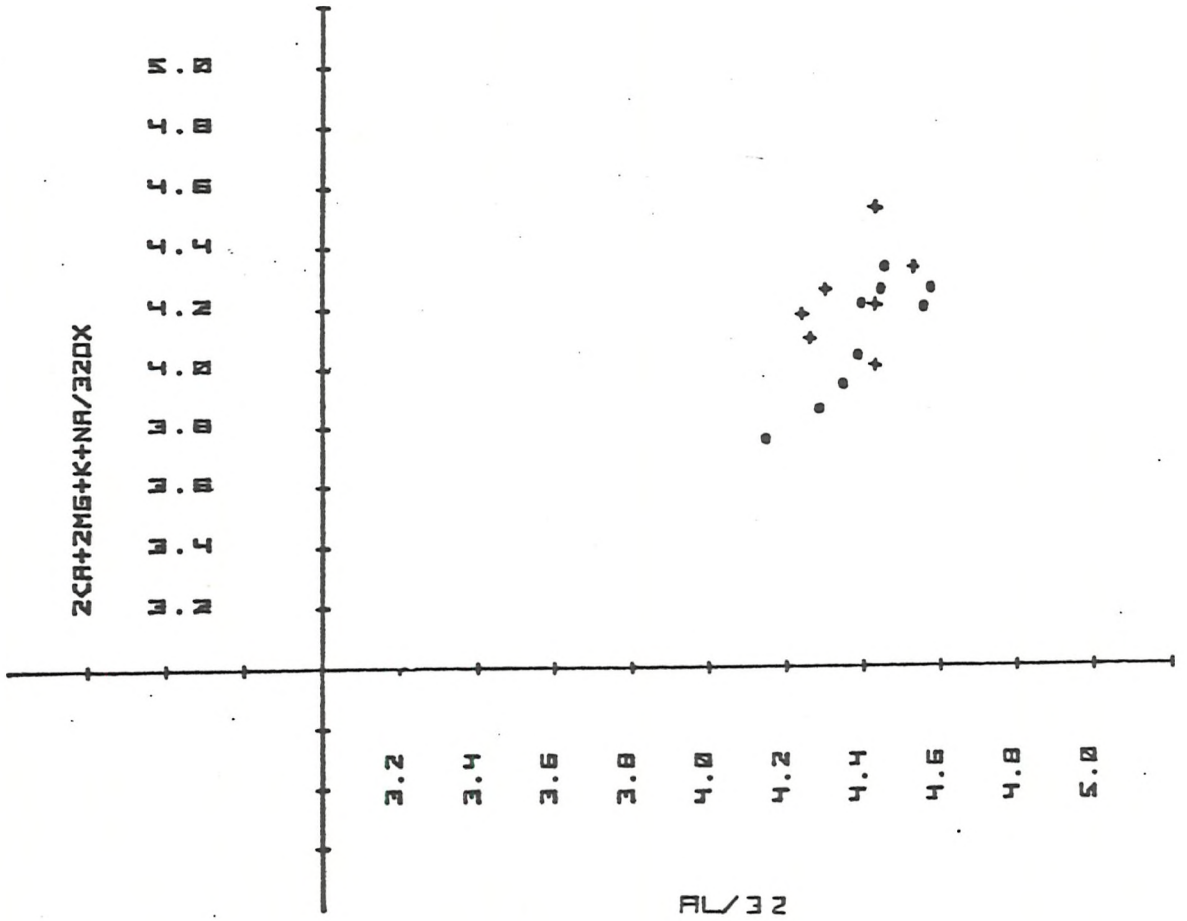

Fig. 5-8b

In the case of the present study, Passaglia's criteria was met in most of the samples (Tables 5-7a & b). Stonecipher (1977) and Steel et al. (1975) suggested that the deviation from the criteria and the balance error of more than 10% could be due to elements which are not accounted for (such as Ba and Sr).

1. Chemistry of zeolites

Stonecipher (1978) reported that deep sea clinoptilolite is more siliceous than sedimentary clinoptilolite and deep sea phillipsite. Both deep sea zeolites (clinoptilolite and phillipsite) are more potassic compared with those found in other environments (sedimentary and igneous rocks). Deep sea phillipsites are alkaline and relatively siliceous as compared with phillipsite from mafic igneous rocks (Sheppard et al., 1970; Stonecipher, 1978).

In the case of the present study, 82% of phillipsites have Si/Al ratios between 2·5 and 2·8, and 80% of clinoptilolites have Si/Al ratios between 4·5 and 5·5. Monovalent cations are in excess of divalent ones. Figures 5-9a and b show the variation of the proportion of monovalent to divalent cations versus Si/Al ratios in clinoptilolite and phillipsite from the deep sea. Fields representing phillipsite and clinoptilolite from other geologic environments and data from Stonecipher's study on deep sea zeolites are also presented. As can be seen, clinoptilolites of the present study are more siliceous than clinoptilolite and heulandite from igneous and sedimentary rocks. Most of them have more alkalis than alkali-earths, except clinoptilolites in association with carbobates which are rich in Ca. Phillipsites have Si/Al ratios intermediate between phillipsites from mafic igneous rocks and phillipsites from saline lacustrine deposits. The majority have K > Na, Ca and Mg. They show lower Si/Al ratio than clinoptilolite. Lacustrine phillipsites have sodium as the dominant cation, whereas those from mafic igneous rocks commonly have a higher percentage of alkali-earths than deep-sea or lacustrine phillipsite (Hay, 1966; Sheppard et al., 1970; Stonecipher, 1978). The present study zeolites show lower alkalis content than that of Stonecipher's study, which could reflect the chemistry of the interstitial water and the glass involved in the formation of zeolites.

In relation with depth, the Na^{+} content of phillipsite at Site 213 decreases as depth increases, whereas the amount of alkali-earths increases;

Fig.5-9a: Plot showing the proportion of monovalent to divalent cations versus Si/Al ratios of clinoptilolite. Key: ● data from Stonecipher (1978), ■ data from Sheppard et al. (1970), + data from present study.

Fig.5-9b: Plot showing the proportion of monovalent to divalent cations versus Si/Al ratios of phillipsite. Symbols same as in Figure 5-9a.

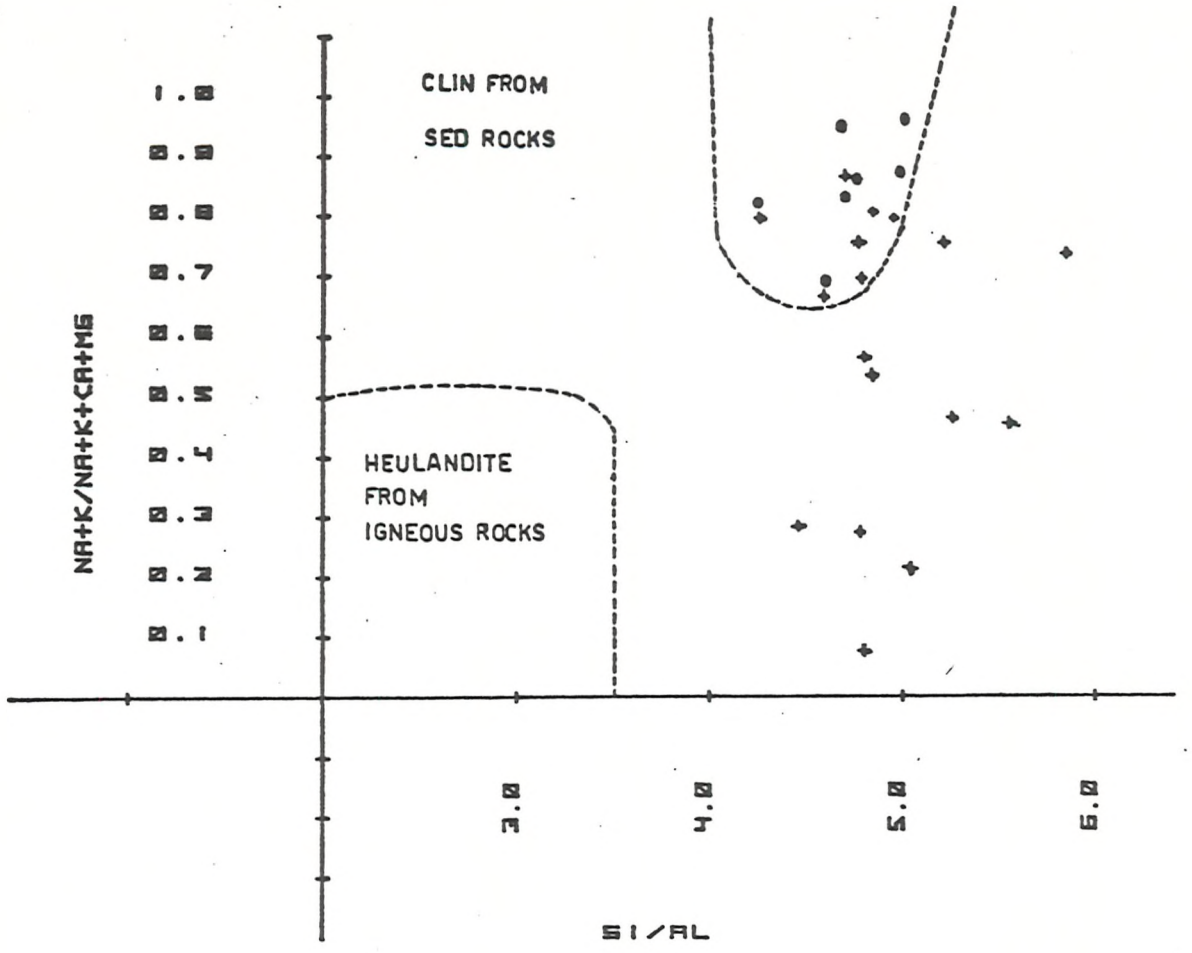

Fig. 5-9a

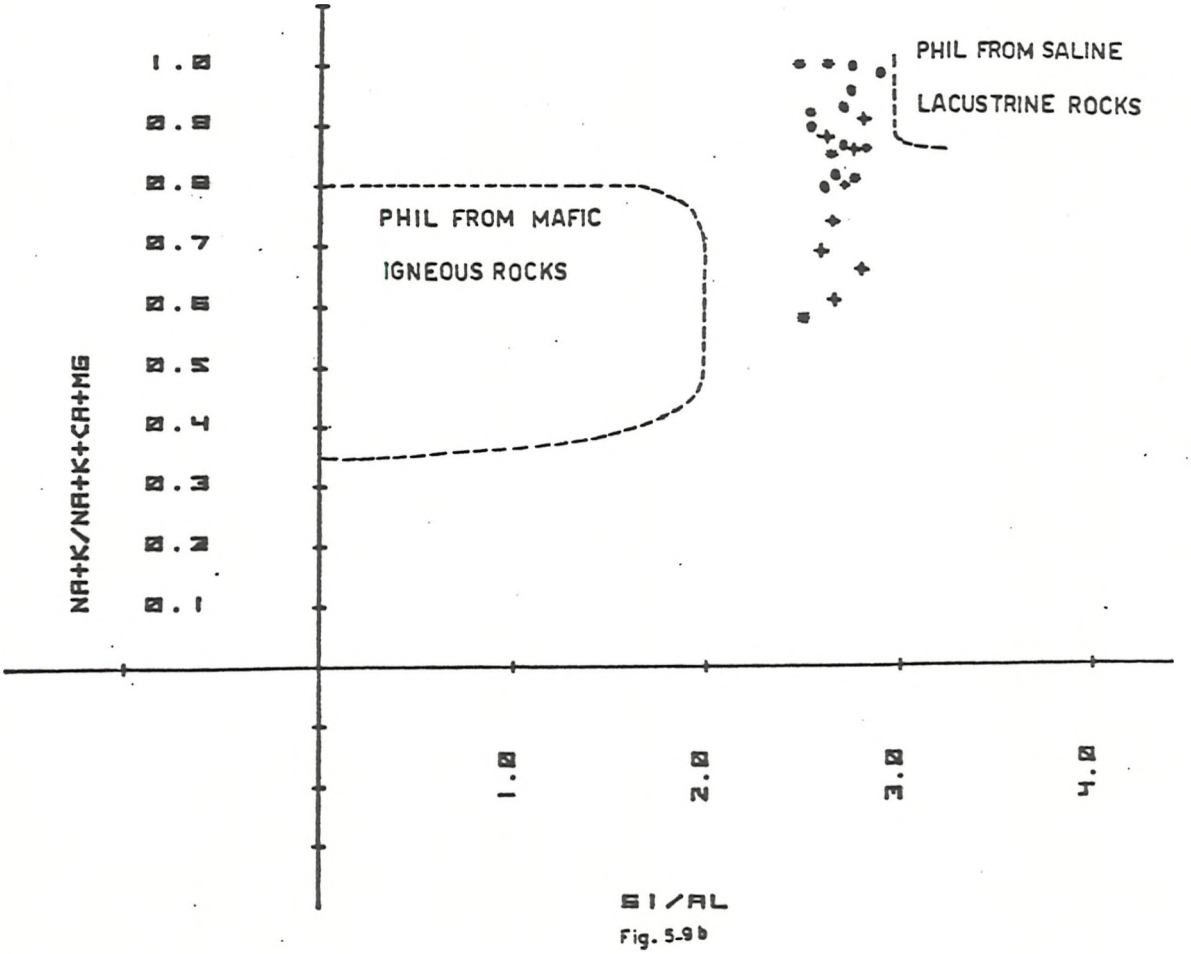

Fig. 5-9b

this coincides with the disappearance of halite. Clinoptilolite also shows an increase in Al and decrease in Si and Na with depth in most of the sites.

2. The relation of mineralogy and chemistry in whole rocks with zeolites

Phillipsite was observed at Sites 213, 239, 246 and 254. It was associated with clinoptilolite in Samples 246/10/2 and 254/25/2. Sample 213/8/5 contained well preserved siliceous fossils (radiolarians). No opal-CT was observed in association with phillipsite. The percentage of plagioclase was higher than K-feldspar in all samples. MLIS was the dominant clay mineral present in all samples. The percentage of E was high at Sites 254 and 246, whereas it varied widely at Sites 213 and 239. At Site 213 mixed-layer IS decreased downward, whereas illite increased. Mixed layer IS did not show any particular trend at the other sites. Volcanic glass was observed at Sites 246 and 254 under SEM. Ti/Al, Cr/TiO_2 and Fe/Ti vs. Al/(Al+Fe+Mn) plots (Figs.4-1,2 & 3) showed that Samples 213/9/4, 213/10/3, 213/11/2 and 246/10/2 plotted close to the rhyolitic line, whereas the rest of the sediments were fell close to the line representing basaltic and silicic material.

Clinoptilolite occurred in the sediments older than the Miocene in the Wharton Basin (Sites 212, 256 and 257), Naturaliste Plateau (Site 258), Ninetyeast Ridge (216),Somali Basin (236), Mozambique Basin (248) and Madagascar Ridge (246). As previously mentioned (Chapter III), it was associated with siliceous fossils (radiolaria) and opal-CT, and occurred in the cavities, which were left after the dissolution of biogenic silica. Plagioclase was dominant compared with K-feldspar. Mixed-layer IS with a high percentage of E was the dominant clay mineral present in association with clinoptilolite. The percentage of E was low where clinoptilolite was in association with palygorskite. Mixed-layer IS, total clay, opal-CT and biogenic silica decreased as clinoptilolite increased. This was further confirmed by the correlation programme (Table 4-5). However, in the presence of palygorskite, MLIS and clinoptilolite decreased as palygorskite increased. Volcanic glass was observed under SEM at Sites 216, 246 and 254. Plots of Ti versus Al, Fe/Ti versus Al/(Al+Fe+Mn) and Cr versus TiO_2 (Figs. 4-1,2 & 3) showed that clinoptilolite-bearing samples contained basaltic and silicic volcanic material contribution, except Sample 246, which contains only silicic volcanic material.

3. Conclusions

Basaltic material, in particular basaltic glass and/or palagonite, is the main precursor of phillipsite (Murray and Renard, 1891; Bonatti, 1963; Rex, 1967; Kolla and Biscaye, 1973b; Stonecipher, 1977; Kastner and Stonecipher, 1978). Smectite, which formed from altered basaltic glass, has also been suggested as a precursor of phillipsite (Bonatti and Arrhenius, 1965; Hay, 1966; Kastner, 1979).

In the case of the present study, well-shaped crystals indicated *in situ* formation of both phillipsite and clinoptilolite. MLIS did not show any relation with phillipsite. Visible volcanic glass and the bulk chemistry indicated the presence of both basaltic and silicic volcanic material, which could suggest the phillipsite formation from volcanic glasses. However, phillipsite - silicic volcanic material association was observed at Sites 213 (Samples 9/4, 10/3 and 11/2) and 246 (Sample 10/2). The question is why a high silica rhyolitic glass precursor yields phillipsite, a low silica zeolite. According to Hay (1966), Sheppard and Gude (1968, 1969), Kastner *et al.* (1978), Stonecipher (1978) and Iijima (1978) in the alkaline saline lake environment, rhyolitic glass is the most common precursor, whereas basaltic glass is in the marine environment. The association of phillipsite with certain silicic tuffs has been reported by Burns *et al.* (1973), Stonecipher (1976), Waterman *et al.* (1973) and Matti *et al.* (1973).

Stonecipher (1976) observed low Ti/Al ratios for some phillipsite-bearing samples and suggested that low Ti/Al ratio is caused by a high proportion of smectites, since smectites generally have a lower Ti/Al ratio compared with illite or kaolinite. Hay (1978) believes that the low silica content of the pore water probably explains why phillipsite was formed from the silicic ashes at hole 199 of Leg 20, which might otherwise be expected to have yielded clinoptilolite.

In the present study, the amount of MLIS did not show any relation with Ti/Al ratio. High percentage MLIS was associated with both low and high Ti/Al ratios (e.g. Samples 236/18/3 with 57% MLIS and 213/9/4 with 59% MLIS showed 0·04 and 0·07 Ti/Al ratios respectively). Unfortunately, no data on the chemistry of the interstitial water of phillipsite and silicic volcanic-bearing sediments is available to test the suggestion made by Hay (1978).

However, the occurrence of phillipsite instead of clinoptilolite in association with silicic volcanic glass could be caused by either the

existence of saline, alkaline interstitial water: Mariner and Surdum (1970) explained the correlation between the alkalinity and zeolite composition experimentally. According to them the Si/Al ratios of the zeolites are controlled by alkalinity. Figure 5-10 demonstrates the decrease in Si/Al ratio of the solution with an increase in alkalinity. In these alkaline solutions, the activity of silica is high, but the activity of alumina increases more rapidly with an increase in alkalinity. As a consequence of increasing pH, zeolites like phillipsite (relatively low Si/Al ratio) would be favoured over zeolites like clinoptilolite (relatively high Si/Al ratio), or basaltic volcanic material might have been present at the time of phillipsite formation and might have been entirely dissolved.

Bulk chemistry and SEM studies of clinoptilolite-bearing sediments suggested the occurrence of volcanic material (basaltic and/or silicic). MLIS with a high percentage of expandable layer was observed in association with clinoptilolite. A high percentage of expandable layer suggested its authigenic origin (Perry et al., 1976a and 1976b; Drever, 1976), and its probable formation from the alteration of volcanic material. Based on the common observed assemblage (i.e. clinoptilolite, high %E MLIS, opal-CT and biogenic silica) and the negative correlation of clinoptilolite with MLIS and B (biogenic silica, opal-CT, volcanic glass and minor minerals), the following reaction is suggested:

MLIS + biogenic silica and/or silicic volcanic $\longrightarrow$ clinoptilolite.

C. Composition of Palygorskite

In the present study, palygorskite (paly) was analysed by Energy Dispersive X-rays (EDX) since it was not possible to obtain a pure mineral specimen using the supercentrifuge. Therefore, the composition of paly was determined using calibration curves derived from other minerals. Details of the preparation of the calibration curves are given in the Technique Chapter (Chapter II).

The chemical analyses of 9 palys are listed in Table 5-9. A comparison of the published analysis of paly (Table 5-10) with the chemistry of the present study paly (Table 5-9) reveals that the present study paly is higher in Fe^{3+}, K^{+} and lower in Mg^{2+} compared with continental paly whereas it is, generally , close to oceanic paly. The sum of the oxides varies between 78·56% and 89·46%, and the average is 86·86%, which is in

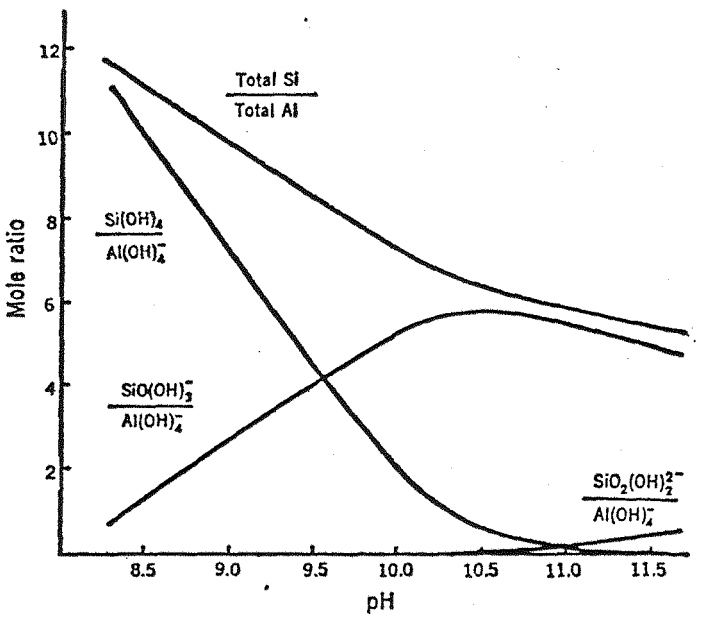

Fig.5-10.Mole ratio of total silica to total alumina and of various silica species in solution to the alumina species in solution,as a function of pH(after Mariner and Surdam,1970).

good agreement with those of the oceanic palys (80·38% - 88·61%). In the continental paly, the sums vary between 76·65% and 84·18%, and the average is 79·30% (Table 5-10).

The structural formula was calculated on the basis of 21 oxygens per formula unit of the dehydrated clay and complete tetrahedral sites occupancy (Table 5-11). There is not enough excess charge in the interlayer to be balanced by deficiencies in both the tetrahedral and octahedral layers. This suggests that an important number of electrical charges are balanced either by H_3O^+ or the elements that are not accounted for. Weaver and Pollard (1973) pointed out that the H^+ content of the octahedral sheet is so speculative that it is impossible to make a reasonable calculation of the layer charge. Couture (1977a) determined the approximate composition of six samples of marine paly by X-ray diffraction. He suggested that deep-sea paly has approximately the composition $Mg_2Al_2Si_8O_{20}(OH)_2(OH_2)_4.4H_2O$, possibly with some iron in octahedral positions. The structure proposed by Bradley (1940) corresponds to the chemical formula $Mg_5Si_5O_{20}(OH)_2(OH_2)_4$. Weaver and Pollard's results (1973) indicate that only four of the five octahedral sites are occupied. Al^{3+} fills from 1·13 to 2·34 of these five sites or between 28% and 59% of the four occupied sites. $Al^{3+} + Fe^{3+}$ values range from 31% to 62%. Divalent cations, largely Mg^{2+}, occupy from 29% to 76% of the four occupied sites. Therefore, as an average, in the four occupied sites approximately half contain trivalent and half divalent cations.

In the present study, four of the five octahedral sites are occupied. Al^{3+} fills from 1·46 to 1·88 of the five octahedral sites, which is between 37% and 47% of the four occupied sites. $Al^{3+} + Fe^{3+}$ occupies from 58% to 71% of the four sites. Mg^{2+} occupies from 22% to 41%. Thus, as an average, the four occupied sites contain 32% Mg^{2+} and 65% $Al^{3+} + Fe^{3+}$. That is, they contain one-third divalent and two-thirds trivalent cations.

According to Couture (1977a), deep sea paly probably has Al/(Al+Fe+Mg) ratios of about 0·4-0·5, and Mg/(Al+Fe+Mg) ratios of 0·4 to 0·6. He could not determine the iron but allowed Fe/(Al+Fe+Mg) values up to 0·1%.

In the present study, paly shows Al/(Al+Fe+Mg) ratios of 0·37-0·51,

Mg/(Al+Fe+Mg) values of 0·22 - 0·42 and Fe/(Al+Fe+Mg) ratios of 0·21-0·31.

Weaver and Pollard (1973) observed that Mg^{2+} content of the octahedral sheet in paly is 2-4 times as abundant as in montmorillonite. In the present study, MLIS from the Ninetyeast Ridge and Madagascar Ridge (Sites 254 and 246) showed high MgO with Mg^{2+} contents in the octahedral sheet (MgO is between 7·71% and 10%, and Mg^{2+} in the octahedral positions is between 0·38 and 0·7). However, the rest of the mixed layers showed a moderate content of Mg^{2+} (MgO varies between 2·47% and 4·79% and Mg in the octahedral position is between 0·07 and 0·39). Therefore, these results showed that the Mg^{2+} content of the octahedral sheet of the present study paly is two to five times as abundant as in the mixed layer (not considering the mixed layer from the ridges). The Mg^{2+} content of the octahedral sheet of paly is between 0·41 and 0·82.

1. Composition of palygorskite-bearing sediments

Table 5-12 shows Mg/Al and MgO/SiO_2 ratios of paly-bearing sediments. Couture (1977b) observed that the montmorillonite and zeolite-rich samples had Mg/Al ratios of 0·26 and 0·34, whereas the most paly-rich samples had higher Mg/Al ratios of 0·34 and 0·40. This ratio was 0·25 in samples poor in paly. The results of Bowles et al. (1971) indicated that paly-rich sediments from seamounts and scarps in the Atlantic have Mg/Al ratios ranging from 0·21 to 0·48. Lomova (1975) reported Mg/Al ratio of 0·64 in paly-rich sediments of the Eastern Atlantic.

In the present study, sediments rich in paly showed Mg/Al ratios of 0·63 (Sample 215/9/2). Sediments from Site 221 showed Mg/Al ratios between 0·34 and 0·36, and the rest of the sediments, which contained a small amount of paly, showed Mg/Al ratios between 0·2 and 0·29. Thus, the Mg/Al and Fe/Al ratios of these sediments (Mg/Al = 0·2 to 0·63, and Fe/Al = 0·6 to 0·9) were in good agreement with ratios in paly (Mg/Al = 0·3 - 0·7 and Fe/Al = 0·7 - 0·9).

Bonatti et al. (1968) observed that the MgO/SiO_2 ratio in paly-bearing samples was between 2 and 3 times higher than in common smectite-bearing sediments, and thus concluded that it was probable that the formation of deep sea paly requires solutions with Mg activities in excess of those which were commonly able to produce smectites on or below the sea

floor. The present study paly-bearing sediments showed similar ratios to the MLIS-bearing sediments. However, sample 215/9/2, which contained the highest amount of paly, showed MgO/SiO_2 ratios two times higher than MLIS-bearing sediments. This ratio is in sympathy with Bonatti's view.

2. Conclusions

The present study palys showed Al content as abundant as that of Weaver et al. (1973), but higher Fe^{3+} and lower Mg^{2+}. The Mg^{2+} content of the octahedral sheet was two to five times as abundant as in MLIS. It also showed lower Fe/(Al+Fe+Mg) and Al/(Al+Fe+Mg) and higher Mg(Al+Fe+Mg) compared with MLIS.

Thus it is evident from the above observation that paly in comparison with MLIS of the present study requires an environment with higher Mg^{2+} activities. Bonatti et al. (1968) also believe that montmorillonite generally forms from volcanic glass on the ocean floor, and since MgO/SiO_2 ratio in paly is higher than in common smectite, a solution with Mg^{2+} activities in excess of those which are commonly able to produce smectites on or below the sea floor is required for the formation of paly.

In the case of the present study, sea water, hydrothermal solution and Mg-bearing minerals, in addition to volcanic glass, could provide the necessary Mg^{2+}. Most of the paly-bearing sediments occur below hiatuses or have slow sedimentation rates which indicate long periods of contact with sea water. Samples at Site 211 (cores 13 and 14) occur between two basalt horizons, which could indicate hydrothermal solution activity, and at Site 245 sediments with high sedimentation rate could obtain the necessary Mg from chlorite. Couture (1977a) believes that the association with hiatuses, which have resulted from bottom water current activity or slow sediment accumulation rates, suggest that extended contact with sea water may be helpful or even necessary for the formation of paly. He suggested that absorption of Mg was made possible by the stirring action of the bottom current.

In summary, MLIS with a low percentage of expandable layer is associated with paly or paly plus clinoptilolite, whereas MLIS with a high percentage of expandable layer is only associated with clinoptilolite. Therefore, it is possible that in the absence of MLIS of detrital origin, the authigenic MLIS would be the sink for Mg^{2+}, and thus no paly would form, but in the presence of MLIS of detrital origin, the Mg^{2+} released from

the alteration of volcanics and sea water reacts with MLIS (detrital) and paly results. On burial, where higher H_2SiO_4 is available as the result of biogenic silica dissolution, both MLIS(authigenic) and paly could transform to clinoptilolite. Therefore, on the basis of the above observation, the following reactions are suggested:

in the presence of MLIS(detrital)

Mg^{2+}(volcanic + sea water or hydrothermal solution or Mg-bearing minerals) + $ML_{(detrital)}$ $\longrightarrow$ paly

on burial (in the presence of high silica)

paly + silica (biogenic or volcanic) $\longrightarrow$ clinoptilolite

in the absence of MLIS (detrital)

Mg^{2+}-rich volcanic material transforms to authigenic MLIS.

On burial (in the presence of high silica)

$ML_{(authigenic)}$ + silica(biogenic or volcanic) $\longrightarrow$ clinoptilolite.

TABLE 5-2: Chemical Analysis of MLIS (L.O.I. = loss on ignition)

	212/17cc	212/18/1	212/18/2	212/23/5	212/27/1	212/27/5	212/35cc	213/11/5	239/16/3
SiO_2	46·96	49·57	56·02	50·09	50·09	44·41	52·09	47·24	56·14
TiO_2	0·38	0·21	0·35	0·21	0·89	0·32	0·64	0·25	0·17
Al_2O_3	15·76	14·49	13·98	10·97	18·77	15·41	18·21	14·12	15·84
Fe_2O_3	13·50	14·25	12·55	10·47	11·27	12·91	10·47	11·29	10·41
MgO	2·92	3·11	4·79	3·87	3·52	2·07	3·79	4·12	4·41
CaO	-	0·04	0·35	-	0·93	-	1·84	2·09	0·46
Na_2O								0·096	
K_2O	0·65	0·08	0·38	0·09	0·99	0·52	1·49	0·88	0·74
P_2O_5	0·36	0·08	0·19	-	0·10	-	0·20	1·69	0·05
L.O.I.	19·70	15·88	12·50	22·25	14·30	24·00	12·00	20·00	11·95

/contd.over

TABLE 5-2 contd.

	246/10/2	254/25/2	<0·08 254/26cc	0·2-0·08 254/26cc	254/27/3	254/28cc	256/8/4	257/5/2	257/4/3
SiO_2	53·92	41·35	43·90	44·13	45·31	45·85	56·67	53·35	54·22
TiO_2	0·52	3·05	2·90	2·32	1·40	1·55	0·25	0·21	0·26
Al_2O_3	14·29	12·03	16·75	17·25	14·49	15·00	16·87	16·08	16·70
Fe_2O_3	9·26	17·56	15·76	15·61	17·67	16·24	7·82	11·20	11·98
MgO	9·06	10·00	7·71	8·56	8·74	9·34	4·28	3·34	3·00
CaO	0·49	1·82	0·83	0·59	-	0·03	0·13	-	-
Na_2O	-	1·65	-	-	-	-	-	0·01	0·01
K_2O	0·85	0·73	0·21	-	-	-	0·89	1·07	1·21
P_2O_5	-	0·04	-		-	0·01	0·016	0·04	-
L.O.I.	11·61	12·60	11·95	11·95	12·30	13·10	13·00	13·80	12·60

/contd.over

TABLE 5-2 contd.

	258/15/1	258/17/2	258/22/4
SiO_2	58·61	54·40	56·47
TiO_2	0·10	0·15	0·13
Al_2O_3	18·33	17·41	20·22
Fe_2O_3	4·95	6·84	5·15
MgO	3·36	2·40	2·47
CaO	0·18	0·46	-
Na_2O	-	-	-
K_2O	-	-	0·07
P_2O_5	0·04	0·01	-
L.O.I.	14·30	18·33	15·20

TABLE 5-4: The Structural Formula on the Basis of 11 Oxygens

	212 /17cc	212/18/1	212/18/2	212/23/5	212/27/1	212/27/5	212/35cc	213/11/5
Octahedral								
Al	1.08	1.04	1.03	1.04	1.19	1.14	1.15	0.98
Fe^{3+}	0.79	0.81	0.65	0.64	0.61	0.79	0.55	0.66
Mg	0.13	0.15	0.32	0.32	0.20	0.07	0.30	0.36
Tetrahedral								
Si	3.64	3.75	3.89	4.00	3.60	3.65	3.65	3.68
Al	0.36	0.25	0.11	-	0.40	0.35	0.35	0.32
Interlayer								
Mg	0.21	0.20	0.17	0.16	0.17	0.18	0.12	0.12
Ca	-	0.003	0.025	-	0.08	-	0.14	0.17
Na	-	-	-	-	-	-	-	0.09
K	0.06	0.004	0.034	0.01	0.10	0.05	0.13	0.01
Tetrahedral charge	0.36	0.25	0.11	-	0.40	0.35	0.35	0.32
Octahedral charge	0.13	0.15	0.32	0.32	0.20	0.07	0.30	0.36
Total charge	0.49	0.40	0.43	0.32	0.60	0.42	0.65	0.68
C.E.C.(meq/100g)	64	52	59	44	80	55	87	90
%E	45	71	58	69	57	45	76	52
Al for Si substitution in tetrahedral	9	6.25	3.25	-	10	8.75	8.75	8

/contd.over

TABLE 5-4 contd.

	239/16/3	246/10/2	<2u 254/25/2	<0·08 254/26cc	0·2-0·08 254/26cc	254/27/3	254/28cc	256/8/4
Octahedral								
Al	1·16	0·92	0·28	0·74	0·73	0·59	0·64	1·29
Fe^{3+}	0·54	0·48	1·02	0·88	0·86	0·98	0·89	0·41
Mg	0·30	0·60	1.05	0·57	0·61	0·64	0·70	0·30
Tetrahedral								
Si	3·86	3·75	3·19	3·27	3·24	3·34	3·35	3·92
Al	0·14	0·25	0·81	0·73	0·76	0·66	0·65	0·08
Interlayer								
Mg	0·15	0·34	0·10	0·29	0·33	0·33	0·33	0·14
Ca	0·04	0·04	0·15	0·067	0·05	-	0·002	0·01
Na	-	-	0·25	-	-	-	-	-
K	0·07	0·08	0·07	0·018	-	-	-	0·08
Tetrahedral charge	0·14	0·25	0·81	0·73	0·76	0·66	0·65	0·08
Octahedral charge	0·30	0·60	0·00	0·00	0·00	0·00	0·00	0·30
Total charge	0·44	0·85	0·82	0·73	0·76	0·66	0·66	0·38
C.E.C. (meq/100g)	59	114	195	145	153	141	146	50
%E	69	67	85	81	81	84	70	68
Al for Si substitution in tetrahedral	3·50	6·25	20·25	19	18·25	16·50	16·25	2·00

/contd.over

TABLE 5-4 contd.

	257/5/2	257/4/3	258/15/1	258/17/2	258/22/4
Octahedral					
Al	1·19	1·19	1·45	1·43	1·59
Fe^{3+}	0·60	0·63	0·29	0·36	0·27
Mg	0·21	0·18	0·26	0·21	0·14
Tetrahedral					
Si	3·83	3·80	3·98	3·98	3·93
Al	0·17	0·20	0·02	0·02	0·07
Interlayer					
Mg	0·15	0·13	0·13	0·06	0·11
Ca	-	-	0·01	0·04	-
Na	0·002	0·001	-	0·03	-
K	0·099	0·11	-	-	0·006
Tetrahedral charge	0·17	0·20	0·02	0·02	0·07
Octahedral charge	0·21	0·18	0·26	0·21	0·14
Total charge	0·38	0·38	0·28	0·23	0·21
C.E.C. ($^{meq}/100g$)	51	50	38	31	29
%E	67	72	81	72	83
Al for Si substitution in tetrahedral	4·25	5·00	0·50	0·50	1·75

TABLE 5-5: Three recognised Groups of MLIS (in %)

	%E	Al_{oct}	Fe^{3+}_{oct}	Mg_{oct}
Group 1	69-83	52-80	14-41	7-16
Group 2	45-58	49-60	31-40	4-18
Group 3	67-76	46-58	24-28	15-30

TABLE 5-6a: Chemical Analyses of Clinoptilolite

	SiO_2	Al_2O_3	MgO	CaO	Na_2O	K_2O
212/18/2	64·87	11·56	0·78	1·67	1·14	3·40
212/37cc	66·74	11·78	0·29	1·81	2·71	2·79
212/38/1	64·15	11·41	1·17	1·92	0·86	2·57
216/34/1	60·57	11·56	-	5·13	0·43	1·00
236/19/2	61·87	10·45	0·78	2·06	0·71	2·09
246/10/2	61·15	12·30	-	2·30	0·86	5·78
248/12/3	66·93	12·13	-	1·63	0·97	6·70
250/22/3	56·70	10·08	2·34	1·75	-	0·31
256/6/3	68·93	11·28	0·59	1·50	1·14	4·13
256/7cc	68·93	11·84	0·49	1·46	1·17	4·26
256/8/4	65·86	11·76	0·49	1·83	0·99	4·85
257/4/3	66·59	10·30	1·56	1·54	0·86	1·27
257/5/2	67·44	11·87	1·27	2·37	0·71	2·82
258/14/1	68·86	10·02	0·49	1·63	1·14	3·34
258/15/1	60·34	9·78	1·27	1·87	0·86	1·32
258/17/2	67·38	12·02	0·20	5·25	0·57	0·85
258/25cc	63·25	11·74	-	3·00	0·43	4·20

TABLE 5-6b: Chemical Analyses of Phillipsites

	SiO_2	Al_2O_3	MgO	CaO	Na_2O	K_2O
213/8/5	46·82	14·41	0·29	0·99	5·14	2·77
213/9/4	47·12	15·54	-	2·04	4·14	4·78
213/9cc	49·00	15·91	0·20	3·25	1·28	5·97
213/11/2	48·16	15·02	-	4·09	0·86	4·95
213/11/5	49·46	15·60	0·49	2·31	2·99	4·68
213/12/5	51·84	16·69	0·29	4·39	-	5·99
213/13/2	52·56	17·28	0·59	3·58	1·99	5·05
246/10/2	48·88	15·21	0·68	1·21	4·00	4·23

TABLE 5-7a: Structural Formulae of Clinoptilolites on the Basis of 72 Oxygens

	Si	Al	Mg	Ca	Na	K	Si/Al	Eb*
212/18/2	29·82	6·27	0·53	0·83	1·10	1·99	4·76	7·34
212/37cc	29·81	6·18	0·19	0·81	2·36	1·61	4·82	3·40
212/38/1	29·85	6·24	0·84	0·95	0·78	1·53	4·78	5·61
236/19/2	30·18	6·00	0·57	1·08	0·67	1·30	5·03	12·00
246/10/2	29·16	6·88	-	1·2	0·80	3·52	4·24	2·33
248/12/3	29·69	6·34	-	0·77	0·83	3·78	4·68	2·99
250/22/3	29·86	6·25	1·83	0·98	-	0·21	4·78	5·83
256/6/3	30·24	5·83	0·40	0·71	0·98	2·32	5·19	5·32
256/7cc	29·98	6·07	0·31	0·68	1·54	2·35	4·93	3·29
256/8/4	29·78	6·27	0·33	0·90	0·87	2·80	4·75	2·23
257/4/3	30·59	5·52	1·07	0·74	0·76	0·74	5·54	7·25
259/5/2	29·84	6·19	0·82	1·12	0·61	1·59	4·82	1·78
258/14/1	30·80	5·28	0·32	0·78	0·99	1·91	5·83	3·41
258/15/1	30·26	5·78	0·95	0·99	0·84	0·84	5·24	3·81
258/17/2	29·78	6·25	0·13	2·49	0·48	0·48	4·76	0·80
258/25cc	29·59	6·48	-	1·49	0·39	2·54	4·57	8·70
216/34/1	29·44	6·63	-	2·66	0·41	0·61	4·44	4·3

*Eb $= [(Al - \Sigma cat) / Al] \times 100$

$\Sigma cat = [2 (Ca + Mg) + K + Na]$

TABLE 5-7b: Structural Formulae of Phillipsites on the Basis of 32 Oxygens

	Si	Al	Mg	Ca	Na	K	Si/Al	Eb
213/8/5	11·76	4·23	0·11	0·27	2·51	0·90	2·78	1·42
213/9/4	11·48	4·42	-	0·53	1·97	1·49	2·59	-2·26
213/9cc	11·62	4·42	0·07	0·83	0·59	1·81	2·62	4·98
213/11/2	11·76	4·25	-	1·07	0·41	1·54	2·77	3·76
213/11/5	11·59	4·33	0·17	0·58	1·37	1·39	2·68	1·62
213/12/5	11·66	4·42	0·09	1·05	-	1·72	2·63	9·54
213/13/2	11·56	4·52	0·20	0·85	0·80	1·42	2·56	4·42
246/10/2	11·70	4·30	0·24	0·31	1·90	1·30	2·72	0·0

TABLE 5-8: A Comparison of the Iron Impurities in Zeolites measured by Different Methods.

(The asterisk sign (*) represents the samples containing clinoptilolite, whereas the plus sign (+) represents those with phillipsite. β-probe + EDX indicate measurements done by either β-probe or EDX. Fe impurities of clinoptilolite were measured by β-probe, whereas those of phillipsite were measured by EDX.)

	Atomic Absorption	β-probe + EDX	
256/7cc	0·32	0·20	*
257/5/2	0·58	0·40	*
213/11/2	0·71	0·74	+
213/11/5	1·33	1·09	+

TABLE 5-9: Chemical Composition of Present Study Palygorskite

	SiO_2	TiO_2	Al_2O_3	Fe_2O_3	MgO	CaO	Na_2O	K_2O	Total
211/14/1	53·47	0·78	15·35	9·29	4·58	-		3·44	86·91
212/37cc	57·19	0·80	12·00	8·50	5·09	1·28		3·70	88·56
215/9/2	55·38	0·82	13·80	8·39	8·34	0·67		2·06	89·46
221/15/2	47·66	0·26	14·90	9·43	4·79	0·36		1·16	78·56
245/5/3	50·81	0·91	16·30	11·07	4·20	0·95		2·82	87·06
248/10/2	49·82	0·52	14·50	10·09	6·53	0·27		2·35	84·08
248/14/1	52·85	0·63	17·58	9·64	4·08	0·48		3·81	89·07
250/22/3	58·87	0·58	13·00	8·00	5·52	0·72	0·12	2·15	88·96
256/7cc	58·83	0·67	13·50	8·65	4·94	0·38		2·13	89·10

TABLE 5-10: Chemical Composition of Palygorskite presented by Some Workers

	SiO_2	TiO_2	Al_2O_3	Fe_2O_3	MgO	CaO	Na_2O	K_2O	Total
1	61•60		6•82	0•87	14•22	0•67	-	-	84•18
2	54•71		13•48	2•10	5•44	2•79	-	-	78•52
3	52 35		15•44	2•12	6•60	0•14	-	-	76•65
4	50•65	0•20	11•97	7•45	7•75	0•14	-	-	78•82
5	55•12		15•70	1•60	6•14	0•41	-	-	80•36
6	57•01	0•41	10•67	3•80	4•56	0•89	-	-	77•24
7	70•47	0•69	6•84	5•65	15•90	0•22	-	0•004	99•77+
8	50•16	0•63	17•76	7•16	4•97	0•85	4•29*	2•32	88•14
9	51•95	0•72	18•70	8•81	3•12	0•71	2•36*	2•24	88•61
10	49•30	-	13•96	4•40	8•87	0•77	2•33	0•75	80•38

1. Heystek and Schmidt (1954): Dorboon, South Africa.
2. Caillere (1934): Taodoni, Algeria.
3. Stephen (1954): Bakkastters, Shetland.
4. Ovcharenko (1964): Cherkassy, Ukraine, U.S.S.R.
5. Huggins et al. (1962): Volhynia, U.S.S.R.
6. Elprince, A.M. et al. (1979): Saudi Arabia.
7. Singer et al. (1974): Australia.

8 and 9. Bowles et al. (1971): Atlantic Ocean (small amounts of halite and quartz impurities are present)

10. Lomova (1975): Atlantic Ocean.

* Halite impurity.

\+ L.O.I. = 13•18

TABLE 5-11: Structural Formula for Palygorskite on the 10·5 oxygen basis.
(oct = octahedral; tet = tetrahedral; Int = Interlayer)

	Al_{oct}	Fe_{oct}	Mg_{oct}	Si_{tet}	Al_{tet}	Ca_{Int}	Na_{Int}	K_{Int}	Al/(Al+Mg+Fe)	Fe/(Al+Fe+Mg)	Mg/(Mg+Al+Fe)
211/14/1	0·90	0·48	0·47	3·66	0·34			0·26	0·49	0·26	0·25
212/37cc	0·79	0·43	0·51	3·84	0·16	0·09		0·30	0·46	0·25	0·29
215/9/2	0·73	0·42	0·81	3·66	0·34	0·05		0·17	0·37	0·21	0·42
221/15/2	0·87	0·53	0·53	3·56	0·44	0·03		0·12	0·45	0·27	0·27
245/5/3	0·83	0·58	0·44	3·50	0·50	0·07		0·25	0·45	0·31	0·24
248/10/2	0·74	0·54	0·69	3·53	0·47	0·02		0·21	0·38	0·27	0·35
248/14/1	0·94	0·50	0·41	3·54	0·46	0·04		0·20	0·51	0·27	0·22
250/22/3	0·85	0·40	0·54	3·85	0·15	0·10	0·02	0·10	0·47	0·22	0·30
256/7cc	0·89	0·43	0·48	3·85	0·15	0·03		0·17	0·49	0·24	0·27

TABLE 5-12: Composition of Paly-bearing Sediments

MgO/SiO_2 (in Paly-bearing sediments)

1	2-3 times higher than in MLIS-bearing sediments (Bonatti et al.,1968).
2	2 times higher than in MLIS-bearing sediments (Present study Paly-rich sample,215/9/2).
3	The same as that of MLIS-bearing sediments (Present study Paly-poor sediments)

Mg/Al (in Paly-bearing sediments)

1.	Deep sea paly (Couture, 1977 b)	0·34 - 0·40
2	Site 12 (Anonymous, 1970, quoted by Couture, 1977a)	0·50
3	Florida (Couture, 1977a)	1·30 - 1·45
4	Atlantic Ocean (Lomova, 1975)	0·64
5	Echo seamount (Bowles et al., 1971)	0·21 - 0·48
6	Barracuda Escapement (Bonatti et al., 1968)	0·33 - 0·36
7	Present study Paly-rich sediments (Sample 215/9/2)	0·63
8	Present study Paly-bearing sediments (Site 221)	0·34 - 0·36
9	Present study Paly-poor sediment	0·20 - 0·29

CHAPTER VI

A THERMODYNAMIC MODEL FOR PREDICTING THE FORMATION OF ZEOLITES, MLIS AND PALYGORSKITE

A. Introduction

In this chapter an attempt is made to assess the stability and inter-relationship of naturally occurring mineral assemblages. Equilibrium diagrams provide guidelines for the interpretation of natural processes, and also commonly reveal limiting conditions for the formation of minerals.

Thermodynamic information enables us to calculate the equilibrium composition of a solution, and to find the maximum useful work done or minimum energy needed for a process (Stumm et al., 1981).

In the present study, it is assumed that the reactions occur in an aqueous medium. The composition of the reactants and products (the pure minerals) were determined by EDX and β-probe, and are listed in Tables 5-2, 6a and 6b). The chemistry of sea water and interstitial waters is listed in Table 6-1. Relative standard free energies of formation ($\triangle G_f^\circ$) selected from the literature are summarized in Table 6-2. According to Rai and Lindsay (1975), since a change of a few Kcal in $\triangle G_f^\circ$ may change the predicted stability drastically, it is imperative to have accurate $\triangle G_f^\circ$ values.

1) The calculation of Gibbs free energy for MLIS

The $\triangle G_f^\circ$ for MLIS was calculated independently using the method suggested by Nriagu (1975), since it will be required later in the calculation of the free energies of the formation of paly and clinoptilolite. In this method Nriagu (1975) assumes that clay minerals are formed by the combination of silicon hydroxides with metal hydroxides. The change in free energy during the polymerization of hydroxides to form silicates plus water is generally small and has been approximated by a one parameter correction term (Nriagu, 1975). Nriagu has illustrated the mechanics of the procedure by considering the formation reaction of a typical montmorillonite as follows:

$$n_1\,NaOH = n_2\,KOH + n_3\,Ca(OH)_2 + n_4\,Mg(OH)_2 + n_5\,Fe(OH)_3$$
$$+ n_6\,Al(OH)_3 + n_7\,Si(OH)_4 \longrightarrow$$
$$Na_{n1}K_{n2}\,Ca_{n3}\,Al_{n6}\,Fe_{n5}\,Mg_{n4}\,Si_{n7}\,O_{10}\,(OH)_2 + (n_i\,Z_{i-12})H_2O \qquad (1)$$

where n_1 is the reaction coefficient of the i-th hydroxide and Z_1 is the change on the i-th cation (including Si). Usually n_1 corresponds to the amount of the i-th cation (or silicon) in the formula unit for the clay mineral. The free energy of formation for the clay mineral whose formation is described by the above reaction is calculated by the expression:

$$\Delta G_f^{\circ} \text{ (montmorillonite)} = \sum n_1 \Delta G_f^{\circ}(ri) - (\sum n_i Z_{i-12})\ \Delta G_f^{\circ}(H_2O) - Q$$

where $\Delta G_f^{\circ}(ri)$ is the free energy of formation of the i-th hydroxide component and Q is an empirical correction factor defined as:

$$Q = S\ (n_i Z_{i-12})$$

i.e. Q is expressed as a function of the number of moles of water released during the reaction. The expression for Q is empirical. According to equation (1), the hydroxides polymerize to form silicate + water, and Q may be envisaged as the sum of the dehydration energies of the water molecules split out. In other words, the dehydration of the hydroxides during the formation of silicates may be analogous to the splitting out of water during the formation of a polymer. Nriagu found during the study that the best fit between the experimental and predicted data was obtained when S was assigned a constant value of 0·39. Thus Q = 0·39 x (the number of moles of water liberated).

In the present study, the method described above, with some modification, was used, since it was decided to use mineral formula in a dehydrated state for thermodynamic calculation. The modification can be illustrated by considering Nriagu's montmorillonite reaction as follows:

$$n_1\ NaOH + n_2\ KOH + n_3\ Ca(OH)_2 + n_4\ Mg(OH)_2 + n_5\ Fe(OH)_3 +$$
$$n_6\ Al(OH)_3 + n_7\ Si(OH)_4 \longrightarrow Na_{n_1}\ K_{n_2}\ Ca_{n_3}\ Al_{n_6}\ Fe_{n_5}\ Mg_{n_4}$$
$$Si_{n_7}O_{11} + (n_i Z_{i-13})\ H_2O$$

therefore Q will be

$$Q = S\ (n_i\ Z_{i-13})$$

and the free energy is calculated as follows:

$$\Delta G_f^{\circ}(\text{MLIS}) = \Sigma n_i \Delta G_f^{\circ}(ri) - (\Sigma n_i Z_{i-13}) \Delta G_f^{\circ}(H_2O) - Q$$

The calculated free energies are represented in Table 6-3 . They are compared with the reported ΔG_f° values for pure smectite and MLIS in Table 6-4. As can be seen, the present study MLIS is more positive than the reported values, which could be the result of

a) calculated free energy on the basis of dehydrated structural formula;

b) the reported values by Tardy & Garrels (1974) were for pure smectite, whereas the present study minerals are MLIS with various %E and crystallinity. Crystallinity and %E could control the chemistry, and thus the free energy. According to Tardy and Garrels (1974) 'poorly crystallized silicates may have ΔG_f° values several kilocalories more positive than well crystallized ones'.

2) H_2O content of zeolites

Breger et al. (1970) have studied the water content in heulandite and clinoptilolite by infra-red spectrophotometer and found that there is not correspondence between the dehydration data obtained for heulandite and clinoptilolite in their work and that based on published DTA and TGA analysis. They believe that a critical factor is the heating rate. Thus, the slow loss of loosely held water followed by the incomplete loss of tightly bound water would tend to obscure both thermal and weight changes in the minerals, unless proper analytical parameters were chosen. Therefore, failure to do so has led to the variety of published DTA and TGA curves, which contribute little or nothing to an understanding of how water is retained by heulandite and clinoptilolite.

It is not clear in zeolites which part of the total water content is significant to the structure. According to Ogawa (1967) and Breger et al. (1970), removal of even the loosely bound water results in a structural contraction. Most of the more loosely bound water in a heulandite studied by Merkle and Slaughter (1968) was found to occupy specific sites in the structure. Boles (1972) believes that both loosely and more tightly bound water is important in these minerals since the naturally occurring specimens show that water contents consistently vary between 19 and 26 H_2O molecules per 72 oxygen unit cells.

Breger et al. (1970) suggested that the correct amount of tightly bound water in a heulandite and a clinoptilolite, which they studied,

would correspond to 8-9 H_2O molecules per 72 oxygen unit cell and this water in heulandite-group zeolites is more firmly held to Ca^{2+} ions than to Na^+ or K^+ ions. Work by Merkle and Slaughter (1968) demonstrated that 5 H_2O molecules are co-ordinated about Ca^{2+} ions in heulandite. Boles (1972) believes that since clinoptilolites are usually rich in Na^+ and K^+ ions and low in Ca^{2+} ions relative to heulandites, and as clinoptilolite usually contains less total water, Na^+ and K^+ may have fewer total number of water molecules co-ordinated about them than do Ca^{2+} ions.

In the present study, thermogravimetric analysis (TGA) was carried out on the purified clinoptilolite. No consistent result for H_2O content was obtained (the H_2O content varied between 6·5% and 9·7%).

Since the present study is concerned with the thermodynamic stability of zeolites in deep sea sediments, the free energy of the reaction was calculated for reactions involving hydrated and dehydrated minerals, so as to determine whether the H_2O content of the minerals has any effect on the free energy of the reaction. For this purpose, a reaction suggested by Cosgrove et al. (1979) was assessed as follows:

a) On a hydrated basis:

$$0{\cdot}7725\ \overset{\text{(smectite)}}{K_{0.66}\ Al_{4.66}\ Si_{7.34}\ O_{20}\ (OH)_4} + 8{\cdot}73\ H_4SiO_4 + 3{\cdot}09\ K^+ \longrightarrow$$

$$3{\cdot}09(H^+) + \overset{\text{(clinoptilolite)}}{K_{3.6}\ Al_{3.6}\ Si_{14.4}\ O_{36}\ .8{\cdot}8\ H_2O} + 8{\cdot}66\ H_2O + 3{\cdot}09\ H^+$$

where the equilibrium constant is:

$$\log K = -3.09 \log ([K^+]/[H^+]) - 8.73 \log [H_4SiO_4]$$

Using values for the concentration of K^+ and H_4SiO_4 in interstitial waters obtained from deep sea cores (represented in Table I in the paper by Cosgrove et al. (1979)

$$\log K = 13{\cdot}99$$

since

$$\Delta G_{reaction} = -1{\cdot}364 \log K \text{ (at } 25^{\circ}C \text{ and 1 atm)},$$

by substitution:

$$\Delta G_{reaction} = -19{\cdot}08 \text{ Kcal/mol.}$$

Further, by substituting the appropriate standard free energy values into the reaction, the free energy of formation of clinoptilolite on a hydrated basis (clinoptilolite + 8·8 H_2O) can be calculated:

$$\Delta G_f^{\circ}\text{clinoptilolite} = -4447{\cdot}00 \text{ Kcal/mol}$$

if 8·8 molecules H_2O content of clinoptilolite is subtracted, the ΔG_f°clinoptilolite on a dehydrated basis would be

$$\Delta G_f^{\circ}\text{clinoptilolite} - 8{\cdot}8\Delta G_f^{\circ}(H_2O) = -3948{\cdot}13 \text{ Kcal/mol.}$$

b) On a dehydrated basis

$$0{\cdot}7725\ K_{0.66}\ Al_{4.66}\ Si_{7.34}\ O_{22} + 3{\cdot}09\ K^{+} + 8{\cdot}73\ H_4SiO_4 \longrightarrow$$

$$K_{3.6}\ Al_{3.6}\ Si_{14.4}\ O_{36} + 15{\cdot}915\ H_2O + 3{\cdot}09\ H^{+}$$

where

$$\Delta G_R^{\circ} = -19{\cdot}08 \text{ Kcal/mol}$$

and

$$\Delta G_f^{\circ}\text{clinoptilolite} = -3934{\cdot}04 \text{ Kcal/mol.}$$

Thus, the free energies remain essentially the same. Therefore, it was decided not to involve the water content of the minerals in the calculations, since it is difficult to assign a particular amount of water to zeolites and also, the water has virtually no effect on the free energy calculations.

3) Method of calculation of free energy of reaction (ΔG_R°)

An equation is written for an equilibrium reaction between two minerals. Balancing of the equation is started by first conserving aluminium, on the assumption that alumina is not an important variable in naturally occurring reactions (Hess, 1966). Then, K^{+}, Na^{+}, H^{+}, H_4SiO_4 and/or H_2O are added in appropriate amounts to satisfy electrical neutrality and to conserve the remaining elements. The standard free energy change of the reaction (ΔG_R°) can then be calculated.

ΔG_R° is the sum of the free energies of formation of the products in their standard states, minus the free energies of formation of the

reactants in their standard states, that is:

$$\Delta G_R^\circ = \Sigma \Delta G_f^\circ \text{ products} - \Sigma \Delta G_f^\circ \text{ reactants.}$$

In turn, the standard free energy change of reaction is related to the equilibrium constant (K°) by

$$\Delta G_R^\circ = -R\ T\ \ln\ K^\circ$$

where R is the gas constant (0·001987 Kcal/deg per mol) and T is the absolute temperature. At 25°C, T = 298·15, the above equation can be written as follows:

$$\Delta G_R^\circ = -1{\cdot}364\ \log\ K.$$

By definition, an equilibrium constant is equal to the products of the activities of the products raised to the power of their numerical coefficients divided by the product of the activities of the reactants raised to the power of their numerical coefficients. The log of the equilibrium constant is taken, and the activities can be arranged into terms of log alkali/H^+, log alkali-earths/H^+, and log H_4SiO_4. These three units are the parameters that characterise an aqueous environment in this system, and are used to describe the phase equilibria (Hess, 1966).

At 25°C and 1 atmosphere, the activities of pure solids are equal to one, and aqueous solutions if very dilute may also be taken as one (Hess, 1966). The ionic strengths of most natural budies of water are less than 1·25, and correspondingly the activity coefficient of H_2O is greater than 0·95 (Garrels, 1960). The activity of water may therefore be considered to be equal to one. With respect to the dissolved ions, the assumption is made that natural aqueous systems are so dilute that molality is equivalent to the activity (Hess, 1966).

B. Mineral Stabilities

1) The stability of clinoptilolite

Clinoptilolite formation and stability can be discussed in the two following ways:

a) clinoptilolite formation via the reaction of MLIS with biogenic silica and/or silicic volcanic glass.

As previously mentioned, clinoptilolite was found commonly associated with authigenic MLIS, opal and opal-CT. It occurred in the pores and cavities, and showed negative correlation with MLIS and B (biogenic silica, opal-CT, volcanic glass and minor elements). This evidence suggests that clinoptilolite could form at the expense of MLIS. Therefore a reaction can be set up as follows:

$$\underset{\text{(MLIS)}}{1{\cdot}025\ K_{0.132}\ Ca_{0.06}\ Mg_{0.7}\ Fe_{0.88}\ Al_{2.916}\ Si_{7.74}\ O_{22}} + 7{\cdot}07\ H_4SiO_4 + 0{\cdot}599\ Ca^{2+} + 0{\cdot}665\ K^{+} + 0{\cdot}37\ Na^{+} \longrightarrow$$

$$\underset{\text{(clinoptilolite)}}{Na_{0.37}\ K_{0.80}\ Ca_{0.66}\ Mg_{0.27}\ Al_{2.99}\ Si_{15.00}\ O_{36}} + 0{\cdot}9\ Fe(OH)_3 + 0{\cdot}448\ Mg^{2+} + 12{\cdot}13\ H_2O + 1{\cdot}32\ H^{+} \qquad (1)$$

using the average formulae for both clinoptilolite and MLIS from samples which contain only clinoptilolite and MLIS. The resulting $Fe(OH)_3$ (perhaps as mineral oxy-hydroxide) could occur as inclusions in clinoptilolite crystals, as observed by A.A and SEM, whereas the Mg^{2+} is probably involved in opal-CT formation. Kastner et al. (1977) demonstrated from hydrothermal experiments that a magnesium hydroxide compound (MHC) serves as a nucleus for opal-CT crystallization at all temperatures.

The equilibrium constant for reaction (1) is related to the products and reactants in the following manner:

$$K = \frac{[H^+]^{1{\cdot}32}\ [Mg^{2+}]^{0{\cdot}448}\ [H_2O]^{12{\cdot}13}\ [Fe(OH)_3]^{0{\cdot}9}\ [\text{clinoptilolite}]}{[K^+]^{0{\cdot}665}\ [Ca^{+2}]^{0{\cdot}599}\ [Na^+]^{0{\cdot}37}\ [H_4SiO_4]^{7{\cdot}07}\ [\text{MLIS}]^{1{\cdot}025}} \qquad (1)$$

When the activities of pure compounds are at unity (by convention), equation (1) becomes:

$$K = \frac{[H^+]^{1{\cdot}32}\ [Mg^{2+}]^{0{\cdot}448}}{[K^+]^{0{\cdot}665}[Ca^{2+}]^{0{\cdot}599}\ [Na^+]^{0{\cdot}37}\ [H_4SiO_4]^{7{\cdot}07}} \qquad (2)$$

The log of Equation (2) is taken:

$$\log K = 1{\cdot}32 \log [H^+] + 0{\cdot}448 \log [Mg^{2+}] - 0{\cdot}665 \log [K^+] - 0{\cdot}599 \log [Ca^{2+}] - 0{\cdot}37 \log [Na^+] - 7{\cdot}07 \log [H_4SiO_4] \qquad (3)$$

and log K is calculated using the data for interstitial water in Table (6-1):

$$\log K = 1.32\ (-7.05) + 0.448\ (-1.62) - 0.37\ (-0.353) - 0.665\ (-2.173) - 0.599\ (-1.67) - 7.07\ (-3.325) \quad (4)$$

and thus,

$$\log K = 16.05$$

By substituting the value of K back into Equation (3), the rearrangement is as follows:

$$16.05 = 1.32 \log[H^+] + 0.448 \log[Mg^{2+}] - 0.665 \log[K^+] - 0.599 \log[Ca^{2+}] - 0.37 \log[Na^+] - 7.07 \log[H_4SiO_4] \quad (5)$$

The regression equation would then be:

$$\log \left(\frac{[K^+]^{0.665}\ [Ca^{2+}]^{0.599}\ [Na^+]^{0.37}}{[H^+]^{1.32}\ [Mg^{2+}]^{0.448}} \right) = -16.05 - 7.07 \log [H_4SiO_4]$$

The above equation is presented as a linear regression in Figure 6-1. The linear regression shows the stability-field boundary between clinoptilolite and MLIS in terms of silica activity against alkali, alkali-earths activity and pH. The slope of the line is -7·07, and the intercept is -16·05.

Figure 6-1 suggests that clinoptilolite is favoured by high activity of H_4SiO_4 compared with MLIS, the slope,being high, indicating that the other ions have limited influence. Sea water and interstitial water are also plotted on the diagram. As expected, the regression line passes through the area of the interstitial water, since activities in interstitial water were used in the calculation of log K. Points representing interstitial water above or to the right of the line indicate that interstitial water is supersaturated with respect to clinoptilolite, and this mineral can precipitate. On the other hand, points below or to the left of the line indicate the under saturation of interstitial water with respect to clinoptilolite, and thus this mineral would dissolve (as can be seen, the point representing sea water falls into the MLIS field, which suggests that MLIS is the stable phase in sea water). In

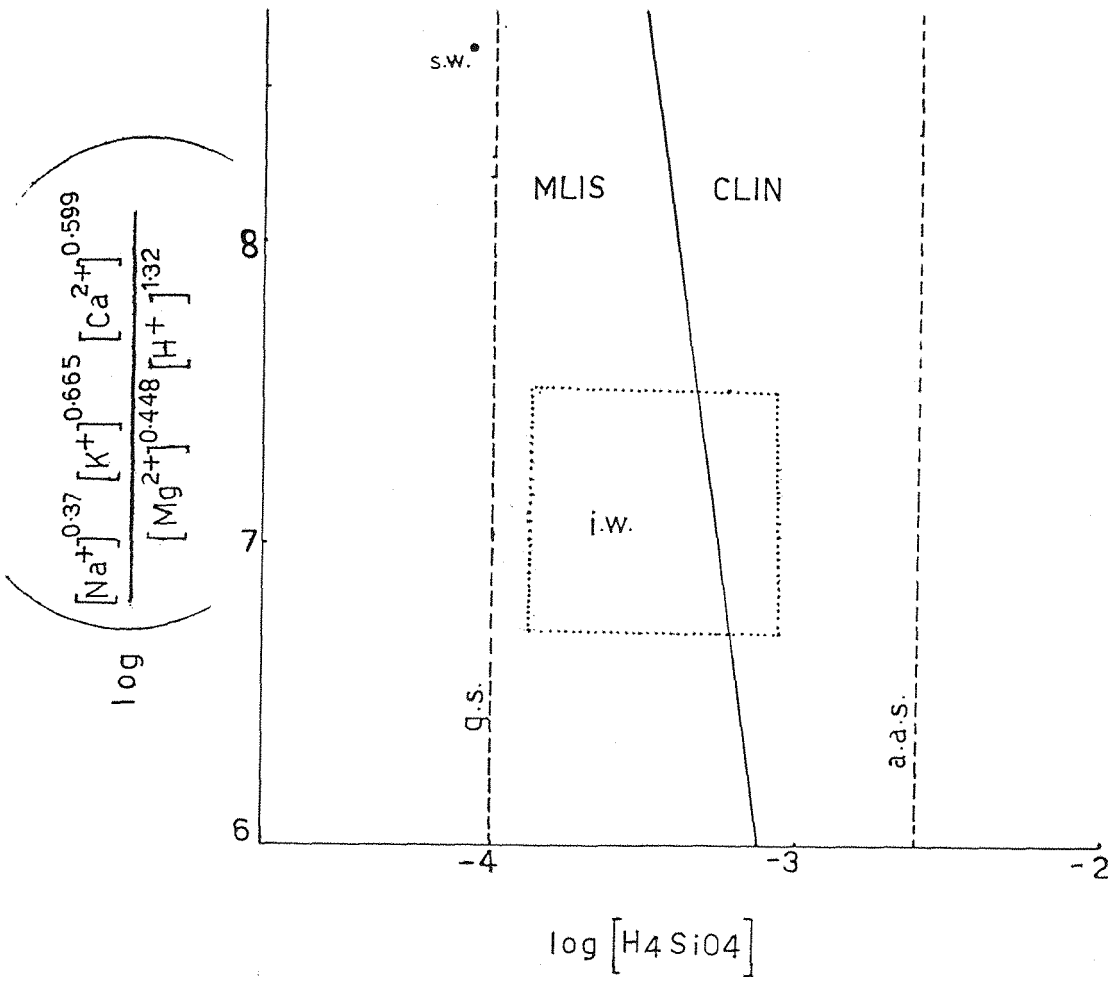

Fig.6-1.Stability fields for MLIS and CLIN.
Key:q.s.=quartz saturation;a.s.s=amorphous silica saturation;s.w.=average sea water; i.w.=interstitial waters(maximum field defined by dotted-line boundary).

order to determine whether reaction (1) is favoured towards the right or left (i.e. whether clinoptolite is the stable phase or MLIS), the free energy of reaction (ΔG_R^o) is calculated as follows:

$$\Delta G_R^o = -1{\cdot}364 \log K \quad (\text{at } 25^oC \text{ and } 1 \text{ atm})$$

by substitution:

$$\Delta G_R^o = -1{\cdot}364\ (16{\cdot}05)$$

and thus,

$$\Delta G_R^o = -21{\cdot}89 \text{ Kcal/mol.}$$

Both the negative ΔG_R^o and the positive log K indicate that reaction (1) is favoured towards the right and that clinoptilolite could form diagenetically as the result of the reaction of MLIS with interstitial water rich in H_4SiO_4, Ca^{2+}, Na^+ and K^+ at low temperatures.

According to many workers (e.g. Krauskopf, 1979; Wood et al., 1976; Stumm et al., 1981) free energy changes can be used to determine accurately how far a given reaction mixture is from equilibrium;in other words, whether the substances will react, and how far the reaction will go. The rules are:

If $\Delta G_R^o < 0$, the reaction will take place spontaneously (although the rate may be slow, so that no reaction is apparent).

If $\Delta G_R^o > 0$, the reaction cannot take place unless energy is supplied from an external source.

If $\Delta G_R^o = 0$, the reaction mixture is at equilibrium.

Krauskopf (1979) suggested a reaction is fairly close to equilibrium as long as ΔG_R^o is less than about 10 Kcal. Therefore, clinoptilolite is the stable mineral phase,compared with MLIS, in conditions of high $[H_4SiO_4]$, $[Na^+]$, $[K^+]$ and $[Ca^{2+}]$.

A similar type of reaction was also suggested by Cosgrove and Papavasiliou (1979). They used the idealised formulae of Boles (1972) and Helgeson et al. (1969) for clinoptilolite and MLIS respectively, and suggested that zeolites could have formed diagenetically by the reaction of smectites with interstitial water rich in H_4SiO_4, Na^+, K^+ at low temperature, which agrees well with the findings of the present study.

As an extension of this approach, the calculation of ΔG_f° for clinoptilolite can be achieved as follows:

$$\Delta G_R^\circ = \Delta G_f^\circ{}_{product} - \Delta G_f^\circ{}_{reactant}$$

Using the standard free energies of formation given in Table 6-2, it follows that:

$$\Delta G_f^\circ{}_{product} = 0{\cdot}448\ (-108{\cdot}8) + 0{\cdot}9\ (-166{\cdot}5) + 12{\cdot}13\ (-56{\cdot}69) + \Delta G_f^\circ{}_{clinoptilolite}$$

$$\Delta G_f^\circ{}_{product} = -886{\cdot}24 + \Delta G_f^\circ{}_{clinoptilolite}$$

$$\Delta G_f^\circ{}_{reactant} = 0{\cdot}37\ (-57{\cdot}279) + 0{\cdot}665\ (-67{\cdot}3) + 0{\cdot}599\ (-132{\cdot}3) + 7{\cdot}07\ (-318{\cdot}6) + 1{\cdot}025\ (-2342{\cdot}71)$$

$$\Delta G_f^\circ{}_{reactant} = -4798{\cdot}98$$

and thus,

$$-21{\cdot}89 = -886{\cdot}24 + \Delta G_f^\circ{}_{clinoptilolite} - (-4798{\cdot}98)$$

$$\Delta G_f^\circ{}_{clinoptilolite} = -3934{\cdot}63 \text{ Kcal/mol.}$$

This value is slightly more positive than that of Cosgrove and Papavasiliou (1979). They calculated the free energy of formation of clinoptilolite on a hydrated basis. In order to be able to compare their ΔG_f° of clinoptilolite with that of the present study, their value was re-calculated on a dehydrated basis as follows:

$$\Delta G_f^\circ{}_{clinoptilolite} - 8{\cdot}8\ \Delta G_f^\circ{}_{(H_2O)} = -3948{\cdot}13 \text{ Kcal/mol}$$

The more positive value of the ΔG_f° of clinoptilolite in the present study is probably due to:

i) Cosgrove and Papavasiliou (1979) used the idealised formulae, which contain either Na^+ or K^+, whereas the present study deals with the naturally occurring minerals which contain Na^+, K^+, Ca^{2+} and Mg^{2+}.

ii) the standard free energies, which were used for Na^+, K^+, H_2O and H_4SiO_4, were different from those used by Cosgrove et al. (1979).

iii) The present study formulae are the result of the semi-quantitative analyses of the minerals (clinoptilolite, phillipsite) by EDX.

b) clinoptilolite formation via the reaction of phillipsite with biogenic silica and/or silicic volcanic glass.

Clinoptilolite, phillipsite and MLIS assemblage was present at Sites 246 (Sample 246/10/2) and 254 (Sample 254/25/2). No trend between phillipsite and the rest of the minerals was observed, since phillipsite was present only in one sample from each site. The absence of any relation between phillipsite and the rest of the minerals was the case everywhere (i.e. Sites 213 and 239). The presence of volcanic glass (basaltic and silicic) was confirmed by the bulk chemistry (Fe/Ti vs Al/(Al+Fe+Mn), Ti vs Al and Cr vs TiO_2) and SEM studies (Plates 3-13 and 3-14). High expandable mixed-layer IS at the above sites suggested their authigenic formation from volcanic glass. The direct formation of phillipsite from volcanic glass was also suggested, since no relation between phillipsite and MLIS was observed.

Clinoptilolite, which usually showed negative correlation with both total clay (Fig.3-7) and MLIS (Fig.3-16) did not show such correlations in the presence of phillipsite. Stonecipher (1976 and 1977) and Couture (1977b) suggested a possible transition of phillipsite to clinoptilolite during post-sedimentation alteration of the sediments, since they found phillipsite in younger sediments (younger than Pliocene) and clinoptilolite in older sediments (Eocene-Cretaceous). The present study zeolites also showed similar vertical stratification. Therefore, on the basis of the above observation, a phillipsite into clinoptilolite transformation is suggested, which can be tested thermodynamically as follows:

$$0{\cdot}80\ \overset{\text{(phillipsite)}}{Na_{1{\cdot}90}\ K_{1{\cdot}30}\ Ca_{0{\cdot}31}\ Mg_{0{\cdot}24}\ Al_{4{\cdot}3}\ Si_{11{\cdot}7}\ O_{32}} + 5{\cdot}22\ H_4SiO_4$$

$$0{\cdot}35\ Ca^{2+} + 0{\cdot}72\ K^{+} + 0{\cdot}08\ H^{+} \longrightarrow$$

$$\overset{\text{(clinoptilolite)}}{Na_{0{\cdot}40}\ K_{1{\cdot}76}\ Ca_{0{\cdot}60}\ Al_{3{\cdot}44}\ Si_{14{\cdot}58}\ O_{36}} + 0{\cdot}19\ Mg^{2+} + 1{\cdot}12\ Na^{+} + 10{\cdot}48\ H_2O \qquad (2)$$

using the formulae for clinoptilolite and phillipsite from Sample 246/10/2.

The equilibrium constant for the above reaction is

$$K = \frac{[Na^+]^{1.12} \quad [Mg^{2+}]^{0.19}}{[H^+]^{0.08} \; [K^+]^{0.72} \; [Ca^{2+}]^{0.35} \; [H_4SiO_4]^{5.22}}$$

The log of the above equation is taken and the average concentration of interstitial water data associated with sediments bearing phillipsite, clinoptilolite and phillipsite + clinoptilolite is used to calculate the log K as follows:

$$\log K = 1.12\ (-0.335) + 0.19\ (-1.448) - 0.08\ (-7.33) - 0.72\ (-2.03) - 0.35\ (-1.87) - 5.22\ (-3.34)$$

and thus,

$$\log K = 19.49$$

The resulting regression equation would then be:

$$\log\left(\frac{[Na^+]^{1.12} \quad [Mg^{2+}]^{0.19}}{[K^+]^{0.72} \; [Ca^{2+}]^{0.35} \; [H^+]^{0.08}} \right) = 19.49 + 5.22 \log[H_4SiO_4]$$

The above linear regression equation is presented in Figure 6-2. The slope of the line is 5·22 and the intercept is 19·49. Figure 6-2 indicates that clinoptilolite is favoured by high activities of $[H_4SiO_4]$, $[K^+]$, $[Ca^{2+}]$ and pH compared with phillipsite, which is the stable phase in sea water.

ΔG_R° could then be achieved as follows:

$$\Delta G_R^{\circ} = -1.364 \log K$$

$$\Delta G_R^{\circ} = -1.364\ (19.49)$$

$$\Delta G_R^{\circ} = -26.58 \text{ Kcal/mol.}$$

The negative ΔG_R° indicates that reaction (2) is favoured towards the right and thus clinoptilolite is stable compared with phillipsite in interstitial water.

Further, the ΔG_f° of phillipsite can be achieved as follows:

$$\Delta G_R^{\circ} = \Delta G_f^{\circ}{}_{\text{product}} - \Delta G_f^{\circ}{}_{\text{reactant}}$$

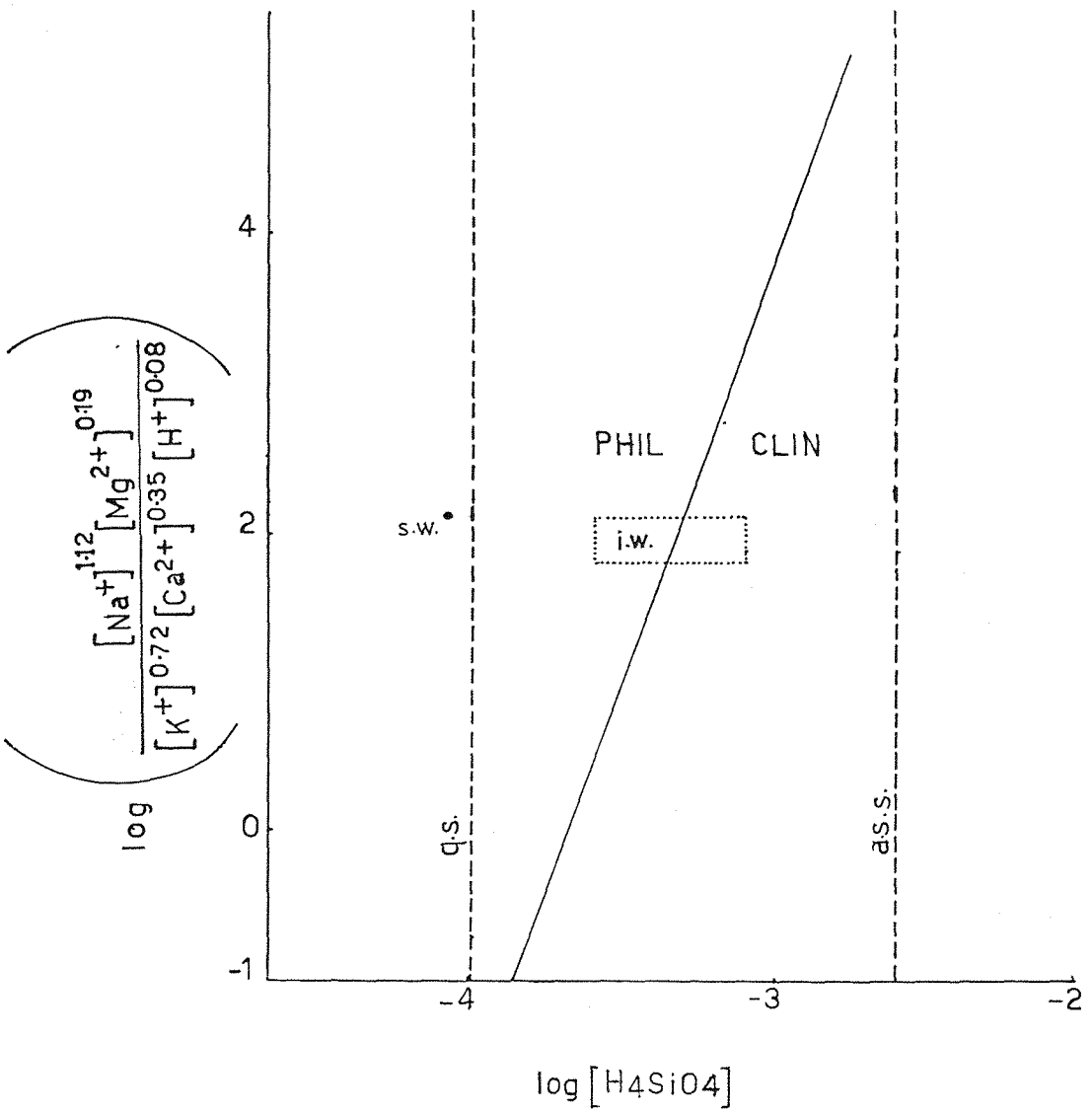

Fig.6-2.Stability fields for PHIL and CLIN.Key:q.s.= quartz saturation;a.s.s.=amorphous silica saturation;s.w.=average sea water;i.w.= interstitial waters(maximum field defined by dotted-line boundary).

$$\Delta G_f^{\circ}{}_{product} = 1{\cdot}12\ (-57{\cdot}279) + 10{\cdot}48\ (-56{\cdot}69) + 0{\cdot}19\ (-108{\cdot}8) + (-3963{\cdot}70)$$

$$\Delta G_f^{\circ}{}_{product} = -4642{\cdot}64 \text{ Kcal/mol}$$

$$\Delta G_f^{\circ}{}_{reactant} = 0{\cdot}72\ (-67{\cdot}3) + 0{\cdot}35\ (-132{\cdot}3) + 5{\cdot}22\ (-318{\cdot}6) + 0{\cdot}80\ \Delta G_f^{\circ}{}_{phillipsite}$$

$$\Delta G_f^{\circ}{}_{reactant} = -1757{\cdot}85 + 0{\cdot}80\ \Delta G_f^{\circ}{}_{phillipsite}$$

and thus,

$$-26{\cdot}58 = -4642{\cdot}64 + 1757{\cdot}85 - 0{\cdot}80\ \Delta G_f^{\circ}{}_{phillipsite}$$

$$\Delta G_f^{\circ}{}_{phillipsite} = -3572{\cdot}76 \text{ Kcal/mol.}$$

$\Delta G_f^{\circ}{}_{clinoptilolite}$ used in reaction (2) was calculated via the following reaction:

$$1{\cdot}18 \underset{\text{MLIS}}{K_{0{\cdot}132}\ Ca_{0{\cdot}06}\ Mg_{0{\cdot}70}\ Fe_{0{\cdot}88}\ Al_{2{\cdot}916}\ Si_{7{\cdot}74}\ O_{22}} + 5{\cdot}447\ H_4SiO_4 + 0{\cdot}53\ Ca^{2+} + 1{\cdot}604\ K^{+} + 0{\cdot}40\ Na^{+} \longrightarrow$$

$$\underset{\text{clinoptilolite}}{Na_{0{\cdot}40}\ K_{1{\cdot}76}\ Ca_{0{\cdot}60}\ Al_{3{\cdot}44}\ Si_{14{\cdot}58}\ O_{36}} + 1{\cdot}038\ Fe(OH)_3 + 0{\cdot}83\ Mg^{2+} + 8{\cdot}634\ H_2O + 1{\cdot}406\ H^{+} \qquad (3)$$

using the average formulae for MLIS and Sample 246/10/2 for clinoptilolite.

The equilibrium constant, ΔG_R°, and $\Delta G_f^{\circ}{}_{clinoptilolite}$ were calculated in the same way as reactions(1) and (2)

$$\log K = 11{\cdot}37$$

$$\Delta G_R^{\circ} = -15{\cdot}50 \text{ Kcal/mol}$$

and thus,

$$\Delta G_f^{\circ}{}_{clinoptilolite} = -3963{\cdot}70 \text{ Kcal/mol.}$$

Taylor et al. (1981) reported a value of -1072·8 Kcal/mol for a phillipsite in the tuffaceous sediments at Teels Marsh, Nevada, with the formula of $K_{0{\cdot}43}Na_{0{\cdot}50}Al_{3{\cdot}1}O_{8{\cdot}2} \cdot 3{\cdot}2\ H_2O$. An approximation for their

ΔG_f^o on a dehydrated and 32 oxygens basis is:

$$-3478{\cdot}6 \text{ (i.e. } (-1072{\cdot}8 - 3{\cdot}2\ H_2O) \times 32/8{\cdot}2 \text{).}$$

Glaccum and Bostrom (1976) suggested a value of -5382·4 Kcal/mol for a phillipsite from deep sea sediments with the formula of $K_6Al_6Si_{14}O_{40}.15\ H_2O$. On a dehydrated and 32 oxygens basis as above, the ΔG_f^o of this phillipsite would be -3625·6 (i.e. (-5382·4 - 15 H_2O) x 32/40). Thus, the difference between the present study value and those reported by others is probably due to the same reasons as mentioned before for ΔG_f^o of clinoptilolite in reaction (1).

2) The stability of palygorskite (paly)

Bonatti et al. (1968), Bowles et al. (1971), Vallier (1974), Weaver et al. (1977) and Couture (1977a) suggested an authigenic origin for paly and believed that the necessary Mg^{2+} for its formation could be provided from either sea water or volcanic ash. Bonatti et al. (1968) believed that a source rich in Mg (richer than volcanic glass) is necessary for paly formation, since paly is richer in Mg than montmorillonite, which usually forms from volcanic glass. According to Donnelly et al. (quoted by Couture, 1977a), the Mg diffused in sediments after burial during a sedimentary hiatus. Couture (op.cit.) pointed out that absorption of Mg^{2+} by the sediment near the sediment-water interface may have been possible by the stirring action of a bottom current. The association of paly with hiatuses and bottom currents or slow sedimentation rates suggested to him that extended contact with sea water may be helpful or even necessary for paly formation. His experimental studies also showed that paly was stable with respect to montmorillonite in sea water at 25°C and pH 7·5 if dissolved silica exceeds roughly 36 ppm.

Couture (op.cit.) also reported a good correlation between authigenic silica and paly and between clinoptilolite and paly in late Cretaceous through to Eocene sediments (Figs. 6-3 and 4).

The above mentioned evidence is in good agreement with the present study observations. Bulk chemistry indicates a volcanic material contribution (basaltic and silicic) to the paly-bearing sediments, which occur either below hiatuses (Fig.6-4a) or have low sedimentation rates. MLIS with a low percentage of expandable layer (detrital), paly, clinoptilolite and opal-CT are associated in late Cretaceous through to Eocene sediments at Site 212

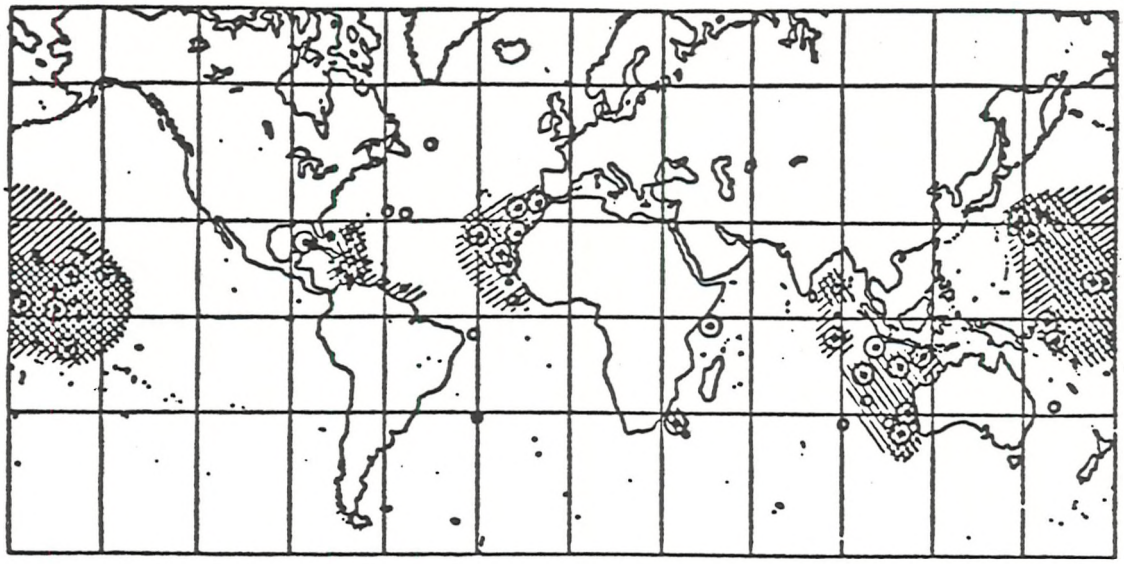

Upper Cretaceous

Fig.6-3. Relation of paly with clino and authigenic silica in the upper Cretaceous. Key: ○ no paly, • paly present, ◎ paly abundant in one or more sample, ⁄⁄ chert, porcelanite, or op-CT, /// clino (after Couture, 1977a).

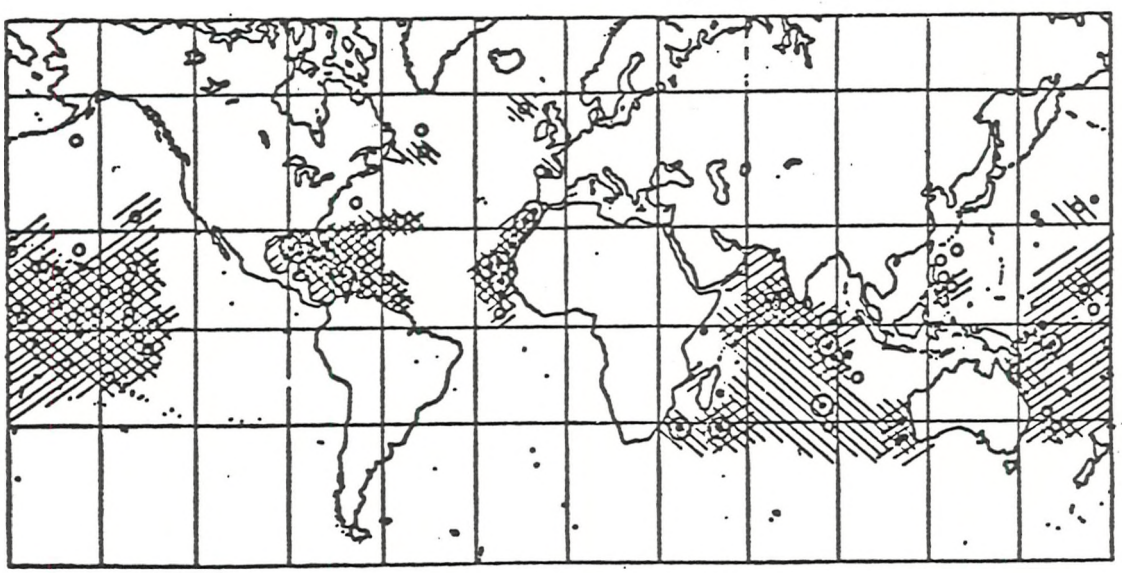

Eocene and Paleocene

Fig.6-4. Relation of paly with clino and authigenic silica in the Eocene and Paleocene. Symbols same as figure 6-3 (after Couture, 1977a).

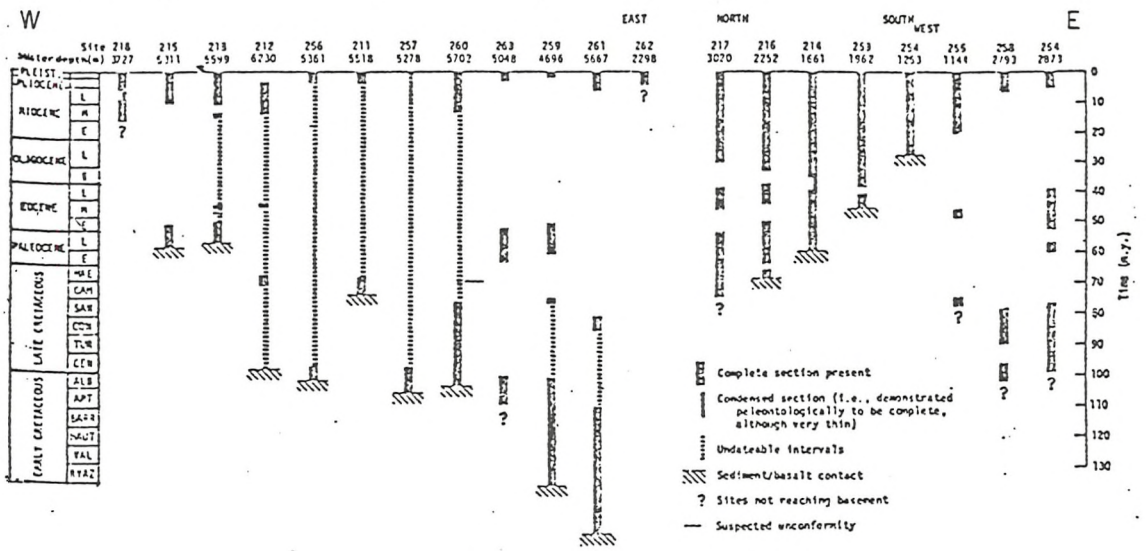

Stratigraphic section sampled at sites in the eastern Indian Ocean. Ridge and plateau sites (right) are separated from the basin sites (left). The basement age for Site 212 is derived from geophysical evidence[17].

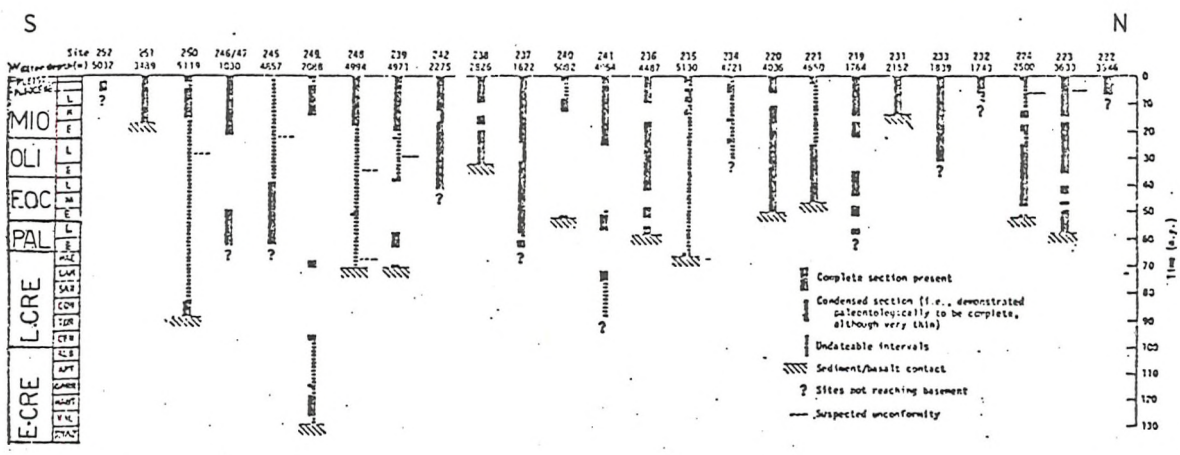

Fig.6-4a. Stratigraphic section sampled at sites in the western Indian Ocean. Sites 243 and 244 are omitted since no cores were recovered from these sites. Basement ages at Sites 248 and 249 were determined radiometrically (after Davies et al., 1975).

(Samples 18/2, 37cc and 38/1), Site 250 (Sample 22/3) and Site 256 (Samples 6/3, 7cc and 8/4), which have slow sedimentation rates since they contain zeolites. Paly-bearing sediments of the Cretaceous to middle Miocene, in the absence of zeolites, were also observed at Sites 212 (cores 27/5 and 37cc), 213 (core 14), 215 (core 9/2) and 248 (core 10/2) (present below hiatuses), 248 (core 14; slow sedimentation rate), 211 (cores 13 and 14; present between diabase sill and basaltic basement), 245 and 245A (cores 1/3 and 2/6 have slow sedimentation rates, whereas cores 6/2 and 5/3 show high sedimentation rates, i.e. > 9m m.y) and Site 221 (slow sedimentation rate).

All the above mentioned sediments could obtain the necessary Mg from volcanic glass, and if the view of Bonatti et al. (1968) is correct, i.e. Mg of volcanic glass is not a sufficient source for paly, then an extra source of Mg (besides volcanic glass) for the above sediments could be provided in the following manner: sediments which have slow sedimentation rates or occur below hiatuses could gain Mg from sea water. Mg for paly formation at Site 211 could have a hydrothermal origin. Sediments with a high sedimentation rate at Site 245 could obtain Mg from chlorite.

At Site 221, a slow sedimentation rate, the occurrence of volcanic glass and similarity of paly composition to those of the other sites suggests an authigenic origin for paly, whereas the proximity of the site to lands rich in paly suggests a terrigenous origin.

It is evident from Figure 6-5 that paly is stable with respect to MLIS in sea water, since the sea water composition falls in the stability field of paly, which is in good agreement with the view of Couture (1977a). In addition, negative correlation exists between MLIS and paly.

On the basis of the above observation, MLIS into paly and paly into clinoptilolite transformations are suggested. It is likely that in the presence of the necessary Mg (sea water + volcanic glass, hydrothermal and Mg-bearing minerals + volcanic glass) and H_4SiO_4, MLIS transforms into paly in sea water or interstitial water (Reaction 4) and then, on moving into the more siliceous interstitial water field on burial, it should transform to clinoptilolite (Reaction 6). The reactions are as follows:

a) MLIS/paly

$$0{\cdot}673\ K_{0{\cdot}20}\ Ca_{0{\cdot}16}\ \overset{\text{MLIS}}{Mg_{0{\cdot}74}\ Fe_{1{\cdot}22}\ Al_{3.18}\ Si_{7.20}\ O_{22}} + 2{\cdot}474\ H_4SiO_4$$

/contd.over

$$+ 0{\cdot}019\ Fe(OH)_3 + 1{\cdot}12\ Mg^{2+} + 0{\cdot}205\ K^{+} \rightleftharpoons$$

$$K_{0{\cdot}34}\ Ca_{0{\cdot}10}\ \overset{paly}{Mg_{1{\cdot}62}}\ Fe_{0{\cdot}84}\ Al_{2{\cdot}14}\ Si_{7{\cdot}32}\ O_{21} + 3{\cdot}76\ H_2O + 2{\cdot}433\ H^{+} \quad (4)$$

using the formulae for MLIS from Sample 212/27/1 and paly from Sample 215/9/2.

The equilibrium constant for the above reaction is

$$K = \frac{[H^+]^{2{\cdot}433}}{[Mg^{2+}]^{1{\cdot}12}\ [K^+]^{0{\cdot}205}\ [H_4SiO_4]^{2{\cdot}474}}$$

Taking the log and substituting the data given in Table 6-1 in the above equation,

$$\log K = 2{\cdot}433\ (-7{\cdot}35) - 1{\cdot}12\ (-1{\cdot}387) - 0{\cdot}205\ (-2{\cdot}13)$$
$$-2{\cdot}474\ (-3{\cdot}55)$$

and thus,

$$\log K = -7{\cdot}11$$

The regression equation would then be:

$$\log\left(\frac{[Mg^{2+}]^{1{\cdot}12}\ [K^+]^{0{\cdot}205}}{[H^+]^{2{\cdot}433}}\right) = 7{\cdot}11 - 2{\cdot}474\ \log[H_4SiO_4]$$

Figure 6-5, which represents the above linear regression equation, shows that the point presenting sea water falls in the stability field of paly, which suggests that paly thermodynamically can be stable in sea water compared with MLIS.

$\triangle G_R^{\circ}$ is calculated as follows:

$$\triangle G_R^{\circ} = -1{\cdot}364\ (-7{\cdot}11)$$

$$\triangle G_R^{\circ} = +9{\cdot}70\ \text{Kcal/mol.}$$

Thus reaction (4) is favoured towards the left (MLIS) although, as $\triangle G_R^{\circ}$ is less than 10 Kcal, it cannot be far from equilibrium.

The free energy of formation of paly could then be calculated in the same way as before:

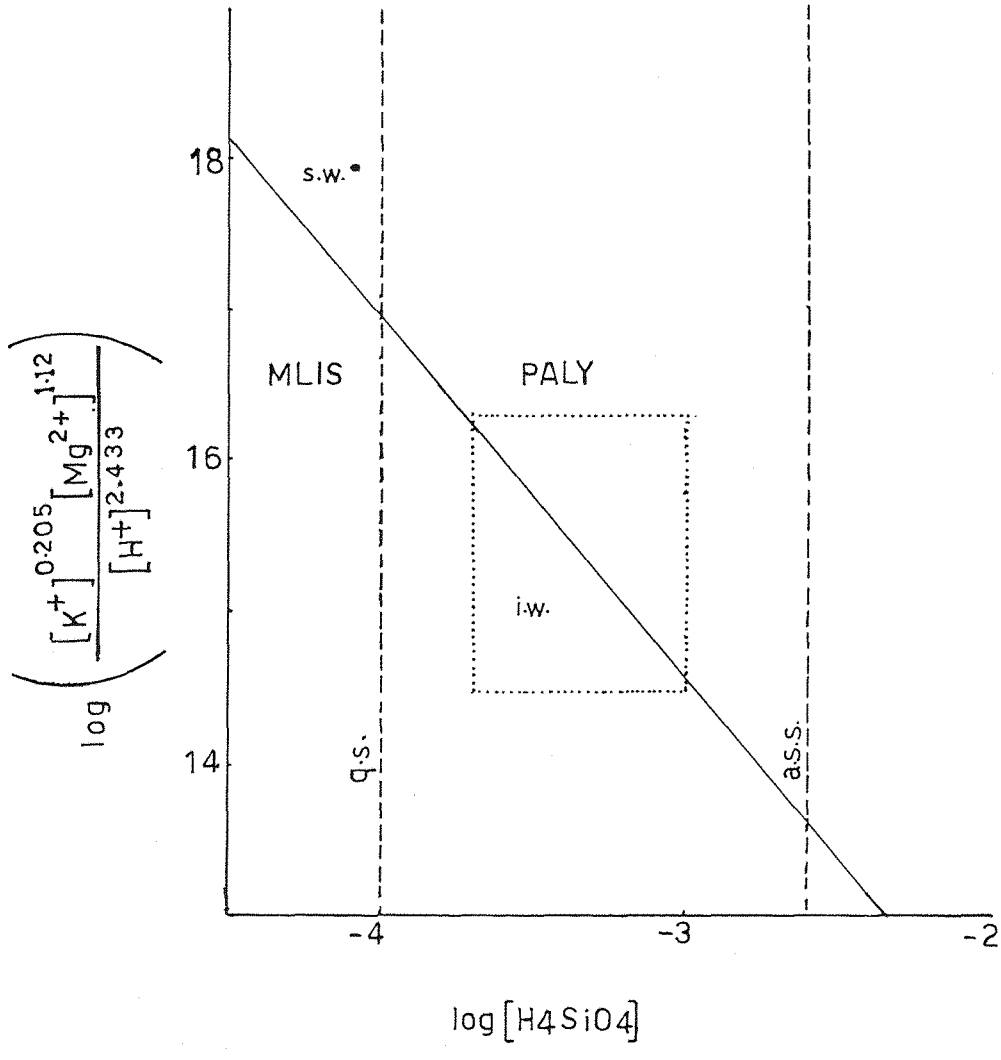

Fig.6-5.Stability fields for MLIS and PALY.Key: q.s.=quartz saturation;a.s.s.=amorphous silica saturation;s.w.=average sea water; i.w.=interstitial waters(maximum field defined by dotted-line boundary).

$$\Delta G_R^{\circ} = \Delta G_f^{\circ}{}_{product} - \Delta G_f^{\circ}{}_{reactant}$$

where,

$$\Delta G_f^{\circ}{}_{product} = -213{\cdot}15 + \Delta G_f^{\circ}{}_{paly}$$

and

$$\Delta G_f^{\circ}{}_{reactant} = -2496{\cdot}57 \text{ Kcal/mol}$$

and thus,

$$\Delta G_{paly_{21}} = -2273{\cdot}72$$

$$\Delta G_f^{\circ}{}_{paly_{10{\cdot}5}} = -1136{\cdot}86 \text{ Kcal/mol}$$

b) Paly/clinoptilolite transformation.

$$1{\cdot}418\ K_{0{\cdot}34}\ \overset{(paly)}{Ca_{0{\cdot}10}}\ Mg_{1{\cdot}62}\ Fe_{0{\cdot}84}\ Al_{2{\cdot}14}\ Si_{7{\cdot}32}\ O_{21} + 4{\cdot}609\ H_4SiO_4$$

$$+ 0{\cdot}198\ Ca^{2+} + 0{\cdot}69\ K^{+} + 0{\cdot}77\ Na^{+} + 2{\cdot}42\ H^{+} \longrightarrow$$

$$\overset{(clinoptilolite)}{Na_{0{\cdot}77}\ K_{1{\cdot}175}\ Ca_{0{\cdot}34}\ Mg_{0{\cdot}155}\ Al_{3{\cdot}035}\ Si_{14{\cdot}99}\ O_{36}} + 1{\cdot}19\ (Fe(OH)_3$$

$$+ 2{\cdot}14\ Mg^{2+} + 8{\cdot}644\ H_2O \qquad (5)$$

using the formulae for paly from Sample 215/9/2 and clinoptilolite from Sample 256/7cc; where the equilibrium constant is:

$$K = \frac{[Mg^{2+}]^{2{\cdot}14}}{[Ca^{2+}]^{0{\cdot}198}\ [K^{+}]^{0{\cdot}69}\ [Na^{+}]^{0{\cdot}77}\ [H^{+}]^{2{\cdot}42}\ [H_4SiO_4]^{4{\cdot}609}}$$

Taking logs and substituting data for interstitial water,

$$\log K = 31{\cdot}02$$

Using the log K, the regression equation would then be:

$$\log \frac{[Mg^{2+}]^{2{\cdot}14}}{[Ca^{2+}]^{0{\cdot}198}\ [K^{+}]^{0{\cdot}69}\ [Na^{+}]^{0{\cdot}77}\ [H^{+}]^{2{\cdot}42}} = 31{\cdot}02 + 4{\cdot}609 \log [H_4SiO_4]$$

Figure 6-6 shows the relative stability of paly and clinoptilolite; the ΔG_R° would then be:

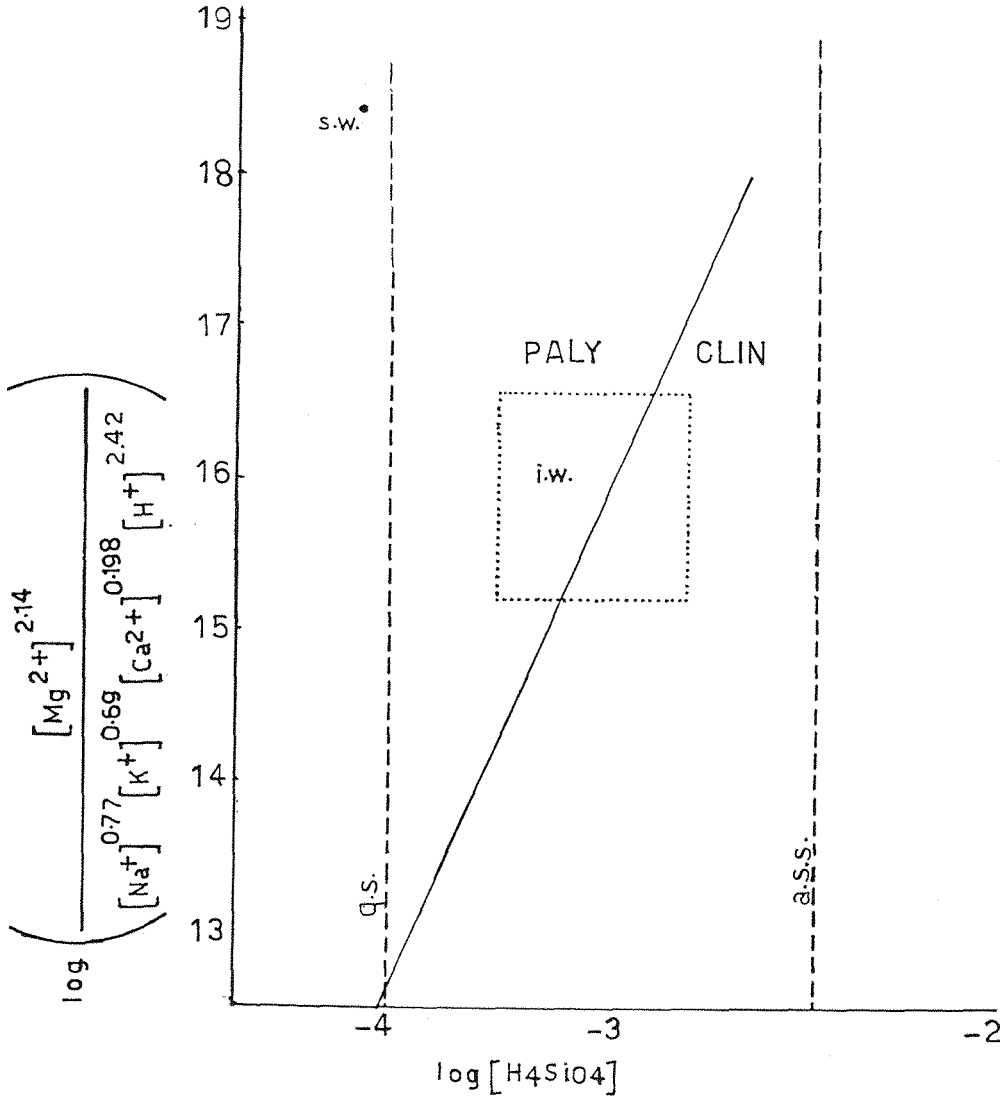

Fig.6-6. Stability fields for PALY and CLIN. Key: q.s.=quartz saturation; a.s.s.= amorphous silica saturation; s.w.= average sea water; i.w.=interstitial waters (maximum field defined by dotted-line boundary).

ΔG_R° = -1·364 (31·02)

ΔG_R° = -42.31 Kcal/mol.

The negative ΔG_R° indicates that clinoptilolite is the favourable mineral compared with paly at high activities of H_4SiO_4, Na^+, K^+, Ca^{+2} and low pH.

The free energy of formation of paly was calculated as follows:

$\Delta G_R^{\circ} = \Delta G_f^{\circ}{}_{product} - \Delta G_f^{\circ}{}_{reactant}$

$\Delta G_f^{\circ}{}_{product} = -920.995 + \Delta G_{clin}$

$\Delta G_f^{\circ}{}_{reactant} = -4809.2996$

$\Delta G_{f\ clin} = -3930.61$ Kcal/mol

The necessary silica for the above reactions could be provided from either biogenic silica or silicic volcanic glass.

Singer et al. (1974) reported a value of -1131·5 Kcal/mol for a soil paly with a formula of $Si_{4.01}\ Al_{0.46}\ Mg_{1.35}\ Fe_{0.24}\ O_{10.5}$. Weaver et al. (1977) also reported values of -2352·78, -2348·91 and -2354·51 Kcal/mol for Na, Mg and Ca exchange forms of marine paly with a formula of $X_{0.48/n}\ (Mg_{1.83}\ Fe_{0.36}\ Al_{1.66})\ (Al_{0.20}\ Si_{7.8})\ O_{20}\ (OH)_2$. An approximation for their ΔG_f° of Mg paly would be -2292.22 (i.e. -2348·91 (-56.69)). The difference between the reported values of the present study and those of others could be due to the same reasons as those mentioned for MLIS.

3) Relative stabilities of clinoptilolite, MLIS, phil and paly

In order to show the relative stabilities of the minerals (clinoptilolite, MLIS, phil and paly), the molar activities of Ca^{2+}, Na^+, K^+ and Mg^{2+} were assumed to be constant, because:

a) they represent different coefficients for every mineral;

b) they serve different purposes, i.e. in clinoptilolite formation Mg^{2+} is released, whereas for paly formation Mg^{2+} is necessary;

c) they show small variations in interstitial waters (i.e. there is not a big difference between minimum and maximum values).

However, variable cation activities would result in small upward or downward shifts of the equilibrium boundaries, indicating only minor effects on the relative stabilities of the minerals. For example, in Figure 6-7, two regression lines are represented which correspond to the minimum and maximum cationic activities found in interstitial water associated with clinoptilolite. As can be seen, the variation is small and also the lines are parallel.

Figure 6-8 shows the stability fields of phil, clinoptilolite, MLIS and paly. The stability field boundaries were established using two variables, pH and H_4SiO_4, from reactions 1, 2,4 and 5. Data from Table 6-1 for cation activities were used to incorporate the constant values in the equations.

The resulting equations are as follows:

MLIS - clinoptilolite (reaction 1)

$$pH = -111{\cdot}52 - 35{\cdot}66 \log [H_4SiO_4]$$

phillipsite - clinoptilolite (reaction 2)

$$pH = 225{\cdot}30 + 65{\cdot}25 \log [H_4SiO_4]$$

MLIS - paly (reaction 4)

$$pH = 3{\cdot}76 - 1{\cdot}02 \log [H_4SiO_4]$$

paly - clinoptilolite (reaction 5)

$$pH = 13{\cdot}46 + 1{\cdot}905 \log [H_4SiO_4]$$

Figure 6-8 shows the occurrence of the following assemblages at different levels of silica activities:

a) at high silica activities the following assemblages are recognised at different pH activities

i) at high pH

paly - clin

ii) at low pH

ML - clin

paly - clin - ML

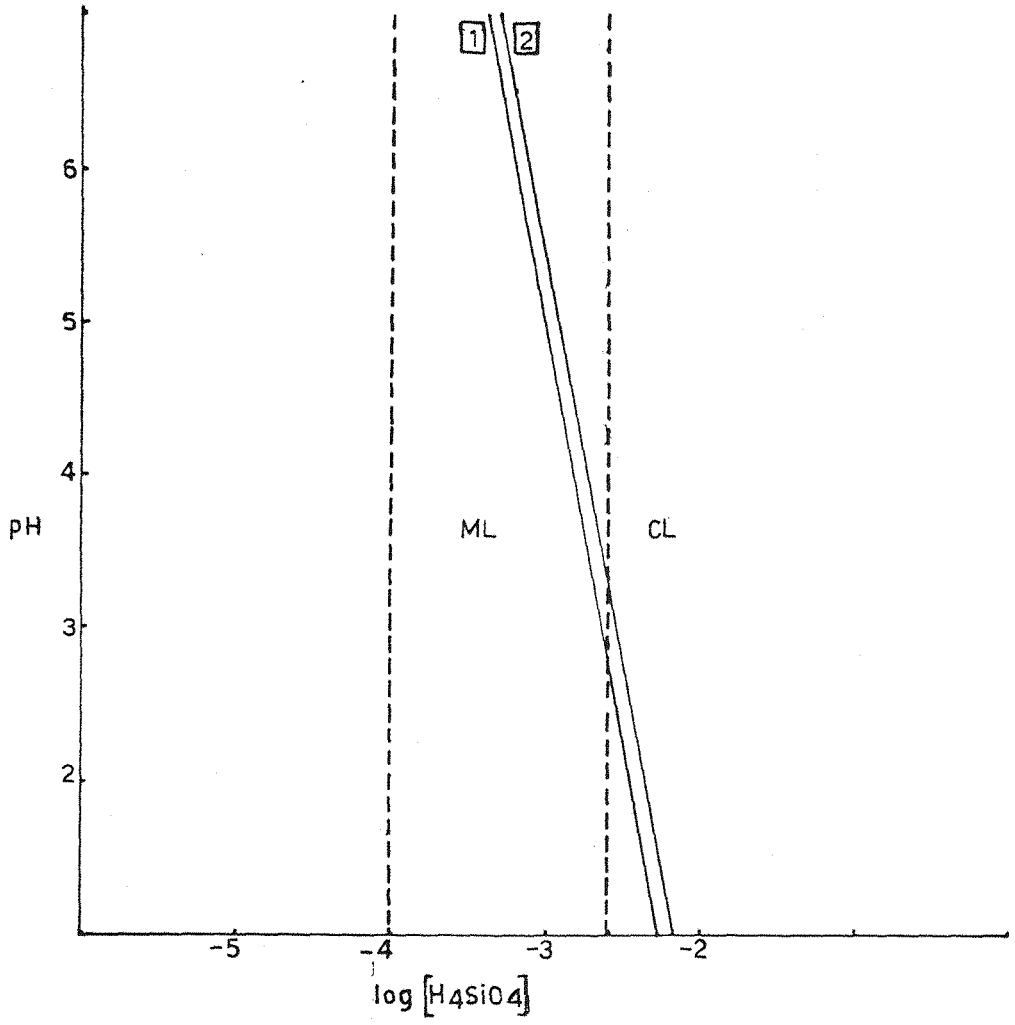

Fig.6-7.Stability of MLIS and clin represented by two regression lines indicating the the minimum(1) and maximum(2) cation activities in interstitial water.

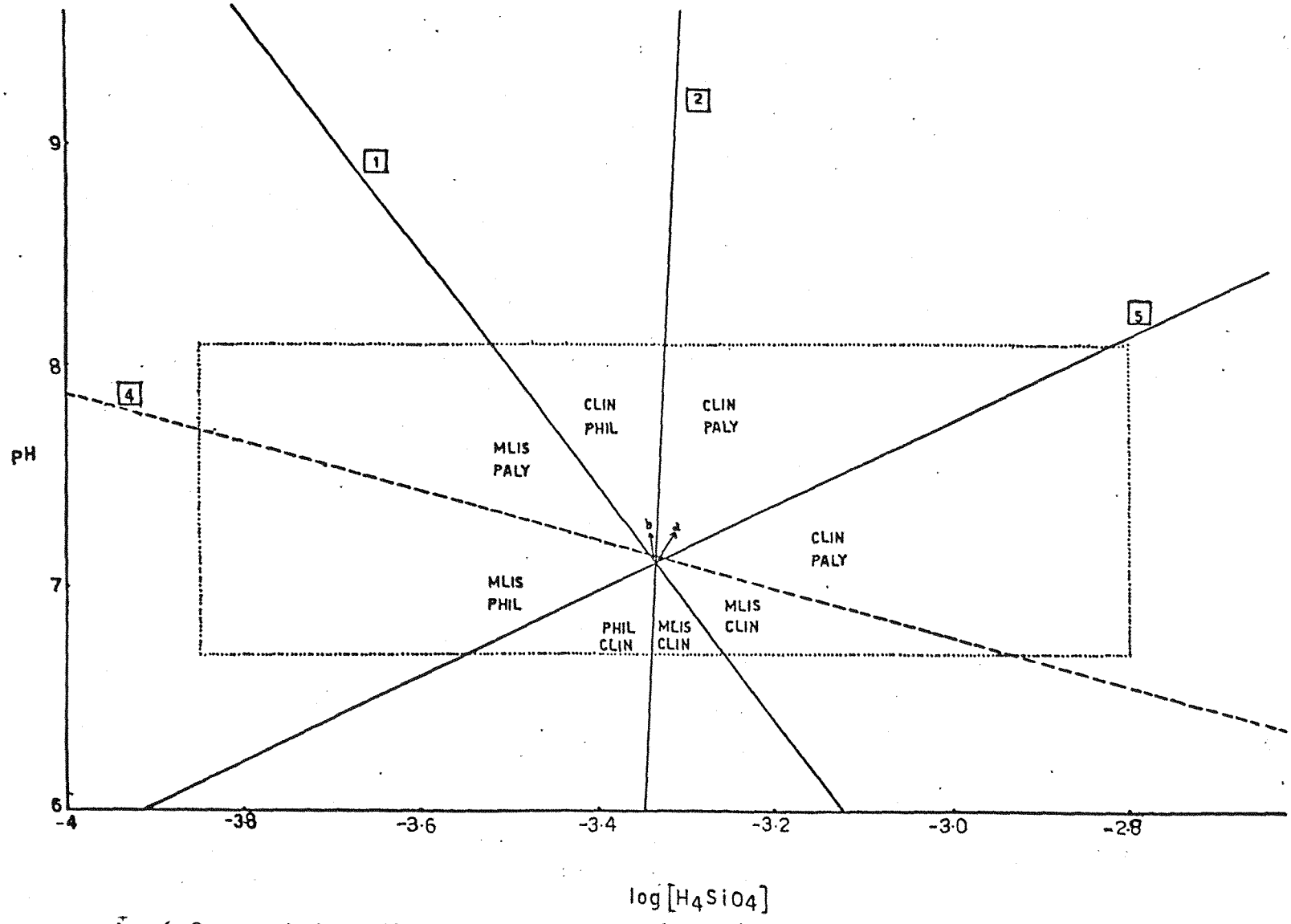

Fig.6-8.Stability fields for MLIS,clin,phill,and,paly.Key:.....interstitial water field, --- reaction with positive ΔGR°, ___ reactions with negative ΔGR°, [1], [2], [4] and [5] indicating MLIS-clin,phil-clin,MLIS-paly and paly-clin reactions respectively. a=MLIS-clin-paly stability field ,b=MLIS-clin-phil stability field.

b) at low silica activities

i) high pH

phil - clin

MLIS - paly

ii) medium pH

MLIS - paly

MLIS - clin - phill

iii) low pH

phill - clin.

It was decided to choose Mg^{2+} as a third variable (i.e. besides pH and H_4SiO_4) in order to show its effect on the stabilities of paly and clin, since Mg^{2+} is an important factor in clinoptilolite and paly formation (clinoptilolite forming reaction releases Mg, whereas paly consumed it).

In order to show the stabilities of paly,clinoptilolite and MLIS as a function of three variables: pH, pMg and pH_4SiO_4, a three dimensional stability diagram was constructed. The method of construction is the same as that represented by Garrels et al. (1965). One variable is taken as constant for each face of the block and then a regression line is plotted as a function of two variables. The considered fixed values are as follows:

front face	pH = 9
back face	pH = 6
left face	$\log[H_4SiO_4] = -4$
right face	$\log[H_4SiO_4] = -2$
top face	$\log[Mg^{2+}] = -1$
bottom face	$\log[Mg^{2+}] = -8$

The three dimensional diagrams were constructed for MLIS-clin, MLIS-paly and paly-clin using reactions 1 (Fig.6-9), 4 (Fig.6-10), and 5 (Fig.6-11) respectively.

From Figure 6-9 it is evident that clinoptilolite is the stable phase on the high silica side of the diagram, and with increasing pH, clinoptilolite stability increases.

Fig.6-9: ML-CL stability fields as a function of three variables (pH, pH_4SiO_4 and pMg).
Key: - - - interstitial water field,
ML = mixed layer illite/smectite;
CL = clinoptilolite.

Fig.6-10: ML-Pa stability fields as a function of three variables (i.e. pH, pH_4SiO_4 and pMg).
Key: - - - interstitial water field,
ML = mixed layer illite/smectite;
Pa = palygorskite.

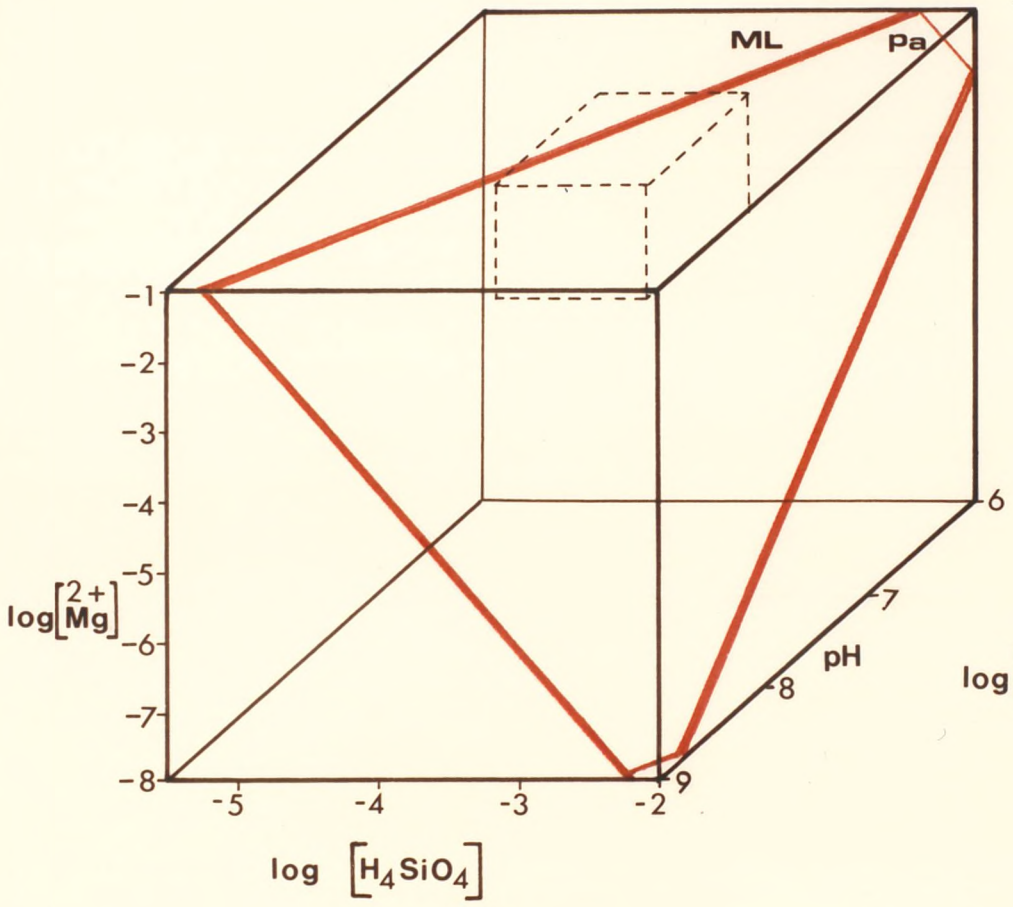

Fig. 6 - 10

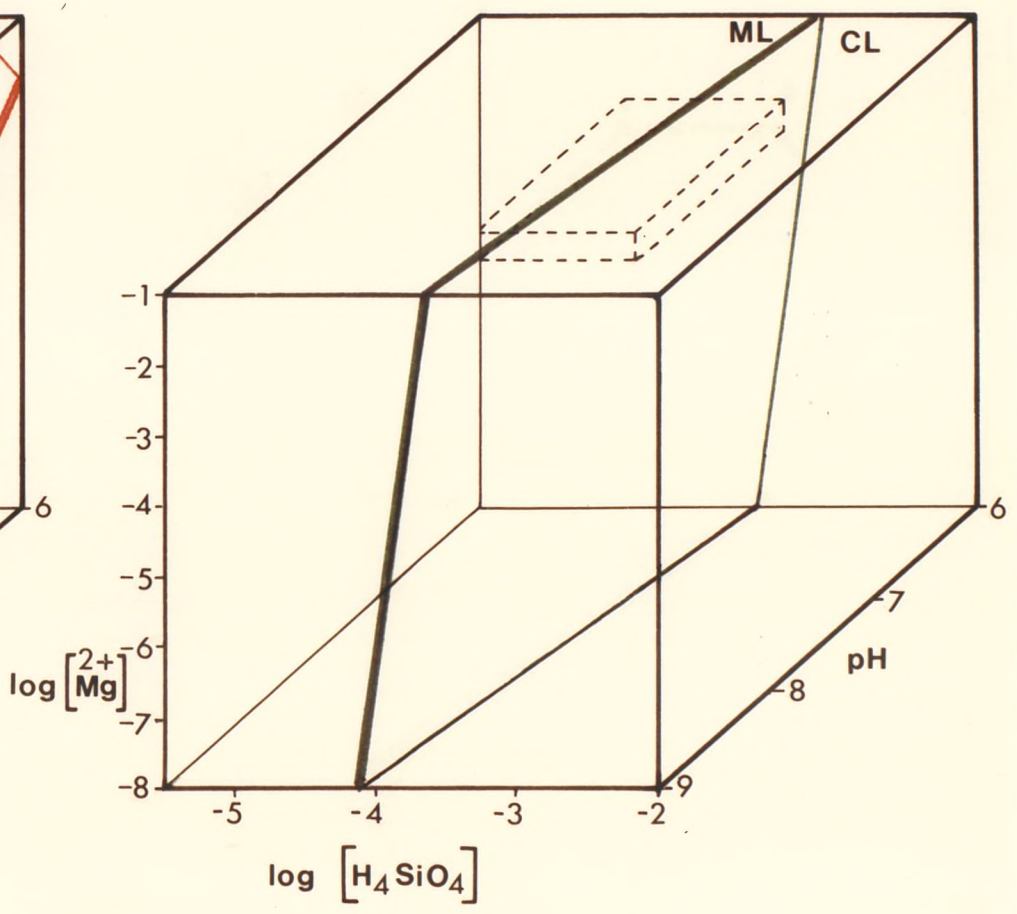

Fig. 6 -9

Figure 6-10 shows that paly is the stable phase at high silica, pH and Mg^{2+} compared with MLIS, and with increasing pH, lower silica activity is required and thus the stability field of paly increases.

Figure 6-11 concerns paly and clinoptilolite stabilities. As can be seen, paly is stable at high Mg^{2+} and low silica compared with clinoptilolite. As pH increases, lower Mg^{2+} and higher silica are required for paly formation.

Figure 6-12, which is a combination of Figures 6-10 and 6-11, was constructed to illustrate the transformation of MLIS into paly, and then paly into clinoptilolite. It is evident from this Figure that paly stability field is small in relation to MLIS + clinoptilolite. It clearly requires moderate to high pH, Mg^{2+} and low to high Si activities for its formation.

4. Conclusions

On the basis of the common occurrence of mineral assemblages and their correlation with each other, a series of reactions occurring in an aqueous solution were suggested for the formation of clinoptilolite-phill and paly (Table 6-5). It is evident from this Table that clinoptilolite-forming reactions all show negative ΔG_R, indicating that the reactions are spontaneous and clinoptilolite is the stable phase, whereas reactions involving paly are almost at equilibrium and show small positive ΔG_R. The reactions also show that paly and clinoptilolite are formed in more basic environments compared with MLIS. Paly also forms in more basic environments compared with clinoptilolite. Both clinoptilolite and paly use up K^+, Na^+ and Ca^{2+}. Mg^{2+}, however, is used up in the paly-forming reaction, whereas it is released in the clinoptilolite-forming reaction.

However, the mineralogical data and stability diagrams suggest that MLIS is the common mineral of normal deep sea environment (either detrital or authigenic). In the absence of detrital MLIS, the alteration of volcanic rock could result in the formation of authigenic MLIS, which becomes a sink for Mg. The MLIS could then transform into clinoptilolite in the presence of K^+, Na^+, Ca^{2+} and H_4SiO_4. In the presence of detrital MLIS, where high pH, H_4SiO_4 and Mg exist, paly formation could take place. The necessary Mg could become available from the alteration of volcanics, sea water,

Fig.6-11: Pa-CL stability fields as a function of three variables. - - - interstitial water field; Pa = palygorskite; CL = clinoptilolite.

Fig.6-12: Paly stability field compared with paly-CL, CL-ML and ML-paly stability fields.
Key: - - - interstitial water field;
paly = palygorskite; clin = clinoptilolite;
ML = mixed layer illite/smectite.

Red plane ML - Paly
Green plane Paly - Clin

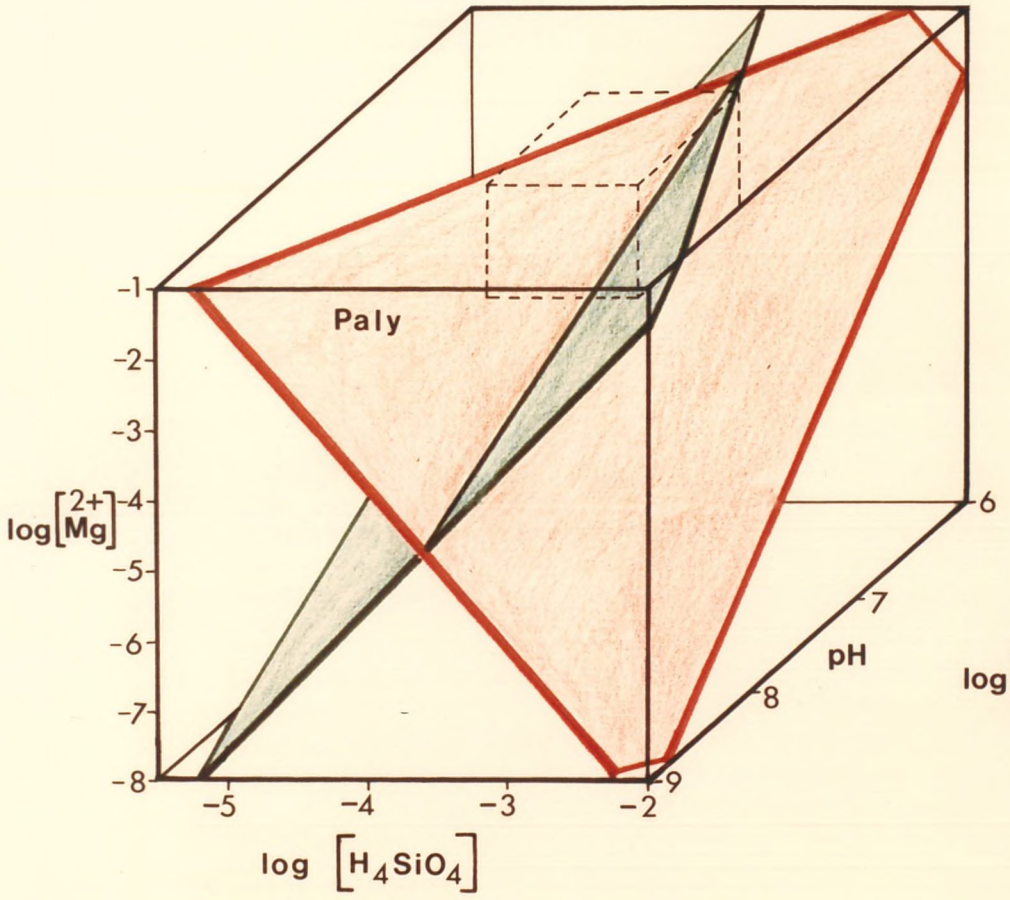

Fig. 6-12

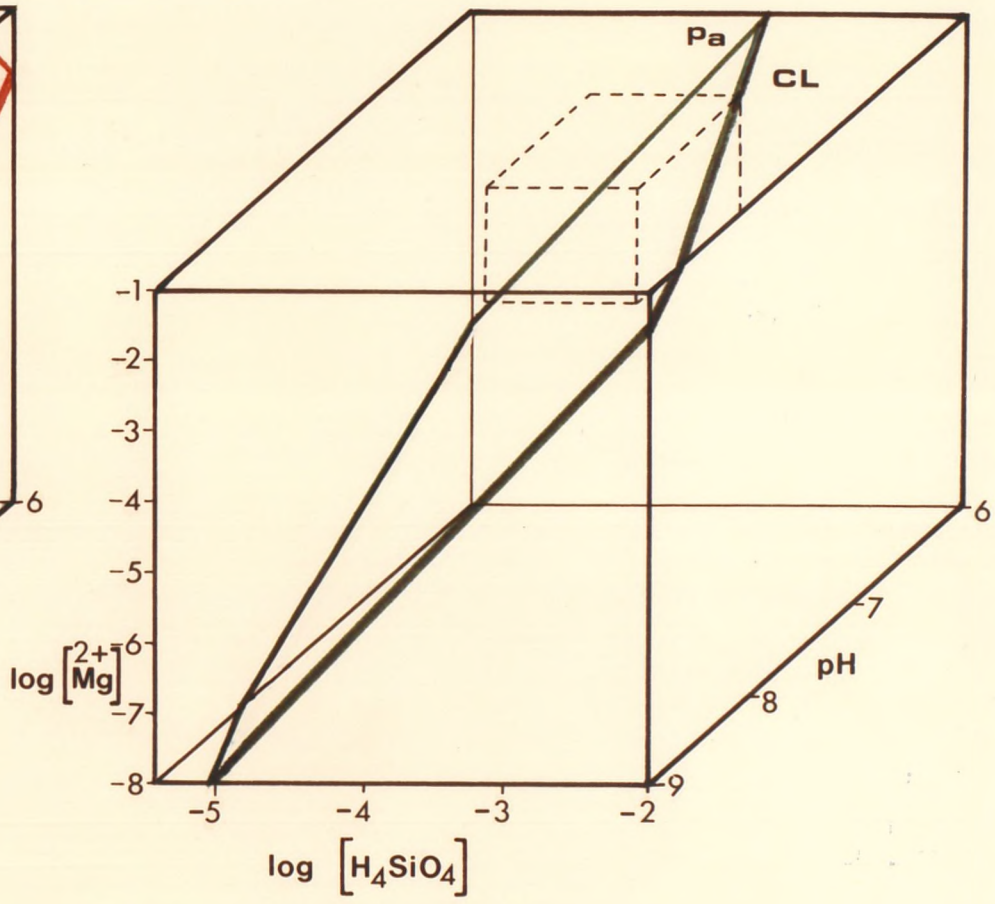

Fig 6-11

TABLE 6-5: Reactions involving Clin, Phill and Paly Formation

	$\triangle G_R^o$	$\triangle G_f^o$ of the mineral marked with *
MLIS - clin (Reaction 1)		
$1{\cdot}025\ MLIS + 7{\cdot}07\ H_4SiO_4 + 0{\cdot}599\ Ca^{2+} + 0{\cdot}665\ K^+ + 0{\cdot}37\ Na^+ \longrightarrow$ clin* $+ 0{\cdot}9\ Fe(OH)_3 + 0{\cdot}448\ Mg^{2+} + 12{\cdot}13\ H_2O + 1{\cdot}32\ H^+$	-21·89	-3934·63
Phill - clin (Reaction 2)		
$0{\cdot}8$ phill* $+ 5{\cdot}22\ H_4SiO_4 + 0{\cdot}35\ Ca^{2+} + 0{\cdot}72\ K^+ + 0{\cdot}08\ H^+ \longrightarrow$ clin $+ 0{\cdot}19\ Mg^{2+} + 1{\cdot}12\ Na^+ + 10{\cdot}48\ H_2O$	-26·58	-3572·76
MLIS - paly (Reaction 4)		
$0{\cdot}673\ MLIS + 2{\cdot}474\ H_4SiO_4 + 0{\cdot}019\ Fe(OH) + 1{\cdot}12\ Mg^{2+} + 0{\cdot}205\ K^+ \rightleftharpoons$ paly* $+ 3{\cdot}76\ H_2O + 2{\cdot}433\ H^+$	+9·70	-2273·72
Paly - clin (Reaction 5)		
$1{\cdot}41$ paly $+ 4{\cdot}609\ H_4SiO_4 + 0{\cdot}198\ Ca^{2+} + 0{\cdot}69\ K^+ + 0{\cdot}77\ Na^+ + 2{\cdot}42\ H^+ \longrightarrow$ clin* $+ 1{\cdot}19\ Fe(OH)_3 + 2{\cdot}14\ Mg^{2+} + 8{\cdot}644\ H_2O$	-42·31	-3930·61

hydrothermal and Mg-bearing minerals, whereas H_4SiO_4 could become available from both biogenic silica and/or volcanics. The necessary high pH is also provided during the volcanics alteration. On moving into more siliceous interstitial water field on burial, and as Mg falls, paly becomes unstable and could transform to clinoptilolite (Mg is cut off on burial if it supplied from sea water).

The above observations suggest a transition from a less complex and dense structure to a more complex and harder structure, i.e. a transition from sheet to double chain-sheets, and finally to half-open tektosilicate (MLIS → paly → clinoptilolite) rather than direct precipitation.

Singer (1979) believes that such transformation is not possible at normal temperatures and pressures, since an input of energies is required, i.e. energies for breaking of octahedral bond (according to Weaver et al., 1977, when appreciable Al is present it is difficult for much Mg to be incorporated in the octahedral positions), and energy for physically inverting Si tetrahedron smectite sheet into the partially inverted tetrahedrons of the paly chain structure. He believes that since the input of energies in the order of 19 Kcal/mol is required for the diagenetic transformation of smectite into illite, during which tetrahedral Si is replaced by Al, there is no reason to believe the breaking of octahedral bonds requires less energy in the case of smectite into paly transformation.

Greene-Kelly (1955) has demonstrated that when Mg-saturated montmorillonites are heated at $\sim 300^{\circ}$ for a few hours, they lose their ability to expand. He speculated that the Mg migrated into the octahedral layer. Later, infra-red studies (Tettenhorst, 1962) suggested the Mg migrated into the hexagonal holes in the tetrahedral sheet. Weaver et al. (1977) considered the above experimental work and suggested that in any event Mg is unique among the more abundant cations in nature, in its ability to enter the montmorillonite layer, and thus environments in which Mg^{2+} has a high activity and temperature is high would tend to favour such a reaction in the natural system.

Matter (1974) believes that the transformation affecting the clay mineral assemblage is primarily temperature dependent and, to a lesser extent, is dependent on pressure, age of the formation, and composition of interstitial water. However, he noticed an illite into MLIS trans-

formation could take place at a temperature of 23·5°C. This temperature is observed in most sites of the present study. Douglas et al. (1973) reported that until the late Eocene the ocean was probably 10-15°C warmer than today.

Weaver et al. (1977) believe that montmorillonite structure allows for an easier transformation of a sheet-structure to a chain-structure clay (Si tetrahedron inversion), since in montmorillonite every other SiO_4 tetrahedron is inverted (Edelman and Favejee , 1940). The results of Weaver et al. (1973) showed that the four occupied sites of paly are occupied by half trivalent and half divalent cations. According to them 2:1 layer structures with predominantly Al and Mg are in the octahedral sites; the minimum occupancy for the poorly crystallized clay minerals is 65%, and the minimum for well-crystallized muscovite is 85%. In the 1:1 layer silicates occupancy values less than 85% are rare. They therefore concluded that when the occupied octahedral sites are more than 65% occupied by Al or by Mg, the layer can adjust to compensate for the internal strain and can grow in two dimensions. The minerals which form larger sheets generally have a larger proportion of their occupied sites filled with Al or Mg than the smaller clay minerals. The occupancy value can be less than 65% when the smaller Fe^{3+} is substituted for Al. When these conditions are not satisfied, the internal strain is such that growth is in only one direction. The width of the sheet is restricted to five octahedral sites. Sufficient strain accumulates within this five-site interval so that the silica tetrahedral sheet is forced to invert to accommodate the strain.

It should be borne in mind that the above relations among the minerals result from the assumption that:

a) the activity of water is unity;

b) the concentration is equivalent to activity;

c) pressure is 1 atmosphere;

d) temperature is 25°C.

According to Hess (1966), the activity-molality approximation is a poor one, especially when dealing with electrolytic solutions.

Kolla et al. (1973b) observed a) zeolites are present in the

areas of relatively thin sediment cover in the Indian Ocean, and b) the sediment thickness in clinoptilolite-rich areas is somewhat higher than in phillipsite areas. They believe that if the thickness of sediment overburden were significant in the genesis of clinoptilolite, one would see indications of it in the degradation and destruction of smectite (Burst, 1969). They observed the abundant smectite and its usually well-crystallized nature in the Cretaceous to Eocene sediments, which suggested to them that no great overburden of the sediment has been involved.

On the basis of the above observation, they suggested therefore that depth of burial is apparently not as critical a factor in the genesis of clinoptilolite as it is on land (Hay, 1966).

Temperature does not deviate much from the assumed values. Sclater et al. (1974b) reported temperature values between 2° and $15^{\circ}C$ for sediments from 0 to 200m depth at Sites 214, 216 and 217 (on the Ninetyeast Ridge).

So, on the basis of the arguments above and the experimental and thermodynamic approach presented in this thesis, the mineral transformation series MLIS $\rightarrow$ paly $\rightarrow$ clin series is largely substantiated.

TABLE 6-1: The Content of Na^+, K^+, Ca^{2+}, Mg^{2+} and Si of Interstitial Water of the DSDP Core Sediments and Sea Water. All the data are in Log Concentrations. Values of Si are equivalent to log $[H_4SiO_4]$.

	Clinoptilolite association 1	Phillipsite association 2	Palygorskite association 3	Paly + Clin association 4	Phill + Clin association 5	Phill + Clin + Paly association 6	Average sea water 7
Na^+	-0·353	-0·324	-0·198	-0·344	-0·328	-0·341	-0·336
K^+	-2·173	-1·985	-2·13	-3·16	-1·939	-1·959	-2·012
Ca^{2+}	-1·67	-1·944	-1·789	-2·42	-1·982	-1·974	-1·94
Mg^{2+}	-1·62		-1·387	-2·09	-1·276	-1·276	-1·28
Si	-3·325	-3·333	-3·55	-3·28	-3·373	-3·36	-4·087
pH	-7·05	-7·35	-7·35	-7·21	-7·59	-7·41	-8·10

1: from Boles and Wise (1978)
2: from Iijima (1978)
3: from Manheim et al. (1974b) and Gieskes (1974)
4: from Manheim et al. (1974a); Presley et al. (1974); Sandstrom et al. (1974); Waterman et al. (1972) and Waterman (1973); Presley et al. (1973).
5 & 6: from Brady et al. (1976)
7: Na^+ and K^+ as 1; Si as 2; pH from Glaccum et al.,(1976).

TABLE 6-2: Selected Values of Standard Gibbs Free Energy of Formation at 25°C and one atmosphere

Chemical Species	ΔG_f° (Kcal/mol)	Reference
$Al(OH)_3$	-274.20	Stumm et al. (1970)
$Fe(OH)_3$	-166.50	"
$Mg(OH)_2$	-202.12	"
$Ca(OH)_2$	-214.22	"
NaOH	-102.60	"
KOH	-114.6	"
H_2O	-56.69	"
H_4SiO_4 (amorphous)	-318.60	"
Na^+	-57.279	Krauskopf (1979)
K^+	-67.30	"
Mg^{2+}	-108.80	"
Ca^{2+}	-132·30	"

TABLE 6-3: Calculated free energies of MLIS by the Method suggested by Nriagu (1975)

Sample No.	Structural Formulae	ΔG_f^o (K cal/mol)
212/17cc	$(K_{0.06}\ Mg_{0.21})\ (Mg_{0.13}\ Fe^{+3}_{0.79}\ Al_{1.08})$ $(Al_{0.36}\ Si_{3.64})\ O_{11}$	-1142.79
212/18/1	$(K_{0.004}\ Mg_{0.20}\ Ca_{0.003})\ (Mg_{0.15}\ Fe^{3+}_{0.81}\ Al_{1.04})$ $(Al_{0.25}\ Si_{3.75})\ O_{11}$	-1135.88
212/18/2	$(K_{0.034}\ Mg_{0.17}\ Ca_{0.025})\ (Mg_{0.32}\ Fe^{3+}_{0.65}\ Al_{1.03})$ $(Al_{0.11}\ Si_{3.89})\ O_{11}$	-1149.16
212/23/5	$(K_{0.01}\ Mg_{0.16})\ (Mg_{0.32}\ Fe^{3+}_{0.64}\ Al_{1.04})$ $(Si_{4.00})\ O_{11}$	-1144.99
212/27/1	$(K_{0.10}\ Mg_{0.17}\ Ca_{0.08})\ (Mg_{0.20}\ Fe^{3+}_{0.61}\ Al_{1.19})$ $(Al_{0.40}\ Si_{3.60})\ O_{11}$	-1166.08
212/27/5	$(K_{0.05}\ Mg_{0.18})\ (Mg_{0.07}\ Fe^{3+}_{0.79}\ Al_{1.14})$ $(Al_{0.35}\ Si_{3.65})\ O_{11}$	-1140.51
212/35cc	$(K_{0.13}\ Mg_{0.12}\ Ca_{0.14})\ (Mg_{0.30}\ Fe^{3+}_{0.55}\ Al_{1.15})$ $(Al_{0.35}\ Si_{3.65})\ O_{11}$	-1176.24
213/11/5	$(Na_{0.01}\ K_{0.09}\ Mg_{0.12}\ Ca_{0.17})(Mg_{0.36}Fe^{3+}_{0.66}Al_{0.98})$ $(Al_{0.32}\ Si_{3.68})\ O_{11}$	-1164.27
239/16/3	$(K_{0.07}\ Mg_{0.15}\ Ca_{0.04})\ (Mg_{0.30}\ Fe^{3+}_{0.54}\ Al_{1.16})$ $(Al_{0.14}\ Si_{3.86})\ O_{11}$	-1164.41
246/10/2	$(K_{0.08}\ Mg_{0.34}\ Ca_{0.04})\ (Mg_{0.60}\ Fe^{3+}_{0.48}\ Al_{0.92})$ $(Al_{0.25}\ Si_{3.75})\ O_{11}$	-1184.48

/contd.over

TABLE 6-3 contd.

Sample No.	Structural Formulae	ΔG_f° (K cal/mol)
254/25/2	$(Na_{0.25}\ K_{0.07}\ Mg_{0.45}\ Ca_{0.15})(Mg_{0.70}Fe^{3+}_{1.02}Al_{0.28})$ $(Al_{0.81}\ Si_{3.19})\ O_{11}$	-1163·58
254/26cc (0·2-0·08)	$(Mg_{0.53}\ Ca_{0.05})\ (Mg_{0.41}\ Fe^{3+}_{0.86}\ Al_{0.73})$ $(Al_{0.76}\ Si_{3.24})\ O_{11}$	-1165·98
254/26cc (< 0·08)	$(K_{0.018}\ Mg_{0.48}\ Ca_{0.067})(Mg_{0.38}\ Fe^{3+}_{0.88}\ Al_{0.74})$ $(Al_{0.73}\ Si_{3.27})\ O_{11}$	-1162·35
254/27/3	$(Mg_{0.54})(Mg_{0.43}\ Fe^{3+}_{0.98}\ Al_{0.59})$ $(Al_{0.66}\ Si_{3.34})\ O_{11}$	-1147·44
254/28cc	$(Mg_{0.55}\ Ca_{0.002})\ (Mg_{0.47}\ Fe^{3+}_{0.89}\ Al_{0.64})$ $(Al_{0.65}\ Si_{3.35})\ O_{11}$	-1157·40
256/8/4	$(K_{0.079}\ Mg_{0.14}\ Ca_{0.008})(Mg_{0.30}\ Fe^{3+}_{0.41}\ Al_{1.29})$ $(Al_{0.08}\ Si_{3.92})\ O_{11}$	-1173·57
257/5/2	$(Na_{0.0019}\ K_{0.099}\ Mg_{0.15})(Mg_{0.21}Fe^{3+}_{0.60}Al_{1.19})$ $(Al_{0.17}\ Si_{3.83})\ O_{11}$	-1157·97
257/4/3	$(Na_{0.0013}\ K_{0.11}\ Mg_{0.13})(Mg_{0.18}\ Fe^{3+}_{0.63}\ Al_{1.19})$ $(Al_{0.20}\ Si_{3.80})\ O_{11}$	-1153·24
258/15/1	$(Mg_{0.14}\ Ca_{0.01})\ (Mg_{0.26}\ Fe^{+3}_{0.29}\ Al_{1.45})$ $(Al_{0.02}\ Si_{3.89})\ O_{11}$	-1181·95
258/17/2	$(K_{0.04}\ Mg_{0.06}\ Ca_{0.04})(Mg_{0.21}\ Fe^{3+}_{0.36}\ Al_{1.43})$ $(Al_{0.02}\ Si_{3.98})\ O_{11}$	-1168·84
258/22/4	$(K_{0.006}\ Mg_{0.11})\ (Mg_{0.14}\ Fe^{+3}_{0.27}\ Al_{1.59})$ $(Al_{0.07}\ Si_{3.93})\ O_{11}$	-1183·58

TABLE 6-4: Calculated Free Energies of Montmorillonite and MLIS from Literature

		ΔG_f^o (Kcal/mol)
Aberdeen mont.	$(Mg_{0.45}\ Fe^{3+}_{0.335}\ Al_{1.29})\ (Al_{0.18}\ Si_{3.92})\ O_{10}\ (OH)_2$	-1225.2^+ -1224.6^*
Mg mont	$(Mg_{0.29}\ Fe^{3+}_{0.22}\ Al_{1.71}\ Si_{3.81})\ O_{10}\ (OH)_2$	-1255.8^+ -1254.7^*
Ca mont	$Ca_{0.167}\ Al_{2.33}\ Si_{3.67}\ O_{10}\ (OH)_2$	-1279.2^+ -1280.8^*
Mixed layers 1/S having 60% smectite layers (Papavasiliou 1979)	$(Na_{0.025}\ K_{0.115}\ Ca_{0.155})_{0.297}\ (Mg_{0.21}Fe^{3+}_{0.535}Al_{1.125}Ti_{0.085})$ $(Al_{0.185}\ Si_{3.815})_4\ O_{10}(OH)_2$	Range -1211.66 to -1221.48
	$(Na_{0.065}\ K_{0.09}\ Ca_{0.2565})_{0.4115}\ (Mg_{0.162}\ Fe^{3+}_{0.56}\ Al_{1.04}\ Ti_{0.065})_{1.88}$ $(Al_{0.16}\ Si_{3.84})_4\ O_{10}\ (OH)_2$	
	$(Na_{0.035}\ Ka_{0.05}\ Ca_{0.11})_{0.195}\ (Mg_{0.155}\ Fe^{3+}_{0.445}\ Al_{1.315}\ Ti_{0.0485})_{1.965}$ $(Al_{0.1}\ Si_{3.90})_4\ O_{10}\ (OH)_2$	
Mont. Weaver & Beck (1977)	$X^{n+}_{0.35/n}\ (Mg_{0.25}\ Fe^{3+}_{0.30}\ Al_{1.45})\ (Al_{0.10}\ Si_{3.90})\ O_{10}\ (OH)_2$	-1246.88 Z_1 -1244.09 Z_2 -1248.17 Z_3

* Data from Nriagu (1975)
\+ Data from others quoted by Nriagu (1975)
X^{n+} refers to exchange cations: Na^+, Mg^{2+}, and Ca^{2+}
mont: montmorillonite

Z_1 Na mont
Z_2 Mg mont
Z_3 Ca mont

CHAPTER VII

CONCLUSION

The present study was concerned with the relationships and stabilities of zeolites (phillipsite and clinoptilolite), mixed-layer illite/smectite (MLIS) and palygorskite (paly) in deep-sea sediments. The combined chemical and mineralogical data of the whole rock and chemistry of the individual minerals were used to characterise their conditions of formation and inter-relations.

Plots of Ti versus Al, Fe/Ti versus Al/(Al+Fe+Mn) and Cr versus TiO_2 were used as indicators of the sediments source (Bostrom, 1971; Bostrom et al., 1973; and Couture, 1977b). These ratios indicated the contribution of terrigenous material (i.e. continental crust + shale, where continental crust consisted of basaltic and/or silicic volcaniclastics and ash), oceanic crust (tholeiitic and alkali basalts) and active ridge sediments (volcanic matter = VM). The log-log diagrams also showed the contribution of biogenic matter to the sediments. Times of both volcanism on land (eastern Africa, Madagascar, parts of India and Indonesian island arc) and activities on the spreading ridges (the Ninetyeast Ridge, Mid-Indian Ocean Ridge, Mozambique Ridge and Carlsberg Ridge) correlate well with the ages of the volcanic sediments.

Terrigenous material was mostly transported by river, although a significant aeolian contribution was possible in certain areas of the Indian Ocean. Aeolian input is possible from the desert regions of northern India and west Pakistan, Iran-Makran region, Arabian Peninsula and Somalia (Kolla et al., 1981). Kolla et al. (1973a) observed the influence of windborne volcanic material from the Indonesian island arc. They noticed the influence of the south-easterly winds on the southern part of the Wharton Basin extending somewhat west of the Ninetyeast Ridge, south of 15°C, which carry kaolinite-rich clays from the lateritic soils of western Australia.

The detrital group of minerals consisted of quartz, K-feldspar, plagioclase, kaolinite, chlorite, some dolomite, MLIS, illite and paly.

Biogenic silica consisted of radiolaria and small quantities of diatoms, and $CaCO_3$ consisted mainly of foraminifera and coccoliths. The authigenic

group of minerals were pyrite, some calcite and dolomite, zeolites (phillipsite and clinoptilolite), opal-CT, and some illite, MLIS and paly.

Pyrite formed authigenically; the reducing conditions being provided by the burial of organic matter.

The necessary Ca^{2+} for dolomite formation was obtained from biogenic $CaCO_3$, whereas Mg^{2+} was gained from altered basalt.

Phillipsite and clinoptilolite were the only zeolites present in the sediments. Although there were only 34 samples, they showed the following patterns. Phillipsite was dominant in brown clay, Miocene sediments and shallow depth (50 - 150m), whereas clinoptilolite was dominant in brown clay, Cretaceous sediments and in 200-250m and 500-550m sediment depths. Phillipsite was associated with Mn micro nodules, whereas clinoptilolite was associated with opal and opal-CT. MLIS was dominant in both types of sediments.

On the basis of the negative correlation of clinoptilolite with MLIS, with a high percentage of expandable layers,and B (biogenic silica, volcanic ash and opal-CT), a MLIS to clinoptilolite transformation was suggested. Silicic ash and basaltic volcaniclastics and ash were suggested as the main source for phillipsite formation. The chemistry of individual minerals showed that 82% of phillipsite contained Si/Al ratios between 2·5 and 2·8, and 80% of clinoptilolite contained Si/Al ratios between 4·5 and 5·5. Monovalent cations were in excess of divalent cations and most of them had K^+ as the dominant cation. The clinoptilolite was more siliceous than clinoptilolite from igneous and sedimentary rocks, and most of it had more alkalis than alkali -earths, except clinoptilolite associated with carbonates, which was rich in Ca^{2+}. Phillipsite had Si/Al ratios intermediate between phillipsite from mafic igneous rocks and phillipsite from saline lacustrine deposits. The majority had $K^+ > Na^+$, Ca^{2+} and Mg^{2+}.

Phillipsite-clinoptilolite association was observed only in two samples where MLIS with high percentage of expandable layers was the only clay mineral present. Clinoptilolite did not show any relation to MLIS in the presence of phillipsite. A phillipsite into clinoptilolite transformation was suggested, since phillipsite was observed in younger sediments and clinoptilolite in older sediments. The negative free energy

of this reaction indicated that clinoptilolite was the stable phase compared with phillipsite in pore waters. Such a transition was also suggested by Stonecipher (1976 and 1977) and Couture (1977b). Although this reaction is thermodynamically possible, it cannot be the only responsible factor for vertical stratification of oceanic zeolites because phillipsite and clinoptilolite appear in different lithologies and have different rates of sedimentation and paragenesis. Lisitsyna et al. (1978) believe that zeolite-forming processes in oceanic sediments are found to be closely associated with the global evolution of the oceans. According to them and Petzing et al. (1979), one of the reasons for vertical stratification of zeolites could be the change in pattern of global volcanicity with time, and consequent change in composition of the volcanic materials available for distribution within the ocean basins and margin. According to many authors (Wozel, 1959; Kennet et al., 1975b and Levitan et al., 1978), the maximum intensity of explosive andesitic volcanism took place in the last 2 million years, i.e. in Pleistocene and Upper Pliocene. Lisitsyna et al. (1978) believe that this is the stage of massive development of phillipsite in the oceans. They also believe that the wide development of clinoptilolite in the Cretaceous and Eocene corresponds to an epoch of intensive silica deposition in the oceans. According to them, the reason for the increased supply of silica into the oceans during this period has been associated by a few authors with volcanic activity (Kolla et al., 1973b), and another leading factor is considered to be change in the climate (Leclaire, 1974 and Nathan et al., 1977).

Authigenic MLIS, which was MLIS with a high percentage of expandable layers, was the result of alteration of volcaniclastics and ash. It is a dioctahedral variety with either Al^{3+} or Fe^{3+} as the dominant cation in the octahedral positions. It was associated with clinoptilolite, whereas detrital MLIS (low per cent expandable layer) was associated with paly or paly plus clinoptilolite.

An authigenic origin for paly was suggested where the following criteria were met:

a) remoteness of the sites of study from the lands rich in paly;

b) presence of volcanic material, Mg-bearing minerals or hydrothermal activity;

c) presence of hiatuses or existence of low sedimentation rates;

d) negative correlation with MLIS of detrital origin;

e) negative relation with clinoptilolite.

Almost all authigenic paly occurred in the Cretaceous to Eocene.

Paly octahedral sites contained one-third divalent and two-thirds trivalent cations. Mg content of the octahedral sheet was 2-5 times as abundant as in MLIS. It also showed lower Fe/(Al+Fe+Mn). The stability diagram showed that moderate to high pH and Mg^{2+}, and low to high Si activities are the necessary conditions for paly formation.

It is evident from the above observation that paly compared with MLIS requires an environment with higher Mg activities. This agrees well with the view of Bonatti et al. (1968). They believe that Mg released from volcanic glass is not a sufficient source for paly formation, and montmorillonite usually forms from volcanic glass on the ocean floor. Therefore, an additional source of Mg^{2+} besides volcanic glass is required. Sea-water could provide the extra Mg^{2+}. Almost all paly-bearing sediments were present below hiatuses or had slow sedimentation rates. Hiatuses resulted from bottom currents (Davies et al.,1975). According to Couture (1977a), the association with bottom current and hiatuses suggests that extended contact with sea-water may be helpful or even necessary for paly formation. However, paly from Site 211, which was located between basaltic basement and diabase sill on the top, might have formed by hydrothermal activity. Two samples from Site 245 (cores 6/2 and 5/3) showed high sedimentation rates and the absence of hiatuses. The necessary Mg could come from chlorite.

The necessity of an extra source of Mg for paly is also confirmed by the equilibrium state of MLIS-paly reaction. On burial, the Mg from sea-water is cut off, and thus the reaction reaches a state of equilibrium. Hydrothermal activity has also stopped at Site 211. According to Krauskopf (1979) the equilibrium state indicates that one of the substances involved in the reaction has been entirely used up. However, on burial, where higher silica is available, clinoptilolite could form. The free energy of such reaction is negative.

In the absence of detrital MLIS, MLIS of authigenic origin becomes a sink for Mg^{2+} released from the alteration of volcanic ash and on burial,

in the presence of silica, clinoptilolite could form.

The necessary silica for the above reactions is obtained from the dissolution of biogenic silica. Opal-CT, which is interlayer tridymite and cristobalite, also forms at the expense of biogenic silica. The necessary Mg^{2+} for its formation becomes available from either volcanic alteration or clinoptilolite forming reaction.

In summary, the following reactions are suggested:

In the absence of MLIS of detrital origin:

Mg-rich volcanic material transforms to MLIS of authigenic origin.

$$MLIS_{(authigenic)} + H_4SiO_4 \xrightarrow{\text{on burial}} \text{clinoptilolite} + Mg^{2+}$$

$$\text{phillipsite} + H_4SiO_4 \longrightarrow \text{clinoptilolite}.$$

In the presence of MLIS of detrital origin:

$$Mg^{2+} + H_4SiO_4 + MLIS_{(detrital)} \rightleftharpoons \text{paly}$$

$$\text{paly} + H_4SiO_4 \xrightarrow{\text{on burial}} \text{clinoptilolite} + Mg^{2+}.$$

Future research on these samples could usefully include combined isotopic and fully quantitative EDX analyses of the pure minerals. This treatment would give a better understanding and more complex picture of the genesis of zeolites and palygorskite.

BIBLIOGRAPHY

ARRHENIUS, G.O.S. (1952) Sediment cores from the East Pacific. Reports of the Swedish Deep-Sea Expedition 1947-48. V.Göteborgs Kungl. Veteskaps.-och Vitterhets - Samhälle, Göteborg.

ASTON, S.R., CHESTER, R., JOHNSON, L.R. and PADGHAM, R.C. (1973): Eolian dust from the lower atmosphere of China sea and sea of Japan. Mar.Geol., v:14, pp.15-28.

BAIG, M.A.A. (1982): The geochemistry and mineralogy of sediments of the Oxford Clay and Kellaways Formations from southern England. Unpublished Ph.D. Thesis, Southampton University.

BAQRI, S.R.H. (1976) The mineralogy and chemistry of some coals and associated sediments from the South Wales coalfield. Unpublished Ph.D. Thesis, Southampton University.

BARBI, N.C. (1981) P.G.T. internal publication.

BASS, M.N., MOBERLY, R. RHODES, J., CHI-YU SHIH and CHURCH, S. (1973) Volcanic rocks cored in the Central Pacific, Leg 17, Deep Sea Drilling Project. In: Initial Reports of Deep Sea Drilling Project, v:17. Washington (U.S.Government Printing Office), pp.429-503.

BELTAGY, A.I., CHESTER, R. and PADGHAM, R.C.P. (1972) The particle-size distribution of quartz in some North Atlantic deep-sea sediments. Mar.Geol., v:13, pp.297-310.

BERGER, W.H. and von RAD, U. (1972) Cretaceous and Cenozoic sediments from the Atlantic Ocean. Initial Reports of the Deep Sea Drilling Project, v:XIV. Washington (U.S.Government Printing Office) pp.

BERNER, R.A. (1964a) Iron sulphides formed from aqueous solution at low temperatures and atmospheric pressure. J.Geol.,v:72, pp.293-306.

_____ (1964b) Stability fields of iron minerals in anaerobic marine sediments. J.Geol., v:72, pp.826-834.

_____ (1970) Sedimentary pyrite formation. Am.J.Sci., v:268, pp.1-23.

BESAIRIE, H. (1972) Géologie de Madagascar, pt.35, Tananarive, Madagascar, pp.463.

BISCAYE, P.E.(1964) Distinction between Chlorite and Kaolinite in Recent sediments by X-ray diffraction. Am.Mineral, v:49, pp.1281-1289.

_____ (1965) Mineralogy and sedimentation of Recent deep sea clay in the Atlantic Ocean and adjacent seas and oceans. Bull.Geol.Soc.Am., v:76, pp.803-832.

BISCHOFF, J.L. and DICKSON, F.W. (1975) Sea water - basalt interaction at 200°C and 500 Bars: implications for origin of sea-floor - heavy metal deposits and regulation of sea water chemistry. Earth Planet.Sci.Letters, v:25, pp.385-397.

BOLES, J.R. (1972) Composition, optical properties, cell dimensions and thermal stability of some heulandite group zeolites. Am.Mineral., v:57, pp.1463-1493.

BOLES, J.R. and WISE, W.S. (1978) Nature and origin of deep-sea clinoptilolite. In: L.B. Sand and F.A. Mumpton (Editors): Natural Zeolites: Occurrence, Properties, Use. Pergamon: Oxford. pp.235-243.

BONATTI, E. (1963) Zeolites in Pacific pelagic sediments. N.Y.Acad.Sci.Trans., Ser.II, v:28, pp.938-948.

_____ (1965) Palagonite, hyaloclastites and alteration of volcanic glass in the ocean. Bull.Volcanol., v:29, pp.257-269.

BONATTI, E. and NAYUDU, Y.R. (1965) The origin of manganese nodules on the ocean floor. Am.J.Sci., v:263, pp.17-39.

BONATTI, E. and JOENSUU, O. (1968) Palygorskite from Atlantic deep sea sediments. Am.Mineral., v:53, pp.975-983.

BOSTROM, K. (1967) The problem of excess manganese in pelagic sediments. In: P.H. Abelson (Editor): Research in Geochemistry. New York: Wiley; London: Chapman & Hall.

_____ (1970) Submarine volcanism as a source for iron. Earth Planet Sci.Letters, v:9, pp.348-354.

BOSTROM, K. and PETERSON, M.N.A. (1969) The origin of aluminium-poor ferromanganon sediments in areas of high heat flow on the East Pacific Rise. Mar.Geol., v:7, pp.427-447.

BOSTROM, K., FARQUHARSON, B. and EYL, W. (1971) Submarine hot springs as a source of active ridge sediments. Chem.Geol.,v:10, pp.189-203.

BOSTROM, K. and FISHER, D.E. (1971) Volcanogenic uranium, vanadium and iron in Indian Ocean sediments. Earth Planet Sci.Lett.,v:11, pp.95-98.

BOSTROM, K., JOENSUU, O., VALDES, S. and RIERA, M. (1972) Geochemical history of south Atlantic Ocean sediments since late Cretaceous. Mar.Geol., v:12, pp.85-121.

BOSTROM, K., KRAEMER, T. and GARTNER, S. (1973) Provence and accumulation rates of opaline silica, Al, Ti, Fe, Mn, Cu, Ni, and Co in Pacific pelagic sediments. Chem.Geol.,v:11, pp.123-148.

BOSTROM, K., JOENSUU, O. and BROHM, I. (1974) Plankton: its chemical composition and its significance as a source of pelagic sediments. Chem.Geol., v:14, pp.255-271.

BOSTROM, K., JOENSUU, O., VALDES, S., CHARM, W. and GLACCUM, R. (1976) Geochemistry and origin of East Pacific sediments, sampled during D.S.D.P. Leg 34. Initial Reports of the Deep Sea Drilling Project, v:34. Washington (U.S. Government Printing Office), pp.559-574.

BOWLES, F.A., ANGINO, E.A., HOSTERMAN, J.W. and GALLE, O.K. (1971). Precipitation of deep-sea palygorskite and septilolite. Earth Planet.Sci.Letters, v:11, pp.324-332.

BRADLEY, W.F. (1940) Structure of attapulgite. Am.Mineral., v:25, pp 405-410.

BRADLEY, W.H. and BRAMLETTE, M. (1942) U.S. Geol.Survey Prof., Paper 196.

BRADY, S. and GIESKES, J.M. (1976) Interstitial water studies, Leg 34. In: Initial Reports of Deep Sea Drilling Project, v:34. Washington (U.S.Government Printing Office), pp.625-628.

BRAMLETT, M.N. and POSNJAK, E. (1933) Zeolitic alteration of pyroclasts. Am. Mineral., v:18, pp.167-171.

BREGER, I.A., CHANDLER, J.C. and ZUBOVIC, P. (1970) An infrared study of water in heulandite and clinoptilolite. Am.Mineral., v:55, p.825.

BROWN, D.A., CAMPBELL, K.S.W. and CROOK, K.A.W. (1968) The geological evolution of Australia and New Zealand. Oxford, Pergamon Press.

BURNS, R.E., ANDREWS, J.E., van der LINGEN, G.J. et al. (1973) Site Report. In: Initial Reports of the Deep Sea Drilling Project, v:21. Washington (U.S.Government Printing Office), pp.57-102.

BURSER, W and GRUTTER (1956) Schweiz . Min.Petrogr.Mitt., v:36, pp.49-62.

BURST, J.F. Jr. (1969) Diagenesis of Gulf Coast clayey sediments and its possible relation to petroleum migration. Bull.Am.Assoc. Petrol.Geologist., v:53, pp.73-93.

CALLEN, R.A. (1977) Late Cainozoic environments of part of north-eastern South Australia. J.Geol.Soc.Aust., v:24, pp.151-169.

CAILLERE, S. (1934) Observations sur la composition chimique des palygorskite. Compt.Rend., v:198, pp.1795-1798.

CAILLERE, S and HENIN, S. (1961) Palygorskite. In: G. Brown (Editor) The X-ray identification and crystal structures of clay minerals. London: Mineralogical Soc.

CALVERT, S.E. and PRICE, N.B. (1970) Composition of manganese nodules and manganese carbonates from Loch Fyne, Scotland. Cont.Mineral.and Petrol., v:29, pp.215-233.

CALVERT, S.E. (1974) Deposition and diagenesis of silica in marine sediments. Spec.Publs.Int.Ass.Sediment., v:1, pp.273-299.

CALVERT, S.E. (1976) The mineralogy and geochemistry of near-shore sediments. In: J.P. Riley and R. Chester (Editors) Chemical Oceanography. London Academic Press, v:6, p.235.

CALVERT, S.E. and PRICE, N.B. (1977) Shallow water, continental margin and lacustrine nodules. In: G.P.Glasby (Editor), Marine Manganese Deposits. Amsterdam: Elsevier, pp.45-86.

CARROLL, D. (1958) Role of clay minerals in the transportation of iron. Geochim Cosmochim Acta., v:14, pp.1-27.

CHANDLER, J.A. (1977) X-ray microanalysis in the electron microscope. North Holland Publishing Company: Amsterdam.

CHESTER, R. (1965) Element geochemistry of marine sediments. In: J.P. Riley and G. Shirrow (Editors) Chemical Oceanography. London Academic Press. v:2, pp.23-80.

CHESTER, R. and ASTON, S.R. (1976) The geochemistry of deep sea sediments. In: J.P. Riley and R. Chester (Editors) Chemical Oceanography. London Academic Press, v:6, pp.281-390.

CHOWDHURY, A.N. (1980) Geochemistry and sedimentology of the Corallian sediments of Southern England. Unpublished Ph.D. Thesis, University of Southampton.

CHRIST, C.L., HATHAWAY, J.C., HOSTETTLER, P.B. and SHEPARD, A.O. (1969) Palygorskite: new X-ray data. Am.Mineral., v:54, pp.198-205.

CHURCH, T.M. and VELDE, B. (1979) Geochemistry and origin of a deep-sea Pacific palygorskite deposit. Chem.Geol., v:25, pp.31-39.

CLARKE, F.W. (1924) Data of geochemistry. U.S.Geol.Surv.Bull., p.770.

CLARKE, F.W. and WHEELER, W.C. (1922) The inorganic constituents of marine invertebrates. U.S.Geol.Survey Prof.Paper 124.

CLARK, S.P. (1966) Composition of rocks. In: Handbook of Physical Constants, Clark, S.P. (ed.) (Geol.Soc.Amer.) pp.1-6.

CLAYTON, T. (1970) Program Factor and Grasp System. Department of Geology, University of Southampton.

COOK, H.E. and ZEMMELS, I. (1972) X-ray mineralogy studies - Leg 9. In: Initial Reports of the Deep Sea Drilling Project, v:9. Washington (U.S.Government Printing Office). pp.707-778.

CORRENS, C.W. (1937) Die sediments des aquatorialen Atlantichen ozeans. Berlin, Walter de Gruyter and Co.,Wiss. Ergeb., Deutsche Atlantische Exped. Meteor (1925-1927). Bd.3. Teil 3, pp.135-298.

_____ (1941) Akad. Wiss Göttingen, Math. Phys., Kl.5, p.219.

COSGROVE, M.E. (1972) The geochemistry of the Red beds of South-West England, including the Permian volcanics. Unpublished Ph.D. Thesis, Southampton University.

COSGROVE, M.E. and PAPAVASILIOU, C.T. (1979) Clinoptilolite in DSDP sediments of the Indian Ocean (Site 223, Leg 23): Its stability conditions and estimation of its free energy. Mar.Geol.,v:33, pp.77-84.

COUTURE, R.A. (1977a) Synthesis of some clay minerals at 25°C, Palygorskite and Sepiolite in the Ocean. Unpublished Ph.D. Thesis, Scripps Institution of Oceanography.

_____ (1977b) Composition and origin of palygorskite-rich and montmorillonite-rich zeolite-containing sediments from the Pacific Ocean. Chem.Geol., v:19, pp.113-130.

CRIDDLE, A.J. (1974) A preliminary description of microcrystalline pyrite from the nannoplankton ooze at Site 251, south-west Indian Ocean. In: Initial Reports of the Deep Sea Drilling Project, v:26. Washington (U.S.Government Printing Office),pp.603-607.

CRONAN, D.S. and TOOMS, J.S. (1967) Geochemistry of manganese nodules from the N.W. Indian Ocean. Deep Sea Res., v:14, pp.239-249.

CURRAY, J.R., EMMEL, F.J., MOORE, D.G. and RAITT, W.R. (1982) Structure, tectonics and geological history of the north-eastern Indian Ocean. In: A.E.M. Nairn and Stehli, F.G.(Editors) The Ocean Basins and Margins. New York: Plenum Press. v:6,pp.399-447.

DALY, R.A. (1925) The geology of Ascension Island. Am.Acad.Sci.Proc. v:60, pp.3-80.

DAVIES, D. (1968) When did the Seychelles leave India? Nature, v:220, pp.1225-1226.

DAVIES, T.A. and SUPKA, P.R. (1973) Oceanic sediments and their diagenesis: Some examples from deep sea drilling. J.Sed.Pet., v:43, pp.381-390.

DAVIES,T.A., LUYENDYK, B.P., RODOLFO, K.S., et al.(1974) Site Reports. In: Initial Reports of Deep Sea Drilling Project, v:26. Washington (U.S.Government Printing Office).

DAVIES, T.A., WESER, O.E., LUYENDYK, B.P. and KIDD, R.B. (1975) Unconformities in the sediments of the Indian Ocean. Nature, v:253, pp.15-19.

DAVIES, T.A. and GORSLINE, D.S. (1976) Oceanic sediments and sedimentary processes. In: J.P. Riley and R. Chester (Editors), Chemical Oceanography, London Academic Press, v:5.pp.47-63.

DEKIMPE, C.R., GASTUCHE, M.C. and BRINDLEY, G.W. (1961) Ionic coordination in alumino-silicic gels in relation to clay mineral formation. Am.Mineral., v:46, pp.1370-1381.

DE LA LAPPARENT, J. (1935) Attapulgite. C.R.Acad.Sci., Paris, v:201. pp.481-483.

DONNELLY, T.W. and WALLACE, J.L. (1976) Major and minor element chemistry of Antarctic clay-rich sediments: Sites 322, 323 and 325, D.S.D.P. Leg 35. In: Initial Reports of the Deep Sea Drilling Project, v:35. Washington (U.S.Government Printing Office) pp.427-446.

DONNELLY, T.W. (1977) Chemistry of Cenozoic sedimentation in the world oceans Geol.Soc.Amer.90th Ann.meet.Abstr.with programs,v:9,p.953.

DOUGLAS, R.G. and SAVIN, S.M.(1973) Oxygen and carbon isotope analyses of Cretaceous and Tertiary foraminifera from the central north Pacific. In: Initial Reports of the Deep Sea Drilling Project, v:17. Washington (U.S.Government Printing Office),pp.591-603.

DREVER, J.I. (1976) Chemical and mineralogical studies, Site 323. In: Initial Reports of the Deep Sea Drilling Project, v:35. Washington (U.S.Government Printing Office) pp.471-478.

DÜING, W. (1970) The monsoon regime of the currents in the Indian Ocean: Honolulu (East-West Cent.Press) p.68.

EDELMAN, C.H. and FAVEJEE, J.C.L. (1940) On the crystal structure of montmorillonite and halloysite.Z.Kristallogr.,v:102,pp.417-431.

ELDERFIELD, H. (1976) Hydrogenous material in marine sediments, excluding manganese nodules. In: J.P.Riley and R.Chester (Editors) Chemical Oceanography. London Academic Press,v:5,pp.137-215.

ELPRINCE, A.M., MASHHADY, A.S. and ABAHUSYNE, M.M. (1979) The occurrence of pedogenic palygorskite to Saudi Arabia.Soil Sci.,v:128,p.211.

EL-SHAHAT, A. (1977) Petrography and geochemistry of a limestone-shale sequence with early and late lithification: the middle Purbeck of Dorset, England. Unpubl.Ph.D.Thesis, University of Southampton.

EL-WAKEEL, S.K. and RILEY, J.P. (1961) Chemical and mineralogical studies of deep sea sediments. Geochim.Cosmochim.Acta.,v:25,pp.110-146.

ENGEL, A.E.J.,ENGEL, C.G. and HAVENS, R.G.(1965) Chemical characteristics of oceanic basalts and the upper mantle. Bull.Geol.Soc.Amer., v:76, pp.719-734.

ENGEL, A.E.J., and ENGEL, C.G. (1970) Mafic and ultramafic rocks. The Sea, v:4, pp.465-519.

ERNEST, W.G. and CALVERT, S.E. (1969) An experimental study of the recrystallization of porcelanite and its bearing on the origin of some bedded cherts. J.Am.Sci.,v:267A, pp.114-133.

ESLINGER, E.V. and SAVIN, S.M. (1976) Mineralogy and O^{18}/O^{16} ratios of fine-grained quartz and clay from Site 323. In: Initial Reports of the Deep Sea Drilling Project, v:35. Washington (U.S.Government Printing Office),pp.489-496.

FALVEY, D.A. (1972) Sea-floor spreading in the Wharton Basin (north-east Indian Ocean) and the break up of eastern Gondwanaland. Aust.Petrol.Exlp.Assoc.J., v:12, pp.86-88.

FERSMANN, A. (1913) Research on magnesian silicates. Mem.Acad.Sci.St.Petersb. v:32, pp.321-430.

FISHER, R.L., BUNCE, E.T., CERNOCK, P.J. et al. (1974) Site Reports. In: Initial Reports of Deep Sea Drilling Project,v:24.Washington (U.S.Government Printing Office).

FITZPATRICK, E.A. (1971) Pedology: a systematic approach to soil science. Oliver & Boyd.

FLEET, A.J. and KEMPE, D.R.C. (1974) Preliminary geochemical studies of the sediments from D.S.D.P., Leg 26, Southern Indian Ocean. In: Initial Reports of Deep Sea Drilling Project, v:26. Washington (U.S.Government Printing Office),pp.541-551.

FLORES, G. (1970) Suggested origin of the Mozambique Channel. Geol.Soc.Africa Trans., v:73, pp.1-16.

FLÖRKE, O.W. (1955) Zur Frage des 'Hoch'. Cristobalites in opalen, Bentoniten und Gläsern. Neues Jb. Miner.Mh., v:10, pp.217-233.

FRAKES, L. and KEMP, E. (1972) Influence of continental positions on early Tertiary climates. Nature, v:240, pp.97-100.

FRENCH, J.W. and ADAMS, J.S. (1972) A rapid method for the extraction and determination of Fe^{2+} in silicate rocks and minerals. Analyst, v:97, pp.828-831.

FÜCHTBAUER, H. and MULLER, G. (1970) Sedimente und sedimentgesteine, p.726. Schweizerbart-verlag, Stuttgart.

FURBISH, W.J. and SAND, T.W. (1976) Palygorskite - by direct precipitation from a hydrothermal solution. Clay Minerals, v:11, p.149.

GARRELS, R.M. (1960) Mineral equilibria. New York: Harper and Bros., p.254.

GARRELS, R.M. and CHRIST, C.L. (1965) Solutions, Minerals and Equilibria. New York: Harper and Row.

GARRISON, R.E., HEIN, J.R. and ANDERSON, T.F. (1973) Lithified carbonate sediment and zeolitic tuff in basalts, Mid-Atlantic Ridge. Sedimentology, v:20, pp.399-410.

GAST, G. (1977) Surface and colloid chemistry. In: Minerals in Soil Environments. (Soil Science Society of America) Dixon, J.B. and Weed, S.B. (Editors)

GIBBS, B.J. (1967) The geochemistry of the Amazon River system; Part I. The factors that control the salinity and the composition and concentration of the suspended solids. Geol.Soc.Amer.Bull., v:78(10), p.1203.

GIESKES, J.M. (1974) Interstitial water studies, Leg 25. In: Initial Reports of Deep Sea Drilling Project, v:25. Washington (U.S.Government Printing Office). pp.361-394.

GIESKES, J.M., KASTNER, M. and WARNER, T.B. (1975) Evidence for extensive diagenesis, Madagascar Basin, Deep Sea Drilling Site 245. Geochim.Cosmochim.Acta., v:39, pp.1385-1393.

GILL, E.D. (1961) The climates of Gondwanaland in Kainozoic times. In: A.E.M. Nairn (Editor) Descriptive Palaeoclimatology. pp.332-354.

GIRDLEY, W.A. and WHITE, S.M. (1974) Preliminary study of terrigenous minerals: light and heavy mineralogy of selected cores, Deep Sea Drilling Project Leg 25. In: Initial Reports of the Deep Sea Drilling Project, v:25. Washington (U.S. Government Printing Office), pp.431-439.

GLACCUM, R. and BOSTROM, K. (1976) (Na,K) phillipsite: its stability conditions and geochemical role in the deep sea. Mar.Geol., v:21, pp.47-58.

GOLDBERG, E.D. and ARRHENIUS, G. (1958) Chemistry of Pacific Pelagic sediments. Geochim.Cosmochim.Acta. v:13, pp.153-212.

GOLDBERG, E.D. (1961) Chemical and mineralogical aspects of deep sea sediments. In: Ahrens, L.H. and Runcorn, S.K. (Editors) Physics and Chemistry of the Earth. v:4. Pergamon Press: Oxford. pp.281-302.

GOLDBERG, E.D. and GRIFFIN, J.J. (1970) The sediments of the northern Indian Ocean. Deep Sea Res., v:17, pp.513-537.

GOLDSCHMIDT,V.M. (1937) The principles of distribution of chemical elements in minerals. J.Chem.Soc., pp.635-673.

GOLDSCHMIDT, V.M. (1954) Geochemistry. Oxford University Press.

GOODEL, H.G. (1973) Sediments. Am.Geog.Soc. Antarct.Map Ser., Folio 17.

GORBUNOVA, Z.N. (1966) Clay mineral distribution in Indian Ocean sediments (English translation). Oceanology, v:6, pp.215-221.

GOTTARDI, G. (1978) Mineralogy and crystal chemistry of zeolites. In: L.B. Sand and F.A. Mumpton (Editors), Natural Zeolites: Occurrence, Properties, Use. Pergamon: Oxford. pp.235-243.

GRIFFINE, J.J., WINDOM, H.L. and GOLDBERG, E.D. (1968) The distribution of clay minerals in the world oceans. Deep Sea Res.,v:15, pp.433-459.

GRIM, R.E. (1953) Clay mineralogy. New York:McGraw-Hill Book Co.

GRIM, R.E. and GÜVEN, N. (1978) Bentonite Geology, Mineralogy, Properties and Uses. Amsterdam: Elsevier.

GREENE-KELLY, R. (1955) Dehydration of the montmorillonite mineral. Mineral. Mag., v:30, pp.604-615.

HANSHAW, B.B., BACK, W. and DEIKE, R.G. (1971) A geochemical hypothesis for dolomitization by ground water. Econ.Geol. v:66, pp.710-724.

HARDER, H. (1972) The role of magnesium in the formation of smectite minerals. Chemical Geol., v:10, pp.31-39.

HART, R.A. (1970) Chemical exchange between sea water and deep ocean basalt. Earth Planet.Sci.Lett., v:9, pp.269-279.

HASSOUBA, H. and SHAW, H.F. (1980) The occurrence of palygorskite in Quaternary sediments of the coastal plain of north-west Egypt. Clay Minerals, v:15, pp.77-83.

HATHAWAY, J.C. and SACHS, P.L. (1965) Sepiolite and clinoptilolite from the Middle Atlantic Ridge. Am.Min., v:50, pp.852-867.

HATHAWAY, J.C., McFARLIN, P.F. and ROSS, D.A. (1970) Mineralogy and origin of sediments from drill holes on the continental margin off Florida. Geological Survey Professional Papers, 581-E.

HAWKINS, D.B. and ROY, R. (1963) Experimental hydrothermal studies on rock alteration and clay mineral formation. Geochim. Cosmochim. Acta., v:27, pp.1047-1054.

HAY, R.L. (1966) Zeolites and zeolitic reactions in sedimentary rocks. Geol.Soc.Amer. Spec.Paper 85.

_____ (1978) Geologic occurrence of zeolites. In: L.B. Sand and F.A. Mumpton (Editors) Natural Zeolites: occurrence, properties, use. Pergamon: Oxford. pp.135-144.

HAYES, J.B. (1973) Petrology of indurated sandstones, Leg 18, Deep Sea Drilling Project. In: Initial Report of Deep Sea Drilling Project, v:18. Washington (U.S.Government Printing Office), pp.903-

HAYES, D.E. and RINGIS, J. (1973) Sea floor spreading in the Tasman Sea. Nature, v:243, pp.454-458.

HEATH, G.R. and MOBERLY, R.J.E. (1971) Cherts from the Western Pacific, Leg 7, Deep Sea Drilling Project. In: Initial Reports of the Deep Sea Drilling Project, v:7(VII). Washington (U.S. Government Printing Office), pp.991-1007.

HEEZEN, B.C. and HOLLISTER, C.D. (1964) Deep Sea current evidence from abyssal sediments. Mar.Geol., v:1, pp.141-174.

HEEZEN, B.C. and THARP, M. (1965) Physiographic diagram of the Indian Ocean (with descriptive sheet). New York. (Geol.Soc.Am.)

HEEZEN, B.C., NESTEROFF, W.D.A., OBERLIN, A. and SABATIER, G. (1965) Decouverte d'attapulgite dans les sediments profonds du Golf d'Aden et de la Mer Rogue. C.r-hebd. Sean,Acad.Sci., Paris, v:260, pp.2819-2821.

HEEZEN, B.C. and HOLLISTER, C.D. (1971) Face of the Sea. Oxford University Press; New York.

HEIN, J.R. and SCHOLL, D.W.(1978) Diagenesis and distribution of late Cenozoic volcanic sediment in the Southern Bering Sea. Geol.Soc.Am.Bull., v:89, pp.197-210.

HEIRTZLER, J.R., DICKSON, G.O., HERRON, E.M., PITMAN, W.C. and LEPICHON, X. (1968) Marine magnetic anomalies, geomagnetic field reversals, motions of the ocean floor and continents, J.Geophys.Res., v:72, pp.2119-2136.

HEIRTZLER, J.R. and BURROUGHS, R. (1971) Madagascar's palaeo-position new data from the Mozambique Channel. Science, v:174, pp.488-490.

HEKININ, R. (1968) Rocks from the mid-ocean ridge in the Indian Ocean. Deep Sea Res., v:15, pp.195-213.

HELGESON, H.C., BROWN, T.H. and LEEPER, R.H. (1969) Handbook of theoretical activity diagrams depicting chemical equilibria in geologic systems involving an aqueous phase at one atm. and 0°C to 300°C. Freeman, Cooper and Company, San Francisco.

HENDRICKS, S.B. and TELLER, E. (1942) X-ray interference in partially ordered layer lattice. J.Chem.Phys., v:10, pp.147-167.

HESS, P.C. (1966) Phase equilibria of some minerals in the K_2O - Na_2O - Al_2O_3 - SiO_2 - H_2O system at 25°C and 1 atmosphere. Am.J.Sci., v:264, pp.289-309.

HEYSTEK, H. and SCHMIDT, E.R. (1954) Palygorskite from Dornboom. Trans.Geol.Soc.S.Afr., v:56, pp.99-115.

HIRST, D.M. (1962) The geochemistry of modern sediments from the Gulf of Paria. I. The relationship between the mineralogy and the distribution of major elements. II. Location and distribution of trace elements. Geochim.Cosmochim.Acta, v:26,pp.1147-

_____ (1974) Geochemistry of sediments from Black Sea cores. In: Degens, E.T. and Ross, D.A. (Editors) The Black Sea: Geology, Chemistry and Biology. Am.Assoc.Petrol.Geol.Mem., v:20, pp.430-455.

HOFMANN, U., ENDELL, K. and WILM, D. (1933) Kristallstrukture und Quellung von Montmorillonite. Zeischer. Krist, v:86, pp.340-348.

HONNOREZ, J. (1978) Generation of phillipsites by palagonitization of basaltic glass in sea water and the origin of K-rich deep sea sediments. In: L.B. Sand and F.A. Mumpton (Editors) Natural Zeolites: Occurrence, Properties, Use. Pergamon: Oxford. pp,245-248.

HONNOREZ, J., BOHLKE, J.K., HONNOREZ, B.M. and PETERSON, N. (1979) Correlation between the changes in the mineralogy, chemistry and magnetic properties of basalts from DSDP Leg 46 with low temperature submarine alteration. In: Initial Reports of the Deep Sea Drilling Project, v:46. Washington (U.S.Government Printing Office), pp.371-

HOWER, J. and MOWATT, T.C. (1966) The mineralogy of illites and mixed layer illite-montmorillonite. Am.Mineral.,v:51, pp.825-854.

HOWER, J. (1967) Order of mixed-layering in illite/montmorillonites. Clays and Clay Miner.,Proc., v:15, pp.63-74.

HUGGINS, C.W., DENNY, M.V. and SHELL, H.R. (1962) Properties of palygorskite, an abestiform mineral. U.S.Bur.Mines, Rept.Invest., v:6071, p.8.

HURD, D.C. (1973) Interactions of biogenic opal, sediment and sea water in the central equatorial Pacific. Geochim.Cosmochim. Acta., v:37, pp.2257-

HURLBUT, J.R. and KLEIN, C. (1977) Manual of mineralogy (19th ed.) John Wiley & Sons: New York.

IIJIMA, A. (1978) Geological occurrences of zeolite in marine environments. In: L.B. Sand and F.A. Mumpton (Editors) Natural Zeolites: Occurrence, Properties, Use. Pergamon: Oxford. pp.175-198.

IRWIN, H. (1980) Early diagenetic carbonate precipitation and fluid migration in the Kimmeridge clay of Dorset, England. Sedimentology, v:27, pp.577-591.

ISPHORDING, W.C. (1973) Discussion of the occurrence and origin of sedimentary palygorskite-sepiolite deposits. Clay and Clay Minerals, V:21, pp.391-401.

JACKSON, M.L. (1956) Soil chemical analysis - Advanced course. Madison,Wis.: University of Wisconsin, Dept.of Soils.

JEDWAB, J. (1967) Mineralization engreigite de debris vegetaux d'une vase recent (Grote Geul). Soc.Belge geologie Bull.,v:76, pp.1-19.

JOHNSON, D.A. (1974) Radiolaria from the eastern Indian Ocean, DSDP Leg 22. In: Initial Reports of Deep Sea Drilling Project. v:22. Washington (U.S.Government Printing Office), pp.521-575.

JOHNSON, B.D., POWELL, C.McA and VEEVERS, J.J. (1976) Spreading history of the eastern Indian Ocean anddgreater India's northward flight from Antarctica and Australia. Geol.Soc.Am.Bull., v:87, pp.1560-1566.

KAPLAN, I.R., EMERY, K.O. and RITTENBENBERG, S.C.(1963) The distribution and isotopic abundance of sulphur in recent marine sediments off southern California. Geochim.Cosmochim.Acta., v:27, pp.297-332.

KASTNER, M., KEEN, J.B. and GIESKES, J.M. (1977) Diagenesis of siliceous oozes. I. Chemical controls on the rate of opal-A to opal-CT transformation - an experimental study. Geochim. Cosmochim.Acta., v:41, pp.1041-1059.

KASTNER, M. and STONECIPHER, S.A. (1978) Zeolites in pelagic sediments of the Atlantic, Pacific and Indian Oceans. In: L.B.Sand and F.A. Mumpton (Editors) Natural Zeolites: Occurrence, Properties, Use. Pergamon: Oxford, pp.199-220.

KASTNER, M. (1979) Zeolites. In: Buris, R.G. (Editor) Marine Minerals. Miner.Soc.of Am., v:6, pp.111-123.

KENNETT, J.P., HOUTZ, R.E., ANDREW, P.B., EDWARDS, A.R. et al.(1974) Development of the circum-Antarctic current. Science, v:186, pp.144-147.

KENNETT, J.P., HOUTZ, R.E., ANDREW, P.B., EDWARDS, A.R. et al.(1975a) Cenozoic palaeoceanography in the south-west Pacific Ocean, Antarctic glaciation, and the development of the Circum-Antarctic Current. In: Initial Reports of the Deep Sea Drilling Project, v:29. (U.S. Government Printing Office: Washington), pp.1155-1169.

KENNETT, J.P. and THUNNEL, R.C. (1975b) Global increase in Quaternary explosive volcanism. Science, v:187, pp.497-502.

KENNETT, J.P. and WATKINS, N.D. (1975) Deep sea erosion and manganese nodule development in the south-east Indian Ocean. Science, v:188, pp.1011-1013.

KENNETT, J.P. and WATKINS, N.D. (1976) Regional deep sea dynamic process recorded by late Cenozoic sediments of the south-eastern Indian Ocean. Geol.Soc.Am.Bull., v:87, pp.321-339.

KIDD, R.B. and DAVIES, T.A. (1978) Indian Ocean sediment distributions since the late Jurassic. Mar.Geol.,v:26, p.4970.

KING, L.C. (1961) The climates of Gondwanaland in Kainozoic times. In: Nairn, A.E.M. (Editor), Descriptive Palaeoclimatology

KOLLA, V. and BISCAYE, P. (1973a) Clay mineralogy and sedimentation in the eastern Indian Ocean. Deep Sea Res., v:20, pp.727-738.

KOLLA, V. and BISCAYE, P. (1973b) Deep sea zeolites: variations in space and time in sediments of the Indian Ocean. Mar.Geol., v:15, pp.11-17.

KOLLA, V. (1974) Mineralogical data from Sites 211, 212, 213, 214, 215 of Deep Sea Drilling Project Leg 22, and origin of non-carbonate sediments in the equatorial Indian Ocean. In: Initial Reports of Deep Sea Drilling Project, v:22, Washington (U.S.Government Printing Office). pp.489-501.

KOLLA, V., HENDERSON, L. and BISCAYE, P.E. (1976) Clay mineralogy and sedimentation in the Western Indian Ocean. Deep Sea Res., v:23, pp.949-961.

KOLLA, V., KOSTECKI, J.A., ROBINSON, F. et al. (1981) Sediments of region of clay minerals and quartz in surface sediments of the Arabian Sea. J.Sed.Pet., v:51, pp.563-569.

KRAUSKOPF, K.B. (1956) Factors controlling the concentrations of thirteen rare metals in sea-water. Geochim.Cosmochim.Acta, v:9, pp.1-32B.

_____ (1967) Introduction to Geochemistry. McGraw-Hill, New York.

KRAUSKOPF, K.B. (1979) Introduction to Geochemistry. McGraw-Hill, New York.

KURBATOV, M.H., WOOD, G.B. and KURBATOV, J.D. (1951) Isothermal adsorption of cobalt from dilute solutions. J.Phys.Colloid Chem., v:55, pp.1170-1182.

LANCELOT, Y. (1973) Chert and silica diagenesis on sediments from the Central Pacific. In: Initial Reports of Deep Sea Drilling Project., v:17. Washington (U.S. Government Printing Office)

LANDERGREN, S. (1964) On the geochemistry of deep sea sediments. Reports of the Swedish Deep Sea Expedition, X, Spec. Investig., v:5, ppl-154.

LARSON, R.L. (1975) Late Jurassic sea-floor spreading in the eastern Indian Ocean. Geology, v:3, pp.69-71.

LARSON, R.L. and HILDE, T.W.C. (1975) A revised time scale of magnetic reversals for the Wharton Basin near the Investigator Fracture Zone. J.Geophys.Res., v:83, pp.773-782.

LARSON, R.L., CARPENTER, G.B. and DIEBOLD, J.B. (1978) A geophysical study of the Wharton Basin near the Investigator Fracture Zone. J.Geophys.Res., v:83, pp.773-782.

LAUGHTON, A.S. MATTHEWS, D.H. and FISHER, R.L. (1971) In: A.E.Maxwell (Editor), The Sea, v:4, Part II, pp.543-586. Interscience Publishers, New York.

LECLAIRE, L. (1974) Late Cretaceous and Cenozoic pelagic deposits. Palaeoenvironment and palaeo-oceanography of the central western Indian Ocean. In: Initial Reports of the Deep Sea Drilling Project, v.25. Washington (U.S.Government Printing Office), pp.418-512.

LEPICHON, X. (1960) The deep sea circulation in the south west Indian Ocean. J.Geophys.Res., v:65, pp.4061-4074.

LEVITAN, M.A. and LISITSYN, A.P. (1978) Distribution of ash beds in the sediments of the Pacific Ocean. Dokl.Akad.Nauk SSSR, v:24.

LISITIZIN, A.P. (1972) Sedimentation in the world oceans. Spec.Pub. Tulsa Soc.Econ.Palaeontol.Mineral. v:17, p.218.

LISITSYNA, N.A. and BUTUZOVA, G.Yu (1978) Authogenic zeolites in oceanic sediments. Lithology and Mineral Resources, v:13, pp.663-671.

LISITZINA, N.A. and BUTUZOVA, G.Yu (1982) Authigenic zeolites in the sedimentary mantle of the world oceans. Sed.Geol., v.31, pp.33-41.

LOMOVA, O.S. (1975) Abyssal palygorskite clays of the eastern Atlantic and their genetic relation to alkalic volcanism (from data of Legs II and XIV of the Glomar Challenger). Lithology and Mineral Resources, v.10, pp.415-430.

LONSDALE, P., NORMARK, W.R. and NEWMAN, W.A. (1972) Sedimentation and erosion on Horizon Guyot. Geol.Soc.Am.Bull., v:83, pp.289-316.

LYNN, D.C. and BONATTI, E.D. (1965) Mobility of manganese in diagenesis of deep sea sediments. Mar.Geol., v:3, pp.457-474.

LUYENDYK, B.P. (1974) Gondwanaland dispersal and the early formation of the Indian Ocean. In: Initial Reports of the Deep Sea Drilling Project, v:26. Washington (U.S.Government Printing Office) pp.945-952.

LUYENDYK, B.P. and DAVIES, T.A. (1974) Results of DSPP Leg 26, and the geologic history of the southern Indian Ocean. In: Initial Reports of the Deep Sea Drilling Project, v:26. Washington (U.S.Government Printing Office), pp.909-948.

MACKENZIE, R.C. (1954) Free iron-oxide removal from soils. J.Soil Sci., v:5. pp.107-109.

MACKENZIE, F.T. and GARRELS, R.M. (1966) Silicon-bicarbonate balance in the ocean and early diagenesis. J.Sediment.Petrol.,v:36, pp.1075-1084.

MALLIK, T.K. (1974) Heavy mineral studies of samples from deep sea drill cores of Sites 223 and 224, Leg 23. In: Initial Reports of Deep Sea Drilling Project, v:23. Washington (U.S.Government Printing Office), pp.497-502.

MANHEIM, F.T., SAYLES, F.L. (1971) Interstitial water studies on small core samples, Deep Sea Drilling Project Leg 8. In: Initial Reports of the Deep Sea Drilling Project, v:8. Washington (U.S.Government Printing Office) pp.857-872.

MANHEIM, F.T. and SAYLES, F.L. (1974) Brines and interstitial brackish water in drill cores from the deep Gulf of Mexico. Science, v:170, pp.57-60.

MANHEIM, F.T., WATERMAN, L.S and SAYLES, F.L. (1974a) Interstitial water studies on small core samples, Leg 22. In: Initial Reports of the Deep Sea Drilling Project, v:22. Washington (U.S.Government Printing Office) pp.657-670.

MANHEIM, F.T., WATERMAN, L.S., CHING CHANG WOO and SAYLES, F.L. (1974b) Interstitial water studies on small core samples, Leg 23 (Red Sea). In: Initial Reports of the Deep Sea Drilling Project, v.23. Washington (U.S.Government Printing Office) pp.955-967.

MANHEIM, F.T. (1976) Interstitial waters of marine sediments. In: J.P. Riley and R. Chester (Editors) Chem.Ocean.,v:6, pp.115-186.

MANSFIELD, G.R. (1940) The role of flourine in phosphate deposition. Am.J.Sci.,v:238, pp.863-879.

MARGOLIS, S.V. and KENNETT, J.P. (1970) Antarctic glaciation during the Tertiary: recorded in sub-Antarctic deep sea cores. Science, v:170, p.1085-

MARINER, R.H. and SURDAM, R.C. (1970) Alkalinity and formation of zeolites in saline alkaline lakes. Science, v:170,pp.977-980.

MARKLE, R.G. (1978) Further evidence for the early Cretaceous break up of Gondwanaland off south-western Australia. Mar.Geol., v.26, pp.41-48.

MARSHALL, C.E. (1935) Layer lattices and base exchange clays. Z.Krist., v:91, pp.433-449.

MARSHALL, B.V. and ERICKSON, A.J. (1974) Heat flow and thermal conductivity measurements, Leg 25, Deep Sea Drilling Project. In: Initial Reports of the Deep Sea Drilling Project, v:25. Washington (U.S.Government Printing Office) pp.357-360.

MASON, B. (1966) Principles of Geochemistry. J. Wiley & Son: New York.

MATHER, P.M. (1970) Principal components and Factor Analysis. Dept.of Geography, University of Nottingham.

MATTER, A. (1974) Burial diagenesis of pelitic and carbonate deep sea sediments from the Arabian Sea. In: Initial Reports of the Deep Sea Drilling Project, v.23. Washington (U.S.Government Printing Office), pp.421-469.

MATTI, J.C., ZEMMELS, I. and COOK, H.E. (1974) X-ray mineralogy data, north-eastern part of the Indian Ocean, Leg 22, Deep Sea Drilling Project, In: Initial Reports of Deep Sea Drilling Project, v.22. Washington (U.S.Government Printing Office) pp.693-710.

MATTI, J.C., ZEMMELS, I. and COOK, H.E. (1973) X-ray mineralogy of sediments from the far western Pacific, Leg 20, DSDP. In: Initial Reports of Deep Sea Drilling Project, v:20. Washington (U.S.Government Printing Office). pp.323-334.

McELHINNY, M.W. (1970) Formation of the Indian Ocean. Nature, v:228, pp.977-979.

McGOWRAN, B. (1978) Stratigraphic records of early Tertiary oceanic and continental events in the Indian region. Mar.Geol., v:26, pp.1-39.

McKENZIE, D. and SCLATER, J.G. (1971) The evolution of the Indian Ocean since the late Cretaceous. Geophys. J.R.Astron.Soc.,v:25, pp.437-528.

MELIERES, F. (1978) X-ray mineralogy studies, Leg 41, Deep Sea Drilling Project, eastern north Atlantic Ocean. In: Initial Reports of the Deep Sea Drilling Project, v:41. Washington (U.S. Government Printing Office).

MERKLE, A.B. and SLAUGHTER, M. (1968) Determination and refinement of the structure of heulandite. Am.Mineral.,v:53, pp.1120-1138.

MERO, J.L. (1960) Minerals on the ocean floor. Sci.Am., v:203, pp.64-72.

MILLIMAN, J.D. and MULLER, J. (1973) Precipitation and lithification of magnesian calcite in the deep sea sediments of eastern Mediterranean Sea. Sedimentology, v:20, pp.29-45.

MILLIMAN, J.D. (1974) Marine carbonates. Springer-Verlag, Berlin: Heidelberg: New York.

MILLOT, G.H., PAQUET, H. and RUELLAN, A. (1969) Neoformation de l'attapulgite dans les sols a carpaces calcaires de la Basse Moulouya (Maroc oriental). Pedologie, v:268,pp.2771-2774.

MOHR, C.J. and van BAREN, F.A. (1954) Tropical soils. New York: Interscience Pub.

MOORE, J.G. (1966) Rate of palagonization of submarine basalt adjacent to Hawaii. In: Geological Survey Research, 1966. U.S.Survey Prof.Pap. 550-D, D163-D171.

MORGAN, W.J. (1972) Deep mantle convection plumes and plate motions. Bull.Amer.Assoc.Petrol.Geol., v:56, pp.203-213.

MORGENSTEIN, M.M. (1967) Authigenic cementation of scoriaceous deep-sea sediments west of the Society Ridge, South Pacific. Sedimentology, v:9, pp.105-118.

MUIR, A. (1951) Notes on Syrian soils. J.Soil Sci.,v:2,pp.163-183.

MULLER, G. (1961) Palygorskite und sepiolite in Tertiaren und Quartaren sediment von Hadramawt (S.Arabian). Oceanology, v:18, pp.177-180.

MUMPTON, F. and ORMSBY, W.C. (1976) Morphology of zeolites in sedimentary rocks by scanning electron microscopy. Clays and Clay Minerals, v:24, pp.1-23.

MUMPTON, F.A. and ORMSBY, W.C. (1978) Morphology of zeolites in sedimentary rocks by Scanning Electron Microscopy. In: L.B. Sand and F.A. Mumpton (Editors) Natural Zeolites, Occurrence, Properties, Use. Pergamon: Oxford. pp.113-132.

MURRAY, J. and RENARD, A.F. (1891) Report on the Scientific Results of the Voyage of 'H.M.S. Challenger' during the years 1873-76; Deep Sea Deposits. Johnson Reprint Co., London. p.525.

NATHAN, Y., BENTOR, V.K. and WURZBURGER, U. (1970) Vein palygorskites in Israel and Sinai: their origin and symmetry. Israel Chem. v:9, pp.469-476.

NATHAN, Y. and FLEXER, A. (1977) Clinoptilolite Paragenesis and Stratigraphy. Sedimentology, v:24, pp.845-855.

NELSON, B.W. and ROY, R. (1954) In: A. Swinefor and N.Y. Plummer (Editors) Clays and Clay Minerals, Proc.2nd Conf. Pergamon Press: Oxford. p.334.

NICHOLLS, G.D., CURL, H. and BOWEN, V.T. (1959) Oceanogr., v:4, p.472.

NRIAGU, J.O. (1975) Thermochemical approximations for clay minerals. Am. Mineral., v:60, pp.834-839.

OGAWA, T. (1967) On the varieties of heulandite. J.Sci. Hiroshima Univ., Japan. v:5, pp.267-285.

OSTROUMOV, E.A. (1953) Different forms of combined sulphur in the sediments of the Black Sea. Akad.Nauk SSSR, Inst.Okeanologii Trudy, v:7, pp.70-90.

OVCHARENKO, F. (1964) The colloid chemistry of palygorskite. Israel Programme for Scientific Translations, Jerusalem.

PAPAVASILIOU, C.T. (1979) The geochemistry and mineralogy of some N.W. Indian Ocean D.S.D.P. cores (Sites 222 and 223, Leg 23, Deep Sea Drilling Project). Unpub. Ph.D. Thesis, Southampton University.

PAPAVASILIOU, C.T. and COSGROVE, M.E. (1981) Chemical and mineralogical changes during basalt sea water interaction: Site 223, Leg 23 D.S.D.P., north-west Indian Ocean. Min. Mag., v:44, pp.141-146.

PAQUET, H. and MILLOT, G. (1972) Geochemical evolution of clay minerals in the weathered products in soils of Mediterranean climate. Proc.Int.Clay Conf.,Madrid, pp.199-206.

PASSAGLIA, E. (1970) The crystal chemistry of chabazites. Am.Mineral., v.55, pp.1278-1301.

PEARSON, R. (1978) Climate and evolution. London:Academic Press.

PERRY, E.A. and HOWER, J. (1970) Burial diagenesis in Gulf Coast pelitic sediments. Clays and Clay Minerals, v:18, pp.165-177.

PERRY, E.A., GIESKES, J.M and LAWRENCE, J.R. (1976a) Mg, Ca, and O^{18}/O^{16} exchange in the sediment pore water system, Hole 149, D.S.D.P., Geochim. Cosmochim. Acta., v:40, pp.413-423.

PERRY, E.A., BECKLES, E.C. and NEWTON, R.M. (1976b) Chemical and mineralogical studies, Sites 323 and 325. In: Initial Reports of Deep Sea Drilling Project, v:35 . Washington (U.S.Government Printing Office) pp.465-470.

PETERSON, M.N.A. and GOLDBERG, E.D. (1962) Feldspar distribution in South Pacific pelagic sediments. J.Geophys.Res., v:67,pp.3477-3492.

PETERSON, M.N.A., EDGAR, N.T., von der BORCH, C.C. and REX, R.W. (1970) Cruise leg summary and discussion. In: Initial Reports of Deep Sea Drilling Project, v:2 (U.S.Government Printing Office) pp.413-427.

PETTIJOHN, F.J. (1957) Sedimentary rocks. Harper and Bros.,New York.

PETZING, J. and CHESTER, R. (1978) Composition and origin of palygorskite-rich and montmorillonite-rich zeolite containing sediments from the Pacific Ocean. Comments.Chem.Geol.,v:21, pp.177-180.

PETZING, H. and CHESTER, R. (1979) Authigenic marine zeolites and their relationships to global volcanism. Mar.Geol.,v:29, pp.253-271.

PIMM, A.C. (1974) Sedimentology and history of the north-eastern Indian Ocean from late Cretaceous to Recent. In: Initial Reports of Deep Sea Drilling Project, v:22. Washington (U.S.Government Printing Office), p.717.

POLUSHKINA, A.P. and SIDORENKO, G.A. (1963) Melnikovite as a mineral species. Zapiski vses. Mineralog.Obshch. v:92, pp.547-554.

POWERS, M.C. (1967) Fluid release mechanisms in compacting marine mudrocks and their importance in oil exploration. Bull.Am. Assoc. Petrol.Geologists. v:51, pp.1240-1254.

PRESLEY, B.J., SIMS, R.R. and FEAGLEY, S.E. (1973) Interstitial water chemistry: Deep Sea Drilling Project Leg 20. In: Initial Reports of Deep Sea Drilling Project, v:20. Washington (U.S. Government Printing Office), pp.427-428.

PRESLEY, B.J., TREFRY, J., ARMSTRONG, D. and NUZZO, M. (1974) Interstitial water chemistry: Deep Sea Drilling Project, Legs 21 and 22. In: Initial Reports of Deep Sea Drilling Project, v:22. Washington (U.S.Government Printing Office) pp.861-864.

PRICE, N.B. (1967) Some geochemical observations on manganese iron oxide nodules from different depth environments. Mar.Geol. v:5, pp.511-538.

_____ (1976) Diagenesis in marine sediments. In: J.P. Riley and R. Chester (Editors) Chemical Oceanography, v:6, Academic Press, London. pp.1-58.

PRICE, N.B. and CALVERT, S.E. (1970) Compositional variation in Pacific Ocean ferromanganese nodules and its relationship to sediment accumulation rates. Mar.Geol., v:9, pp.145-171.

PYTKOWITZ, R.M. (1970) On the carbonate compensation depth in the Pacific Ocean. Geochim.Cosmochim.Acta., v:34, pp.836-839.

RAI, D. and LINDSAY, W.L. (1975) A thermodynamic model for predicting the formation, stability and weathering of common soil minerals. Soil Science Soc.Am.Proc.,v:39, pp.991-996.

RATEEV, M.A., EMELYANOV, E.M. and KHEIROV, M.B. (1966) Conditions for the formation of clay minerals in contemporaneous sediment conditions of the Mediterranean Sea. Lithology and Mineral Resources (English translation), p.4418.

REX, R.W. (1967) Authigenic silicates formed from basaltic glass by more than 60 million years' contact with sea water. Clays and Clay Minerals. Proc.15th Natl.Conf. (S.W. Bailey, ed.) pp.195-203. Pergamon: Oxford.

RIECH, V. (1979) Diagenesis of silica, zeolites and phyllosilicates at Sites 397 and 398. In: Initial Reports of Deep Sea Drilling Project, v:47. Washington (U.S.Government Printing Office) pp.741-

REYNOLDS, C.R.and HOWER, J. (1970) The nature of interlayering in mixed layer illite-montmorillonite. Clays and Clay Minerals, v:18, pp.25-36.

RICKARD, D.T. (1969) The chemistry of iron sulphide formation at low temperatures. Stockholm contr. Geology, v:20, pp.67-95.

RINALDI, R., PLUTH, J.J. and SMITH, J. (1974) Zeolites of the phillipsite family. Refinement of the crystal structure of phillipsite and harmotome. Acta cryst.series, v:30, pp.2426-2433.

ROBERSON, H.E., WEIR, A.H. and WOODS, R.D. (1968) Morphology of particles in size fractionated Na-montmorillonites. Clays and Clay Minerals, v:16, pp.239-247.

SABATIER, G. (1969) Palygorskite from the Deep Sea. A discussion. Am.Mineral., v:54, pp.567-568.

SANDSTROM, M. and GIESKES, J. (1974) Interstitial water studies, Leg 24. In: Initial Reports of Deep Sea Drilling Project,v:24. Washington (U.S.Government Printing Office) pp.799-810.

SASS, E. (1965) Dolomite-calcite relationships in sea water: theoretical considerations and preliminary experimental results. J.Sed.Pet., v:35, pp.339-347.

SCHEIDGGER ,K.F. and STAKES, S. (1977) Mineralogy, chemistry and crystallization sequence of clay minerals in altered tholeiitic basalts from the Peru Trench. Earth and Planet.Sci.Lett., v:36, pp.413-422.

SCHLICH, R. SIMPSON, E.S.W., GIESKES, J. et al. (1974) Site Reports. In: Initial Reports of Deep Sea Drilling Project, v:25, Washington (U.S.Government Printing Office)

SCHOTT, G. (1935) Geographie der Indischen und Stillen Ozeans, Verlag vonc.Boysen, Hamburg.

SCHWARZBACH, M. (1963) Climate of the Past: an introduction to Palaeo-climatology; translated from the German and edited by R.O. Muir.

SCLATER, J.G., von der BORCH, C.C., VEEVERS, J.J. et al. (1974a) Regional synthesis of the deep sea drilling results from Leg 22 in the eastern Indian Ocean. In: Initial Reports of Deep Sea Drilling Project, v:22. Washington (U.S.Government Printing Office).

SCLATER, J.G., ERICKSON, A.J. (1974b) Geothermal measurements on Leg 22 of the D/V Glomer Challenger. In: Initial Reports of Deep Sea Drilling Project, v:22. Washington (U.S.Government Printing Office) pp.387-

SCLATER, J.G. and FISHER, R.L. (1974c) Evolution of the east central Indian Ocean, with emphasis on the tectonic setting of the Ninetyeast Ridge. Geol.Soc.Am.Bull., v:85, pp.683-702.

SHEPPARD, R.A. and GUDE, A.J.,3rd.(1968) Distribution and genesis of authigenic silicate minerals in tuffs of Pleistocene Lake Tecopa, Inyo County, California. U.S.Geol.Surv.Prof.Paper 597, 38pp.

SHEPPARD, R.A. and GUDE, A.J. 3rd. (1969) Diagenesis of tuffs in the Barstow formation, mud hills, San Bernardino County, California. U.S.Geol.Surv.Prof.Paper 634, 35 pp.

SHEPPARD, R.A. and GUDE, A.J. (1970) Chemical composition and physical properties of phillipsite from the Pacific and Indian Oceans. Am.Mineral., v:55, pp.2053-2062.

SIMPSON, E.S.W., SCHLICH et al. (1974) Site reports: In: Initial Reports of Deep Sea Drilling Project, v:25. Washington (U.S. Government Printing Office).

SINGER, A., GAL, M and BANIN, A. (1972) Clay minerals in sediments of lake Kinneret (Tiberias), Israel. Sediment.Geol., v:8, pp.289-308.

SINGER, A. and NORRISH, K. (1974) Pedogenic palygorskite occurrence in Australia. Am.Mineral., v:59, p.508.

SINGER, A. (1979) Palygorskite in sediments: detrital, diagenetic or neoformed (a critical review). Geologische Rundschau.,v:69, pp.997-1007.

STATHOM, P.J. (1979) Measurement and use of peak-to-background ratios in X-ray analysis. Mikrochimica Acta., v:8, pp.229-242.

STEELE, I.M., SMITH, J.V., PLUTH, J.J. and SOLBERG, T.N. (1975) Quantitative analysis of zeolites using an energy dispersive system. In: Proc.10th Annual Conf.,Microbeam Anal.Soc., Las Vegas, Nevada: 37 ± 37D.

STEPHEN, I. (1954) Palygorskite from Shetland. Mine. Mag., v:30, pp.471-480.

STEPHENS, W.E., WATSON, S.W. (1975) Element associations through a lower Palaeozoic graptolitic shale sequence in the southern uplands of Scotland. Chem.Geol., v:16, pp.269-294.

STEWART, R.A., PILKEY, O.H. and NELSON, B.W. (1965) Sediments of the northern Arabian Sea. In: Marine Geology. New York (Elsevier publ.) no.3, pp.411-427.

STONECIPHER, S.A. (1976) Origin, distribution and diagenesis of phillipsite and clinoptilolite in deep sea sediments. Chem.Geol.,v:17, pp.307-318.

_____ (1977) Origin, distribution and diagenesis of deep sea clinoptilolite and phillipsite. Unpubl.Ph.D. Thesis, Scripps Inst.Oceanogr.

_____ (1978) Chemistry of deep sea phillipsite, clinoptilolite and host sediments. In: L.B. Sand and F.A. Mumpton (Editors), Natural Zeolites: Occurrence, Properties, Use. Pergamon: Oxford, pp.235-243.

STRAKHOV, N.M. (1967) Principles of lithogenesis, v:1. S.I.Tomkeieff and J.E. Hemingway (Editors). Consultants Bureau, New York; Oliver and Boyd, Edinburgh - London.

STUMM, J.W. and MORGAN, J.J. (1970) Aquatic chemistry. Wiley:Interscience, New York.

STUMM, J.W. and MORGAN, J.J. (1981) Aquatic chemistry. Wiley:Interscience, New York.

SUBBARO, K.V., KEMPE, D.R.C., REDDY, V.V., REDDY, G.R. and HEKINIAN (1979) Review of the geochemistry of Indian and other oceanic rocks. In: Ahrens (ed.) Origin and Distribution of Elements: Second Symposium, Physics and Chemistry of the Earth, v:II. Pergamon: Oxford. pp.367-

SULIMAN, A.M. (1972) The geochemistry of the Namurian argillites of Ireland. Unpubl. Ph.D. Thesis, Southampton University.

SUMMERHAYES, C.P. (1967) Manganese nodules from the south-western Pacific. J.Geol.Geophys., v:10, pp.1372-1381.

_____ (1969) Marine geology of New Zealand: Sub-Antarctic sea floor. Dep.Sci.Ind.Res.Bull., v:190.

TARDY, Y. and FRITZ, B. (1981) An ideal solid solution model for calculating solubility of clay minerals. Clay Minerals, v:16, pp.361-373.

TARDY, Y and GARRELS, R.M. (1974) A method of estimating the Gibbs energies of formation of layer silicates. Geochim.Cosmochim. Acta., v:38, pp.1101-1116.

TARLING, D.H. (1971) Gondwanaland, palaeomagnetism and continental drift. Nature, v:229, pp.17-21

TAYLOR, M.W. and SURDAM, R.C. (1981) Zeolite reactions in tuffaceous sediments at Teels Marsh, Nevada. Clays and Clay Minerals, v:29, pp.341-352.

TCHERNIA, P. (1980) Descriptive regional oceanography.Pergamon Marine Series, v:3. Pergamon Press (English translation).

TETTENHORST, R. (1962) Cation migration in montmorillonite. Am.Mineral., v:42, pp.769-773.

TOOMS, J.S., SUMMERHAYES, C.P. and CRONAN, D.S. (1969): Oceanogr.Mar.Biol. Ann.Rev., v:7, p.49.

TUREKIAN, K.K. and WEDEPHOL, K.H.(1961) Distribution of elements in some major units of the earth crust. Bull.Geol.Soc.Am.,v:72, pp.175-189.

TUREKIAN, K.K. (1964) The marine geochemistry of strontium. Geochim. Cosmochim.Acta., v:28, pp.1479-1496.

_____ (1965) Some aspects of the geochemistry of marine sediments. In: J.P. Riley and G. Skirrow (Editors): Chem. Ocean., v:2. Academic Press, London. pp.81-126.

UDINTSEV, G.B. (1965) New data on the bottom topography of the Indian Ocean. Okeanologiya, v:5, pp.993-998.

UPTON, B.G.J. (1982) Oceanic islands. In: A.E.M. Nairn and F.G.Stehli (Editors) The Ocean Basins and Margins. New York: Plenum Press. v:6, pp.585-643.

VALLIER, T.L. (1974) Volcanogenic sediments and their relation to land-mass volcanism and sea floor-continent movements, western Indian Ocean, Leg 25, Deep Sea Drilling Project. In: Initial Reports of Deep Sea Drilling Project, v:25. Washington (U.S.Government Printing Office) pp.515-542.

van der MERWE, C.R. and HEYSTEK, H. (1956) Clay minerals of South Africa soil groups: IV. Soils of the temperate regions. Soil Science, v:81, pp.399-414.

van STRAATEN, L.M.J.V. (1954) Composition and structure of Recent sediments of the Netherlands. Leidse Geol.,Mededel. v:19,pp.1-110.

VEEVER, J.J., HEIRTZLER, J.R. (1974) Tectonic and palaeogeographic synthesis of Leg 27. In: Initial Reports of Deep Sea Drilling Project, v:27. Washington (U.S.Government Printing Office) pp.1049-1059.

VOLKOV, I.I. (1961) Iron sulphides, their interdependence and transformation in the Black Sea bottom sediments. Akad.Nauk SSSR, Inst. Okeanologii Trudy, v:50, pp.68-92.

von der BORCH, C.C., SCLATER, J.G. et al. (1974) Site Reports. In: Initial Reports of Deep Sea Drilling Project, v:22. Washington (U.S.Government Printing Office).

von RAD, U. and ROSCH, H. (1972) Mineralogy and origin of clay minerals, silica and authigenic silicates in Leg 14 sediments. In: Initial Reports of the Deep Sea Drilling Project, v:14. Washington (U.S.Government Printing Office) pp.737-751.

von RAD, U. and ROSCH, H. (1974) Petrography and diagenesis of deep sea cherts from the central Atlantic. In: Pelagic Sediment: on land and under the sea. Spec.publs.Int.Ass.Sediment, 1. pp.323-347.

WATERMAN, L.S., SAYLES, F.L. and MANHEIM, F.T. (1972) Interstitial water studies on small core samples, Leg 14. In: Initial Reports of Deep Sea Drilling Project, v:14. Washington (U.S. Government Printing Office), pp.753-762.

WATERMAN, L.S. (1973) Interstitial water studies on small core samples, Leg 20. In: Initial Reports of Deep Sea Drilling Project, v.20. Washington (U.S.Government Printing Office) pp.423-425.

WATKINS, N.D. and KENNETT, J.P. (1971) Antarctic bottom water: major change in velocity during the late Cenozoic between Australia and Antarctica. Science, v:173, pp.813-818.

WATKINS, N.D. and KENNETT, J.P. (1972) Regional sedimentary disconformities and upper Cenozoic changes in bottom water velocities between Australia and Antarctica. Antarct.Res.Ser., v:19, pp.273-294.

WATKINS, N.D. and KENNETT, J.P. (1977) Erosion of deep sea sediments in the southern ocean between longitude 70 E and contrasts in manganese nodule development. Mar.Geol., v:23, pp.103-111.

WATTENBERG, H., TIMMERMANN, E. (1936) Uber die Sattigung des Seewassers an $CaCO_3$ und die anorganogene Bildung von Kalksedimenten. Ann.Hydrog.Marit.Meteorol.,v:64, pp.23-31.

WEAVER, C.E. (1968) Mineral facies in the Tertiary of the continental shelf and plateau. South-eastern Geology, v:9, pp.57-63.

WEAVER, C.E. and BECK, K.C. (1977) Miocene of the S.E. United States: a model for chemical sedimentation in a peri-marine environment. Sediment.Geol., v:17, pp.1-234.

WEAVER, C.E. and POLLARD, L. (1973) The chemistry of clay minerals. Elsevier, Amsterdam.

WEISSEL, J.K. and HAYES, D.E. (1971) A symmetric sea floor spreading south of Australia. Nature, v:231, pp.518-522.

WESER, O.E. (1974) Sedimentological aspects of strata encountered on Leg 23 in the northern Arabian Sea. In: Initial Reports of Deep Sea Drilling Project, v:23. Washington (U.S. Government Printing Office) p.503.

WHITEMARSH, R.B., WESER, O.E., ROSS, D.A. et al. (1974)

In: Initial Reports of the Deep Sea Drilling Project, v:23. Washington (U.S.Government Printing Office).

WIERSMA, J. (1970) Provenance, genesis and palaeogeographical implications of microminerals occurring in sedimentary rocks of the Jordan Valley area. Publ.Fys.Geog.Bodemkd.Lab. Univ., Amsterdam. No.15, p.240.

WINDOM, H.L. (1976) Lithogenous material in marine sediments. In: J.P. Riley and R. Chester (Editors) Chemical Oceanography. London Academic Press, v.5; pp.103-136.

WOOD, B.J. and FRASER, D.G. (1976) Elementary thermodynamics for geologists. Oxford Univ.Press.

WORZEL, I.L. (1959) Extensive deep sea sub-bottom reflections identified as white ash. Proc.Natl.Acad.Sci., v:45, pp.73-81.

WYRTKI, K. (1971) Oceanographic Atlas of the International Indian Ocean Expedition. Washington National Science Foundation, p.531.

YAALON, D.H. and WIEDER, M. (1976) Pedogenic palygorskite in some arid brown (calciorthid) soils of Israel. Clay Miner.,v:11, pp.73-80.

YODER, H.S. and EUGSTER, H.P. (1955) Synthetic and natural muscovites. Geochim. Cosmochim. Acta., v:8, pp.225-280.